

44014

Joint Institute for Nuclear Research

C3431(04) N-50

# NEUTRON SPECTROSCOPY, NUCLEAR STRUCTURE, RELATED TOPICS

XVI International Seminar on Interaction of Neutrons with Nuclei

Dubna, June 11-14, 2008

Proceedings of the Seminar

Объединенный институт ядерных исследований БЦБДДОЛБКА УДК 539.125.5(042) ББК 22.383.2я431+22.383.5я431+22.383.25я431 N48

# Organizing Committee

W. I. Furman (co-chairman), V. N. Shvetsov (co-chairman),
E. N. Rusakovich (seminar coordinator), M. V. Frontasyeva,
V. A. Khitrov, Yu. N. Kopatch, S. V. Kozenkov, P. V. Sedyshev,
A. M. Sukhovoj

Secretariat: O. E. Karpova, N. A. Malysheva, V. S. Rumyantseva, S. F. Yarovikov

The contributions are reproduced directly from the originals presented by the Organizing Committee.

Neutron Spectroscopy, Nuclear Structure, Related Topics: Proceedings N48 of the XVI International Seminar on Interaction of Neutrons with Nuclei (Dubna, June 11–14, 2008). — Dubna: JINR, 2009. — 434 p.

ISBN 978-5-9530-0206-6

This collection of papers reflects the current status of neutron-aided investigations of the properties of the nucleus, including fundamental symmetries, properties of the neutron itself, neutron-excited reactions and the parameters of the nucleus that determine the reaction cross section, as well as the latest theoretical development of all these problems. The works on experimental investigations in the physics of fission by neutrons of various energies are presented in great detail. The state of the art of experiments on the physics of ultracold neutrons and facilities to obtain them is described at length. The status achieved by now of the latest (from the viewpoint of technique) experiments and environment studies is covered as well.

**Нейтронная** спектроскопия, структура ядра и связанные вопросы: Труды XVI Международного семинара по взаимодействию нейтронов с ядрами (Дубна, 11–14 июня 2008 г.). — Дубна: ОИЯИ, 2009. — 434 с.

ISBN 978-5-9530-0206-6

В сборнике представлено современное состояние исследований свойств ядра с помощью нейтронов: фундаментальных симметрий и свойств самого нейтрона, возбуждаемых им реакций и параметров ядра, определяющих их сечения, а также последние теоретические разработки всех этих вопросов. Очень детально представлены работы по всем аспектам, связанным с экспериментальными исследованиями физики деления ядра нейтронами различных энергий. Достаточно полно описано современное состояние экспериментов по физике ультрахолодных нейтронов и установок для их получения, а также достигнутый к настоящему времени статус методически новейших экспериментов и результатов экологических исследований.

УДК 539.125.5(042) ББК 22.383,2я431+22.383.5я431+22.383.25я431

> © Joint Institute for Nuclear Research, 2009

### CONTENTS

UCN, Fundamental properties of the neutron, fundamental symmetries
Neutron-electron scattering length extraction from the neutron diffraction data measured on noble gases  Mitsyna L.V., Nikolenko V.G., Parzhitski S.S., Popov A.B., Samosvat G.S
Constraints on extra-short-range interactions from neutron scattering experiments  Nesvizhevsky V.V., Pignol G., Protasov K.V
Small angle scattering of fast neutrons and nucleon "atmosphere" of heavy nuclei  Alexandrov Yu.A., Anikin G.V
Storage of very cold neutrons in a trap with nano-structured walls  Lychagin E.V., Muzychka A.Yu., Nekhaev G.V., Nesvizhevsky V.V., Pignol G.,  Protasov K.V., Strelkov A.V
Current status of the experiment on direct measurement of neutron-neutron scattering length at the reactor YAGUAR  Furman W.I., Muzychka A. Yu., Crawford B.E., Howell C.R., Kandiev Ya., Levakov B.G., Litvin V.I., Lychagin E.V., Lyzhin A.E., Mitchell G.E., Nekhaev G.V., Sharapov E.I., Shvetsov V.N., Stephenson S.L., Strelkov A.V., Tchernukhin Yu.I., Tornow W 45
On a coincidence measurement in the YAGUAR nn-experiment Crawford B.E., Sharapov E.I., Stephenson S.L
Analytical calculation of the neutrons spectrum for direct measurement of n-n scattering at pulsed reactor YAGUAR  Ignatovich V.K
Status of the experiments on radiative branch of neutron decay  Khafizov R.U., Tolokonnikov S.V., Solovei V.A., Kolhidashvili M.R 69
Determination of n-e scattering length from neutron diffraction on a tungsten isotopic mixture in magnetic field  Alexandrov Yu.A., Oprea C., Oprea A.I
Measurement of the P-odd asymmetry of $\gamma$ -quanta from the $^{10}\mathrm{B}(n,\alpha)^7\mathrm{Li}^* \to ^7\mathrm{Li}(\mathrm{g.st.})$ reaction at heightened frequency of neutron polarization switching Vesna V.A., Gledenov Yu.M., Nesvizhevsky V.V., Petukhov A.K., Sedyshev P.V., Soldner T., Shul'gina E.V., Zimmer O

# Nuclear data, Methodical aspects

The development of segmented high resolution fast neutron spectrometer Abdurashitov J.N., Gavrin V.N., Matushko V.L., Mustafin M.F., Shikhin A.A., Veretenkin I.E., Yants V.E., Nico J.S., Thompson A.K	
The investigation of the resonance structure of the neutron cross-sections with the time-of-flight spectrometers at the Moscow meson factory Grigoriev Yu. V., Pavlova O.N., Zhuravlev B.V., Alekseev A.A., Berlev A.I., Koptelov E.A., Khlustin D.V., Mezentseva Zh.V	
Production cross-sections for the residual radionuclides from the $^{\mathrm{nat}}\mathrm{Pd}(p,x)$ and $^{\mathrm{nat}}\mathrm{Cd}(p,x)$ processes up to 40 MeV Khandaker M.U., Kim K., Lee M., Kim K., Kim G.N	
Measurement of excitation functions of proton induced reactions on nat Mo, nat W, and nat Zn up to 40 MeV  Kim G.N., Khandaker M.U., Kim K., Kim K.S., Uddin M.S., Lee M.W	
A method for the direct measurement of mean squre radius for excited nuclei  Panteleev Ts. Ts., Borzakov S.B., Simeonova-Panteleeva L.Ts	
Compilation of neutron resonance parameters NRF-3 Soroko Z.N., Sukhoruchkin S.I., Sukhoruchkin D.S	
Study of neutron emission in high-energy reactions with lead nuclei  Yurevich V.I	
Nuclear structure	
The search for the singlet deuteron in the radiative capture of the thermal neutrons by protons  Borzakov S.B., Gundorin N.A., Pikelner L.B., Rebrova N.V., Zhdanova K.V	
Level density and radiative strength functions of the $^{237}$ U nucleus from the $(\overline{n}, \gamma)$ reaction  Khitrov V.A., Sukhovoj A.M., Maslov V.M	
Status and problems of experimental study of excited nucleus superfluidity Sukhovoj A.M., Furman W.I., Khitrov V.A	
Parameters of distribution of the primary gamma-transition intensities following resonance neutron capture and some properties of compound nuclei <sup>157,159</sup> Gd	
Sukhovoj A.M., Khitrov V.A	

Possibility of experimental determination of reliable parameters of the compound-state gamma-decay and some errors of analysis:  96 Mo as an example
Sukhovoj A.M., Khitrov V.A
Radiative capture of thermal and resonance neutrons, main parameters of the gamma-decay process and properties of the <sup>174</sup> Yb nucleus Sukhovoj A.M., Khitrov V.A
Parameters of cascade gamma-decay of compound-nuclei $^{146}$ Nd, $^{156}$ Gd, $^{172}$ Yb, $^{182}$ Ta, $^{184}$ W, $^{191}$ Os, $^{231,233}$ Th, $^{239}$ U, $^{240}$ Pu from experimental data of reaction $(\overline{n}, \gamma)$ Sukhovoj A.M., Khitrov V.A.
Nuclear interaction dynamics in $^{56}$ Fe $(\alpha, xn)$ reaction Zhuravlev B.V., Titarenko N.N., Trykova V.I
$(n,p), (n,\alpha)$ reactions
Cross section measurement for the $^{147}\mathrm{Sm}(n,\alpha)^{144}\mathrm{Nd}$ reaction at $E_n=5.0$ and $6.0~\mathrm{MeV}$
Gledenov Yu.M., Sedysheva M.V., Stolupin V.A., Guohui Zhang, Jiaguo Zhang, Li-an Guo, Hao Wu, Jinxiang Chen, Guoyou Tang, Khuukhenkhuu G., Szalanski P.J. 248
The systematic study of $(n,p)$ cross sections for 18 and 20 MeV Khuukhenkhuu G., Gledenov Yu.M., Sedysheva M.V., Odsuren M
Nuclear Analytical Methods in the Life Sciences
Possibility of some radionuclides production using high energy electron bremsstrahlung
Baljinnyam N., Belov A.G., Ganbold G., Gerbish Sh., Maslov O.D., Shvetsov V.N261
Heavy metals and REE in bottom sediments and dreissenids of the Rybinsk reservoir
Goryaynova Z.I., Frontasyeva M.V., Pavlov S.S., Pavlov D.F
Determination of major and minor elements in sediments of some central and northern Mongolian rivers using INAA
Gerbish Sh., Baljinnyam N., Ganbold G., Ganchimeg G274
WDXRS of minor and trace element contents in soils of the Khamar-Daban mountain range
Grosheva E., Zaichick D., Lyapunov S., Schevchenko E
Neutron activation analysis of trace element contents in the crowns of human permanent teeth
Zaichick V

Role of nuclear analytical methods in the environmental health elementology  Zaichick V., Ermidou-Pollet S., Pollet S
Theory
Symmetries and spin-angular correlations in neutron induced reactions: elastic, radiative and fission channels  Barabanov A.L
The rotation of the fissioning compound nucleus in reactions induced by polarized neutrons  Bunakov V.E., Kadmensky S.G
The mechanism of excitation of giant resonances in nuclear fission and T-odd correlations for prescission gamma-quanta  Bunakov V.E., Kadmensky S.G., Kadmensky S.S
Low-energy scattering of a polarized neutron on a polarized proton Lyuboshitz V.L., Lyuboshitz V.V
Fission
ROT – effect in binary fission induced by polarized neutrons  Danilyan G.V., Granz P., Krakhotin V.A., Mezei F., Novitsky V.V., Pavlov V.S.,  Russina M., Shatalov P.B., Wilpert T
Detailed study of the effects following from rotation of the scissioning nuclei in ternary fission of <sup>235</sup> U by cold polarized neutrons ("ROT" and "TRI" effects)
Gagarski A., Petrov G., Guseva I., Zavarukhina T., Gönnenwein F., Mutterer M., von Kalben J., Trzaska W., Sillanpää M., Kopatch Yu., Tiourine G., Soldner T., Nesvizhevsky V
TRI- and ROT- effects in ternary fission as a new way of investigating fission dynamics at low excitation energies  Petrov G.A., Gagarski A.M., Guseva I.S.,, Gönnenwein F., Mutterer M.,  Bunakov V.E
The estimation of scission neutron parameters from $n$ - $f$ and $n$ - $n$ angular correlations in $^{235}$ U( $n_{\rm th}$ , $f$ ) reaction Guseva I.S., Gagarski A.M., Sokolov V.E., Petrov G.A., Krinitsin D.O., Val'sky G.V., Vorobyev A.S., Scherbakov O.A.
Left-right and angular asymmetry of fission neutron emission  Kornilov N.V., Hambsch FJ., Fabry I., Oberstedt S., Simakov S.P

Exotic high neutron multiplicity modes in <sup>252</sup> Cf(sf)
Pyatkov Yu.V., Tyukavkin A.N., Kamanin D.V., Falomkina O.V., Lavrova J.E., Falomkin I.I., Pyt'ev Yu.P., Sokol E.A., Kuznetsova E.A
Measuring of the fragments nuclear charges at the mini-Fobos spectrometer Tyukavkin A.N., Pyatkov Yu.V., Kamanin D.V., Kopach Yu.N., Alexandrov A.A., Alexandrova I.A., Borzakov S.B., Voronov Yu.N., Denisov S.V., Efimov G.L., Zhuchko V.E., Kondratiev N.A., Kuznetsova E.A., Lavrova Yu.E., Mitrofanov S.V., Panteleev Ts., Salamatin V.S., Tsurin I.P.
Reports received after deadline
A statistical analysis of regional oil impacts on environment  Oprea C., Gustova M.V., Maslov O.D., Oprea A.I., Szalansky P.J
Impact evaluation of the toxic and biologic active elements consumed through food crops on the consumer's health using nuclear methods and neural network technique  Oprea C., Maslov O.D., Gustova M.V., Belov A.G., Oprea A.I., Mihul A.,  Loghin V., Nicolescu C., Gorghiu G
Comparison of inorganic chemical constituents of different herbal medicines
Oprea C., Gustova M.V., Maslov O.D., Belov A.G., Oprea A.I., Pirvutoiu C., Vladoiu D
Asymmetry effects in the $^{19}$ F $(p,\alpha)$ reaction Oprea A.I., Oprea C.D
Photon neutron activation analysis of the sea lettuce algae from the Black Sea, Romania  Oprea C., Gustova M.V., Maslov O.D., Belov A.G., Oprea A.I., Ion I.,  Nedelcu M.G., Pirvutoiu C., Vladoiu D
ISINN-16 Program

The 16th International Seminar on Interaction of Neutrons with Nuclei: "Fundamental Interactions & Neutrons, Nuclear Structure, Ultracold Neutrons, Related Topics" (ISINN-16), was organized by the Frank Laboratory of Neutron Physics of the Joint Institute for Nuclear Research (Dubna, Russia). The Seminar continues the tradition of the FLNP annual workshops and seminars in the field. ISINN-16 was held in Dubna, Russia from June 11 to 14, 2008. 108 participants attended ISINN-16 representing leading scientific centers of Belgium, Bulgaria, Byelorussia, China, Czech Republic, France, Germany, India, Italy, Japan, Poland, Republic of Korea, Romania, Russia, Serbia, Sweden, Switzerland, Turkey and USA. The numerous delegation of JINR scientists included speakers and participants from the Frank Laboratory of Neutron Physics (FLNP), Flerov Laboratory of Nuclear Reactions (FLNR), Veksler-Baldin Laboratory of High Energy Physics (VBLHEP). More than 90 oral and poster reports were presented at the Seminar.

Scientists of different generations from leading laboratories carrying out investigation with neutrons aimed at fundamental and applied nuclear physics attended the Seminar. It became traditional to discuss within Seminar the problems of Life Sciences also. Special two sessions dedicated to the Nuclear Analytical Methods in the Life Sciences were held.

As usual the opening session was devoted to recent development of neutron sources. An impressive progress was achieved at Munich FRM-II reactor. In course of ultracold neutron session first information on very recent observation of neutron quantum states in the field of centrifugal forces was reported. Another new result related to an acceleration matter effect in neutron optics was presented at the same section. Both reports gave rise to very alive response and discussion.

Traditional topics were presented during sessions on fundamental properties of the neutron and fundamental symmetries; nuclear data and nuclear structure; nuclear fission and development of new experimental methods. Last two topics were considered during two pithy sessions each. The results of first test experiment on neutron EDM search by crystal-diffraction method were reported. A key topic of the fission session was recently discovered time non-invariant and rotational effects in ternary fission. Many new experimental and theoretical results were presented and discussed actively. More than 30 papers were presented at special poster session that gave rise to large interest of Seminar participants.

Many informal discussions and contacts took place in free time during the Welcome Party, long enough coffee breaks and traditional picnic held at the bank of Dubna river.

Favorable conditions for the Seminar were provided by the JINR Directorate. A hospitality and effective support of leadership and personnel of Dubna branch of Nuclear Physic Institute of Moscow State University ensured very comfortable atmosphere of the Seminar.

We would like also to acknowledge the traditional support of the Seminar by the Russian Foundation for Basic Research (grant # 08-02-06060-a). This allowed many scientists from Russia to take part in the Seminar and made it possible to publish the Seminar Proceedings.

We wish to thank all the members of the Advisory Committee for their fruitful propositions concerning the scientific program of the Seminar, the Organizing Committee and the Secretariat for their efforts in preparation and holding of the Seminar.

ISINN-16 Co-chairmen

W.I. Furman V.N. Shvetsov

# Neutron-electron scattering length extraction from the neutron diffraction data measured on noble gases

L.V.Mitsyna, V.G.Nikolenko, S.S.Parzhitski, A.B.Popov, G.S.Samosvat

Frank Laboratory of Neutron Physics, Joint Institute for Nuclear Research, 141980, Dubna, Russia

#### Abstract

The proposed new method for extraction of the neutron-electron scattering length  $b_{ne}$ , which is connected directly with the fundamental physical value of neutron mean squared charge radius, from the slow neutron diffraction on noble gases was developed and performed by analysis of literature data on structure factors for gases Kr,  $^{36}$ Ar and liquid Kr.

For the most part, different variants of analysis of these experimental data allow us to obtain  $b_{ne}$  value with the statistical accuracy 10–20 %, but in some of them the real possibility for the accessible accuracy no worse than 2–3% was shown. In order to remove some systematical errors and to reach such good accuracy the execution of the comparative diffraction measurements is proposed with a pair of gases having close atomic properties and different n,e-scattering contributions, such as  $Ar - {}^{36}Ar$  or Xe - Kr.

PACS. 28.20.-v, 61.12.-q, 14.20.Dh,13.40.-f

### 1. Introduction

History of the n,e-interaction investigations began nearly 70 years ago, the first mention of this effect was made by D.Ivanenko in 1941 [1]. However, in spite of existence of a dozen of the most precise experimental  $b_{ne}$  values with errors  $< 0.05 \cdot 10^{-3}$  fm obtained by different methods (see, for example [2]) there were doubts about the validity of their declared accuracy, as they differed by ~5 standard errors. In all methods there are principal troubles connected with the necessity of introducing large corrections, whose size of order of the investigated effect. Thus, further investigations of this problem with the aim to adjust  $b_{ne}$  value are desired and required as before.

The intrigue is that in the interval about  $\pm 10\%$  all  $b_{ne}$  values were scattered around the so-called Foldy scattering length

$$b_F = -\frac{\mu e^2}{Mc^2} = -1.468 \cdot 10^{-3} \text{ fm},$$

which, according to the Dirac generalized equation for neutron, is connected with the interaction between the neutron anomalous magnetic momentum and electric field. One may note that the terms attached to  $div\vec{E}$  in the Dirac generalized equation for neutron and in the Dirac equation for electron have the same structure

$$[\varepsilon + \frac{\hbar}{4Mc}(\frac{e\hbar}{2Mc} + 2\mu)]div\vec{E}$$

and depend on the particle magnetic momentum  $\mu$  only, and parameter  $\varepsilon$  appears just in the equation for neutron. In case of  $b_{ne}$  and  $b_F$  values the coincidence parameter  $\varepsilon$  must be equal to zero. Possible equality of  $b_{ne}$  and  $b_F$  values would be surprising, as it signifies that

the charge distribution of a neutron scattered on the outside charge becomes displayed through magnetic momentum only. So closeness of  $b_{ne}$  and  $b_F$  values will confirm this non-trivial phenomenon.

From the point of view of comprehension of all corrections introduced into the experimental data for masking effects the simplest experiment to obtain  $b_{ne}$  value is the slow neutron scattering by noble gas. Nevertheless, in these experiments it is impossible to ignore the diffraction on nuclei of neighboring atoms even at low gas densities. So, weak dependence of  $b_{ne}$  value obtained from the data of [3] on the gas pressure was noticed and taken into account in [4], whereupon the extracted  $|b_{ne}|$  values were decremented by ~10% for Kr and by ~5% for Xe.

Seemingly, the negative role of neutron diffraction at the observation of n,e-interaction effect was noticed first by A.I.Akhieser and I.J.Pomeranchuk [5] soon after appearance of the classical paper by E.Fermi and L.Marshall [6], which was one of the pioneering attempts to discover n,e-scattering. The warning [5] was evidently known to the authors of one of the most accurate results for the n,e-scattering length obtained in [3]. The authors of [3] used gases at low pressures 0.33-1.68 atm just to detect possible diffraction distorting the result.

The new method to obtain  $b_{ne}$  value proposed in Dubna [7] permits to use much more dense gases, inasmuch as the diffraction can be taken into account with satisfactory accuracy when extracting the n,e-effect. Our method is based on two facts:

- 1) diffraction and n,e-interaction contributions to scattering cross section have very different dependences on the momentum transfer  $\hbar q$  (oscillating and monotonous);
- 2) diffraction contribution to the scattering is proportional to a gas density n (or even has a term with  $n^2$ ), but the nuclear and n,e-scatterings do not depend on n.

Investigations of the neutron diffraction in monatomic gases in quest of interatomic interaction potentials are progressing in the last decades. As for gas densities, the pressures up to hundreds atmospheres are used in these experiments. So, the effect of n,e-scattering in them is essentially more than in the researches like [3].

#### 2. Basic relations

According to conceptions accepted in literature we describe the neutron scattering intensity per one target atom and unity neutron flux with the accuracy enough for our purposes by the following expression

$$\frac{dI(q)}{d\Omega} = \frac{\sigma_s}{4\pi} \left\{ F_s(V_0, q, A)(1+B) + \frac{nC(q)}{1 - nC(q)} F_s(V_0, q, 2A) \left( \frac{\sigma_{coh}}{\sigma_s} + B \right) \right\},\tag{1}$$

where  $B = \frac{8\pi a_{coh}b_{ne}Zf(q)}{\sigma_s}$ , q is the wave number of momentum transfer,  $\sigma_s$  and  $\sigma_{coh}$  are the total and coherent nuclear cross sections,  $a_{coh}$  is the length of coherent nuclear scattering, Z is the number of electrons in atom,  $f(q) = \left[1 + 3(q/q_0)^2\right]^{-1/2}$  is the electron form factor of an atom,  $q_0$  is the Hartree-Fock's constant, which characterizes atomic properties (see [8]). For taking into account the influence of the atoms thermal motion on the neutron scattering distribution in expression (1) we did not use the Placzek corrections, which are generally applied in the works for diffraction investigations, but more correct (see [9]) kinematic description. It was used in [3] and set out in detail in V.Turchin's book [10]. The thermal motion effect is described by function  $F_s$ 

$$F_{s}(V_{0}, \theta, A) = \frac{(A+1)^{2}}{A^{2}\sqrt{\pi}V_{0}U_{0}} \int_{0}^{\infty} \frac{V^{2}}{\sqrt{V_{0}^{2} + V^{2} - 2V_{0}V\cos\theta}} \times$$

$$\times \exp \left\{ -\frac{\left(V^{2} - V_{0}^{2} \frac{A - 1}{A + 1} - \frac{2V_{0}V\cos\theta}{A + 1}\right)^{2}}{4\left(\frac{A}{A + 1}\right)^{2} U_{0}\left(V_{0}^{2} + V^{2} - 2V_{0}V\cos\theta\right)} \right\} dV. \tag{2}$$

In expression (2)  $\theta$  is the scattering angle of neutron in the laboratory reference frame,  $V_0$  and V are the initial neutron velocity and its velocity after scattering, A is the atom mass number,  $U_0 = \sqrt{\frac{2kT}{mA}} = 128.9 \sqrt{\frac{T}{A}}$  [m/s], T is the gas temperature in K.

Function C(q) is connected with the structure factor S(q) by formula

$$S(q) - 1 = \frac{nC(q)}{1 - nC(q)}.$$
(3)

The peculiarity of expression (1) applied by us is the use of the function  $F_s$  attached to diffraction term with doubled atom mass, as the diffraction, first of all, is connected with the interaction between the neutron and pair of atoms having coincident velocity vectors.

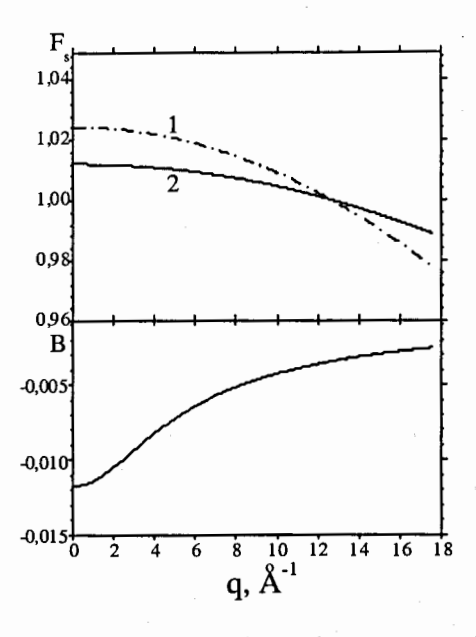


Fig.1. Contributions of thermal motion corrections to the neutron scattering intensity for Kr calculated for neutron diffraction scattering on single atom (curve 1) and on two atoms (curve 2) and calculation of n,e-contribution.

The values of separate effects for gaseous krypton are shown in Fig.1 and Fig.2. It is seen, that n,e-contribution to nuclear scattering is ~1% or less and does not depend on the

gas density. And the diffraction amplitudes rise strongly with the gas density increase at preserving positions of their maximums and minimums.

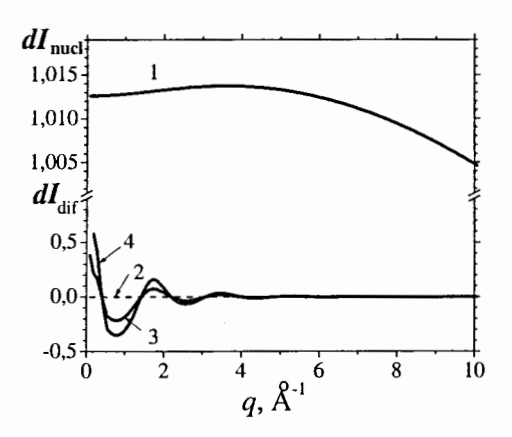


Fig.2. Calculation for Kr of the nuclear and n,e-scattering term contribution to the neutron intensity, which does not depend on the gas density - curve 1 and diffraction term dependent on the gas density: curve 2 - at the pressure 1 atm., curve 3 - at 100 atm., curve 4 - at 200 atm.

The problem of  $b_{ne}$  value determination comes to accurate separating the n,e-contribution from the diffraction waves with taking into account the thermal motion of atoms.

Unfortunately, for diffraction description there is no strict theory yet, so in our analysis we used different expressions describing relaxing oscillations of the correlation function C(q), such as

$$C(q) = (A_1 - A_2 n) \exp(-A_3 q) \sin(\frac{2\pi q}{A_4} + A_5), \tag{4}$$

where one or two out of five parameters  $A_1 - A_5$  are sometimes fixed.

Testing the different phenomenological formulas for C(q) description including hard-core model approach (as in [2]) adjudicated that all considered variants with the exception of the last one fit to the experimental data satisfactorily.

### 3. Results

The experimental data of [11-13] were used, where the S(q) values were obtained for gaseous Kr, isotope <sup>36</sup>Ar and for liquid Kr, in order to test the proposed method of the  $b_{ne}$  value obtaining. Moderate accuracy ( $\sim 5 \cdot 10^{-3}$ ) of these experimental S(q), which was sufficient to obtain information about interatomic interaction potentials, nevertheless, allowed us to extract  $b_{ne}$  value with the accuracy  $\sim 10 - 20$  %. To achieve better accuracy it is desirable to measure the scattered neutron intensity for noble gases with the relative accuracy  $3 \cdot 10^{-4} - 10^{-4}$ .

### 3.1. Gaseous Kr

In [14] we used experimental data S(q,n) measured for gaseous Kr and published in [11]. The structure factors were obtained for 17 gas densities  $n = (0.26-6.19)\cdot 10^{21}$  cm<sup>-3</sup> and 78 values of q up to 4 Å<sup>-1</sup>. To normalize the neutron scattering intensity the authors of [11] used vanadium, assuming that its scattering cross section is isotropic in the interval of q from 0 up to 4 Å<sup>-1</sup>, and the calculated S(q,n) value using the expression

$$\frac{dI(\vartheta)}{d\Omega} = \frac{\sigma_s}{4\pi} \left[ 1 + B_0 f(q) \right] \cdot \left\{ \left[ S(q, n) - 1 \right] \gamma + 1 + P_1(q) \right\},\tag{5}$$

where  $B_0$  is the correction for n,e-scattering with  $b_{ne} = -1.34 \cdot 10^{-3}$  fm,  $P_1(q)$  is the well known Placzek correction, which is usually applied to describe thermal motion of atoms in solid state experiments. We used all S(q,n) from [11] and described them by fitting formula, which ensued after equating the right parts of equations (1) and (5) and finding a solution of combined equation relative to the experimental S(q,n) from (5). We kept the normalizing multiplier  $\alpha$  before the fitting formula to take into account inaccurate knowledge of krypton and vanadium cross sections. In our expression (1) term with  $n^2$  appeared in diffraction dependency on gas pressure due to linear in n function  $C(q) = C_0(q) - nC_1(q)$ . Thus, in the fitting formula for describing the experimental S(n,q) values for all n for each q there were three varied parameters:  $C_0, C_1$  and B.

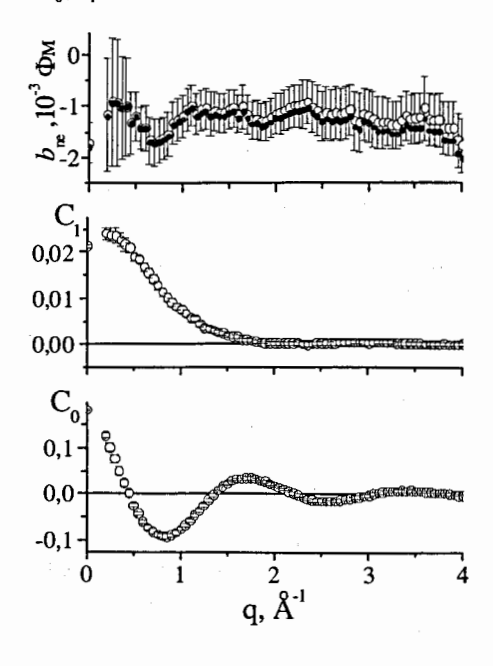


Fig.3. Fitted parameters  $b_{ne}$ ,  $C_0$  and  $C_1$  with F-corrections and  $\alpha = 0.975$  (light points) and with the Placzek corrections and  $\alpha = 1$  (black points).

The results of fits are shown in Fig.3. The upper picture shows a constancy of  $b_{ne}$  parameter within the error bars, which means good quality of the experimental data described with the accuracy  $3 \cdot 10^{-3}$ .

The performed fits with replacement of functions  $F_s$  by Placzek's  $P_1(q)$  showed that parameters  $C_0$  and  $C_1$  (see Fig.3) are practically indistinguishable, but  $b_{ne}$  systematically differ by  $\sim 0.1 \cdot 10^{-3}$  fm. This circumstance denotes once more the importance of correct calculation of atomic thermal motion influence on the extracted  $b_{ne}$  estimations.

Furthermore, the experimental data for all q and all n simultaneously were fitted by ten parameters:  $\alpha$ ,  $b_{ne}$  and eight parameters  $A_i$  for describing functions  $C_0$  and  $C_1$  by formula (4) (assuming that  $A_2$ =0). Examples of experimental data describing for four chosen gas densities demonstrate the satisfactory quality of this fitting at the lower part of Fig.4. The result obtained with free parameter  $\alpha$  is placed in the first line of Table.

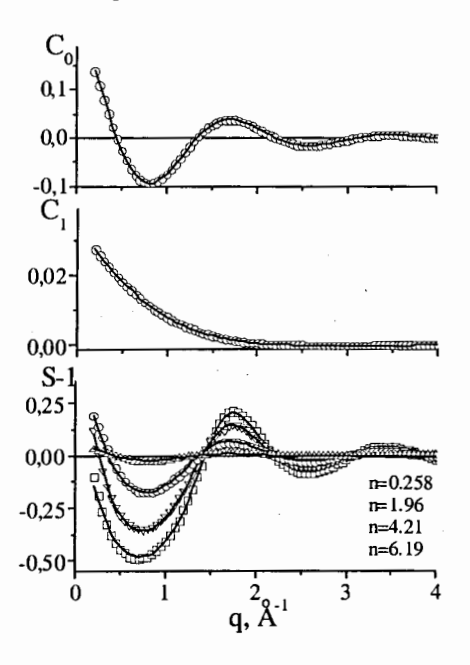


Fig.4. The result of simultaneous fitting to the data for all q and all n.

Thereby, in the proposed method the diffraction on neighboring atoms does not disturb obtaining the  $b_{ne}$  value, and that differentiates our method profitably from the researches with liquid metals [2], where correction for diffraction, which is more than n,e-effect, is calculated analytically.

# 3.2. Gaseous isotope <sup>36</sup>Ar

As  $^{36}$ Ar has an anomalously large scattering cross section  $\sigma_s \approx 78$  b, and n,e-effect for it must be ~10 times less than for natural Ar, so extracting  $b_{ne}$  value from the  $^{36}$ Ar diffraction data we made a check of our method sensitivity.

In [15] we used S(q) data obtained in the Institute Laue-Langevin in Grenoble [12] for  $q = (0.24-10.1) \text{ Å}^{-1}$  at four densities of gaseous isotope <sup>36</sup>Ar with the accuracy from 0.06% up to 0.2%.

Small number and narrow range of densities n did not allow us to get  $b_{ne}$  value for each given q separately (as in the case of gaseous Kr, see 3.1). We fitted these data for each density of  $^{36}$ Ar in the wide interval of q values using formulae (1) and (4). The authors of [12] normalized experimental S(q) values on the data at large q neglecting the diffraction there and not taking into account n,e-scattering. Their thermal motion corrections differed from  $F_s$ -corrections (2) by a constant multiplier close to 1 only, so their intensity we described by expression (1) with  $F_1 = F_2 = 1$  and with varied multiplier  $\alpha$  taking into account the difference of normalizations.

During data processing a strong correlation took place between  $b_{ne}$  value and  $\alpha$  ( $\Delta \alpha \sim 10^{-3}$  changed  $b_{ne}$  by 10%), and insufficient precision of normalization did not allow us to get  $b_{ne}$  value with the accuracy better than 10 %.

We could describe experimental data of S(q) satisfactorily at  $q \ge 3$  Å<sup>-1</sup>only. Moreover, all the data for the lowest density of argon were rejected because of large  $\chi^2$  criterion. The weighted average result for the rest three densities is shown in Table (line 2) with the statistical error. However, the systematic error of normalization evaluated over a wide interval q = (8-10) Å<sup>-1</sup> turned out two times more than the statistical one.

## 3.3. Liquid Kr

Although  $b_{ne}$  value extracting from the neutron scattering on liquid is not so clear in comparison with the scattering on gases because of the problem of adequate consideration of thermal motion for atoms of liquid, the  $b_{ne}$  value was also obtained from the diffraction data measured in Grenoble [13] for seven close densities of liquid Kr in the wide range  $q \sim (0.4-17) \text{ Å}^{-1}$ . We used these experimental data to verify different versions of  $b_{ne}$  value extracting. They were described in detail in [16,17].

Out of ~5000 experimental data presented in [13] we used S(n,q) in the interval  $q = 4 - 16 \,\text{Å}^{-1}$ , because we could not get fits with  $\chi^2 \le 1$  analyzing all the data (with  $q < 4 \,\text{Å}^{-1}$ ).

Simultaneous fitting of all seven densities with the same parameters  $A_i$  of function C(q) gave the result  $b_{ne} = -(1.39 \pm 0.04) \cdot 10^{-3}$  fm. The result of fitting is shown in Fig.5. However, the correlation between  $b_{ne}$  value and normalizing constant  $\alpha$  led to  $b_{ne}$  values spread up to  $\pm 30\%$ .

Using individual diffraction parameters fitted for each of seven samples and fixing them afterwards in the following fitting with free  $b_{ne}$  value and with seven different normalizing parameters  $\alpha_i$  we obtained  $b_{ne} = -(1.63 \pm 0.02) \cdot 10^{-3}$  fm. This error is 10-15 times less than for gaseous Kr and  $^{36}$ Ar, where it is caused by correlation between  $b_{ne}$  and  $\alpha$ . We succeeded in the break off correlation here due to wider region of q reached  $q > 16 \text{ Å}^{-1}$ , where n,e-contribution is negligible. This example demonstrates future prospects of obtaining  $b_{ne}$  value with the accuracy  $\sim 2\%$  by means of performing similar measurements with gaseous samples.

Unfortunately, this result can not be accepted as significant one on account of essential change of the extracted  $b_{ne}$  value at varying the limits of the working q-interval. It

can be evidently explained by insufficiently satisfactory description of neutron diffraction in liquid state of Kr.

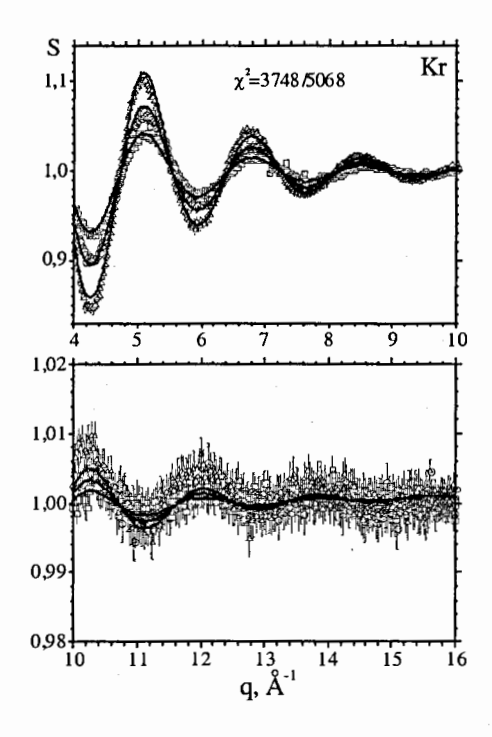


Fig.5. The simultaneous fitting for S(n,q) of liquid Kr for seven densities. The data for three densities n = 11.86, 14.57 and 17.01 nm<sup>-3</sup> are shown only. Points are experimental data, curves are fitting results.

Table

Target	Fittings	$< b_{ne} > 10^3$ , fm
Kr	for all $q$ and all $n$ simultaneously	-1,53±0,24
<sup>36</sup> Ar	averaged value of simultaneous fits for each n	-1,33±0,28±0,57
liquid Kr	average value obtained by interval dividing	-1,38±0,27
	average value of fits for three samples with similar $n$	-1,40±0,10

To escape safely a correlation between  $\alpha$  and  $b_{ne}$  we separated n,e-part in our fitting function (details see in [16]):

$$p(q) = \alpha[1 + Bf'(q)] = S^{\exp}(q)/\{1 + \gamma[S^{ft}(q) - 1]\},$$

where  $S^{\exp}(q)$  are the experimental and  $S^{\operatorname{fit}}(q)$  are the fitted structure factors, and after dividing the working q interval into six parts, which corresponded to six visible periods of the diffraction, obtained three  $b_{ne}$  values from the sum ratios  $p_i/p_j$  for i/j = 1/4, 2/5 and

3/6 (indexes i, j belong to different parts of the interval). Thus, we exclude  $\alpha$ . The average of three obtained  $b_{ne}$  values is placed in the third line of Table.

The averaged result of fittings to the experimental data for three groups of samples with similar densities, which were done in [17], is presented in the 4-th line of Table.

# 4. Conclusion

Possibilities of the new method to extract the n,e-scattering length from the measured structure factors were entirely shown with the data of experiments [11-13]. The data analysis for gaseous Kr demonstrated two variants of the data processing for  $b_{nr}$  value extracting: with the use of n- and q-dependences of experimental structure factors.

Fundamental capability to solve the problem of  $b_{ne}$  obtaining by new method was also shown by the model experiment performed by the Monte Carlo procedure [18], where angle distributions of neutrons with the energy 0.0143 eV scattered by gaseous Kr were considered. Calculations allowed us to come to a conclusion that having the data for 20 or more angles at a few gas densities in the range from  $0.0269 \cdot 10^{21} \text{cm}^{-3}$  to  $2.69 \cdot 10^{21} \text{cm}^{-3}$  with the relative accuracy of experimental points  $\sim 3 \cdot 10^{-3}$ , we could extract the  $b_{ne}$  value with the accuracy no worse than 5%.

High sensitivity of the new method to the ne-scattering length extracting was also shown in the work with <sup>36</sup>Ar, where n,e-effect is 10 times less than for natural argon.

A problem of the extracted neutron-electron scattering length precision in the proposed method depends not only on the statistical accuracy of the measured angle distributions of neutrons scattered by gas but also on an extent of diffractometer isotropy the constancy of the product of detector efficiency and the solid angle at all angles.

The exclusion of the dependency of neutron probability registration by the detectors on a scattering angle is fundamentally important task. In [11] this problem was solved by O normalizing the angle distribution of neutrons scattered by gaseous krypton on such Maistribution of neutrons scattered by vanadium. However, the order of vanadium isotropy is not known with the accuracy, which would be sufficient for our purposes (see [19,20]).

To obtain  $b_{ne}$  value with the accuracy ~ 2% the facility anisotropy must be less than ~3·10<sup>-4</sup>, that is practically impossible condition. The only possibility of this trouble avoidance is to realize relative measurements of two noble gases with strongly different n,econtributions to scattering cross sections, for example Ar and <sup>36</sup>Ar, which have n.econtributions 1.7% and 0.2%, or Xe and Kr, whose ones are 2.1% and 1.2%. correspondingly.

The authors are grateful to Dr. Renato Magli for valuable discussions and for his kind sending to us the numerical data for <sup>36</sup>Ar and liquid Kr, and also to Dr.Yu.A. Alexandrov for useful discussions.

The work is supported by RFBR, grant №07-02-00410.

#### References

- 1. D.Ivanenko, ZhETF, 11, 197(1941) (in Russian).
- 2. S.Kopecky, J.A. Harvey, N.W. Hill, M. Krenn, M.Pernicka, P. Riehs, and S. Steiner, Phys. Rev., C56, 2229(1997).
- 3. V.E. Krohn, G.R. Ringo, Phys. Rev., 148, 1303(1966); Phys. Rev., D8, 305(1973).
- 4. L.V.Mitsyna, V.G.Nikolenko, A.B.Popov and G.S.Samosvat, in X International Seminar on Interaction of Neutrons with Nuclei, Dubna, May 22-25, 2002, JINR, E3-2003-10 (Dubna, 2003), p.100.
- 5. A.Akhiezer and I.Pomeranchuk, ZhETF, 19, 558(1949)( in Russian). 06ъединенный институт

ядерных иселедований БИБЛИОТЕКА

- 6. E.Fermi and L.Marshall, Phys.Rev. 72, 1139(1947).
- L.V.Mitsyna, V.G.Nikolenko, S.S.Parzhitski, A.B.Popov and G.S.Samosvat, Preprint E3-2003-183, JINR(Dubna, 2003).
- 8. V.F. Sears, Phys. Reports, 141, 282(1986).
- 9. V.G.Nikolenko, A.B.Popov, Eur. Prys J., A34, 443(2007).
- 10. V.F.Turchin, Medlennye nejtrony (Gosatomizdat, Moscow, 1963)( in Russian).
- 11. A.Teitsma and P.A. Egelstaff, Phys. Rev., A21, 367(1980).
- H.Fredrikze, J.B. van Tricht, Ad A. van Well, R.Magli, P.Chieux and F.Barocchi, Phys. Rev., Lett., 62, 2612(1989).
- F.Barocchi, P.Chieux, R.Magli, L.Reatto and M.Tau, J.Phys. Condens. Matter, 5, 4299(1993).
- L.V.Mitsyna, V.G.Nikolenko, S.S.Parzhitski, A.B.Popov and G.S.Samosvat, Eur.Phys.J., C40, 473(2005).
- R.Magli, L.V.Mitsyna, V.G.Nikolenko, S.S.Parzhitski, A.B.Popov and G.S.Samosvat, in XIII International Seminar on Interaction of Neutrons with nuclei, Dubna, May 25-28, 2005, JINR, E3-2006-7 (Dubna, 2006), p.114.
- R.Magli, L.V.Mitsyna, V.G.Nikolenko, S.S.Parzhitski and G.S.Samosvat, Preprint E3-2006-139, JINR(Dubna, 2006).
- R.Magli, L.V.Mitsyna, V.G.Nikolenko, S.S.Parzhitski, A.B.Popov and G.S.Samosvat, in XIV International Seminar on Interaction of Neutrons with Nuclei, Dubna, May 24-27, 2006, JINR, E3-2007-23 (Dubna, 2007), p.183.
- L.V.Mitsyna, V.G.Nikolenko, A.B.Popov and G.S.Samosvat, JINR Communications, P3-2003-232(Dubna, 2003) (in Russian).
- 19. J.R.Granada, F. Kropff and R.E.Mayer, Nucl. Instr. Meth., 200, 547(1982).
- 20. Mayers, Nucl. Instr. Meth., 221, 609(1984).

# Constraints on extra-short-range interactions from neutron scattering experiments

V. V. Nesvizhevsky

Institute Lauc Langevin, 6 rue Jules Horowitz, F-38042, Grenoble, France G. Pignol, K. V. Protasov

Laboratoire de Physique Subatomique et de Cosmologie, UJF - CNRS/IN2P3 - INPG, 53 Av. des Martyrs, Grenoble, France

#### Abstract

The available data on neutron scattering were reviewed to constrain a hypothetical new short-range interaction. We show that these constraints are several orders of magnitude better than those usually cited in the range between 1 pm and 5 nm. This distance range occupies an intermediate space between collider searches for strongly coupled heavy bosons and searches for new weak macroscopic forces. We emphasise the reliability of the neutron contraints in so far as they provide several independent strategies. We have identified a promising way to improve them.

# 1 Introduction

The existence of other forces in nature, mediated by new bosons, has been extensively discussed in the literature, given their possibility in many of the extensions to the standard model of particle physics [1]. New bosons for example are predicted by most of the Grand Unified Theories embedding the standard model, with a coupling constant of  $\approx 10^{-1}$ . These strongly coupled bosons would have to be heavier than  $\approx 1$  TeV if they were not to conflict with present observations; heavier bosons will be searched for at the Large Hadron Collider. Lighter bosons could however have remained unnoticed, provided they interact weakly with matter. Such bosons would mediate a finite range force between two fermions:

 $V(r) = Q_1 Q_2 \frac{g^2 \hbar c}{4\pi r} e^{-r/\lambda} \tag{1}$ 

where g is the coupling constant,  $Q_1$  and  $Q_2$  the charges of the fermions under the new interaction, and the range of this Yukawa-like potential  $\lambda = \frac{\hbar}{Mc}$  is inversely proportional to the boson mass M. In the following we consider the interactions of neutrons with nuclei of atomic number A: the charge of the atom under the new interaction is equal  $Q_1 = A$ ; the neutron charge is equal unity  $Q_2 = 1$ . A new boson could even be massless, as has been suggested by Lee and Yang [2] well before the birth of the standard model, to explain the conservation of the baryon number. This additional massless boson would mediate a new infinite-range force, and could be seen in searches for violation of the equivalence principle at large distances. The presence of very light bosons ( $M \ll 1$  eV) would be shown by deviations from the gravitational inverse square law. Gravity has been probed down to distances of 0.1 mm [3]; new bosons lighter than  $2 \times 10^{-3}$  eV must thus have a coupling constant lower than the gravity strength between nucleons,  $g^2 < 10^{-37}$ .

Theories with extra large spatial dimensions [4, 5, 6, 7, 8, 9] provide strong motivation to search for such forces. If a boson is allowed to travel in large extra-dimensions, with a

strong coupling constant in the bulk, it behaves in our 4D world as a very weakly coupled new boson, the coupling being diluted in the extra-dimensions. The light dark matter hypothesis also argues in favour of the existence of new short range interactions [10].

While gravity experiments are most competitive in the distance range > 10  $\mu$ m, the measurements of the Casimir or Van der Waals forces (for a review, see e.g. [11]) give the best constraints in the nanometer range (10 nm <  $\lambda$  < 10  $\mu$ m), and antiprotonic atoms constrain the domain below 1 pm [12, 13], it has been suggested that experiments with neutrons could be competitive in the intermediate range [14, 15, 16, 17, 13, 18]. Neutrons could also probe spin-dependent interactions in a wider distance range [19], or spin-independent interactions in the range of several micrometers [20, 18, 21].

In this contribution we give the quantitative constraints on the parameters of the additional interaction,  $\lambda$  and g using the existing data on neutron scattering at nuclei. A detailed analysis is presented in [22].

# 2 Slow neutron / nuclei interaction with extra-shortrange interactions

The scattering of slow neutrons on atoms is described by the scattering amplitude  $f(\mathbf{q})$ ; this can be represented by a sum of a few terms [23]:

$$f(\mathbf{q}) = f_{\text{nucl}}(\mathbf{q}) + f_{ne}(\mathbf{q}) + f_V(\mathbf{q}) \tag{2}$$

The first and the most important term represents the scattering due to the nuclear neutron-nucleus interaction. At low energies discussed in this article, it is isotropic and energy-independant, because the nuclear radius is much smaller than the wavelegth of slow neutrons:

$$f_{\text{nucl}}(\mathbf{q}) = -b. \tag{3}$$

The coherent scattering lenght b is the fundamental parameter describing the interaction of slow neutrons with a nucleus [24].

The second term is the amplitude of so-called electron-neutron scattering due to the interaction of the neutron charge distribution with the nucleus charge and the electron cloud. This amplitude can be written as

$$f_{ne}(\mathbf{q}) = -b_{ne}(Z - f(Z, \mathbf{q})), \tag{4}$$

where  $f(Z, \mathbf{q})$  is the atomic form-factor measured in the X-rays experiments and  $b_{ne}$  is a constant called the electron-neutron scattering length, which is directly related to the neutron charge radius [23] and to the neutron electromagnetic form-factor  $G_E(\mathbf{q}^2)$  by

$$b_{ne} = -\frac{2}{a_0} \frac{m}{m_e} \frac{dG_E(\mathbf{q}^2)}{d\mathbf{q}^2} \bigg|_{\mathbf{q}^2 = 0}, \tag{5}$$

m and  $m_e$  being the neutron and electron masses,  $a_0$  the Bohr radius. This contribution to the total scattering amplitude is as small as a per cent for heavy nuclei.

In the presence of a new interaction (1), the scattering for a center of mass momentum  $\hbar k$  due to the extra interaction, within the Born approximation, is given by

$$f_V(\theta) = -A \frac{g^2}{4\pi} \hbar c \frac{2m\lambda^2/\hbar^2}{1 + (g\lambda)^2} \tag{6}$$

where  $q = 2k \sin(\theta/2)$ ,  $\theta$  is the scattering angle.

Any other possible contributions to the scattering amplitude  $f(\mathbf{q})$ , due to non zero nuclear radius, nucleon polarizability, etc. are very small in the energy range discussed here [23].

The nuclear scattering lengths are measured for almost all stable nuclei, using a variety of methods. A review of the different methods and a complete table of the measured scattering lengths can be found in [25]. We can distinguish two classes of method, with different sensitivities to a new interaction.

The first class – including the interference method, the total reflection method, the gravity refractometer method – measures the forward scattering amplitude  $f(\mathbf{q}=0)$ . These methods actually measure the mean optical potential of a given material, called the Fermi potential, due to the coherent scattering of neutrons at many nuclei. The Fermi potential is related to the *forward* scattering amplitude.

In the presence of the new force, the measured scattering lenght can be separated into a nuclear and an additional term

$$b_{\text{opt}} = -f(\mathbf{q} = 0) = b + A \frac{mc^2}{2\pi\hbar c} g^2 \lambda^2 \tag{7}$$

The second class of method – including the Bragg diffraction method and the transmission method – uses non-zero transferred momentum. In the Bragg diffraction method, the scattering amplitude for a momentum transfer of  $q_{\rm BD}=10~{\rm nm}^{-1}$  is measured. One actually extracts, besides the nuclear term, an extra contribution according to (6)

$$b_{\rm BD} = b + A \frac{mc^2}{2\pi\hbar c} g^2 \frac{\lambda^2}{1 + (q_{\rm BD}\lambda)^2} \tag{8}$$

In the case of the transmission method, the total cross-section is measured. Generally, neutrons with energies of about 1 eV are used; they are much faster than slow neutrons, and no coherent scattering can be observed. An additional interaction would manifest itself by an energy dependance of the extracted scattering length

$$b_{\rm TR}(k^2) = \sqrt{\frac{\sigma_{\rm tot}}{4\pi}} = b + A \frac{mc^2}{2\pi\hbar c} g^2 \lambda^2 \frac{\ln(1 + 4(k\lambda)^2)}{4(k\lambda)^2}$$
 (9)

Finally, we should also mention the very popular Christiansen filter technique; this measures *relative* scattering lengths, so we do not consider this data.

# 3 Random potential nuclear model

A simple and robust limit on the additional Yukawa forces can be easily obtained by neglecting the small term due to the neutron-electron scattering and by studing the general

A-dependence of the scattering amplitude. In the domain of  $\lambda \leq 1/q_{\rm BD}$ , the optical and Bragg diffraction methods are sensitive to the same amplitude

$$b_{\text{Meas}} = -f(\mathbf{q} = 0) = b + A \frac{mc^2}{2\pi\hbar c} g^2 \lambda^2$$
 (10)

as clear from (7) and (8). The presence of additional forces would be apparent from the linear increase of the measured scattering length as a function of A in addition to the A-dependence of the nuclear scattering length.

There exists a simple and elegant semi-phenomenological approach that describes the nuclear dependence [27]. It assumes that a nucleus can be presented as an attractive "square well" potential, with radius  $RA^{1/3}$  and depth  $V_0$  for slow neutrons. The scattering length would then be equal to

$$b(A) = RA^{1/3} \left( 1 - \frac{\tan(X)}{X} \right), \tag{11}$$

where  $X = \frac{RA^{1/3}}{\hbar} \sqrt{2mV_0}$  is supposed to be a random variable distributed uniformly over the range  $[\pi/2, 5\pi/2]$ ; the lower value corresponds to the appearance of a bound state and the upper limit is set sufficiently large not to influence the results of the present analysis; more details can be found in [27].

This model describes well the distribution of all experimental data; the value of the only free parameter in this model is estimated to be  $R=1.44\pm0.05$  fm at the 68 % C.L. The likelihood function at its maximum satisfies  $\ln(L)=-254$  for 216 degrees of freedom.

With a short-range new interaction included in the analysis we have to consider the random variable

$$b_{\text{Meas}} = RA^{1/3} \left( 1 - \frac{\tan(X)}{X} \right) + b_{\text{Extra}} A. \tag{12}$$

where the effect of the extra interaction is the slope  $b_{\text{Extra}} = \frac{mc^2}{2\pi\hbar c} g^2 \lambda^2$  of the linear term. The linear term is compatible with zero, as expected. We thus obtain a quantitative constraint for the coupling  $g(\lambda)$  [22]:

$$q^2 \lambda^2 \le 0.016 \text{ fm}^2 \text{ at } 95\% \text{ C.L.}$$
 (13)

This result is presented in fig. 1 for the distance range of interest,  $10^{-12} - 10^{-10}$  m.

# 4 Constraint from comparaison of forward and backward scattering of neutrons

Another way to constrain on aditional Yukawa forces consists in comparing the scattering lengths measured by different methods.

As explained above, the scattering lengths measured using the Bragg diffraction method  $b_{BD}$  and the interference method  $b_{opt}$  do not show the same sensitivity to a new

short-range interaction. According to (7) and (8), the ratio of the two values should deviate from unity in the presence of an additional interaction

$$\frac{b_{\text{opt}}}{b_{\text{BD}}} \approx 1 + \frac{A}{b} \frac{mc^2}{2\pi\hbar c} g^2 \lambda^2 \frac{(q\lambda)^2}{1 + (q\lambda)^2}$$
 (14)

We found a set of 13 nuclei for which both measurements exist. Taking into account systematic errors in those experiments as described in [22], we obtain the constraint

$$g^2 \lambda^2 \frac{(q\lambda)^2}{1 + (q\lambda)^2} \le 0.0013 \text{ fm}^2 \text{ at } 95\% \text{ C.L.}$$
 (15)

corresponding to the bold limit in fig. 1.

# 5 Electromagnetic effects

Up to now, the amplitude due to a new additional interaction  $f_V(\mathbf{q})$  has been compared to the nuclear one  $f_{\text{nucl}}(\mathbf{q})$  (see (2)). One could compare it to a smaller amplitude due to an electromagnetic interaction  $(f_{ne}(\mathbf{q}))$ . This idea was first proposed in ref. [14].

One could repeat the previous analysis using measurements of the total cross-section at energies of  $\approx 1$  eV (1/k=5 pm) instead of the Bragg diffraction. If the range of a new interaction is larger than 1 pm, the scattering length extracted would be free of any extra contribution. However, the residual electromagnetic effects due to the neutron square charge radius can mimick in this case an extra-force contribution in the quantity  $b(1 \text{ eV}) - b_{\text{opt}}$ , as this contribution is energy-dependent and proportional to the charge number of the atoms. The extracted difference  $b(1 \text{ eV}) - b_{\text{opt}}$  therefore contains the two contributions:

$$b(1 \text{ eV}) - b(0) = Zb_{ne}$$

$$- A \frac{mc^2}{2\pi\hbar c} g^2 \lambda^2 \left( 1 - \frac{\ln(1 + 4(\frac{\lambda}{5 \text{ pm}})^2)}{4(\frac{\lambda}{5 \text{ pm}})^2} \right)$$
(16)

Unfortunately, there is very clear disagreement between the two groups of values for  $b_{ne}^{\text{exp}} = \frac{b(1 \text{ eV}) - b(0)}{Z}$  known as the Garching-Argonne and Dubna values [28]

$$b_{ne}^{\rm exp} = (-1.31 \pm 0.03) \times 10^{-3} \text{ fm [Gartching-Argonne]}$$
  
 $b_{ne}^{\rm exp} = (-1.59 \pm 0.04) \times 10^{-3} \text{ fm [Dubna]}$  (17)

The discrepancy is much greater than the quoted uncertainties of the experiments and there evidently an unaccounted for systematic error in at least one of the experiments.

In order to overcome this difficulty we could determine  $b_{nc}$  from the experimental data on the neutron form factor (5). The simplest way to do this consists in using a commonly accepted general parametrization of the neutron form factor [29]:

$$G_E(\mathbf{q}^2) = -a\mu_n \frac{\tau}{1+b\tau} G_D,\tag{18}$$

where  $\mu_n = -1.91\mu_B$  is the neutron anomalous magnetic moment,  $\tau = q^2/4m^2$  and

$$G_D(\mathbf{q}^2) = \frac{1}{(1 + \mathbf{q}^2/0.71 (\text{GeV/c})^2)^2},$$
 (19)

is so-called dipole form factor; a and b being fitting parameters.

A fit of an existing set of the neutron form factor experimental data [30] yields the following values for the parameters:

$$a = (0.77 \pm 0.06)$$
  
 $b = (2.18 \pm 0.58)$ 

with  $\chi^2/\text{NDF} = 15.3/27$ . The  $b_{ne}$  determined in this way is

$$b_{ne} = (-1.13 \pm 0.08) \times 10^{-3} \text{ fm.}$$
 (20)

Our principal conclusion consists in the observation of (underestimated) systematical uncertainties in the presented experiments. Therefore a single experiment/method can not be used for any reliable constraint. A conservative estimate of the precision of the  $b_{ne}$  value could be obtained from analysing the discrepancies in the results obtained by different methods; it is equal to  $\Delta b_{ne} \leq 6 \times 10^{-4}$  fm. The corresponding contraint at the  $2\sigma$  level [22]

$$\frac{mc^2}{2\pi\hbar c} g^2 \lambda^2 \left( 1 - \frac{\ln(1 + 4(\frac{\lambda}{5 \text{ pm}})^2)}{4(\frac{\lambda}{5 \text{ pm}})^2} \right) \leqslant \Delta b_{ne}$$
 (21)

is represented by the dot-dashed line in fig. 1 and 2.

# 6 Asymmetry of scattering

As is clear from fig. 1, the best constraint was obtained from the analysis of the energy dependence of the neutron scattering lengths in the  $b_{ne}$  measurements inspite of systematic errors in these experiments. However, the precision here is limited by the correction for the  $b_{ne}$  value itself. An obvious proposal for improving this constraint would be to set up experimental conditions free of the  $b_{ne}$  contribution. This is indeed possible, because neutron-electron scattering is essential for fast neutrons only, and is absent for slow neutrons.

We propose improving the experiment [26] and measuring the forward-backward asymmetry of the scattering of neutrons at atoms of noble gases, in the following way: the initial velocity of the neutrons should correspond to the range of very cold neutrons (VCN); the double differential measurement of neutron velocity before/after scattering should be used to calculate the transferred momentum for every collision.

The measurement described above could provide an accuracy of at least  $10^{-3}$  for the ratio of forward to backward scattering probabilities and a corresponding constraint for the additional short-range interaction shown in fig. 1. The relative drop in sensitivity at a few times  $10^{-11}$  m is due to the appearance of neutron electron scattering; the range of interest for this possible constraint is  $10^{-11} - 10^{-8}$  m.

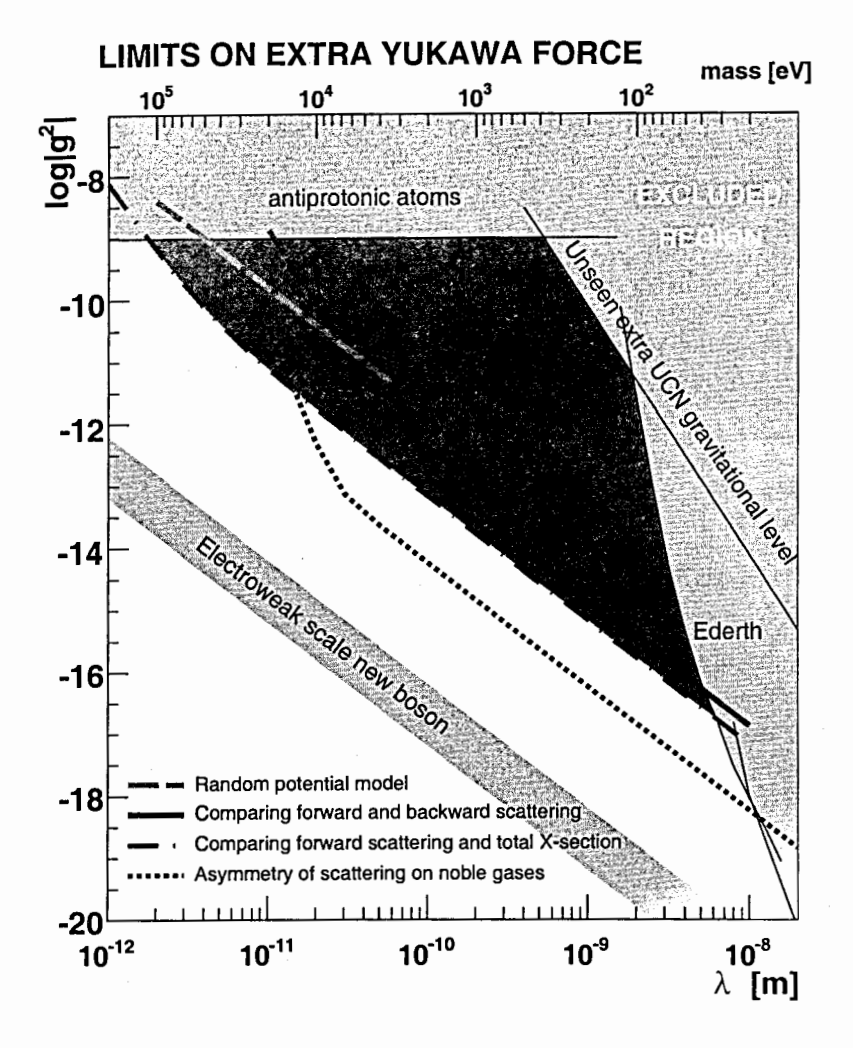


Figure 1: The shaded regions correspond to current experimental limits on extra Yukawa interaction. It includes constraint at 95 % C.L. (dashed, dot-dashed and bold lines) obtained in this article, and the existing constraints [11, 13]. The dotted line is an estimation of the sensitivity of proposed experiment.

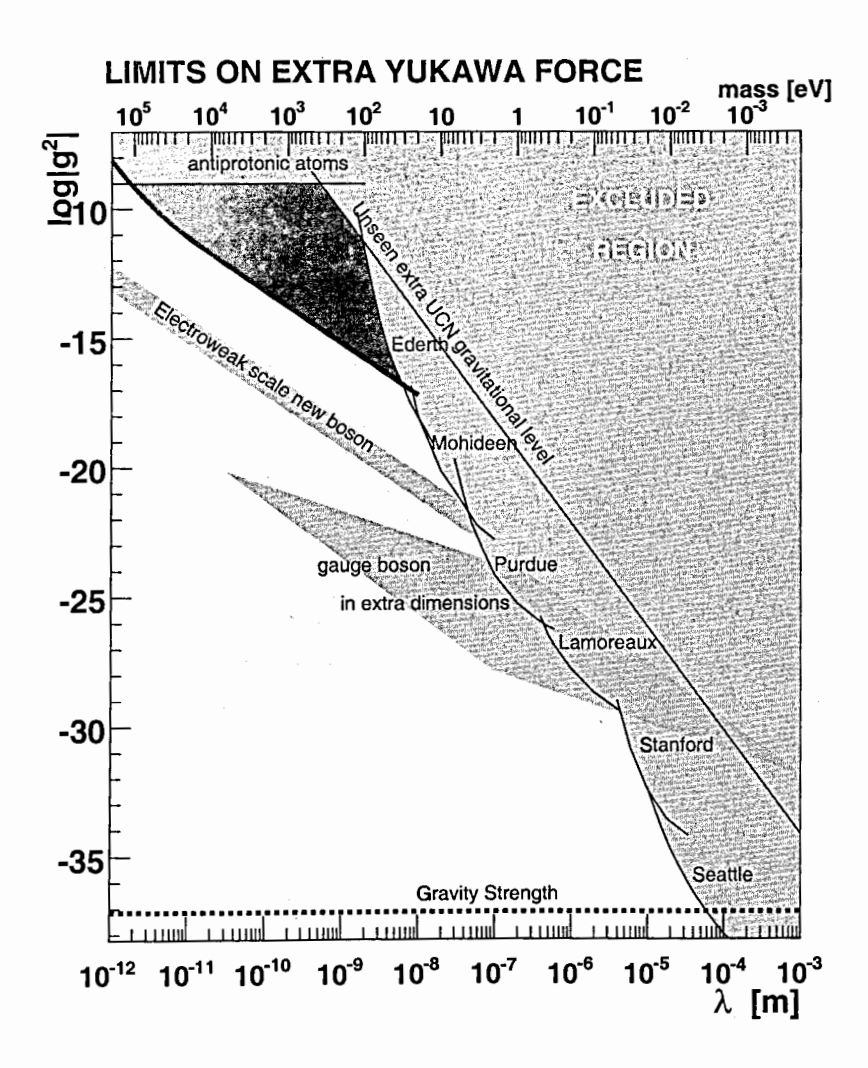


Figure 2: Experimental limits on extra interactions including the best neutron constraint obtained in this article (bold line). Two theoretical regions of interrest are shown: new boson with mass induced by electroweak symmetry breaking [10], and new boson in extra large dimensions [4].

# 7 Conclusion

We analysed the constraints for extra short-range interactions on the basis of the existing data on neutron scattering. These constraints are several orders of magnitude better than those usually cited in the range between 1 pm and 5 nm. The reliability of these constraints was supported by the application of several independant methods with comparable accuracy, as well as by the use of a major fraction of known neutron scattering lengths and treatment of the data in a most conservative way. One constraint obtained within the random potential nuclear model was based on the absence of an additional linear term in the mass dependance of the neutron scattering lengths. It would be difficult to improve this constraint in either experimental or theoretical terms. Another constraint was derived by comparing two types of neutron scattering experiments with different sensitivities to the extra short-range interactions. These are interference experiments measuring forward neutron scattering and the Bragg diffraction. The accuracy here is limited by the relatively poor precision of the Bragg scattering technique. Significant improvements in the accuracy of such experiments would be particularly interesting. Further constraints were estimated using the energy-dependence of the neutron scattering lengths at heavy nuclei. They are limited by the precision of our knowledge of the neutron-electron scattering length. An elegant method for further improving such constraints would consist in achieving experimental conditions free of  $b_{ne}$  contribution. This is indeed possible, given that neutron-electron scattering is essential for fast neutrons only. The experiment would consist in scattering very cold neutrons at rare noble gases and in measuring precisely the differential asymmetry of such scattering as a function of the transferred momentum.

# References

- [1] W.-M. Yao et al., J. Phys. G 33, 1 (2006).
- [2] T. D. Lee and C. N. Yang, Phys. Rev. 98, 1501 (1955).
- [3] C. D. Hoyle et al., Phys. Rev. D 70, 042004 (2004);
   D. J. Kapner et al., Phys. Rev. Lett. 98, 021101 (2007).
- [4] N. Arkani-Hamed, S. Dimopoulos and G. R. Dvali, Phys. Lett. B 429, 263 (1998); Phys. Rev. D 59, 086004 (1999).
- [5] I. Antoniadis et al., Phys. Lett. B 436, 257 (1998).
- [6] V. A. Rubakov and M. E. Shaposhnikov, Phys. Lett. B 125, 136 (1983); Phys. Lett. B 125, 139 (1983).
- [7] M. Visser, Phys. Lett. B 159, 22 (1985).
- [8] I. Antoniadis, Phys. Lett. B 246, 377 (1990).
- [9] J. D. Lykken, Phys. Rev. D 54, 3693 (1996).

- [10] P. Fayet, Phys. Rev. D 75 115017 (2007);P. Fayet, arXiv:hep-ph/0111282.
- [11] M. Bordag, U. Mohideen and V. M. Mostepanenko, Phys. Rept. 353, 1 (2001).
- [12] M. Hori et al., Phys. Rev. Lett. 91, 123401 (2003).
- [13] V. V. Nesvizhevsky and K. V. Protasov, Class. Quant. Grav. 21, 4557 (2004).
- [14] H. Leeb and J. Schmiedmayer, Phys. Rev. Lett. 68, 1472 (1992).
- [15] A. Frank, P. van Isacker and J. Gomez-Camacho, Phys. Lett. B 582, 15 (2004).
- [16] P. J. S. Watson, arXiv:hep-ph/0406308.
- [17] G. L. Greene and V. Gudkov, Phys. Rev. C 75, 015501 (2007).
- [18] V. V. Nesvizhevsky, G. Pignol and K. V. Protasov, Proceedings of the 42th Rencontres de Moriond (2007).
- [19] S. Bacßler, V. V. Nesvizhevsky, K. V. Protasov and A. Y. Voronin, Phys. Rev. D 75, 075006 (2007).
- [20] O. Bertolami and F. M. Nunes, Class. Quant. Grav. 20, L61 (2003).
- [21] V. V. Nesvizhevsky et al., Nature 415 297 (2002).
- [22] V. V. Nesvizhevsky, G. Pignol and K. V. Protassov, Phys. Rev. D 77, 034020 (2008).
- [23] V.F. Sears, Phys. Reports 141, 281 (1986).
- [24] E. Fermi, L. Marshall, Phys. Rev. 71, 666 (1947).
- [25] L. Koester, H. Rauch and E. Seymann, Atomic Data and Nuclear Data Tables 49, 65 (1991).
- [26] V. E. Krohn and G. R. Ringo, Phys. Rev. 148, 1303 (1966).
- [27] M. Peskhin and G. R. Ringo, Am. J. Phys. 39, 324 (1971).
- [28] S. Kopecky, J. A. Harvey, N. W. Hill, M. Krenn, M. Pernicka, P. Riehs, and S. Steiner, Phys. Rev. C56, 2229 (1997).
- [29] S. Glaster et al., Nucl. Phys. B 32, 221 (1971);
   A. F. Krutov and V. E. Troitsky, Eur. Phys. J. A 16, 285 (2003).
- [30] http://www.jlab.org/cseely/formfactor-data.txt

# Small angle scattering of fast neutrons and nucleon "atmosphere" of heavy nuclei

Yu.A.Alexandrov
FLNP, Joint Institute for Nuclear Research, Dubna, Russia
G.V.Anikin
Institute of Physics and Power Engineering, Obninsk, Russia

**Abstract:** The neutron excess of heavy nuclides may lead to a slow downing nucleon density at the nuclear perifery. Such an "atmosphere" can affect the small angle scattering cross sections of fast neutrons. The anomaly connected with nuclear "atmosphere" must be taken into account in calculation of neutron polarizability the last potential being presented as  $C_{pol}/r^4$ . The  $Z^2$ -dependence of  $C_{pol}$  must be investigated as well. Some attempts are presented to account for these effects.

The fifties of XX century, the time of intensive development of nuclear theories, were also the time of beginning of search for long-range interaction effects between neutron and nucleus, which could determine thin structure of the first diffraction maximum in the pattern of neutron scattering by nuclei (first of all, by heavy ones). The interaction of neutron magnetic moment with electric field of nucleus predicted by Schwinger [1] was detected, in which it moved in the process of scattering. The Schwinger cross section burst at scattering angles less than 3 degree is traced most clearly in papers [2,3], when the nuclear reactor was used as a powerful neutron source, which allowed one to apply a very high degree of collimation of neutron flux.

In paper [3] it was proposed to estimate the contribution of another effect of electromagnetic type – the scattering of induced electric dipole moment in the neutron (the so-called neutron "polarizability") into the small angle neutron scattering. The measurements of neutron scattering cross sections by heavy nuclei for small angles (less than 20-25 degree) were carried out in the wide energy range (0.5-15 MeV, see, for example, papers [2,4-7]). After that, it became possible to trace that the deviations of experimental cross sections from the calculation with nuclear short-acting potential (for example, in the Woods-Saxon form) correlate with the real part of amplitude of nuclear scattering pointing to its interference with the amplitude of long-range interaction unaccounted in the calculation.

If we attribute all these deviations to electric polarizability of a neutron, then too large value of the polarizability factor (around  $1.5\cdot10^{40}$  sm<sup>3</sup>) turns out for it. There occurred a supposition that other effects [2, 5] admix to the long-range interaction. All these problems are discussed in detail in review [8], where the results of study by Pokotilovsky et al. are also considered [9], in which contribution of the long-range interaction potential in the form of  $C_0 \cdot R^n/r^n$  in the cross section of small angle scattering of fast neutrons is analyzed. In paper [9] it was shown that at the increase of constant  $C_0$  by a factor of 1.5 deviations of small angle cross sections from the calculation with purely nuclear potential at the index n=6 are very close to those, which occur at n=4, i.e. at the electromagnetic long-range interaction related, for example, with the neutron polarizability  $\alpha$ =1.5·10<sup>-40</sup>cm<sup>3</sup>. It may be pointed out that simultaneously in paper [9] such reserves as taking into account the influence of nuclear "atmosphere" at the nuclear surface and dependences of small angle anomalies in cross sections on the nuclear charge are used insufficiently to estimate the value and physical nature of the long-range interaction.

The "atmosphere" apparently related to the excess of neutrons in heavy nuclei may imitate long-range interaction only at the limited interval of distances from the nuclear surface. It may be called the intermediate long-range interaction  $V_{\rm in}$ . If we denote the true (for example, electromagnetic) long-range interaction as  $V_{\rm e}$ , then the three-component representation of the neutron scattering potential will have the form:

$$V = V_0 + V_{in} + V_e$$

where  $V_0$  – the ordinary nuclear potential, for example in the Woods-Saxon form. The analysis of neutron scattering with two-component potential  $V=V_0+V_{long}$  automatically includes the intermediate potential into the long-range interaction  $V_{long}=V_{in}+V_e$  and the steepness of its decrease  $1/r^n$  may be considerably greater (n=6, for example), since  $V_{in}$  may be rather large.

Statement on the presence of "atmosphere" was made in the papers by Wilkinson and Burhop [10-12], who analyzed K-meson capture in the vicinity of nuclear surface. Cluster composition of the "atmosphere" was indicated in percentage terms (deuterons, bineutron, alpha-particles). It was traced not only in the nuclei of average atomic weight but also in lead. Another paper, which reported on the excess of the real part of potential at the nuclear periphery, was the paper by Anand et al. [13]. There this excess was added in the form of derivative from the Woods-Saxon potential. Finally, in paper [14], where the authors studied thin structure of the neutron-optical potential for lead, some excess of the mean depth of potential well was observed outside the radius of 8 fermi. In our Fig. one of the variants of periodic (layered) potential of paper [14] is reproduced (curve A). In itself this potential is interesting by the fact that many resonance structures in cross sections of heavy nuclei were reproduced with it. In the upper part of the Fig. (curve B) the total neutron cross section for lead at the estimation by BROND-2 [15] is presented. The correlation of structural elements of the potential and intervals of the neutron wavelengths is seen, in which the greatest bursts of cross section are observed. Physical interpretation of details of the potential needs further consideration. Perhaps, it points to the space division of nucleon shells. Appearance of the potential of complicated shape can hardly be regarded as totally unexpected. The features of layering of properties of optical potential were observed for a long time and in papers by many authors.

Despite the indication of the theory that maxima of imaginary and spin-orbit parts must be, where the derivative from the real part is maximum, in many cases they are situated either in the "inner" nuclear region, or beyond its bounds. This is easy to understand if the Woods-Saxon potential describes only on average the shape of decline of the potential at the nuclear surface and the real potential has bursts in the vicinity of nuclear surface. Near these bursts as shown in paper [14] maxima of the imaginary and spin-orbit parts of the potential are located. Moreover, in our attempts to describe angular distributions of fast neutrons [4-6] at the sequential transition from one neutron energy to another abrupt changes of radial address of maximum of the imaginary part of potential were observed, and in paper [7] three maxima of the imaginary part were obtained at once.

Broken curve (A') on the presented figure is close to the mean level of structural potential and is expressed by the formula:

$$-V(r) = V_0/\{1 + \exp[(r-R)/a]\} + V_{np} \cdot \exp[-(r-R_{np})^2/b^2]$$

Here the Woods-Saxon potential has the parameters:  $V_0$ =44 MeV, R=7.5 fermi, a=0.3 fermi. Gaussian is added to it with the parameters:  $V_{np}$ =25 MeV,  $R_{np}$ =8.6 fermi, b=0.4 fermi. There proves to be something like the Anand potential.

Apparently, it would be of interest to repeat the analysis of small angle neutron cross sections carried out in paper [9] but with the application, for example of the Anand potential with the excess of the real part at the nuclear periphery, as purely nuclear interaction. It would

be interesting to compare the results of such analysis with the calculations of neutron scattering cross sections (especially at the neutron energy in the region of 1 MeV) when the structural nuclear potential from paper [14] is used.

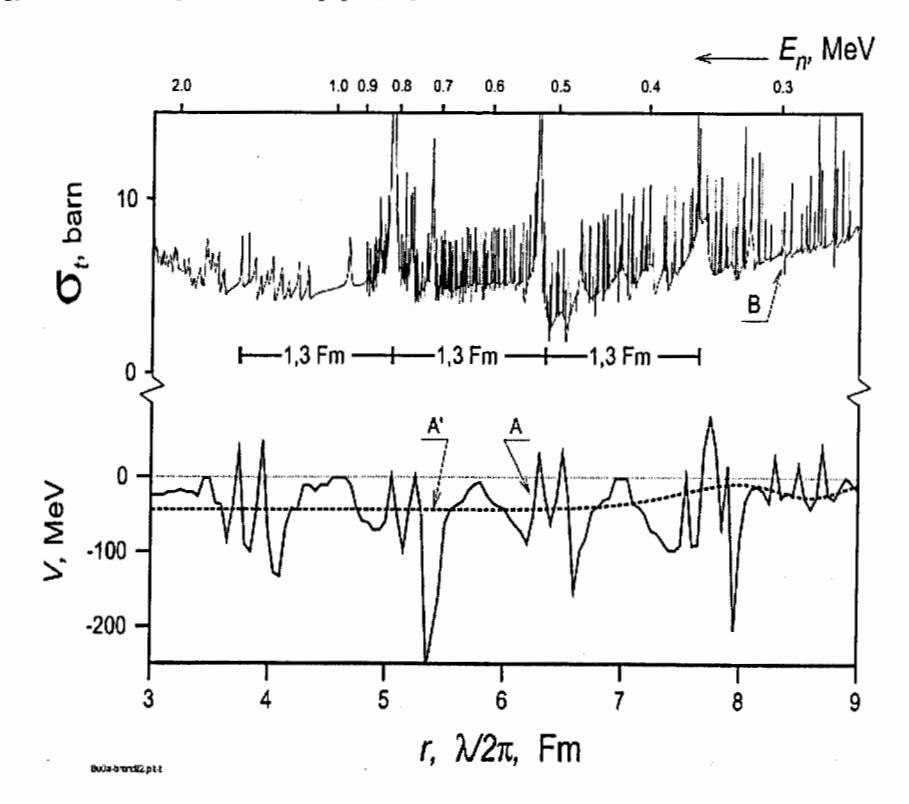


FIG: The real part of potential from paper [14] (curve A), as compared to the structure of total neutron cross section of lead (the upper curve, B). Comment is in the text.

As for the study of dependence of anomalies in scattering of neutrons for small angles from the charge of nucleus, some results in this direction were obtained in 1974 in paper [16]. These data were not presented quite widely and were not included into consideration in review [8].

In short, the contents of the given study may be presented as follows. Within the framework of the unified approach to describe optical potential including long-range interaction, the fitting of calculated angular distributions was carried out in the wide range of angles and total cross sections for the experiment for four elements: bismuth, thorium, uranium and plutonium. Experimental data were used in the neutron energy range 0.5 –14 MeV, with 4+6 energies for each element.

The calculated optical potential  $V_0$  included, along with the purely nuclear  $V_{nuc}$ , the Schwinger  $V_{sch}$  and the unknown additional long-range interaction  $V_{long}$  (which was called  $V_{pol}$  in paper [16])

$$V_0 = V_{\text{nuc}} + V_{\text{sch}} + V_{\text{long}}$$

The potential  $V_{\text{nuc}}$  contained two Woods-Saxon expressions, which changed each other at the radius  $r=R_1$ .

$$-V_{nuc}(r) = \begin{cases} V_1 (1 + \exp[(r-R_1)/a_1])^{-1}, & r \leq R_1 \\ V_2 (1 + \exp[(r-R_1)/a_2])^{-1}, & r > R_1 \end{cases}$$

The values of parameters of the given potential changed little with the transition from one element to another with the exception of the parameter of smearing of edges of the potential well  $a_2$ . It increased for heavier elements, apparently, reflecting a change of the nuclear "atmosphere" and was approximated by the formula  $a_2$ =0.47+0.03·(A - A<sub>mag</sub>)  $^{1/3}$  (A<sub>mag</sub> =208).

The unknown long-range interaction is presented as follows:

$$-V_{long}(r) = \begin{cases} V_D \cdot R_1^{n} / r^n & r > R_1 \\ V_D & r \le R_1 \end{cases}$$

At fitting the potential parameters to describe cross sections of each element separately the long-range interaction constants were obtained: for bismuth  $V_D(Bi)$ =0.18 MeV; for plutonium  $V_D(Pu)$ =0.22 MeV. The relations  $V_D(Pu)/V_D(Bi)$ =1.22 and  $Z^2(Pu)/Z^2(Bi)$ =1.27 are rather close. Although, Z-squared relationship of long-range interaction was not introduced analytically into the potential at the search of the average for all elements of  $V_D$  value. For index n at the search the value n=3.95 was obtained. Later on similar work must be carried out using specific small angle scattering cross sections of fast neutrons at  $E_n$ = 1+2 MeV and  $E_n$ = 7+8 MeV, i.e. there, where it is possible to expect the maximum sensitivity to long-range interaction of the above-mentioned amplitude.

Similarly, one may consider the results of paper [7], in which the parameters of optical potential and long-range interaction were compared for two nuclei – lead and uranium. The real part of potential for each nucleus was a sum of three Woods-Saxon potentials. Their radial parameters R<sub>L</sub>and parameters of smearing of edge of the well a<sub>L</sub>were as follows:

$$R_1$$
=7.47;  $a_1$ =0.26;  $R_2$ =7.79;  $a_2$ =0.59;  $R_3$ =2.56;  $a_3$ =0.1 (x10<sup>-13</sup>cm)  
For uranium:

$$R_1=7.51$$
;  $a_1=0.41$ ;  $R_2=8.00$ ;  $a_2=0.64$ ;  $R_3=2.75$ ;  $a_3=0.1$  (x10<sup>-13</sup>cm)

Those results, where the parameter R<sub>2</sub> and smearing of edge of the well (parameter a<sub>2</sub>) in the case of uranium prove to be greater than in the case of lead, show that "atmospheric" characteristics of these nuclei prove to be accounted for to some extent. In paper [7] the long-range interaction was introduced in the form:

$$-V_{long}(r) = 1/2 \cdot \alpha \cdot Z^2 \cdot e^2 \cdot 1/r^4 \ (r > R_2)$$

Thus, the  $Z^2$ -dependence of this potential was introduced into the calculation analytically and electric polarizability coefficient  $\alpha$  of a neutron also introduced into this formula proved to be very close at its determination both for lead

$$(\alpha=1.3\cdot10^{-40}\text{cm}^3)$$
 and for uranium  $(\alpha=1.5\cdot10^{-40}\text{cm}^3)$ .

Summing up the consideration of two papers [7, 15], one might say that there are at least two pairs of elements: lead and uranium, as well as bismuth and plutonium, in which the long-range interaction addition to the potential is proportional to the value  $Z^2/r^4$ . Moreover, a decrease of small angle distortions of cross sections for copper pointed out already in paper [4] is also compatible with the Z-quadratic dependence of these distortions. If we talk about

the whole considered facts concerning small angle neutron scattering with the energy of 0.5-15 MeV, it is compatible only with the idea of large neutron polarizability ( $\alpha$ ~1.5·10<sup>-40</sup>cm³), although it may be accounted for by introduction of the long-range interaction dipole-dipole (at  $\alpha$ ≈1.5x10<sup>-42</sup>cm³) addition (see paper [8]). The question on the nature of the potential proportional to 1/ r⁴ and not attaching too much importance to the neutron polarizability still remains open.

We thanks P.P.Djachenko and other colleagues from IPPI for useful discussions.

### References

- 1. Schwinger J. Phis. Rev. 1948, v.75, p.407.
- Alexandrov Yu.A. Zh. Eksp. Teor. Fiz. 1957, v.33, p.294, see also Nuclear. Reactions at Low and Moderate Energies (Proc. All.-Union Conf... Nov. 1957) M.1958, p. 206.
- 3. Alexandrov Yu.A., Bondarenko I.I.. Zh.Eksp.Teor.Fiz. 1956,v.31.,p.726.
- 4. Anikin G.V., Alexandrov Yu.A., Soldatov A.S. Proc. of the Intern.Conf. Study of Nuclear Structure with Neutrons. Antwerp., Belgium, 1965.
- 5. Anikin G.V., Kotukhov I.I Yad.Fiz 1971, v.14,iss.2,p.269.
- 6. Anikin G.V., Kotukhov I.I. Yad.Fiz 1989, v.49,iss.1,p.101.
- 7. Anikin G.V., Kotukhov I.I. VANT, ser: Nuclear Constants, iss.4,1989, p.58.
- 8. Alexandrov Yu.A. Phys. Part. Nucl. 2001, v.32, iss.6, p.1405.
- 9. Konnova S.V., Lyboshitz V.V., Pokotilovski Yu.N. | Proc. of the VII Intern. Seminar on Interaction of Neutrons with Nuclei, Dubna, May 25-28, 1999. Dubna 1999, p.325.
- 10. Wilkinson D.H. Phil. Mag., 1959. 4, p.215.
- 11. Wilkinson D.H. Proc. of the Rutherford Jubilee Intern. Conf. Manchester, 1961. London, 1961, p.339.
- 12. Burhop E.H.S. Nucl. Phis. B1, 1967, p. 438.
- 13. Annand J.R.M. at al. Nucl. Phis., 1985, A443, p.249.
- 14. Anikin G.V., Anikin V.G, Preprint IPPE-3031, Obninsk-2004.
- 15. Blokhin A.I., Ignatyuk A.V., Manokhin V.N. и др. || (BROND-2)-VANT ser. Nuclear Constants, 1991, v.3, p.131-235.
- 16. Anikin G.V., Kotukhov I.I., Prokhorova L.I | VANT ser. Nuclear Constants, 1974, iss. 17, p.3.

# STORAGE OF VERY COLD NEUTRONS IN A TRAP WITH NANO-STRUCTURED WALLS

E. V. Lychagin<sup>1</sup>, A. Yu. Muzychka<sup>1</sup>, G. V. Nekhaev<sup>1</sup>, V. V. Nesvizhevsky<sup>2</sup>, G. Pignol<sup>3</sup>, K. V. Protasov<sup>3</sup>, A. V. Strelkov<sup>1</sup>

<sup>1</sup>JINR, 6 Joliot-Curie, Dubna, Moscow reg., Russia, 141980 <sup>2</sup>ILL, 6 rue Jules Horowitz, Grenoble, France, F-38042 <sup>3</sup>LPSC (UJF, CRNS/IN2P3, INPG), 53, rue des Martyrs, Grenoble, France, F-38026

#### Abstract

We report on storage of Very Cold Neutrons (VCN) in a trap with walls containing powder of diamond nanoparticles. The efficient VCN reflection is provided by multiple diffusive elastic scattering of VCN at single nanoparticles in powder. The VCN storage times are sufficiently long for accumulating large density of neutrons with complete VCN energy range of up to a few times  $10^4 \, \text{eV}$ . Methods for further improvements of VCN storage times are discussed.

### Keyword

Very cold neutrons; diamond nanoparticles; neutron scattering; fundamental particle physics.

#### Introduction

Recently we showed that powders of nanoparticles could be used efficiently as first reflectors of Very Cold Neutrons (VCN) in velocities range up to 160 m/ [1], thus bridging the energy gap between efficient reactor reflectors [2] for thermal and cold neutrons, and effective Fermi potential for ultracold neutrons (UCN) [3].

The possibility to use medium with nanoparticles like a reflector of VCN has been treated in [4]. If a neutron comes in such a medium then its velocity direction changes many times due to scattering on the particles. In the issue neutron can live this medium back. In other words, the neutron is reflected from the medium. In [4] was shown that the reflector is more effective if the particles size is close to the neutron wavelength. A large number of diffusive collisions needed to reflect VCN from powder constrains the choice of materials: only low-absorbing ones with high effective Fermi potential are appropriate. Thus, diamond nanoparticles were an evident candidate for such VCN reflector. The formation of diamond nanoparticles by explosive shock was first observed more than forty years ago [5]. Since then very intensive studies of their production and of their various applications have been performed worldwide. These particles measure a few nanometers; they consist of a diamond nucleus (with a typical diamond density and Fermi quasipotential) within an onion-like shell with a complex chemical composition [6] (with lower Fermi quasipotential). A recent review of the synthesis, structure, properties and applications of diamond nanoparticles can be found in [7].

The first experiments on the reflection of VCN from nano-structured materials as well as on VCN storage were carried out in the seventies in [8] and later continued in [9]. In [1] we extended significantly the energy range and the efficiency of VCN reflection by exploiting diamond nanoparticles. A reflector of this type is particularly useful for both UCN sources using ultracold nanoparticles [4, 10] and for VCN sources; it would not be efficient however for cold and thermal neutrons, as shown in [11].

In order to measure precisely the VCN reflection probability from powder of diamond nanoparticles and to explore feasibility of VCN storage in traps with nano-structured walls, we carry out a dedicated experiment described in the present article. In fact, the measuring procedure used here is equivalent to that typically used in experiments on UCN storage in traps (see for example [12, 13]). The difference consists in a type of trap walls and in characteristic values of the reflection probability.

## The experimental setup

This experiment was carried out at the VCN beam, PF2, ILL. The installation scheme is shown in Fig. 1.

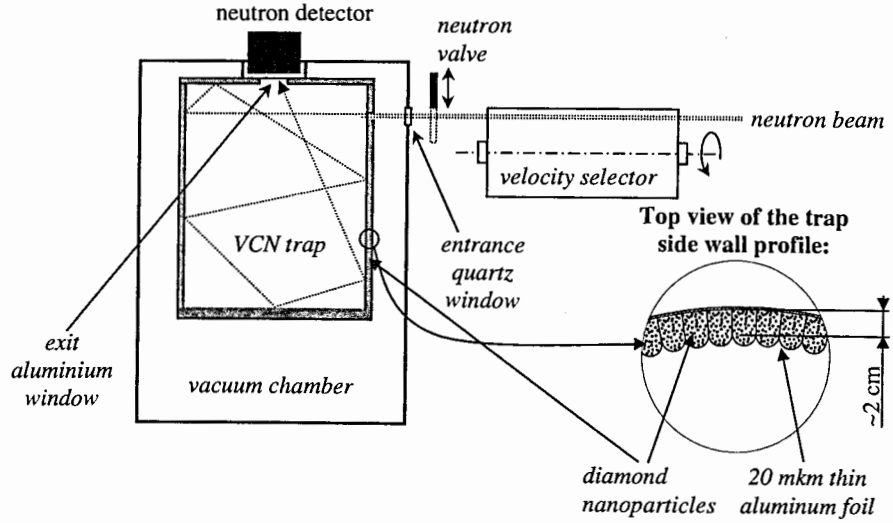


Fig.1 The installation scheme.

The VCN trap has cylindrical shape with a diameter of 44 cm and a height of 47 cm. VCN could enter the trap through a small square window of 2 cm by 2 cm in its side wall. The VCN beam diameter is ~1 cm. VCN could be reflected many times from the trap walls. Thus they could find an exit circular window with a diameter of 6~cm in the trap cover and enter into a detector behind the window. The VCN beam could be opened or closed using a fast cadmium valve with a thickness of 0.2 mm. The VCN velocity could be chosen using a velocity selector in front of the valve. The trap is placed inside a vacuum chamber with an entrance quartz window with a thickness of 3 mm and an exit aluminum window with a thickness of 1 mm. When the VCN beam is closed the detector count rate decreases exponentially following the VCN density in the trap. Thus we could measure the VCN storage times as a function of their velocity.

The neutron detector is a gaseous proportional  $^3$ He counter (the thickness of its sensitive layer is 5 cm, the  $^3$ He partial pressure is 200 mbar) with an entrance aluminum window with a thickness of 100  $\mu$ m and a diameter of 9 cm. The electrical detector signals are analyzed using the time and amplitude information.

The velocity selector consists of a cylinder with a length of I=40 cm and a diameter of D=19 cm. Curved plastic plates with a thickness of 1 mm are installed at the side surface of the cylinder in such a way that they form screw-like slits with a width of d ~4.5 mm and the screw length of L=480 cm. The cylinder rotates around its axis with the period T. Neutrons could scatter at hydrogen atoms in the plate's material; those neutrons leave the neutron beam. The rotation period defines the velocity of neutrons passing through the selector. Neutrons with low angular divergence and with momentum parallel to the selector axis pass through the selector screw slits, thus avoiding scattering by the plates only if the neutron velocity is equal to:

 $v = L \frac{2\pi}{T} \left( 1 \pm \frac{dL}{2\pi Dl} \right).$ 

The selector allowed us to choose the neutrons with a velocity in the range of 30-160 m/s. The velocity resolution was measured using time-of-flight method; the some results are shown in Fig. 2.

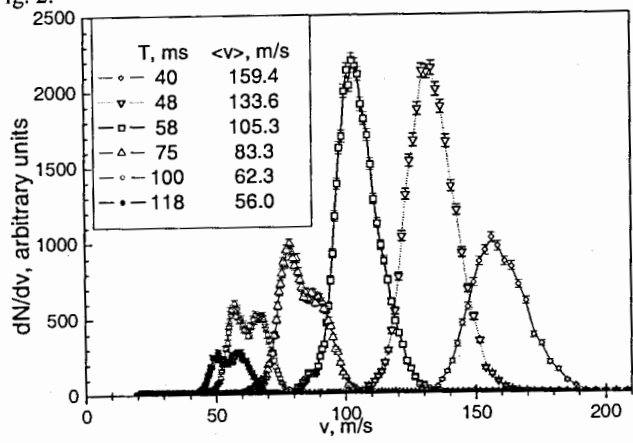


Fig. 2 Experimental time-of-flight neutrons spectra after the velocity selector are presented (neutron chopper resolution is different for various curves). Labels at the figure indicate the rotation period of the velocity selector and average velocity in the spectra.

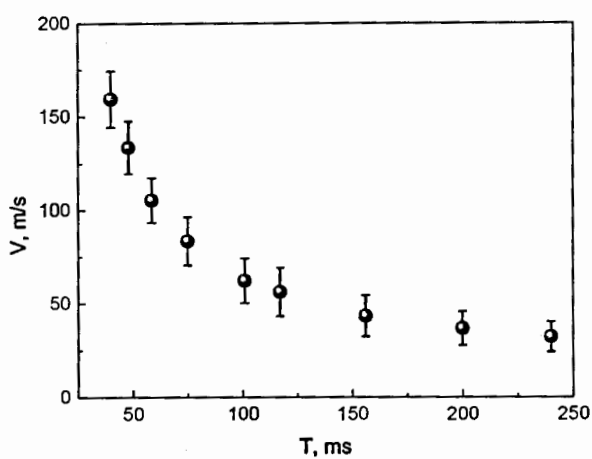


Fig. 3 The neutron average velocities at the velocity selector exit are shown as a function of its rotation period. Error bars indicate the half width of velocity distribution in the beam after selector (because these distributions are not Gaussians).

Fig. 3 summarizes the time-of-flight measurements results. It presents neutrons average velocity at the velocity selector exit as a function of its rotation period. Error bars indicate the half width of velocity distribution in the beam after selector. Neutron chopper resolution has been took into account and subtracted.

The neutron flux at the selector exit is shown in Fig. 4.

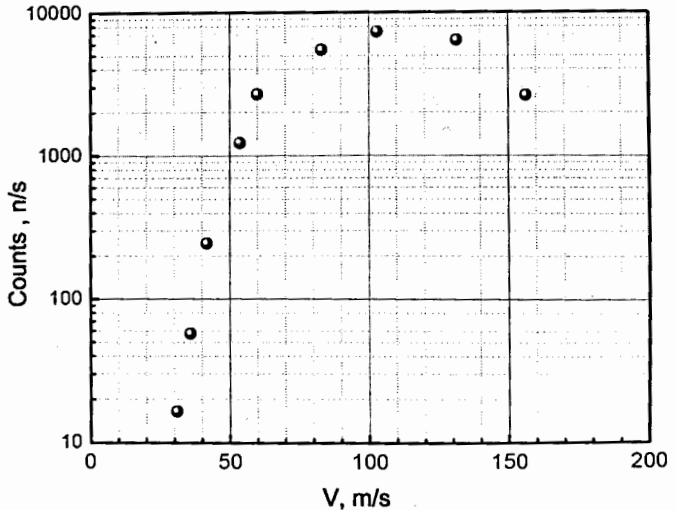


Fig. 4 The neutron flux at the selector exit is shown as a function of neutron velocity

The valve is controlled by an electro-magnet governed with an electric pulse generator. The time of opening and closing the valve was measured in a separate experiment with a light beam; it is equal to 5 ms in both cases.

The trap is built using powder of diamond nanoparticles. To build the trap side walls from the powder we decided to fill nanoparticles into aluminum tubes, and to assemble them into a cylinder as shown in Fig. 1 and in Fig. 5. Thus the walls are not quite homogeneous. VCN reflect many times from the trap walls, thus they pass many times through aluminum walls of the tubes. In order to avoid significant losses of VCN in aluminum, we have to decrease the aluminum wall thickness to a minimum value. Therefore the tubes are built using 20  $\mu$ m thick aluminum foil. We fill in the tubes with powder and compressed it. The compressed powder density is 0.4 g/cm<sup>3</sup>. The trap cover is shown in Fig. 6. It was design like a tambourine with height of 3 cm and 30  $\mu$ m thickness aluminum foil membrane. This "tambourine" is filled by powder with density of 0.3 g/cm<sup>3</sup>. A window in the cover center (see Fig. 6) allows us to count VCN in the detector. The cover is installed on top of the trap side wall; thus an eventual slit between the side wall and the cover surface is minimized. The trap bottom is covered with powder with a thickness of 3 cm compressed to a density of 0.3 g/cm<sup>3</sup>.





Fig. 5 The VCN trap. The cover is open.

Fig 6 The cover with a window in its center.

Electro-heaters are rolled around the trap; the trap and the electro-heaters are covered by many aluminum foil layers in order to provide thermal isolation of the trap. The trap temperature could be raised using the electro-heaters and measured with two thermo-pairs attached to the massive aluminum parts of the trap bottom and the cover respectively.

# The experimental results

When the valve is open VCN fill in the trap as long as needed to reach a saturation VCN density. Then we close the valve and measure the time constant of the exponential decrease of the VCN density in the trap. The detector count rate is proportional to the VCN density in the

trap. Such a measuring cycle is repeated many times in order to accumulate sufficient statistics.

An example of the neutron count rate during one cycle is shown in Fig. 7; a background is subtracted. The solid line in Fig. 7 shows the light signal, in arbitrary units, used to synchronize the valve with the measuring cycle. A pulse generator starts the cycle at time t=0, opens the valve at t=50 ms, and closes the valve at t=250 ms. When the valve is open the trap could be filled in with VCN up to a saturation density. When the valve is closed, the VCN density decreases exponentially. The characteristic time of this decrease is equal to a convolution of the VCN storage time and empting time. The dominant loss factor is associated with the trap walls, as the area of the entrance and exit windows is smaller than 0.3% compared to total area of the trap surface. The storage time in Fig. 7 is equal to  $\tau_{st}^{VCN} = (19.0 \pm 0.5)$  ms.

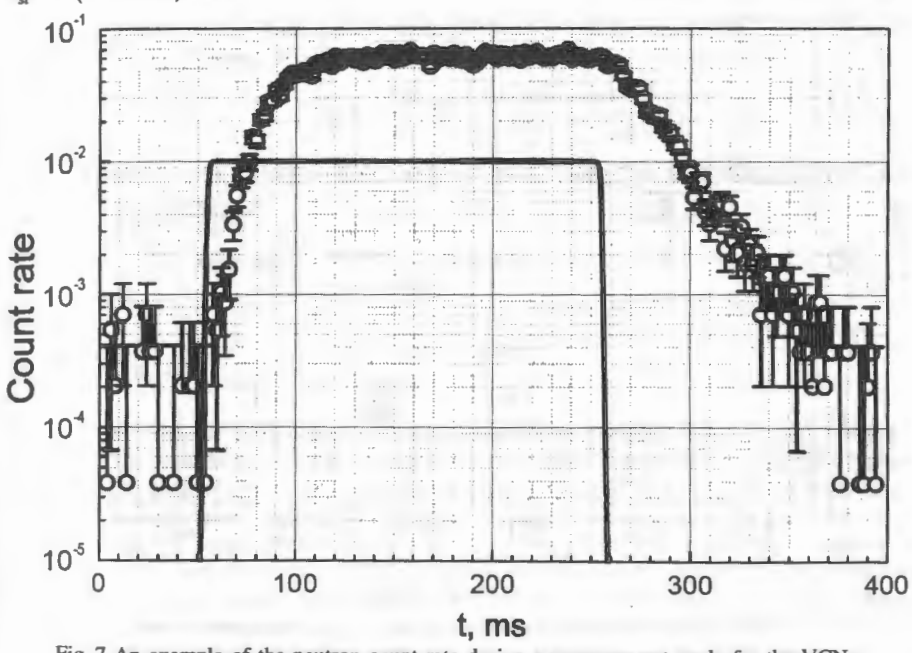


Fig. 7 An example of the neutron count rate during a measurement cycle for the VCN velocity of 85 m/s. The solid line shows the light signal, in arbitrary units, used to synchronize the valve with the measurement cycle.

Analogous measurements were carried out for this and other VCN velocities in 3 series of measurements. First, we pumped out the trap during 12 hours then measured the VCN storage times at room temperature. Second, the vacuum chamber was filled in with argon at a pressure of 1 bar then the trap was heated to a temperature of ~120°C and kept at this temperature during 3 hours. After that argon was pumped out, the trap was slowly cooled to a room temperature then VCN storage times were measured. Third, we heated the trap to a temperature of ~145°C on permanent pumping. The measurement started when the temperature (measured with the two termo-pairs) had got stabilized. Besides, the detector

count rate (with the valve open and the neutron velocity equal to 160 m/s) had to get stabilized as well. The later process is delayed because of slow heating of internal zones of powder.

The results of all these 3 series of measurements are shown in Fig. 8. Storage times were not measured for fast neutrons in the third series, because they are too short.

As it possible to see from the Fig. 8 the degassing of the trap not leads to increasing of the neutron storage time to compare with the pumped trap. Though increasing the trap temperature up to 150°C (30% in absolute scale) has led to decreasing of neutron storage time at 30% approximately. It looks like increasing of neutron losses due to inelastic scattering by hydrogen bounded strongly (it is not removed by 150°C degassing) to the diamond.

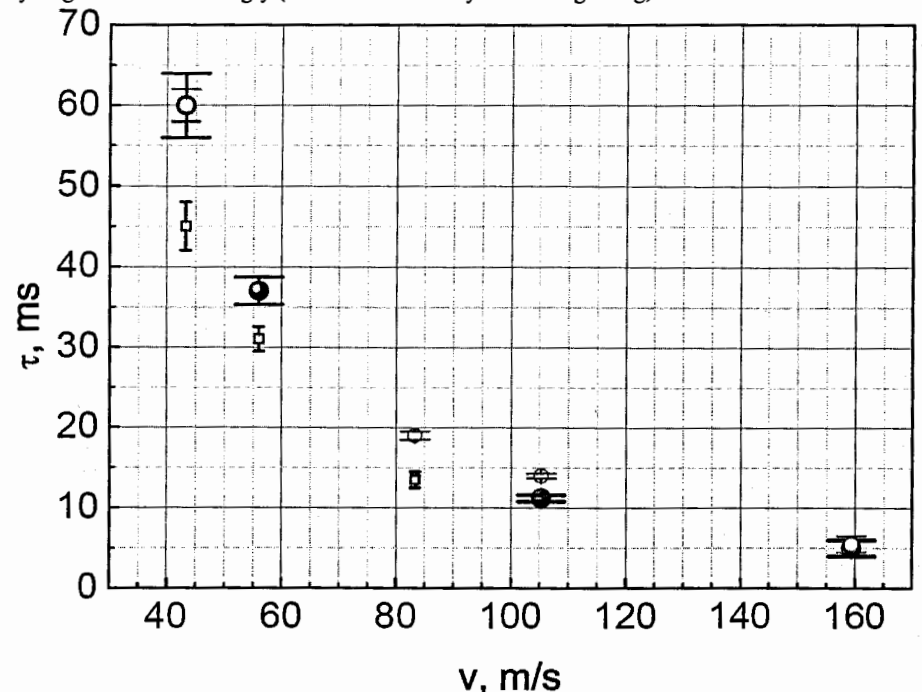


Fig. 8 The VCN storages times as a function of their velocity. Black circles correspond to measurements at room temperature after 12 hour pumping. Empty circles show measurements at room temperature after heating the trap at 120°C in argon. Boxes indicate results obtained at a temperature of 150°C under permanent pumping.

### Analysis of the experimental results

For the trap geometry described above we calculate a VCN mean free path for all neutron velocities:

 $\Delta x = 22 \pm 1 \, cm$ 

neglecting small gravitational corrections. Thus the probability of VCN reflection from the trap wall could be estimated from equation:

$$P(v) = 1 - \frac{\Delta x}{\tau_{+}^{VCN}(v) \cdot v} \cdot (1 - \varepsilon)$$
 (1)

where  $\varepsilon$  accounts for VCN losses in the entrance and exit windows and amounts to  $\varepsilon = 3.5 \cdot 10^{-3}$ . The errors in this estimation are defined by storage time uncertainty (see Fig. 8), mean flight pass uncertainty and neutron velocity uncertainty (see Fig. 3).

This probability represents the reflectivity for the walls actually used in this experiment. It thus includes losses in the aluminium foil, and effects of the geometrical shape of the trap walls. This estimation supposes isotropic angle distribution of neutrons in the trap that is not quite true for more fast neutrons.

On the other hand, we have in hand a model for the propagation of neutrons in the nanoparticle powder. The method used here to describe the reflection of VCN at a layer of nanoparticles is similar to that in [1]. Namely, we neglected the relatively complex internal structure of the nanoparticle and modeled it as a uniform sphere. The neutron-nanoparticle elementary interaction was calculated using the first Born approximation. The amplitude for a neutron with the energy  $(\hbar k)^2/2m$  to be scattered at a spherical nanoparticle with the radius R and Fermi potential V, at an angle  $\theta$  is equal:

$$f(\theta) = -\frac{2m}{\hbar^2} V R^3 \left( \frac{\sin(qR)}{(qR)^3} - \frac{\cos(qR)}{(qR)^2} \right),$$

where  $q = 2k\sin(\theta)$  is the transferred momentum. The total elastic cross section is equal correspondingly:

$$\sigma_{s} = \int \left| f \right|^{2} d\Omega = 2\pi \left| \frac{2m}{\hbar^{2}} V \right|^{2} R^{6} \frac{1}{(kR)^{2}} I(kR),$$

where

$$I(kR) = \frac{1}{4} \left( 1 - \frac{1}{(2kR)^2} + \frac{\sin(4kR)}{(2kR)^3} - \frac{\sin^2(2kR)}{(2kR)^4} \right).$$

The chemical composition of the nanoparticle is complex and includes carbon (up to 88% of the total mass), hydrogen (1%), nitrogen (2.5%), oxygen (up to 10%) [14]. Moreover, a certain amount of water covers a significant surface area of the nanoparticles. In general, the hydrogen in the water and on the surface of the nanoparticles scatters the neutrons up to the thermal energy range (*up-scattering*); thermal neutrons do not interact as efficiently with nanoparticles and therefore traverse powder. The hydrogen quantity in the powder was measured by  $(n,\gamma)$  method and composition  $C_{15}H$  was found for degassed and non degassed powder in the vacuum and composition  $C_{8}H$  was found for powder in the air.

To compare the experimental results to the model of independent nanoparticles, we further corrected the measured reflectivity from VCN loss in aluminum foils and from a dead zone in the wall structure in between each cylinder (this correction is about 1%). The corrected reflectivity is shown in Fig. 9 for measurements at room temperature (averaged through two series of measurements); together with the Monte-Carlo calculation. The only parameter of this calculation concerns inelastic scattering on hydrogen. In the Monte-Carlo simulation, the quantity of hydrogen is fixed according to the  $C_{15}H$  chemical composition (0.5% of the total mass). Besides, the cross section for inelastic scattering is assumed to follow the 1/v rule, and the value of the cross section  $\sigma_H$  for neutron velocity of 2200 m/s is considered as an effective parameter. The calculation reproduces the velocity dependance of the reflectivity well, and the effective parameter is fitted at the approximate value of  $\sigma_H = 1.3$  barn.

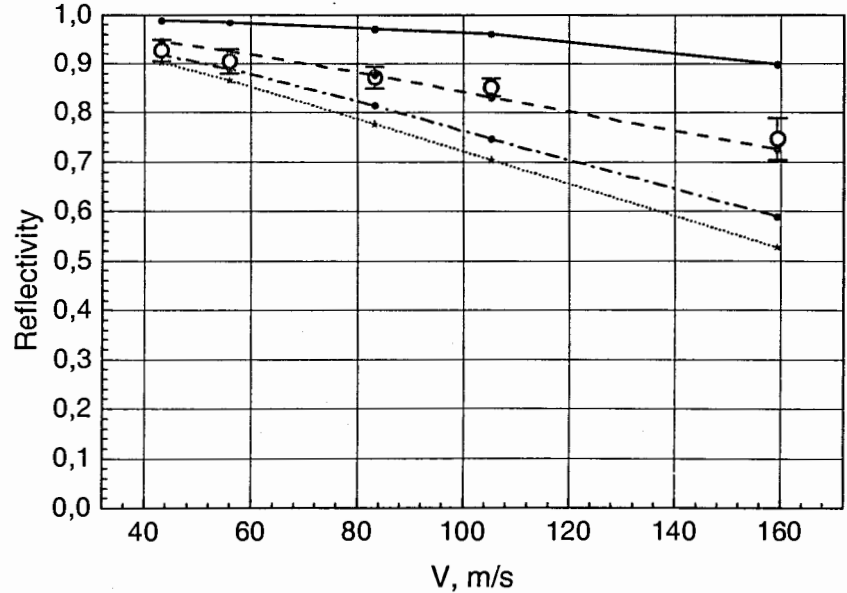


Fig. 9 The probability of VCN reflection from a layer of nanoparticles as a function of their velocity. Open circles correspond to measurements at room temperature. Thin lines correspond to Monte-Carlo calculations, taking into account upscattering at hydrogen, the quoted cross section corresponds to neutron velocity of 2200 m/s: 4 barn for dotted line, 3 barn for dot-dashed line, 1.3 barn for dashed line and 0 barn for plain black line.

### Conclusion

We have observed for the first time storage of VCN with the velocity 40-160 m/s (the energy up to  $10^{-4}$  eV) in a trap with walls containing powder of diamond nanoparticles. The VCN storage will allow us to accumulate significant number (density) of VCN in a trap (much larger than that typical for UCN). Further improvement of the VCN storage times could be achieved by removing a part of hydrogen from powder (it could not be removed by degassing at 150°C) to suppress inelastic up-scattering of VCN. Another option could consist in replacing the diamond nanoparticles by O<sub>2</sub>, D<sub>2</sub>, D<sub>2</sub>O, CO<sub>2</sub>, CO or other low-absorbing nanoparticles, free of hydrogen and other impurities with significant VCN loss cross-section.

The probability of cold neutron isotropic flux reflection from diamond nano particles is compared with others well know reflectors in Fig. 11. As it can be seen from Fig. 11, the maximum energy of the reflected VCN and the reflection probability far exceeds the corresponding values for the best supermirrors available [15]. Thus nanoparticle reflector bridges the energy gap between efficient reactor reflectors for thermal and cold neutrons, and the effective Fermi potential for UCN. This phenomenon has a number of applications. Such a reflector can be used for VCN and UCN sources, for the more efficient guiding of VCN and, probably, of even faster neutrons at "quasi-specula" trajectories.

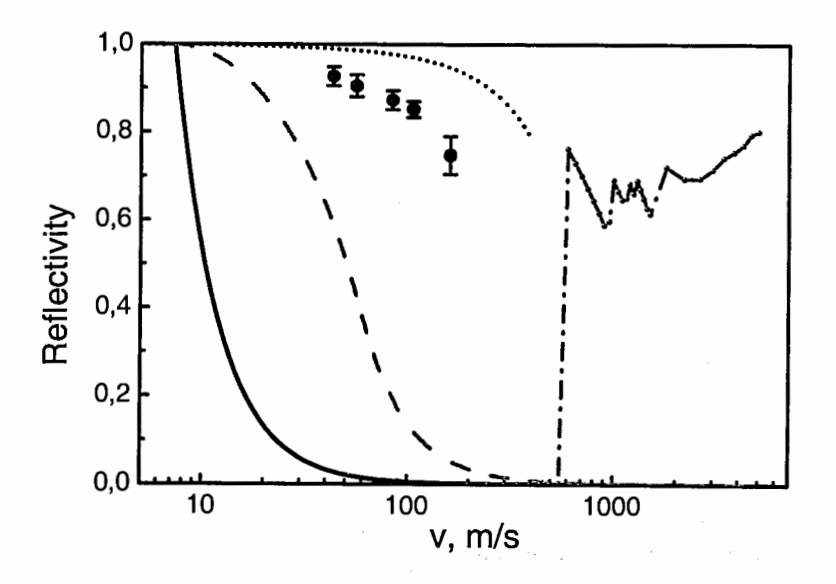


Fig. 11. The elastic reflection probability for isotropic neutron flux is shown as a function of the neutron velocity for various carbon-based reflectors: 1) Diamond-like coating (DLC) (thin solid line). 2) The best supermirror [15] (dashed line). 3) Hydrogen-free ultradiamond [16] powder with the infinite thickness (dotted line). Calculation. 4) VCN reflection from ~3 cm thick diamond nanopowder at room temperature (points), with significant hydrogen contamination [this paper]. Experiment. 5) MCNP calculation for reactor graphite reflector [17] at room temperature with the infinite thickness.

### References

- 1 V.V.Nesvizhevsky E.V.Lychagin, A.Y.Muzychka, A.V.Strelkov, G.Pignol and K.V.Protasov "The reflection of very cold neutrons from diamond powder nanoparticles," // Nucl. Instrum. Meth. A 595, 631 (2008).
- 2 E.Fermi, "A course in neutron physics" in "Collected papers", The University of Chicago Press, Chicago (1965).
- 3 V.I.Luschikov, Yu.N.Pokotilovsky, A.V.Strelkov and F.L.Shapiro, JETP Lett. 9 (1), 23-26 (1969).
- 4 V.V.Nesvizhevsky, "Interaction of neutrons with nano-particles" // Phys. At. Nucl. 65, 400 (2002). [Yad. Fiz. 65, 426 (2002)].
- 5 P.J.De Carli and J.C. Jamieson, Formation of Diamond by Explosive Shock Science 133, 1821 (1961).
- 6 A.E.Aleksenskii, M.V.Baidakova, A.Y.Vul' and V.I.Siklitskii, "The structure of diamond nanoclusters." // Physics of Solid State 41, 668 (1999).
- 7 V.Yu.Dolmatov, "Detonation-synthesis nanodiamond: synthesis, structure, properties and applications" // Russian Chemistry Review 76, 339 (2007).
- 8 A.Steyerl and W.-D.Trüstedt, "Experiments with a neutron bottle" // Z.Physik 267, 379 (1974).
- 9 S.S.Arzumanov, L.N.Bondarenko, P.Geltenbort, V.I.Morozov, Yu.N.Panin, "Cold-Neutron Storage Owing to Diffusion Reflection" // Phys. At. Nucl. { 68, 1141 (2005).
- 10 V.V.Nesvizhevsky, G.Pignol and K.V.Protasov, "Nanoparticles as a possible moderator for an ultracold neutron source." IJN 6 (6), 485 (2007).
- 11 V.A.Artem'ev, "Estimation of neutron reflection from nanodispersed materials" // Atomic Energy 101, 901 (2006).
- 12 V.K.Ignatovich, "The Physics of Ultracold Neutrons", Oxford University Press (1990) ISBN 0198510152
- 13 R.Golub, D.Richardson and S.K.Lamoreaux, "Ultra-Cold Neutrons", Adam Higler (1991). ISBN 07503 0115 5
- 14 A.L. Vereschagin, G.V.Sakovich, V.F.Komarov, and E.A.Petrov, "Properties of ultrafine diamond clusters from detonation synthesis." // Diamond and Related Materials 3, 160 (1993).
- 15 R. Maruyama, et al., Thin Solid Films 515 (2007) 5704
- 16 http://www.ultradiamondtech.com
- 17 E. Fermi, "A course in neutron physics" in "Collected papers" (The University of Chicago Press, Chicago, 1965).

# CURRENT STATUS OF THE EXPERIMENT ON DIRECT MEASUREMENT OF NEUTRON – NEUTRON SCATTERING LENGTH AT THE REACTOR YAGUAR

W.I. Furman<sup>1</sup>, A.Yu. Muzychka<sup>1</sup>, B.E. Crawford<sup>2</sup>, C.R. Howell<sup>3</sup>, Ya. Kandiev<sup>4</sup>, B.G. Levakov<sup>4</sup>, V.I. Litvin<sup>4</sup>, E.V. Lychagin<sup>1</sup>, A.E. Lyzhin<sup>4</sup>, G.E. Mitchell<sup>5</sup>, G.V. Nekhaev<sup>1</sup>, E.I. Sharapov<sup>1</sup>, V.N. Shvetsov<sup>1</sup>, S.L. Stephenson<sup>2</sup>, A.V. Strelkov<sup>1</sup>, Yu.I. Tchernukhin<sup>4</sup> and W. Tornow<sup>3</sup>

<sup>1</sup> Joint Institute for Nuclear Research, 141980 Dubna, <sup>2</sup>Gettysburg College, Box 405, Gettysburg PA, USA 17325, <sup>3</sup>Duke University and Triangle Universities Nuclear Laboratory, Durham NC, USA 27708-0308, <sup>4</sup>RFNC- All-Russian Research Institute of Technical Physics, P.O. Box 245, 456770 Snezhinsk, Russia, <sup>5</sup> North Carolina State University, Raleigh NC, USA 27695-8202 and Triangle Universities Nuclear Laboratory, Durham NC, USA 27708-0308

Abstract. It is proposed in 2002 the new experiment on the first direct measurement of neutron-neutron scattering on the powerful pulsed reactor YAGUAR placed at Snezhinsk, Ural region, Russia. After that an extensive work has been done for modeling of background conditions and an optimization of the set-up design. To make the experiment feasible it was necessary to suppress the background of various origins for more than 16 (for thermal neutrons) and 14 (for fast neutrons) orders of magnitude. In 2003 it had been drilled under reactor and equipped a channel for time-of-flight measurements. During next two years at this channel there were carried out a series of test experiments aimed at checking out an accuracy of background condition modeling. A good agreement of the measured results with the calculated values allowed us to realize the final design of full scale set-up. During 2005-2006 it has been manufactured and after vacuum tests at JINR the set-up has been mounted at YAGUAR reactor hall. In 2006-2007 the calibration measurements with noble gases have been carried out. The obtained results confirmed a validity of the full scale experiment modeling and allowed to verify necessary calibration. The first preliminary experiments for nn-scattering were performed at April 2008. The results are discussed.

Keywords: Nuclear physics, charge invariance of nuclear forces, nucleon-nucleon scattering lengths.

### INTRODUCTION

A main motivation for performing the direct neutron-neutron scattering (nn) measurements is the issue of charge symmetry violation in the nuclear force; the size of this symmetry breaking remains an open fundamental problem in nuclear physics. One way to study this problem is the comparison of the neutron-neutron,  $a_{nn}$ , and proton-proton,  $a_{pp}$ , scattering lengths. Although the pp-scattering length is well measured, existing indirect m-data (from nuclear reactions with two neutrons and a third particle in the final state) for many years contradicted each other [1-4] in both the magnitude and sign of the difference between the nn- and pp-scattering lengths. This value is rather essential for verification of QCD at low energy.

An idea how to measure *nn*-scattering directly is discussed in detail in ref. [5]. There it is shown that a direct measurement of the neutron scattering length with 3% accuracy (0.5 fm) may resolve the above mentioned contradictions.

### STRATEGY OF EXPERIMENT

As it is shown in ref. [5] only possibility at present to measure nn-scattering directly is to use the pulsed reactor YAGUAR, VNIITF, Snezhinsk. The main parameters of the respective

experiment are: energy of YAGUAR pulse is up to ~30 MJ, a repetition rate is one per day, number of neutrons, flied out from the reactor per pulse  $\sim 10^{18}$ , duration of the pulse is  $\sim 1$  ms, the thermal neutron flux density in central cavity of the reactor reaches ~10<sup>18</sup> n/cm<sup>2</sup>/s. Effective density of "neutron target" could be ~ 10<sup>13</sup> n/cm<sup>3</sup>, number of n-n collision per pulse estimates as ~107 and an expected number of n-n scattered neutrons, counted by the detector (100+300) per pulse. The basic idea of the experiment is to use time-of-flight (TOF) method for separating of nn-scattering events from all other false effects. For such limited statistics a providing of appropriate background conditions is crucial for realization of the experiment.

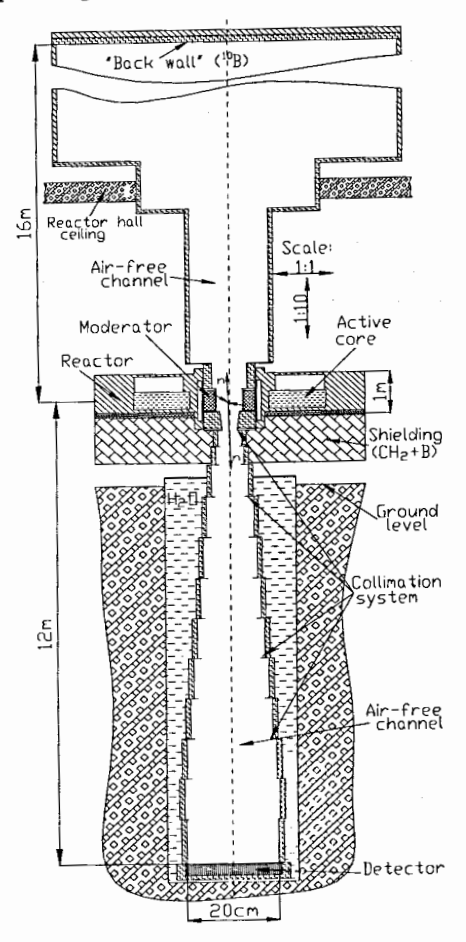


FIGURE 1. The layout of the experimental setup.

For realization of the nn-experiment was chosen the following strategy: its preparation and an execution were broken for some stages. In doing so each next stage started to implement only after a successful completion of the previous one.

First of all the detailed calculations of neutron fields within the reactor through channel have been done. The results of these calculations coincided well with the spatial, energy and time distributions of neutron measured in special precise experiments [5]. After that it was formulated full mathematic model of the set-up and as result it was obtained the quantitative estimation of numbers of n-n scattered neutrons, counted by the detector.

If we wish to reach the 5% accuracy in the nn-cross-section (2.5% in  $a_{nn}$ ) so the effect/background ratio should be not more than 40-50%. It results immediately that a thermal neutron background must be suppressed for sixteen orders of magnitude. Due to the fact that the YAGUAR pulse has long tail related to delayed neutrons with flux ~10<sup>14</sup> n/cm<sup>2</sup>/s it needs to take special measures for elimination of a very high background of fast neutrons. The modeling with such level of background suppression did not carried out up to now. But necessary calculations have been successfully done [6] in parallel by two independent groups from JINR and RRITP, Snezhinsk using MCNP and PRIZMA codes respectively.

In fig.1 the lay-out of the set-up is shown. Thermal neutrons escaped from the inner surface of the reactor cavity covered by moderator in thin aluminum case scatter on

other neutrons placed there and move after collision up and down by the respective evacuated flight passes. In chosen design of set-up first scattered thermal neutrons reach the detector ~ 2ms after the reactor pulse whereas the thermal neutrons reflected by "the back wall" (the lid of upper flight pass) after collision in reactor cavity have time delay about 10 ms. It allows one to detect nn-scattering events in the time window (2-12) ms. In this situation TOF method could diminish the background from fast neutrons emitted during YAGUAR pulse at least for four order of magnitude.

The first conic collimator just under reactor core serves for exclusion of a direct visibility of the moderator surface by the detector. Beside that the collimation system has to prevent neutrons reach the detector after first scattering on walls of the lower flight pass. To diminish effect of multiple scattering of thermal neutron on the walls the inner surfaces of both flight passes these were covered by cadmium sheets of 1mm thick. To decrease a number of neutrons scattered on the back wall and hit the detector the surface of this wall is covered by

A thick borated polyethylene shield under the reactor core and water surrounding the lower flight pass serve for suppression of fast neutron background. Part of the fast delayed neutrons can penetrate the shielding and induce background during the

time interval allocated for detecting thermal neutron collision during the reactor pulse. A suppression of this background could be achieved by used shielding and specially designed

detector with low sensitivity to fast neutrons.

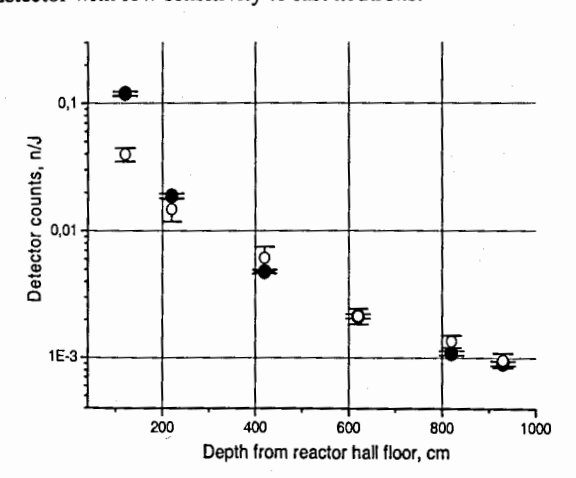


FIGURE 2. The count of the fast neutron detector normalized for one Joule of the reactor energy is presented in dependence of the shaft depth. The black and open cycles are the results of the measurements and calculations respectively.

The calculations have shown that it is possible to obtain satisfactory background conditions with expected effect/background ratio near 30% if the vacuum within scattering cavity will be as low as 10<sup>-6</sup> mb. Here it is appropriate to note that beside of all abovementioned sources of background that is possible consider quantitatively another kind of background exists that could spoil the vacuum condition within central cavity just after reactor pulse. This is so called a radiation degassing of the cavity and the first collimator walls. The effect was studied [7] for steady reactor. The preliminary

qualitative estimations gave us some hopes that this background has not to be essential for our

Before completion of these calculations there was no any confidence in the feasibility of the planned experiment. For verification of modeling results there were carried out the special test measurements. It was dug the under-reactor shaft of 11m depth, manufactured and installed the moderator, the first massive conical collimator and the under reactor shield. It was studied the spatial and depth distributions of thermal and fast neutrons inside of the mine filled by air. In comparison with the planned experiment there were no any vacuumed flight passes and whole collimation system. It was used a neutron detection system prepared specially for this experiment. In fig. 2 the results of test measurements for fast neutrons ( $E_n > 0.5 \text{ MeV}$ ) are shown together with the results of special modeling carried out for the abovementioned experimental conditions.

The respective comparison of the results for thermal neutrons was good too but it was verification of only special modeling of this experiment. But for fast neutrons as it follows from modeling the absolute value and energy dependence of the background are very close to the same obtained for the main experiment.

So the good agreement between experimental results and calculations demonstrated in fig. 2 gave us the firm grounds for final design of whole set-up and the neutron detector in particular.

The upper flight pass was manufactured and tested at Dubna. It was drilled a special



FIGURE 3. The vacuum tests of the set-up at Dubna

whole in the ceiling of the reactor hall and after that this flight pass has been installed on the roof of the YAGUAR building. In parallel the middle part of the set-up and the lower flight pass were manufactured and installed at Dubna for vacuum tests.

Inside of scattering chamber and surrounding vacuumed channel it was achieved the pressure 10-6 mb that was a satisfactory value for carrying out of *nn*-scattering. After completion of all tests the whole set-up was installed at the reactor hall.

Due to some technical problems the used collimation system was not optimal. Instead of pure <sup>10</sup>B ceramic collimators we were forced to use ones prepared with the mixture of <sup>10</sup>B and sulfur. The characteristics of such collimator are about three times worse than the designed ones. So the respective background/effect ratio was expected at the level of 70-80%.

But with these collimators it was possible to verify whole experimental technique and to measure the cross-section of nn-scattering with the accuracy  $\sim 20\%$ .

Consider in more detail what requirements the neutron detector should match in real conditions of the experiment. In measurement of *nn*-scattering as modeling shows [6] for one reactor pulse during TOF interval (2-12) ms about 200 neutrons have to go throughout of the

entrance detector window. At the same time a flux of fast neutrons and  $\gamma$ -quanta on the detector could reach  $\sim 10^4$  and  $\sim 10^5$  respectively. In calibration measurements with noble gases (He and Ar) the expected count rate at the detector is about  $10^4$  of scattered neutrons for one reactor burst. As a result of this consideration the neutron detector has to match the following rather strict requirements:



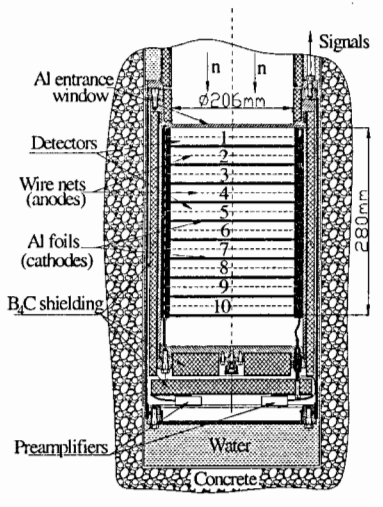
FIGURE 4. The installation of the set-up at the reactor

1) the maximal effectiveness( $\sim 100\%$ ) to thermal neutrons; 2) a very low sensitivity to fast neutrons and  $\gamma$ -quanta; 3) the high count rate  $\sim 10^6$  n/s; 4) the satisfactory amplitude resolution ( $\leq 20\%$ ).

The last condition is essential for a suppression of the background of fast neutrons and  $\gamma$ -quanta. The good enough amplitude resolution is necessary for precise determination of the effectiveness of the detector.

Only possibility to satisfy the abovementioned requirements is to use the gas proportional counter. But it was very difficult to match the condition 3 and 4 simultaneously. This task has been solved using special multi-section design and very fast flux preamplifiers shown in fig. 5. The each section forms practically the independent detector filled by the mixture of  $^3$ He  $(0.5 \text{ b}) + + \text{CF}_4$  (0.7 b) with 4.5 kV electric supply and the separate preamplifier. The anodes are one layer grid with parallel needles of  $20\mu\text{m}$  thickness spaced by 3mm.

Its effectiveness for thermal neutrons consists of 86% with the duration of detector signal ≤100 ns. An each signal is digitized and read out for following off-line analysis. Using the high enough coefficient of gas amplification ~10³ in combination with the fast current preamplifiers we have managed to get rather satisfactory amplitude resolution about 10%. In fig. 6 a typical signal from one section of the detector induced by thermal neutron from YAGUAR reactor pulse is presented.



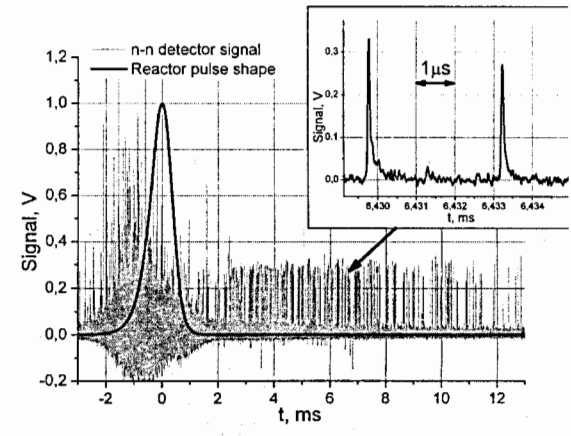


FIGURE 6. A signal from neutron detector (thin grey lines) in dependence on TOF. Each peak corresponds to neutron registration event. A black curve shows a time dependence of the reactor power during the pulse

FIGURE 5. The layout of the neutron detector

### EXPERIMENT WITH NOBLE GASES

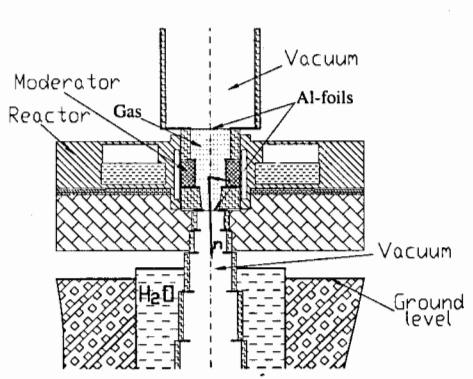


FIGURE 7. The scheme of measurements with noble gases

The last preliminary stage before the nncross-section measurement was experiments with noble gases. The measurements ofthermal neutron scattering on <sup>4</sup>He and Ar gases allow us to verify the whole experimental procedure and the method of data analysis. To reach this goal it is necessary to measure the respective cross-sections with accuracy much better than it was planned to get for main nn-experiment (~5%). Beside that these measurements should be realized with minimal number YAGUAR bursts. So the density respective gaseous targets has to be as much as necessary to ensure  $\approx 10^4$ 

detector counts per one burst. Taking into account known scattering cross-sections for  $^4\text{He}$  and Ar the respective pressure of the targets should be  $\sim 10^{-1}$  mb. But at this very small pressure the essential uncertainties could arise due to degassing of scattering chamber walls. So the effectiveness of the detector for thermal neutrons was decreased in  $10^3$  times by changing of its filling ( $^3\text{He}$  (0.5 mb) + $^4\text{He}$  (0.5 b) + CF<sub>4</sub> (0.7 b)). At the same time all other detector characteristics were preserved.

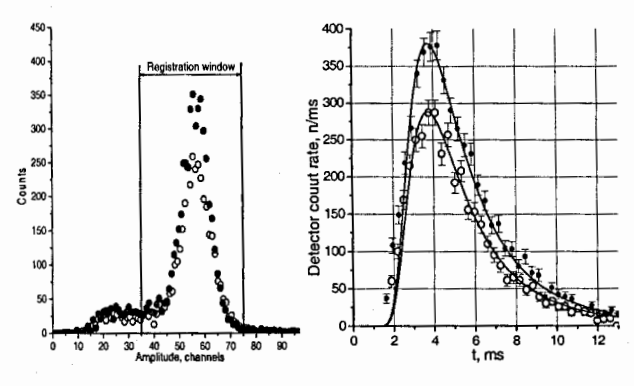


FIGURE 8. The amplitude (left) and TOF spectra of neutrons scattered by <sup>4</sup>He (black points) and Ar (open points) targets at 200mb pressure.

quanta to the detector count.

In fig. 9 the normalized detector counts are presented in dependence on the pressure of gas targets at 20°C.

The linear dependence in fig.9 of <sup>4</sup>He data corresponds fully to the results of modeling. The background in these measurements relates to scattering on Al foils. The special measurement without foils and with vacuum in the channel gave a result 0.05±0.05 n/MJ.

The detailed analysis of these data results in the ratio of the measured scattering cross-sections  $\omega = \sigma(^4\text{He})/\sigma(\text{Ar}) = 1.236 \pm 0.046$  instead of the known value [8]  $\omega = 1.2 \pm 0.03$ . A good agreement of these two ratios confirms an overall validity of the developed experimental technique and the method of data analysis.

The special measurements in stationary mode of the YAGUAR operation showed that the fast neutron background for

The scheme of gas measurements is shown in fig. 7. The gas target is separated from the rest vacuum volume by  $40 \mu m$  aluminum foils.

In fig. 8 the results of measurements on 4He for two reactor pulses summed over all ten detector sections are shown. The threshold in TOF measurements 1.6ms. For fixed at the amplitude spectra the registration window was chosen to decrease maximally a contribution of fast neutrons and gamma

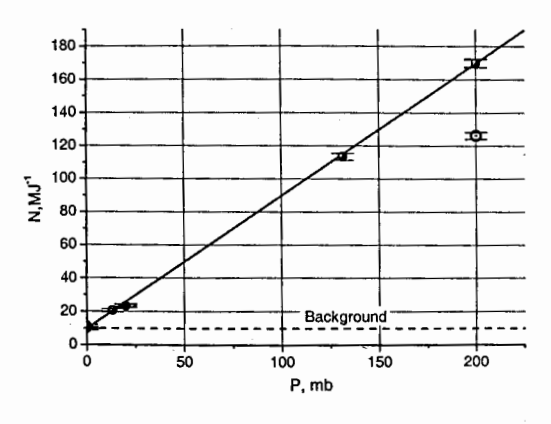


FIGURE 9. The results of measurements with noble gases normalized to 1MJ of the reactor energy release. Black points are for <sup>4</sup>He, the open one is for Ar.

realistic conditions of nn-experiment is not higher than 10 events for maximal (30MJ) pulse energy of the reactor. It consists of less than 10% of the expected effect of nn-scattering.

### FIRST ATTEMPT OF MAIN EXPERIMENT

After successful completion of calibration measurement the detector was refilled for its original content, the whole volume was pumped out for high vacuum and the first measurements of *nn*-scattering have been done in April 2008. In fig. 10 it is shown TOF spectra for two reactor energies.

These spectra are very similar to the same shown in fig. 8. So it indicates that the detected neutrons are thermal ones. But the count rate is  $\sim 20 \div 30$  times higher than expected number for nn-scattering.

The last number could be expressed in form [5]:

$$N_{m} \sim \iint \frac{\Phi^{2}(t,\vec{r})}{v_{0}} \sigma_{m} dt dV \sim \frac{F^{2}}{Tv_{0}} \sigma_{m} V$$

Here t is time, T is the burst duration,  $\Phi(t, \vec{r})$  is the instantaneous neutron flux

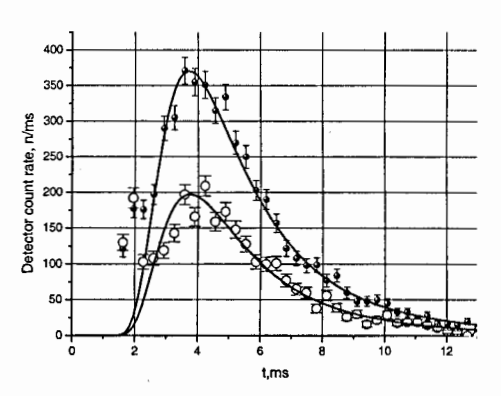
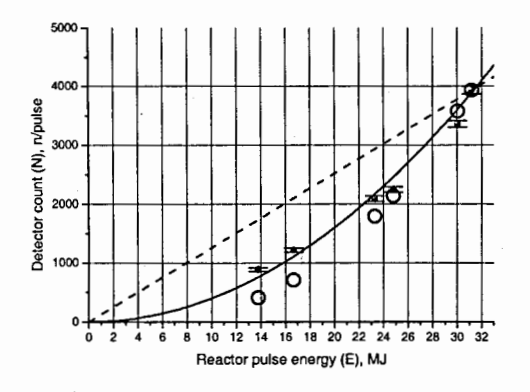


FIGURE 10. The TOF spectra measured with vacuumed scattering chamber for 31 MJ (black points) and 25MJ (open circles). The curves are a fit with Maxwellian distribution.

density,  $F = \int \Phi(t)dt$  is the neutron fluence,  $v_0 = 2200 \text{ m/s}$ , and  $\sigma_{nn}$  is the nn scattering cross section. In a case of neutron burst duration depending on the burst energy, it is the fluence that is proportional to the burst energy.



**FIGURE 11.** The black points are neutron counts N for different reactor energies E. The dashed line is  $N \sim E$ ; the solid curve represents the dependence  $N \sim E^2$  and open circles corresponds to the reactor energy dependence of the calculated  $N_{nn}$  values normalized conditionally to the measured number at 31MJ point.

We see that the total number N<sub>nn</sub> of the nn-scatterings is proportional to fluence squared (or to the burst energy squared) and is also reverse proportional to the pulse duration T. The latter for the reactor YAGUAR case, is in turn the reverse proportional to the duration As the result, the N<sub>nn</sub> number of counts is expected to follow approximately the 3-rd power of the burst energy. In contrary, the number of scatterings from the channel walls and the from collimator edges proportional to  $\Phi(t, \vec{r})$  and, therefore, should have the linear dependence of the pulse energy.

In fig. 11 it is presented the results of all measurements with vacuumed scattering chamber. The total count of thermal neutrons detected in the proper time window for one reactor burst is shown in dependence of reactor energy.

It is clear that experimental points have approximately square energy dependence. A distinction from linear dependence indicates that during reactor pulse a number of objects on which thermal neutrons scatter is changed. In the case quadratic energy dependence the number of such objects is proportional the energy of the reactor pulse but not the neutron flux density. So these objects are accumulating within the reactor cavity during its pulse. The most probable candidates for these are gas molecules ejecting from the cavity walls due to its neutron and gamma irradiation during reactor burst. It is rather plausible that we have observed the effect of the radiative desorbtion.

### CONCLUSION

As the result of six years hard work of DIANNA collaboration the full scale set-up aimed at the direct measurement of the cross-section of neutron-neutron scattering has been designed, manufactured and installed at the YAGUAR reactor hall. The planned technical parameters of the set-up have been achieved. The calibration measurements with noble gases have demonstrated that preliminary modeling was reliable and that the developed procedure of data analysis allows one to extract the respective cross-section with necessary accuracy.

The first attempt of *nn*-measurement has been done. The unexpected background of thermal neutrons proportional to a square of the reactor pulse energy was observed. It seems that this effect is connected with the radiative desorbtion of gas molecules from the walls of the central reactor cavity under neutron and gamma irradiation. The nature of this background and possible ways of its suppression has to be studies in nearest future.

### ACKNOWLEDGMENTS

Authors express their gratitude to the YAGUAR reactor staff for kind assistance and long patience during many years of our collaboration. We are very obliged to the directorates of JINR, Dubna and VNIITF, Snezhinsk for their informal attitude to this project and for support of our activity.

This work was supported by the ISTC grant #2286 and the grant of RFBR # 05-02-17636.

### REFERENCES

- 1. C.R. Howell, Q. Chen, T.S. Carman, et al., *Phys. Lett.* B 444, 252 -254 (1998)
- 2. D.E. González Trotter, F. Salinas, Q. Chen, et al., Phys. Rev. Lett. 83, 3788 (1999)
- 3. G.A. Miller, B.M.K. Nefkens, I. Slaus, Phys. Reports 194, 1(1990)
- 4. V. Huhn, L. Wätzold, Ch. Weber, A. Siepe, W. von Witsch, H. Witala, W. Glöckle, *Phys. Rev.* C 63, 014003, (2001)
- W.I. Furman, E.V. Lychagin, A.Yu. Muzichka, et al., J. Phys. G: Nucl. Part. Phys. 28, 2627 (2002)
- 6. A.Yu. Muzichka, W.I. Furman, E.V. Lychagin et al., Nuclear Physics A 789, 30-45 (2007)
- 7. R. Dobrozemsky, Nucl. Instrum. Methods 118, 1-23 (1974)
- 8. S.F. Mughabghab, Atlas of Neutron Resonances, N.Y. Elsevier, 2006

# ON A COINCIDENCE MEASUREMENT IN THE YAGUAR NN-EXPERIMENT

B. E. Crawford, E. I. Sharapov, S. L. Stephenson,

<sup>1</sup>Gettysburg College, 300 N. Washington Street, Gettysburg PA 17325, USA <sup>2</sup>Joint Institute for Nuclear Research, 141980 Dubna, Russia

### Abstract

A hypothesized improvement for the signal-to-noise ratio in the DIANNA nnscattering experiment at the pulsed YAGUAR reactor would be to measure coincidences between the existing detector located below the scattering volume and an additional detector equidistant but above the scattering volume. Here we determine and compare the relative size of the coincidence count rate with the single detector count rate. We present an analytical estimate and results of Monte Carlo modeling with the modified code PZSIM [1] previously developed to calculate the detector counts and neutron spectra after nn-scattering. Results suggest a coincidence efficiency of 10<sup>-5</sup> to 10<sup>-6</sup> relative to a single detector geometry, where the range of values depends on the detection options. This coincidence rate is too low to be statistically informative.

# 1 Introduction

Motivated by a desire to understand charge symmetry breaking of the nuclear force, the neutron-neutron scattering length,  $a_{nn}$ , has been actively pursued for several decades [2]. Current values of  $a_{nn}$  come from the indirect measurements of the  ${}^{2}H(\pi^{-},\gamma n)n$ ,  ${}^{2}H(n,nn)p$ ,  ${}^{2}H(n,np)n$  reactions. Current values from these experiments are  $a_{nn} = -18.6 \pm 0.3$  fm [3],  $a_{nn} = -18.8 \pm 0.5$  fm [4], and  $a_{nn} = -16.1 \pm 0.4$  fm [5], respectively.

To help resolve the current discrepancies between these values, the Direct Investigation of  $a_{NN}$  Association (DIANNA) is using the aperiodic pulsed Yaguar reactor at Snezhinsk, Russia, which can produce pulsed neutron fluxes of  $\Phi \simeq 10^{18}/\mathrm{cm}^2\mathrm{s}$  [6] to directly measure  $a_{nn}$  from neutron-neutron scattering with an accuracy of a 3% [7]. The experimental nnsetup is shown schematically in Fig. 1. The original reactor through channel has been modified with a CH<sub>2</sub> cylindrical moderator. A 12-m evacuated, collimated flight path with neutron detector has been assembled below the reactor itself. The detector diameter is 20 cm, with a solid angle of  $3\times 10^{-6}$  in  $4\pi$  and is nearly 100% efficient to thermal neutrons. Reducing the neutron background and correcting the nn-scattering signal for residual background counts is the primary experimental challenge; a <sup>10</sup>B "back wall" absorber and a special collimator system have been installed for this purpose. With these in place, extensive modeling and test measurements have shown that a signal-to-background ratio of three is achievable [8]. Nonetheless, any ideas for improving this ratio warrant consideration.

One such suggestion has been to replace the <sup>10</sup>B "back wall" absorber with a second detector in order to measure coincidences between neutrons that scatter back-to-back

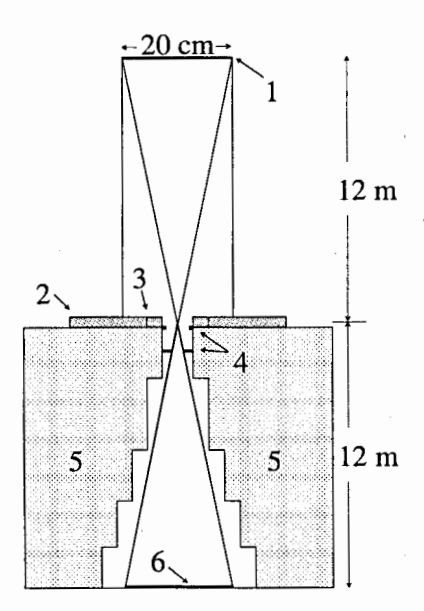


Figure 1: Schematic of experimental setup (not to scale).  $1 - {}^{10}B$  back wall or upper neutron detector for coincidence measurement, 2 - reactor core, 3 - polyethylene moderator, 4 - collimators with a minimal apperture of 3 cm, 5 - shielding, 6 - main neutron detector of with 20-cm diameter.

toward and away from the main detector. We describe here analytic estimates and Monte-Carlo modeling of the coincidence rate in that scenario.

# 2 Analytic estimate

Fig. 2 shows the geometry for the analytical calculations of the nn experiment. Neutrons leave source points  $Q_1$  and  $Q_2$  with velocity vectors  $\vec{v}_1$  and  $\vec{v}_1$  and collide at point P. The vector  $\vec{v}_{cm}$  is the center of mass velocity for these two neutrons. The final velocities of interest  $\vec{v}_f$  lie in the detector solid angle  $d\Omega_{det}$  along the z-axis. The opening angle of  $d\Omega_{det} = \theta_{det}$ , has a value of about 1°. To simplify the present analytical calculations we assume that all neutrons have the same speeds v and that vectors  $v_{cm}$  are distributed uniformly in space. The final speeds  $v_{1f}$  and  $v_{2f}$  are calculated as

$$v_{1f}^{2} = v_{cm}^{2} + (v^{*})^{2} + 2v_{cm}v^{*}\cos\theta^{*}$$

$$v_{2f}^{2} = v_{cm}^{2} + (v^{*})^{2} - 2v_{cm}v^{*}\cos\theta^{*},$$
(1)

and their cosines with respect to the direction of  $\vec{v}_{cm}$  are

$$\cos \theta_{1f} = (v_{cm} + v^* \cos \theta^*) / \sqrt{v_{cm}^2 + (v^*)^2 + 2v_{cm}v^* \cos \theta^*} \cos \theta_{2f} = (v_{cm} - v^* \cos \theta^*) / \sqrt{v_{cm}^2 - (v^*)^2 + 2v_{cm}v^* \cos \theta^*}.$$
 (2)

The angle  $\theta_{1f}$  is the angle in the laboratory frame between the velocity  $\vec{v}_{1f}$  and the center-of-mass velocity  $\vec{v}_{cm}$ . The quantities in the center-of-mass frame are marked by an asterisk, \*, so  $v^*$  is the speed of the particle and  $\theta^*$  is the scattering angle in the center-of-mass frame. We represent the uniform distribution of  $\cos \theta^*$  in the range  $[-1\ 1]$  by

$$\cos \theta^* = 1 - 2r,\tag{3}$$

where random numbers r are uniformly distributed in the range [0 1]. For our monoenergic  $(v_1 = v_2 = v)$  case, the quantities are:  $\sqrt{2}v_{cm} = v\sqrt{1 + \cos\theta_{12}}$ , and  $\sqrt{2}v^* = v\sqrt{1 - \cos\theta_{12}}$ , where  $\theta_{12}$  is the collision angle between the velocity vectors  $\vec{v_1}$  and  $\vec{v_2}$ . Therefore, the equations are simplified; in particular

$$\cos \theta_{1f} = \frac{\sqrt{1 + \cos \theta_{12}} + \cos \theta^* \sqrt{1 - \cos \theta_{12}}}{\sqrt{2}\sqrt{1 + \cos \theta^* \sin \theta_{12}}} \tag{4}$$

and

$$\cos \theta_{2f} = \frac{\sqrt{1 + \cos \theta_{12}} - \cos \theta^* \sqrt{1 - \cos \theta_{12}}}{\sqrt{2} \sqrt{1 - \cos \theta^* \sin \theta_{12}}}.$$
 (5)

These equations, Eq. 4 and 5, together with an assumed uniform spatial distribution of vectors  $\vec{v}_{cm}$ , serve as the basis for the numerical analysis of the coincidence probability. First, from inspection of Eq. 4 and 5 it can be shown that for collision angles  $\theta_{12} < 90^{\circ}$ , the final velocities,  $\vec{v}_{1f}$  and  $\vec{v}_{2f}$  are always directed at acute angles to  $\vec{v}_{cm}$ . For example, Fig. 3 shows  $\theta_{1f}$  and  $\theta_{2f}$  for  $\theta_{12} = 85^{\circ}$ . For such a case both outgoing neutrons are directed into the same hemisphere with respect to the center-mass velocity vector and therefore no coincidence is possible.

For collision angles  $\theta_{12} > 90^{\circ}$  the final velocity vectors are directed at obtuse angles to  $\vec{v}_{cm}$ , so detector coincidences are possible but only if two conditions are fulfilled simultaneously: 1) the vector  $\vec{v}_{cm}$  lies along the z-axis inside  $\Delta\Omega_{det}$  and 2) the corresponding angles  $\theta_{1f}$ ,  $\theta_{2f}$ , of the two final velocity vectors are about 0° and 180° within the range of  $\theta_{det} \approx 1^{\circ}$ . Fig. 4 presents plots  $\theta_{1f}$  and  $\theta_{2f}$  as a function of  $\theta^{*}$  for different values of obtuse  $\theta_{12}$  angles. The coincidences are possible for  $\theta^{*}$  near zero, which rarely happens.

Since  $\Delta\Omega_{det}$  is defined as the relative solid angle, it also gives the probability for meeting the first condition above, that is when the vector  $\vec{v}_{cm}$  lies along the z-axis inside  $\Delta\Omega_{det}$ . The probability governing the second condition is determined from the range of random numbers,  $\Delta r$ , in Eq. 3, which describes the isotropic scattering in the center-of-mass frame. Therefore, if the total number of collisions inside the YAGUAR through-channel is  $N_{nn}$ , then the number of two-detector coincident counts is

$$N_{coinc}^{det} = 2 \times N_{nn} \times \Delta \Omega_{det} \times \Delta r, \tag{6}$$

while the number of single detector counts [7] is given by

$$N_{single}^{det} = 2 \times N_{nn} \times \Delta\Omega_{det}, \tag{7}$$

which leads us to the final estimate of the probability of coincidences relative to the single detector counts,

$$P_{coinc} = \Delta r. (8)$$

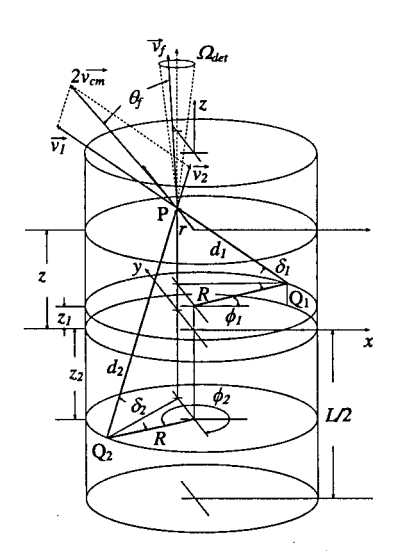


Figure 2: Diagram of scattering geometry. Neutrons leaving source points  $Q_1$  and  $Q_2$  on the internal surface of the neutron moderator (not shown), collide at point P, with initial velocities  $\vec{v}_1$  and  $\vec{v}_1$  and the collision angle  $\theta_{12}$ . Final velocities in the laboratory frame,  $\vec{v}_{1f}$  and  $\vec{v}_{2f}$  make angles  $\theta_{1f}$  and  $\theta_{2f}$  with the center-of-mass velocity  $\vec{v}_{cm}$ .

By applying Eq. 4 and 5, we find that condition 2) is fulfilled nearly independent of the obtuse  $\theta_{12}$  values, for the range of random numbers r in the interval  $[0.7.6 \times 10^{-5}]$  while the total range of r for all possible scattering angles  $\theta^*$  is [0.1]. Therefore, our analytical estimate for two-detector coincidences if  $P_{coinc} \approx 0.8 \times 10^{-4}$ . This value is an upper limit because it does not include the collimation system or the time-of-flight window which would further reduce the expected coincidence rate.

# 3 Monte-Carlo modeling with code PZSIM

In order to investigate the coincidence rate with the full geometry and the neutron energy distribution, we modified the PZSIM (Production in **Z SIM**ulation) code used to model the nn-experiment in [1] to include a second detector of either 20 cm or 200 cm diameter placed 12 m above the reactor, mirroring the placement of the original 20-cm diameter detector 12 m below the reactor. No collimators were assumed for the upper detector, but the same simplified collimation system used in [1] and shown in Fig. 1 was assumed for the main detector. As explained in [1] the PZSIM code uses the Amaldi analytical expressions for the scattering kinematics [9]. The code chooses a collision point within the scattering volume (YAGUAR through channel), chooses neutron starting positions along the internal wall of the cylindrical moderator, and chooses energies from a Maxwellian distribution with an epithermal tail. Based on the initial trajectories, the velocities are transformed to the center-of-mass system where scattering is isotropic. The new velocities

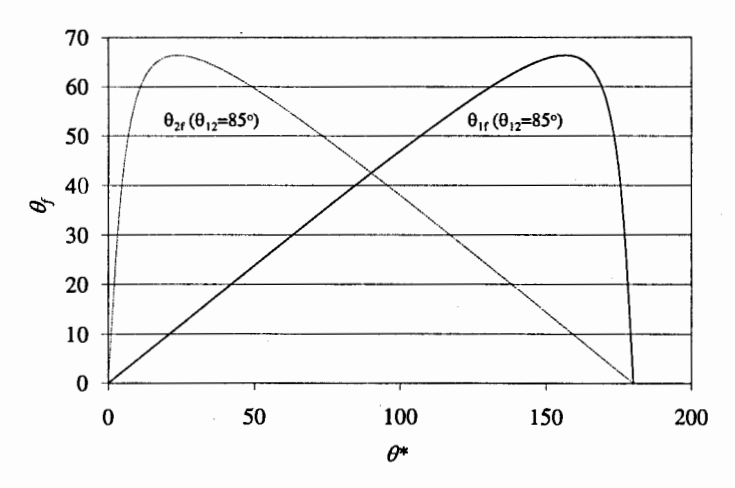


Figure 3: Plot of  $\theta_{1f}$  (dark line) and  $\theta_{2f}$  (light line) for  $\theta_{12} = 85^{\circ}$ . For any  $\theta_{12} = 85^{\circ}$  the angles  $\theta_{1f}$  and  $\theta_{2f}$  are both in the same hemisphere with respect to the center-mass velocity vector. Therefore, coincidence counts in opposite detectors are impossible.

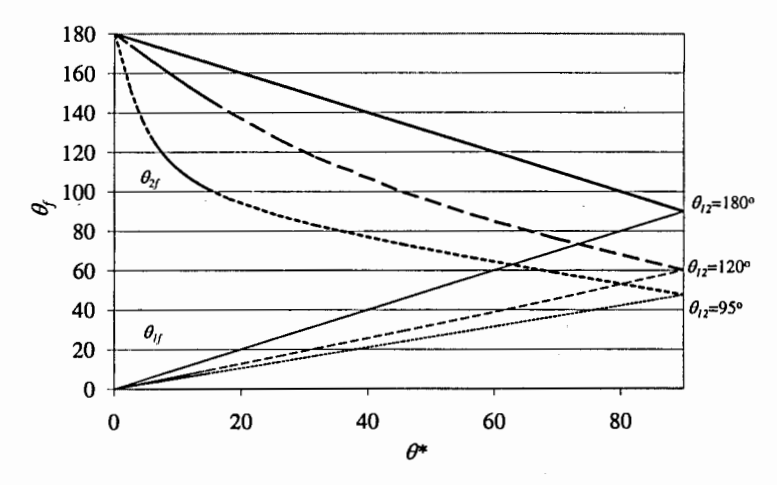


Figure 4: Plot of final angles with respect to the center-of-mass velocity,  $\theta_{1f}$  (upper light lines) and  $\theta_{2f}$  (lower dark lines), as a function of  $\theta^*$  for different scattering angles,  $\theta_{12}$ . Coincidence counts are possible. However, for the YAGUAR geometry as dicussed in the text,  $\theta_{1f}$  must be within about 1° of 0° and  $\theta_{2f}$  must be within about 1° of 180°. This rarely occurs.

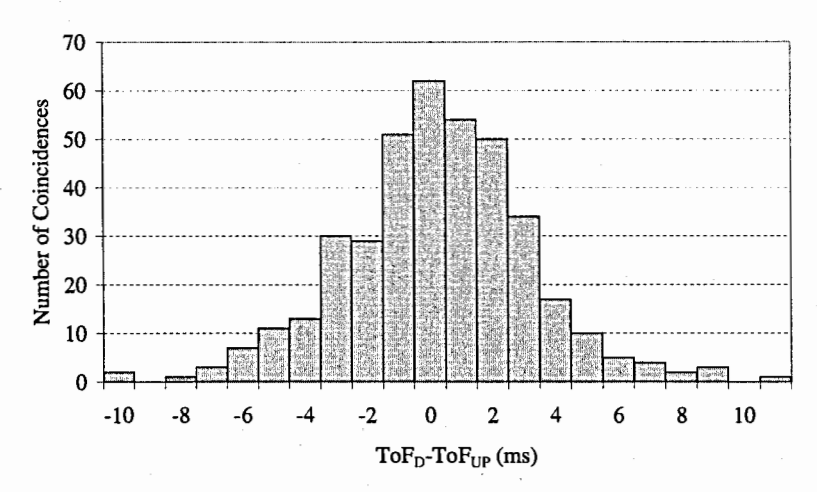


Figure 5: Histogram of the difference between arrival time-of-flight at the main detector and the upper detector for the case of a 200-cm upper detector and 20-cm main detector. There were 398 coincidences out of  $1.4 \times 10^6$  main detector hits.

of both neutrons after scattering are transformed back to the laboratory frame by adding the center-mass velocity vector. Each neutron is then followed along its path until it collides with the moderator wall, a collimator, or the detectors.

Running the modified PZSIM code with a 20-cm diameter upper detector we find that only a few of the  $10^6$  neutrons which reach the main, bottom detector have a partner that makes it to the second, top detector at any time of flight, though the statistics of this result are quite poor. To improve the statistics the upper detector by a factor of 100, the diameter of the detector was increased to 200 cm. The coincidence rate for this rather large detector is  $3\times 10^{-4}$  of the main detector count rate. Scaling this result down to the more reasonable detector size of 20 cm in diameter, we get  $3\times 10^{-6}$ . This result is quite reasonable when one considers the fact that not only do most neutrons collide with the moderator walls, but also the vast majority (98% in our simulation) of neutrons that reach the main detector originate from a collision between two neutrons that happen to both be traveling with their initial z-component of velocity towards the main detector.

The reality of time-of-flight is not included in the above coincidence probability. Of the very small fraction of detector counts that have a coincidence partner reaching the other detector, the time-of-flight for the two neutrons can vary drastically given the wide range of neutron energies involved in the collisions. The time-of-flight for the coincidences range over  $\sim 10$  ms (which corresponds with the time-of-flight interval of the Maxwellian spectrum), as shown in Fig. 4. By limiting the coincidence window to 1 ms, the overall probability for coincidences is  $< 10^{-6}$ .

## 4 Conclusion

We conclude that the coincidence rate in a hypothetical two-detector YAGUAR nnexperiment is far too low to be of any pratical use in the direct measurement of the nn-singlet scattering length. The main reason for such a small effect is the conservation of energy and momentum in the interaction between two particles of equal mass. Even though the particles go in opposite directions in the center-of-mass frame, only relatively rare head-on collisions with the center-of-mass velocity close to zero are relevant for coincidences in the lab frame. An additional reason for the low coincidence rate is the wide dispersion of neutron arrival times to the two detectors due to the broad thermal energy spectral range.

# 5 Acknowledgments

This work was supported in part by the International Science and Technology Center under project No. 2286, the Russian Foundation for Basic Research Grant No. 05-02-17636, and the US National Science Foundation Low Energy Nuclear Science RUI Award No. 0555652.

#### References

- [1] B. E. Crawford et al., J. Phys. G: Nucl. Part. Phys. 30 (2004) 1269.
- [2] Slaus I., et al., Physics Reports 173, No. 5 (1989) 257.
- [3] C. R. Howell et al., Phys. Lett. B 444 (1998) 252.
- [4] D. E. González Trotter et al., Phys. Rev. C 73 (2006) 034001.
- [5] V. Huhn, et al., Nuclear Physics A 684 (2001) 632.
- [6] B.G. Levakov, et al., Physics, Safety and Applications of Pulsed Reactors, Washington DC (1994) 67.
- [7] W. I. Furman, et al., J. Phys. G: Nucl. Part. Phys. 28 (2002) 2627.
- [8] Muzichka, A. Yu., et al., Nucl. Phys. A 789 (2007) 30.
- [9] E. Amaldi, in: S. Flügge, (Ed.), Handbuch der Physik, XXXVIII/2, Springer-Verlag, Berlin, 1959, p.1.

### ANALYTICAL CALCULATION OF THE NEUTRONS SPECTRUM FOR DIRECT MEASUREMENT OF N-N SCATTERING AT PULSED REACTOR YAGUAR

V. K. Ignatovich<sup>1</sup> FLNP JINR Dubna 141980 RF

#### Abstract

Analytical calculation of a single neutron detector counts per YAGUAR reactor pulse is presented and comparison with coincidence scheme is given.

# 1 Introduction

There is a project to measure directly n-n collision for checking charge symmetry of nuclear forces [1]. It is accepted that the best neutron source to perform such measurements is the Russian pulsed YAGUAR reactor. Some preliminary measurements and numerical simulations for expected experimental geometry had been performed [2]. We want to show here an analytical approach to calculations. First we obtain analytical momentum spectrum of scattered neutrons, then the time of flight spectrum of neutrons detected by a single counter. After that we consider coincidence scheme where we have two detectors, and calculate time of flight spectrum for one detector and delay time spectrum for the second one. We considered coincidence scheme because from the very beginning of discussions about the project, and all the time during preparation of the experiment, many people continue to express the opinion that the coincidence scheme has an advantage comparing to the single detector measurement. They claim that loss of intensity, which they usually estimated at the level of 20%, will be surpassed by much higher suppression of background. We show here analytically that in the coincidence scheme effect is so much suppressed, that the question about the background level becomes irrelevant.

# 2 Estimation of the effect

The scheme of the experiment is presented in Fig. 1 borrowed from [1]. The YAGUAR reactor 1 gives a pulse of length  $t_p = 0.68$  ms, during which a huge amount of neutrons with flux density  $\Phi = 0.77 \times 10^{18}$  n/cm<sup>2</sup>s is released. After a moderator at room temperature T neutrons in the thermal Maxwellian spectrum arrive at the volume 2 (V = 1.13 cm<sup>3</sup>), where they collide with each other and some of them after collision fly along the neutron guide 3 with collimators 4, and arrive at the detector 5, where they are registered with  $\sim 100\%$  efficiency. The collimators 4 determine the solid angle  $\Delta\Omega = 0.64 \times 10^{-4}$ , at which the volume V is visible by the detector. The estimated number of neutrons that can be registered at a single pulse is equal to

$$N_e = 2n^2 V t_p v_T |b|^2 d\Omega, \tag{1}$$

where factor 2 takes into account that the detector can register scattered neutron or neutron-scatterer. The square of the scattering amplitude  $|b|^2$  is defined as:  $|b|^2 = |b_0|^2/4$ ,

<sup>&</sup>lt;sup>1</sup>e-mail ignatovi@nf.jinr.ru

where  $b_0$  is the singlet scattering amplitude, which is accepted to be 18 fm, and factor 1/4 is statistical weight of the singlet scattering. Therefore  $|b|^2=8.1\times 10^{-25}$  cm<sup>2</sup>. The speed  $v_T$  corresponds to the thermal speed  $v_T=2200$  m/s, and the factor  $v_T|b|^2$  determines number of collisions in the neutron gas per unit time. The factor  $n^2$  is the square of the neutron density:  $n=\Phi/v_T=3\times 10^{12}$  cm<sup>-3</sup>. After substitution of all the parameters into (1) we find  $N_e\approx 170$  neutrons per pulse. However it is the estimation number. To find real number counted by the single detector,  $N_s$ , it is necessary to calculate the scattering process. Calculation shows that  $N_s=FN_e$ , where factor F is of the order unity. Monte Carlo calculations in [1] give F=0.83. Analytical calculations presented below give F=0.705. The number of neutrons per pulse counted at coincidence, if the neutrons trap 6 is replaced by another detector, can be estimated as

$$N_{ec} = N_s d\Omega \tau / t_T, \tag{2}$$

where  $\tau$  is the width of the coincidence window,  $t_T=L/v_T$  is the average length of measurement time after the reactor pulse, and  $L\approx 12$  m is the average distance between collision volume and the detectors. In the experimental scheme of Fig. 1 the time  $t_T$  is of the order 5 ms. If we accept  $\tau\approx t_p=0.5$  ms, then the ratio  $\tau/t_T$  is 0.1. The factor  $d\Omega$  is included in (2), because only neutrons in this solid angle will be registered by the second detector. The total factor, which suppresses the estimated number of neutrons registered per single pulse in coincidence scheme, is of the order  $10^{-5}$ , therefore the estimated number of counts in coincidence scheme will be  $10^{-3}$ , so the experiment becomes non feasible, and the level of the background, which is determined by neutron scattering on the residual gas atoms present at even very good vacuum conditions, becomes irrelevant. The analytical calculations, presented below, show that the real number of counted neutrons in coincidence scheme contains even additional small factor  $F_c=0.15$ .

# 3 The analytical calculation of neutron scattering in the thermal neutron gas

Our calculations will be based on the standard scattering theory of neutron scattering in the atomic gas. Our main feature is that we shall make calculations directly in the laboratory reference frame without transition to the center of mass system. First we remind all the definitions of the standard scattering theory and then present analytical calculations of all the required integrals.

# 3.1 The standard scattering theory

The standard scattering theory starts with the Fermi golden rule, according to which one can write down the probability of the neutron scattering per unit time on an arbitrary system as

$$dw(\mathbf{k}_i \to \mathbf{k}_f, \lambda_i \to \lambda_f) = \frac{2\pi}{\hbar} \left| \langle \lambda_f, \mathbf{k}_f | U | \lambda_i, \mathbf{k}_i \rangle \right|^2 \delta(E_{fk} + E_{f\lambda} - E_{ik} - E_{i\lambda}) \rho(E_{fk}), \quad (3)$$

where  $|k_i\rangle$ ,  $|\lambda_i\rangle$  are initial,  $|k_f\rangle$ ,  $|\lambda_f\rangle$  are final states of the neutron and system with energies  $E_{ik}$ ,  $E_{i\lambda}$ ,  $E_{fk}$ ,  $E_{f\lambda}$  respectively, U is the neutron-system interaction potential,

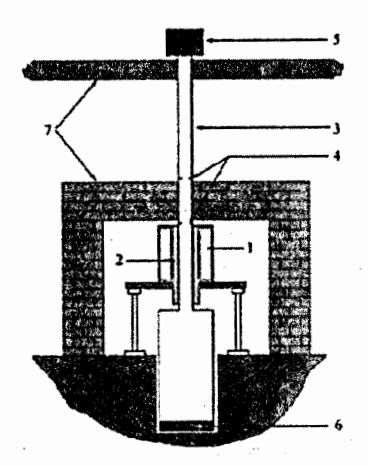


Figure 1: Scheme of the experiment on direct measurement of n-n scattering [1]. 1 — reactor core; 2 — volume of collisions; 3 — neutron guide; 4 — collimators; 5 — detector; 6 — neutrons trap.

which in the neutron atom scattering is accepted in the form of the Fermi pseudo potential

$$U = \frac{\hbar^2}{2m} 4\pi b \delta(\mathbf{r}_1 - \mathbf{r}_2). \tag{4}$$

Here  $r_1$ ,  $r_2$  are positions of the neutron and the system,  $\rho(E_{fk})$  is the density of the neutron final states

$$\rho(E_k) = \left(\frac{L}{2\pi}\right)^3 d^3k,\tag{5}$$

 $E_k = \hbar^2 k^2/2m$ , m is the neutron mass, and L is the size of some arbitrary space cell.

We suppose that the system is an atom with mass M=m, and momentum p. The initial and final states of the neutron and atom are described with similar wave functions

$$|\mathbf{k}_{i,f}\rangle = \frac{1}{L^{3/2}} \exp(i\mathbf{k}_{i,f}\mathbf{r}), \qquad |\lambda_{i,f}\rangle \equiv |\mathbf{p}_{i,f}\rangle = \frac{1}{L^{3/2}} \exp(i\mathbf{p}_{i,f}\mathbf{r}),$$
 (6)

where  $k_{i,f}$  and  $p_{i,f}$  are initial and final neutron and atom momenta respectively.

The flux density of the single incident neutron is

$$j_i = \hbar k_i / mL^3. \tag{7}$$

The scattering cross section at the given initial and final states is the ratio

$$d\sigma(\mathbf{k}_i \to \mathbf{k}_f, \mathbf{p}_i \to \mathbf{p}_f) = \frac{1}{j_i} dw(\mathbf{k}_i \to \mathbf{k}_f, \mathbf{p}_i \to \mathbf{p}_f). \tag{8}$$

At the next step we need to sum this cross section over final states of the system and average over initial states. In our case summation over the system final states is the integration over density of the atomic final states

$$\rho(E_{pf}) = \left(\frac{L}{2\pi}\right)^3 d^3 p_f. \tag{9}$$

This integration gives the cross section for the given initial states as

$$d\sigma(\mathbf{k}_i \to \mathbf{k}_f, \mathbf{p}_i)$$

$$=2\frac{2\pi m}{\hbar^2 k_i} \frac{L^9 d^3 k_f}{(2\pi)^6} \int d^3 p_f \left| \langle \mathbf{p}_f, \mathbf{k}_f | U | \mathbf{p}_i, \mathbf{k}_i \rangle \right|^2 \delta(E_{fk} + E_{fp} - E_{ik} - E_{ip}), \tag{10}$$

where  $E_p = \hbar^2 p^2 / 2M$ ,  $E_k = \hbar^2 k^2 / 2m$ , and the additional factor 2 means that the atom and neutron are the same particles, therefore we can detect with the same probability the scattered neutron in the phase element  $d^3k_f$  or an atom in the element  $d^3p_f$ .

For our experiment we need not a cross section, but the number of the neutrons  $dN(\mathbf{k}_i, \mathbf{p}_i, \mathbf{k}_f)$  scattered in the element  $d^3k_f$ . This number is determined by the number of collisions of neutrons with atoms, so the number of scattered neutrons is equal to

$$dN(\mathbf{k}_i, \mathbf{p}_i, \mathbf{k}_f) = dn_a(\mathbf{p}_i)dn_n(\mathbf{k}_i)Vdt_p vd\sigma(\mathbf{p}_i, \mathbf{k}_i \to \mathbf{k}_f), \tag{11}$$

where  $dn_a(p_i)$ ,  $dn_n(k_i)$  are the number densities of atoms and neutrons with initial momenta  $p_i$  and  $k_i$  respectively,  $v = \hbar |p_i - k_i|/m$  is the relative neutron-atom velocity, and V,  $dt_p$  are volume and time, where collisions create detectable neutrons.

Since our atoms and neutrons have the same Maxwellian distribution with the temperature T, the densities  $dn_a(p_i)$  and  $dn_n(k_i)$  are

$$dn_a(q) = dn_n(q) = n \frac{d^3q}{(2\pi T)^{3/2}} \exp\left(-\frac{q^2}{2T}\right),$$
 (12)

where n is the average neutrons density, the letter T denotes reduced temperature  $T = mk_B[T]/\hbar^2$ , and [T] is the temperature in Kelvin degrees. To find the total number of neutrons  $dN(\mathbf{k}_f)$  scattered into element  $d^3k_f$  of the final momentum space we must integrate (11) over  $dn_a(p_i)dn_n(k_i)$ , after which we get

$$dN(\mathbf{k}_f) = 2n^2 V dt_p \frac{1}{(2\pi T)^3} \frac{L^9 d^3 k_f}{(2\pi)^6} \frac{2\pi}{\hbar} \frac{2m}{\hbar^2} \int d^3 k_i \int d^3 p_i \frac{|\mathbf{p}_i - \mathbf{k}_i|}{k_i}$$

$$\times \exp\left(-\frac{p_i^2 + k_i^2}{2T}\right) \int d^3p_f \left| \langle \boldsymbol{p}_f, \boldsymbol{k}_f | V | \boldsymbol{p}_i, \boldsymbol{k}_i \rangle \right|^2 \delta(k_f^2 + p_f^2 - k_i^2 - p_i^2). \tag{13}$$

The matrix element of the potential (4) is

$$\langle \mathbf{p}_f, \mathbf{k}_f | V | \mathbf{p}_i, \mathbf{k}_i \rangle = 4\pi b \frac{\hbar^2}{2m} \frac{(2\pi)^3}{L^6} \delta(\mathbf{p}_i + \mathbf{k}_i - \mathbf{p}_f - \mathbf{k}_f), \tag{14}$$

and its square is

$$\left| \langle \boldsymbol{p}_f, \boldsymbol{k}_f | V | \boldsymbol{p}_i, \boldsymbol{k}_i \rangle \right|^2 = |4\pi b|^2 \left( \frac{\hbar^2}{2m} \right)^2 \frac{(2\pi)^3}{L^9} \delta(\boldsymbol{p}_i + \boldsymbol{k}_i - \boldsymbol{p}_f - \boldsymbol{k}_f). \tag{15}$$

After substitution of (15) into (13) we can extract  $|b|^2$  from the square of the matrix element,  $d\Omega$  from  $d^3k_f$  and introduce the thermal speed  $v_T = \hbar\sqrt{2T}/m$ . As a result we obtain

$$dN(\mathbf{k}_f) = N_e g(\mathbf{k}_f) \frac{dk_f}{\sqrt{2T}}, \qquad (16)$$

where  $N_e$  is given in (1), and  $g(\mathbf{k}_f)$  is

$$g(\mathbf{k}_f) = \frac{2}{\pi^3} \frac{k_f^2}{(2T)^3} \int d^3k_i \int d^3p_i \frac{|\mathbf{p}_i - \mathbf{k}_i|}{k_i}$$

$$\times \int d^3p_f \exp\left(-\frac{p_f^2 + k_f^2}{2T}\right) \delta(\mathbf{p}_i + \mathbf{k}_i - \mathbf{p}_f - \mathbf{k}_f) \delta(k_f^2 + p_f^2 - k_i^2 - p_i^2). \tag{17}$$

Integration over  $d^3p_i$  gives

$$g(\mathbf{k}_f) = \frac{2}{\pi^3} \frac{k_f^2}{(2T)^3} \int d^3 p_f \exp\left(-\frac{p_f^2 + k_f^2}{2T}\right) \int d^3 k_i \frac{|\mathbf{P} - 2\mathbf{k}_i|}{k_i} \delta(k_f^2 + p_f^2 - k_i^2 - (\mathbf{P} - \mathbf{k}_i)^2), \tag{18}$$

where  $P = p_f + k_f$  is the total momentum of two particles.

With all these definitions in hands we can directly calculate the spectrum of scattered neutrons

# 3.2 Analytical calculation of the integrals

First we calculate the integral

$$Q(k_f, p_f) = \int d^3k_i \frac{|P - 2k_i|}{k_i} \delta(k_f^2 + p_f^2 - k_i^2 - (P - k_i)^2)$$

$$= 2 \int \frac{d^3k_i}{k_i} |2k_i - P| \delta((k_f - p_f)^2 + (2k_i - P)^2).$$
(19)

After change of variables  $2k_i - P = u$  we obtain

$$Q(\mathbf{k}_f, \mathbf{p}_f) = \frac{1}{2} \int u \frac{d^3 u}{|\mathbf{u} + \mathbf{P}|} \delta(u^2 - q^2), \tag{20}$$

where  $q^2 = (\boldsymbol{k}_f - \boldsymbol{p}_f)^2$ .

After representation  $ud^3u = (u^2du^2/2)d\varphi d\cos\theta$ , where polar axis is chosen along the vector P, we can integrate over  $d\varphi$  and  $d(u^2)$ . As a result we get

$$Q(k_f, p_f) = \int_{-1}^{1} \frac{\pi q^2 d \cos \theta}{2\sqrt{q^2 + 2Pq \cos \theta + P^2}}.$$
 (21)

Integration over  $d\cos\theta$  gives

$$Q(k_f, p_f) = \frac{\pi q}{2P} (q + P - |q - P|). \tag{22}$$

The last factor is equal to 2q, if q < P, and it is equal to 2P, if q > P. Which one of these inequalities is satisfied depends on the angle  $\theta_f$  between vectors  $\mathbf{k}_f$  and  $\mathbf{p}_f$ . Inequality q < P is satisfied, when  $\cos \theta_f > 0$ , and inequality q > P is satisfied, when  $\cos \theta_f < 0$ . Therefore Eq. (22) is representable in the form

$$Q(\mathbf{k}_f, \mathbf{p}_f) = \pi q \left( \Theta(\cos \theta_f < 0) + \Theta(\cos \theta_f > 0) \frac{q}{P} \right), \tag{23}$$

where  $\Theta(x)$  is the step function equal to unity, when inequality in its argument is satisfied, and to zero in the opposite case.

## 3.3 The spectrum of neutrons, counted by a single detector

Substitution of (23) into (18) gives

$$g(\mathbf{k}_f) = \int d^3 p_f w(\mathbf{k}_f, \mathbf{p}_f), \tag{24}$$

where

$$w(\mathbf{k}_f, \mathbf{p}_f) = \frac{2}{\pi^3} \frac{k_f^2}{(2T)^3} \exp\left(-\frac{p_f^2 + k_f^2}{2T}\right) Q(\mathbf{k}_f, \mathbf{p}_f). \tag{25}$$

To obtain spectrum of neutrons counted by a single detector we represent  $d^3p_f = p_f^2 dp_f d\Omega_f$ , and integrate Q(k, p) over  $d\Omega_f$ . As a result we obtain (in the following we omit subscripts f of variables)

$$I(k,p) = \int Q(k,p)d\Omega = 2\pi^{2} \left( \int_{-1}^{0} d\cos\theta |k-p| + \int_{0}^{1} d\cos\theta \frac{(k-p)^{2}}{|k+p|} \right)$$

$$= 2\pi^{2} \left( \int_{0}^{1} d\cos\theta |k+p| + \int_{0}^{1} d\cos\theta \left[ \frac{2(k^{2}+p^{2})}{|k+p|} - |k+p| \right] \right)$$

$$= \frac{(2\pi)^{2}}{pk} (p^{2} + k^{2})(p + k - \sqrt{p^{2} + k^{2}}). \tag{26}$$

Substitution of (26) into (25) and change of variables x = p/k,  $y = k/\sqrt{2T}$  gives

$$g(\mathbf{k}_f) \equiv f(y) = \frac{2}{\pi} \exp(-y^2) y^2 J(y),$$
 (27)

where

$$J(y) = 2y^4 \int_0^\infty 2x dx \exp(-x^2 y^2) (1+x^2) \left[ (x+1) - \sqrt{x^2 + 1} \right]. \tag{28}$$

Integration by parts gives

$$J(y) = 2y^2 \int_0^\infty dx \exp(-x^2 y^2) (1 + 2x + 3x^2 - 3x\sqrt{x^2 + 1}) = y\sqrt{\pi} + J_1(y), \tag{29}$$

$$J_1(y) = 2y^2 \int_0^\infty x dx \exp(-x^2 y^2) (2 + 3x - 3\sqrt{x^2 + 1}) = -1 + 3\frac{\sqrt{\pi}}{2y} \{1 - e^{y^2} [1 - \Phi(y)]\}, (30)$$

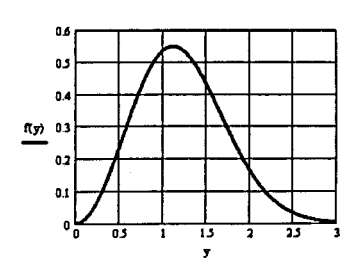


Figure 2: Spectrum  $y^2F(y)\exp(-y^2)$  of the neutrons detected by a single detector in dimensionless units  $y=v/v_T$ .

where  $\Phi(y) = \int_0^y \exp(-x^2) 2dx / \sqrt{\pi}$ . Substitution of (30) into (29) gives

$$J(y) = y\sqrt{\pi} - 1 + 3\frac{\sqrt{\pi}}{2y} \{1 - e^{y^2} [1 - \Phi(y)]\}.$$
 (31)

The momentum spectrum f(y) from Eq. (27) with account of (31) is shown in Fig. 2. Numerical integration of this function gives  $F = \int_0^\infty f(y)dy = 0.705$ .

# 3.4 Time of flight spectrum of a single detector

In the experiment the time of flight (TOF) spectrum is measured. To transform (27) into TOF spectrum we multiply it by unity

$$1 = dt\delta(t - L/v_T y), \tag{32}$$

where L is the distance between scattering volume and the detector, and integrate over dy. After that we obtain

$$\dot{N}_{s}(y(t)) = f(L/v_{T}t) \frac{L}{v_{T}t^{2}} = f(y) \frac{y}{t}.$$
 (33)

# 4 Registration by two detectors in coincidence

Let's consider the case, when neutrons are registered in coincidence by two detectors on the opposite sides of the collision volume. It means that the angle between  $k_f$  and  $p_f$  is approximately 180°. Since we register both neutrons, we should not integrate (23) over  $d^3p_f$ . Instead we should accept  $k_fp_f < 0$ ,  $p_f \approx -k_f$ , and  $d^3p_f = p_f^2dp_fd\Omega$  with the same  $d\Omega$  as in  $d^3k_f$ . Taking into account Eq. (16), (24) and (25) we can represent the number of neutrons counted by two detectors as

$$dN(\mathbf{k}_f, \mathbf{p}_f) = N_e d\Omega_{pf} \frac{2}{\pi^2} \frac{k_f^2 dk_f}{(2T)^{7/2}} q p_f^2 dp_f \exp\left(-\frac{p_f^2 + k_f^2}{2T}\right). \tag{34}$$

After transformation to dimensionless variables  $y = k_f/\sqrt{2T}$  and  $z = p_f/\sqrt{2T}$  we get

$$dN(\mathbf{k}_f, \mathbf{p}_f) = N_e d\Omega_p G(y, z) dy dz, \tag{35}$$

where  $G(y,z) = \exp(-y^2 - z^2)2y^2z^2(y+z)/\pi^2$ , and we replaced q by  $k_f + p_f$ .

To get TOF spectrum in one detector and coincidence count in the second one with coincidence window  $\tau$  we must multiply (35) by the unit  $1 = dt\delta(t - L/v_T y)dt'\delta(t' - L/v_T z + t)$  and integrate over dydz. As a result we obtain

$$\dot{N}_c \equiv dN(\mathbf{k}_f, \mathbf{p}_f)/dt = N_0 d\Omega_p G\left(\frac{L}{v_T t}, \frac{L}{v_T (t + t')}\right) \frac{dt' L^2}{v_T^2 t^2 (t + t')^2}.$$
 (36)

After integration over dt' in the range of the coincidence window  $\tau$  we can put  $z \approx y$ , and finally get

$$\dot{N}_c \approx N_0 d\Omega_p \frac{4y^7}{\pi^2} \exp(-2y^2) \frac{\tau}{t^2}.$$
 (37)

For comparison of TOF spectrum of two and single detectors it is useful to find ratio of (37) to (33). This ratio is

$$W = \frac{\dot{N}_c}{\dot{N}_s} = d\Omega_p \frac{\tau}{t} R(y), \tag{38}$$

where  $R(y) = \frac{4y^6}{\pi^2 f(y)} \exp(-2y^2) 4y^6/\pi^2 f(y)$  is shown in Fig. 3. Its integral  $\int dy R(y)$  is equal to 0.15. So we can tell that the ratio is approximately  $W \approx 0.1 d\Omega \tau/t$ , as is said in section 2.

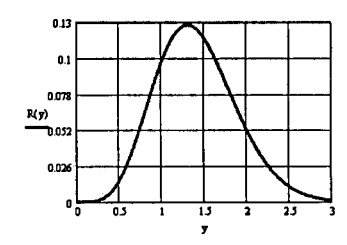


Figure 3: Dependence of R(y) on  $y = k/\sqrt{2mT}$ .

# 5 Conclusion

We have shown that the effect of n-n scattering experiment and spectrum of detected neutrons in a single detector can be calculated analytically with the standard scattering theory without transformation to center of mass system. Analytically calculated factor F=0.705 is close to that F=0.83, calculated by Monte Carlo method. The difference can be attributed to slightly different spectra of neutrons in the collision volume. In Monte Carlo calculations spectrum contained Maxwellian part and epithermal tail, while for analytical calculations we used only Maxwellian part. We did not calculated background which is related to scattering of neutrons on gas molecules, but we claim that it also can be calculated analytically. One of the main conclusions of this paper is that coincidence scheme for this type of experiment is absolutely impractical, because the effect becomes so low, that the level of the background is irrelevant.

# Acknowledgments

I am grateful to A.Strelkov for introduction to the problem, to W.Furman, E.Lychagin, A.Muzychka for discussion, to Yu.Kopach, P.Sedyshev and V.Shvetsov for support.

# References

- [1] W.I.Furman, E.V.Lychagin, A.Yu.Muzichka, et al, J. Phys. G 28,2627(2002).
- [2] B.E.Crawford, S.L.Stephenson, C.R.Howell, et al, J. Phys. G 30,1269(2004).

# STATUS OF THE EXPERIMENTS ON RADIATIVE BRANCH OF NEUTRON DECAY

Khafizov R.U.a, Tolokonnikov S.V.a, Solovei V.A.b, Kolhidashvili M.R.b

<sup>a</sup> RRC Kurchatov Institute, 123182 Moscow, Russia
 <sup>b</sup>Petersburg Nuclear Physics Institute, 188350 Gatchina, Russia

#### Abstract

This report is dedicated to the investigation of radiative neutron decay. The theoretical spectrum of radiative gamma quanta, calculated within the framework of the standard electroweak interaction model, is compared with our experimental value of branching ratio (B.R.) for radiative neutron decay. It is noted that the study of radiative branches of elementary particle decay occupies a central place in the fundamental problem of searching for deviations from the standard electroweak model. Particular attention is paid to analyzing the results of the experiment conducted at the FRMII reactor of the Technical University of Munich [1] in 2005.

#### Introduction.

Characteristics of the ordinary decay mode are currently measured with precision of tenths of a percentage point. Under these circumstances experimental data obtained by different groups of experimentalists can be reconciled only by taking into account the corrections calculated within the framework of the standard theory of electroweak interactions. This means that experimental research of the ordinary mode of neutron decay has exhausted its usefulness for testing the standard model. To test the theory of electroweak interaction independently it is necessary to move from the research of the ordinary decay branch to the next step, namely, to the experimental research of the radiative decay branch.

The radiative decay branch, where an additional particle, the radiative gamma quantum, is formed along with the regular decay products, has been discovered for practically all elementary particles. This has been facilitated by the fact that among the rare decay branches the radiative branch is the most intensive, as its value is proportional to the fine structure constant  $\alpha$  and is only several percent of the intensity of the regular decay mode (in other words, the relative intensity B.R. of the radiative decay branch has the value of several hundredths of a unit.)

However, for the neutron this decay branch had not been discovered until recently. Our experiment conducted in 2005 at the FRMII reactor of Munich Technical University became the first experiment to observe this elementary process [1]. We initially identified the events of radiative neutron decay by the triple coincidence, when along with the two regular particles, beta electron and recoil proton, we registered an additional particle, the radiative gamma quantum

$$n \rightarrow p + e + v + \gamma$$

and so could measure the relative intensity of the radiative branch of neutron decay B.R.= (3.2+-1.6) 10<sup>-3</sup> ( with C.L.=99.7% and gamma quanta energy over 35 keV; before this experiment we had measured only the upper limit on B.R. at ILL [2] ).

If we compare neutron decay with the well known radiative muon decay ( see ref. in [3] ),

the research of radiative neutron decay gives significant advantages. First, the presence of intensive cold neutron beams with intensity of  $10^9 - 10^{10}$  n/s/cm<sup>2</sup> allows to research this rare mode of neutron decay in flight, without the stop target. In the muon case, the research of this rare decay mode requires the use of the stop target, the material of which creates a significant background of the bremsstrahlung gamma quanta. This background becomes significant at the low energies of the registered gamma-quanta, so at the present the muon B.R. is well researched only for the high energy part of the spectrum, with the energy of the registered gamma-quanta over several Mev. When researching the neutron decay on intensive beams, the stop target is absent, which allows to study the radiative gamma quanta of exceptionally low energies, up to the light photons. This, in turn, allows to experimentally test a phenomenon well known in theory - the infrared convergence. Secondly, neutron life time is several orders of magnitude longer than the longest-lived elementary particle of muon. This, along with the presence of the intensive cold neutron beams, allows to research the characteristics of the radiative neutron decay with much greater precision than it has been done before, even for the muon. Thus, conducting a precise experiment on the radiative neutron decay allows to hope to discover a deviation from the standard electroweak model.

The current status and perspectives for research of the neutron and muon radiative decay modes will be discussed in detail in a separate work. In this report we will only mention that while numerous experiments have been dedicated to the research of the radiative decay mode over the past few decades, the radiative decay mode of neutron in particular has been researched only recently and by only two experimental groups. Below we will analyze and compare the results of our experiment on radiative neutron decay to the attempt to identify radiative events in the decay of neutron by a NIST experimental group. We will also compare the results of our experiment with the experiment conducted by emiT group in NIST in 2000 to measure the ordinary decay mode [4].

In the first experiment we conducted at ILL to identify radiative events we can measure only upper limit on B.R. [2]. In the second experiment we conducted at FRMIII to measure the relative intensity of the radiative branch of decay, we received an average value for B.R. that exceeds the theoretical value we obtained within the framework of the electroweak model [5]. However, due to the presence of a significant experimental error, we cannot make any final conclusions about a deviation from the standard model. Thus, our next step is to measure the characteristics of the radiative neutron decay, and especially the B.R., with greater precision. Almost a year after we published our results on the internet [6] and at JETP Letters [1], another experimental group announced the discovery of the radiative neutron decay mode and cited its own value B.R. = (3.13±0.34)·10<sup>-3</sup> with C.L.=68% and gamma quanta energy from 15 to 340 keV [7]. However, as we demonstrated later [8] the use of strong magnetic fields of several tesla prevents the identification not only of the radiative decay events, but also the events of ordinary neutron decay.

To summarize the main distinctions of our experiment [1] and compare them with the experiment conducted at NIST [7]. Both equipments are comparable in size and about 1 meter. The diagram of our equipment is given on Fig. 1. The size of our equipment is also comparable to the equipment used by emiT group at NIST in 2000 to measure coefficient D for the ordinary decay branch, an experiment to which we will also refer and with which we will compare our results [4].

Our spectrum of double coincidences of electron and recoil protons is given on Fig. 2 and its main characteristics are similar to an analogous spectrum published by emiT group ( see Fig.11 in ref. [4] ). This is an important point and requires a detailed comparison of our spectrum and the spectrum of the emiT group on double coincidences of electron and recoil proton in neutron decay. As Fig 2 and Fig 11 reference [4] show, there are two distinct peaks

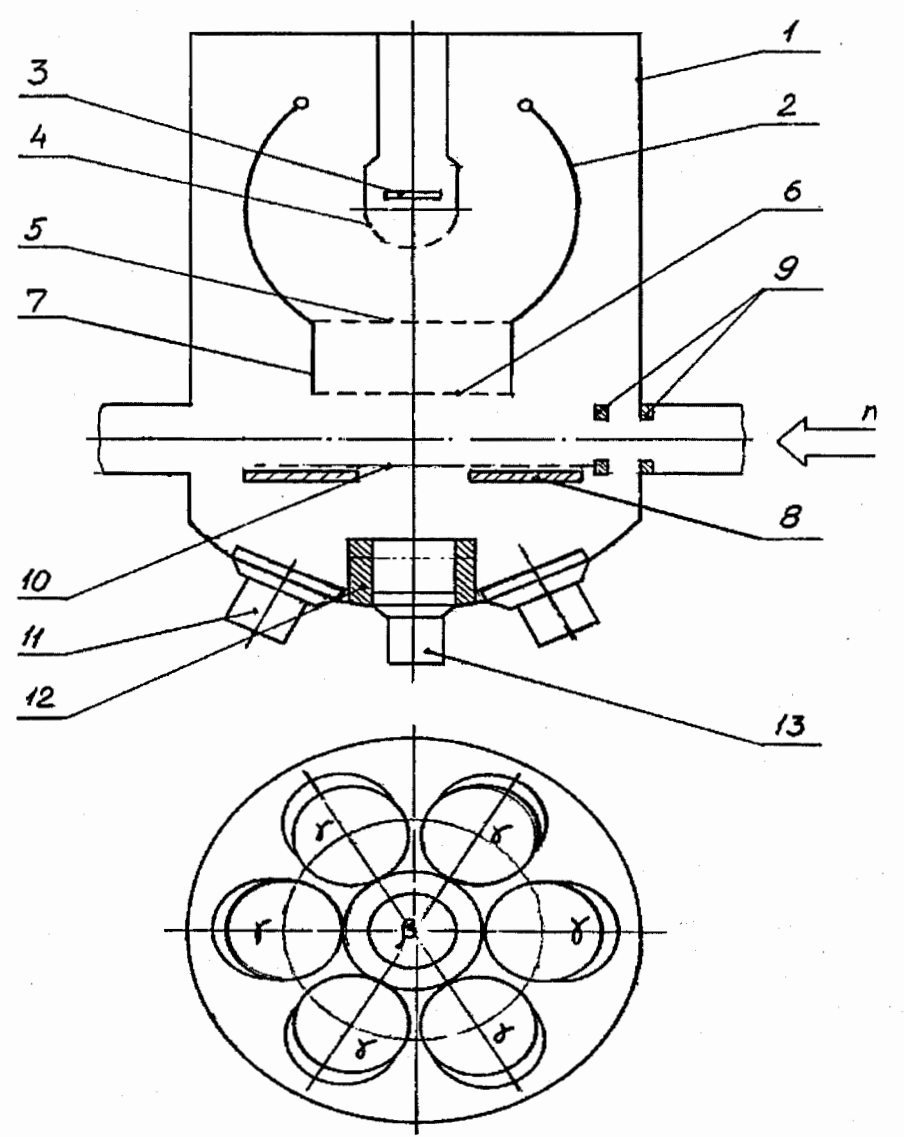


Fig.1. Schematic layout of the experimental set-up. (1) detector vacuum chamber, (2) spherical electrodes (at 18-20 kV) to focus the recoil protons on the proton detector (3) ( at ground potential), (4) grid for proton detector (at ground potential), (5) & (6) grids for time of flight electrode, (7) time of flight electrode (at 18-20 kV), (8) plastic collimator (5 mm thick, diameter 70 mm) for beta-electrons, (9) LiF diaphragms, (10) grid to turn the recoil proton backward (at 22-26 kV), (11) six photomultiplier tubes for the CsI(Tl) gamma detectors, (12) lead cup, (13) photomultiplier tube for the plastic scintillator electron detector.

in the spectra. As we can see on Fig.2 and Fig. 11 in ref [4] two peaks are eliminated on both

spectra. The first narrow peak is located in the middle of the time window where the electron opens the two equal backward and forward time windows.

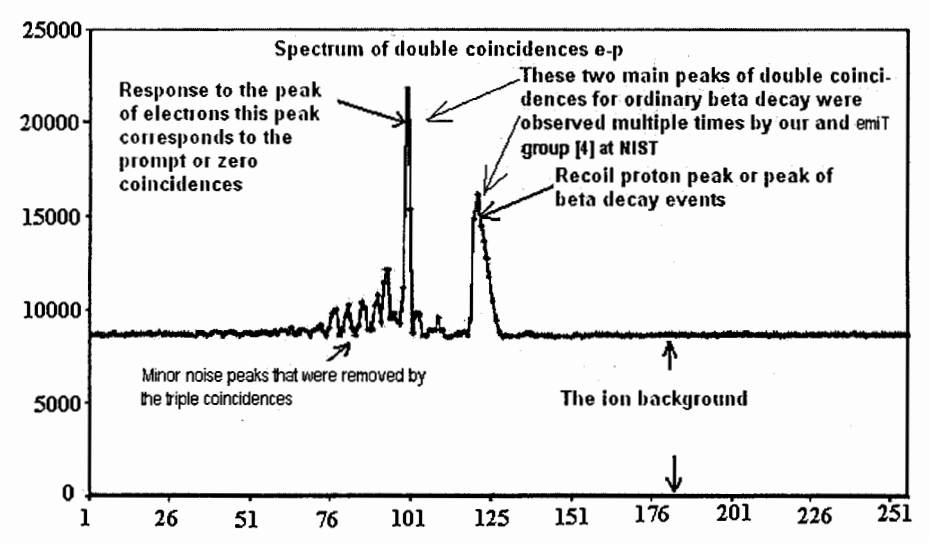


Fig.2. Timing spectrum for e-p coincidences. Each channel corresponds to 25 ns. The peak at channel 99-100 corresponds to the prompt ( or zero ) coincidences. The coincidences between the decay electrons and delayed recoil protons (e-p coincidences) are contained in the large peak centered at channel 120 ( delay time is about 500 ns ). Minor noise peaks before the peak of zero coincidences were not stable during statistics collection, disappearing at nighttime and on weekends, when the noise in the electric circuits was minimal.

In essence, this first peak is the response to the registration of beta electrons in the electron detector channel. The second peak is located to the right of the first at about the same distance in both our spectrum and the spectrum emiT group from NIST. This peak is created by the decay protons which in turn were pulled out from the decay zone by the electric field. Thus, the events that got into this peak are beta decay events; we first register the beta electron in the electron channel and then after a slight delay register the recoil proton in the proton channel. It is namely the number of events in this peak that determines the total number of registered neutron beta-decays, necessary in our experiment to measure B.R.. In our equipment protons traveling from the decay zone cross a distance several times greater than in the emiT group equipment, but proton speed is also several times higher than in emiT group experiment. From this we deducted that proton delay time in relation to electrons in both experiments is comparable. The width of the proton peak in emiT group experiment is also comparable to the width of the proton peak in our spectrum of double coincidences, as this width is primarily determined by the size of the decay zone and proton speeds. In our experiment the thickness of decay zone was 3 cm while the diameter of the decay zone in the emiT experiment was slightly greater than 6 cm, which explains why the peak width in their case is roughly twice the size of ours. Here it is important to emphasize that initial speed of recoil protons is the same in both our the emiT group experiments and that the maximum speed is determined by the maximum kinetic energy equal to 750 eV. However, in our experiment protons leaving the decay zone immediately get picked up by the external electrostatic field and their final speed is determined by the difference of potentials between the focusing electrodes and the grounded grid of the proton detector (see Fig. 1 to compare it with Fig. 5 and 7 in ref. [4]), which is why flight time to the proton detector was approximately equal in both our and the emiT group experiments, even though in our case the distance between the decay zone and the proton detector was several times greater than in the emiT group experiment.

Our double coincidences spectrum and the results of the emiT group are also similar in regard to the ion background. In both experiments the value of the background in the time window opened backward and located to the left of the sharp response peak (on Fig. 11 ref. [4] see value of background in window 1) is equal to the value of the ion background in the window opened forward (see Fig. 11 in ref. [4] see value of background in window 2) and located to the right of that peak. Most importantly, in both experiments the value of the background was comparable to the value of the beta-decay peak itself, which in turn means that in such experiments the background cannot be disregarded and that to determine the number of double coincidences it is necessary to distinguish this peak from the background.

To measure B.R. of the radiative neutron decay it is necessary to first identify the events of ordinary neutron decay and determine the number of double coincidences of beta electron with recoil proton N<sub>D</sub> and then to identify the events of radiative decay and determine the number of triple coincidences of electron, recoil proton and gamma-quantum N<sub>T</sub>. That is exactly what we did in our experiment and obtained two spectra, the spectrum of triple coincidences, used to identify events of radiative neutron decay distinguishing the radiative peak from the background, and the double coincidences spectrum, used to identify events of ordinary neutron decay distinguishing beta decay peak from the background. Unfortunately the NIST team measuring B.R. for the radiative neutron decay did not publish the experimental spectrum of double coincidences [7], which meant that they also did not present the peak of ordinary neutron decay observed by both our team and the emiT group in the double coincidences spectra. The absence of the peak is obvious as the experiment on radiative decay conducted at NIST used strong magnetic fields with values of several tesla (while the emiT group also used a magnetic field, its value was negligible and was just several millitesla), and strong magnetic fields wash out the peak of ordinary decay so that it practically fades into the ion background and it becomes impossible to distinguish. As we noted above, both our group and the emiT group obtained a background value comparable to the value of the beta decay peak ( scc Fig. 2 ), thus in principle it is possible to fit the experimental result to the B.R. value we calculated within the QED framework over 10 years ago by simply cutting out a time window in the ion background. As shown on Fig. 3, such manipulations with the ion background are absolutely unacceptable, as it is necessary to first observe the beta decay peak against the ion background on the double coincidences spectrum (see Fig. 2) and only then determine the number of ordinary beta decay events N<sub>D</sub> by subtracting the ion background from the obtained double coincidence spectrum [1].

Delays of recoil protons, published by the NIST group in [7] (see Fig. 3) are greater than 10 microseconds and are in sharp contradiction to the elementary estimates (see Fig. 4 and 5) and to the experimental spectra, obtained by us and by the emiT group [4] at NIST. Thus, instead of identifying beta decay events, the NIST experiment on BR measurements identified events of double coincidences of the background ions with beta electrons, while as we pointed out earlier (see Fig. 3), experiment authors could use only the very long delay times, characteristic for ions, but not for protons. Here it is necessary to note that ions could be created inside the equipment (vacuum chamber, neutron guide) not only because of the high intensity or a neutron beam, but also because of radioactive emissions, created due to activation of media inside of the experimental set up as the gamma quanta energy of the emission substantially exceeds the energy of ionization.

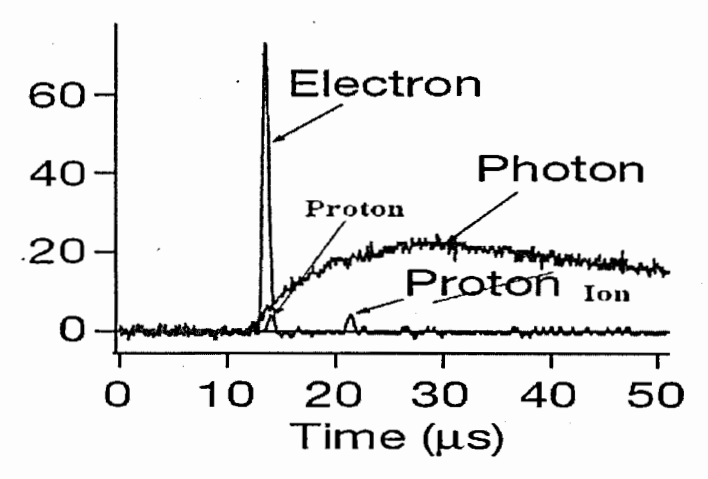


Fig.3. The photon line shows the shape of pulses from the gamma detector of the NIST experiment, built on avalanche diodes, and the electron line shows the shape of pulses from the combined electron-proton detector ( see ref. [7] ) The signal from the decay proton has to be delayed by less than one microsecond, which is why it is located at the base of the electron pulse and so cannot be registered by the combined electron-proton detector of NIST experiment. The pulses that are delayed by longer than 1 microsecond are pulses not from decay protons, as it was indicated in ref. [7], but rather from ions, formed in the decay zone ( see Fig. 2, which shows that the delay time between proton peak and the peak of prompt events is about 500 ns, and the ion background is significant because it has the same value as the proton peak ).

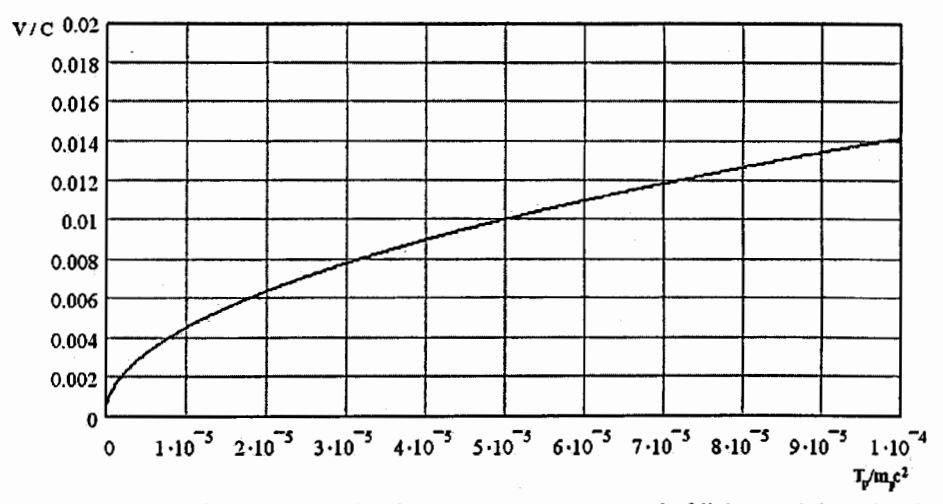


Fig.4. Relationship between the ratio of proton velocity v to speed of light c and the ratio of kinetic proton energy Tp to its mass  $m_p c^2$ 

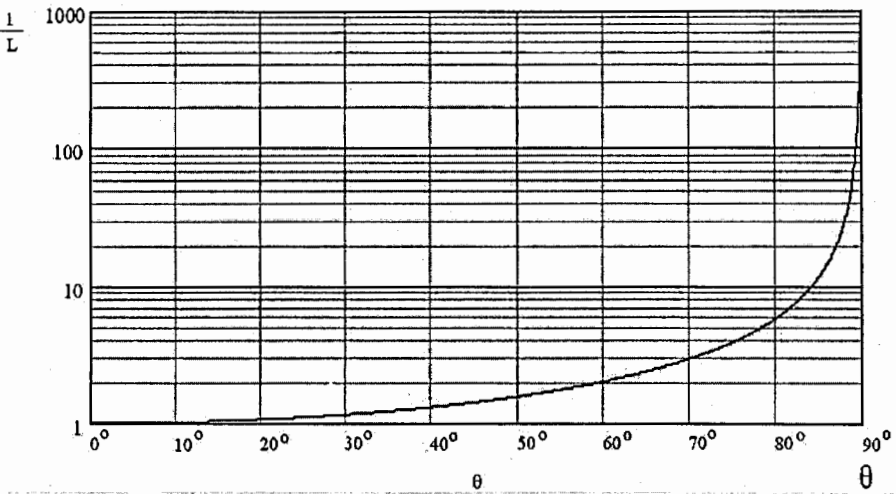


Fig.5.. Relationship between the ratio of the trajectory length l of charged particles moving in the magnetic field to distance L between the point of decay and the detector and the angle between the velocity of this particle and the direction of the magnetic field  $\theta$ . In beta decay, the beta-electrons and the protons can fly out under any angle  $\theta$ , therefore the magnetic field can increase the time of delay by several orders of magnitude only for a negligible portion of the charged particles. Even this negligible number of particles that flew out at an almost 90 degree angle to the direction of the magnetic field that coincides with the direction of the narrow neutron guide will most likely end up on the walls of the neutron guide rather than reach and hit the detector due to the presence of the strong electrostatic field.

Now we'll move to discuss the spectrum of triple coincidences, beta electron, recoil proton and radiative gamma quantum, created by radiative neutron decay. Our spectrum of triple coincidences is shown on Fig. 6, where the radiative peak is slightly shifted and located before the response to the beta-electron peak. The problem is that we observed the radiative peak not against a uniform horizontal background, but rather against a background of two peaks, which in their turn are responses to the two peaks in the spectrum of double coincidences in Fig. 2. Thus it is necessary to first distinguish the narrow radiative peak from this heterogeneous background using the method of response function. The number of events in this peak is what determines the number of radiative neutron decays, while the error arises from statistic fluctuations of the background, which can be seen on the horizontal parts of the spectrum of triple coincidences on Fig. 6. The final value of radiative events, namely the value of triple coincidences  $N_T$ , in our experiment with an error of  $3\sigma$  was equal to  $N_T$  = 360±180 events. After we obtained the number of beta-decay events forming the beta decay peak on the spectrum of double coincidences ND and calculated the geometric factor of the experimental equipment k [1], we obtained the B.R. =  $k \cdot N_T / N_D$  value of B.R. = (3.2+-1.6) 10<sup>-3</sup> (with C.L.=99.7% and gamma quanta energy over 35 keV). It is necessary to note that the average B.R. value is greater than the theoretical value, calculated within the framework of electroweak interaction. However, due to the significant error we cannot conclude that we observe a deviation from the standard model.

Coming back to the comparison of our results to the findings of the NIST experimentalists claiming to observe radiative decay events: as in the case with double coincidences, the NIST group has not published the initial experimental spectrum of triple coincidences. Instead, they demonstrate a single wide gamma peak, shifted by 1.25 microseconds before the beta-electrons. This value deviates from the estimates and the value of the leftward shift of the radiative peak from the response to the electron peak shown on our experimental spectra by several orders of magnitude. The location of the radiative peak is determined by the distance from the decay zone to detectors L and the speed of the registered articles. These distances in both experiments are roughly the same at about 1 meter and the presence of strong magnetic fields cannot lengthen spiral for the absolute majority of charged particles in this experiment even twofold (see Fig. 4), and the speed of beta electrons is comparable to the speed of light (see Fig. 5). Thus the radiative peak should be delayed by several tens of nanoseconds at most and definitely should not be delayed by microseconds.

A delay of 1.25 microseconds is huge in comparison to this estimate, and to obtain such a delay the size of the equipment should be hundreds of meters. Besides, during our experiment we did not obtain such a peak before the arrival of beta electron, and as can be seen from Fig. 6 the background before the peak responding to electron registration is horizontal and against it only negligible statistical fluctuations are visible. We can reconcile our spectra of triple coincidences with the one isolated peak observed at NIST [7] only if we assume that at NIST, the gamma-quanta were registered after the beta-electron (see Fig. 6).

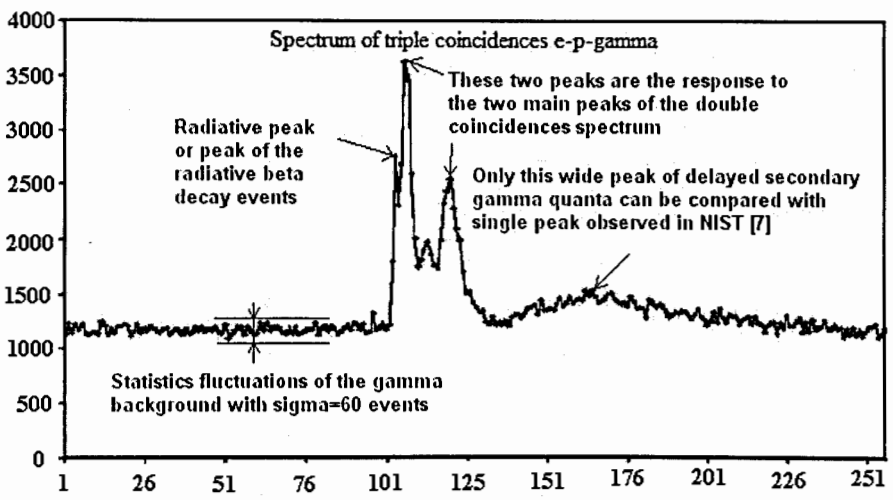


Fig.6. Timing spectrum for triple e-p-g coincidences. Each channel corresponds to 25 ns. In this spectrum, three main peaks in channels 103, 106 and 120 can be distinguished. The leftmost peak in 103 channel among these three main peaks is connected with the peak of radiative decay events. This peak was always stable, it never "migrated" to a different channel and it grew at a stable rate, regularly collecting the same number of events during the same stretch of time.

In this case the huge shift of 1.25 microseconds obtained by the NIST experimentalists fully corresponds to the shift of the wide peak we obtained in the spectrum of triple coincidences located to the right of the peak responding to beta electron registration, as this peak is formed

by gamma quanta delayed in relation to the beta electron. In comparing these peaks it is also necessary to note that their widths are identical. A radiative peak, on the other hand, could not be so wide as to be comparable to 1 microsecond, as the width is primarily determined by the size of the observed decay zone and the speed of the gamma quanta, which are parts of a nanosecond. Thus our radiative peak is very narrow and occupies one channel, the minimal time interval accommodated by our electronic equipment. If we return to the double coincidences spectrum, we will see that the second wide beta decay peak is quite wide in both our experiment (see Fig. 2) and the emiT group experiment (see fig. 11 in reference [4]), and that its width in both experiments corresponds well to the elementary estimate, arrived at by simply dividing the size of the observed decay zone by the speed of the recoil proton. Even at recoil proton speeds substantially below the speed of light – the speed of radiative gamma quanta, the width of the proton peak of double coincidences [1, 4] is less than the width of the radiative peak obtained in the NIST experiment [7].

It is necessary to note that both our Western collaborators and the authors of the radiative decay experiment in NIST [9] perfectly understood that the only peak published in Nature, the wide peak, corresponds primarily to our wide peak in the triple coincidences spectrum formed by gamma quanta registered after the registration of beta electrons, as throughout our experiment we never observed a wide peak before the registration of beta electrons. Namely this understanding heightened the NIST experimentalists' interest in explaining the wide peak in our spectrum of triple coincidences. It is obvious both from the position and the width of the peak that it is not the radiative peak [10]. Instead, it is formed by delayed secondary gamma quanta emitted by the media inside of experimental chamber activated by the detected beta-electron. According to our estimates, the value of the peak corresponds namely to the emission intensity of the secondary radioactive gamma quanta with energies above 35 keV, created when the equipment environment is activated by beta electrons. The value of the peak in the NIST experiment was greater namely because they selected the lower energy limit for the registered gamma quanta, 15 keV.

Conclusions. From the arguments laid out above it follows that the authors of the NIST experiment did not identify the peak of beta decay in the spectrum of double coincidences. One reason for this is the use of strong magnetic fields in several tesla, as well as detectors with resolution several orders of magnitude worse than those used in our experiment. On the other hand, the main parameters of our spectrum of double electron-proton coincidences identifying the events of ordinary neutron decay fully coincide with an analogous spectrum published by emiT group in Phys. Rev. [4] ( see Fig. 2 and Fig. 11 in ref. [4]).

Unfortunately we cannot say same for another experiment measuring the radiative neutron decay conducted in NIST. Our results are in sharp contradiction to the results they published in Nature [7]. Particularly vexing is the authors' unsubstantiated assertion that they observe their only wide peak of gamma quanta before the registration of beta-electrons. Both the position and the width of this peak are located in sharp contradiction to both the elementary estimates [8], and the results of our experiment [1]. In the course of our entire experiment we did not observe such a wide gamma quanta peak in the triple coincidences spectrum, located before the arrival of electrons at a huge distance of 1.25 microseconds (see Fig. 6). However, it is possible to reconcile our spectra of triple coincidences with the one isolated peak observed at NIST [7] if we assume that at NIST, the gamma-quanta were registered after the beta electrons. Only in this case does the NIST peak almost completely coincide with the peak we observed in the spectra of triple coincidences with the maximum in channel 163 (see Fig. 6), both in terms of the huge delay of 1.25 microsecond and in terms of its huge width. It is obvious that this peak is in no way related to the radiative peak, as the gamma quanta are registered after the beta electrons. This peak is created by the delayed

secondary radioactive gamma-quanta, arising from the activation of the media inside experimental chamber, which was the real object of the NIST experimentalists' observation. From this it follows that the authors of the NIST experiment knowingly mislead the physics community when they assert that the peak they observed is formed by the radiative gamma quanta registered before the registration of beta electron, when in reality their peak, shifted by 1.25 microseconds and based on comparable with this shift width is formed by delayed radioactive gamma quanta, the nature of which has nothing in common with the radiative gama quanta formed in radiative neutron decay, which is the subject of our research.

The main result of our experiment is the discovery of the radiative peak namely in the location and of the width that we expected. The location and the width of the radiative peak correspond to both estimates and the detailed Monte Carlo simulation of the experiment. Thus, we can identify the events of radiative neutron decay and measure its relative intensity, which was found to be equal B.R. =  $(3.2+-1.6)\ 10^{-3}$  (with C.L.=99.7% and gamma quanta energy over 35 keV). At the same time, the average experimental B.R. value exceeds the theoretical value by 1.5 times. However, due to a significant error we cannot use this result to assert that we observe a deviation from the standard model. Therefore, our most immediate goal is to increase experiment precision, which we can improve by 10% according to estimates.

The authors would like to thank the President of RRC "Kurchatov Institute" Academician E.P. Velikhov, Prof. Yu. V. Gaponov and V. P Martemyanov for their support of our work. The research is conducted with the financial support of RFBR (grant N 1a - 00517).

#### References

- [1] R.U. Khafizov et al., JETP Letters, v. 83(1), (2006), p. 5.
- [2] M. Beck et al., JETP Letters v. 76(6), 2002, p. 332.
- [3] W.-M. Yao et al., Journal of Physics, G 33, 1 (2006).
- [4] L.J. Lising, et al., Phys. Rev. C. v.6, 2000, p. 055501.
- [5] Yu.V. Gaponov, R.U. Khafizov, Phys. Lett. B 379(1996), p. 7.
- [6] R.U. Khafizov et al., e-print arXiv: nucl-ex /0512001
- [7] J. Nico et al., Nature, v. 444 (2006) p. 1059.
- [8] R.U. Khafizov et al., e-print arXiv: nucl-ex /0710.1389
- [9] N. Severijns, et al., e-print arXiv: nucl-ex/0607023; J. Nico, private communication
- [10] R.U. Khafizov, V.A. Solovei, e-print arXiv: nucl-ex /0608038

# DETERMINATION OF N-E SCATTERING LENGTH FROM NEUTRON DIFFRACTION ON A TUNGSTEN ISOTOPIC MIXTURE IN MAGNETIC FIELD

Yu. A. Alexandrov, C. Oprea, A.I. Oprea

JINR, Dubna, Russian Federation

Abstract. We would like to continue measurements n-e interactions begun in 70s years [1], by the method of diffraction with neutrons of 1Å (10<sup>-10</sup>m) on a sample-ball by a diameter of 5 mm from a mixture of wolfram isotopes, having a very small nuclear scattering length (of about 0.3 Fm). Owing to the smallness of nuclear scattering length, it is possible to achieve an increasing of the measured n-e interaction till 20-30% (instead of the usual 1-1.5%). The dependence of scattering length  $b = a + Z Fa_{ne}$  determined in 1974 for two isotopic mixtures of wolfram  $(b_1>0)$  and  $b_2<0)$  has shown, that there is an additional scattering giving the contribution in Bragg peaks. The analysis of such scattering has shown, that the scattering carries most likely magnetic character and it is caused by formation of clusters from wolfram atoms around the impurities of cobalt atoms available in analysed samples. The account of such magnetic scattering had as a result  $a_{ne} = -1.60(5) \times 10^{-3} \text{ Fm}$ . Following this value it is possible to receive the average square of electrical internal radius of the neutron less than zero that is in the consent with the meson theory of Yukawa. Let's notice that an average square of electrical internal radius of the neutron >0 at  $|a_{ne}| < 1.468 \times 10^{-3} \ Fm$ contradicts the theory of Yukawa, though on this fact why that do not pay usually attention. If we'll perform experiences of neutron diffraction on a sample in magnetic field in the scattering plane, then it is possible to avoid or strongly reduce the magnetic scattering.

1. INTRODUCTION. The interaction of the thermal neutron with the electron in the atoms is one of the important source of information about the structure of the neutron. At the interaction of the thermal neutron with the atoms when the process can be considered elastic the total scattering length has the form:

$$a(\theta) = \frac{2}{3} \frac{MR^3}{h^2} V_0 Z f\left(\frac{\sin \theta}{\lambda}\right) \tag{1}$$

3  $h^2$   $\lambda$  )
where: M = the reduced mass of the system,  $V_0 = \text{the depth of the well describing the}$ 

interaction,  $R = \frac{e^2}{mc^2}$  = the radius of the well and equal to the classical radius of the

electron, Z = the electric charge of the electrons,  $f\left(\frac{\sin\theta}{\lambda}\right)$  = the form factor of the electrons

known from the scattering of the X-rays on the atoms.

If we take into account only the n-e interaction we can write:

$$a(\theta) = a_{ne} Z f\left(\frac{\sin \theta}{\lambda}\right) \tag{2}$$

where :  $a_{ne} =$  the neutron – electron interaction length.

2. Experimental methods of the measurement of the neutron – electron interaction. The differential cross section of the thermal neutron coherent scattering scattering on the atoms [2]:

$$\sigma(\theta) = \left| a + a_F + a_{ne} Z f \left( \frac{\sin \theta}{\lambda} \right) \right|^2$$
 (3)

 $a_F = \frac{Z\mu_n e^2}{2Mc^2} = Z \cdot 1.468 \cdot 10^{-16} \, \mathrm{cm}$  = the Foldy term due to the relativistic interaction of the anomal magnetic moment of the neutron with the electrostatic field of the nucleus Ze, a = the length of the nuclear scattering ( $a \sim 10^{-12}$ ) m.

For heavy nuclei the ratio  $\frac{Za_{ne}}{a} f\left(\frac{\sin \theta}{\lambda}\right) \approx 1\%$  so it is possible in principle to measure this

ratio. There are a few methods for the measurement of neutron – electron scattering length

A. The first method is based on the measurement of the very small asymmetry of the
scattered neutrons due to the term. The asymmetry is conditioned by n-e interaction, by the
interaction of the magnetic fields generated by the electrons with the magnetic moment of the
neutron. To avoid the magnetic interaction were used atoms with full electronic shells
(monoatomic noble gases). The n-e scattering length is extracted from the following

$$\varepsilon = \frac{1 + 4\pi (2R)^3 n f(\varphi_1)}{1 + 4\pi (2R)^3 n f(\varphi_2)}, \ \varphi_1 = 45^0, \varphi_2 = 135^0, \tag{4}$$

R = radius of the atoms, n = density of the atoms

experimental measured value

$$a_{ne} = (-1.34 \pm 0.03) \cdot 10^{-16} \, cm \rightarrow V_0 = (-3720 \pm 90) eV$$
 (5)

**B.** Another method for the measurement of the n-e scattering length is based on the dependence of the total cross section of the scattered neutrons by the neutron wave length  $\lambda$ . Were used neutrons with  $\lambda \approx 1$ . The length of nuclear scattering is constant and the modification of the cross section is given by the form factor  $f\left(\frac{\sin\theta}{\lambda}\right)$ . Were effectuated measurements on Lead (Pb) and Bismuth (Bi).

$$a_{ne} = (-1.49 \pm 0.05) \cdot 10^{-16} cm \rightarrow V_0 = (-4340 \pm 140) eV$$
 (6)

C. A more reliable method for evaluation of the n-e scattering length is the method of compensation of the nuclear length by reflection of the neutron on a mirror. It is known that the refraction index for the neutrons depends of the neutron wave length  $\lambda$ .

$$n^2 = 1 - \frac{\lambda^2}{\pi} \sum_i a_i N_i$$
,  $a_i = \text{coherent scattering length on the } i \text{ atom type, } N_i = \text{number of atoms of } i \text{ type on cm}^3$ .

Were used two type of atoms (A and B) for precise measurements of the critical angle  $\theta_{cr}^2 = n_A^2 - n_B^2$ ,  $\theta_{cr} << 1$ . For liquid oxygen and bismuth we have:

$$\frac{\pi}{\lambda^{2}} \theta_{cr}^{2} = N_{Bi} a_{Bi} \left( \frac{N_{O} a_{O}}{N_{Bi} a_{Bi}} - 1 \right) - N_{O} Z_{O} a_{ne} \left( \frac{N_{Bi} Z_{Bi}}{N_{O} Z_{O}} - 1 \right)$$
(7)

$$a_{ne} = (-1.39 \pm 0.13) \cdot 10^{-16} cm \rightarrow V_0 = (-3860 \pm 370) eV$$
 (8)

3. Measured experimental valus of the n-e scattering length. From different experiment were obtained the following values for n-e scattering length [3], [4], [5]:

$$a_{ne} = (-1.30 \pm 0.03) \cdot 10^{-16} cm$$

$$a_{ne} = (-1.56 \pm 0.04) \cdot 10^{-16} cm$$

$$a_{ne} = (-1.427 \pm 0.023) \cdot 10^{-16} cm$$
(9)

In the  $a_{ne}$  the main contribution is given by the Foldy term related with the magnetic momentum of the neutron. Until now it is not clear if there are also other contribution given by the internal structure of the neutron, due to the electrical mean square radius.

One of the important problem of the measurement described in [3-5] is the smallness of the effect due to the n-e scattering in comparison with the nuclear scattering ( $\approx 1\%$ ).

In [3] and the references from [3] it is described a new method for the extraction of the n-e scattering length  $a_{ne}$ , by diffraction of the thermal neutrons on some mono crystals of Wolfram 186 (Tungstem). Using this method the n-e effects will be increased from some percents till tens of percents.

It is proposed to repeat the diffraction method at intense neutron sources.

4. The method of extraction of n-e scattering length by diffraction on 186 Wolfram mono crystals. The mixture of the Wolfram isotopes with negative scattering amplitude can give a very small coherent amplitude. For the experiment were prepared two small spheres from isotopes of Wolfram with diameter of 5 mm each. One sphere is prepared from 90.7 % of <sup>186</sup> W with coherent amplitude:

$$b_{1,0} = (-0.0466 \pm 0.0006) \cdot 10^{-12} cm \text{ for } \lambda = 15 \text{ } A$$
 (10)

The second sphere is prepared with <sup>186</sup>W isotopes and 14% natural Wolfram with known coherent amplitude

$$b_{nat} = (0.471 \pm 0.0013) \cdot 10^{-12} cm. \tag{11}$$

The coherent amplitude for the second sphere is  $b_{1,0} = 0.0267 \cdot 10^{-12} cm$  for  $\lambda = 15 \text{ Å}$ . Where measured 8 integral intensities of the following reflections: (110), (200), (220), (310), (400), (330), (420), (510). The n-e scattering length were extracted from:

$$\left[\frac{I_{hkl}Sin2\theta\exp(2W)}{A_{hkl}K} - \gamma^2ctg^2\theta(1-f)^2\right]^{\frac{1}{2}} = a + Zfa_{n\epsilon} = b - \text{linear function on } Zf$$
 (12)

where: W = Debye - Waller factor,  $\gamma = \frac{1}{2} \mu_n \frac{h}{Mc} \frac{Ze^2}{hc} = \text{parameter due to the Schwinger}$ scattering,  $a_{re} = (-1.55 \pm 0.02) \cdot 10^{-16} \, cm$ 

5. Discussions. As hypothesis was proposed the presence of a supplementary scattering giving his contribution in the Bragg peaks. This supplementary scattering is a result of the neutrons interaction with the existing ranges in the Wolfram probe with ordered magnetic moments. Later this hypothesis was confirmed in the other experiments realized by teams from Institute for Nuclear Physics from Leningrad (former USSR) and Prague. Activation analysis realized in Dubna showed that the probes of Wolfram contain micro impurities (part of percent) of Cobalt. Around these impurities is forming magnetic clusters from some hundred of Wolfram atoms. In this way Wolfram can exist in hetero phases state and in consequence to have the symmetry properties of two phases, the paramagnetic and

ferromagnetic phases. Taking into account the formation of the magnetic clusters the relation (12) is changing to:

$$\left[\frac{I_{hkl}Sin2\theta\exp(2W)}{A_{hkl}K} - \gamma^2ctg^2\theta(1-f)^2 + p^2\right]^{\frac{1}{2}} = a + Zfa_{ne} = b$$
(13)

where:  $p^2$  = parameter counting the ferromagnetic scattering.

The processing of the experimental data allow us to obtain the neutron – electron scattering length  $a_{n\epsilon}=-1.55\cdot 10^{-16}\,cm$  and also the  $p^2$  parameter. It is possible to avoid or to neglect the magnetic scattering using a method form [6]. The  $p^2$  function contains terms with  $\sin^2\alpha$ , where  $\alpha$  is the angle between the scattering vector perpendicular to the scattering surface and vector of magnetization. If the magnetic moments are perpendicular on the reflecting surface then the angle  $\alpha=0$  and consequently also  $p^2=0$ . In conclusion the measurements must be realized in an applied external magnetic field of order of 0.1 T. The diffraction can be eliminated in these conditions using the formula (12).

#### References.

- [1] Yu. A. Alexandrov, Fundamental properties of the neutron, EnergoAtomIzdat, Moskva, 1982 (in Russian)
- [2] Yu. A. Alexandrov, O znake I velichine srednego kvadrata vnutrennogo zariadogo radiusa neytrona, Fizika Elementarnyh Chastits I Atomnogo Yadra, vol. 30, issue 1, 1999 (in Russian)
- [3] Yu. A. Alexandrov, T. A. Machekhina, L. N. Sedlakova, L.E. Fykin, Preprint Dubna, P3-7745, 1974 (in Russian)
- [4] V. E. Krohn, G. R. Ringo, 148, 1303, 1966; Phys. Rev. D8, 1305, 1973
- [5] E. Melkonian, B. M. Rustad, W.W. Havens, Phys. Rev., 114, 1571, 1959
- [6] G.E.Bacon, Neutron Diffraction, Oxford, Clarendon Press, 1955

# MEASUREMENT OF THE P-ODD ASYMMETRY OF γ-QUANTA FROM THE <sup>10</sup>B(n,α)<sup>7</sup>Li\*→Li(g.st.) REACTION AT HEIGHTENED FREQUENCY OF NEUTRON POLARIZATION SWITCHING

V. A. Vesna<sup>1</sup>, Yu. M. Gledenov<sup>2</sup>, V. V. Nesvizhevsky<sup>3</sup>, A. K. Petukhov<sup>3</sup>, P. V. Sedyshev<sup>2</sup>, T. Soldner<sup>3</sup>, E. V. Shul'gina<sup>1</sup>, O. Zimmer<sup>3</sup>

Petersburg Nuclear Physics Institute RAS, Gatchina, Russia
 Joint Institute for Nuclear Research, Dubna, Russia
 Institut Laue-Langevin, Grenoble, France

#### Abstract.

We present results of a measurement of P-odd asymmetry  $\alpha_r$  of  $\gamma$ -quanta emission in the nuclear reaction  $^{10}\text{B}(n,\alpha)^7\text{Li}^* \to \gamma \to ^7\text{Li}(\text{g.st.})$  with polarized cold neutrons. The experiment was carried out using a new version of the integral measuring method. The frequency of neutron spin-flip is higher in this method than the typical reactor power noise frequency; this condition decreases experimental uncertainties. The result is  $\alpha_r = (0.8 \pm 3.9) \cdot 10^{-8}$ ; the results of previous experiments and a "zero" experiment are taken into account. Using this value, we constrain the neutral current coupling constant in the framework of the cluster consideration for light nuclei  $f_\pi \leq 2.4 \cdot 10^{-7}$  (at 90% c.l.). This constraint does not contradict the estimation obtained from the P-odd asymmetry in the reaction  $^6\text{Li}(n,\alpha)^3\text{H}$ :  $f_\pi \leq 1.1 \cdot 10^{-7}$ . However, both these constraints contradict the DDH "best value" of  $f_\pi = 4.6 \cdot 10^{-7}$ .

#### Introduction.

The main prediction of the standard model of electroweak interactions is the weak neutral current. The parity violation in the nucleon-nucleon interaction in various processes with few-nucleon systems and nuclei has to include both charged and neutral currents. The weak neutral current however has not yet been observed in such interactions.

The nuclear reaction of light nuclei (A = 6-10) with polarized slow neutrons is probably the most promising candidate for the study of weak neutral current properties in nucleon-nucleon (NN) processes. Such nuclei could be described in the framework of cluster and multi-cluster models [1, 2], if the excitation energy is < 25-30 MeV. P-odd effects could thus be estimated at least for the nuclear reactions with  $^{10}B$  and  $^{6}Li$ .

Using this method the authors of refs. [3, 4] have calculated the P-odd asymmetry of  $\gamma$ -quanta emission in the transition  $^7\text{Li}^* \rightarrow ^7\text{Li} + \gamma$ ,  $E_{\gamma} = 0.478$  MeV resulting from the reaction  $^{10}\text{B}(n,\alpha)^7\text{Li}$  with polarized cold neutrons (Fig. 1.). The P-odd asymmetry can be presented in terms of the meson exchange constants [4]:

$$\alpha_{\nu} = 0.16 f_{\pi} - 0.028 h_{\rho}^{0} - 0.009 h_{\rho}^{1} - 0.014 h_{\omega}^{0} - 0.014 h_{\omega}^{1} . \tag{1}$$

Here  $f_{\pi}$  corresponds to  $\pi$ -meson exchange, i.e. the weak neutral current. The calculation of the asymmetry using expr. (1) and the "best values" of the meson exchange constants [5]

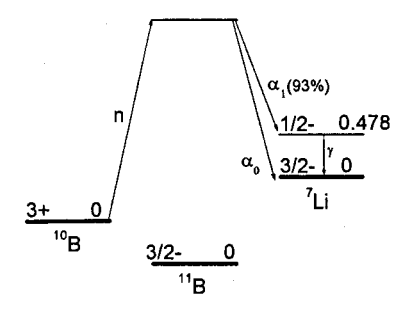


Fig. 1. Scheme of the  ${}^{10}$ B $(n,\alpha)^7$ Li reaction with slow neutrons.

yields the value:  $\alpha_{\gamma} = 1.1 \cdot 10^{-7}$ . Note that it is dominated by  $f_{\pi}$  and would be equal to  $\alpha_{\gamma} = 3 \cdot 10^{-8}$  if the weak neutral constant is zero. Two previous experiments (with a total measuring time of 47 days [6, 7]) have provided a P-odd asymmetry value in the  $^{10}\text{B}(n,\alpha)^7\text{Li}^* \to \gamma \to ^7\text{Li}(g.\text{st.})$  reaction equal to  $\alpha_{\gamma} = (2.7 \pm 3.8) \cdot 10^{-8}$ .

The P-odd effect in the nuclear reaction  $^6\text{Li}(n,\alpha)^3\text{H}$  has also been calculated [8] in terms of the meson exchange constants

$$\alpha_{l} \approx -0.45 f_{\pi} + 0.06 h_{\rho}^{0} \tag{2}$$

and measured in ref. [9, 10]:  $\alpha = (-8.6 \pm 2.0) \cdot 10^{-8}$ . If the charged weak constant were equal to the DDH "best value" of  $h_\rho^{\ 0} = -11.4 \cdot 10^{-7}$ , the weak neutral constant would be equal to  $f_\pi \approx (0.4 \pm 0.4) \cdot 10^{-7}$ , or, at 90% confidence level, to  $f_\pi < 1.1 \cdot 10^{-7}$ . However, this value is smaller than the DDH "best value"  $f_\pi = 4.6 \cdot 10^{-7}$  [5]. This contradiction could be verified independently if the asymmetry  $\alpha_r$  for  $^{10}$ B could be measured more precisely.

#### Experiment.

In the light of the above, we have carried out another experiment on the PF1B beam of polarized cold neutrons [11] at the Institut Laue-Langevin (ILL) in Grenoble, France. A typical scheme of experiment is shown in Fig. 2. The average neutron wavelength at the PF1B was  $\langle \lambda_n \rangle = 4.7$  Å. The neutron beam cross-section at the sample position was  $80 \times 80$  mm. The total neutron flux at the sample was equal to  $\sim 3 \cdot 10^{10}$  c<sup>-1</sup>. The neutron polarization was  $P = (92\pm2)\%$ . The neutron spin  $\vec{\sigma}_n$ , the  $\gamma$ -quantum momentum  $\vec{p}_\gamma$ , and the neutron momentum  $\vec{p}_n$  were set as follows:  $\vec{\sigma}_n || \vec{p}_\gamma \perp \vec{p}_n$ . The P-odd effect could be observed in the asymmetry of the angular distribution of the  $\gamma$ -quanta emission:

$$\frac{dN_{\gamma}}{d\Omega} \sim 1 + \alpha_{\gamma} \cos \theta , \qquad (3)$$

where  $\theta$  is the angle between the neutron spin and the  $\gamma$ -quantum momentum.

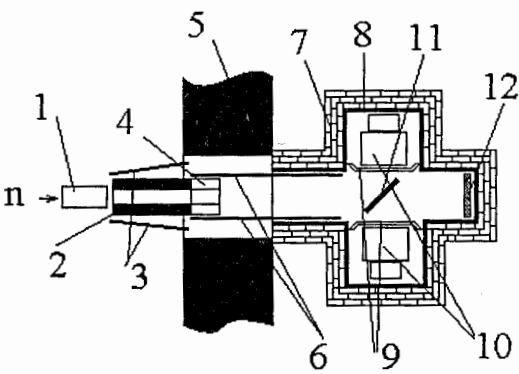


Fig. 2. A typical scheme of experiment: 1-polarizer; 2-adiabatic spin-flipper; 3,6-magnetic plates of guide field; 4-lead collimator; 5-concrete wall; 7-lead shield, 8-B4C-shield; 9-Helmgoltz coils; 10-detectors; 11-sample; 12-Li beam stop

The magnetic field guiding the neutron spin and the  $\gamma$ -quantum momentum was set parallel to each other with an accuracy of  $10^{-2}$  sr. This is sufficiently precise, as the left-right asymmetry in the  $\gamma$ -quantum emission is zero [12]; it does not therefore contribute to the P-odd effect

We used two detectors in the electric current mode and a method to compensate for any possible false effects described in refs. [13]. The guiding magnetic field is produced by Helmholtz coils; it is reversed periodically during the measurement.

The sample was produced from an amorphous powder  $^{10}B$ ; its isotopic purity was 85%. It was enclosed in an aluminium case measuring  $160\times180\times5$  mm. The sample was covered with an aluminium foil 14  $\mu$ m thick on the neutron entrance side. The total sample weight was 50 g. The sample was installed in the centre of the neutron beam; the angle between the neutron beam axis and the sample surface was 45°. Most of the neutrons were absorbed by the sample; an absorption event results in the emission of an  $\alpha$ -particle and  $\gamma$ -quantum. The distance between the sample centre and the centre of each detector is 75 mm.

Each  $\gamma$ -quanta detector consists of an NaI(Tl) crystal with a diameter of 200 mm and thickness of 100 mm. "Hamamatsu" S3204-03 photodiodes sized 18×18 mm were used to detect scintillation photons. The detectors were inserted into aluminium-alloy cases placed symmetrically on two opposite sides of the sample. The setup was surrounded with lead protection 15 cm thick. The internal surface of the lead shielding was covered with borated rubber or a polyethylene cover. The polarizer and the spin-flippers were protected by boron collimators. The detectors were protected with boron rubber. We used boron for the protection, but avoided <sup>6</sup>Li, as the  $\beta$ -decay asymmetry of <sup>8</sup>Li (the energy of 12-14 MeV results from a 10% admixture of <sup>7</sup>Li) is as high as  $\alpha_{P-odd}^{*Li} \sim 3\%$  [14]. This could compromise the results with a false P-odd effect. Background scattering (with no sample) was found to be as low as 5% compared to scattering by the sample. Neutron absorbtion in other-than-sample materials does not produce P-odd asymmetry of  $\gamma$ -quanta emission as the neutron scattering is nearly completely incoherent.

A new version of the integral measuring method was first used to measure P-odd asymmetry in ref. [15]: the frequency of neutron spin flip was higher than the typical frequency of the reactor power noise.

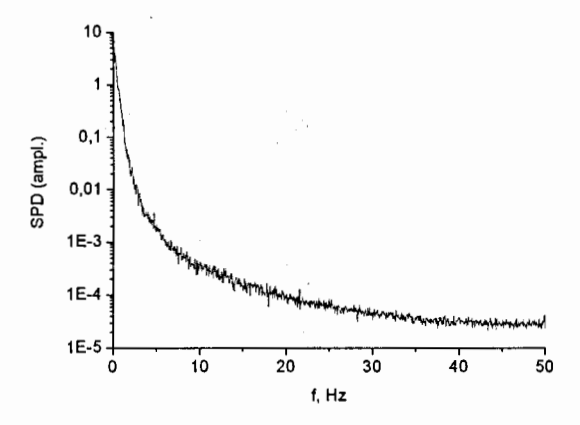


Fig. 3. SPD is a spectral density of the ILL reactor power fluctuations (in a.u.) as a function of frequency.

Fig. 3 shows the spectral density of the noise of the reactor power as a function of frequency f measured during the experiment at PF1B. Analogous distributions have been measured previously in experiments at other reactors [16]. It has been shown (ref. [16]) that uncertainty in the asymmetry measurement is only due to frequencies higher than the frequency of spin-flip. The spectral noise density decreases sharply at high frequency; so the corresponding systematics could generally be suppressed.

A significant fraction of light is lost in  $\gamma$ -detectors, as the photodiode sensitive area is much smaller than the diameter of an NaI(Tl) crystal; we therefore had to enhance the electronic signals significantly in order to measure them. This caused a "microphone effect" in an electronic channel because of the mechanical vibration of the preamplifiers. The effect varies with the different electronic channels. It is therefore not subtracted by the measuring procedure described in refs. [13]. Spin-flipping with high frequency "cuts" the low-frequency non-correlated frequency of two signals and therefore reduces the corresponding uncertainty. In order to suppress the microphone effect, we built a new electronic system to measure current. It is adapted to the neutron spin-flip frequency of 0.01-50 Hz. The uncertainty of measurement of the P-off effect in the  $^{10}\text{B}(n,\alpha)^7\text{Li}^* \to \gamma \to ^7\text{Li}(g.st.)$  is shown in Fig. 4 as a function of neutron spin flip frequency. One can see that this method reduces uncertainties in single channels as well as in the subtracted signal. The decrease in uncertainty is due to the suppression of the "microphone effect".

Additionally, new system were tested with a  $^{137}$ Cs  $\gamma$ -source (Fig. 5.). It should give homogeneous distribution of spectral density – "with noise". However, Fig. 5. shows a declination of spectral density for frequency more then  $\sim 50$  Hz. The reason of it is that the system detector + preamplifier is not ideal current to voltage converter, but it works as low pass filter.

In main measurements the frequency of neutron spin flip was equal to 5 Hz. The measurements were carried out in series of ~4 minutes. In order to reduce the effects of apparatus asymmetry and radio noise, we reversed the direction of the guiding magnetic field at the sample in every series using Helmholtz coils.

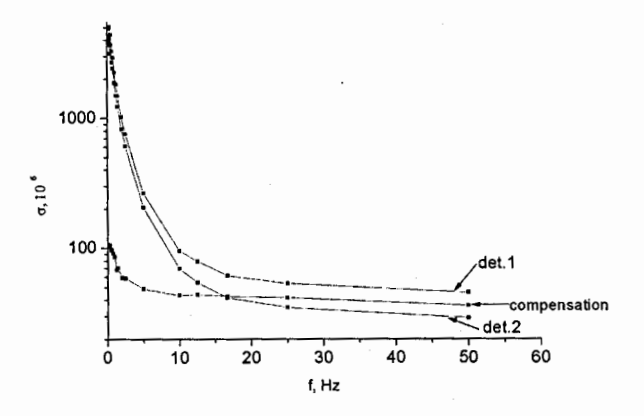


Fig. 4. The uncertainty  $\sigma$  of the measurement of the P-odd effect in the reaction  ${}^{10}\mathrm{B}(n,\alpha)^7\mathrm{Li}^* \to \gamma \to {}^7\mathrm{Li}(\mathrm{g.st.})$  as a function of the frequency of the neutron spin flip: det.1, det. 2 – the uncertainty of the asymmetry measurement for the detectors 1, 2; "compensation" – the uncertainty of the measurement of the subtracted signal (the reactor power fluctuations are compensated) multiplied by  $*\sqrt{2}$  (for comparison with single channels).

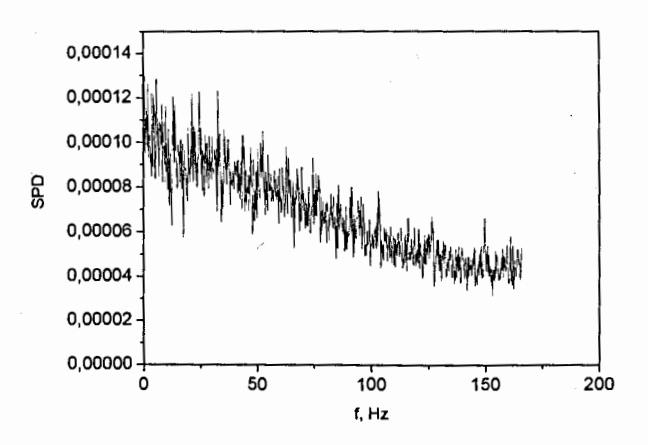


Fig. 5. SPD of signal from the 137Cs source

We measured an equal number of series for two field directions in analogy to ref. [9]. This reversed the neutron spin and the sign of the measured asymmetry respectively. The subtracted signal thus contains double asymmetry; in contrast, apparatus-related false asymmetries are subtracted. As the spin-flip frequency was not high enough to minimize the

measurement uncertainty, we also used the scheme of compensation for reactor power fluctuations.

After measuring the asymmetry for ~20 days we obtained the following result

$$\alpha_{\nu} = (3.1 \pm 3.8) \cdot 10^{-8}$$
.

It is corrected for the neutron beam polarization P and for the average cosine of the detection angle  $\theta$ :  $P < cos \theta > 077$ . Table 1 shows the P-odd asymmetry values in the reaction  ${}^{10}B(n,\alpha)^7Li^* \rightarrow \gamma \rightarrow {}^7Li(g.s.)$  measured during two ILL runs (no cut for the data applied).

Table 1.  $\alpha_{P-odd}^{^{10}B}$  asymmetry values measured during 2 runs at the ILL.

Run	$\alpha_{P-odd}^{^{10}B}$	Ref.	
2001-2002	+(2.7±3.8)·10 <sup>-8</sup>	[6, 7]	
2007	+(3.1±3.8)·10 <sup>-8</sup>		
Average	$+(2.9\pm2.7)\cdot10^{-8}$		

#### Test experiments.

An appropriate "zero" experiment is described in [10] for measurements with  $^6$ Li. Aluminium foil was used to cover the sample, to prevent the charged particles penetrating from the sample to the ionization chamber. We cannot carry out an analogous experiment in the integral current mode with a  $^{10}$ B sample, as the  $\gamma$ -quanta from the neutron reaction with boron cannot be separated from those from other reactions with impurity nuclei. We therefore performed two other kinds of test experiment.

One test consisted in performing measurements with an aluminium foil covering the sample, or with no sample in the neutron beam. In these circumstances the neutrons interact with the material behind the sample position and produces mainly  $\gamma$ -quanta (in the main experiment the neutrons are otherwise absorbed by the sample). This is not a true "zero" test, but a check for false P-odd asymmetry related to the construction material of set-up. The statistical accuracy of such measurements is not higher than in the main experiment. The measurement with the aluminium foil provided the result:

$$\alpha_{test}^{0} = (0.6 \pm 4.0) \cdot 10^{-8}$$
.

The second test involves replacing the  $^{10}B$  sample with a different target sample which has high neutron scattering cross section and low  $(n,\gamma)$  cross section. The scattered neutrons can be absorbed by the apparatus materials and emit  $\gamma$ -quanta. If  $\gamma$ -quanta emission in impurities in the apparatus materials is P-odd asymmetric, the corresponding false P-odd asymmetry is greatly enhanced (thanks to the highly enhanced flux of the scattered neutrons). Graphite is an "ideal" scatterer. Its absorption cross-section is  $\sigma_{n\gamma} = 3.8 \cdot 10^{-3}$  b; its scattering cross-section is  $\sigma_{s} = 4.8$  b. We used a target of natural graphite scattered ~43% neutrons; these scattered neutrons were absorbed by the apparatus materials. The scattering is not complete because the graphite scattering cross-section is not as large as the boron absorption cross-section. The result of this test is

$$\alpha_{test}^{graph} = (1.7 \pm 1.9) \cdot 10^{-6}$$
.

Using this value, and taking into account the cross-sections of absorption and scattering in boron, as well as the values of the constant parts of the detector signals in the experiments

with boron and graphite, we were able to calculate the contribution of false P-odd effect due to neutron scattering in boron and the consequent absorption in the apparatus materials:

$$\alpha_{scatB} = (2.7 \pm 3.0) \cdot 10^{-9}$$
.

As it is seen, the corresponding correction is small.

Besides, ~0.002 of neutrons scatters in the air in the vicinity of the sample. An additional false effect, in analogy to the estimation for boron scatter, is equal to:

$$\alpha_{scat.air} = (3.5 \pm 3.9) \cdot 10^{-8}$$
.

This is the most significant possible admixture to the measured P-odd effect.

The estimation resulting from the "zero" experiment is:

$$\alpha_0^{tot} = (2.1 \pm 2.8) \cdot 10^{-8}$$
.

The false P-odd effect caused by eventual impurities in the  $^{10}\mathrm{B}$  sample is estimated at  $\alpha_{imn}^{est} < 10^{-8}$ .

The small size of this effect is explained by the large cross-section of neutron absorption, the small fraction of impurities ( $\sim 10^{-5}$ ), and the small asymmetry values of the reactions with the impurities.

We also measured the possible false P-odd effect caused by parasite electromagnetic signals. The effect was small in all measurements:

$$\alpha_{noise} < 10^{-8}$$
.

#### Results and discussion.

Finally, the coefficient of P-odd asymmetry is equal to:

$$\alpha_{\rm r} = (0.8 \pm 3.9) \cdot 10^{-8}$$

taking into account the background/test measurements.

Using this value, eq. (1) and supposing that other weak coupling constants are equal to the DDH "best values", we estimated the weak  $\pi$ -meson constant in a fashion similar to our estimations in ref. [10]:

$$f_{\pi} = -(1.5 \pm 2.4) \cdot 10^{-7}$$
,

or, at 90% confidence level:

$$f_{\pi} < 2.4 \cdot 10^{-7}$$
.

We intend to increase the accuracy in future experiments, taking advantage of the new system of measurement of detector current, which provides experimental uncertainty close to the best possible statistical value. However, the existing data is already sufficiently precise to be able to state that the weak neutral current constant in the reaction  $^{10}B(n,\alpha)^7Li^* \rightarrow \gamma \rightarrow$   $^7Li(g.st.)$  is smaller than the DDH "best value". As mentioned above, the constraint for the weak neutral constant obtained in the reaction with  $^6Li$  [10] in the framework of the cluster model [8]  $f_{\pi} < 1.1 \cdot 10^{-7}$  is also smaller than the DDH "best value".

Finally, we can conclude that the two measured constraints (with  $^{10}$ B and  $^{6}$ Li) for the weak neutral constant agree with each other but contradict the DDH "best value"  $f_{\pi} = 4.6 \cdot 10^{-7}$ .

We are grateful for the support provided by the RFBR grant No 07-02-00138-a.

#### References.

- 1. V. I. Kukulin, et al. Nucl. Phys. A417 (1984) 128.
- 2. T. Kajino, et al. Nucl. Phys. A413 (1984) 323.
- 3. V. A. Vesna et al. Phys. At. Nucl. 62 (1999) 522.
- 4. S. Yu. Igashov, A. V. Sinyakov, Yu. M. Tchuvil'sky. In: Proc. ISINN-11, Dubna (2004) 34.
- 5. B. Desplanques, et al. Ann. Phys. 124 (1980) 449.
- 6. V. A. Vesna, Yu. M. Gledenov, et al. Bulletin of the Russian Academy of Sciences: Physics 67(1) (2003) 125.
- 7. V. A. Vesna, Yu. M. Gledenov, et al. In: Proc. ISINN-11, Dubna (2004) 52.
- 8. M. M. Nesterov, I. S. Okunev. JETP Letters 48(11) (1988) 621.
- 9. V. A. Vesna, Yu. M. Gledenov, et al. JETP Letters 82(8) (2005) 463.
- 10. V. A. Vesna, Yu. M. Gledenov, et al. Phys. Rev. C 77 (2008) 035501.
- 11. H. Abele, et al. NIM A 562 (2006) 407.
- 12. A. L. Barabanov, V. E. Bunakov et al. Bulletin of the Russian Academy of Sciences: Physics 66(5) (2002) 715.
- 13. Yu. M. Gledenov, I. S. Okunev, et al. NIM A350 (1994) 517.
- 14. Y. G. Abov et al. Nucl. Phys. 34 (1962) 506.
- V. A. Vesna, E. V. Shulgina. Instruments and Experimental Techniques 48(1) (2005)
   47.
- 16. E. A. Garusov, K. A. Konoplev, et al. Kernenergie 26(2) (1983) 68.

# THE DEVELOPMENT OF SEGMENTED HIGH RESOLUTION FAST NEUTRON SPECTROMETER.

J. N. Abdurashitov<sup>a</sup>\*, V. N. Gavrin<sup>a</sup>, V. L. Matushko<sup>a</sup>, M. F. Mustafin<sup>a</sup>, <u>A. A. Shikhin</u><sup>a</sup>†, I. E. Veretenkin<sup>a</sup>, V. E. Yants<sup>a</sup>, J. S. Nico<sup>b</sup>, A. K. Thompson<sup>b</sup>

<sup>a</sup> Institute for Nuclear Research, Russian Academy of Sciences Moscow, 117312, Russia

b National Institute of Standards and Technology Gaithersburg, MD 20899 USA

#### Abstract

We present the development of a spectrometer based on full energy absorption using liquid scintillator doped with enriched <sup>6</sup>Li. Of specific interest, the spectrometer is expected to have good pulse height resolution, estimated to lie in the range (10-15)% for 14 MeV neutrons. It should be sensitive to fluence rates from  $10^{-4}$  cm<sup>-2</sup> s<sup>-1</sup> to  $10^2$  cm<sup>-2</sup> s<sup>-1</sup> above a threshold of 500 keV in an uncorrelated  $\gamma$ background of up to  $10^2$  s<sup>-1</sup> ( $E_{\gamma} > 100$  keV). The detector's efficiency is determined by the volume of the scintillator ( $\sim$ 1.2 l) and is estimated to be (0.2-0.5)% for 3 MeV neutrons. The good pulse height resolution is achieved by compensation of the nonlinear light-yield of the scintillator due to the use of optically separated segments, which collect scintillations from each recoil proton separately. We have constructed a pilot version of the detector using undoped liquid scintillator, and we demonstrate here the response of the detector to neutrons from a Pu- $\alpha$ -Be source, whose energies range up to 10 MeV and the response of the detector to 14.1 MeV neutrons from a D-T source also. Initial testing indicates a low threshold (\$\approx600 \text{ keV}) and good spectral response after requiring a multiplicity of three segments. Such a spectrometer has applications for low-background experiments in fundamental physics research. characterizations of neutron fluence in space, and the health physics community.

# 1 Introduction

Because the neutron is a neutral particle, it does not produce direct ionization in matter, and thus one cannot measure its energy as one does with charged particles. Nevertheless, it can scatter on nuclei and transfer some part of initial energy to recoil particles.

<sup>\*</sup>Corresponding author: jna@inr.ru

<sup>†</sup>e-mail: shikhin@inr.ru

Those recoils, however, do produce significant ionization and are able to ionize a detector medium. Therefore, in measuring the ionization of a medium irradiated with neutrons, one is able to estimate its initial energy. In organic media a neutron with an energy in the range of 1 MeV to 30 MeV loses its energy primarily through collisions with hydrogen. Due to the simple kinematics of elastic scattering, it is the most common medium for looking at recoil events. In recent decades, techniques based on full absorption of neutrons in organic scintillators that have been doped or mixed with an isotope with a large neutron capture cross section, such as <sup>6</sup>Li or <sup>10</sup>B, have undergone significant development [1, 2]. The detection of prompt scintillations from recoil protons in the medium followed by delayed neutron capture ensures that the energy released by the recoils corresponds to the full absorption of neutron. Such devices are referred to as capture gated fast neutron spectrometers.

The most significant obstacle to obtaining good energy resolution in such a detector is the poor pulse height resolution. The response to monoenergetic neutrons usually consists of two clearly distinguishable peaks [2]. Moreover, it reveals some of the dynamics. In particular, the relative intensities of the peaks change with the energy of incident neutrons. This behavior has been explained from the point of view of the multiplicity of recoil protons in combination with the nonlinear light-yield of the medium [3].

To illustrate the concept, consider the moderation of monoenergetic neutrons with an energy  $E_n$  in organic medium containing only hydrogen. Those neutrons transmit their energy to recoil protons  $E_{p_i}$  by elastic scattering. If a neutron was captured, the condition

$$E_n = \sum_i (E_{p_i})$$

is satisfied. Due to the kinematics in each collision, the neutron loses on average half of the energy that it had before the collision. The number of recoil protons, as well as distribution of their energy in each particular moderation event, differ in statistical weight and depend on  $E_n$  only. For example, 14.1 MeV neutrons decelerating to 0.5 MeV (the detection threshold) will produce recoil protons with a multiplicity distribution that is on average 4–5 recoils with FWHM  $\sim$ 100%.

Due to quenching effects, the specific light-yield in organic scintillators is not proportional to the energy of a recoil proton. Therefore, from the point of view of total light yield, the moderation process proceeds by two primary modes. In the first, multiple recoils occur and the total light yield depends strongly on the how the energy of each neutron was distributed among the recoil protons. The diffusion of the total light yield corresponds to a multiplicity distribution with a broad asymmetric peak. In the second mode, a neutron loses all (or almost all) its energy in a single collision. In this case the light is emitted by single recoil proton. The total light yield is unambiguous because the energy of that recoil is fixed; therefore, this mode of moderation will contribute to the pulse height response as a separate and relatively narrow peak. This peak always appears above the multiple one because in this mode the recoil proton has its highest energy.

Thus, capture-gated spectroscopy does not lend itself well to performing spectroscopy with good resolution. The relationship between the intensities of the two peaks corresponds to relative probability of two modes of moderation. One can understand the dynamics of the energy response also. For example, in a large detector all possible combinations of recoils and their energy will be realized. The multiplicity distribution will

be wide, and the contribution of a single recoil mode will be small. In a sufficiently small detector, the probability for neutron to lose all its energy in a single collision will increase significantly in comparison to that of moderation with multiple recoils, but the total probability for a neutron to be captured will decrease. If the neutron did not lose all its energy in the first collision, it will most probably leave detector medium, i.e., in a small detector there is little chance for the neutron to make a second collision before capture.

Monte-Carlo simulations of this process are consistent with the explanation, and we proposed a procedure for correcting the measurement of the total energy of a neutron [3]. It is necessary to measure amplitude of the scintillation from each recoil proton  $I(E_{p_i})$ . Although the light-yield function  $I(E_p)$  is nonlinear, it is still single-valued and is known (or can be measured). The function  $E_p(I)$  can be understood as the inverse, and the value of  $E_{p_i}$  can be calculated. Thus, the neutron energy can be expressed as

$$E_n = \sum_{i} (E_p(I_i)).$$

The pulse height response using such an approach will have a single peak, and the energy resolution will be determined primarily by the photoelectron statistics and will be significantly better.

# 2 Design of a Segmented Spectrometer

# 2.1 Principle of Design

To achieve the goal of compensating for the nonlinear light yield, it is necessary to distinguish the individual contributions from a common signal into separate recoil protons. Since neutron with an energy of a few MeV loses 90% of its energy within 10 ns in the scintillator, a time that is comparable to characteristic time of scintillation light, identification of these contributions using pulse shape of the signal from scintillator is practically impossible. To circumvent that problem, we divided the volume scintillator into optically independent segments, small enough that the probability of two scatters on hydrogen in one segment will be small (<10%). With such a partition, the majority of stopping neutrons create no more than one recoil proton in each segment. Using the amplitude of the signal from each photomultiplier tube (PMT), the energy of a recoil proton  $E_p(I_i)$  in each hit segment is calculated, and summing  $E_{p_i}$ , one obtains the initial energy of the captured neutron. Note that more than 90% of the energy lost by a neutron occurs in the first few collisions with protons.

# 2.2 Individual Section Design

The pilot version of the spectrometer consists of 16 single segments. Each segment consists of a 3-cm diameter quartz tube with a 2-mm thick wall. The tubes are 15 cm in length with 1.2-cm quartz light guides glued at both ends of the tube. It is filled with 80 ml of

whitespirit-based scintillator with a light-yield about 40% of anthracene and a hydrogento-carbon ratio of  $\sim 1.8$ . In this pilot version of the detector, there is no  $^6 \text{Li}$  added to the scintillator. Instead of capture on  $^6 \text{Li}$ , a special mode of operation is used (and discussed below). The outer surface of each tube is carefully polished, so the light is collected at the ends is due to internal reflection. Each segment is viewed by two PMTs at the end of the tube. The PMTs are FEU-85 produced by the MELZ company (Moscow, Russia) and have 15% of quantum efficiency at 420 nm. Each PMT is supplied with high voltage produced by bases (cells) from the HV-System company (Dubna, Russia) [4]. The nonuniformity of light collection along the tube was measured to be within  $\pm 5\%$ . In order to optically isolate the segments, each tube is wrapped with aluminized mylar.

# 2.3 Data Acquisition System

The design of the data acquisition system (DAQ) depends on the logic of neutron event selection in a background of  $\gamma$ -events. We consider a typical fast neutron event in the sectioned spectrometer with full deceleration in the scintillator and its capture on  $^6$ Li.

PMT signals that are characteristic of proton recoil appear in sections simultaneously with a spread of less than 10 ns. Signals that are the result of slow neutron capture in the reaction  $n+^6\mathrm{Li} \to \alpha+^3\mathrm{H} + 4.8$  MeV will occur later in a single section; the capture time depends on  $^6\mathrm{Li}$  concentration and is in the range (20–30)  $\mu\mathrm{s}$  for our case. The amplitude of the signal is approximately 450 keV on the electron scale. The signals from both capture events and recoil events have large slow components and can be distinguished from each other and from  $\gamma$ -events by using of the pulse shape analysis (discrimination factor is  $\sim 10^3$ ).

Thus, the neutron event in the sectioned spectrometer has an unique signature. The selection criteria of neutron events are 1) the number of triggered sections is greater than one; 2) the presence of two events in a time interval of 30  $\mu$ s; 3) the slow component in the first and second signals corresponds to heavy particles; and 4) the amplitude of the second signal corresponds to energy release of a neutron capture on <sup>6</sup>Li. The joint application of these criteria allows one to achieve discrimination factor of >10<sup>8</sup> at  $\gamma$ -background of  $10^2$  s<sup>-1</sup>.

The electronics and logic diagram that incorporates these criteria is shown in Figure 1. All channels function identically, and therefore one channel only is shown. The system is composed of commercial NIM and CAMAC equipment and a computer-based digital oscilloscope card. The PMT anode signals enter a low-noise mixer through matched 50-ohm coaxial cables. The impedance of the mixer inputs is 50-ohm DC, and its gain is unity. The output of the mixer enters the input of a fast buffer voltage amplifier with variable gain, which is necessary for gain matching the individual channels.

One output of the buffer amplifier enters a fast integral discriminator; the second output enters the input of a fast linear gate through a broadband coaxial 40 ns delay line in order to record of the initial slope of the waveform. The gate together with a delay line, discriminator, level translator (LT), and fast 16-channel mixer forms a linear multiplexer permitting a reduction in the electronic noise by a factor of  $\sqrt{n}$ , where n is the number of sections of the detector. The linear gate is controlled by a signal from a discriminator. Thus, the linear gate is open only when there is a control signal. The duration of the signal is 130 ns, corresponding to the pulse width and a time to compensate for the

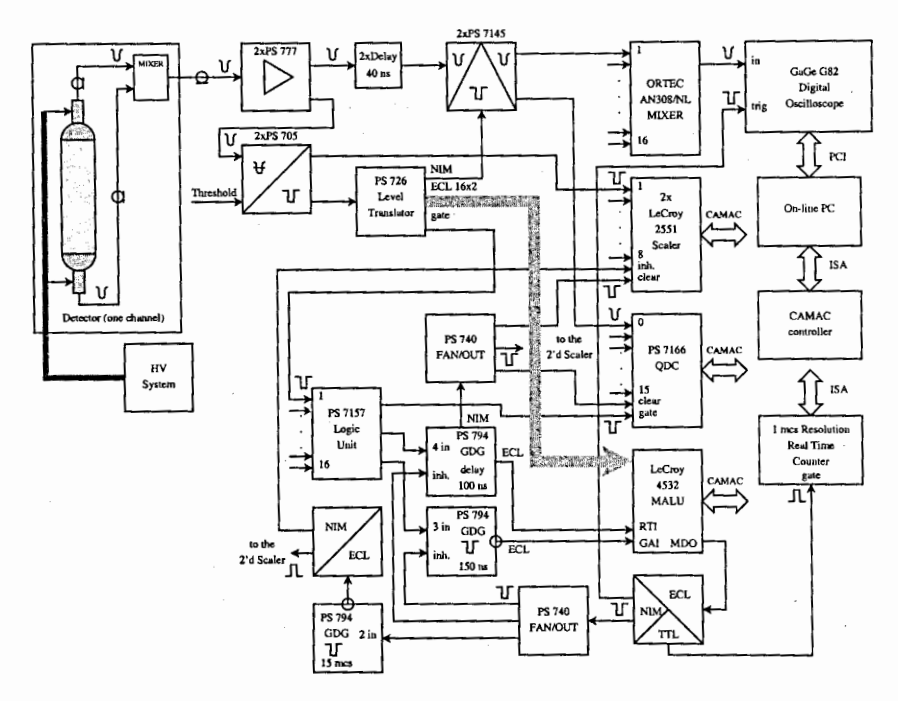


Figure 1: The functional diagram of the data acquisition system.

non-simultaneity of the signals from different sections.

From a linear gate, one output enters the input of the digital oscilloscope (DO) via a fast mixer, and a second output enters a multichannel integrating (charge-sensitive) QDC, which has 12-bit resolution. A conversion for all 16 channels in the QDC is produced by a gate signal from the OR operation of LT pulses in a logic unit.

The duration of the gate signal sets limits on the integration of the input signal. Of course, the duration of control signals for the linear gate and QDC are equal and exceed the duration of the PMT signals. The start of the DO is performed by the leading edge of a trigger produced by a MALU (Majority Logic Unit) from its MDO (Majority Discriminated Output) socket over an ECL/NIM level translator. The DO is set to a 32 kB frame size of the buffer memory; hence, a 1 ns of digitizing period corresponds to a time interval about 32  $\mu$ s. In addition, another output of the discriminator enters a fast scaler, and paraphase pulses of ECL levels are input to the MALU unit. A real time counter with 1  $\mu$ s resolution is used for precise system dead time measurement.

### 2.4 Acquisition Algorithm

In the initial state of the DAQ, operation of the scaler is inhibited by a logic 1 level, and the QDC is ready for conversion. The MALU, which operates in the memory enable mode, is already put in an open state by the logic 1 level on its gate input from the

inverted output of a gate and delay generator, which operates here as a NIM/ECL level translator for the trigger signal from the OR of a logic unit. The gate closes over a very short time interval, typically a few nanoseconds after accepting signals to its data inputs. This time interval is caused by the difference in cable delays. During the time when the gate is open, the internal register of the MALU collects signals from the appropriate inputs. After the gate closes, the data in this register are frozen, and an MDO level can be generated depending on the setting of the majority threshold  $M_{\rm thr}$ . This threshold is adjustable and usually is set to a value greater than one for true neutron detection. The reset input of the MALU is controlled by the same trigger signal from the logic unit after being delayed by another gate and delay generator, which operates in the delay mode and uses the ECL output. The same signal from its NIM output enters to the clear inputs of the scaler and QDC through an active signal splitter module.

As a fast neutron decelerates in the scintillator, some number of discriminators corresponding to the detector sections will trigger simultaneously. For the detection of a gamma ray, however, typically one section will fire. PMT signals from triggered sections enter only the appropriate inputs of the QDC, and their sum is input to the DO. The QDC begins the conversion process immediately after the gate signal, thus latching the gate input.

In the case of  $\gamma$ -ray detection, the number of hits in the MALU register is one. An MDO level is not generated, and after 100 ns all the units (scaler, QDC and MALU) receive and external fast clear from a delayed trigger signal that is active at their appropriate inputs. The acquisition continues without software participation, and dead time is very small.

In the case of fast neutron detection, the number of hits in the MALU register is more than one. The MDO level is generated after a few tens of nanoseconds, starts the record at the DO, and inhibits the operation of the gate and delay generators, which is responsible for the generation of the reset and gate signals for the MALU and the generation the clear signal for the scaler and QDC. The third gate and delay starts with an MDO signal and enables operation of the scaler for  $\simeq 30~\mu s$ . If the slow neutron capture occurs during this interval, the scaler will increment one, which is one more selection criterion. The digitizing process at the QDC and the record at the DO will continue to the end. The acquisition software checks the LAM signal from the MALU, after which it waits for readiness of the QDC and DO, saves the data, and clears MDO output. Upon completion of the sequence, the system is reset to the initial state and acquisition continues. Obviously, the amplitude of all signals in the event, except for initial one, can be only defined by the record of the oscilloscope. This is not a problem because with the capture of a neutron, the correlation between the light yield and energy of the particles ( $^3$ H and  $^4$ He) is unambiguous.

The DAQ system is ready for the full operation of the detector, but without  $^{6}$ Li doped scintillator in the segments, the application of the DO is superfluous. In the current operation for fast neutron detection, the  $M_{thr}$  is set greater than one and the operation of the scaler is not inhibited. The total dead time of the acquisition is significantly lower in this mode.

# 2.5 Principle of Operation

There are two main modes of operation. First, in the case of  $M_{thr} = 1$ , the system is triggered by any hit segment, so one measures the scintillation in segments independently. The response of the detector looks like the response of an individual segment that is simply 80 ml of organic scintillator. Each section is designed so that both background  $\gamma$ -rays and neutrons of an intermediate energy range undergo, on average, a single scattering in a single segment. Thus, the response of the detector gives a Compton scattering distribution for monoenergetic  $\gamma$ -rays interaction and a flat step for monoenergetic neutrons. In the second mode, the system is triggered by three or more segments hit  $(M_{thr} = 3)$  within a few tens of nanoseconds. In this case the probability of the interaction being due to  $\gamma$ rays is drastically decreased in comparison to that a fast neutron interaction. In addition, since the neutron loses on average about 90% of its initial energy after three collisions, it is a close approximation to the detector's operation when the scintillator is doped with <sup>6</sup>Li and requires the neutron capture. In this mode the neutron energy is obtained as a sum of recoil energies. Those energies are derived from the individual QDC values of each segment that fired and corrected by the electron-equivalent energy scale and the lightyield function. This is the main mode of operation for the pilot version of the detector for fast neutron measurements.

# 3 Response Function and Pulse Height Resolution

#### 3.1 Calibration Sources

To measure the response of the detector on  $\gamma$ -rays, we used a  $^{40}\mathrm{K}$  source with a single 1.46 MeV line. The activity of the source was  $10^3$  Bq, and the distance between the detector and the source was 15 cm. The Compton edge of the line appears at 1.24 MeV, thus giving the electron equivalent energy scale.

The response to fast neutrons was measured with a Pu- $\alpha$ -Be source. It emits neutrons with a wide distribution of energies up to 10 MeV. In addition, 60% of neutron emission is accompanied by 4.44 MeV  $\gamma$ -rays (with a Compton edge at 4.2 MeV), so a sheet of 3-cm tungsten was used to shield the detector. The shield decreased the gamma intensity by a factor of 20 but does not distort the neutron spectrum significantly. The neutron emission rate of the source was  $10^7 \, \mathrm{s}^{-1}$ , and the distance between the detector and source was 80 cm.

The response function of the detector was measured using monoenergetic 14.1 MeV neutrons from a D-T source (commercial model UNG-1, Russia). Its principle of operation is based on fusion reaction  ${}^{3}H(d,n){}^{4}He$ . The emission rate of source was about  $10^{3}$  s<sup>-1</sup>, the distances were  $\approx 0.2$  m from the source to the detector and  $\approx 1$  m to the wall of room.

# 3.2 Pu-α-Be source: Response and Resolution

Irradiation of the detector in  $M_{thr} = 1$  mode by the  $^{40}$ K  $\gamma$ -source shows a clear Compton edge at 1.24 MeV (see Figure 2) at approximately channel 700 of the QDC. The resolution

of the step is estimated to be (10-15)% and is a result of the dispersion in the response of an individual segment and the photoelectron statistics.

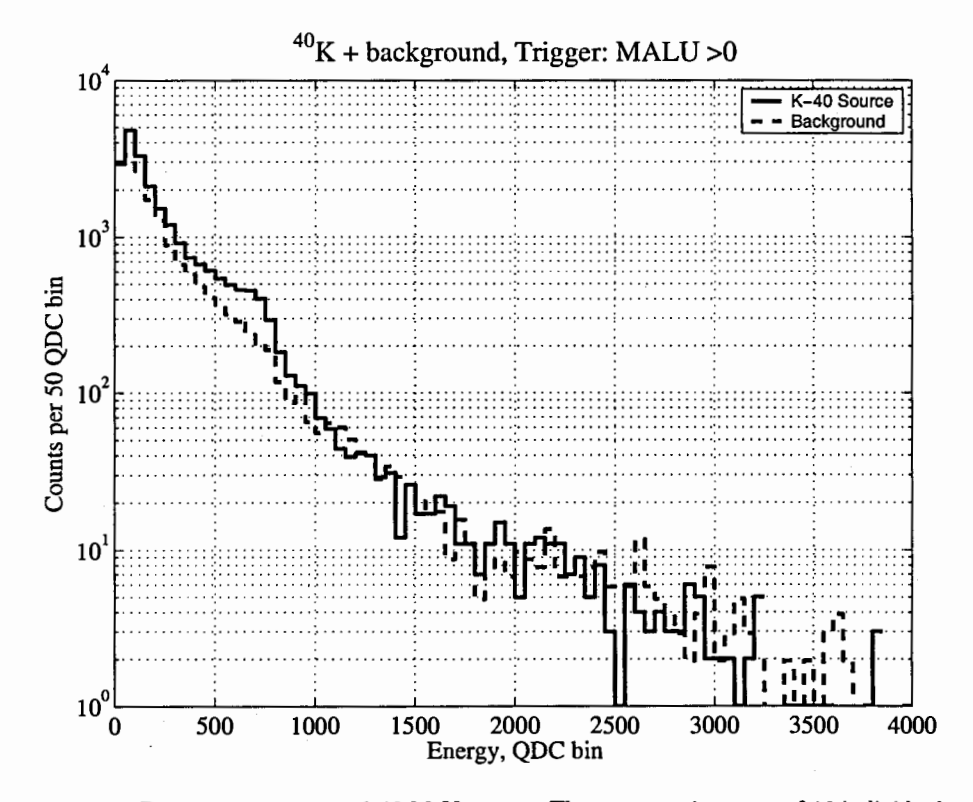


Figure 2: Detector response to 1.46 MeV  $\gamma$ -rays. The response is a sum of 16 individual responses from each segment.

When irradiated with  $Pu-\alpha$ -Be source in the same mode without the shield, the response reveals a weak Compton edge of 4.44 MeV  $\gamma$ -rays also. In Figure 3 ones sees a small excess in the proper 4.2 MeV location (upper curve) in comparison with shielded response (middle curve). Another feature of the response is a threshold of individual segments for recoil protons. It occurs around 100 keV in the electron-equivalent energy scale, corresponding to 600 keV of recoil energy.

In the mode of  $M_{thr}=3$ , there is essentially no evidence of a  $^{40}$ K  $\gamma$ -source. When irradiated with the  $Pu-\alpha$ -Be source, the neutron energy is obtained as the sum of the recoil energies derived from the individual QDC value of each hit segment. Without the tungsten shielding, occasionally a random coincidence can occur from one segment hit by the 4.44 MeV  $\gamma$ -ray and two segments hit by a single neutron. The QDC value of the segment hit by the  $\gamma$ -rays obviously distorts the final neutron energy. This is why the response of the unshielded source looks flat in the energy range of 2 MeV to 8 MeV,

# Pu-Be + background, w and w/out shield, Trigger: MALU >0

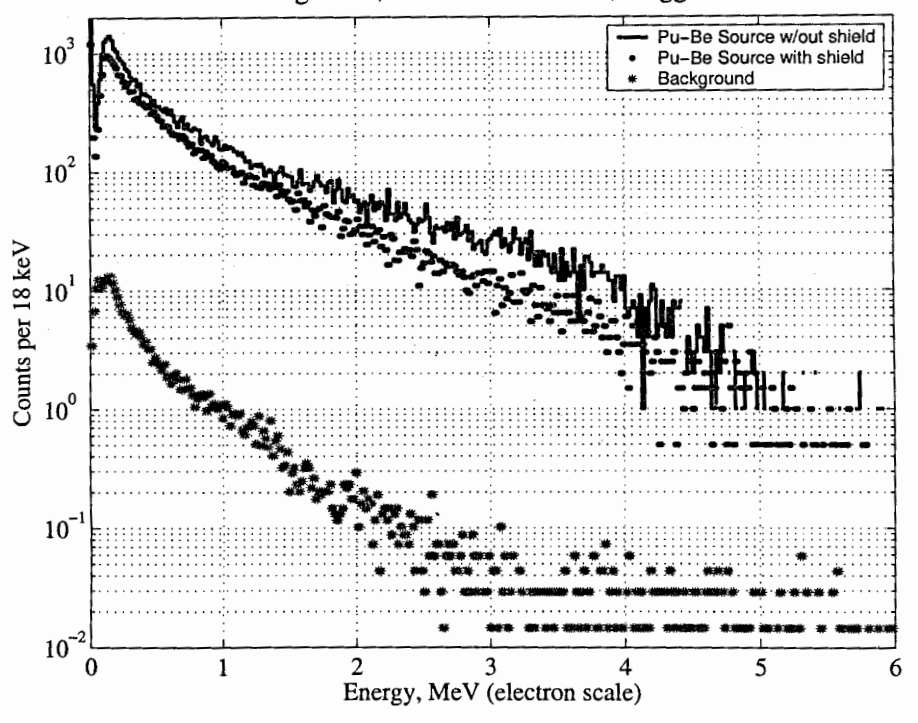


Figure 3: Detector response to a Pu- $\alpha$ -Be source,  $M_{thr}=1$ .

as seen in the upper curve of Figure 4. The tungsten shielding strongly suppresses the contribution of the accompanying  $\gamma$ -rays, and one can see the undiluted response to neutrons (middle curve).

The effective neutron threshold in the  $M_{thr}=3$  mode differs from that of 600 keV in the  $M_{thr}=1$  mode. The minimal neutron energy that can be detected is  $3\times600$  keV = 1.8 MeV. The probability that the energy will be uniformly distributed among three recoils is rather small. It is much more probable to encounter, for example, recoils with energies of 600 keV, 1200 keV, and 2400 keV producing 4.2 MeV of neutron energy. Hence, one would expect that an effective neutron threshold should exist somewhere in the middle of those values. The measured response in Figure 4 indicates that the threshold lies around 3 MeV, which is in agreement with this consideration.

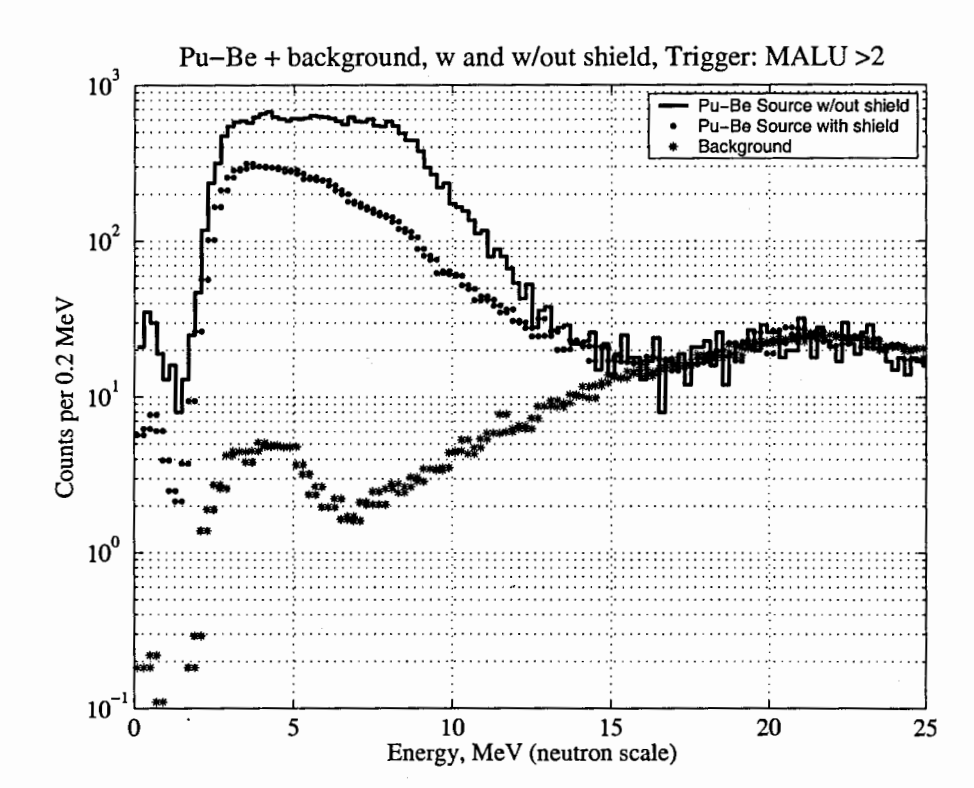


Figure 4: Detector response to a Pu- $\alpha$ -Be source,  $M_{thr} = 3$ .

# 3.3 14.1 MeV neutrons source: the Response Function measurement

There were made four measurements. Their statistical data are shown in Table 1, where Run — data file number,  $M_{\rm thr}$  — MALU threshold, Thr — hardware threshold,  $N_{\rm ev}$  — number of events in the run, Rate — average rate of events in the run and Rate<sub>sc</sub> — summary scaler rate for all sections. The details of the measurements are described below.

First, we measured response of single sections ( $M_{\rm thr}=1$ ) that gave us the energy scale. Before the measurements we decreased the gain to set the step in 3/4 of full QDC scale and increased the hardware threshold at five times to record the step in more detail. The middle of the step appears at 2900 QDC bin (Figure 5), and it corresponds to 8.0 MeV of electron energy scale due to light-yield curve, which is given in [5] and can be expressed as (1):

$$E_{\rm ee} = 0.95 E_{\rm p} - 8.0 \left[ 1 - \exp(-0.1 E_{\rm p}^{0.9}) \right],$$
 (1)

where  $E_{\rm ee}$  and  $E_{\rm p}$  are in MeV for energies of electrons and protons accordingly. This

Table 1: Response Function measurement: statistical data

Run	M <sub>thr</sub> ,	Source,	Thr,	Live Time,	$N_{ m ev}$	Rate,	Rate <sub>sc</sub> ,
	hits	MeV	mV	S		$s^{-1}$	$s^{-1}$
094303	1	-	100	1157	27215	23.5	30
101459	1	14.1	100	167	89835	538	542
104231	3	14.1	20	2481	11305	4.6	865
114105	3		20	9260	18676	2.0	114

equation yields negative light yield for  $E_{\rm p} < 0.2$  MeV, but it is not a problem in our case because a 20 mV threshold for individual segments corresponds to 0.8–1.0 MeV of recoil energy.

14.1 MeV neutrons + background, Trigger: MALU>0 One section Background 10<sup>3</sup> Counts per 50 bins  $10^2$ 10<sup>1</sup> 10<sup>0</sup> 500 1000 1500 3500 2000 2500 3000 4000 Energy, QDC bin

Figure 5: Step response for 14.1 MeV neutrons.  $M_{thr} = 1$ 

The resolution of the step is mainly due to dispersion of each PMT, which is follows from comparison of the step responses from all sixteen sections and the single section of

the detector in Figure 5. The main reason of dispersion is obviously that they are not proper glued to lightguides. Another reason is that HV-cells have poor resolution in set values.

Second, we measured the pulse height response of the detector on 14.1 MeV neutrons with  $M_{\rm thr}=3$ . It appeared to be like clear peak even on wide muon background distribution (Figure 6). With application of the correction curve for energy determination of recoil protons, which was obtained according to procedure described in Section 1, we have got the response at neutron energy scale.

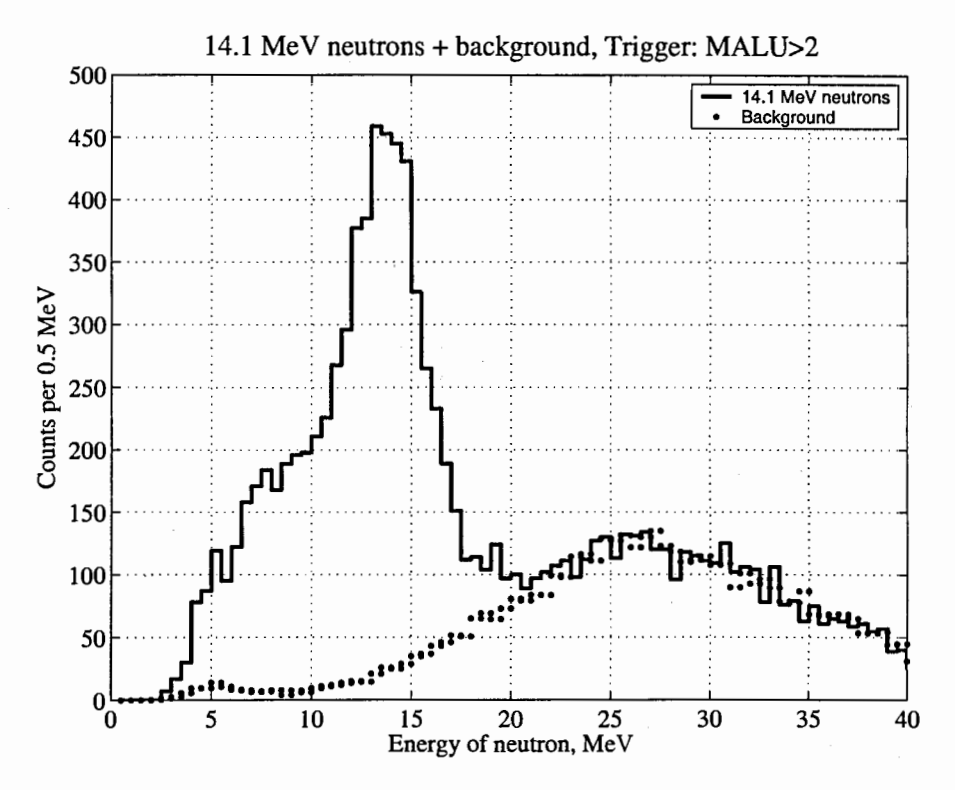


Figure 6: 14.1 MeV neutrons energy distribution on cosmic muons background

Clear distribution of cosmic muon background was obtained at the measurement with same conditions, but without neutron irradiation of the detector. It is shown in Figure 6 by the bold dots.

The pulse height resolution looks rather poor (FWHM  $\simeq$ 30%), but definitely it can be greatly improved. The effective neutron threshold is 3 MeV, which corresponds to our estimations for these conditions.

### 4 Conclusions

The first test of the pilot version of the segmented fast neutron spectrometer has demonstrated that it operates in accordance with expectations. Its response to neutrons over a broad energy range shows no unexpected behavior. The response function of the detector on 14.1 MeV neutrons from D-T fusion is obtained and is presented at first time. The measured pulse height resolution is about 30%. One of the reasons for the relatively poor resolution is the absence of <sup>6</sup>Li as an effective capture material.

The effective neutron threshold is about 3 MeV. There are several things which determine the threshold. First, it is obviously an apparatus threshold of single section. Right now it is 20 mV and it corresponds to 0.8-1.0 MeV of recoil energy. It can be easily decreased twice but it requires some improvement in discriminator module. Now it looks to be not so stable and at low level signals with noise it may produce several consequent gates. Second, an improved PMT and HV-cell combination as well as an improved segment design will allow one to make the sections much more uniform. It will improve the resolution of the step (and pulse height resolution of the detector response function also) and as a result will allow one to put the middle of step in 4/5 of QDC full scale (instead of 3/4 now). Obviously it will decrease threshold. Another reason here is the noise of PMT — now it looks not so good. Last, one should remember that the threshold of single section is not direct threshold just because of that a normal MALU threshold is now 3 or more hits. It increases the effective threshold according to average lose of 1/2 of intitial neutron energy in each collision up to 3-4 MeV that we see at real spectrum. Thus, introducing 6Li or other capturer in the detector we may trigger with 2 or even 1 hits, drastically decreasing the effective threshold.

# Acknowledgments

This research was made possible by Award No. RP2-2277 of the U.S. Civilian Research & Development Foundation for the Independent States of the Former Soviet Union (CRDF).

# References

- Kamykowski et al, NIM A 317 (1992) 559.
- [2] Aoyama et al, NIM A 333 (1993) 492.
- [3] Abdurashitov et al, NIM A 476 (2002) 318.
- [4] Mailto: astakhov@sunhe.jinr.ru
- [5] Scintillators for the physical sciences. Brochure No. 126P, Nuclear Enterprises Inc., Feb. 1980.

# THE INVESTIGATION OF THE RESONANCE STRUCTURE OF THE NEUTRON CROSS-SECTIONS WITH THE TIME-OF-FLIGHT SPECTROMETERS AT THE MOSCOW MESON FACTORY

Yu.V. Grigoriev, O.N. Pavlova, B.V. Zhuravlev Institute of Physics and Power Engineering, Obninsk, Russia

A.A. Alekseev, A.I. Berlev, E.A. Koptelov, D.V. Khlustin Institute for Nuclear Research RAN, Troitsk, Russia

Zh.V. Mezentseva Joint Institute for Nuclear Research, Dubna, Russia

Abstract In 2007-2008 measurements of the time-of-flight spectra of different multiplicities coincidences of the gamma-rays have been carried out for  $^{55}$ Mn,  $^{93}$ Nb, Mo, In,  $^{148}$ Sm,  $^{165}$ Ho,  $^{181}$ Ta, W and  $^{238}$ U. For these measurements the 8-section liquid (n,  $\gamma$ )-detector and  $^{3}$ He neutron detector have been installed at 50 m flight path of the REPS setup of the Moscow Meson Factory (MMF). They have revealed 5 new resonances in the neutron radioactive capture cross-section of W at the energies of 4 eV and 18 eV and of  $^{55}$ Mn at the energies of 228 eV, 359.4 eV and 375.2 eV.

On the basis of the 12 m proton ion guide and of the Rb target of the isotope complex of the MMF an original time-of-flight neutron spectrometer has been designed placed at the 18 m flight path. It allows to investigate the neutron cross-sections resonance structure and some fundamental neutron characteristics in the broad energy range.

To investigate the resonance structure of the neutron cross-sections the time-of-flight spectra measurements have been carried out at 50 m flight path of the REPS setup shown in Fig 1. [1] and at 18 m flight path of the radiochemical complex (RCC) of the MMF (see Fig. 2)

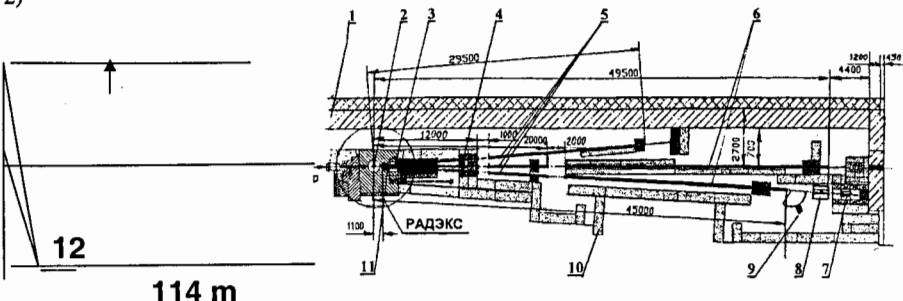


Fig.1. A schematic view of the time-of-flight neutron spectrometer: 1- brick wall, 2- tungsten target with a water moderator, 3- concrete biological shielding of the neutron source RADEKS, 4 - cast-iron shielding form neutrons and gamma-rays, 5 - neutron guide in the form of steel vacuum tube, 7- <sup>3</sup>He neutron detector, 8 - multisectional liquid (n,γ) - detector, 9 - multiangular setup to investigate an neutron scattering, 10 - concrete shielding of the neutron spectrometer, 11- gate of a neutron beam, 12 - <sup>3</sup>He counter (SNM-18)

The measurements were performed by means of the 8-section liquid  $(n, \gamma)$ -detector and neutron detectors with <sup>3</sup>He counters. The metal targets made from a natural tungsten with a thickness of 7 cm were used as the pulse neutron sources (at the RADEKS setup) [2]. At the RCC the metal targets made from a natural Rb with a thickness of 6 cm were in use with the same purpose [3]. Targets were illuminated by a proton beam with an energy of 209 MeV at the RADEKS setup and with an energy of 160 MeV at the RCC. The operated parameters

were the following: the average pulse current I = 5 - 10 mA and an proton bursts repetition frequency f = 1-50 Hz with a duration of  $\Delta t = 1-200$   $\mu s$ .

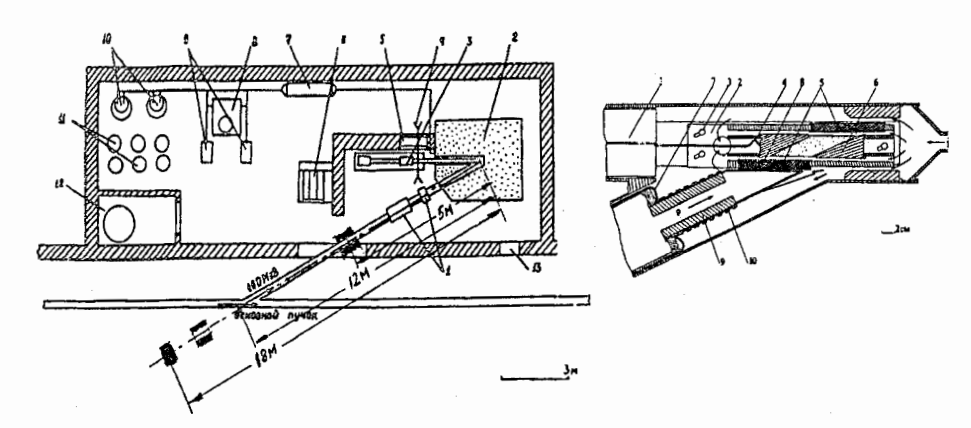


Fig. 2. A schematic view of the neutron setup with a Rb target: 1 – proton ion guide with equipments for a beam control, 2 – cast-iron cube shielding for a target placement, 3- equipment for a target movement, 4..12 – functional elements of the RCC, 13 – entrance into a target hall. A detailed view of the target construction is shown on the right.

The radiator-samples and filter-samples were served metal and oxide disks made from  $^{55}\text{Mn}, ^{93}\text{Nb}, \text{Mo}, \text{In}, ^{148}\text{Sm}, ^{165}\text{Ho}, ^{181}\text{Ta}, \text{W} \text{ and } ^{238}\text{U}$  with a diameter from 50 mm to 80 mm of different thickness. An intensity level of a neutron beam at the REPS setup was controlled by a  $^3\text{He}$  counter (SNM-18) installed at 114 m flight path before a tungsten target of the RADEKS source. At the RCC a  $^{10}\text{B}$  counter (SNM-13) was in use before a Rb target. The data acquisition was realized by means of measurement modules on the basis of PC with two analog software at 1  $\mu s$  time channel width (author T.G. Petukhova FLNP JINR) and 0.01  $\mu s$  (development of INR Troitsk and JINR, [4]). The main feature of these measurements is the usage of ion guide as neutron guide. This allowed to perform new experiments requiring more time measurement and higher energy resolution.

In 2007-2008 measurements of the time-of-flight spectra of different multiplicities coincidences of the gamma-rays have been carried out at a radioactive neutron capture by nuclei of 55Mn, 93Nb, Mo, In, 148Sm, 165Ho, 181Ta, W and 238U. For these measurements the 8section liquid (n, γ)-detector with o total volume of 40 l and <sup>3</sup>He neutron detector have been installed at 50 m flight path of the REPS setup of the Moscow Meson Factory (MMF). A duration of analog pulses was 35 ns and 1 µs from the (n,  $\gamma$ )-detector and from the <sup>3</sup>He neutron counter respectively. The registration efficiency of the (n, γ)-detector was determined using  $\gamma$ -lines of  $^{60}$ Co source and was equal to 30 % at the energy resolution of 30 %. The registration efficiency of thermal neutrons of <sup>3</sup>He neutron counter was approximately 95 %. The experimental time-of-flight spectra are shown in Fig. 3, 4, 5, 6, and 7 (x-axis corresponds to the energy). The background components in time-of-flight spectra are the result of the gamma-rays and neutrons scattered in the experimental hall. These components were measured by resonance filters which have so-called deep "black resonances" like Al (35 keV), Mn (2.4 keV and 336 eV) and W(20 eV). It should be stressed that protons falling to the target cause neutrons which have a broad energy spectrum with a 15 % fraction of fast neutrons in the energy range from 15 MeV to 209 MeV after moderation. These neutrons fly from the target mainly forward where detectors of the REPS setup are located and result in background increase and in overload of spectrometric electronic equipment. At 18 m and 114

m flight paths, where proton ion guides were used as neutron guides, the fraction of background neutrons less because these neutrons fly towards the proton beam.

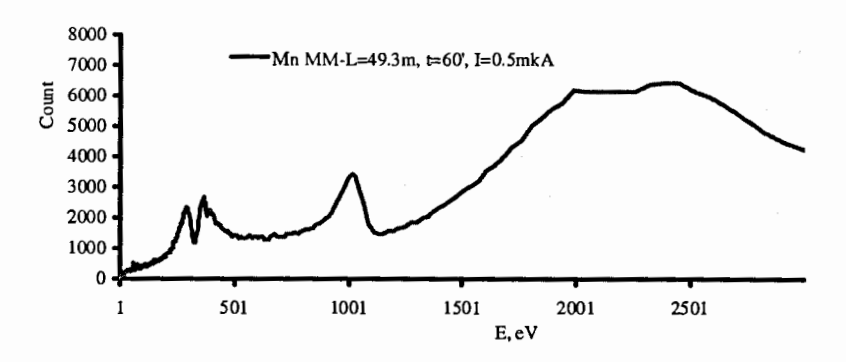


Fig. 3 Time-of-flight spectrum of the neutron radioactive capture by  $^{55}$ Mn sample (d=2 mm), measured by the liquid (n, $\gamma$ )-detector at 49.3 m flight path. Parameters of proton beam are  $E_n$ =209 MeV,  $I_n$ =5 mA, f=50 Hz,  $\Delta t$ =1  $\mu$ s,  $dt_{ch}$ =1  $\mu$ s

As one can see from the Fig.3, a more complicated resonance structure is observed in the radioactive capture cross-section of a natural Mn for the first time. So instead of one resonance 3 resonances are observed at the energy of 336 eV with  $E_0$ =228 eV, 359.4 eV and 375.2 eV. Also two resonances instead one are observed around 2375 eV. Moreover, the resonance structure with several weak resonances exists in the energy region from 20 eV to 80 eV. In the previous measurements at the REPS setup new resonances of a natural W have been observed at the energy of 7 eV and 18 eV. These results are very interesting in respect to the nucleus theory and its practical applications.

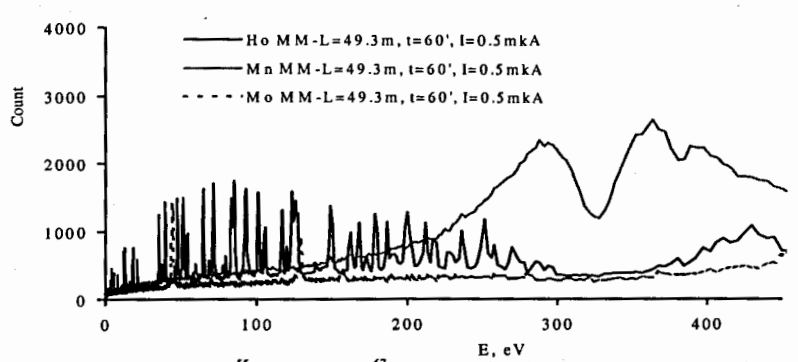


Fig. 4 Time-of-flight spectra of  $^{55}$ Mn (d=2 mm),  $^{67}$ Ho (d=5 mm) and Mo (d=0.4 mm) transmissions, measured by the liquid (n, $\gamma$ )-detector at 49.3 m flight path. Parameters of proton beam are E<sub>p</sub>=209 MeV, I<sub>p</sub>=5 mA, f=50 Hz,  $\Delta$ t=1.5  $\mu$ s, dt<sub>ch</sub>=1  $\mu$ s.

To obtain resonance parameters of new mentioned resonances of Mn one needs to repeat such measurements with better statistical precision and with higher energy resolution.

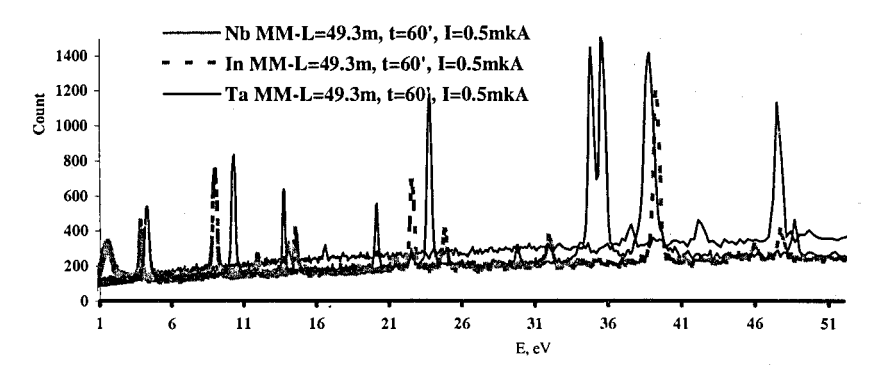


Fig. 5. Time-of-flight spectra of  $^{93}$ Nb (d=2 mm),In(d=0.5mm),  $^{181}$ Ta(d=0.2 mm) transmissions, measured by the liquid (n, $\gamma$ )-detector at 49.3 m flight path. Parameters of proton beam are E<sub>p</sub>=209 MeV, I<sub>p</sub>=5 mA, f=50 Hz,  $\Delta t$ =1.5  $\mu$ s, dt<sub>ch</sub>=1  $\mu$ s.

It should be mentioned that new resonances for other materials except Mn and W were not observed in the energy range from 1 eV to 3 keV.

To determine fluxes from thermal neutrons time-of-flight spectra measurements were carried out at 20 m, 50 m and 114 m flight paths of the neutron source RADEKS and at 18 m flight path of the isotope complex by means of  $^3$ He counter at a neutron burst duration of  $\Delta t = 65 \,\mu s$  and 200  $\mu s$  and at a frequency repetition of  $f = 1 \,Hz$  and 50 Hz.

In Fig. 6-8 time-of-flight spectra, measured at 50 m and 114 m flight paths of the neutron source RADEKS and at 18 m flight path of the isotope complex, are presented.

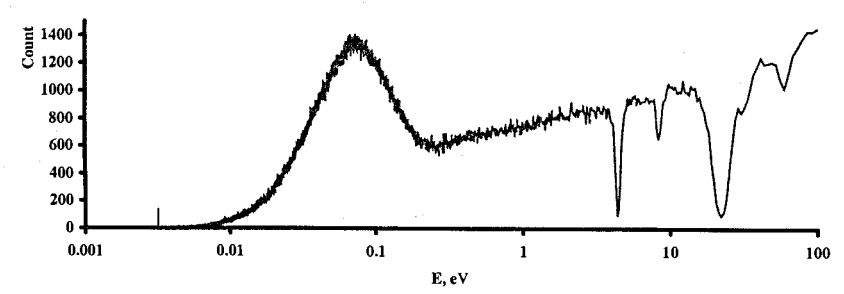


Fig. 6 Time-of-flight spectra of W (d=0.4 mm) transmissions, measured by the  $^3$ He counter at 51 m flight path of the REPS setup. Parameters of proton beam are  $E_p$ =209 MeV,  $I_p$ =5 mA, f=1 Hz,  $\Delta t$ =65  $\mu$ s,  $dt_{ch}$ =16  $\mu$ s,  $t_{mes}$  = 60 min

As one can see from the Fig. 6 a maximum peak of thermal neutrons is situated at the energy of 0.062 eV and a spectrum of thermal neutrons is located in the energy range from 0.0032 to 0.25 eV. It is important that a thin W sample installed in the neutron beam practically did not decrease the neutron beam intensity. It allowed to estimate the background components in this energy region using W resonances with a precision of 3 %.

Since the registration efficiency of thermal neutrons by <sup>3</sup>He counter was approximately 95 % and an illuminated detector surface came to 30 cm<sup>2</sup> that an averaged flux of thermal

neutrons will be  $\Phi_{max} = 3000 \text{ n/cm}^2$  at 51 m flight path of the REPS setup at the proton beam parameters  $E_p = 209 \text{ MeV}$ ,  $I_p = 10 \text{ mA}$ , f = 50 Hz,  $\Delta t = 200 \mu s$ . This flux corresponds approximately to the thermal neutrons flux at the IBR-30 reactor and about 100 times less than at the IBR-2 reactor at JINR, Dubna [5].

The test measurements were performed using the <sup>3</sup>He counter at 18 m flight path of the isotope complex with the Rb target (see Fig.2). The neutron counter was placed by a flank to the neutron flux to achieve the registration efficiency of thermal neutrons of 94 % at a flank surface of 7 cm<sup>2</sup>. Because of copper plates with a thickness of 3 cm located behind the ion guide in the neutron beam the neutron flux decreased by an order of magnitude 10. In this case the thermal neutrons flux was 600 n/cm<sup>2</sup> s. That is why the neutron detector should be well shielded from neutrons and gamma-rays at 27-degree turn of the ion guide and precisely adjusted along the neutron beam rigidly collimated by the ion guide.

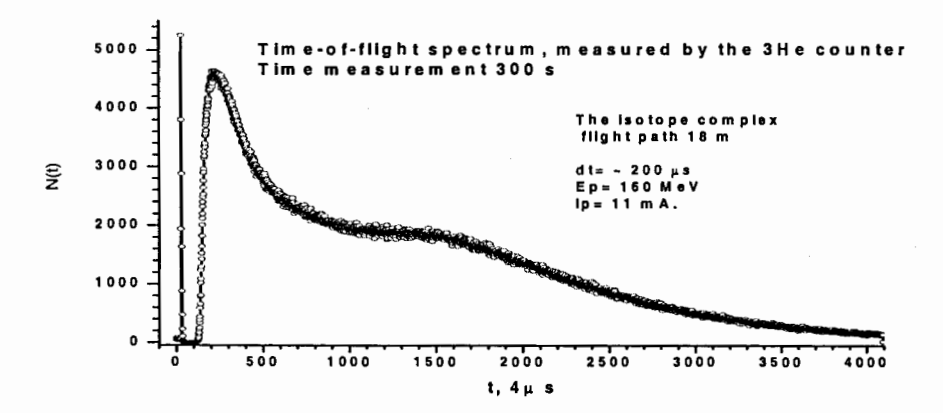


Fig. 7 Time-of-flight spectrum of an opened beam, measured by the  $^3$ He counter at 18 m flight path of the isotope complex at  $E_p=160$  MeV,  $I_p=11$  mA, f=50 Hz,  $\Delta t=200$   $\mu s$ ,  $dt_{ch}=16$   $\mu s$ ,  $t_{mes}=5$  min.

If we suppose that thermal neutrons are emitted in  $^3$ He counter direction installed at a distance of 18 m from the target surface of 3 cm², than the thermal neutrons flux at the source surface should be approximately  $10^{11}$  n/cm²s. Evidently the thermal neutrons flux will be  $3*10^4$  n/sm²s at a distance of 3 m from the neutron source where the ring monitor detector was placed.

It would be possible to carry out investigations of the (n,n) and (n,p) scattering by the method of incoming beams and overtaking neutrons [6] using of W and U targets to increase the neutron beam intensity.

#### Conclusion

During the last two years 2007-2008 several experiments on the resonance structure investigation of neutron cross-sections at time-of-flight spectrometers of the MMF were carried out. Time-of-flight spectra of Mn, Cr, Nb, Mo, In, Ta, W and U metal samples were measured at the REPS setup using the 8-section liquid  $(n,\gamma)$ -detector and  $^3$ He counter. The averaged group total transmissions and cross-sections were extracted from the experimental spectra in the energy range from 1 eV to 10 keV.

Two new resonances in the radioactive capture for natural W were revealed at the energies of 4 eV and 17 eV and three new resonances for <sup>55</sup>Mn at the energies of 228 eV, 359.4 eV and 375.2 eV.

The new time-of-flight neutron spectrometer was constructed on the basis of 12 m ion guide of the radioisotope complex of the MMF. Test measurements were carried out to determine its characteristics. Similar test measurements were also carried out at the 114 m ion guide before the neutron source RADEKS. These original spectrometers allow to increase time measurement of nuclear-physical values in the thermal and resonance neutron energy region.

Authors thank the director of INR RAS academician V.A. Matveev, vice-director L.V. Kravchuk for their support and also leader of linear proton accelerator of the MMF A.V. Feshchenko, V.L. Serov, M.I. Grachev for their help. Authors also express thanks to A.A. Bergman, B.I. Fursov, V.M. Kochanyuk and other colleagues for help and assistance.

#### Literature

- Berlev A.I., Grigoriev Yu.V., The REPS setup for the investigation of the neutron cross Sections structure and fundamental characteristics of neutron: Preprint INR RAS №1183/2007. – Moscow: INR RAS, 2007.
- 2. Benetsky B.A., Vahetov F.Z., Grachev M.I. e.a., Program of experimental researches on device RADEX: Preprint INR RAS № 1058/2001. Moskow: INR RAS, 2001.
- 3. Juikov B.L., Kohanuk V.M., Gabrielants Ju.G. etc., Device for production of radio nuclei on 160 Mev beam removal of Moskow Meson Factory // Radiochemistry. 1994. V.36. Release 6. P. 499-504.
- 4. Berlev A.I., System for registration, gathering and accumulation of experimental data from nuclear physical installations by time of flight method: Preprint INR RAS № 1189/2007, Moscow: INR RAS, 2007.
- Frank I.M., Development and scientific researches application of pulsed reactor IBR // 94AA. – V.2. Release 4, P. 805 – 860.
- 6. Grigoriev Yu.V., Method for determination cross-sections of neutron neutron interaction: Pat. USSR № 549023. Moscow, 1976.

# Production Cross-sections for the Residual Radionuclides from the $^{nat}Pd(p,x)$ and $^{nat}Cd(p,x)$ Processes up to 40 MeV

Mayeen U. KHANDAKER, Kwangsoo KIM, Manwoo LEE, Kyungsook KIM, and Guinyun KIM \*

Department of Physics, Kyungpook National University, Daegu 702-701, Korea \*) Contact information: Tel. +82(53)950-5320, E-mail: gnkim@knu.ac.kr

#### Abstract

Independent and cumulative production cross-sections of the  $^{nat}Cd(p,x)^{109g,111g,114m}In$  and  $^{nat}Pd(p,x)^{105}Rh$  nuclear processes have been reported from 40 MeV down to their threshold energy by using a stacked-foil activation technique combined with high purity germanium  $\gamma$ -ray spectrometry. Measured data were compared with the available literature data and the theoretical data from the model calculations by the TALYS and ALICE-IPPE codes. Integral yields were also deduced for all the measured radionuclides. The measured cross-sections have a significance for various practical applications; nuclear medicine, nuclear technology, radioactive waste handling etc.

Keywords: Indium and Rhodium radionuclides, natural cadmium and palladium targets; 42
MeV proton; stacked-foil technique; excitation functions; medical applications.

#### 1. Introduction

The study of light ion-induced nuclear reactions leading to the production of various radionuclides is finding increasing importance for medical and technological applications. The versatile ion-accelerating machine cyclotrons are employed to produce these radionuclides. The physical basis of a radionuclide production could be optimized by using data on nuclear cross-sections. Therefore, excitation functions and/or nuclear cross-sections have great significance in the production and the quality control of desired radionuclides for various practical applications, especially in nuclear medicine [1].

Cadmium (Cd) and Palladium (Pd) are ideal target materials for the production of medically important radionuclides, such as 109,111,114mIn, and 105Rh, respectively. The radionuclide <sup>11</sup>In is widely used in diagnostic nuclear medicine [2]. The radionuclide <sup>109</sup>In is used for diagnostic purposes using PET. It is interesting to note that, 114mIn and its daughter radionuclide 114 In are usually regarded as undesirable long-lived impurities in 111 In -labeled radiopharmaceuticals for a diagnostic use. However, there is increasing interest in studying 114mIn to determine the long-term stability and bio kinetics of indium-labeled pharmaceuticals as well as for radionuclide therapy at a low-energy [3-4]. On the other hand, the 105Rh radionuclide is a promising candidate for targeted radiotherapy [5-6]. The emission of beta  $(E_{R}$  = 570 keV 70%, 250 keV 30%) and  $\gamma$ -ray (318.9 keV 19%) with a moderate energy, and medium half-life (1.44 days) make this radionuclide attractive for the dosimetry and the pharmacokinetic perspective [6]. Currently, a large amount and a high specific activity <sup>105</sup>Rh radionuclide is produced by a nuclear reactor using an enriched 104Ru target through the indirect  $^{104}$ Ru $(n,\gamma)^{105}$ Ru $\rightarrow$   $^{105}$ Rh process. But, an unsolved problem with the current production methods is the high level of Ru impurity associated with the radiochemical separation method used [7]. It is also possible to obtain very large quantities of <sup>105</sup>Rh as a fission product, if required [8]. But, the radiochemical work involved in the separation of fission products is rather cumbersome. However, alternatively this <sup>105</sup>Rh radionuclide can be produced in a no carrier added (NCA) form by a using medium energy cyclotron through the proton irradiations on a palladium target.

A general survey of the literature [1, 9-12] revealed that only a few earlier investigations have been carried out for the production of medically and technologically important radionuclides from a proton bombardment on natural and/or enriched Cd (or Pd) targets but considerable discrepancies are found among them. Therefore, new experimental data is required to reduce these discrepancies and also to prepare a recommended database for an optimal production of important radionuclides. Hence, we have measured the production cross-sections of residual radionuclides from the natCd(p,x) 109g,111g,114m and natPd(p,x) 105Rh nuclear processes up to 40 MeV by using a stacked-foil activation technique and using an Azimuthally Field Varying (AVF) MC-50 cyclotron at the Korea Institute of Radiological and Medical Sciences (KIRAMS).

#### 2. Experimental procedure

The irradiation technique, the activity determination and the data evaluation procedures were similar to our previous works [13]. Some important features relevant to this work are discussed as follows. A well established stacked-foil activation technique combined with a high-resolution γ-ray spectrometer was employed to determine the excitation functions of the  $^{\text{nat}}$ Cd(p,x) $^{109g,111g,114m}$ In and  $^{\text{nat}}$ Pd(p,x) $^{105}$ Rh nuclear processes. High purity Cd ((>99.98%, 50 μm thick) and Pd (>99.99%, 50 μm thick) foils with natural isotopic composition was used as the targets for the irradiation. Several foils of copper (100 µm thick) and aluminum (100 µm thick) were also assembled in the stack to monitor the beam intensity and to degrade the beam energy, respectively. The stacked-foils were irradiated for 60 minutes by a proton energy of 42.1 MeV with a beam current of about 100 nA from an external beam line of the MC-50 cyclotron at the KIRAMS. The spectrum analysis was done using the Gamma Vision 5.0 (EG&G Ortec) program. The photo peak efficiency curve of the gamma spectrometer was calibrated with a set of standard point sources. The proton beam intensity was determined by using the monitoring reaction of  $^{\text{nat}}\text{Cu}(p,x)^{62}\text{Zn}$  with known cross sections from the ref. [14]. The proton energy degradation along the stacked foils was calculated by using the computer program SRIM-2003 [15]. The activation cross-sections for the <sup>nat</sup>Cd(p,x) and <sup>nat</sup>Pd(p,x) processes were determined using a well-known activation formula [13]. The decay data of the radioactive products were taken from the NUDAT database [16], and presented in Table 1.

The uncertainty of the proton energy for each point were estimated from the uncertainty of the incident beam energy, the target thickness, and the beam straggling. On the other hand, the uncertainty of the cross-sections were estimated using the uncertainty propagation formula by considering the following uncertainties; statistical uncertainty of the  $\gamma$ -ray counting (~10 %), uncertainty in the monitor flux (~7 %), uncertainty in the detector efficiency (~4 %), and so on. The overall uncertainties of the measured cross-sections were in the range of 8-15 %.

#### 3. Theoretical calculations

The excitation functions of the  $^{\rm nat}$ Cd(p,x) $^{\rm 109g,111g,114m}$ In and  $^{\rm nat}$ Pd(p,x) $^{\rm 105}$ Rh nuclear processes at proton energies up to 100 MeV were theoretically calculated using the model calculations by the TALYS [17] and ALICE-IPPE [18] codes. In the case of the TALYS code, the present results were mostly evaluated using the default values of various models, but the very important inputs like the optical model parameters, discrete energy levels and level

densities of the nuclides involved in the calculations have been taken care of in a proper way during the calculations. Furthermore, the data of the ALICE-IPPE code were taken from the IAEA (www-nds.iaea.org), where it is compiled as the MENDL-2P database.

Table 1 Decay data for the  $^{nat}Cd(p,x)$  and  $^{nat}Pd(p,x)$  nuclear processes

Nuclei	Half-life	Decay	Eγ	Ι <sub>γ</sub>	Contributing	Q-value	Threshold
	T <sub>1/2</sub>	mode (%)	(keV)	(%)	reactions	(MeV)	(MeV)
109gIn	4.2 h	EC	203.5	73.5	110Cd(p, 2n)	-12.718	12.8347
		(100)	426.25	4.12	$^{111}Cd(p, 3n)$	-19.693	19.8729
			623.7	5.5	$^{112}Cd(p, 4n)$	-29.092	29.3542
			1149.1	4.3	$^{113}Cd(p, 5n)$	-35.632	35.9505
IIIgIn	2.81	EC	171.28	90	$^{111}Cd(p, n)$	-1.6477	1.66276
	d	(100)	245.39	94	$^{112}Cd(p, 2n)$	-11.046	11.1454
					$^{113}Cd(p, 3n)$	-17.586	17.7432
					114Cd(p, 4n)	-26.629	26.8646
114mIn	49.51	IT+EC	190.29	14.74	114Cd(p, n)	-2.2342	2.25401
	d	(100)	558.46		$^{110}Cd(p, 3n)$	-17.075	17.2238
<sup>105</sup> Rh	1.47	β-	318.9	19.1	$^{106}Pd(p, 2p)$	-9.3470	9.4360
	ď	(100)			$^{108}$ Pd(p, $\alpha$ )	3.18925	0.0
					<sup>110</sup> Pd(p, 2nα)	-11.781	11.889

#### 4. Results and discussion

#### 4.1 The <sup>nat</sup> $Cd(p,x)^{109g}$ In processes

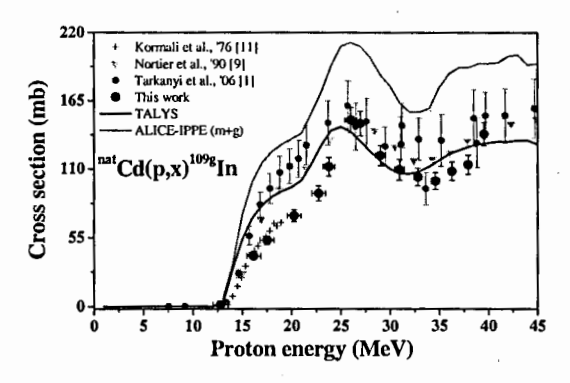


Fig. 1 Excitation function for the natCd(p,x)109gIn processes

<sup>109</sup>In has one long-lived ground state radionuclide <sup>109</sup>gIn ( $T_{1/2}$ = 4.20 h), and two short-lived excited state radioisomers <sup>109m</sup>In ( $T_{1/2}$ = 1.34 m) and <sup>109n</sup>In ( $T_{1/2}$ = 0.21 s). Both of the isomers completely decay to their ground state <sup>109</sup>gIn through a 100% IT decay process. As the γ-ray counting process was started after a cooling time of about 1.5 h, the measured production cross-sections of the <sup>109</sup>gIn radionuclide are considered as cumulative ones. The measured excitation function of the <sup>109</sup>gIn is shown in Fig. 1 in comparison with the available literature data and the theoretical data by the model code calculations. The first maximum obtained at around 25 MeV signifies the direct contribution of the (p, 2n) and (p, 3n) reactions. The measured data revealed a very good agreement with the data reported by Kormali et al.

obtained with the Nortier et al. [9], Tarkanyi et al. [1], and also with the theoretical data from the TALYS code for the whole investigated energy region. The ALICE-IPPE code predicted data with a similar shape for the measured excitation function, but overestimated the absolute values by about 20%.

# 4.2 The nat Cd(p,x)111g In processes

<sup>111</sup>In has a long-lived ground state radionuclide <sup>111g</sup>In (T<sub>1/2</sub>=2.80 d) and a short-lived isomer <sup>111m</sup>In (T<sub>1/2</sub>=7.70 m), whereas the isomeric state radionuclide completely decays to its ground state by an IT process. Therefore, the measured cross-sections of the <sup>111g</sup>In radionuclide is a cumulative one. The measured excitation function of <sup>111g</sup>In is shown in Fig. 2 together with the available literature values and the data from the model calculations. The formation of the <sup>111g</sup>In radionuclide is also contributed to by the direct reactions collected in Table 1. The contribution of the (p,n), (p,2n) and (p,3n) reactions formed a sharp maximum at around 24 MeV, whereas the second maximum at around 40 MeV is from the contribution of the <sup>114</sup>Cd(p,4n) reaction. The present results are in good agreement with the measured data reported by Tarkanyi et al. [1], Nortier et al. [9], and the deduced normalized values from the IAEA recommended data [19]. However, the data reported by Zaitseva et al. [10] is different from any other measurements. The data calculated by the TALYS and ALICE-IPPE codes revealed a good agreement for both the shape and magnitude with the measured data.

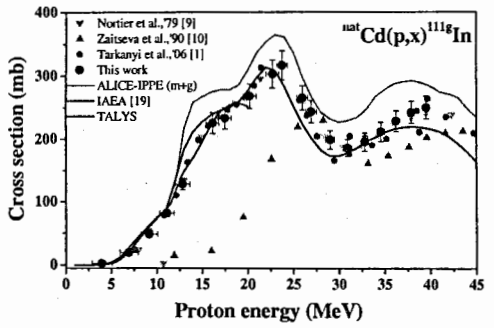


Fig. 2 Excitation function for the natCd(p,x)111gIn processes

# 4.3 The nat Cd(p,x)114m In processes

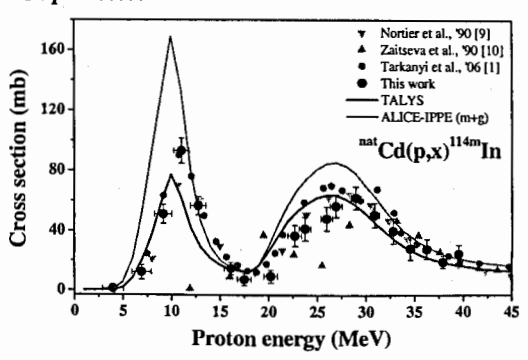


Fig. 3 Excitation function for the natCd(p,x)114mIn processes

Except for the short-lived ground state radionuclide  $^{114g}$ In ( $T_{1/2}$ = 1.20 m),  $^{114}$ In has two isomeric states  $^{114m}$ In ( $T_{1/2}$ = 49.51 d) and  $^{114n}$ In ( $T_{1/2}$ = 0.0431 s). Under the present experimental conditions, we could only measure the  $^{114m}$ In radionuclide. The measured data is shown in Fig. 3 together with the available literature data and the theoretical data from the model code calculations. The two maximums at around 12 MeV and 29 MeV are from the independent contributions of the  $^{114}$ Cd(p, n) and  $^{116}$ Cd(p, 3n) reactions, respectively. We found a good overall agreement with the Tarkanyi et al. [1] and Nortier et al. [9] reported data but the data reported by Zaitseva et al. [10] revealed a discrepancy due to a significant energy shift. The TALYS code reproduced a nicely fitted excitation function with the measured ones, whereas the ALICE-IPPE code produced a similar shape but overestimated the magnitudes.

# 4.4 The nat Pd(p,x)105Rh processes

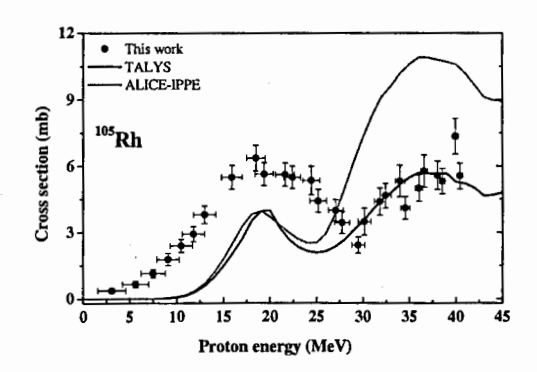


Fig. 4 Excitation function for the <sup>nat</sup>Pd(p,x)<sup>105</sup>Rh processes

The long-lived radionuclide  $^{105}Rh$  ( $T_{1/2}{=}1.47$  d) has a short-lived meta-stable state  $^{105m}Rh$  ( $T_{1/2}{=}40.0$  s), which completely decays to its ground state by an IT process before starting our measurement. Therefore, the formation of the  $^{105}Rh$  radionuclide follows a cumulative process. The radionuclide  $^{105}Rh$  was identified using its strong and independent gamma line,  $E_{\gamma}{=}318.9$  keV ( $I_{\gamma}{=}19.1\%$ ). The direct contributing channels for the formation of this radionuclide are the  $^{106}Pd(p,\ 2p)$ , the  $^{108}Pd(p,\ \alpha)$  and the  $^{110}Pd(p,\ 2n\alpha)$  reactions. We couldn't compare the present results with any previous measurements due to the lack of available literature data. The measured excitation function of this radionuclide formation is shown in Fig. 4 and compared with the value predicted from the TALYS and the ALICE-IPPE codes, and we found a partial agreement with the TALYS prediction above 30 MeV whereas ALICE-IPPE overestimates it in this energy region.

#### 5. Integral yield

The integral yields were deduced using the measured cross-sections of the radionuclides over the energy range from their threshold to 40 MeV by taking into account that the total energy is absorbed in the targets. The deduced yields are expressed as  $MBq-\mu A^{-1}$ -h<sup>-1</sup>, and are presented in Fig. 5.

#### 6. Conclusions

Production cross-sections for the natCd(p,x)109g,111g,114mIn and natPd(p,x)105Rh nuclear processes have been reported from 40 MeV down to their threshold energy with an overall uncertainty of about 15%. Standardization and validation of the measured data were done using the available literature data, and the theoretical data from the TALYS and ALICE-IPPE codes. The present measured cross-sections of <sup>111</sup>In from a natural cadmium target could be used for a validation of the IAEA recommended data. But, the production of this radionuclide from a natural cadmium target is not suitable due to a contamination from a simultaneously produced 114mIn radionuclide in our investigated energy range. However, highly enriched 111, <sup>112</sup>Cd targets could be used to obtain a suitable production of the <sup>111</sup>In radionuclide with a minimum impurity level. On the other hand, the deduced thick target yield showed that a low energy (<20 MeV) medical cyclotron and highly enriched <sup>108,110</sup>Pd targets could be used for a profitable production of <sup>105</sup>Rh with a minimum impurity from <sup>101m</sup>Rh, even though under the above conditions the production of a <sup>101m</sup>Rh impurity is not possible, energetically. Above all, the present investigation is the first report on a cyclotron production of a carrier free 105Rh radionuclide as an alternative route to the currently used neutron activation process by a nuclear reactor. In addition, the present experimental results will play an important role in the enrichment of the literature data base for the  $^{nat}Cd(p,x)^{109g,111g,114m}In$  and  $^{nat}Pd(p,x)^{105}Rh$ nuclear processes leading to various applications.

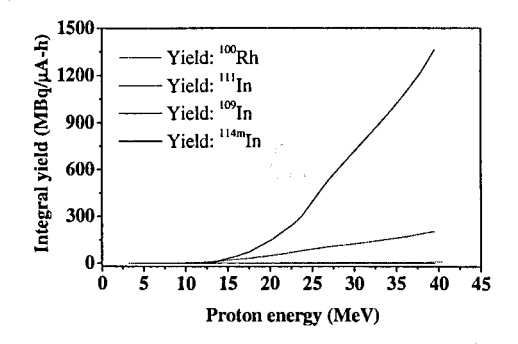


Fig. 5 Integral yields for the <sup>100</sup>Rh and <sup>109g,111g,114m</sup>In radionuclides

### Acknowledgments

This work was partly supported by the Korea Science and Engineering Foundation (KOSEF) through a grant provided by the Korean Ministry of Education, Science and Technology (MEST) in 2008 (Project No. 08M040001110), and by the Science Research Center project through the Center for High Energy Physics, Kyungpook National University.

#### References

- [1] F. Tarkanyi et al., Nucl. Instr. and Meth., B 245, 379 (2006).
- [2] M.L. Thakur, A.D. Nunn, Int. J. Appl. Radiat. Isot., 23, 139 (1972).
- [3] W.J. Nieckarz, A.A. Caretto, Phys. Rev., 178(4), 1887 (1969).
- [4] J. Zweit, Phys. Med. Biol., 41, 1905 (1996).
- [5] R.C. Brooks et al., Nucl. Med. Biol., 26, 421 (1999).

- [6] S. M. Qaim, Radiat. Phys. and Chem., 71, 917 (2004).
- [7] D. E. Troutner, Int. J. Radiat. Appl. Inst., Part B. Nucl. Med. Biol., 14, 171 (1987).
- [8] F. Ta'rka'nyi et al., Radiochim. Acta, 93, 1 (2005).
- [9] F.M. Nortier et al., Appl. Radiat. Isot., 41, 1201 (1990).
- [10] N.G. Zaitseva et al., Appl. Radiat. Isot., 41, 177 (1990).
- [11] S.M. Kormali et al., J. Radioanal. Chem., 31, 437 (1976).
- [12] F. Ditrói et al., J. Radioanal. Nucl. Chem., 272(2), 231 (2007).
- [13] M.U. Khandaker et al., Nucl. Instr. and Meth. B, 262, 171 (2007).
- [14] F. Tarkanyi et al., IAEA-TECDOC-1211, Available from <a href="http://www-nds.iaea.org/medical/">http://www-nds.iaea.org/medical/</a>>.
- [15] J.F. Ziegler et al., SRIM 2003 code, Available from <a href="http://www.srim.org/">http://www.srim.org/</a>>.
- [16] NUDAT data base, Available from <a href="http://www.nndc.bnl.gov/nudat2/">http://www.nndc.bnl.gov/nudat2/</a>
- [17] A.J. Koning et al., TALYS: Comprehensive nuclear reaction modeling, in *Proc. Int. Conf. Nucl. Data for Sci. and Tech.* ND2004, Santa Fe, USA, AIP vol. 769, p.1154, 2005.
- [18] A.I. Dityuk et al., New Advanced Version of Computer Code ALICE-IPPE, INDC (CCP) 410, IAEA, Vienna, 1998.: MENDL-2P, <a href="http://www-nds.iaea.org/nucmed.html">http://www-nds.iaea.org/nucmed.html</a>.
- [19] S. Takacs et al., Nucl. Instr. and Meth., B 240, 790 (2005).

# Measurement of excitation functions of proton induced reactions on <sup>nat</sup>Mo, <sup>nat</sup>W, and <sup>nat</sup>Zn up to 40 MeV

G. N. Kim at, M. U. Khandaker K. Kim, K. S. Kim, M.S. Uddin b, M.W. Lee

#### Abstract

Excitation functions for the production of various radioisotopes from proton bombardment on <sup>nat</sup>Mo, <sup>nat</sup>W, and <sup>nat</sup>Zn were measured using the stacked-foil activation technique for proton energies up to 40 MeV. A new data set has been given for the formation of the investigated radioisotopes. The present results were compared with the earlier reported experimental data and theoretical data taken from the ALICE-IPPE code, and found good agreement with some well measured literature values in the overlapping energy region. The thick target integral yields were also deduced from the measured cross sections. The deduced yield values compared with the directly measured thick target yield values, and found acceptable agreement. The measured cross sections of the investigated radioactive products have much importance in the field of a nuclear medicine, a thin layer activation analysis, and a trace element analysis.

#### 1. Introduction

Radioisotopes with a variety of half-lives (few seconds ~ few years) are widely used in medical, agricultural, and industrial research and applications. The charged particle accelerators, especially the medium energy cyclotrons are used to produce these radioisotopes. In principle, charged particle activation experiments are carried out leading to the production of high specific activity radioisotopes, reduction of impurities, and effective use of start-up materials.

Natural molybdenum (Mo), tungsten (W), and zinc (Zn) can be used as the ideal target materials for the production of medically important radioisotopes  $^{99}\text{Mo}/^{99\text{m}}\text{Tc}$ ,  $^{186}\text{Re}$ , and  $^{67}\text{Ga}$ , respectively. The radionuclide  $^{99\text{m}}\text{Tc}$  from  $^{99}\text{Mo}/^{99\text{m}}\text{Tc}$  generator is used extensively in radio-diagnostics due to its moderate half life, suitable  $\gamma$ -energy, absence of  $\beta$ - activity, and its ability to form various complexes which have specific affinity to different organs of the human system. About 80% of the diagnostic nuclear medicine procedures are performed using  $^{99\text{m}}\text{Tc}$  labeled compounds [1]. The parent radionuclide  $^{99}\text{Mo}$  can be produced in principle in

 <sup>&</sup>lt;sup>a</sup> Department of Physics, Kyungpook National University, Daegu 702-701, Korea.
 <sup>b</sup> Institute of Nuclear Science and Technology, Atomic Energy Research Establishment, Savar, GPO Box No.3787, Dhaka-1000, Bangladesh.

Corresponding author: Tel.: +82-53-950-5320, e-mail: gnkim@knu.ac.kr.

various ways. Currently, the dominant route is neutron fission of natural or isotopically enriched  $^{235}$ U (so-called "fission-moly"), while the activation of natural or isotopically enriched Mo is the second important route. Recent survey has shown that  $^{186}$ Re is an ideal candidate for radioimmunotherapy [2-4] of its moderate  $\beta$ <sup>-</sup> particle energies at 1.07 and 0.933 MeV, low- abundance (9%)  $\gamma$  emission at 137 keV, which allows for in vivo tracking of the radiolabeled biomolecules and estimation of dosimetry calculation. The suitable 3.7-day half-life allows sufficient time for the synthesis and shipment of potential radiopharmaceuticals. On the other hand, the metallic radionuclide  $^{67}$ Ga forms strong metal complex and is of considerable interest in diagnostic nuclear medicine, particularly for tumor localization.

Several investigations [5-15] were carried out for the determination of reaction cross-sections leading to radionuclide production; but large discrepancies are found among these data set. On a practical level, it is very difficult to estimate the causes of discrepancies among the data sets. These inconsistencies severely limit the reliability of data evaluations. However, nowadays only a few groups are engaged with the systematic investigations by using modern experimental techniques and methods. Until now, no recommended data are available for the mentioned radionuclides in the literature. We therefore, investigated the production cross sections of the medically important radionuclides <sup>99m</sup>Tc, <sup>186</sup>Re, and <sup>67</sup>Ga from the proton bombardment of natural Mo, W, and Zn, respectively, by using the MC-50 cyclotron at the Korea Institute of Radiological and Medical Sciences (KIRAMS). The integral yields were also obtained from the respective threshold for the produced radionuclides by using the measured excitation functions as a function of proton energy.

### 2. Experimental Procedure

#### 2.1. Targets and Irradiations

Excitation functions for the proton-induced reactions on natural target elements (Mo, W, Zn) were measured by using the well established stacked foil activation technique. High purity metallic form of molybdenum (>99.99%), tungsten (99.99%), zinc (99.98%), copper (>99.98%) and aluminum (99.999%) foils with natural isotopic compositions were assembled in stacks. Al and Cu foils were used as monitor as well as energy degraders. An Al foil (200 µm thickness) was placed as the front foil of each stack (where the beam energy is well defined) to accurately measure the beam flux.

Special care was taken in preparation of uniform targets with known thickness, determination of proton energy and intensity along the stacks, and also in determination of the activities of the samples. The thickness of Mo, Zn, Cu, and Al foils was 100 µm but that of W was 200 µm. Several and individual stacks of natural Mo, Zn, and W with monitors were assembled and separately irradiated by 42 MeV collimated proton beam of 10 mm diameter from the external beam line of the MC-50 cyclotron at KIRAMS. The beam intensity was kept constant during irradiation. It was necessary to ensure that equal areas of monitor and

target foils intercepted the beam. The irradiation geometry was kept in a position so that the foils get the maximum beam line. To avoid errors in the determination of the beam intensity and energy, excitation functions of the monitor reactions were measured simultaneously with the reactions induced on natural molybdenum.

#### 2.2. Measurement of Radioactivity

After the irradiations and appropriate waiting time the samples were taken off, and the induced gamma activities emitted from the activation foils were measured by using a gamma spectrometer. The gamma spectrometer was an n-type coaxial ORTEC (PopTop, Gmx20) high-purity germanium (HPGe) detector. The HPGe detector was coupled with a 4096 multi-channel analyzer (MCA) with the associated electronics to determine the photo peak area of the gamma-ray spectrum. The spectrum analysis was done using the program Gamma Vision 5.0 (EG&G Ortec). The energy resolution of the detector was 1.90 keV full width at half maximum (FWHM) at the 1332.5-keV peak of <sup>60</sup>Co. The photopeak efficiency curve of the gamma spectrometer was calibrated with a set of standard sources: <sup>109</sup>Cd (88.03 keV), <sup>57</sup>Co (122.06 keV and 136.47 keV), <sup>137</sup>Cs (661.65 keV), <sup>54</sup>Mn (834.85 keV), <sup>22</sup>Na (511.01 keV and 1274.54 keV), <sup>60</sup>Co (1173.24 keV and 1332.50 keV), and <sup>133</sup>Ba (80.99 keV, 276.39 keV, 302.85 keV, 356.02 keV, and 383.82 keV). The measured detection efficiencies were fitted by using the following function:

$$\ln \varepsilon = \sum_{n=0}^{7} a_n \ln E^n, \qquad (1)$$
 where  $\varepsilon$  is the

detection efficiency,  $a_n$  represents the fitting parameters, and E is the energy of the photo peak. The detection efficiencies as a function of the photon energy were measured at 10 cm and 20 cm distances from the end-cap of the detector. Since most of the sources <sup>133</sup>Ba, <sup>60</sup>Co, <sup>57</sup>Co and <sup>22</sup>Na emit more than one gamma ray; there is a certain probability of coincidence losses of cascade gamma rays when the sources are put closer to the detector [16]. For this reason, all samples were counted at distances of 10 cm and 20 cm from the end-cap of the detector to avoid coincidence losses, to assure low dead time (<10%) and point like geometry.

The proton beam intensity was determined from the measured activities induced in aluminum and copper monitor foils at the front position of each stack using the reactions  $^{27}$ Al(p,x) $^{24}$ Na and  $^{nat}$ Cu(p,x) $^{62}$ Zn, respectively. The use of the multiple monitor foils decreases the probability of introducing unknown systematic errors in activity determination. It was considered that the loss of proton flux was very small and very hard to deduce practically. The beam intensity was considered constant to deduce cross sections for each foil in the stack. The loss of proton beam energy for each foil in the stack was calculated by using the computer program SRIM-2003 [17].

The excitation functions for the <sup>99m</sup>Tc, <sup>186</sup>Re, and <sup>67</sup>Ga radionuclides were determined in the proton energy range 2.5~42 MeV by using the well-known activation formula [18].

Most of the decay data regarding induced radioactivity, such as the half-life ( $T_{1/2}$ ), the  $\gamma$ -ray energy ( $E_{\gamma}$ ) and the  $\gamma$ -ray emission probability ( $I_{\gamma}$ ), were taken from the Table of Radioactive Isotopes [19], and are furnished in Table 1. The threshold energies given in Table 1 were taken from the Los Alamos National Laboratory, T-2 Nuclear Information Service on the internet [20]. The standard cross section data for the monitors were taken from internet service [21].

Table 1 Decay data of the produced radioisotopes.

Nuclei	Half-life	Decay	Eγ,	Intensity(I <sub>γ</sub> )	Contributing reactions	Q-value
	T <sub>1/2</sub>	mode	(keV)	(%)		(MeV)
<sup>99</sup> Mo	2.74 d	β	140.511	4.52	100Mo(p, pn)	-8.29
			181.0	6.07	<sup>100</sup> Mo(p, d)	-6.07
			739.5	12.13	$^{100}$ Mo(p, 2p) $^{99}$ Nb $\rightarrow$ $^{99}$ Mo	-11.14
<sup>99т</sup> Тс	6.02 h	IT+	140.5	89.06	<sup>100</sup> Mo(p, 2n)	-7.71
		β			<sup>100</sup> Mo(p, pn) <sup>99</sup> Mo→ <sup>99m</sup> Tc	-8.29
					$^{100}$ Mo(p, d) $^{99}$ Mo $\rightarrow$ $^{99m}$ Tc	-6.06
186Re	3.72 d		137.16	9.42	<sup>186</sup> W(p,n)	-1.36
<sup>67</sup> Ga	3.26 d	EC	184.6	21.2	<sup>67</sup> Zn(p, n)	-1.81
			300.2	16.8	<sup>68</sup> Zn(p, 2n)	-12.16
					<sup>70</sup> Zn(p, 4n)	-28.08
<sup>62</sup> Zn	9.186 h	EC	548.35	15.2	<sup>63</sup> Cu(p, 2n)	-13.27
			596.7	25.7	<sup>65</sup> Cu(p, 4n)	-31.09
<sup>65</sup> Zn	244.26 d	EC	1115.5	50.6	<sup>65</sup> Cu(p, n)	-2.13
<sup>24</sup> Na	14.96 h	β	1368.598	100	$^{27}$ Al(p,p+ $^{3}$ He)	-23.71
					<sup>27</sup> Al(p, 2p+d)	-29.20
					<sup>27</sup> Al(p, 3p+n)	-31.43
<sup>22</sup> Na	2.60 y	EC	1274.53	99.94	$^{27}$ Al(p, d+ $\alpha$ )	-20.29
					<sup>27</sup> Al(p,α+pn)	-22.51

The theoretical data were taken from the MENDL-2P database [22] calculated by using the ALICE-IPPE code. It is an 'a-priori' model calculation. The calculation of cross-section using this code was based on the evaporation Weisskopf-Ewing model and geometry dependent hybrid exciton model [23]. Pre-equilibrium cluster emission calculation is included in this code. The lack of angular momentum and parity treatments in the Weisskopf-Ewing formalism used in these codes makes independent treatment of isomeric states impossible, only total production cross-sections were calculated.

In the present experiment, all the errors were considered as independent. Consequently, they were quadratically added according to the laws of error propagation to obtain total errors. However, some of the sources of errors are common to all data, while others individually affect each reaction. The estimated major sources of errors considered in deduction of cross-sections are as follows; statistical error (1-13%), error of the monitor cross sections  $(2\sim4\%)$ , error due to the beam flux  $(2\sim4\%)$ , error due to the beam energy (0.5-1%), error due to the detector efficiency (0.5-3%), and error due to the gamma ray intensity  $(1\sim2\%)$ . The overall uncertainty of the cross-section measurements is around 12%. The total

uncertainties of the measured cross-sections were calculated by combining the statistical uncertainties ( $\delta_{m}$ ) and other uncertainties ( $\delta_{ab}$ ).

#### 3. Results and Discussion

The stable isotopes of molybdenum, tungsten, and zinc transmute to the corresponding  $^{99m}$ Tc,  $^{186}$ Re, and  $^{67}$ Ga radioisotopes through the (p, xn) process, respectively. In some cases, two or more  $\gamma$ -rays were used for the measurement of each reaction cross-section, and the average value is presented. The detailed situations of the individually studied nuclides are discussed in the following section. The excitation functions of the investigated radioactive products are presented together with the available literature data and ALICE-IPPE prediction [22]. The numerical data with errors are collected in Table 1. The integral yields were deduced using the measured cross-sections taking into account that the total energy is absorbed in the targets.

# 3.1. Production of 99mTc

The production cross-section of medically important radionuclide 99mTc is determined through the analysis of 140.51 keV gamma-ray peak. Basically, this radionuclide can be produced in two processes. One is direct process through the reaction <sup>100</sup>Mo(p, 2n)<sup>99m</sup>Tc and the other is indirect process via <sup>100</sup>Mo(p, pn)<sup>99</sup>Mo  $\rightarrow$  <sup>99m</sup>Tc reaction. Also theoretically, the reaction  $^{98}$ Mo(p,  $\gamma$ ) $^{99m}$ Tc has little contribution in the production cross section of  $^{99m}$ Tc. The present result of 99mTc radionuclide formation is shown in Fig. 1. We didn't find agreement with the data reported by Lagunas-Solar [7]. In the lower energy region (<28 MeV) the trend of peak formation agrees with our data, but at higher energy it seems to us that he didn't separate the contribution of <sup>99</sup>Mo and <sup>90</sup>Nb radionuclides from 140.5 keV gamma-ray peak. At higher energy (>28 MeV), the radionuclides <sup>99</sup>Mo and <sup>90</sup>Nb have more contribution than <sup>99m</sup>Tc at 140.5 keV gamma line. This may be the possible reason to get the complete disagreement compare to our data in the higher energy region. The data reported by Scholten et al. [6] show general good agreement with our data. In their experiment, they worked with the 97.4% and 99.5% enriched <sup>100</sup>Mo and <sup>98</sup>Mo sample, respectively, but we performed the present experiment using natural molybdenum target and normalized the data for <sup>100</sup>Mo. The data reported by Levkovskji [24] showed agreement at 20-30 MeV proton energy but at lower energy (<20 MeV), a clear disagreement exists not only with our data but also with the other literature values. The present measurement showed very good agreement with the recent literature data reported by Takacs et al. [25] up to 27 MeV but after then an acceptable disagreement is found, and we could not determine any possible reason. Our previous data [26] were consistent with the present data except one point around 17 MeV. Although the <sup>99m</sup>Tc radionuclide has great practical importance, the production cross-sections measured by several groups showed considerable discrepancies. An accurate experimental data base is thus crucial to consider the feasibility of this reaction for a possible production of <sup>99m</sup>Tc at a cyclotron.

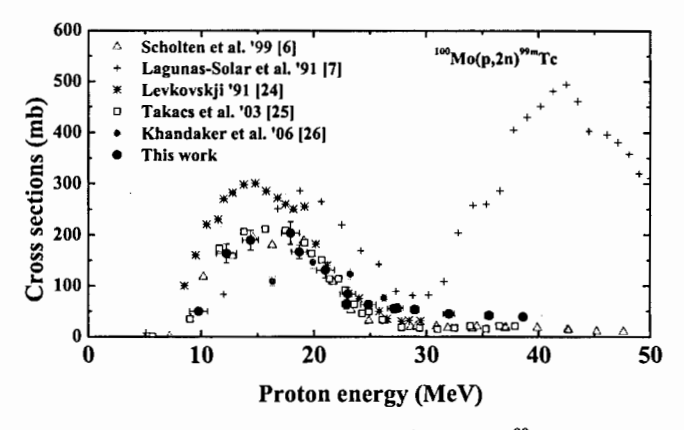


Fig. 1. Excitation function of the nat Mo(p, xn) 99m Tc reaction.

# 3.2. Production of 186Re

The most suitable reaction path for the production of <sup>186</sup>Re from the proton bombardment on natural tungsten is <sup>186</sup>W(p, n)<sup>186</sup>Re (Q= -1.069 MeV). The measured excitation function for the production of neutron rich therapeutic radionuclide <sup>186</sup>Re has shown in Fig. 2 together with the available experimental values and theoretical data taken from ALICE-IPPE code [22]. We found a very good agreement with the data reported by Lapi et al. [11], Tarkanyi et al. [27], Szelecsenyi et al. [28], and Shigeta et al. [10] in the investigated energy region. The data reported by Zhang et al. [12] and ALICE-IPPE prediction [22] showed lower values in the peak formation region at 6-13 MeV.

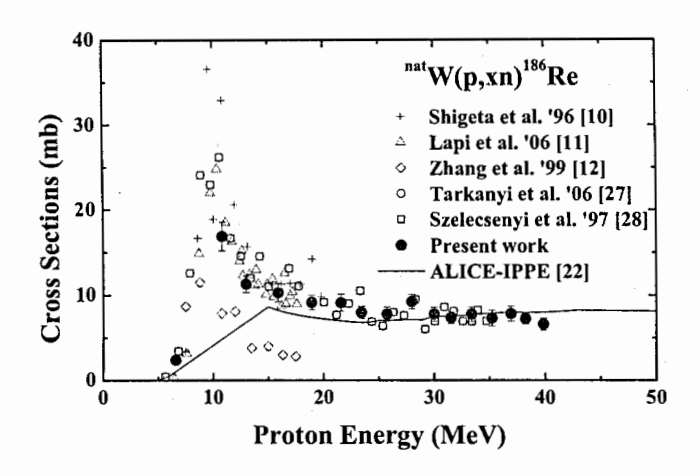


Fig. 2 Excitation function of the <sup>nat</sup>W(p, xn) <sup>186</sup>Re reaction

# 3.3. Production of 67Ga

The radionuclide <sup>67</sup>Ga is formed via the (p.2n) reactions on <sup>68</sup>Zn. Targetry and chemical processing problems have been well studied. For the production on a small scale the (p,n) reaction on <sup>67</sup>Zn has also been utilized. The <sup>67</sup>Ga nuclei emitted several strong gammarays with different energies (184, 300, 393 keV), the activities were evaluated separately by using all these gamma-lines and the average of the individual values were taken. In the case of the  $^{nat}$ Zn(p,xn) $^{67}$ Ga process three reactions,  $^{67}$ Zn(p,n) $^{67}$ Ga (Q=-1.8MeV),  $^{68}$ Zn(p,2n) $^{68}$ Zn(p,2n 12.15 MeV) and <sup>70</sup>Zn(p,4n)<sup>67</sup>Ga (O=-27.7 MeV) contribute to the formation of <sup>67</sup>Ga over the investigated proton energy range. The cross section values for the <sup>nat</sup>Zn(p,xn)<sup>67</sup>Ga process measured in this work from 4 to 40 MeV are shown in Fig. 3 compared with the results of the previous works [13-15, 29-33] and the theoretical calculation using the ALICE-IPPE code [22]. The maximum cross section for the <sup>nat</sup>Zn(p,xn)<sup>67</sup>Ga process was found at around 20 MeV. The <sup>68</sup>Zn(p,2n)<sup>67</sup>Ga process has a large contribution to the <sup>67</sup>Ga nuclide formation in peak region at about 20 MeV. Due to the low isotopic abundance of <sup>67</sup>Zn in the natural zinc target, the <sup>67</sup>Zn(p,n)<sup>67</sup>Ga process has lower contribution than <sup>68</sup>Zn(p,2n)<sup>67</sup>Ga. Comparing the present results with the available previous works it can be concluded that the values of Hermanne et al. [14, 29] are systematically higher than the present ones as well as the other investigators [15, 30, 31] above 15 MeV, but their results are in excellent agreement both with this work and Kopecky [30] below 15 MeV. The present measurement for the <sup>nat</sup>Zn(p,xn)<sup>67</sup>Ga process agrees well with the measurements of Tarkanvi et al. [15], Kopecky [30], and Nortier et al. [31]. The theoretical calculation using the ALICE-IPPE code [22] and this work agrees well except three points in maxima.

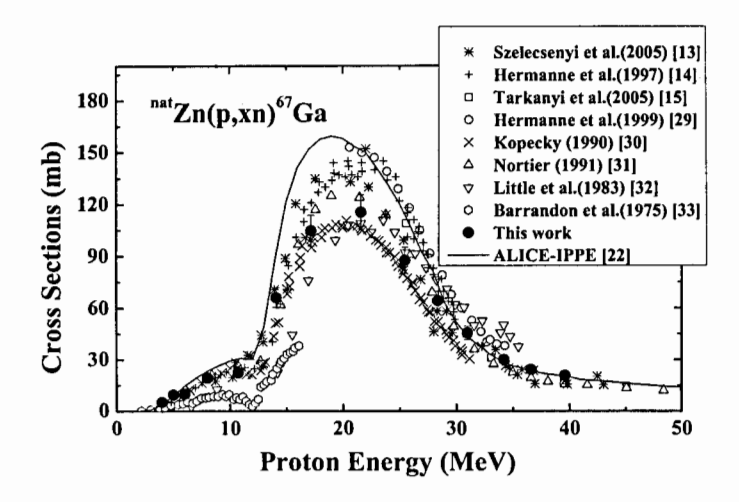


Fig. 3 Excitation function of the <sup>nat</sup>Zn(p, xn)<sup>67</sup>Ga reaction.

#### 4. Integral yield

The integral yield of the radionuclides from a nuclear process was deduced using the excitation function and stopping power of  $^{nat}Mo$ ,  $^{nat}W$ , and  $^{nat}Zn$  over the energy range from threshold upto 40 MeV. It is expressed as MBq  $\mu A^{-1}h^{-1}$ , i.e. for an irradiation at beam current of 1  $\mu A$  for 1 hour. The obtained results are shown in Figs. 4-5 as a function of proton energy. Dmitriev et al. [34] reported thick target yields of the  $^{67}Ga$  radionuclide measured by irradiating thick natural zinc target with 22 MeV proton beam. The used target was thick enough to cover the energy range from threshold to 22 MeV. Our results as shown in Fig. 5 are consistent with the directly measured values of Dmitriev et al. [34]. We couldn't compare the yield of  $^{99m}Tc$  and  $^{186}Re$  due to the lack of available literature values.

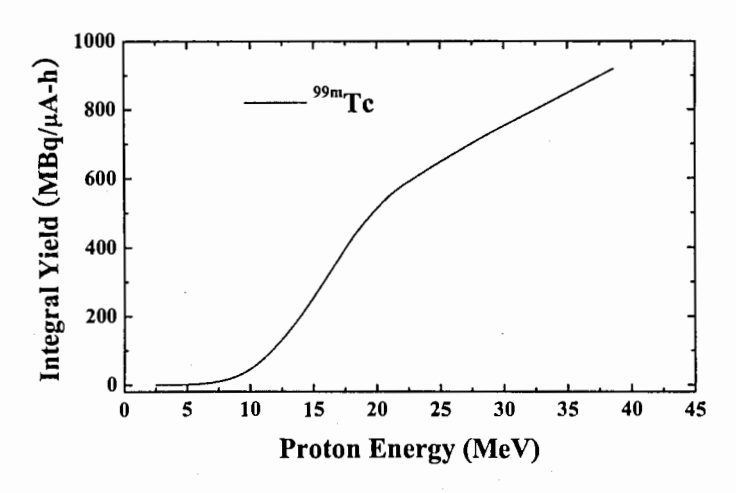


Fig. 4 Integral yield for the production of 99mTc radionuclide

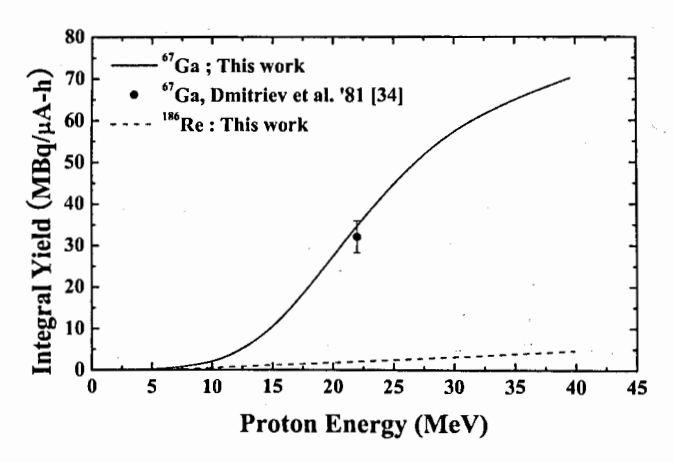


Fig. 5 Integral yields for the production of <sup>186</sup>Re and <sup>67</sup>Ga radionuclides

#### 5. Conclusions

A new cross sections data set for the formation of <sup>99m</sup>Tc, <sup>186</sup>Re, and <sup>67</sup>Ga radionuclides have been reported in the energy range 2.5 - 40 MeV using the stacked-foil activation technique with an overall uncertainty of about 12%. The present experimental data were compared with the available literature values in order to select the most reliable data sets for optimization of production routes. A considerable discrepancies still exists among the

available literature data for the production of medically (SPECT) important <sup>99m</sup>Tc radionuclide, which demands more and more experimental data to obtain a recommended data set, and the present data is important in this regard. Rhenium-186 (<sup>186</sup>Re) is one of the most useful radionuclide for internal radiotherapy in nuclear medicine. The measured production cross sections data of this radionuclide will help effectively to optimize the production conditions. Significant amount of <sup>67</sup>Ga can be produced at low energy accelerators using natural zinc as a target, but the possibility to involve impurity of gamma emitting radionuclides is very high. The present experiment reported a reliable data set for these radionuclides in the whole investigated energy region, and these data could help in the prediction, optimization and evaluation of the radiochemical purity.

The thick target integral yields for each radionuclide were deduced using the respective measured cross-sections data. We could not compare the present values of <sup>99m</sup>Tc and <sup>186</sup>Re radionuclides due to the lack of available directly measured thick target yield (TTY) values in the literature. It should be mentioned that our calculated yield values can be used for the optimization of production yields of corresponding radionuclide with minimum impurity contamination. Above all, the present experimental results will play an important role in enrichment of literature data set for all of the investigated radio radionuclides.

#### Acknowledgements

The author would like to express their sincere thanks to the staffs of the MC50 Cyclotron Laboratories for their cordial help in performing the experiment. This work was partly supported by the Korea Science and Engineering Foundation (KOSEF) through a grant provided by the Korean Ministry of Education, Science and Technology (MEST) in 2007 and 2008 (Project No. M2 07B020000810, M2 07M040001110, and M2 08M040001110).

#### References

- [1] W. C. Eckelman, W. A. Volkert, Int. J. Appl. Radiat. Isot. 33 (1982) 945.
- [2] S. Kinuya, K. Yokoyama, M. Izumo, T. Sorita, T. Obata, H. Mori, K. Shiba, N. Watanabe, N. Shuke, T. Michigishi, N. Tonami, Cancer Lett. 219 (2005) 41.
- [3] S. Kinuya, K. Yokoyama, M. Izumo, T. Sorita, T. Obata, H. Mori, K. Shiba, N. Watanabe, N. Shuke, T. Michigishi, N. Tonami, J. Cancer Res. Clin. Oncol. 129 (2003) 392.
- [4] E. J. Postema, P. K. Borjesson, W. C. Buijs, J. C. Roos, H. A. Marres, O. C. Boerman, R. de Bree, M. Lang, G. Munzert, G. A. V. Dongen, W. J. Oyen, J. Nucl. Med. 44 (2003)1690.
- [5] S. M. Kormali, D. L. Swindle, E. A. Schweikert, J. Radiat. Chem. 31 (1976) 437.
- [6] B. Scholten, R.M. Lambrecht, M. Cogneau, H. Vera Ruiz, Appl. Radiat. Isot. 51 (1999) 69.

126

- [7] M. C. Lagunas-solar, P. M. Kiefer, O. F. Carvacho, C. A. Lagunas, Y. P. Cha, Appl. Radiat. Isot. 42 (1991) 643.
- [8] F. Roesch, S. M. Qaim, Radiochim. Acta. 62 (1993) 115.
- [9] N. C. Schoen, G. Orlov, R. J. McDonald, Phys. Rev., Part C 20 (1979) 88.
- [10] N. Shigeta, H. Matsuoka, A. Osa, M. Koizumi, M. Izumo, K. Kobayashi, K. Hashimoto, T. Sekine, R. M. Lambrecht, J. Radioanal. Nucl. Chem. 85 (1996) 205.
- [11] S. Lapi, W.J. Mills, J. Wilson, S. McQuarrie, J. Publicover, M. Schueller, D. Schyler, J. J. Ressler, T. J. Ruth, App. Radiat. Isot. 65 (2007) 345.
- [12] X. Zhang, W. Li, K. Fang, W. He, R. Sheng, D. Ying, W. Hu, Radiochim. Acta 86 (1999) 11.
- [13] F. Szelecsenyi, G. F. Steyn, Z. Kovacs, T. N. Van der Walt, K. Suzuki, K. Okada, K. Mukai, Nucl. Instr. Meth. B 234 (2005) 375.
- [14] A. Hermanne, Private communication, reported in Szelecsenyi et al. (1998), Appl. Radiat. Isot. 49 (1997)1005.
- [15] F. Tarkanyi, F. Ditroi, J. Csikai, S. Takacs, M. S. Uddin, M. Hagiwara, M. Baba, Yu. N. Shubin, A. I. Dityuk, Appl. Radiat. Isot. 62 (2005) 73.
- [16] A. Wyttenbach, J. Radioanal. Nucl. Chem. 8 (1971) 335.
- [17] J. F. Ziegler, J. P. Biersack, U. Littmark, SRIM 2003 code, Version 96.xx. The stopping and range of ions in solids. Pergamon, New York. Available at <a href="http://www.srim.org/">http://www.srim.org/</a>
- [18]G. Gilmore, J.D. Hemingway, Practical Gamma-Ray Spectrometry, John Wiley & Sons, England, Chapter 1, 1995, p. 17.
- [19] E. Browne, R. B. Firestone, Table of Radioactive Isotopes, in: V.S. Shirley (ed.), Wiley, New York, (1986).
- [20] Reaction Q-values and thresholds, Los Alamos National Laboratory. Available from
  <a href="http://t2.lanl.gov/data/qtool.html">http://t2.lanl.gov/data/qtool.html</a>>
- [21] Monitor cross-section data. Available at < http://www-nds.iaea.org/medical/>
- [22] A. I. Dityuk, A. Yu. Konobeev, V. P. Lunev, Yu. N. Shubin, New Advanced Versi on of Computer Code ALICE-IPPE, INDC(CCP)-410, IAEA, Vienna (1998); Med ium Energy Activation Cross Sections data: MENDL-2P, Available at: <a href="http://wwww-nds.iaea.org/nucmed.html">http://www-nds.iaea.org/nucmed.html</a>>
- [23] M. Blann, H. K. Vonach, Phys. Rev. C28 (1983) 1475.
- [24] V. N. Levkovskij, Middle Mass Nuclides (A=40-100) Activation Cross-sections by Medium Energy (E=10-50MeV) Protons and Alpha Particles (Experiment and Syst ematics). Inter-vesi, Moscow (1991).
- [25]S. Takacs, Z. Szucs, F. Tarkanyi, A. Hermanne, M. Sonck, J. Radioanal. Nucl. C hem. 257 (2003) 195.
- [26] M. U. Khandaker, A. K. M. M. H. Meaze, K. Kim, D. Son, G. N. Kim, Y.S. Lee, J. Korean Phys. Soc. 48 (2006) 821.

- [27] F. Tarkanyi, S. Takacs, F. Szelecsenyi, F. Ditroi, A. Hermanne, M. Sonck, Nucl. Instr. Meth. B 252 (2006) 160.
- [28]F. Szelecsenyi, S. Takacs, F. Tarkanyi, M. Sonck, A. Hermanne, in: J.R. Heys, D.G. Mellilo, Chichester, et al. (Eds.), Proceedings of the Sixth International Symposium on Synthesis and Applications of Isotopically Labelled Compounds, Philadelphia, USA, 14–18 September, 1997, John Wiley and Sons, 1998, p. 701
- [29] A. Hermanne, F. Szelecsenyi, M. Sonck, S. Takacs, F. Tarkanyi, P. Van der Winkel, J. Radioanal. Nucl. Chem. 240 (1999) 623.
- [30] P. Kopecky, Appl. Radiat. Isot. 41 (1990) 606.
- [31] F. M. Nortier, S. J. Mills, G. F. Stevn, Appl. Radiat. Isot. 42 (1991) 353.
- [32] F. E. Little, M. C. Lagunas-Solar, Int. J. Appl. Radiat. Isot. 34 (1983) 631.
- [33] M. Yagi, K. Kondo, Int. J. Appl. Radiat. Isot. 30 (1979) 569; J. N. Barrandon, J. L. Debrun, A. Kohn, R. H. Spear, Nucl. Instr. and Meth. 127 (1975) 269.
- [34] P. P. Dmitriev, G. A. Molin, Vop. At. Nauki i Tekhn., Ser. Yadernye Konstanty 44 (1981) 43 (in Russian).

# A Method for the Direct Measurement of Mean Square Radius for Excited Nuclei

Ts. Ts. Panteleev', S. B. Borzakov', and L. Ts. Simconova-Panteleeva'

<sup>a</sup> Joint Institute for Nuclear Research, Dubna, Russia

Institute for Nuclear Research and Nuclear Energy, Bulgarian Academy of

Sciences, Sofia, Bulgaria

Abstract—In this work, the energy shift of X-ray photons at two-photon transition, depending on conversion (either at transition between the second and first excited states or at transition from the first to the ground level), is studied. It is possible to very precisely determine the energy shift of an X-ray photon (on the order of 1 eV) by registering the X-ray photon in coincidence with an X-ray photon of another transition with high resolution detectors; this allows one to determine the change of the mean square radius of the nucleus in the excited state.

The electrostatic monopole interaction, depending on the mean square radius of the nucleus and electron density in the region of the nucleus, changes the binding energy of the system nucleus-electrons; therefore, it influences the energy of atomic and nuclear transitions. The result is the isotopic shift in optical spectra and isomeric energy shift of optical and nuclear transitions [1, 2]. Many works are devoted to investigation of these effects giving information on the nuclei properties. Methods of laser spectroscopy allow one to obtain vast information on the difference of charge radii of high-spin isomers [3]. Experimental studies of chemical shifts of neutron resonances were performed at the Laboratory of Neutron Physics of the Joint Institute for Nuclear Research in the 1970s–1980s. The values of the measured chemical shifts of neutron resonances turned out to be equal to  $(10^{-5}-10^{-4})$  eV [4, 5].

One of the consequences of electrostatic monopole interaction is the isomeric shift of X-ray photon energy arising when the hole is filled in the K shell, which is formed as a result of internal conversion of gamma ray photon [6]. Since the hole is filled much faster for heavy nuclei (within  $10^{-17}$  s [7]) than the lifetime of the nuclear level  $(10^{-12}-10^{-10}$  s), the energy of atomic levels corresponds to the mean square radius of the nucleus in the final state. If the nucleus still remains in the excited state after internal conversion of the photon, the energy of the X-ray photon depends on the instantaneous size of the nucleus at this level. Thus, the energy of the X-ray photon is linearly related to the mean square radius of the nucleus. In order to investigate the difference of mean square radii of the nucleus in the

ground and excited states, it is necessary to compare the energy of X-ray photons at transition, for example, from the second to the first excited state  $(E_{r_1})$  with the energy of the similar photon formed at transition from the first level to the ground state  $(E_{r_0})$ .

In this work, methods for experimentally studying in order to obtain data on variations of mean square radius of the nucleus in excited states are proposed. The difference is related to the deformation of the nucleus.

The difference of energies  $E_{r1}$  and  $E_{r0}$  can be represented in the form

$$\delta E = \Delta E \frac{\delta \langle R^2 \rangle}{\langle R^2 \rangle} \tag{1}$$

where  $\Delta E$  is the energy shift of the X-ray line due to the finite size of the nucleus

$$\Delta E = \frac{2}{3}\pi e^2 Z \left| \Psi(0) \right|^2 \left\langle R^2 \right\rangle \tag{2}$$

In [6] the values of  $\Delta E$  were calculated depending on Coulomb charges of some relatively heavy nuclei. Figure 1 shows the basic result of this work in the graphic form.

Taking into account the data presented above and expecting that the mean square radius is changed by several percent, we obtain an estimate of the energy shift of X-ray lines on the order of several electronvolt.

If, as a result of transition from one excited state to another one (or to the ground state), the time it takes nucleons to reorganize in the nucleus is comparable with the short life time of the K vacancy, this process influences the peak shape. The peak broadens, and its symmetry can be violated.

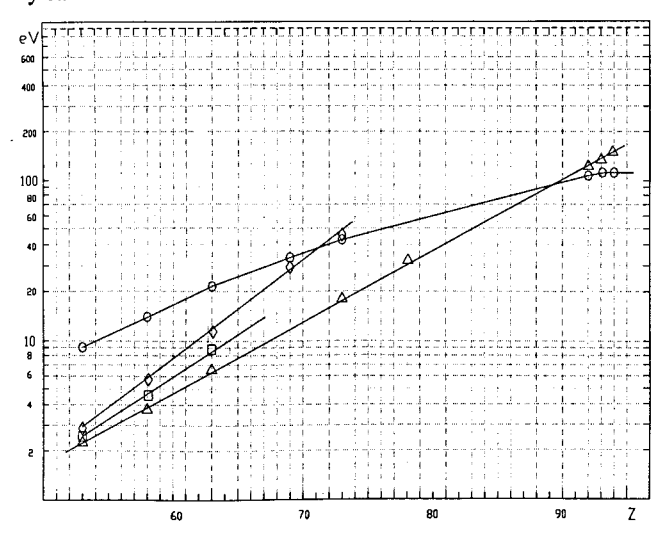


Fig. 1.  $\Delta E$  as a function of nuclei charge Z [6]. Calculations were performed using the following methods: Hartree- Fock-Slater; relativistic Hartree-Fock-Slater; nonrelativistic Hartree-Fock; and nonrelativistic hydrogen-like atom.

The screening influence of the remaining electrons of the atom on  $\Delta E$  for the K shell was calculated in [8]. The obtained results showed that this influence can be neglected.

The motion of conversion electrons through electron shells of the atom excites them and causes some "smearing" of isomeric shifts. Therefore, the velocity of knocked out electrons should be such that they leave the L and even M layers earlier than the X-ray photons are emitted. Otherwise, the peak shape will be changed under the action of the atom.

When measuring the relative variations of superfine effects, it is necessary to perform measurements in such a way that the sought effect and the reference (in this case, the centroid of the X-ray peak in the ground state of the nucleus) are measured simultaneously. If this is impossible, these measurements should be performed in turn and with as little change in the equipment load intensity and geometry of experiment as possible. Figure 2 illustrates this principle. The two-cascade decay of an excited nucleus is considered. The photon initiating the process knocks out the electron from the K shell of the atom, and the nucleus transits to the first excited level. The X-ray photon produced as a result of internal conversion is registered by the thin HP Ge detector only under the condition that it coincides with the momentum of the secondary photon registered by the large volume HP Ge detector. In the second case, this detector also registers the primary photon coinciding with the X-ray photon of the converted transition to the ground state of the nucleus. Thus, the two-dimensional amplitude spectrum of photons and X-quanta in the coincidence scheme is accumulated: the photons are related to the primary  $\gamma$  transition and reflect  $\langle R^2 \rangle$  for the excited state, and the X-quanta are related to characteristic X-ray spectrum of the atom in which the nucleus is in the ground state. The data processing consists of determining the centers of X-ray peaks of these two transitions. The value of  $\delta(R^2)$  is determined by the experimentally measured isomeric shift  $\delta E$  of X-ray photons using (1).

The absolute values of isomeric shifts of X-ray photons are very small even for heavy nuclei. Modern spectrometers based on bent crystals provide an energy resolution of 0.3 eV for a photon energy of about 100 keV;

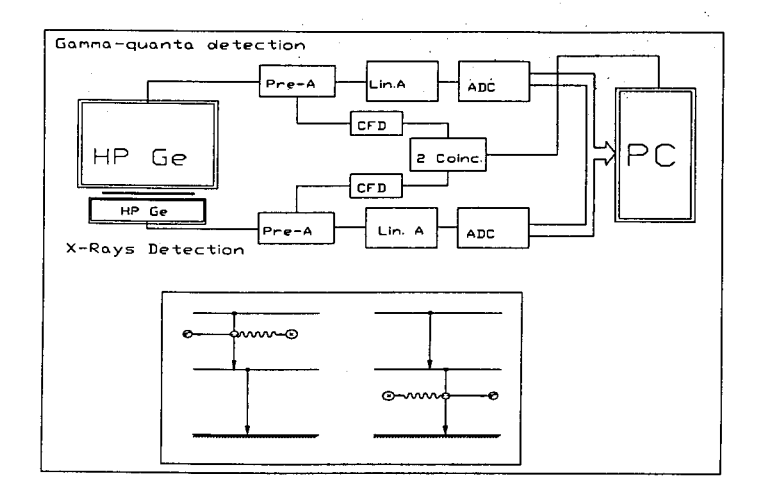


Fig. 2. Schematic diagram of experiment with two-cascade decay of excited nucleus.

however, this detection method is not used here for the following reasons:

- (i) its extremely small event registration efficiency and
- (ii) the geometry of the experimental setup makes this approach practically inapplicable for the measurement method proposed in this work.

In [9] experimental data on the natural widths of X-ray transitions to the K shell of actinide and transuranic atoms were presented. In particular, for  $^{236}$ U, for  $KL_2$  and  $KL_3$  transitions these widths are equal, respectively, to 94.656 and 98.435 eV. The conclusion can be made from these data that the natural width of  $K_\alpha$  line for U atoms is comparable with the energy resolution of high quality HP Ge detectors of X-ray photons.

The precision of measuring the centroid of the peak in the amplitude spectrum was estimated. Let there exists a spectrum corresponding to the peak which consists of the set of counts  $N_i$  in the channel with the number i and the error  $\Delta N_i$ . Then the peak center is determined by the formula

$$\overline{N} = \frac{\sum_{i}^{i} iN_{i}}{\sum_{i}^{i} N_{i}}.$$
 (3)

The error of determining the centroid of the peak can be calculated using the known formula to determine the error of a function of many variables:

$$\Delta \overline{N} = \sqrt{\sum_{i} \left(\frac{\partial \overline{N}}{\partial N_{i}} \Delta N_{i}\right)^{2}}$$
 (4)

Calculating derivatives, we obtain

where S is the peak area, 
$$S = \sum_{i=i \, \text{min}}^{i \, \text{max}} N_i$$
.

(6)

If it is assumed that  $\Delta N_i = \sqrt{N_i}$ , we obtain:

$$\Delta \overline{N} = \frac{\sqrt{\sum_{i} (i - \overline{N})^{2} N_{i}}}{\sum_{i} N_{i}}$$

The table presents the calculated accuracies of determining the centroids of the peaks under the following conditions:

- (i) the number of registered events (peak area) is equal to  $10^6$  and  $2 \times 10^6$ , respectively;
- (ii) the peak shape is symmetric Gaussian;
- (iii) the X-ray photon energy is 100 keV; channel division of amplitude analyzer corresponds to 0.1 keV;
- (iv) the calculations were performed for different energy resolutions of the detector of X-ray photons (0.3, 0.5, 0.7, and 1.0 keV).

An analysis of the data obtained from the table allows one to come to the conclusion that applying the X-ray detector with medium energy resolution can solve the problem of measuring isomeric shifts of the X-ray K transitions of atomic shells.

In [10] the results of the precise determination of the position of the centroid of the peak of photon with an energy of about 100 keV, measured using a high resolution Ge detector, were presented. The weighted mean precision of the determination of the centroid was 0.5 eV.

Table 1.

	Pe	ak	area	10 <sup>6</sup>	Pe	ak area	2x10 <sup>6</sup> e	vents
	event	s						
The detector resolution, keV	1.0	0.75	0.5	0.3	1.0	0.75	0.5	0.3
The peak accuracy, eV	0.9	0.73	0.5	0.3	0.64	0.52	0.35	0.21

The further development of formulating experiments assumes an increase in the number of studied excited levels of separate nuclei by including into consideration  $\gamma$  cascades which follow electron capture processes,  $\beta^+$ ,  $\beta^-$  (and possibly,  $\alpha$ ) emission of radioactive nuclei, and decays of high spin isomeric states.

The measurement of superfine effects (which corresponds to this type of experiments) is often accompanied by the requirement of extremely thorough account of the background. For this reason it is necessary to perform multidimensional analysis and record information on the maximum number of parameters using specific equipment developed specially for these experiments. The example of this formulation is shown in Fig. 3.

First of all, it is necessary to develop and manufacture a pair of compound HP Ge spectrometers, each of which consisting of an independently operating thin detector (for the X-ray photon spectrometry) and a large volume detector for the spectrometry of cascade photons.

Information from each X-ray detector is recorded by separate amplitude analyzers (ADCs) in the presence of the enabling signal from the coincidence scheme, which is triggered by the discriminated pulses from this X-ray detector and from any other  $\gamma$  detector. Pulses from  $\gamma$  detectors are processed in a similar way, but these pulses are also applied to the linear summing unit; from this unit they are applied to the separate ADC. The objective of this operation is to obtain peaks from any combinations of the total energies of the cascade with maximum efficiency. The absence of energy of a certain transition in the peak of the total summarized energy of the cascade means that it is highly probable that it has undergone internal conversion.

Uncorrelated background of X-ray peaks results from accidental coincidences of the external photoeffect on target atoms with the pulses from  $\gamma$ -channels. Further, this background contains a part which may be considered with high accuracy as a constant within the peak region, i.e., this part is approximated as a straight line. The most important is to provide exact normalizations of the background area under the peak and the area of the spectrum near the X-ray peaks.

A precise determination of the contribution of correlated background is a complicated problem. The life time of a  $\gamma$  cascade is  $10^{-12}$ – $10^{-10}$  s; therefore, applying the method of delayed coincidences is unacceptable. Figures 4 and 5 show the diagrams of

radioactive decay of two heavy nuclei <sup>180m</sup>Hf and <sup>192</sup>Ir whose investigation is interesting and promising. Problems of correlated background can be demonstrated using the decay of these nuclei as an example.

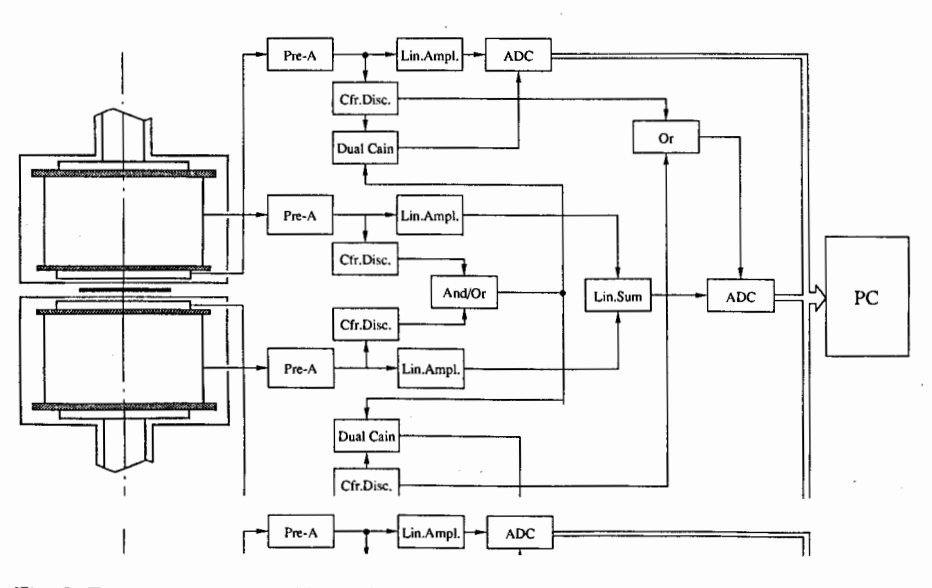


Fig. 3. Experimental setup with maximum efficiency and capability of identifying particular cascade transitions

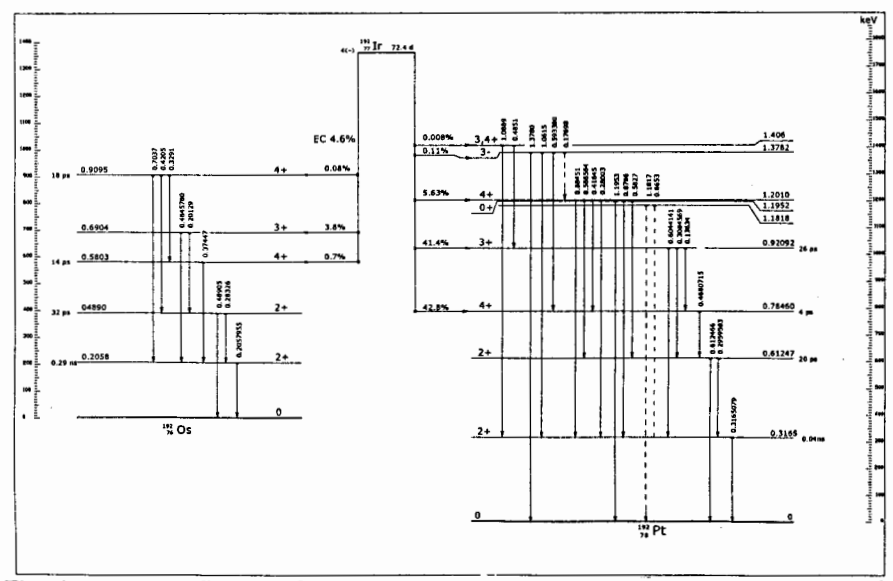


Fig. 4. Schematic diagram of decay of radioactive nucleus "Ir. For determination of the conversion coefficients for isotopes 76Os 192

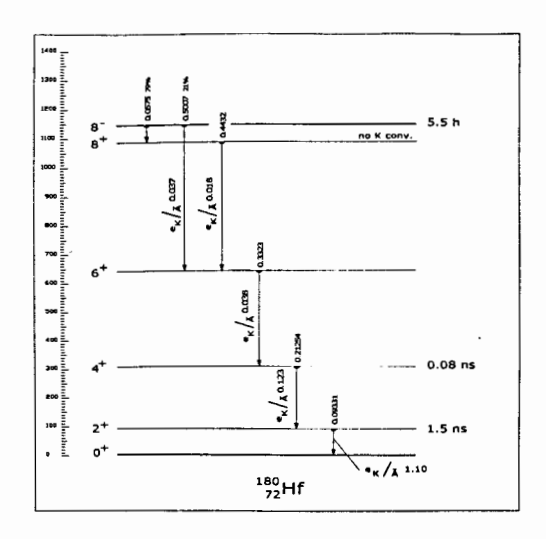


Fig. 5. The decay scheme for isomer state of <sup>180m</sup>Hf.

The measurement of X-ray line shift in experiments with fissionable nuclei is of special interest. Figure 6 shows all four channels via which the excitation energy of the nucleus can be dissipated after neutron capture: (i) radiation capture; (ii) instantaneous fission; (iii)  $(n, \gamma f)$  process: an excited nucleus emits soft photon and undergoes fission after that; (iv) isomeric fission: the nucleus emits the cascade of photons and turns out to be in the ground state at the bottom of the second potential well after that delayed fission takes place. The probability of this process is  $10^{-4}$  of the total fission probability. In the last two channels, photons preceding to fission can be converted and give information on the deformation of highly excited states of nuclei. These measurements can answer the question whether the process of delayed fission is the shape isomerism effect. In [11] measurements of variation of the mean square radius  $\delta \langle R^2 \rangle$  for spontaneously fissionable isomer  $\frac{240}{4}$  Am with respect to  $\frac{240}{4}$  in the ground state of Am nuclei were performed. The method of optical pumping using a laser with a variable wavelength was used in the experiment (laser induced nuclear polarization).

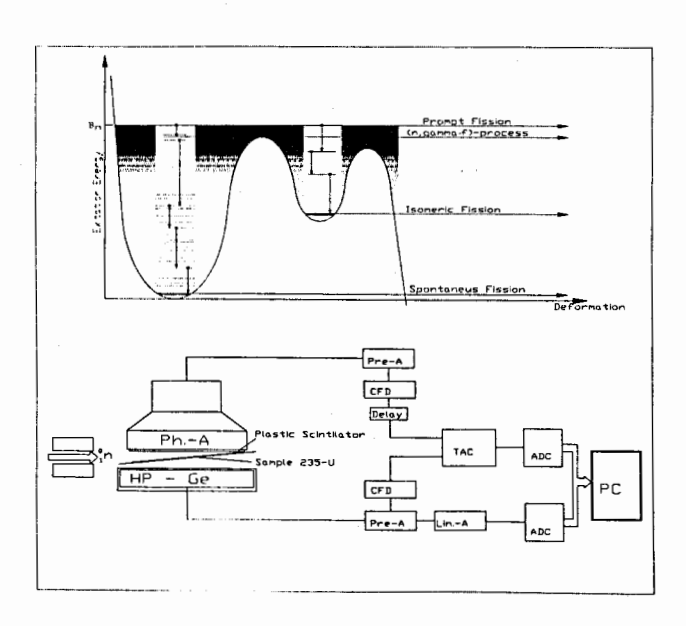


Fig. 6. Schematic diagram of experiment with fissionable nuclei. Two-hump barrier and nuclear fission channels are shown in the upper part.

In this work it is proposed that  $\delta(R^2)$  be measured using the method of isomeric shifts of X-ray photons. This method can be applied for nanosecond half-lives and can be complimentary to laser methods of investigation.

Figure 6 shows the proposed schematic diagram of experimental setup. The fission is registered by the thin plastic scintillator, and the X-ray photon is registered by HP Ge detector. Signals from both detectors are sent to the time-amplitude converter, where the signal from the HP Ge detector serves as the start signal and the delayed pulse from the scintillator serves as the stop signal. This is necessary due to the fact that there are much more fission acts than X-ray photons. Measurements can be performed using a beam of thermal neutrons with a <sup>235</sup>U target. It is known that isomeric fission takes place in this case with a probability of 10<sup>-4</sup>. The lifetime of <sup>236</sup>U\* in the second well is 165 ns [12].

ACKNOWLEDGMENTS We thank G. G. Bunatyan for stimulating this work.

#### REFERENCES

- 1 G. Kopfermann, Nuclear Moments (Academic Press, New York, 1958; Inostr. Liter., Moscow, 1960).
- 2 N. N. Delyagin et al., *Hyperfine Interactions and Nuclear Radiations* (Mosk. Gos. Univ., Moscow, 1985) [in Russian].
- 3 Yu. P. Gangrskii, Pis'ma Fiz. Elem. Chastits At. Yadra 4, 518 (2007) [Phys. Part. Nucl. Lett. 4, 304 (2007)].
- 4 V. K. Ignatovich, Yu. M. Ostanevich, and L. Cher, Soobshch. OIYaI R4-7296 (Dubna, 1973).
- 5 A. Meister, D. Pabst, L. B. Pikelner, and K. Seidel, Nucl. Phys. A 362, 18 (1981).
- 6 V. K. Ignatovich, Yu. M. Ostanevich, and Ts. Panteleev, Soobshch. OIYaI R4-7695 (Dubna, 1974).
- 7 E. E. Berlovich, S. S. Vasilenko, and Yu. N. Novikov, Lifetime of Excited States of Atomic Nuclei (Nauka, Leningrad, 1972).
- 8 E. E. Fradkin, Zh. Eksp. Teor. Fiz. **42**, 777–788 (1962) [Sov. Phys. JETP **15**, 543 (1962)].
- G. Barreau et al., Z. Phys. A 308, 209–213 (1982).
- 10 C. E. Bemis et al., Phys. Rev. Lett. 43, 1854 (1979).
- 11 O. A. Shcherbakov, Fiz. Elem. Chastits At. Yadra 21, 419 (1990) [Sov. J. Part. Nucl. 21, 177 (1990)].

#### COMPILATION OF NEUTRON RESONANCE PARAMETERS NRF-3

Z.N. Soroko, S.I. Sukhoruchkin, D.S. Sukhoruchkin

Petersburg Nuclear Physics Institute, Gatchina, Russia

#### Abstract

This compilation LB I/24 is a continuation of the previous publication LB I/16B,I/16C. The largest part of it is formed by the recent data. Special chapters of the Introduction are prepared by V.Pronyaev and F.Gunsing on the reactor based transmutation and on the numerous measurements at CERN n-TOF, correspondingly. A great number of new resonance parameters comes from measurements at RPI-linac and GELINA as well as from BNL-325 and ENDF/B-VII. A special chapter is devoted to the study of the nonstatistical effects.

#### 1 Introduction

Three years ago we described [1] motivation for production of compilation of neutron resonance parameters needed for nuclear models development and for better understanding of nuclear reactors dynamics: reactions which take place in the reactor components and in its fuel after the compaign. Recently published BNL-325 used in the Evaluated Nuclear Data File ENDF/B-VII [2] contains performed by S. Mughabghab revisions of old data. his own recalculations of neutron widths, new spin assignments. But the presence of large effects from capture of scattered neutrons in  $\gamma$ -ray detectors, the so-called high neutron sensitivity of used earlier capture detectors (discussed by F. Corvi in Introduction to the previous compilation NRF-2 [3]) prevented the production of high-quality capture cross section. First at GELINA, later at CERN n-TOF facility and at ORELA, new results were obtained which were not included in the last BNL-325. The NRF-3 file published as vol.I/24 in Springer Landoldt-Böernstain Library contains many new results from CERN n-TOF in addition to data from other facilities and files from ENDF/B-VII. Special chapters devoted to CERN n-TOF, capture detectors and R-matrix analysis were written by F. Gunsing and a special chapter about reactor-based transmutation method is written by V. Pronyaev. In the separate chapter "Few-nucleon effects in neutron resonance positions" the following topics are considered in subchapters:

- 1) Nonstatistical effects in nuclei around N=82 (Z=58) and N=50.
- 2) Observation of nonstatistical effects in <sup>206</sup>Pb resonances by G.Rohr.
- 3) Door-way states at high-energy excitations of <sup>233</sup>Th.
- 4) Correlations in positions of neutron resonances of <sup>74</sup>As, <sup>123</sup>Sb and other heavy nuclei observed by K.Ideno, M.Ohkubo and F.Belyaev. The introduction to this separate chapter and two last subchapters 3) and 4) are reproduced below.

The contents of NRF-3 is presented in Table 1. Only new data are included in the book, the ratios of numbers of resonances in the book  $N_b$  to the total numbers of all known resonances in the electronic Supplement  $N_s$  are given in Table as a ratio  $N_b/N_s$ .

The NRF-3 file together with the files of proton/alpha resonances (LB vol. I/19A1,2) and nuclear bound states excitations (CRF, Combined Reaction File, LB vols. I/19BC) were used in a study of stable nuclear energy intervals coinciding with (or rational to) the electromagnetic mass differences of the nucleon  $(D_o=\delta_N=m_p-m_p=1293 \text{ keV})$ , the pion

 $(\delta_{\pi}=4.595~{\rm keV}\approx 9m_e=4.599~{\rm keV})$  and the electron  $(2m_e=\varepsilon_o=1022~{\rm keV})$ . For example, nucleon spin-flip effects in the light near-magic nuclei  $^{10}{\rm B}$  and  $^{14}{\rm N}$  (splitting between  $J^{\pi}=0^+, {\rm T=1}$  and  $J^{\pi}=1^+, {\rm T=0}$  levels) have values D=1021.8(2) keV (coincides with  $\varepsilon_o$ ) and D=2312.80 keV (close to  $\varepsilon_o+D_o=2315.3~{\rm keV}$ ). This so-called tuning effect in nuclear excitations and nuclear binding energies, was considered [4-8] as the manifestation of an influence of the nucleon structure in accurately known nuclear data. This is in accordance with the suggested by S.Devons [9] analogy between fine effects in nuclear data and well-known empirical spectroscopic systematics resulted in the quantum atomic physics.

Table 1. Contents of neutron resonance parameters compilation NRF-3.

Isotope	$N_{ m B}/N_{ m S}$	Isotope	$N_{ m B}/N_{ m S}$	Isotope	$N_{\rm B}/N_{\rm S}$	Isotope	$N_{\rm B}/N_{\rm S}$
<sup>9</sup> Be	11/11	<sup>41</sup> K	6/283	<sup>75</sup> As	23/247*	<sup>100</sup> Ru	3/91
$^{10}\mathrm{B}$	4/16	<sup>40</sup> Ca	$\frac{0}{203}$ $\frac{2}{257}$ *	<sup>76</sup> Se	5/22	<sup>101</sup> Ru	4/174
11B	$\frac{4}{10}$ $\frac{17}{35}$	$^{42}Ca$	2/257	<sup>77</sup> Se	2/58	102Ru	4/144
$^{12}C$	6/60	$^{45}Sc$	$\frac{2}{93}$ $\frac{23}{199}$	78Se	2/21	104Ru	4/107
<sup>13</sup> C	1/38	46Ti	3/113	80Se	$\frac{2}{21}$ 3/15	103Rh	26/294
<sup>14</sup> N	34/62	47′]'i	4/118	<sup>82</sup> Se	$\frac{3}{19}$	104Pd	1/326
15 N	$\frac{34}{62}$ $\frac{26}{47}$	<sup>48</sup> Ti	9/87	<sup>79</sup> Br	19/341*	105Pd	$\frac{1}{320}$ $\frac{3}{322}$
<sup>16</sup> O	60/92	<sup>49</sup> Ti	5/79	81Br	$\frac{19}{341}$ $\frac{21}{330}$	106Pd	$\frac{3}{322}$ $\frac{3}{20}$
<sup>17</sup> O	$\frac{60}{92}$	<sup>50</sup> Ti	2/34	<sup>78</sup> Kr	$\frac{21}{330}$ $\frac{5}{27}$	107Pd	1/320 $1/133$
<sup>18</sup> O	$\frac{2}{6}$ 1/21	51 V	6/1073	80Kr	5/27 $5/32$	108Pd	1/133 $1/243$
<sup>19</sup> F		<sup>50</sup> Cr	$\frac{6}{1073}$ $\frac{2}{382}$	82Kr	$\frac{3}{32}$ $\frac{3}{2}$	110Pd	0/231
<sup>20</sup> Ne	23/77	<sup>52</sup> Cr	$\frac{2}{382}$ $\frac{2}{341}$	84Kr	1/207	107Ag	$\frac{0}{231}$ $\frac{4}{439}$
<sup>21</sup> Ne	$\frac{3}{102}$	<sup>53</sup> Cr	$\frac{2}{341}$	86Kr		109Ag	
<sup>22</sup> Ne	2/39	<sup>54</sup> Cr		$^{85}$ Rb	2/817	110Cd	3/459*
<sup>23</sup> Na	$\frac{3}{26}$ $\frac{4}{250}$	<sup>55</sup> Mn	345/345 $23/175$	87Rb	$\frac{21}{348}$ $\frac{19}{100}$	111Cd	$\frac{3}{103}$ $\frac{3}{156}$
<sup>24</sup> Mg		<sup>54</sup> Fe	3/894	86Sr	7/74	112Cd	$\frac{3}{130}$
<sup>25</sup> Mg	. 23/42	<sup>56</sup> Fe	$\frac{3}{694}$ $\frac{2}{1242}$	87Sr	3/116	113Cd	2/514*
<sup>26</sup> Mg	12/35	<sup>57</sup> Fe	$\frac{2}{1242}$ $\frac{2}{127}$	88Sr	20/444	114Cd	5/86
<sup>26</sup> Al	$\frac{5}{12}$	<sup>58</sup> Fe	$\frac{2}{127}$ $\frac{20}{83}$	89Y	2/693	116Cd	4/53
<sup>27</sup> Al	1/378	<sup>59</sup> Co	20/03	90Zr ~	2/093 45/250*	113In	$\frac{4}{3}$
<sup>28</sup> Si		<sup>58</sup> Ni	$\frac{218}{774}$ $\frac{3}{1991}$	91Zr	157/530	115 In	3/76 $3/259$
<sup>29</sup> Si	52/261	<sup>59</sup> Ni	3/1991 4/15	92Zr	3/148	116Sn	3/218
<sup>30</sup> Si	30/34	<sup>60</sup> Ni	2/2601	$^{93}Zr$	3/148	117Sn	$\frac{3}{218}$
31P	26/31	61Ni		$^{94}\mathrm{Zr}$	$\frac{3}{141}$	118Sn	4/86
32S	23/375*	<sup>62</sup> Ni	181/1693	<sup>96</sup> Zr		119Sn	$\frac{4}{80}$
<sup>33</sup> S	3/105	<sup>64</sup> Ni	1/80	93Nb	8/30	120Sn	
<sup>34</sup> S	2/58	<sup>63</sup> Cu	24/56	94Mo	21/240	122Sn	3/348
<sup>35</sup> Cl	6/82	<sup>65</sup> Cu	23/548	95Mo	30/60	124Sn	3/361
<sup>36</sup> Cl	268/274	<sup>64</sup> Zn	14/450		59/109	121Sb	4/192
<sup>37</sup> Cl	17/17	<sup>66</sup> Zn	2/402	<sup>96</sup> Mo <sup>97</sup> Mo	75/75	123Sb	9/300*
<sup>37</sup> Ar	140/144	<sup>67</sup> Zn	2/400	981/4	107/107	122Te	9/260*
40 A	4/4	687_	7/505	<sup>98</sup> Mo	159/159	<sup>123</sup> Te	15/396
<sup>40</sup> Ar	6/313	<sup>68</sup> Zn	17/292	<sup>100</sup> Mo	102/125	124TD-	3/361
$^{39}\mathrm{K}$	4/207	$^{70}\mathrm{Zn}$	5/192	<sup>99</sup> Tc	22/693	<sup>124</sup> Te	4/442

Table 1. (continued) Asterisks mark the data considered in this work.

Isotope	$N_{\rm B}/N_{\rm S}$	Isotope	$N_{\mathrm{B}}/N_{\mathrm{S}}$	Isotope	$N_{\mathrm{B}}/N_{\mathrm{S}}$	Isotope	$N_{ m B}/N_{ m S}$
<sup>125</sup> Te	6/297	<sup>148</sup> Nd	12/160	$^{170}\mathrm{Tm}$	0/13	$^{208}\mathrm{Pb}$	3/129
<sup>126</sup> Te	5/321	$^{150}\mathrm{Nd}$	11/92	<sup>168</sup> Yb	7/7	$^{209}\mathrm{Bi}$	35/134
<sup>128</sup> Te	5/40	<sup>147</sup> Pm	20/42	<sup>169</sup> Yb	2/22	$^{226}\mathrm{Ra}$	1/41
<sup>130</sup> Te	4/23	<sup>144</sup> Sm	129/207	<sup>170</sup> Yb	2/24	$^{229}{ m Th}$	1/31
<sup>127</sup> I	729/729	<sup>147</sup> Sm	144/222	<sup>171</sup> Yb	2/170	<sup>230</sup> Th	1/30
129 <sub>I</sub>	406/406	148Sm	26/26	<sup>172</sup> Yb	2/101	$^{232}\mathrm{Th}$	920/1260*
<sup>124</sup> Xe	5/5	<sup>149</sup> Sm	3/160	<sup>173</sup> Yb	2/167	$^{231}$ Pa	3/138
<sup>126</sup> Xe	5/5	<sup>150</sup> Sm	3/25	<sup>174</sup> Yb	2/79	$^{232}$ Pa	1/33
<sup>128</sup> Xe	15/15	<sup>151</sup> Sm	525/526	<sup>176</sup> Yb	2/69	$^{233}$ Pa	93/93
<sup>129</sup> Xe	2/71	<sup>152</sup> Sm	0/92	<sup>175</sup> Lu	3/449	$^{232}{ m U}$	0/44
<sup>130</sup> Xe	19/19	<sup>154</sup> Sm	0/36	<sup>176</sup> Lu	2/59	$^{233}{ m U}$	0/770*
<sup>131</sup> Xe	24/48	<sup>151</sup> Eu	2/106	<sup>174</sup> Hf	11/11	$^{234}{ m U}$	2/144
<sup>132</sup> Xe	1/7	<sup>152</sup> Eu	2/25	<sup>176</sup> Hf	7/128	$^{235}{ m U}$	0/3184*
<sup>134</sup> Xe	1/7	<sup>153</sup> Eu	2/77	$^{187}\mathrm{Re}$	5/399	<sup>236</sup> U	12/297
<sup>135</sup> Xe	1/1	<sup>154</sup> Eu	3/20	<sup>186</sup> Os	4/133*	$^{237}{ m U}$	0/36
<sup>136</sup> Xe	1/36	<sup>155</sup> Eu	7/7	<sup>187</sup> Os	2/311	$^{238}\mathrm{U}$	3302/3606*
<sup>133</sup> Cs	324/327	$^{152}\mathrm{Gd}$	20/129	<sup>188</sup> Os	2/115	<sup>236</sup> Np	1/41
<sup>134</sup> Cs	1/8	$^{153}\mathrm{Gd}$	3/10	<sup>189</sup> Os	1/713	$^{237}\mathrm{Np}$	2/1214
<sup>135</sup> Cs	2/7	$^{154}\mathrm{Gd}$	20/162	<sup>190</sup> Os	1/24	$^{238}\mathrm{Np}$	1/17
130Ba	2/41	$^{155}\mathrm{Gd}$	96/122	<sup>192</sup> Os	1/20	<sup>236</sup> Pu	2/2
<sup>132</sup> Ba	3/18	<sup>156</sup> Gd	10/87	<sup>191</sup> Ir	3/63	<sup>238</sup> Pu	1/64
<sup>133</sup> Ba	6/6	<sup>157</sup> Gd	58/89	<sup>192</sup> Ir	2/11	<sup>239</sup> Pu	4/1040*
<sup>134</sup> Ba	21/311	<sup>158</sup> Gd	5/96	<sup>193</sup> Ir	2/54	<sup>240</sup> Pu	6/430*
<sup>135</sup> Ba	90/156	<sup>160</sup> Gd	2/58	<sup>192</sup> Pt	156/156	<sup>241</sup> Pu	35/243
136Ba	3/295	<sup>159</sup> Tb	3/504	<sup>194</sup> Pt	5/8	<sup>242</sup> Pu	0/255*
<sup>137</sup> Ba	2/82	$^{160}\mathrm{Tb}$	4/4	<sup>195</sup> Pt	3/45	<sup>244</sup> Pu	0/35*
$^{138}$ Ba	3/147	<sup>156</sup> Dy	4/20	<sup>196</sup> Pt	6/6	<sup>241</sup> Am	35/195
138La	2/11	<sup>158</sup> Dy	7/7	<sup>198</sup> Pt	5/5	<sup>242</sup> Am <sup>m</sup>	4/106
<sup>139</sup> La	86/181	<sup>160</sup> Dy	5/114	<sup>197</sup> Au	265/265	<sup>243</sup> Am	16/241
<sup>136</sup> Ce	1/10	<sup>161</sup> Dy	9/256	<sup>198</sup> Hg	1/73	<sup>242</sup> Cm	0/13
<sup>140</sup> Ce	1/199*	$^{162}\mathrm{Dy}$	8/142	<sup>199</sup> Hg	2/88	<sup>243</sup> Cm	0/105
<sup>141</sup> Ce	0/7	<sup>163</sup> Dy	3/131	<sup>200</sup> Hg	3/45	<sup>244</sup> Cm	0/68
<sup>142</sup> Ce	1/77	<sup>164</sup> Dy	6/117	<sup>201</sup> Hg	2/86	<sup>245</sup> Cm	1/91
141Pr	16/350	<sup>165</sup> Ho	4/374	<sup>202</sup> Hg	2/38	<sup>246</sup> Cm	1/17
<sup>143</sup> Pr	3/6	<sup>162</sup> Er	2/18	<sup>204</sup> Hg	1/23	<sup>247</sup> Cm	1/44
142Nd	95/98	<sup>164</sup> Er	2/19	<sup>203</sup> Tl	6/139	<sup>248</sup> Cm	1/51
<sup>143</sup> Nd	15/151	<sup>166</sup> Er	2/175	<sup>204</sup> Tl	2/2	<sup>249</sup> Bk	2/40
144Nd	102/102	<sup>167</sup> Er	6/277	$^{205}{ m Tl}$	6/445	<sup>249</sup> Cf	1/63
<sup>145</sup> Nd	24/213	<sup>168</sup> Er	0/130	<sup>204</sup> Pb	540/829	<sup>250</sup> Cf	4/4
146Nd	2/119	<sup>170</sup> Er	0/125	<sup>206</sup> Pb	321/772	<sup>251</sup> Cf	4/4
<sup>147</sup> Nd	1/12	<sup>169</sup> Tm	1/431	<sup>207</sup> Pb	29/950	<sup>252</sup> Cf	22/37
			,	l			-,

### 2 Few-nucleon effects in neutron resonance positions

Neutron resonances correspond to the highly excited nuclear states. At the first approximation the statistical model provides the description of general properties of measured neutron resonance spectra, but there are numerous observation of the presence of nonstatistical effects in such complex spectra. To understand these effects a look at the dynamics of the interaction of an incoming neutron with the target nucleus is needed. In Fig.1 [10] a sequential series of nucleon interaction during the neutron capture are shown schematically. Direct radiative capture and  $\gamma$ -transitions in the compound nucleus are shown in the bottom part. The first interaction of the incoming neutron with nucleons of the target nucleus shown in the upper part of Fig.1 results in formation of particle-hole excitation which serves as the "doorway state" mechanism considered by Feshbach. Complicated structures shown at right is the first steps of the compound nucleus formation.

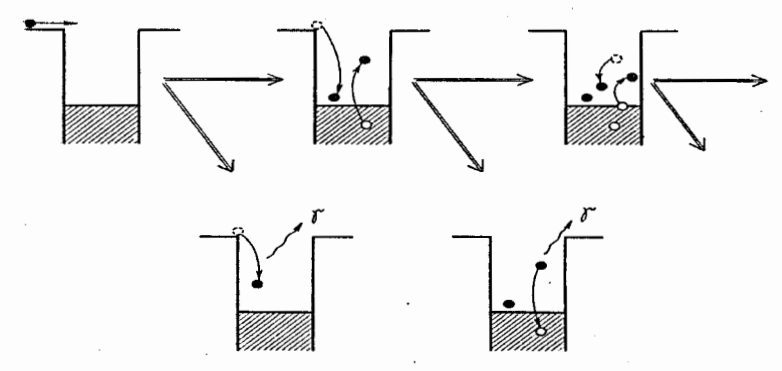


Fig. 1. Formation of the doorway state of the type two particle-one hole with its radiative decay (below) or transformation into a more complex state (three particle-two holes).

The parameters for description of doorway state effects can be estimated from the known splitting of low-energy states in near-magic nuclei. According to the doorway state model even at high-energy excitation one can see intervals due to quasi-particle excitation. They can be noticed in shift of strong resonances relative to the neutron binding energy or as the stable splitting between resonances. Quasi-particle excitation can be observed also as stable spacing in spectra of bound levels. The combined analysis of these effects could be useful for the development of microscopic models. For example, during the neutron cross section measurement of 140Ce (isotope with the magic neutron number N=82 and closed proton subshell Z=58) it was noticed by Ohkubo [11] that an exact rational relation 9:4 exists between positions of strongest neutron resonances 21.4 keV/(9.5 keV= $\delta$ ). The first interval was found also in spacing of all s-resonances of the same 141Ce [1,4] (seen as maxima at 21.7, 43 and 86 keV= $9\delta'$  in D-distribution). The few-nucleon origin of this effect is supported by the fact that the real residual interaction of three valence neutrons above the closed-shell core Z=58,N=82 derived from the observed small splitting of <sup>143</sup>Ce ground state, namely,  $E_1^*=18.9(1)$  keV= $2\delta'$  and 42.3(1) keV are exactly twice the positions of resonances considered by Ohkubo (intervals  $D=n\delta'$  were found also in other nuclei).

## 3 Door-way states at high-energy excitations of <sup>233</sup>Th

Ohkubo, Weigman and Rohr directly connected nonstatistical effects in neutron resonance data with the doorway states mechanism which was considered also by several authors for explaining nonstatistical character of PNC-effect in <sup>232</sup>Th resonances [3]. Correlations of signs in PNC parameters  $P_i$  in <sup>232</sup>Th was clearly seen: all ten the first resonances had the same sign of the parameter P<sub>i</sub> and the occasional probability of such situation was found to be very small. Correlation in  $P_i$ -signs was considered as an example of an influence of fewnucleon doorway states effect [3] due to the fact that in the thorium (Z=90) a subshell  $2f_{7/2}$  is filled up with 8 protons above the core  $Z_o=82$  and hence few-nucleon effects might be directly seen even in the resonance spectrum. Really, nonstatistical character of D<sub>i</sub>-distribution was discussed by Havens. Results of the analysis of the recent data on s-resonances of <sup>232</sup>Th are shown in Fig.2 (left). Maximum at 22 eV corresponds to the effect found by Havens but here all spacing  $(D_{i,j})$  are considered (not only spacing between neighbor resonances  $D_{i,i+1}$ ). In such distributions long-range correlations could be observed. By selection of the relatively strong resonances ( $\Gamma_a \geq 1 \text{meV}$ ) the longrange correlation with D=570 eV appears (Fig.2 right). Analogous effects were found in <sup>123</sup>Sb (Fig.2 bottom), <sup>79</sup>Br, <sup>89</sup>Sr, <sup>133</sup>Cs [1]. The ratios between observed D, namely, 748:594:571:373:22 eV=34.0: 27.0: 26.0: 16.95: 1 are close to integers of the 22 eV. Grouping effects in resonance spacing with similar parameters D=748-749 eV and two-fold values 1495-1497 eV were found [1] in the neighbor compound nuclei 104Rh and 105Pd.

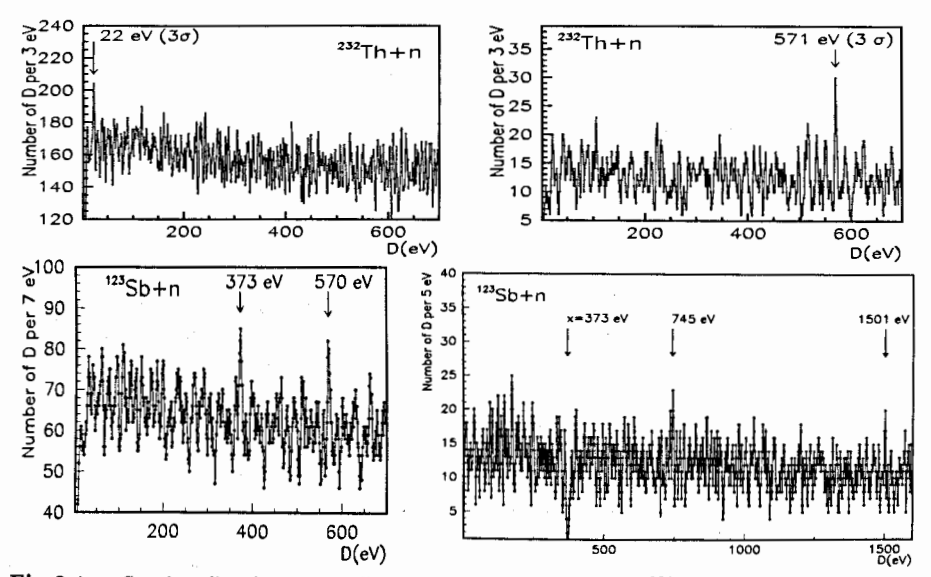
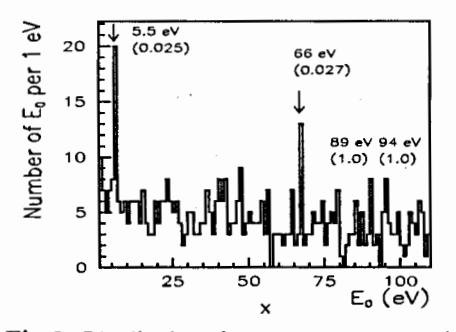


Fig. 2 top: Spacing distribution in all and in strong resonances of  $^{232}$ Th. bottom: Spacing distribution in all resonances of  $^{123}$ Sb and distribution of intervals  $D^{AIM}$  adjusted to fixed D=373 eV (a maximum in D-distribution); the appearance of maxima at multiple values 745 eV=2×373 eV and 1501 eV=4×373 eV shows the stable character of D=373 eV.

# 4 Correlations in positions of resonances of <sup>75</sup>As, <sup>123</sup>Sb, other nuclei observed by Ideno, Ohkubo, Belyaev

The discussed value 22 eV, its threefold value 66 eV and 5.5 eV=22 eV/4 were found earlier as parameters of grouping effects in positions of resonances in all nuclei [12,13] (see Fig.3). For example Ohkubo noticed nonstatistical character of resonance positions in  $^{184}$ W [14], while in the neighbour  $^{187}$ Os all four first resonances (with  $E_o$  <130 eV) are situated at integers of the period  $2\delta''=22$  eV ( $E_o=22.4$ , 44.7, 66.3, 89.7 eV).



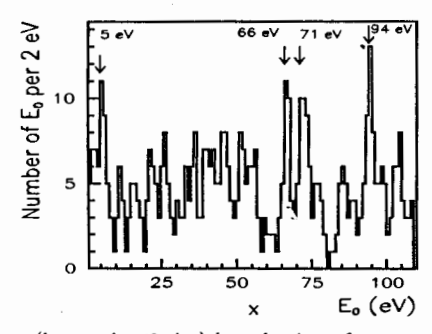


Fig.3. Distribution of neutron resonance positions (known in 70-ties) by selection of one resonance (max  $\Gamma_n^0$ ) in intervals 10 eV, 100 eV; n=1,12,13,17 of the period 5.5 eV are marked.

It was suggested by Izumo [15] that results of the study of D-distribution performed by Ideno, Ohkubo and Belyaev [16,17] can be summarized as the existence of the common period of 5.5 eV (or Poincare cycle  $7.5\times10^{-16}$  s) in the  $^{108}$ Ag,  $^{124}$ Sb,  $^{128}$ I,  $^{134}$ Cs,  $^{139}$ La,  $^{144,146}$ Nd compound nuclei, the period of  $11 \text{ eV}=2\times5.5 \text{ eV}=\delta''$  ( $3.7\times10^{-16}$  s) in the  $^{145,149}$ Nd,  $^{153}$ Sm,  $^{161}$ Gd,  $^{167}$ Sr,  $^{171}$ Er,  $^{239}$ U compound nuclei, the period of 37 eV=143 eV/4 ( $1.12\times10^{-16}$  s) in the  $^{128}$ I,  $^{145}$ Nd,  $^{153}$ Sm,  $^{167,171}$ Er,  $^{175}$ Yb,  $^{196}$ Pt. The Poincare cycles are mainly determined in terms of the elementary interactions among the nucleons inside the nucleus rather than the nuclear size. The cycle is proportional to the number of two-body interactions, that is  $t_n\approx (1/2)n(n-1)t_0$ , where  $t_0$  is the parameter given by the two-body interaction  $t_0\approx 10^{-22}$  s [15,18] ( $\delta''=11 \text{ eV}-a$  common fundamental parameter).

The correlation program "Period" was developed by Ideno and Ohkubo to study a recurrence in spacing distributions in neutron resonances. Response function for each period "x" and multiplicity "k" in it reflects a deviation from statistical expectation for varying value of the interval "x" or integers of " $n \times x$ " (Muradyan noticed that standard deviations  $\sigma$  are unapplicable here due to the lack of independence of values  $n \times x$ ).

Results of application of "Period"-program to resonances of <sup>76</sup>As are shown in Fig.4, top. Distribution of spacing in all resonances in the energy region of 1.8-6.2 keV (multiplicity k=1) given at left is usual histogram with the step of 1 eV and averaging interval 9 eV. At right the response function with k=10 is shown, see also [19] where a periodical disposition of 12 resonances with a period  $2\times143$  eV= $13\times22$  eV=286 eV was found to have an occasional probability less then 1%. The intervals D=572 eV in  $^{232}$ Th and  $^{123}$ Sb (Fig.2) and grouping in positions of strong resonances in all nuclei with Z=33-56 at the same energy 572 eV [1] correspond to four-fold value of the period D=143 eV= $13\delta''$ .

It was noticed [16] that in several cases strong resonances are divided by intervals  $n\times143$  eV formed by spacing between weak resonances (Fig.4 center). The intervals D=143 eV in <sup>76</sup>As and D=213 eV in <sup>141</sup>Pu (see Fig. 4 bottom) form the ratio 2:3 [20].

Systematic character of the  $E_n$  disposition as the recurrence of intervals 55 eV and 88 eV found in <sup>124</sup>Sb [11,16] is shown in Fig.5, top. From this picture one can conclude that strong resonances are located at energies  $E_n$  represented as integers n=9-13-17 of the period of 88 eV/2=44 eV=4 $\delta$ ". Numbers n=13 and 17 correspond to maxima in D-distribution in the same nucleus at D=570 eV and 2×373 eV=745 eV (Fig.2 bottom).

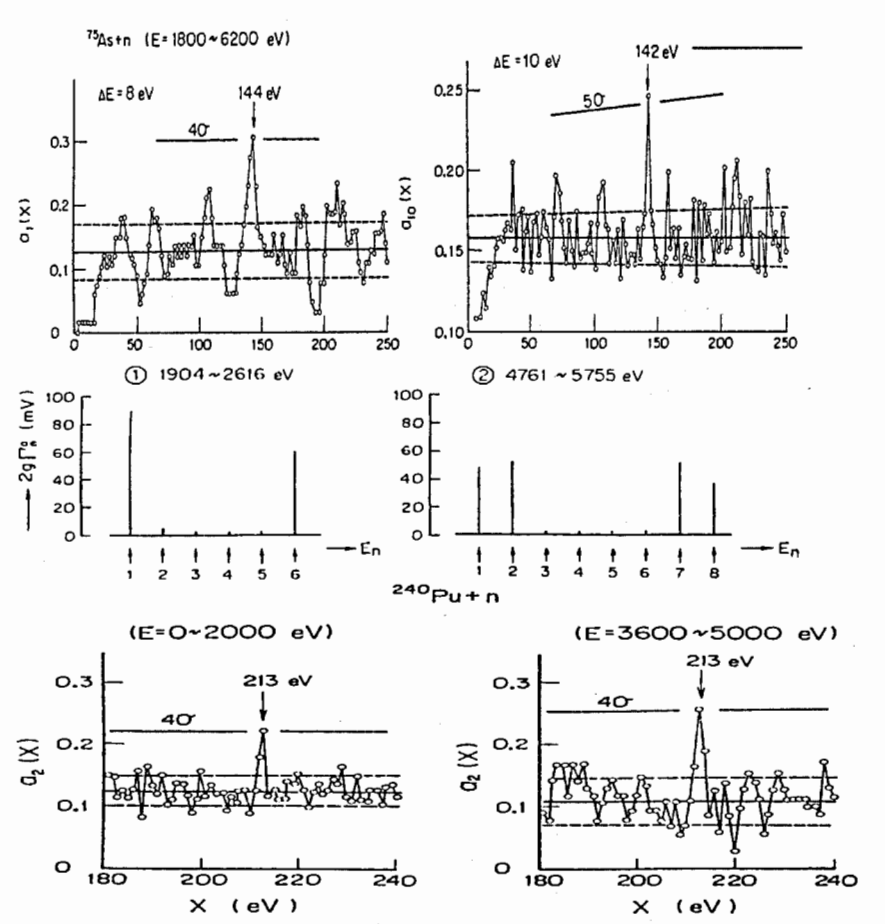


Fig. 4 (from [16]). Top: Results of application of "Period"-program to positions of <sup>76</sup>As resonances with multiplicity factors k=1 (left) and k=10 (see correct estimates in [21]). Center: Correlation in positions of <sup>75</sup>As resonances and reduced neutron widths. Bottom: Application of the "Period"-program to <sup>240</sup>Pu resonances in two energy regions.

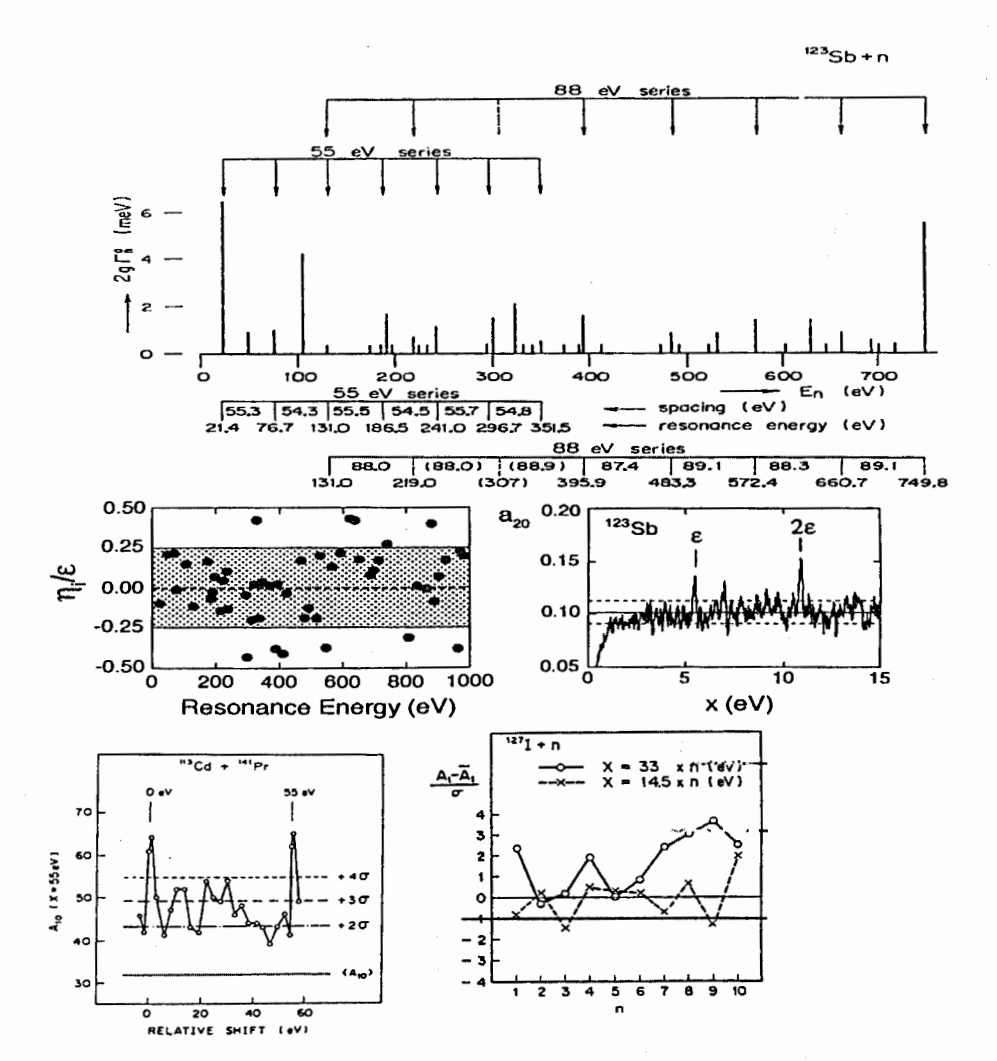


Fig. 5. Top: Positions and reduced widths of neutron resonances in <sup>123</sup>Sb with respect to the periods of 55 eV= $5\delta''$  and 88 eV= $8\delta''$  considered by Ohkubo [11,16].

Center and bottom: Results of application of different correlation programs developed by Ideno: [22-24,16] to different files of neutron resonance data:

center: Differences between resonance positions in  $^{123}\mathrm{Sb}$  and integers of 5.5 eV= $\delta^{\prime\prime}/2.$ 

bottom left: Correlations in positions of resonances <sup>113</sup>Cd and <sup>141</sup>Pr; spectra of resonances in these nuclei are summarized after one of them is shifted on the variable value (displayed along the horizontal axis);

bottom right: Period 33 eV= $3\delta''$  in resonances of  $^{127}$ I and dependence of correlation effect in positions of  $^{127}$ I resonances on the multiplicity parameter in the program "Period". The maximum at n=9 corresponds to D= $9\times33$  eV=297 eV found independently by Belyaev [17].

Three methods of correlation analysis of nonstatistical effects in neutron resonance positions were developed by Ideno [22-25,17].

- 1). In Fig.5 (center) a search for the grouping effect around the period (with the varying value x) is demonstrated in case of  $^{124}$ Sb-resonances (period x=11 eV=2× $\varepsilon$ = $\delta''$ ).
- 2). A study of the combined data with positions of resonances belonging to different isotopes ( $^{114}$ Cd and  $^{142}$ Pr in the case shown in Fig.5 bottom left) resulted in the determination of common stable interval of 55 eV=5 $\delta''$ .
- 3). The complex study of data on resonances of  $^{235}$ U-target [25] and the selection of multiplicity factor k in the "Period"-program (here 33 eV=3 $\delta$ " period in  $^{128}$ I presented in Fig.4 bottom right) are explained in the original works.

The general idea in the analysis of superfine-structure effects (stable intervals of the scale of tens or hundreds of eV, period 11 eV= $\delta''$  [18]) as well as fine-structure effects (stable intervals of the scale of tens or hundreds of keV, period 9.5 keV= $\delta'$  [11] discussed earlier) is a check of relations between interval's values. Izumo-Ohkubo phenomenology in the description of common effects in different nuclei is the first step in this direction.

The great number of new resonance parameters collected in NRF-3 permits expansion of the above discussed data analysis. We describe first results obtained for heavy deformed nuclei (Table 2, Fig.6), after that we consider briefly results for resonances in <sup>114</sup>Cd, <sup>110</sup>Ag, <sup>122,124</sup>Sb and finally, for resonances in <sup>32</sup>P. Correspondingly, in three separate sections of Table.3 positions of maxima in D-distributions for these nuclei are displayed.

### 5 Analysis of data from NRF-3 compilation

Heavy deformed nuclei have many common excitations in their spectra. In Table 2 a stable character of excitations  $E^*(2^+)$  and  $E^*(8^+)$  in ground state bands of Z=90-94 isotopes can be seen and similar stable intervals D were found in spacings [8]. The ratio 1:12 between boxed  $E^*$ =42.5 keV and 510 keV corresponds to a constant inertial parameter 7.2 keV=6 $\varepsilon'$  (expected ratio  $J^8(J^8+1)/J^2(J^2+1)$ =72/6=12 in  $J^2$ -dependence).

Table 2. Excitations in heavy nuclei close to 42.5 keV= $\varepsilon_o/24$  and m(85 keV= $\varepsilon_o/12$ ).

Nucleus	<sup>229</sup> Th	<sup>230</sup> Th	<sup>230</sup> Th	<sup>231</sup> Th	$^{232}{ m U}$		<sup>234</sup> U			<sup>236</sup> U	
$J_o^\pi, J_i^\pi$	$\frac{5}{2} + \frac{7}{2} +$	0+,8+	D	$\frac{5}{2} + \frac{7}{2} +$	0+,2+	0+,12+	2+	8+	12+	$0^{+},2^{+}$	8+
$E^*$ , keV	42.5	594	594	42.0	47.6	1111	43.5	497	1024	45.2	[522]
m	1/2	7	7	1/2	(1/2)	13	1/2	6	12	1/2	12
m⋅85 keV	42.5	595	595	42.5	42.5	1112	42.5	511	1022	42.5	511
Nucleus	<sup>236</sup> U		<sup>237</sup> U	<sup>238</sup> U			<sup>239</sup> U				<sup>240</sup> Ü
$J_o^{\pi}, J_i^{\pi}$	D	D	$\frac{1}{2} + \frac{17}{2} +$	0+,2+	8+	D	$\frac{5}{2} + \frac{7}{2} +$	D	D	D	0+,2+
$E^*$ ,keV	512	1022	518	44.9	518	512	42.5	43	87	170	45(1)
m	6	12	6	1/2	6	6	1/2	1/2	1	2	(1/2)
m.85  keV	511	1022	511	42.5	511	511	42.5	42.5	85	170	42.5
Nucleus	<sup>236</sup> Pu		<sup>236</sup> Pu		<sup>240</sup> Pu		<sup>241</sup> Pu	<sup>242</sup> Pu		<sup>244</sup> Pu	
$J_o^{\pi}, J_i^{\pi}$	0+,2+	8+	$0^+,2^+$	8+	0+,2+	8+	$\frac{5}{2} + \frac{7}{2} +$	$0^{+},2^{+}$	8+	2+	8+
$E^*$ ,keV	44.6	516	44.1	514	42.8	497	42.0	44.5	518	44.2	535
m	1/2	6	1/2	6	1/2	6	1/2	1/2	6	1/2	. 6
m⋅85 keV	42.5	511	42.5	511	42.5	511	42.5	42.5	•511	42.5	511

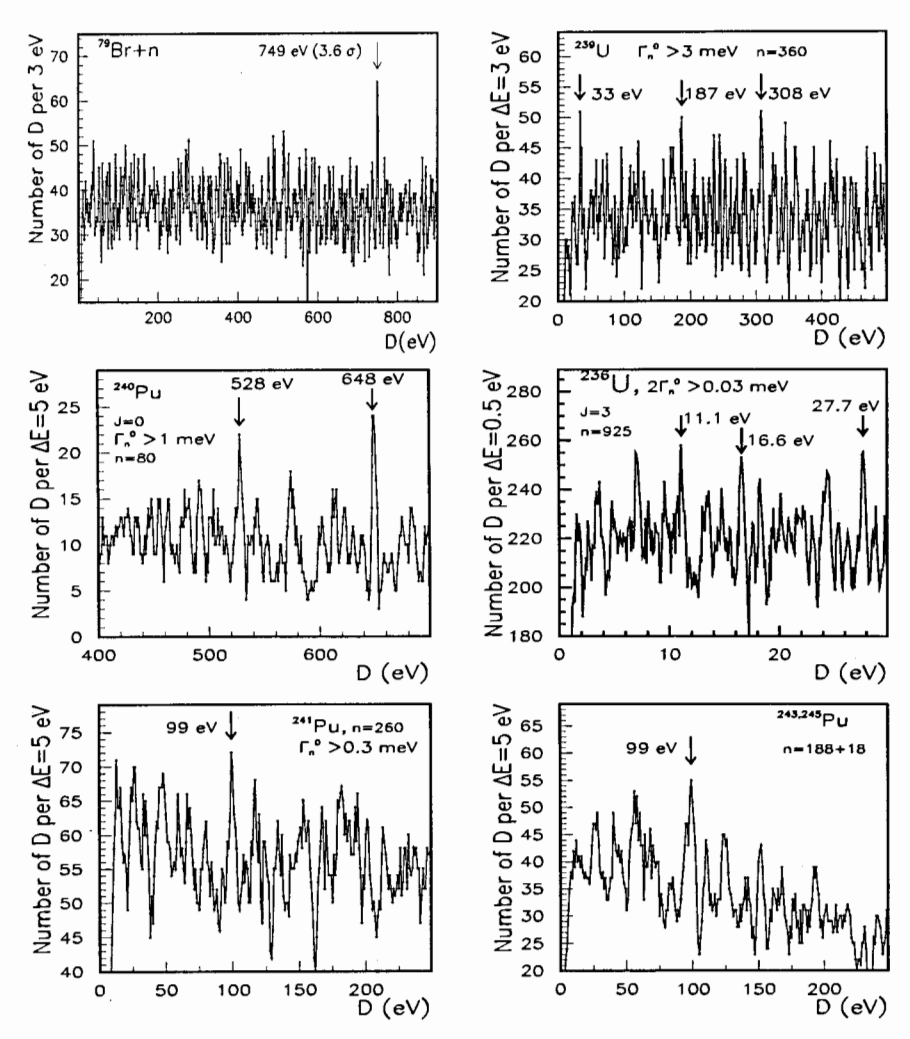


Fig. 6 Top: Spacing distribution in all resonances of <sup>79</sup>Br (target). Top right: Spacing distribution of relatively strong ( $\Gamma_n^o \ge 3$  meV) resonances of <sup>238</sup>U (target). Center: Spacing distributions of relatively strong ( $\Gamma_n^o \ge 1$  meV) 0<sup>+</sup> resonances of <sup>239</sup>Pu and relatively strong ( $\Gamma_n^o \ge 0.03$  meV) 3<sup>+</sup> resonances of <sup>235</sup>U (target). Bottom: Spacing distribution of relatively strong ( $\Gamma_n^o \ge 0.3$  meV) resonances of <sup>240</sup>Pu and sum distribution of all resonances of <sup>242</sup>Pu and <sup>244</sup>Pu (targets).

Table 3. Representation of parameters of tuning effect in particle masses (upper part) and stable mass/energy intervals in nuclear data by expression  $(n\times 16m_e(\alpha/2\pi)^x)\times m$  with the parameter  $\alpha=137^{-1}$  [26]. Boxed are the values interconnected by the same factor with the parameter  $\alpha_Z=129^{-1}$  for the short distances [4-8]. Asterisk marks stable nuclear fine structure intervals seen at low energy excitations and in resonances of Ca,Zr and Ce [1,4,27]. Results obtained with data from NRF-3 compilation are given in four bottom sections: 1) stable intervals shown in Figures 2-5 of this work and in [27]; 2) preliminary results on intervals in heavy nuclei; 3) the same for some near-magic nuclei; 4) the bottom section contains results of the correlation analysis of resonance positions in  $^{32}$ P obtained with data by Rohr at GELINA. The selection of the relatively strong resonances (with the threshold values of widths  $2\Gamma_n^l$  given at right) was found to be necessary for observation of the groupings in D.

$\overline{x}$	m 1	$1=\frac{1}{8}$	n=1	n=13	n=16	n=17	n=18	$^{A}\mathrm{Z},2\mathrm{g}\Gamma_{n}^{l}$
-1	1			$M_Z = 91.2$	$M_{H} = 115$			
GeV	3			_	$2m_t = 348$			
0	1	$\varepsilon_o$	$\delta = 16m_e$	$m_{\mu} = 105.7$	$f_{\pi}$	$m_{\pi}-m_{e}$	$147 = \Delta M_{\Delta}$	
MeV	1						$147 = \Delta E_B$	
	3				$M_q''=m_\omega/2$	$M_q' = 420$	$M_q = 441$	
	3						$441=\Delta E_B$	
1	1	$\varepsilon'$	$\delta' = 9.5*$	123*	152*	161*	$170*=\varepsilon_o/6$	
keV	2		19*	246*		324*	341*	$^{41,43}{ m Ca}$
	3			368*	455*	481*	$511=\varepsilon_o/2$	
	8	9.5*	76*	984*	1212*	$1293 = D_o^*$		<sup>91</sup> Zr, <sup>97</sup> Pd
	9		85*					<sup>141</sup> Ce
2	1		$\delta''=11$	144(4)	176(2)	187(1)		<sup>76</sup> As, <sup>88</sup> Sr, <sup>239</sup> U
eV	$^{2}$		22(1)	286				<sup>232</sup> Th, <sup>76</sup> As
	4	5.5		572(1)	704(2)	750, 749		<sup>232</sup> Th (1 meV), <sup>79</sup> Br
	6		66(1)					$\Sigma E_o$ , Fig.3
	8	11.1	88			1500, 1497		<sup>124</sup> Sb, <sup>104</sup> Rh, <sup>105</sup> Pd
	9		99(2)					oddPu, Fig.6
2	22	.8(2)	)					$^{234}U, \ge 0.2 \text{ meV}$
eV	3				523(2)		595(2)	$^{239}U, \ge 3 \text{ meV}$
	45	.6(2)	) .		1 ( )		791(2)	$^{239}{\rm U}, \ge 3 {\rm meV}$
	6						1185(1)	<sup>241</sup> Pu n=425
	8					1501(1)	( )	$^{239}U, \ge 5 \text{ meV}$
2	1						198(2)	<sup>124</sup> Sb n=259
eV	2						396(2)	$^{110}{ m Ag}, \ge 1 { m meV}$
	2				350(1)		. ,	<sup>114</sup> Cd n=481
	8		87(1)		` '	1503(1)		<sup>114</sup> Cd n=481
	9		97(1)			` '		<sup>114</sup> Cd n=481
	10		, ,	1446(3)				$^{122}\mathrm{Sb}, \geq 1~\mathrm{meV}$
	10			1432(1)				114Cd n=481
	12		132(1)	1722(1)			* :*	<sup>114</sup> Cd n=481
1	14						2314=	$^{32}$ P EXFOR $(\sigma_o)$
keV	16					$2584 = 2D_o$		$^{32}P n=485$

Results of the analysis of spacing of neutron resonances in heavy nuclei [8] and in  $^{80}$ Br are shown in Fig.6. Stable intervals  $D=n\delta''=n\cdot11$  eV with n=3,17,28 in compound nucleus  $^{239}$ U (top right), n=48,59 in strong  $J=0^+$  resonances of  $^{240}$ Pu and  $n=1,\frac{3}{2},\frac{5}{2}$  in  $^{236}$ U (center) as well as n=9 in  $^{241,243,245}$ Pu (bottom) can be compared with the structure observed in resonance positions (Fig.3, period 5.5 eV) and discussed by Izumo and others.

The second step in such a common approach to the nonstatistical effects in resonances consists in comparison of their values with the known stable excitations and intervals in low-lying levels. The factor  $1.16\cdot10^{-3}$  close to  $1/(32\times27)$  and to QED radiative correction  $\alpha/2\pi$  was found in [26,28]. Within such a model the superfine effect in resonances could be used for a check of the tuning effect in nuclear excitations and binding energies. By the later extrapolation we come to the observed long-range correlation in nuclear binding energies  $\Delta M_{\Delta}$  of the scale tens and hundreds of MeV (shown in Table 3 top) and to the tuning effect in particle masses discussed in [4-8]. The suggestion by Devons [9] that in fine nuclear effects one can see the hadronic structure is in line with the proposal by Nambu [29] to search for correlations in particle masses needed for Standard Model development.

#### References

- 1. Z.N.Soroko et al., Proc. ISINN-13, 2006, JINR E3-2006-7, p.205, ibid p.83.
- 2. S.F.Mughabghab, Neutron Resonance Parameters, BNL-325. Elsevier, 2006.
- 3. A.Brusegan et al., L-B New Series, vol. I/16C, Springer, 2004. Ed. H.Schopper.
- 4. S.I.Sukhoruchkin, Proc. Int. Conf. Nucl. Data for Science and Technol., Nice, 2007, p. 179; Z.Soroko, S.Sukhoruchkin, D.Sukhoruchkin, J. Nucl. Sci. Techn., Suppl. 2 Aug. (2002) 64.
- 5. S.I.Sukhoruchkin, Proc. CGS-13, Koeln, 2008. AIP, 2009 (to be publ.)
- 6. S.I.Sukhoruchkin, Int. Review of Physics, August Issue, 2008, Praise Worthy Prize publ.
- 7. S.I.Sukhoruchkin, Proc. 6-th Int. Conf. Persp. Hadr. Phys., Trieste, 2008, AIP 1056, p.55.
- 8. S.I.Sukhoruchkin, Proc. 17th Int. Spin Phys. Symp., Kyoto, 2006, AIP 915, p.272.
- 9. S.Devons, Proc. Rutherford Jubilee Int. Conf., Manchester, Ed.J.Birks, Heywood, p.611.
- 10. S.I.Sukhoruchkin, At. Energ. 29 (1970) 187.
- 11. M.Ohkubo, M.Mizumoto, Y.Nakajima, Report JAERI-M-93-012, 1993.
- 12. S.I.Sukhoruchkin, Proc. IAEA Conf. Nucl. Data for Reactors, Paris, 1966, v.1, p. 159.
- 13. S.I.Sukhoruchkin, Proc. Conf. Neutr. Cross Sections and Techn., Wash., 1968, v.2, p. 923.
- 14. M.Ohkubo, Yu.Kawarasaki, J. Nucl. Sci. Techn. (Tokyo) 21 (1984) 805.
- 15. K.lzumo, Prog. Theor. Phys. 54 (1975) 1378.
- 16. K.Ideno, M.Ohkubo, J. Phys. Soc. Japan 30 (1971) 620; K.Ideno ibid, 37 (1974) 581.
- 17. F.N.Belyaev, S.P.Borovlev, Yad. Fiz. 27 (1978) 289; Sov. J. Nucl. Phys. 27 (1978) 157.
- 18. M.Ohkubo, Phys. Rev. C 53 (1996) 1325.
- 19. S.I.Sukhoruchkin, Proc. ISINN-2, Dubna, 1994, JINR publ. E3-94-419, p.326.
- 20. M.Ohkubo, Proc. Symp. Nucl. Data, 2002, Tokai, JAERI-Conf. 2003-006, p.259.
- 21. M.Ohkubo et al., J. Phys. Soc. Japan 33 (1972) 1185.
- 22. K.Ideno, Proc. Int. Conf. Neutr. Research, Crete, 1997. SPIE Proc. Ser. Vol. 2867, p.398.
- 23. K.Ideno, Proc. Int. Conf. Nucl. Struct, Tokyo, Int. Ac. Pr. Co., Japan, 1977, p.478.
- 24. K.Ideno, Proc. Int. Conf. Nucl. Data Sci. Techn., Mito, 1988, p.783, Saikon Publ.
- 25. K.Ideno, Proc. 17th Int. Spin Phys. Symp., Kyoto, 2006, AIP 915, p.819.
- 26. S.I.Sukhoruchkin, Proc. Int. Conf. on Stat. Prop. Nucl., Albany, Plen. Press (1972), p.215.
- 27. S.I.Sukhoruchkin, Proc. ISINN-8, 2000, JINR E3-2000-192, p.420.
- 28. S.I.Sukhoruchkin, Proc. ISINN-3, 1995, JINR E3-95-307, p.182.
- 29. Y.Nambu, Nucl. Phys. A629, 3c (1998).

#### STUDY OF NEUTRON EMISSION IN HIGH-ENERGY REACTIONS WITH LEAD NUCLEI

#### V.I. Yurevich Laboratory of High Energy Physics, JINR, Joliot Curie 6, 141980 Dubna, Russia

During last two decades many experiments were dedicated to investigation of neutron production in proton-nucleus and nucleus-nucleus collisions in energy range above 100 MeV per nucleon. The interest is explained by (i) importance of these results for understanding of particle emission process in high-energy reaction, (ii) a key role of neutrons in various applications of accelerators in science and technology, (iii) importance of the neutron data for space research and development of theoretical codes for particle emission process simulation.

Investigation of the very hot nuclei is currently one of the most challenging topics of nuclear physics. An effective way to produce the hot nuclei with minimum excitation of collective modes is collisions of energetic hadrons and light nuclei with heavy nuclei.

Reactions with lead nuclei were studied in different laboratories with proton beam in energy range up to several GeV. In JINR/RI experiment [1,2], the neutron emission in p, d, <sup>4</sup>He, C+Pb collisions at 1-2 GeV/nucleon was investigated in TOF measurements with scintillation detectors in angular interval between 30° and 150°. The measurements of neutron energy spectra and yields for lead target are presented in table 1.

The aim of this neutron data analysis included

- · Description of neutron emission process with a phenomenological model,
- · Model fitting of neutron production double differential cross sections,
- · Dependence of neutron multiplicity on projectile energy,
- · Beam energy fraction coming to neutron production,
- Selection and study of neutrons emitted by hot nuclei,
- Determination of hot nucleus temperature.

Table 1. Experiments studied neutron production with lead target.

Laboratory	Beam	Energy (GeV)	Year	Data	Ref.
ITEP (Russia)	p	0.4 - 8.1	1983	ES	[3]
PSI/KfK (Germany)	p	0.6	1987	ES	[4]
LANL (USA)	p	0.1 - 0.8	1989-1993	ES	[5-10]
MRTI (Russia)	p	0.4 - 3.2	1995	Y	[11]
KEK (Japan)	· p	0.8, 1.5, 3	1995	ES	[12,13]
CERN (Switzerland)	p	1.2 -4.1	1997-1998	Y	[14,15]
Saclay (France)	p	0.8, 1.2, 1.6	1999	ES	[16,17]
Julich (Germany)	р	0.4 -2.5	2000, 2006	. Y	[18,19]
ITEP (Russia)	p	0.8, 1, 1.6	2003	ES	[20,21]
JINR/RI (Russia)	<i>p</i> , <i>d</i> , He, C	2, 2, 4, 24	2006	ES	[1,2]

ES - energy spectra of neutrons, Y - neutron yield.

The dependences of neutron multiplicity and energy coming to neutron production on projectile energy were estimated for p+Pb reaction by integration of the TOF results, listed above in the table, over energy and solid angle. Also the direct measurements of neutron yield were added. The found experimental values are shown in fig. 1 together with fit curves. The multiplicity data are good described by a fit expression

$$M = 39(1 - \exp(-0.22E_p))^{0.55},$$
 (1)

where  $E_p$  is the proton energy in GeV. This dependence is close to the Cugnon's formula [22] shown as dashed curve. Also the mean multiplicity of neutrons with energies above 20 MeV is given in fig.1. As one can see, a saturation of the mean neutron multiplicity value with the proton energy is observed above 1 GeV.

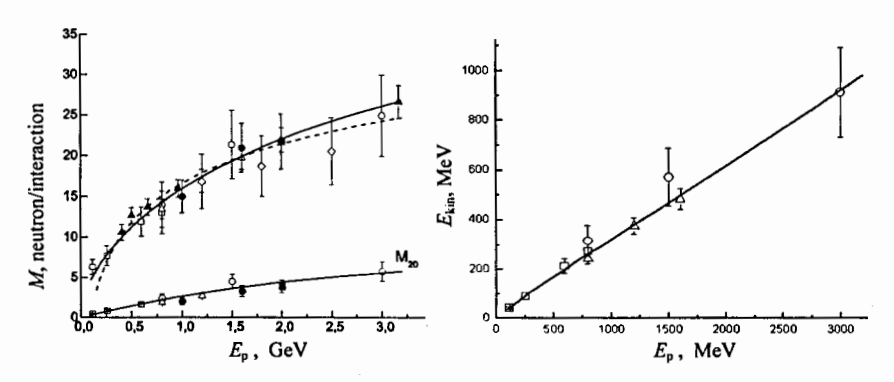


Fig.1. Energy dependences of (left) the mean neutron multiplicity for all neutrons and neutrons with E>20 MeV ( $M_{20}$ ) and (right) the neutron production energy for the reaction p+Pb:  $\blacksquare -[1,2]$ ,  $\square [5-10]$ ,  $\circ [12,13]$ ,  $\bullet [20,21]$ ,  $\Delta [16,17]$ ,  $\triangle [11]$  (corrected on high-energy neutron leakage),  $\Diamond [18,19]$ , the solid curves – the fits, the dashed curve – the formula from [22].

The total kinetic energy of emitted neutrons is approximately proportional to energy of incident protons, and it takes about 31% of the proton energy in GeV range. The main contribution of ~27% is given by neutrons with energies above 20 MeV. The neutron production energy can be found by adding the neutron separation energy, and it is estimated as  $W_n \sim 0.4E_p$ . Thus, the neutron emission plays important role in the reaction energy balance.

In high-energy collisions two processes, change-exchange reaction and projectile nucleus fragmentation, lead to emission of very energetic neutrons in forward direction, along beam trajectory, and form high-energy part of neutron spectra at small angles.

The neutron spectra in large angle region, above 30°, are formed by target nucleus decay. Here the traditional cascade-preequilibrium-evaporation approach is usually applied for experimental neutron data analysis. The fission is included to the evaporation mode. This idea was used for development of a phenomenological model with corresponding three moving sources, and the model was applied for neutron spectra fitting in reactions with protons at energies up to 3 GeV [23].

At the same time, recent investigations of light charged particle (LCP) and intermediate mass fragment (IMF) emission from hot nuclei, formed in central collisions of hadron and light nucleus with heavy nucleus at GeV energies, showed existence of new fast decay modes: hot non-equilibrium stage and thermal multifragmentation. Naturally, one can expect a multiple emission of neutrons at these both decay stages. It became a motivation to revise the neutron emission model and to add the new mechanisms to the modified moving source model (MSM).

A scheme of the nuclear system decay in central and peripheral collisions with emission of neutrons is shown in fig.2. This picture demonstrates the model conception where four neutron sources correspond to the main decay modes: (1) cascade, (2) hot source (fireball) decay, (3) fragmentation or multifragmentation, and (4) evaporation. It was made the assumption that the pre-equilibrium emission, taking place before the evaporation stage, is the second order process and gives a negligible contribution in comparison with the other four sources.

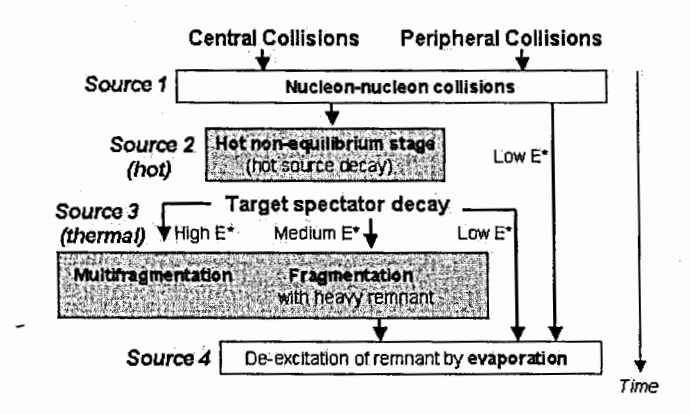


Fig.2. A scheme of the nuclear system evolution in central and peripheral collisions with heavy nuclei in GeV energy range.

The MSM is based on the traditional assumption that in a source frame the neutron emission is isotropic and the spectrum is described by Maxwellian-like distribution. The Lorentz transformation to the lab. frame gives the following formula for the model with four independent sources

$$\frac{d^2\sigma}{dEd\Omega} = \sum_{i=1}^4 pA_i \exp\{-(\frac{E+m-p\beta_i\cos\theta}{(1-\beta_i^2)^{1/2}} - m)/T_i\},\tag{2}$$

where the neutron momentum is calculated as  $p = (E^2 + 2Em)^{1/2}$ , E – the kinetic energy of neutron in lab. frame (MeV), m – the neutron rest mass (MeV),  $\theta$  – the angle of emitted neutron in lab. frame. There are three parameters for each the source: the amplitude  $A_i$ , the temperature  $T_i$  and the velocity  $\beta_i = V_i/c$ . In accordance with the picture of the decay processes (Fig.2), one can expect the following relations between the temperature and velocity parameters:  $T_1 > T_2 > T_3 > T_4$  and  $\beta_1 > \beta_2 > \beta_3 > \beta_4$ .

The model formula (2) was applied for fitting to the experimental neutron production double differential cross sections with selection of the source contributions. The fit curves and the neutron energy spectra measured with proton beam in KEK (1.5 and 3.0 GeV) [12,13] and in Dubna (2.0 GeV) [1,2] at angles of 30°, 90°, and 150° are presented in fig.3. The contributions of the different sources to the neutron spectra in reactions <sup>4</sup>He+Pb and <sup>12</sup>C+Pb [1] are shown in fig.4.

It is clearly seen that the MSM approach perfectly describes the experimental data considered in this analysis. The contributions of hot nucleus decay modes (sources 2 and 3) dominate in the middle part of the neutron spectra, in intervals 5-25 MeV and 25-70 MeV respectively.

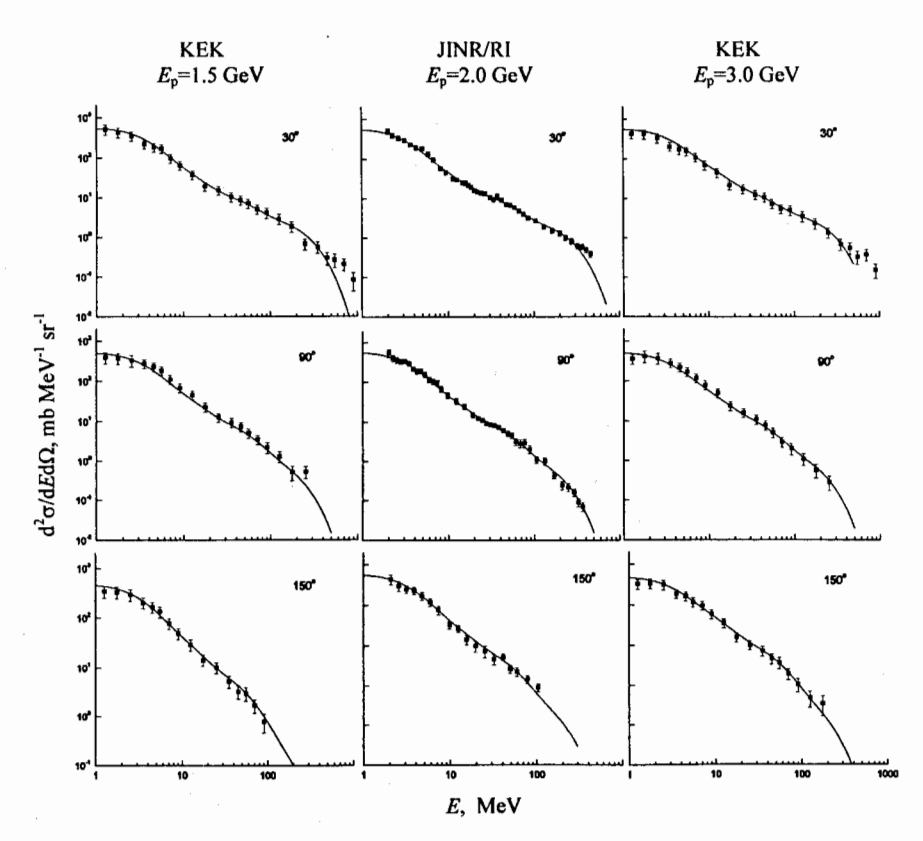


Fig. 3. Neutron energy spectra for reaction Pb(p,nx) at proton energies 1.5, 2.0, and 3.0 GeV: the points – the KEK [12,13] and JINR/RI [1,2] data, the curves – the fit (2).

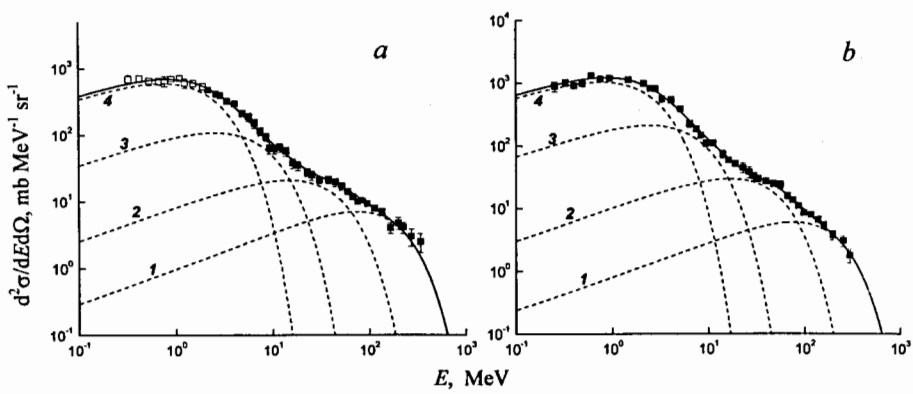


Fig.4. Contributions of the different sources to the neutron energy spectra measured in [1] with 1-AGeV  $^4$ He ( $\blacksquare -30^\circ$ ,  $\Box -60^\circ$ ) (a) and 2-AGeV  $^{12}$ C (53°) (b). The curve numbers – the source numbers.

The energy dependences of the source parameters are shown in fig.5 and fig.6. The temperatures weakly depend on energy and type of the projectile, and the values are practically constant in GeV region. The temperature decreases with the source number, or with a time of the nuclear system decay and de-excitation. The amplitude parameters monotonically increase with the beam energy and the source number. The velocity of source 1 is about 0.2, the 3<sup>rd</sup> source moves with the velocity of 0.005±0.002, and it is about zero for the 4<sup>th</sup> source. The hot source velocity goes down with proton energy, but in a case of the carbon projectile the value is somewhat higher of the magnitudes shown in fig.6 for the incident protons.

Thus, practically only 5 parameters (four source amplitudes and  $\beta_2$ ) have essential energy dependence and the approximations, shown in the figures, can be used for prediction of the neutron distributions. Here, it is important to note that the hot and fragmentation sources appear only if the proton energy exceeds ~0.5 GeV. Its contribution to the neutron production increase with energy and in GeV-energy range it reaches ~40% of total mean yield of neutrons in the reactions with lead nuclei.

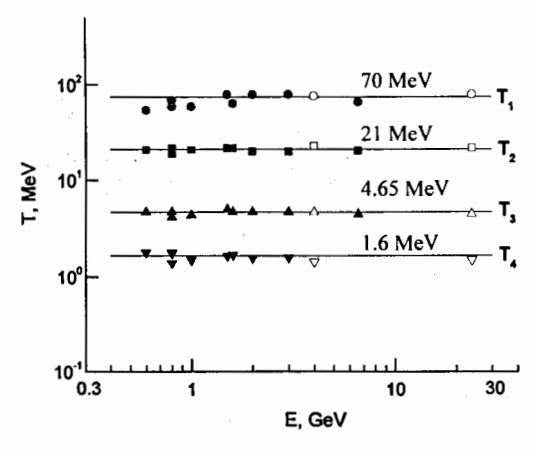


Fig. 5. Energy dependence of the source temperatures: the points – the found parameter values (the black symbols – the proton beam, the open symbols – the He and C beams), the curves – the fits.

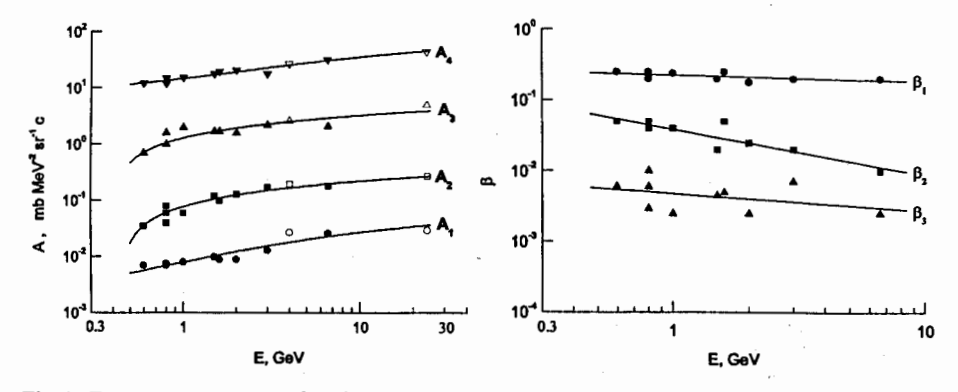


Fig.6. Energy dependences for the source amplitudes (left) and velocities (right): the points – the found parameter values, the curves – the fits.

The mean multiplicities of neutrons in collisions of 4-GeV <sup>4</sup>He and 24-GeV C with Pb nuclei, obtained as a sum of the source contributions, are 22.5±3.5 and 29.1±4.5 neutron/reaction respectively. These magnitudes are close to the predicted ones with the formula (1) for p+Pb reaction.

A comparison of the neutron production cross sections for the different decay modessources is shown in fig.7. The right figure presents the values for 1-GeV protons and 1-GeV/nucleon <sup>4</sup>He, and the left one gives the results for 2-GeV protons and 2-GeV/nucleon C. In the both cases the nuclear beams produce the neutrons with higher cross sections than the incident protons.

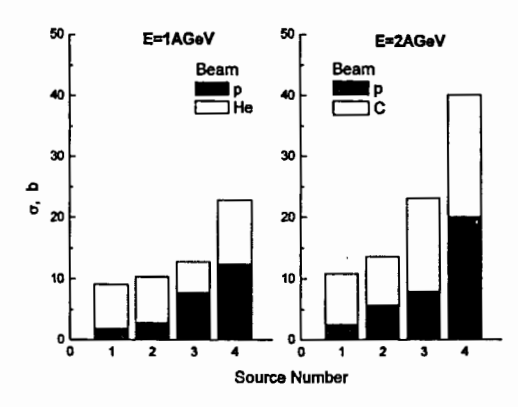


Fig. 7. Neutron production cross sections for the different decay modes, neutron sources, in reactions 1-AGeV p, <sup>4</sup>He + Pb (left) and 2-AGeV p, C + Pb (right).

The observed good agreement of the temperatures and the velocities for the neutron sources and the LCP and IMF sources proves the same particle origin. This is important conclusion because it demonstrates that the MSM is adequate to space-time picture of the high-energy reactions that was mainly investigated via study of charged particle and fragment emission.

Table 3. The estimations of the freeze-out temperature made with the different nuclear thermometers for the collisions of GeV light nuclei with heavy nuclei.

Year	Thermometer	$T_{\rm f}({ m MeV})$	Ref.
1998	$T_{He-DT}$	4.7±0.4	EOS [24]
1998	$T_{\text{slope}}(Z=2)$	4.5±0.3	Saclay [25]
2004	$T_{He-DT}$	5.0±0.5	ISiS [26]
2007	T <sub>He-Li</sub>	4.9±0.2	CHICSi [27]
	Neutron thermometer	4.65±0.15	

The multifragmentation phenomenon is often considered in terms of liquid-gas phase transition characterized by a freeze-out temperature  $T_f$ . This temperature corresponds to a moment when the decayed nuclear system becomes a system of independent nucleons and fragments. The estimation of the third neutron source temperature on slopes of the neutron energy spectra is effective direct method for determination of the  $T_f$  magnitude. By this method

we measure the value averaged over events with different excitation energies of the residues. Nowadays, several different nuclear thermometers based on (1) double ratios of isotopic yields, (2) slopes of kinetic-energy spectra of LCPs and thermal bremsstrahlung photons, (3) relative populations of excited states, and (4) isospin thermometer are widely used for this purpose. The numerical values of  $T_{\rm f}$  estimated with the *Neutron thermometer* and with the other methods in the EOS, ISiS, CHICSi, and Saclay experiments are listed in table 2 for comparison.

The first conclusion – the results very good agree with the magnitude  $T_{t,}$ =4.7 MeV. The second conclusion is a large potential of the *Neutron thermometer* method. Certainly, the potential of the *Neutron thermometer* method will be higher in measurements with selection of the central collisions by a special trigger. In this case the neutron yield from the hot and fragmentation sources will essentially exceed the contributions of the cascade and evaporation neutrons.

#### References

- 1. Yurevich V.I. et al. Yadernaya Fizika, 2006, V.69, P.1531.
- 2. Yurevich V.I. et al. Particles & Nuclei, Letters, 2006, V.3, P.49.
- 3. Bayukov Yu.D. et al. Preprint ITEP-172, M., 1983.
- 4. Cierjacks S. et al. Phys. Rev. C, 1987, V.36, P.1976.
- 5. Meier M.M. et al. Nucl. Sci. Eng., 1989, V.102, P.310.
- Meier M.M. et al. Nucl. Sci. Eng., 1992, V.110, P.289.
- 7. Stamer S. et al. Phys. Rev. C., 1993, V.47, P.1647.
- Meier M.M. et al. Proc. Int. Conf. on Nuclear Data for Basic and Applied Science. Santa Fe. 1985.
- 9. Amian W. B. et al. Nucl. Sci. Eng., 1993, V.115, P.1.
- 10. Amian W. B. et al. Nucl. Sci. Eng., 1992, V.112, P.78.
- 11. Vasilkov R.G. et al. Atomnaya Energiya, 1995, V.79, P.257.
- Nakamoto T. et al. Memoris of the Faculty of Engineering. Kyushu Univ., 1995, V.55, P.361.
- 13. Nakamoto T. et al. J. Nucl. Sci. Technol., 1995, V.32, P.827.
- 14. Pienkowski L. et al. Phys. Rev. C, 1997, V.56, P.1909.
- 15. Hilscher D. et al. Nucl. Instr. and Meth. A, 1998, V.414, P.100.
- 16. Ledoux X. et al. Phys. Rev. Lett., 1999, V.82, P.4412.
- 17. Leray S. et al. Phys. Rev. C, 2002, V.65, P.044621.
- 18. Letourneau A. et al. Nucl. Instr. and Meth. B, 2000, V.170, P.299.
- 19. Herbach C.-M. et al. Nucl. Instr. and Meth. A, 2006, V.562, P.729.
- 20. Trebukhovsky et al. Preprint ITEP 3-03, M., 2003.
- 21. Trebukhovsky et al. Yadernaya Fizika, 2005, V.68, P.4.
- 22. Cugnon J. et al. Nucl. Phys. A, 1997, V.625, P.729.
- 23. Kitsuki H. et al. J. Nucl. Sci. and Tech., 2001, V.38(1), P.1.
- 24. Hauger J.A. et al. Phys. Rev. C, 1998, V.57, P.764.
- 25. Ledoux X. et al. Phys. Rev. C, 1998, V.57, P.2375.
- 26. Bracken D.S. et al. Phys. Rev. C, 2004, V.69, P.034612.
- 27. Jakobsson B. et al. Phys. Lett. B, 2007, V.644, P.228.

# The search for the singlet deuteron in the radiative capture of the thermal neutrons by protons

S.B. Borzakov, N.A. Gundorin, L.B. Pikelner, N.V. Rebrova, K.V. Zhdanova

#### Frank Laboratory of Neutron Physics, JINR, Dubna, Russia

The first attempt to search for the singlet deuteron in the radiative capture of the thermal neutrons by protons with two gamma quanta emitted is described. The measurements have been made on IBR-2 reactor with help of HpGe detector. The obtained value of the upper limit of the cross-section is equal to 50 µb.

The nucleon-nucleon interaction at low energy is possible in two different spin-isospin states: J = 0, I = 1 and J = 1, I = 0, where J is the total momentum of the system and I is the isotopic spin. The singlet and triplet spin states are possible in the case of np-interaction only. The scattering lengths are known with high accuracy for both states. The unusually big value of singlet scattering length (-23.7 Fm) can be explained with help of idea about existing of metastable state with isotope spin I = 1 and total spin J = 0 [1-4]. These ideas contradict to the traditional description of the singlet interaction with the help of the virtual level which was obtained as a consequence of the effective range model [5]. But this model describes the scattering only and does not give the possibility to determine in a experiment the position of the virtual level. This feature is the considerable shortcoming of this model.

So, according to number of works, the quasistationary state which consists from the neutron and the proton with the isotope spin I = 1 and total spin J = 0 (the singlet deuteron), can exist. The mass of this quasistationary state is little less than to the sum of neutron and proton masses. If the singlet quasistationary exists the radiative capture of the thermal neutrons by protons with two gamma quanta is possible  $p(n_{tho}2\gamma)d$ . The first gamma quantum corresponds to the M1 transition from the continuous spectrum ( ${}^{3}S_{1}$ ) to the metastable singlet state ( ${}^{1}S_{0}$ ) and second gamma quantum - to the M1 transition from exited level to the ground state of the deuteron  ${}^{3}S_{1}$ . The main line in the reaction  $p(n_{tho}\gamma)d$  is the M1 transition with the

energy 2223.3 keV which is practically equal to the deuteron binding energy:  $E_{\gamma 0} = B_d - \Delta E$ , where  $B_d$  is the deuteron binding energy and  $\Delta E$  is the recoil energy (approximately 1 keV). The cross-section value of this reaction is known with the excellent accuracy:  $\sigma_{\gamma} = 334 \pm 0.5 mb$  [6]. For the investigated reaction the energy of first quantum is equal to the difference between deuteron binding energy and energy of exited level (66-90 keV [3], 66 keV [4]). The energy of the second quantum approximately is equal to 2134-2158 keV [3] or 2157 keV [4]. The sum of energies for two gamma-quanta is equal to the deuteron binding energy. According to the calculations made by R. Hackenburg the cross-section of the reaction  $p(n_{th},2\gamma)d$  is equal to 27 µb [4]. This value less than cross-section with the main transition in  $1.2 \times 10^4$  times.

The task of this work is the search for the two gamma-quanta channel of the radiative capture of the neutrons by hydrogen and the determination of the probability of this process. The solving of this task allows us to receive the experimental confirmation for the metastable state of nuclear system neutron and proton with the zero total momentum (so named singlet deuteron) or to determine the value of the high level of the cross-section for this process. The compton scattered gamma quanta from the main transition give us the background which is the base difficulty to solve this problem. The number of lines which have arisen as a result of the neutron radiative capture by elements surrounding the detector and the target (Al, Mn, Fe et al.) create the difficulties to solve this problem also.

The principal scheme of used combined correlative gamma spectrometer COCOS is shown on the Fig. 1. The neutron flux after the collimator with the diameter 15 mm falls in the target. The semiconductor HpGe detector with relative efficiency 34% and energy resolution 2.5 keV (for energy 1333 keV) was used to select and identify lines from exited levels of compound nuclei which have arisen after radiative neutron capture. Crystal BGO-scintillators which surround the target and HpGe detector have energy resolution 15-20% (for energy 511 keV) and absolute efficiency about 50%. They allow us to detect the cascade gamma-quanta and Compton scattered gamma-quanta from HpGe detector. The gamma spectrometer can work in coincidence regime and in the anticompton regime.

The measurements have been carried out at the neutron channel of the IBR-2 pulsed reactor (Dubna). The neutron flux density was equal to the value of  $5\times10^5$  n/sm<sup>2</sup> sec. The sample which was made from polyethylene was used for these measurements. The length of the sample was 40 mm and the diameter was 10 mm. The aluminium container which

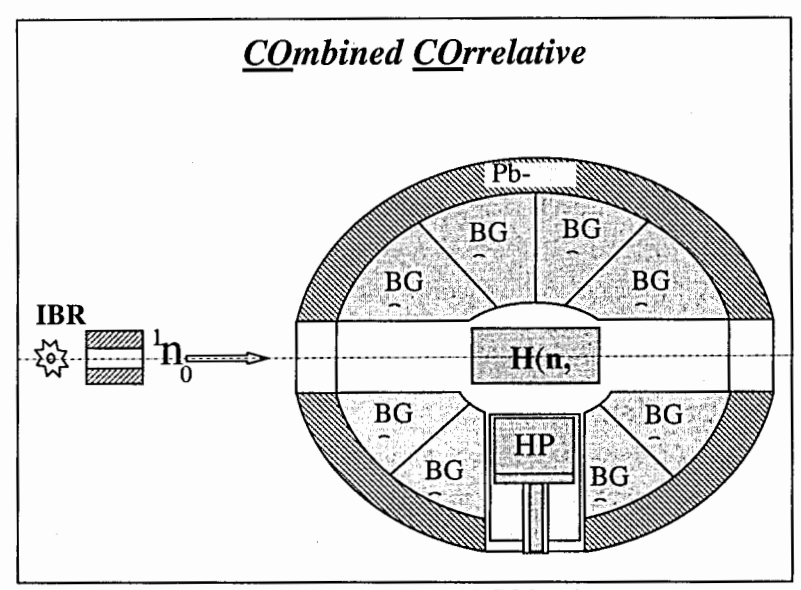


Fig. 1. The correlative gamma-spectrometer COCOS scheme.

contains the hydrogen sample have been placed at the distance of 15 cm from the HpGe detector. The detector was shielded from scattered neutrons by the 2 cm thick <sup>6</sup>LiF filter. The lead and polyethylene with boron (it is not shown in the Fig. 1) were used as the shield from background gamma-quanta and neutrons. The measurement time was 68 hours. The measurement of the background with the graphite sample was carried out. The graphite sample which scatters the neutrons approximately as the main sample was used. It had the length 38 mm and the diameter 13 mm. The measurement time was 93 hours. The computer program writes the codes from the HpGe detector and BGO-detectors for each event. The integral spectra for the control were obtained in the on-line regime. The final analysis was carried out in the off-line regime. The events which correspond to the thermal neutron capture have been selected.

The part of the spectrum from the HpGe detector is shown on the Fig. 2. The most intensive line in the picture is the hydrogen line 2223.3 keV with the peak area 1.8×10<sup>6</sup>. The number of the gamma lines from another elements have been observed. These lines are arisen

as the result of the prompt radiative capture or from activation of the elements surrounding the sample (see the table 1).

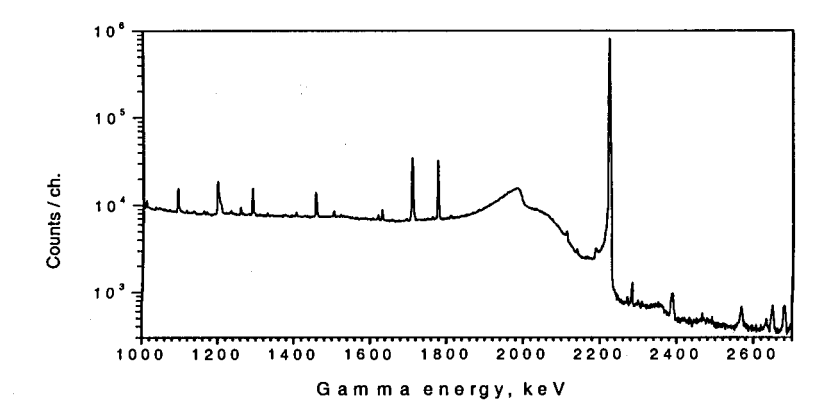


Fig. 2. The gamma quanta spectrum from the radiative capture of neutrons by the polyethylene sample.

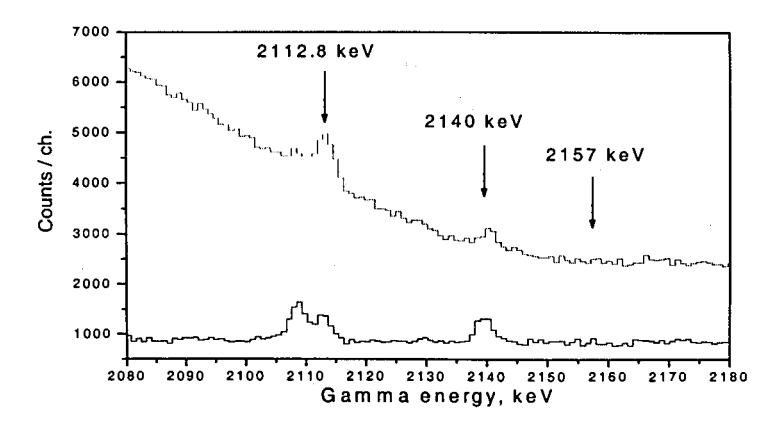


Fig. 3. The part of the gamma- quanta spectrum with the polyethylene and graphite (low histogram) samples.

The identification of the lines was carried out according to the photon energy and relative intensity of different transitions for one isotope. The data about these characteristics were taken from IAEA site [7] for thermal neutrons and from [8] for activation lines. The lines which are the result of activation are signed by the letter A in the table. We are searching

for the lines which exist in the spectrum with polyethylene sample but which don't arise in the background spectrum with the graphite sample.

The part of the spectrum where one can expect the line which we search for according to [3,4] is shown in the Fig. 3. The background lines (see the Table 1) are shown in this figure. The gamma energy predicted in the work [4] is shown also. One can see that statistically meaningful peak is absent. Consequently one can obtain the high level for the value of the cross-section for the  $\sigma(n+p \rightarrow d+2\gamma)$  reaction.

The table 1.

The number of	The gamma	The peak area	The isotope	Comment
amplitude	energy, keV	and its statistical		
channel.		error		
621	511.0		Annigilation	
718.5	595.4	30321 ± 716	Ge	
1006	844	14472 +/- 434	56Mn	A
1163.5	984.0	1541+/-255	27Al, (F?)	
1296	1099	12939 +/-354	59Fe	
1384	1171.5	1015+/-740	60Co	A
1417	1201.3	24211+/-419	DE(H)	
1567	1332	1091+/-257	60Co	
1902.4	1622.5	2117+/-188	27A1	
2005.4	1712.3		SE(H)	
2083	1778.9	53176+/-485	Al	A
2120	1810.6	1894+/-340	56Mn	A
2470	2112.8	600 +/- 200	56Mn	A
2501	2140	610 +/- 170	27A1	
2598.6	2223.3	1817211 +/- 5278	1H	

This evaluation have been made according to the formula:  $\sigma_{2\gamma} = \frac{3 \times \sqrt{N_2}}{N_1} \sigma_{\gamma} \frac{\varepsilon_1}{\varepsilon_2}$ , where  $N_I$  – is the peak area which corresponds to the main transition,  $N_2$  – is the area in the interval near hypothetical line with the energy 2134-2158 keV (interval width is equal to

three values of the detector resolution).  $\sigma_{\gamma}$  – is the cross-section for main transition,  $\varepsilon_{l}$ ,  $\varepsilon_{2}$  – are the efficiencies of the gamma-quanta. Because transition energies are approximately equal the difference of the efficiencies can be neglected. The obtained value of the high limit of the cross-section is equal to 50 µb.

We show in this work that the search for the singlet deuteron in the reaction  $p(n_{th}, 2\gamma)d$  does not need big neutron flux. The new experiments with the samples which contain the hydrogen are needed. The level of the sensitivity to the investigated line can be improved in several times with help of the methods of suppressing of Compton scattered gamma quanta.

The authors are grateful to D-r Yu.N. Pokotilovsky for the stimulated discussions of this problem.

#### Literature.

- K. Maltman, N. Isgur, Phys. Rev., D29, No. 5, p.952, 1984;
- 2. S.B. Borzakov, Physics of Atomic Nuclei, v. 57, p. 517, 1994;
- A.N. Ivanov et al., e-ArXiv:nucl-th/0407079, 2004;
- R. Hackenburg, Preprint BNL-77483-2007-JA, 2007;
- V.L. Lyuboshitz, V.V. Lyuboshitz, Report on ISINN-15, Dubna, 2007, Proceedings, p.37, Dubna, 2008.
- 6. Cox A.F., Wynchank A.R., Collie C.H., Nucl. Phys. 1965, v. 74, p. 497.
- 7. http://www-nds.iaea.org
- G. Erdman, W. Soyka, The Gamma Rays of the Radionuclides, Verlag Chemie, Weinheim, New York, 1979.

# LEVEL DENSITY AND RADIATIVE STRENGTH FUNCTIONS OF THE $^{237}$ U NUCLEUS FROM THE $(\overline{n}, \gamma)$ REACTION

V.A. Khitrov<sup>1</sup>, A.M. Sukhovoj<sup>1</sup>, V.M. Maslov<sup>2</sup>

<sup>1</sup>Joint Institute for Nuclear Research, Dubna, Russia <sup>2</sup>Joint Institute for Nuclear and Energy Research, Minsk-Sosny, Belarus

#### Abstract

The independent analysis of the published data on the intensities of the primary  $\gamma$ -quanta following resonance neutron capture in  $^{236}U$  has been performed. Distribution of these intensities about the mean value was approximated in different energy intervals of the primary gamma-transitions and neutrons. Extrapolation of the obtained functions to the zero registration threshold of the primary gamma-transition intensity allowed us to estimate (independently on the other experimental methods) expected level number of both parities for spin values J=1/2, 3/2 and sum of radiative widths for both electric and magnetic dipole gamma-transitions to levels with excitation energy up to  $\approx 2.3$  MeV. Level densities and sums of radiative strength functions determined in this way confirm characteristic behavior of analogous data derived from intensities of the two-step cascades following thermal neutron radiactive capture in nuclei from the mass-region  $40 \le A \le 200$ . Besides, this permits one to estimate sign and magnitude of systematic uncertainties for their model predicted values, at least, below one half of the neutron binding energy. Comparison with the model notions of level density testifies to super-liquid phase of this nucleus for the main part of excited levels, at least, below 2.3 MeV.

PACS: 21.10.Ma, 23.20.Lv, 27.90.+b

### 1 Introduction

Precise models of level density  $\rho$  and radiative strength functions  $k = \Gamma/(E_{\gamma}^3 D_{\lambda} A^{2/3})$  of the populated them primary dipole gamma-transitions at the neutron radiative capture are necessary for estimation of experimental neutron cross-sections and their calculation at lack of experimental data. First of all, it is necessary for actinides.

Available [1] models, most probably, do not satisfy modern requirements to these data [2]. Their insufficient quality is conditioned by clearly small volume of reliable experimental data on level density and emission probability, for example, of gamma-quanta. This results from significant errors of experiments performed up to now. Underestimation of uncertainties is largely caused by the use of obsolete notions of a nucleus for analysis of experiment.

An increase of reliability level of the experimental data on  $\rho$  and k demands one to develop new methods for their determination at obliged minimization of number of any assumptions and hypotheses of mechanism of used nuclear reaction.

This condition is in high extent satisfied in analysis of the two-step gamma-cascade intensities following thermal neutron capture [3]. By means of this analysis it was observed for the first time the clearly expressed step-wise structure with a width of  $\sim 2$  MeV in the level density  $\rho$  below  $\approx 0.5B_n$  in a large set of nuclei. Further development of this method [4] brought to an additional determination of unknown fact of strong dependence of partial widths  $\Gamma_{if}$  of not only primary but also following gamma-transitions on the energy of the excited levels f in the region of the structure mentioned above.

Intensities  $I_{\gamma\gamma}$  were measured up to now only for the case of thermal neutron capture. Accumulated experimental data allowed one to determine the  $\rho$  and k values for 42 nuclei [3] (in the framework of standard hypothesis [5, 6] on independence of radiative strength functions on nuclear excitation energy). For two tens of them these data were obtained at relatively realistic accounting for function  $k(E_{\gamma}, E_{ex})$ , experimentally estimated below excitation energy  $E_{ex} \sim 3-5$  MeV [4].

It should be noted that the observed in [4] considerable diviation of relation  $R = k(E_{\gamma}, E_{ex})/k(E_{\gamma}, E_{ex} = B_n) = 1$  indirectly and relatively weekly influences the determined parameters of the cascade gamma-decay. This conclusion is true for the analysis of the intensities of the two-step gamma-cascades to the final levels with excitation energy  $E_{ex} < 1$  MeV. In this case, the maximum change in the calculated total radiative width of cascade intermediate level (with accounting for function  $k(E_{\gamma}, E_{ex})$  derived from experiment) brings to decrease in the obtained according to [4] value of  $\rho$  in region of step-wise structure by a factor not more than 2 as compared with [3]. Therefore, method [4] provides the  $\rho$  and k values with the least at present systematic errors [7].

Nevertheless, obviously observed dependence of cascade intensity on the structure of all three levels included initial compound-state [8] stipulates for necessity to get new experimental data on  $\rho$  and k from the other experiments devoted to investigation of gamma-decay. In addition, the methods [3, 4] belong to class of reverse problems (determination of unknown parameters of functions measured in experiment) and, that is why, they require maximum possible verification and revealing all sources of systematic errors. In practice, this condition stipulates for necessity to get additional set of data on  $\rho$  and k from the maximum number of independent experiments. It is necessary also to solve the problem of estimating possible dependence of found according to [3, 4] gamma-decay parameters of high-lying levels on energy of neutron resonances  $\lambda$  and probable influence of their structures on the process under study. On the whole, analysis of the tendencies in determining  $\rho$  and k from solution of reverse tasks points to necessity in further investigations aimed to:

- · estimation of adequacy of model notions of gamma-decay process to experiment and
- direct accounting for the coexistence and strong interaction between Fermi- and Bose-systems in the radiative strength function models. This must be done also in more details and more precisely in the level density models for nuclei of any mass and type.

# 2 Experimental data from the $(\overline{n}, \gamma)$ reaction and method of their analysis

Both solution of the problem of correctness of model notions and necessity to study influence of the structure of the initial compound-states on the cascade gamma-decay process is up to now the primary aim of experiment. At present, this can be done in analysis of experimental intensities of the primary gamma-transitions following capture of "filtered" neutrons with energy 2 and 24 keV (or by any averaging over resolved resonances).

The most complete set of these data among actinides is accumulated for compound nucleus <sup>237</sup>U. Unfortunately, authors of corresponding experiments [9] used their data practically only for determination of spin and parity of excited levels on the base of notions of the limited "statistics" theory of gamma-decay. I.c., in the framework of the hypotheses:

- on independence of k(E1) and k(M1) on structure of decaying  $(\lambda)$  and excited (f) nuclear levels and
- applicability of the Porter-Thomas distribution [10] for describing random deviations
  of the gamma-transition partial widths in any interval of their energy from mean
  values.

There are no experimental evidences of hypothesis [5, 6, 10] for the data like [9] (concrete nucleus, given set of gamma-transition intensities). Therefore, the method of analysis must take into account possibility of non-execution of assumptions mentioned above.

#### 2.1 Algorithm of analysis

The analysis is based on the following statements:

- the number of the primary dipole transitions observed in the  $(\bar{n}, \gamma)$  reaction is less than or equal to the value  $\rho \times \Delta E$  for any excitation energy interval  $\Delta E$  and spin window determined by the selection rule on multipolarity;
- the sum of widths of the observed transitions is less than or equal to the summed width of all the possible primary gamma-transitions;
- the likelihood function of approximation of distribution of random intensity deviations from the mean value has the only maximum;
- the experimental values of  $\rho\Delta E$  and sum  $\Gamma_{\lambda,f}$  can be determined with acceptable uncertainty from extrapolation by curve which approximates distribution of the random gamma-transition intensities to zero threshold of their registration;

• the averaging of random fluctuations of the primary gamma-transition widths over the initial compound states decreases dispersion of their distribution independently on reliability of hypothesis [10]. I. e., any set of gamma-transition intensities from the  $(\bar{n}, \gamma)$  reaction can be approximately described by the  $\chi^2$ -distribution with unknown number of degrees of freedom  $\nu$ . (In practice this distribution is close to normal one with dispersion  $\sigma^2 \approx 2/\nu$ .)

This means that the number of the primary gamma-transitions from reaction  $(\bar{n}, \gamma)$  with intensity lying below detection threshold of experiment [9] in any case considerably decreases as compared with analogous data obtained for decay of the only compound-state. In this case, determination of the primary gamma-transition intensity distribution parameters provides maximum possible precision for extrapolation of function of intensities random values distribution into the region below the detection threshold.

Therefore, precision in estimating the number of unobserved gamma-transitions and sum of their partial widths from the data [9] must be much higher than it can be reached by analysis of intensities of primary gamma-transitions following thermal neutron capture. Corresponding technique was developed earlier and tested on large set of the data on the two-step cascade intensities in [11].

The problem of principle importance in the analysis of such kind is really unknown law of distribution of dispersion of random widths about mean value. The fact of discrepancy between dispersion of random intensities of primary gamma-transitions and expected for a given nucleus value of  $\nu$  at the capture of 2 keV neutrons was first pointed out in [12]. But up to now attempts to solve this problem were undertaken up to now.

The Porter-Thomas distribution correctly describes distribution of the random partial widths of the tested gamma-transitions only when their amplitudes have normal distribution with zero mean value. Therefore, they must be the sum of large number of items of different signs and the same order of magnitude. This condition must be fulfilled if wavefunctions of the levels connected by gamma-transition contain a large amount of items with different signs and comparable magnitudes. Just these components are contained in matrix element for amplitude of gamma-transition.

# 2.2 Some aspects of modern theoretic ideas of gamma-transition probability

On the whole, existing theoretic developments, for example, quasiparticle-phonon nuclear model (QPNM) [13, 14] call some doubts about applicability of mentioned above primitive ideas of gamma-decay. In particular, the regularities of fragmentation of the different complicated states studied in the frameworks of QPNM [15] directly point to presence of items with considerable component of wave functions in the primary transition amplitudes. First of all, this concerns wave functions of excited levels [16], but it is not excluded that the wave-functions of decaying compound states (neutron resonances) also have large components [13]. This directly results in potential possibility of

rather considerable violation of the Porter-Thomas distribution. These violations can appear themselves in limited [15] energy intervals of final levels and change dispersion of real distribution as compared with [10]. Correlation between absolute values of items in amplitude of any gamma-transition and their signs for the data like [9] are unknown. Therefore, the suggested below analysis of available experimental data must take into account possibility of strong dependence of the primary transition partial widths on structure and, correspondingly, energy of excited levels and cover all spectrum of their random deviations from the mean value. At least, it must guaranty obtaining the minimum possible estimation for  $\rho$  and the maximum possible – for k. Just this sign of deviation of their experimental values from the practically used [1] model ideas is provided by the analysis [3, 4].

According to theoretical notions of QPNM, the amplitude of gamma-transition from high-excited nuclear state (neutron resonance) is a sum of different in structure elements [13]. Schematically [17] they consist from a number of items which correspond to the following components of wave-functions of decaying and excited levels connected by the gamma-transition:

- (a) n-quasiparticle,
- (b) n-quasiparticle ⊗ phonon,
- (c) n-quasiparticle ⊗ two phonons and so on.

I. e., amplitude of given gamma-transition can be determined by some components of physically different types. In common case they can have considerably different scale. And concrete values are determined by degree of fragmentation of the nuclear states enumerated above. The types of dominant components in the wave-functions of final levels excited by primary gamma-transitions can be different in principle, especially at low excitation energy of levels [16].

The first part of amplitude (see, for example, [17]) for many rather high-lying levels is determined by a number of items of different sign and, on the average, comparable magnitude. This qualitative explanation follows from calculation of structures of low-lying levels of deformed nuclei performed by authors [16] and the most general principles of fragmentation of nuclear states of complicated structure as increasing excitation energy [15].

The following items in the gamma-transition amplitude (at sufficient energy of excited level) account for contribution of those components which cause change in wave functions by one phonon. I.e., it follows from main theses of QPNM, for example, that the all multitude of the primary gamma-transition amplitudes cannot be reduced to one limited case as it was suggested in [10].

## 2.3 Some peculiarities of experimental data

Experimental investigations of various target-nuclei were performed in BNL. But only even-odd target-nucleus <sup>236</sup>U was chosen for the analysis presented below. This choice is stipulated by maximum interval of the primary gamma-transition energies listed in [9].

Even-odd compound-nucleus has an only possible spin at capture of s-neutrons and two possible – for p-neutrons. Analysis of intensities in the last case requires one to introduce and then determine the number of parameters corresponding to even-even nucleus. Even-odd compound nucleus at its excitation by s-neutrons represents methodically a particular case of the task considered in [18].

The width FWHM=850 eV of filtered neutron beam with the energy of 2 keV in the performed experiments was determined by interference minimum in the total cross section of scandium. The average spacing between neuron resonances in <sup>236</sup>U equals 12 eV and this provides minimum number of the primary gamma-transitions whose intensities are less than detection threshold.

If one does not account for:

- (a) the change in neutron flux in the energy interval mentioned above;
- (b) the possible strong correlation of partial radiative widths and
- (c) the presence of noticeable statistic errors in experimental data

then dispersion  $\sigma^2 = 2/\nu$  of their expected distribution can be not less than  $\sim 0.03$ . In presence of absolute correlation between reduced neutron width and partial radiative widths one can estimate maximum possible dispersion from the folding of two  $\chi^2$  dispersions by the value  $\sigma^2 = 8/\nu \ge 0.12$ .

I.e, the main part of the primary gamma-transition intensities observed in the nucleus under consideration must exceed experimental detection threshold. Therefore, expected errors of extrapolation must be small enough.

It is assumed in analysis that all the distributions of the primary gamma-transition intensities from reaction  $(n, \gamma)$  have only the following unknown parameters:

- (a) the averaged reduced intensity  $\langle I_{\gamma}^{max}/E_{\gamma}^{3}\rangle$  of gamma-transitions populating levels J=1/2,3/2;
- (b) the portion  $B = \langle I_{\gamma}^{min} \rangle / \langle I_{\gamma}^{max} \rangle$  of reduced intensities of gamma-transitions to levels J = 5/2 relatively to that to levels J = 1/2, 3/2 (practically for intensities of primary transitions following capture of neutrons with energy of 24 keV;
- (c) the ratio  $R_k = k(M1)/k(E1)$  which is independent on spin values of the levels populated by the primary transitions;
- (d) the expected and equal numbers  $N_{\gamma}$  of gamma-transitions to levels J=1/2,3/2 and J=5/2;
  - (e) as well as the dispersion  $\sigma^2$  measured in units of degree of freedom  $\nu.$

Naturally, these parameters are to be determined independently for each energy interval of the primary gamma-transitions.

The presence of statistical errors in determination of each experimental value of  $\langle I_{\gamma}/E_{\gamma}^3 \rangle$  automatically increases experimental dispersion  $\sigma^2$  of distribution and decreases the  $\nu$  value. It is assumed that their relative systematic errors in each energy interval are practically equal.

Of course, this notion assumes that the structures of initial compound-state and a

group of levels in rather narrow interval  $\Delta E$  of excitation energy connected by the primary gamma-transitions of the same type weekly influence the mean reduced intensities  $\langle I_{\gamma}/E_{\gamma}^3 \rangle$  of these quanta.

Both performed in [8] approximation and interpretation of experimental data on k(E1) + k(M1) and ideas of modern nuclear theories show that this assumption can contain considerable uncertainty (especially for wide energy intervals of the primary gamma-transitions under study). But the maximum accuracy in determination of the most probable values of  $N_{\gamma}$ , B,  $R_{k}$ ,  $\nu$  and  $\langle I_{\gamma}^{max} \rangle$  can be achieved, in principle, by recurrent optimization of the primary gamma-transition energy intervals where are determined these parameters.

One more problem is due to small volume of the set and difference in numbers of electric and magnetic dipole gamma-transitions in concrete intervals  $\Delta E$ . Therefore, it is necessary to introduce and fix in analysis some assumption about number of levels of positive and negative parity in a given energy interval of nuclear levels. Below is used the hypothesis of equality of number of electric and magnetic gamma-transitions. In practice, this ratio can be varied for any possible hypotheses of ratio between level densities with different parity for any given excitation energy interval. The problem of difference in level density of different parity disappears for values of  $R_k \approx 1$ , the maximum error in determination of  $N_{\gamma}$  in case  $R_k \approx 0$  corresponds to the lowest intensity transitions and insignificantly distorts desired sum  $\sum \langle I_{\gamma}/E_{\gamma}^3 \rangle$ . In intermediate case, error of approximation will be stipulated, first of all, by difference in level densities of positive and negative parity – it will decrease as increasing excitation energy (as it was on the whole predicted by modern theoretical calculation of this nucleus parameter [19]).

Approximation of the mixture of the different type random values with respect to mean parameters by any distribution cannot determine their belonging to certain type without using additional information. But, accounting for the known fact that the magnetic gamma-transitions to the lowest levels are by order of magnitude weaker than electric transitions, one can extrapolate inequality  $R_k = k(M1)/k(E1) < 1$  for the nuclei under study up to excitation energy where  $R_k = 1$ . There is not excluded that at higher energies of gamma-quanta k(M1)/k(E1) > 1.

Strength function of p-neurons  $S_1=2.3(6)$  in isotope <sup>236</sup>U noticeably exceeds strength function of s-neutrons  $S_0=1.0(1)$  [20]. Authors of [21] estimated that in this case the portion of captures of p-neutrons with energy of 2 keV equals approximately 15%. If one does not account for possible irradiation of small group of the primary dipole gammatransitions following capture of p-neutrons and terminating at the levels with spin values J=5/2, then the presence of this capture appears itself, most probably, as change in the  $R_k$  values for different energies of excited levels and corresponding increase of  $\nu$ . Therefore, the presence of small number of the 2 keV p-neutron captures must not noticeably influence accuracy in determination of the expected values of  $N_{\gamma}$  and sum k(E1)+k(M1).

There is no problem of p-neutron capture for the data on the intensities of primary gamma-transitions for resolved resonances. Absolute normalization of partial widths for each resonance performed in [9] allows one to provide for the most effective averaging of them. Unfortunately, arithmetic mean value of  $\Gamma_{if}$  inevitably shifts to lower values by

different for each gamma-transition quantity  $M \times \Delta \Gamma_{if}$ . Partial width  $\Delta \Gamma_{if}$  of each from M gamma-transition with intensity lying below registration threshold in given resonance varies from zero to some maximum magnitude. That is why, averaging over resonances additionally has this unknown specific error.

Approximation of distribution of random values  $I_{\gamma}/E_{\gamma}^3$  was performed by analogy with [11] for cumulative sums in function of increasing values of intensities.

# 3 Results of analysis

The examples of experimental distributions of cumulative sums of the primary transition reduced intensities  $\sum I_{\gamma}/E_{\gamma}^{3} = F(\langle I_{\gamma}/E_{\gamma}^{3} \rangle, N_{\gamma}, \nu, R_{k})$  were calculated for different values of concrete parameters and given in [18].

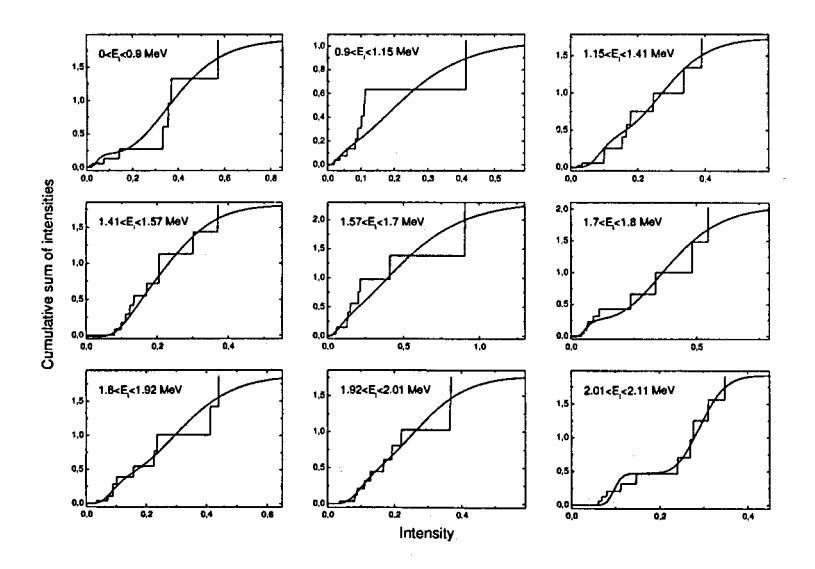


Fig. 1. The histogram represents experimental cumulative sum of reduced relative intensities  $\langle I_{\gamma} \rangle / E_{\gamma}^3$  for <sup>237</sup>U. Smooth curve shows the best approximation. The intervals of excitation energy  $E_i$  of final nuclear levels are shown in figures. Experimental data for neutron energy  $5 \leq B_n \leq 125$  eV.

This was done only under condition of correspondence between experiment and accepted hypotheses of the distribution form of the primary transition random intensities. The presence of functional dependence of the primary transition intensities on some "hidden" parameter can result in maximal errors of approximated values of the most probable number of gamma-transitions and dispersion of their deviation from mean value. Mod-

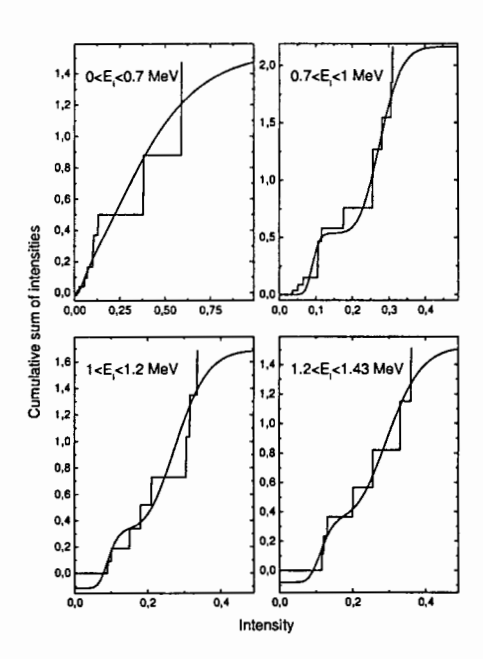


Fig. 2. The same, as in Fig. 1, for  $E_n \approx 2 \text{ keV}$ .

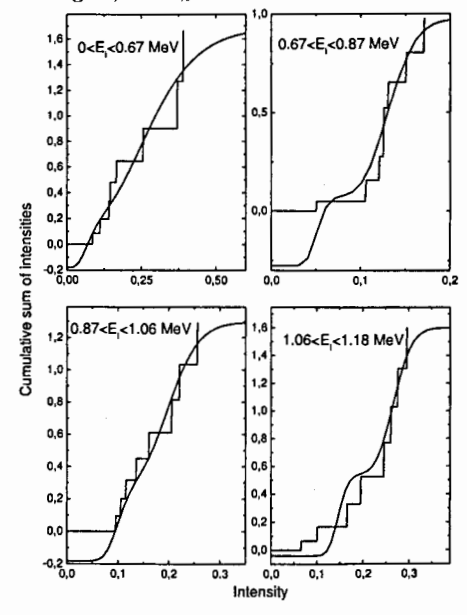


Fig. 3 The same, as in Fig. 1, for  $E_n \approx 24 \text{ keV}$ .

ern nuclear theory does not consider this possibility; there are no experimental data on existence of "hidden" dependence, as well. Therefore, it is not taken into account below.

Experimental cumulative sums of the  $\langle I_{\gamma}/E_{\gamma}^3 \rangle$  relative values are shown in figs. 1-3 together with their best approximation. The data are presented so that the expected total intensity of gamma-transitions lying below detection threshold corresponds to the most probable value of cumulative sum for  $\langle I_{\gamma}/E_{\gamma}^3 \rangle = 0$ .

At low energy  $E_i$  of final levels, accuracy in determination pf parameters of approximating curve must get worse due to inequality of level density with different parity. Most probably, this increases error of extrapolation of gamma-transition intensities to zero value. This can result in overestimating of  $N_{\gamma}$  values.

The best values of fitting parameters  $\nu$  and  $R_k$  are are given in figs. 4 and 5. Noticeable change in these parameters of approximation for  $0.7 < E_i < 1.2$  MeV points to considerable change in structure of given even-odd isotope in this excitation energy region.

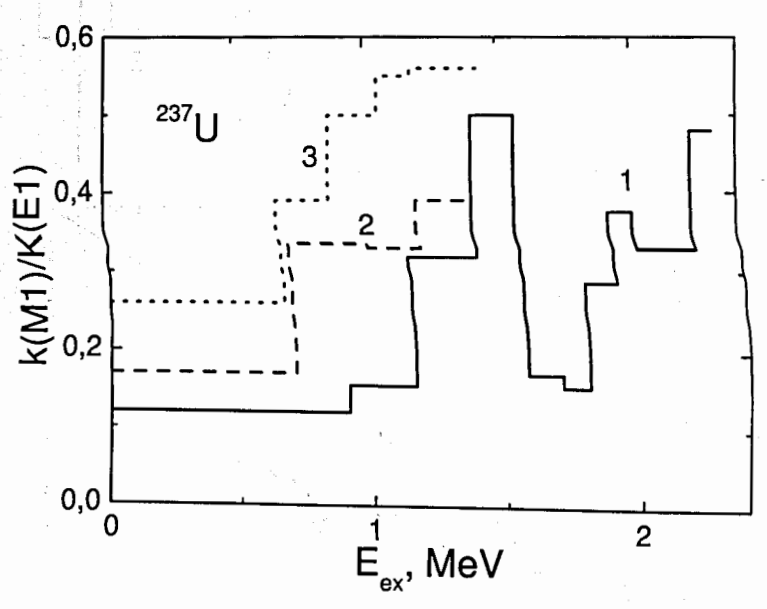


Fig. 4. The histograms represent the best values of ratio k(M1)/k(E1) for different excitation energies of levels populated by dipole gamma-transitions. Line 1 represents data for  $5 < E_n < 125$  eV, line 2 - for  $E_n \approx 2$  keV and line 3 - for  $E_n \approx 24$  keV.

The best values of level density  $\rho = \sum_{J,\pi} N_{\gamma}/\Delta E$  and summed radiative strength functions  $\sum \langle I_{\gamma} \rangle / (E_{\gamma}^3 N_{\gamma})$  are given in figs. 6 and 7. Normalization of intensities and strength functions in both [3] and [9] was done to their absolute values. Because gammatransition intensities following capture of "filtered" neutrons are listed in [10] in relative units than corresponding strength functions Fig.7 are combined with "resonance" values under assumption of their approximate equality.

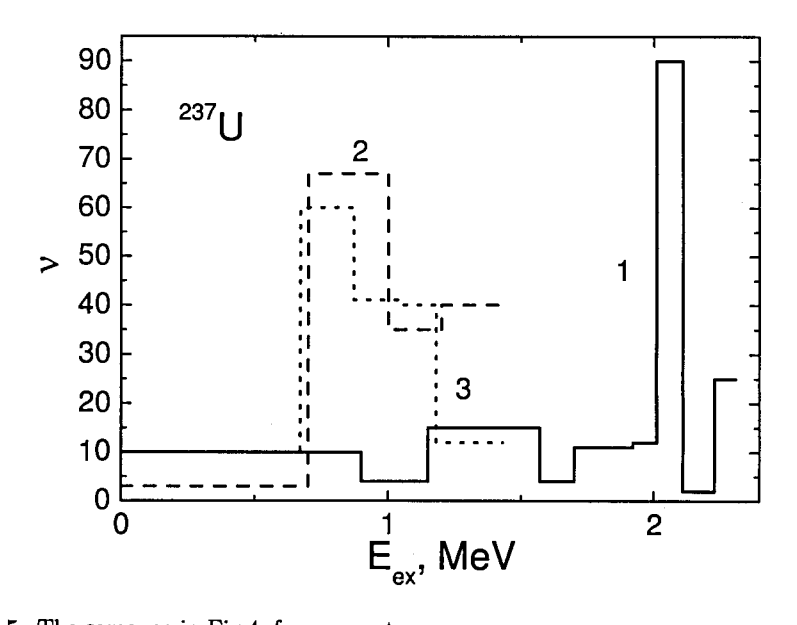


Fig. 5. The same, as in Fig.4, for parameter  $\nu$ .

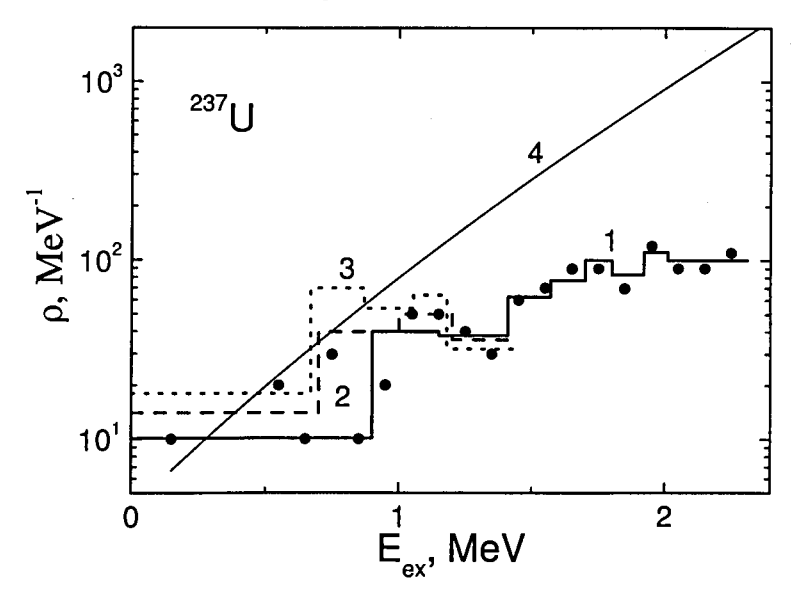


Fig. 6. The same, as in Fig. 4, for the density of excited levels. Line 4 represents calculation within model [22] for spin values J=1/2 and 3/2. Points correspond to number of levels observed in resolved resonances.

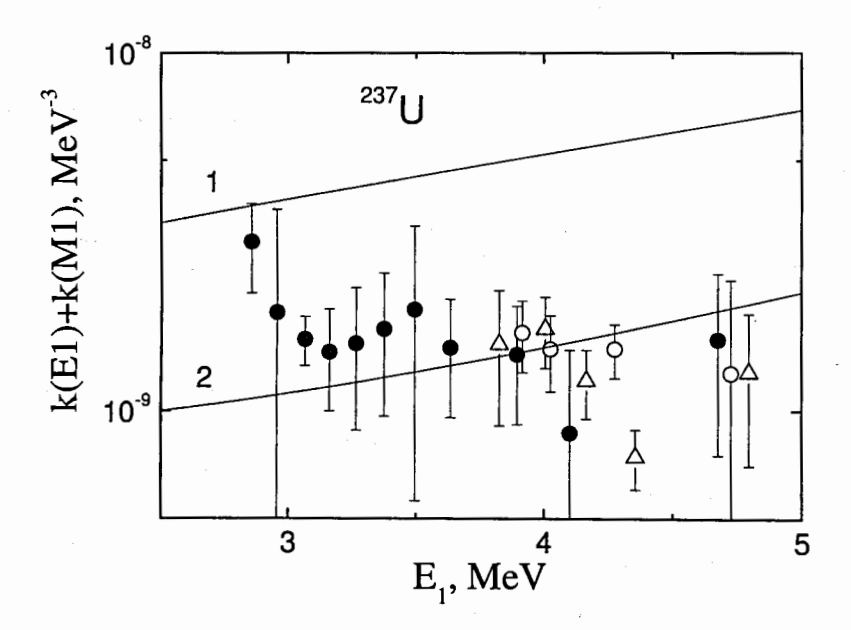


Fig. 7. The summed radiative strength functions derived from the data on capture of neutrons with different energies  $E_n$ : black points –  $5 < E_n < 125$  eV, open points –  $E_n \approx 2$  keV, triangles –  $E_n \approx 24$  keV. Line 1 represents calculation within model [5], line 2 – calculation within model [23] together with k(M1)= const.

#### 3.1 Some sources of systematic errors

Absolute minimum of  $\chi^2$  for all used sets of intensities is achieved practically for the only  $N_{\gamma}$  value. Change in this parameter by  $\pm 1$  brings to significant increase in  $\chi^2$ . This allows one to neglect possibility of considerable (for example, 10-20%) error of determined level density.

Main problems in determination of nuclear parameters and their systematic errors, most probably, are stipulated by:

- (a) the use of assumptions on the distribution form of the random intensity deviations from the unknown mean value and
  - (b) possible presence of significant errors in the set of the intensities under analysis.
- 1. The Porter-Thomas distribution allows very considerable random deviations of partial widths. But the measured gamma-transition intensities are always limited by finite value of the total radiative width of decaying state. Therefore, the set of the best values of parameters depends on the total width of region for approximation of cumulative sums. Mainly this concerns the best value of parameter  $\nu$ . In the performed analysis, intensities were normalized so that their maximum value would not exceed 50-70% of the approximation region width.
- 2. The main error of analysis can be related only to the "loss" of gamma-transitions whose intensities exceed threshold value and/or due to mistaken identification of the secondary gamma-transitions as the primary one. The probability of overlapping of two peaks corresponding to neighbouring levels was estimated in [24]. As it follows from the data presented by authors, this effect is rather small and, most probably, cannot explain considerable (several times) discrepancy between level density determined by us and predictions of the Fermi-gas level density model [22].

Considerable uncertainty could be due to even and significant loss of observed peaks corresponding to intense primary transitions (exceeding their detection threshold) owing to their grouping in multiplets with rather narrow ( $\sim 1-2$  keV) spacing between peaks. But this possibility is not predicted by modern nuclear models.

3. In principle, there is possible the situation when gamma-transitions in all or larger part of chosen intervals of primary transition energies (with the width of some hundreds keV) have different mean values. Moreover, probability of relatively low-intense transitions strongly but smoothly increases as decreasing their intensities. Potentially, this effect can be due to by fragmentation mechanism of states over concrete neighbouring nuclear levels.

Apparently, only such hypothesis can be alternative potential explanation of "stepwise" structure in level density in analysis performed in this work. Application of this hypothesis to the level densities determined according to [3, 4] requires that the main portion of levels with the same  $J^{\pi}$  below  $\approx 0.5B_n$  would not be excited by the primary gamma-transitions. Besides, some Cooper nucleon pairs would break simultaneously at low in comparison with  $B_n$  nuclear excitation energy. We cannot suggest other possibility for precise reproduction of the two-step gamma-caseade intensities in calculation.

#### 3.2 Interpretation of the obtained results

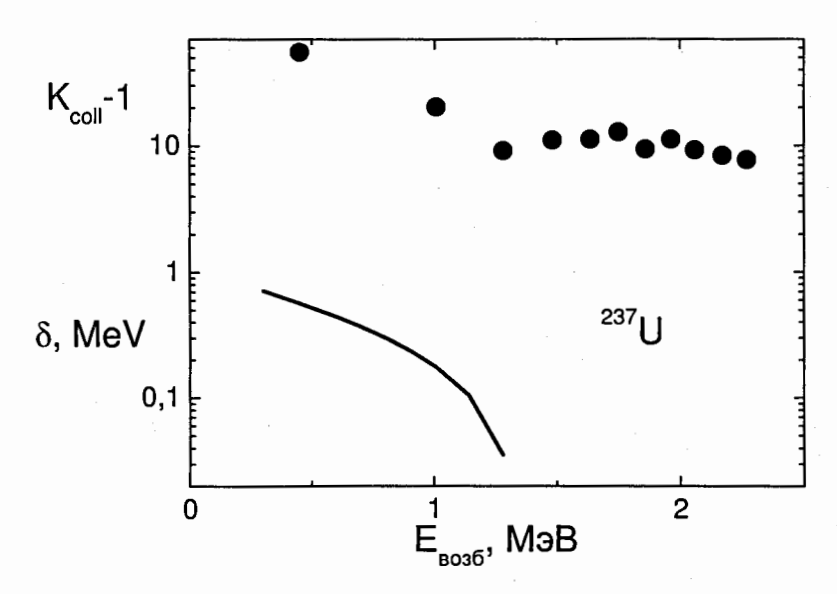


Fig. 8. The points represent the coefficient of collective enhancement of level density, the line shows the values of parameter  $\delta_1$  used in [3, 27] for calculating partial density of three-quasiparticle levels.

The physics important information on level structures below  $\approx 0.5 B_n$  can be extracted from the values of coefficient of collective enhancement of level density:

$$\rho(U, J, \pi) = \rho_{qp}(U, J, \pi) K_{coll}(U, J, \pi). \tag{1}$$

According to modern notions,  $K_{\rm coll}$  determines in deformed nucleus [1] a degree of enhancement of level density of pure quasi-particle excitations  $\rho_{\rm qp}(U,J,\pi)$  due to its vibrations and rotation. In very narrow spin window considered here one can accept in the first approach that, to a precision of small constant coefficient, it equals coefficient of vibration increase in level density  $K_{\rm vibr}$ . On the whole, the last is determined by change in entropy of a nucleus  $\delta S$  and redistribution of the nuclear excitation energy  $\delta U$  between quasi-particles and phonons at nuclear temperature T:

$$K_{\text{vibr}} = exp(\delta S - \delta U/T).$$
 (2)

The experimental data at hand on level density and existing model notions of it do not allow one unambiguous and reliable determination of the  $K_{\text{vibr}}$  value for arbitrary nuclear excitation energy U even at zero systematic error in determination of function  $\rho(U, J, \pi)$ .

Now is no possibility for ambiguous experimental determination [25] of breaking threshold  $E_N$  of the first, secondary and following Cooper pairs, value and form of correlation functions  $\delta_N$  of Cooper nucleon pair number N in heated nuclei. The main uncertainty of  $E_N$  is caused by the lack of the experimental data on function  $\delta_N = f(U)$ , the secondary – by uncertainty of level density of single-particle levels g in model [26]. So, in three different, model dependent approximations of level density in large set of nuclei of different type [25] and [27], the threshold  $E_2$  of five-quasi-particle excitations differs by a factor of 1.5-2.

In practice, for estimation of  $K_{vibr}$  from the data [21] we used the second variant of notions of correlation function of Cooper pair in heated nucleus [25]. In calculation were used the values  $\delta$ =0.83 MeV, g=14 MeV<sup>-1</sup>. The best value of breaking threshold for the first Cooper pair was found to be equal to  $E_1 = 0.55$  MeV when using the assumption on independence of  $K_{vibr}$  on nuclear excitation energy. At low excitation energy this assumption is, most probably, unreal (see Fig.8).

Parameter  $K_{coll} - 1$  determined from comparison between the calculated in this way density of three-quasiparticle excitations (J=1/2, 3/2) and its most probable experimental value is shown in Fig. 8 together with calculated value of  $\delta_1$ .

Significant correlation of this coefficient with  $\delta_1$  from [27] and from the second variant of the analysis [25] is observed in the excitation energy interval below approximately 1.2 MeV. At higher excitation energy, decrease in degree of correlation can be related to both considerable contribution of five-quasiparticle excitations in the function  $\rho_{qp}(U, J, \pi)$  and less than it is accepted in [25, 27] rate of function  $\delta_1$  at U > 1.2 MeV.

The data presented permit one to make the following conclusions:

- 1. The study of the  $^{237}{\rm U}$  nucleus excited in reaction  $(\overline{n},\gamma)$  by neutrons with energies 0.005-0.12, 2 and 24 keV allow us to observe the same properties as those revealed for  $\sim 40$  nuclei from the mass region  $40 \le A \le 200$ . There are: step-wise structure in level density and local enhancement of radiative strength functions of the primary gamma-transitions to corresponding levels.
- 2. In the excitation energy region about 0.7-1.5 MeV occurs abrupt change in level structures. This appears itself in considerable enhancement of the k(M1)/k(E1) values and in strong difference of their distribution from normal distribution of random amplitudes of gamma-transitions.
- 3. Experimental ratios k(M1)/k(E1) can be used for obtaining more unique values of strength functions of E1- and M1-transitions and data on relations between density of levels with different parity in the frameworks of methods [3, 4].
- 4. The majority of the primary gamma-transitions observed in reaction  $(\bar{n}, \gamma)$  correspond, probably, to excitation of levels with large and, maybe, weakly fragmented phonon components of wave functions.

#### 4 Conclusion

Analysis of the available experimental data on the primary gamma-transitions from reaction  $(\overline{n}, \gamma)$  in compound nucleus <sup>237</sup>U has demonstrated step-wise structure in level density and increasing radiative strength functions of transitions to levels lying in the region of this structure, at least, for the primary dipole transitions. I.e., it confirmed main conclusions of [3, 4]. It showed also a necessity to reveal and remove systematic errors of experiment in alternative methods for determining only level density and simultaneously—all the parameters of the cascade gamma-decay. Very important for this are both correct accounting for effect of level structures on probability of emission of evaporated nucleons and cascade gamma-quanta in investigation of nuclear reactions at beams of accelerators and considerable reduction of systematic errors of experiment.

Abrupt increase in dispersion (decrease in the  $\nu$  parameter) of random deviations of intensities from the mean (expected according to [10]) values allows one to suppose the presence in their structure of considerable components of weakly fragmented nuclear states being more complicated than the three-quasiparticle states. Approximation of the obtained level density by Strutinsky model confirms considerable ( $\approx$  10 times) increase in level density due to excitations of mainly vibration type [27]. Comparison of the data presented in figs. 6, 7 with those obtained from analysis of two-step gamma-cascades permits one to make preliminary conclusion that the sharp change in structure of decaying neutron resonances, at least, in their energy interval  $\approx$  24 keV is not observed. And there are no reasons to expect serious change in determined according to [3, 4] level density and shape of energy dependence of radiative strength functions for the primary gamma-transitios from resonance to resonance. Further reduction of systematic errors of these nuclear parameters determined from the two-step gamma-cascade intensities undoubtedly requires reliable estimation of functions  $k(E_{\gamma}, E_{ex})$  for all energy interval of levels excited at neutron capture.

The analysis performed in this work and its results point to necessity of experimental determination of  $\rho$  and k by the method [4] in all practically important for nuclear energetics nuclei from the region of actinides.

#### References

- Reference Input Parameter Library RIPL-2. Handbook for calculations of nuclear reaction data. IAEA-TECDOC, 2002;
  - http://www-nds.iaea.or.at/ripl2;
  - Handbook for Calculation of Nuclear Reactions Data, IAEA, Vienna, TECDOC-1034, 1998.
- V.M. Maslov, Yu.V. Porodzinskij, M. Baba, A. Hasegawa, Nucl. Sci. Eng. 143 (2003)
   1.
- E. V. Vasilieva, A. M. Sukhovoj, V. A. Khitrov, Phys. At. Nucl. 64, 153 (2001).

- [4] A. M. Sukhovoj, V. A. Khitrov, Physics of Paricl. and Nuclei, 36(4), 359 (2005).
- [5] P. Axel, Phys. Rev. 126, 671 (1962).
- [6] D. M. Brink, Ph. D. thesis, Oxford University (1955).
- V. A. Khitrov, Li Chol, A. M. Sukhovoj, in: XI International Seminar on Interaction of Neutrons with Nuclei, Dubna, May 2003, E3-2004-9, (Dubna, 2004), p. 98;
   V. A. Khitrov, Li Chol, A. M. Sukhovoj, nucl-ex/0404028.
- [8] A. M. Sukhovoj, W. I. Furman, V. A. Khitrov, JINR preprint E3-2007-49, Dubna, 2007.
- [9] T. von Egidy et al., Phys.Rev. C 20, 944 (1979).
- [10] C. F. Porter, R. G. Thomas, Phys. Rev. 104, 483 (1956).
- [11] A. M. Sukhovoj, V. A. Khitrov, Phys. At. Nucl. 62, 19 (1999).
- [12] R. C. Greenwood, C. W. Reich, Nucl. Phys. A 252, 260 (1975).
- [13] V. G. Solovev, Fiz. Elem. Chastits At. Yadra, 3, 770 (1972).
- [14] V. G. Soloviev, *Theory of atomic Nuclei: Quasiparticles and Phonons*, (Institute of Physics Publishing, Bristol and Philadelphia, 1992).
- [15] L.A.Malov, V.G.Soloviev, Sov.J. Nucl. Phys. 26, 384 (1977)
- [16] F. A. Gareev, S. P. Ivanova, V. G. Solovev, S. I. Fedotov, Sov.J.Particles Nucl. 4, 148 (1974).
- [17] S.T.Boneva, E.V.Vasilieva, L.A.Malov et al., Yad.Fiz., 49, 944 (1989).
- [18] A. M. Sukhovoj, Physics of atomic nuclei, **71** (2008) 1907.
- [19] A.I. Vdovin et al., Sov. J. Part. Nucl. 7(4) (1976) 380.
- [20] S. F. Mughabghab, Neutron Cross Sections, V.1, part B, (N.Y., Academic Press, 1984).
- [21] R.E. Chrien, J.Kopecky, Nucl. Phys. A414 (1984) 281.
- [22] W. Dilg, W. Schantl, H. Vonach, M. Uhl, Nucl. Phys. A 217, 269 (1973).
- [23] S. G. Kadmenskij, V. P. Markushev, V. I. Furman, Sov. J. Nucl. Phys., 37, 165 (1983).
- [24] V.L. Stelts, R.E. Chrien, M.K. Martel, Phys. Rev. C, 24(4), 1419 (1981).
- [25] A. M. Sukhovoj, V. A. Khitrov, Preprint N° E3-2005-196, JINR (Dubna, 2005).
- [26] V. M. Strutinsky, in Proc. of Int. Conf. Nucl. Phys., (Paris, 1958), p. 617.
- [27] A. M. Sukhovoj, V. A. Khitrov, Physics of Paricl. and Nuclei, 37(6), 899 (2006).

# STATUS AND PROBLEMS OF EXPERIMENTAL STUDY OF EXCITED NUCLEUS SUPERFLUIDITY

#### A.M. Sukhovoj, W.I. Furman, V.A. Khitrov

Joint Institute for Nuclear Research, 141980 Dubna, Russia

#### Abstract.

Modern nuclear models assume a coexistence of normal and superfluid phases of nuclei, as a minimum, up to the excitation energy of neutron resonances. Experiment, accordingly, has to reveal important details of interconnection of these phases. First of all, this concerns large-scale details. An effective method to study this problem is an investigation of neutron radiative capture. The most relevant characteristics of this interconnection are energy dependence of excited level density (in given spin window) and radiative strength function of primary gamma-transitions from a compound-state to low lying states. These values have to be extracted from respective experimental data with maximal reliability and minimal systematic uncertainties. To reach this goal it is necessary to depart in data analysis from obsolete models of radiative strength function and density. The two-step  $(n, 2\gamma)$ -reaction and in general various multi-step reactions provide favorable possibilities for such type of investigations.

On the basis of practically modeless approach there was obtained the phenomenological information on radiative strength function of primary gamma-transitions and level density for wide range of nuclei  $40 \le A \le 200$ . Very important fact established in this study was a discovery of step-like behavior of level density below excitation energy  $E \le 0.5B_n$ . Besides, it was revealed a presence of highly excited levels of vibrational nature in range of normal many quasi-particle excited levels.

In this paper an attempt was made to expand this approach derived for analysis of  $(\overline{n}, \gamma)$ -reaction measured for actinide nuclei with keV neutrons. The obtained results give some evidence for similarity of general behavior of level density and radiative strength function in these wide region of investigated nuclei.

#### 1. Introduction

Density of excited levels  $\rho$  and emission probability  $\Gamma$  of any product of nuclear reaction are the main sources of experimental information on properties of nuclear matter. Id est, to a high extent there is a base for both theoretical notion and concrete models of nuclear parameters. Precise nuclear models of  $\rho$  and  $\Gamma$  are absolutely necessary for estimation and calculation of practically important nuclear-physics constants. This determines a necessity of their predictions with maximum possible accuracy.

Just theoretical analysis of reliable experimental data on the  $\rho$  and  $\Gamma$  values can provide irreplaceable information on fundamental quantum-mechanical process of coexistence and interaction of two states of nuclear matter – fermion and boson types, i.e., usual and superfluid nuclear states. Final sizes of nucleus, presence of deformation, closed magic nucleon shells and so on allow one to hope for obtaining new in principle information on this process, as a minimum, up to the region of neutron resonances. Experiment, correspondingly, must reveal details of their interaction (in the first turn – large-scale details).

But, for the majority of nuclei excited in nuclear reaction, the  $\rho$  and  $\Gamma$  values cannot be determined in direct experiments of classical nuclear spectroscopy: mean spacing  $D_{\lambda}$  between

excited levels is comparable or much less than energy resolution (FWHM) of existing spectrometers. Correspondingly, these parameters can be extracted only from the spectra measured with "bad" resolution for the nucleus excitation energy above several MeV. It is also desirable to determine level density and radiative strength functions of the excited by them primary gamma-transitions, for example, in a given variable spin window. Up to now, the  $\rho$  and  $\Gamma$  values were determined in one-step reactions. And only in the last time corresponding information on these parameters was derived from two-step reaction  $(n,2\gamma)$  [1,2].

#### 2. Difference of principle between one- and two-step reactions

Intensity of the spectra registered in experiment – products of one-step nuclear reaction in all the possible interval of their energies is proportional to product of parameters discussed here:

$$I_1 \propto \rho \Gamma / \sum (\rho \Gamma)$$
 (1)

Energy region where is satisfied the condition  $D_{\lambda}$ >FWHM, as a rule, is a small part of that studied in experiment. In this region, both  $\rho$  and  $\Gamma$  can be determined separately by the use of the nuclear spectroscopy methods. The result is usually used for normalization of the  $\rho$  and  $\Gamma$  relative values. The known data from the neutron resonance region are used for this aim as well. In the region  $D_{\lambda}$ < FWHM determination of  $\rho$  from nucleon evaporation spectra, for example, is impossible in principle without using calculated probabilities of their emission  $\Gamma$ . They should be calculated for wide energy interval of the nuclear reaction products and excitation energies of final nuclei. Up to now, the ideas and potentials of the nucleus optical model are used for this aim. Moreover, the authors of corresponding experiments use without fail the hypothesis (not verified experimentally up to now) [3] on independency of the reverse reaction cross section on excitation energy of final nucleus. (Or its variant for partial widths  $\Gamma$  of gamma-transitions [4,5]).

Comparison between forms of functional dependency of the  $\rho = f(E)$  and  $\Gamma = \varphi(E)$  values obtained in one-step reactions (spectra of evaporated nucleons, different gamma-spectra) [6,7] and the data from two-step reactions (cascades of gamma-transitions) points to their principal incompatibility. It appears itself in presence [1] or absence [7] of sharp changes in determined parameters when change nuclear excitation energy and energy of registered product. This comparison allows one also to determine in the first approach the sources of systematical errors and to evaluate their magnitudes for different experimental methods.

Therefore, one can conclude that quality of extracting  $\rho$  and  $\Gamma$  values from the spectra of one-step reactions changes to the worse to unknown extent due to following reasons:

- 1. the maximum possible transfer coefficients of errors  $\delta S$  of the spectra S measured in one-step reaction onto the errors  $\delta \rho$  and  $\delta \Gamma$ ;
- 2. the use of unverified hypotheses (first of all, on independence of the reverse reaction cross sections on excitation energy of final nucleus);
- 3. inevitable subjectivity in performed analysis (selection [7] of type and parameters of optical potential by determining  $\rho$  from evaporation spectra).

In the case of the two-step reaction (process of interest – two emitted gamma-quanta) distortion of the observed  $\rho$  and  $\Gamma$  values owing to two first reasons considerably decreases, and inevitable ambiguity in determination of parameters from degenerated systems of nonlinear equations is comparable with required accuracy in determination of nuclear parameters. This principle difference is due to another form of energy dependence for the second registered product than (1). Here is supposed that both the first and the second steps

orrespond to excitation of either individual final level or group of final levels limited by experimental conditions.

So, intensities of the two-step gamma-cascades following thermal neutron capture are etermined for fixed initial compound state  $\lambda$ , group of several low-lying levels f and all atermediate levels i lying in a given energy interval  $\Delta E_j$  number j. In these experimental conditions, probability of a given secondary step of reaction

$$I_2 = \Gamma_{ij} / \sum_j \Gamma_{ij} \tag{2}$$

is inversely proportional to level number  $M = \sum \rho \Delta E$  excited at decay of levels i.

Products  $I_1*I_2$  measured in all the possible excitation energy intervals can be eproduced by infinite set of different  $\rho$  and  $\Gamma$  values. But all their values are physically mitted by some region of possible magnitudes

$$\rho_1 \le \rho \le \rho_2$$

$$\Gamma_1 \le \Gamma \le \Gamma_2 \tag{3}$$

or arbitrary excitation energy interval. Really this limitation is not hard and simple. But tarting from some values of system (3), parameter  $\chi^2$  very quickly increases as both acreasing maximum and decreasing minimum  $\rho$  and  $\Gamma$  values. Its least value, as it was btained for the total set of experimental data analyzed in [1,2] was observed for  $\rho_2 - \rho_1 / \rho \approx 20$ -40% and  $(\Gamma_2 - \Gamma_1) / \Gamma \approx 20$ -40%. But only under observation of the oblowing obligatory conditions:

- (a) unambiguously given rule of ratio between radiative strength functions of the primary and secondary gamma-transitions with the same multipolarity and energy;
- (b) extracting two-step reaction intensities from the experimental spectra in function on nergy of their product at the first step.

Possible values of parameters determining intensities  $I_1$ , satisfy this condition, but heir minimum (index 1) and maximum (index 2) values equal zero and infinity, respectively, ust this mathematical condition provides for significantly larger reliability of the parameters erived from two-step reaction as compared with one-step reaction from one hand, and ossibility for model free, practically unique simultaneous determination of both  $\rho_1$ ,  $\rho_2$  and  $\Gamma_1$ ,  $\rho_2$ . Distribution of  $I_1 * I_2$  can be measured with high precision for different types of registered fraction products. For the same reaction products (two successive gamma-quanta, for example) the component corresponding to the first step of reaction must be selected from experimental spectrum although with some systematical error. This approximate ecomposition [8] can be done due to different forms of dependence of  $\rho$  and  $\Gamma$  on energy of evels i.

Nevertheless, a necessity to test method of simultaneous determining  $\rho$  and  $\Gamma$  even at a favorable for its study cases calls no doubts. From the one hand always exist ordinary externatical errors in determination of cascade intensities, on the other hand – it is necessary to use some generally accepted notions on nuclear properties. This can be, for example, the dea of independency of the level decay modes on way of its excitation for lifetime of about everal femtoseconds and so on.

#### 3. The most important results of studying the two-step $(n,2\gamma)$ reaction

Comparison of the  $\rho$  and  $\Gamma$  values obtained from the two-step cascade intensities with nown experimental data and model ideas [9] permits one to conclude:

1. It is necessary to test experimentally the hypothesis [3] in application to calculation of interaction cross sections of evaporated nucleons for different excitation energies of final nuclei. In case of incorrectness of this hypothesis, all the  $\rho$  values derived earlier from evaporation spectra must be re-determined. Just the use of hypothesis [3] brings the main and really unknown error in value of level density extracted from spectra of evaporation nucleons. Evident and very strong violation [3] (in variant [4,5] for the cascade gamma-decay process) can be easily revealed [2] from comparison between intensities  $i_1$ ,  $i_2$  of the primary  $E_1$  and secondary  $E_2$  gamma-transitions following thermal neutron capture and intensities  $i_{1} = i_{1} \times i_{2} / \sum_{i} i_{2}$  of the two-step gamma-cascades.

Determined from ratio  $P=i_1 \cdot i_2/i_{\gamma\gamma}$  total or only cascade's  $P-i_1$  population of individual levels is recurrent folding of interaction cross-section of gamma-quanta with excited nucleus (beginning with maximum excitation energies of levels of final nucleus). This is the only found up to now possibility for indirect testing hypothesis [3] (realized in [2]).

Model notions of Qusiparticle-Phonon Nuclear Model [10] of matrix elements of emission of gamma-quantum and, for example, neutron show that their values are determined by type and value of the wave function components of decaying and excited levels. It is sufficient condition for advance of alternative (with respect to [3]) hypothesis and for the case of emission of nucleon products in nuclear reaction. Its indirect examination can be done in the only way: comparison between the  $\rho = f(E)$  functions obtained in different experiments.

Therefore, extrapolation of conclusions made in [2] on inapplicability of ideas of [3-5] for reactions with nucleon emission calls doubts about all the level densities obtained from evaporation spectra.

2. Averaged sums of the radiative strength functions of the dipole primary gammatransitions over nuclei with different masses but the same parities of neutrons and protons point to existence of two excitation regions below  $B_n$  where occurs rather sharp change in values of this gamma-decay parameter (Fig. 1). Analogous averaging of level density deviations from the simplest exponential interpolation of this parameter in the region between low-lying levels and neutron resonances completely confirms (Fig. 2) this conclusion.

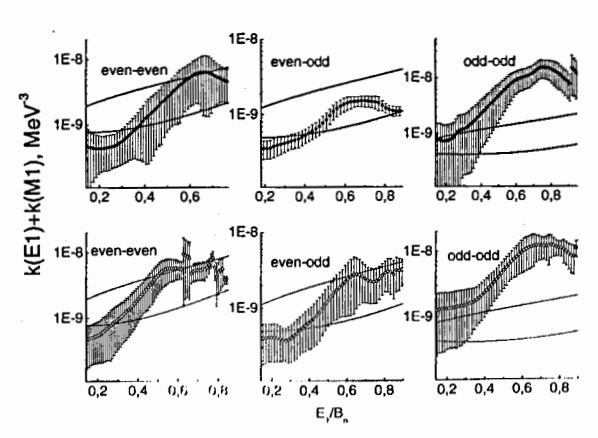


Fig. 1. Comparison between the averaged radiative strength function sums for nuclei with different parities of neutron and proton numbers. Full circles with errors represent nuclei with determined [2] level density. Open circles show results of analysis [1] without accounting for difference in energy

dependence of primary and secondary gamma-transitions. The upper and lower curves represent predictions according to models [4] and [11] in sum with k(M1)=const, respectively.

Approximation (Fig. 3) of the experimental  $\rho$  values by density of n-quasiparticle excitations [13] and radiative strength functions by the semi-phenomenological approach [14] (Fig. 4) allows one to connect [15] this effect partially or completely with break of, as minimum, one and, most probably, two or several Cooper's nucleon pairs.

3. There is a potential possibility for unambiguous determination of dependence of correlation functions  $\Delta_N$  for nucleon pairs (N=1, 2, 3...) on excitation energy of heated nuclei. By now, corresponding functions were obtained in Obninsk [16] only on the data on level density derived from the nucleon evaporation spectra. Due to this reason they have unknown systematical uncertainty.

Approximation of experimental level density from the data [1,2] is ambiguous. Parameters of this fitting by density of n-quasiparticle levels (breaking threshold for next pair, coefficients of collective enhancement, necessary number of breaking pairs below a given excitation energy) depend on form of functional relation of enumerated parameters with nucleus excitation energy.

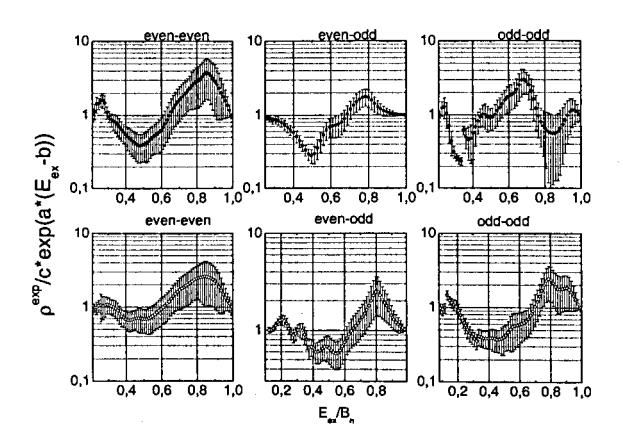
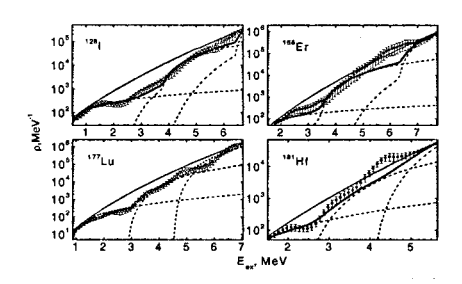


Fig. 2. The mean relative variations of level density. The notations are the same, as in Fig. 1.

Unambiguous choice requires, as minimum, additional development of the radiative strength function models

$$k = f/A^{2/3} = \Gamma/(D_1 E_r^3 A^{2/3})$$

accounting for coexistence, interaction and different influence of quasiparticle and phonon excitations of nucleus on the primary gamma-transition strength functions and determination of parameters of required models. One can expect that joint model reproduction of the  $\Gamma$  values together the level density parameters for different dependences  $\Delta_N = f(E_{ex})$  will allow revealing of main peculiarities of this nuclear parameter, at least, for 2-3 Cooper pairs of nucleons. The basis for this is strong correlation of regions of maximum change in the  $\rho$  and  $\Gamma$  values.



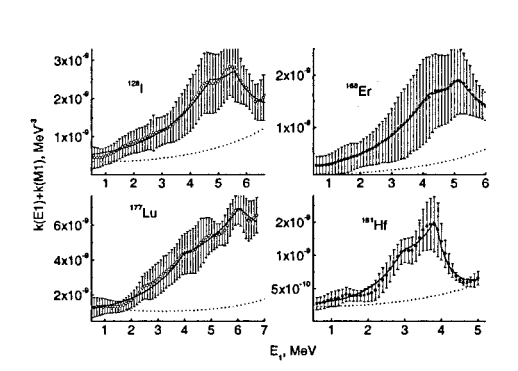


Fig. 3. The examples of approximation of the experimental data for <sup>128</sup>I, <sup>168</sup>Er, <sup>177</sup>Lu and <sup>181</sup>Hf by partial level densities in analogous to [15] variant of analysis under condition *g=const*. Closed points with errors represent experimental data [2], open points – data [1]. Thin dashed curves show partial densities, thick curve demonstrates the sum of partial densities. Solid thin curve corresponds to predictions according to model [12].

Fig. 4. The most probable radiative strength function sums and interval of their values corresponding to minimal values of the  $\chi^2$  parameter for the <sup>128</sup>l, <sup>168</sup>Er, <sup>177</sup>Lu and <sup>181</sup>Hf nuclei. Solid curve shows the best fit, dotted curve represents the component corresponding to expression (5a): open points show data [1], full points – data [2].

#### 4. Requirements to experimental data on two-step reaction

Guarantied reliability of notions of  $\rho$  and  $\Gamma$  being enough for the practical use requires one to determine these parameters with minimum possible systematical errors. For example, overestimation or underestimation of these parameters must not exceed a factor of ~2 in the region of maximum total uncertainty. This region for available information on density of low-lying levels, neutron resonances and other reference data [17] is located at  $\approx 0.5 B_n$ . Achievement of this very high for real situation precision demands, first of all, to exclude not grounded and obviously obsolete hypotheses from analysis of experimental data. Such hypotheses must be replaced by experimental data. Potential possibility to solve this task is measurement of cross-sections and spectra of reactions with different number of steps.

Maximum decreasing in systematical errors of determination of both form of dependence of the two-step reaction spectra on energy of the reaction first step product and absolute partial cross-sections of  $I_1*I_2$  for the fixed initial and final levels practically waits for its solution.

On the whole, the transition from measuring cross-sections of any one- and two-step nuclear reactions to maximum variety of multi-step reactions seems to be desirable and absolutely necessary. It is necessary to use different methods of experiment and its maximum correct analysis for investigation of the same nucleus. Considerable error transfer coefficients of the measured spectra onto the nucleus parameters under study require very careful evaluation of them and necessary reduction of the largest systematical errors of experiment.

#### 5. Verification of results obtained in two-step reactions

Investigation of two-step gamma-cascades in nuclei from the mass region  $40 \le A \le 200$  allowed us to reveal [15,18] the region of the dominant phonon type excitations. It manifests itself as the clearly expressed step-wise structure in level density with a width of  $\approx 2 \Delta_0$  below probable threshold of four- or five-quasiparticle excitations. Analogous conclusions about relation between the levels of quasiparticle and phonon types for higher excitation energy cannot be done – the coefficient of collective enhancement of level density is determined [9] by the ratio

$$\rho(U,J,\pi) = \rho_{an}(U,J,\pi)K_{coll}(U,J,\pi). \tag{4}$$

Therefore, for the unambiguously determined experimental level density, the  $\rho_{qp}$  values for two- or three-quasiparticle excitations are determined with some ambiguity, as well. And the  $\rho_{qp}$  values with 4 and more quasiparticles for a given U, due to strong energy dependence [9,13] depend on breaking thresholds of the second and following Cooper pairs. Therefore, the  $K_{coll}$  values anti-correlate with the birth thresholds of multi-quasiparticle levels. Its value for "step-wise" structure averages [15,18] 10-20. (Concrete values depend on form of function  $\Delta_N = F(E_{ex})$  used for calculation of the n-quasiparticle excitation density in model [13].) But, both the primary and following cascade quanta terminating at the nuclear levels lying in region of this structure are considerably enhanced with respect to any other gammatransitions of the same energy. This conclusion was made by approximation [14] of the experimental data on the primary gamma-transition strength functions [1,2] by the following function:

$$k(E1, E_{\gamma}) + k(M1, E_{\gamma}) = w \frac{1}{3\pi^{2} \hbar^{2} c^{2} A^{2/3}} \frac{0.7 \sigma_{G} \Gamma_{G}^{2} (E_{\gamma}^{2} + \kappa 4\pi^{2} T^{2})}{E_{G} (E_{\gamma}^{2} - E_{G}^{2})^{2}} + (5a)$$

$$+P\delta^{-}\exp(\alpha(E_{\gamma}-E_{p}))+P\delta^{+}\exp(\beta(E_{p}-E_{\gamma})). \tag{5b}$$

The first item is the radiative strength function [11] weighed over probable contribution of quasiparticle excitations in the experimental strength function (with accounting for nuclear temperature, being less than thermodynamics value). The second and the third items describe the left  $(\delta)$  and right  $(\delta^+)$  respectively, parts of peaks in strength functions which are absent in existing [9] model notions. Location of peaks at some energies of the primary gamma-transitions can be explained only by strong difference in structure of levels at different excitation energy of a nucleus under study.

Change of existing [4,5] notions of the  $\Gamma$  values for gamma-transitions of the same energy and multipolarity on excitation energy of studied nucleus by realistic experimental evaluation [2] reduces the most important systematical error in determination of the cascade gamma-decay parameters from the spectra of two-step reaction. But, absolute lack of experimental data on population of levels above  $\approx 0.5B_n$ , practically, in all the studied nuclei does not allow one to remove this error at all.

The obtained  $\rho$  and  $\Gamma$  values are additionally distorted by ordinary experimental errors. Although, for example, variation of the cascade intensity in limits  $\pm 25\%$  changes the obtained  $\rho$  value by a factor not more than 2, as maximum [19]. But reliability of the made conclusions on the determined in [1,2]  $\rho$  and  $\Gamma$  values needs in additional verification.

Usually performed calculation of the gamma-transition spectra and neutron capture cross-sections does not provide for absolute guarantee of absolute reliability in determining  $\rho$ 

and  $\Gamma$  due to small magnitude of the error transport coefficients of these parameters on calculated spectra and cress-sections. Nevertheless, comparison [20] between calculation for different sets of  $\rho$  and  $\Gamma$  and experimental data permits one to reveal the parameter's set having the smallest systematical errors. There is necessary but insufficient condition for reliability of the  $\rho$  and  $\Gamma$  values obtained in experiment.

#### 6. Direct model-less estimation of level density and radiative strength functions

At present, the most precise but incomplete test of results obtained in two-step nuclear reactions can be done only by means of maximum model-free analysis of the primary gammatransitions from reaction  $(\bar{n}, \gamma)$  (capture in "averaged" resonances). Analogous results can be obtained also in any accelerator beam experiment in the fixed (several keV) excitation energy interval and (it is desirable) in limited and known spin window of excited levels of studied nucleus. Practical possibility for this is provided by established in [1,2] fact of relatively small level density in nuclei of any type below  $\approx 0.5B_n$  excited by the dipole primary gammatransitions following decay of compound-states with one or two possible spins.

Resolution of modern HPGe-detectors permits one to determine parameters of corresponding peaks with negligibly small statistical error up to the values  $\rho\sim100\text{-}200~\text{MpB}^{-1}$ . The presence of step-like structure in level density below  $\approx0.5B_n$  provides execution of this condition for even-odd deformed compound nucleus, for example, up to excitation energy  $\sim3$  MeV.

Random character of amplitudes ( $I^{I/2}$ ) of any primary gamma-transition was verified experimentally by studying neutron capture in neutron resonances. Therefore, averaging of partial widths over larger or lesser set of decaying initial levels decreases partial width fluctuations for any distribution of their deviations from the average and decreases portion of the primary gamma-transitions whose intensities are lying below the experimental detection threshold.

In this situation, verification of the experimental data on level densities from one- and two-step reactions at minimum number of hypothesis used must and can be done by approximation of distribution of these averaged intensities above registration threshold and its extrapolation in the intensity region below detection threshold.

In dependence on spin values, experimental distribution can be superposition of two and more individual distributions. The desired parameters for each of them are the most probable number of intensities, mean value, dispersion and their detection threshold.

Authors of experiments performed up to now have analyzed the data in frameworks of notions of limited "statistical" theory of the gamma-decay. The data [1,2,14] unambiguously require their re-analysis within apparatus of mathematics statistic with accounting for possibility of:

- (a) strong dependence of the gamma-transition intensities on structure of excited levels;
- (b) violation of the Porter-Thomas distribution [21] for larger or lesser part of experimental data and
- (c) significant variation of mean widths and their dispersion for gamma-transitions of different multipolarity as changing the level excitation energy.

The necessary re-analysis calls no difficulties:

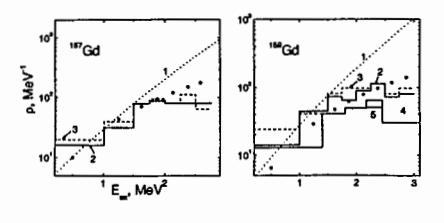
- (a) the random intensity distribution is easily approximated in integral form (cumulative sum of reduced intensities in function of current intensity value) even for small sets of experimental values;
- (b) the best value of the distribution dispersion is set in form  $\sigma^2 = 2/\nu$  with the desired parameter  $\nu$ ;

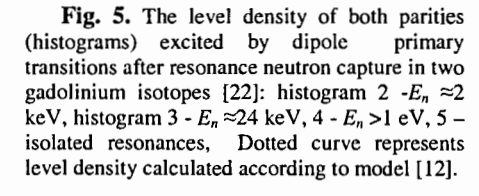
(c) detection threshold for gamma-transition registration and the most probable number of of gamma-transitions of a given multipolarity (the same for the dipole E1- and M1-transitions) is unambiguous enough.

Only the determination of ratio  $R_k$  for mean reduced intensities of M1- and E1-transitions in every 200-300 keV excitation energy intervals can be ambiguous. But near  $R_k$ -0 and  $R_k$ -1 they are indiscernible for approximation procedure (but, correspondingly they differ by two times in desired number of gamma-transitions).

Unfortunately, the data on  $\rho$  and  $\Gamma$  obtained in this way can be to the more or less extent doubtful. This can be due to significant systematical errors in determined experimental sets of the primary transition intensities or due to analysis performed within unverified hypothesis that gamma-transitions of equal multipolarity, the same spin values of decaying compound-states and excited levels have practically equal mean values, at least, in the narrow excitation energy intervals.

If this hypothesis is true in wide enough energy interval of the observed primary gamma-transitions, then such verification confirms [22] presence of step-wise structure and increasing in probability of gamma-transitions to corresponding levels. Moreover, one can conclude that the level densities in [1,2] are considerably overestimated because of underestimation of intensity of the secondary gamma-transitions to these levels.





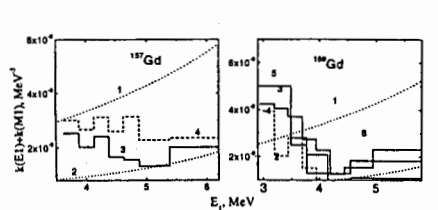


Fig. 6. The sum of the probable radiative strength functions of E1- and M1-transitions. The upper (1) and lower (2) dotted curves represent calculation within the models [4] and [11] in sum with k(M1)=const, respectively. The histograms show the data [22]: 3 — for  $E_n \approx 2$  keV, 4 – for  $E_n \approx 24$  keV, 5 – for  $E_n > 1$  eV and histogram 6 – for isolated neutron resonances.

The data existing for set of actinides [23] on  $(\overline{n}, \gamma)$  reaction allow one to expect level densities and radiative strength functions for them (figs. 7,8) analogous to those obtained for lighter nuclei [1,2]. Experimental data from reaction  $(\overline{n}, \gamma)$  give unique possibility for experimental determination of ratio between the level densities with different parity in rather wide excitation energy region of nuclei studied in  $(\overline{n}, \gamma)$  reaction. Strong correlation between the strength functions of the different multipolarity gamma-transitions and density of levels of different parity does not allow one to get in [1,2] unambiguous ratios k(M1)/k(E1) and  $\rho(\pi=-)/\rho(\pi=+)$ . But, as it was obtained in [22], the ratios k(M1)/k(E1) are determined experimentally. And due to strong correlation of parameters under consideration, this provides for direct experimental determination and of ratio  $\rho(\pi=-)/\rho(\pi=+)$  in the iterative process [1,2].

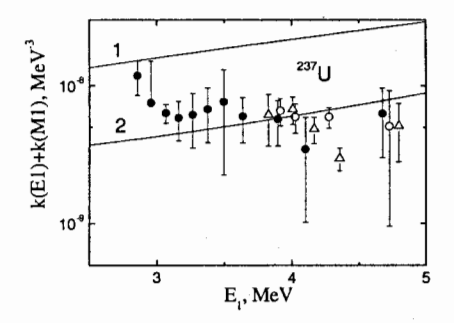


Fig. 7. The sum of the radiative strength functions of E1- and M1-transitions for  $^{237}$ U. Black points represent data for the neutron energy region  $5 < E_n < 125$  eV, open points – for  $E_n \approx 2$  keV, triangles – for  $E_n \approx 24$  keV. The upper and lower curves show predictions of the models [4] and [11] in sum with k(M1)=const, respectively.

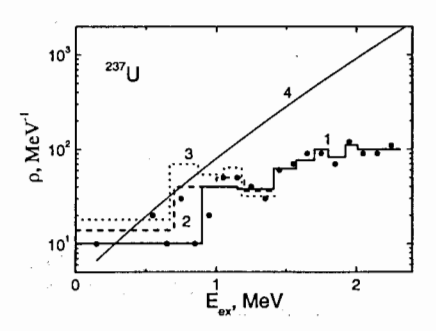


Fig. 8. The same, as in Fig. 5, for density of excited levels. The solid curve corresponds to predictions according to model [11] for spin values J=1/2 and 3/2. Points show the numbers of levels observed in resolved resonances.

#### 7. Aims and possibilities of future experiments

Comparison between the experimental data on  $\rho$  and  $\Gamma$  derived from the spectra of two-step reactions with realistic enough model ideas provides [14,15,18] for potential possibility for obtaining the most reliable data on correlation functions of nucleons in heated nuclei. Id est., for practical studying superfluidity in such rather specific system as heated nuclei.

For maximal decrease in systematical errors in determination of nuclear parameters, it is necessary, first of all, to improve experimental methodology. It can be done in the following directions:

- (a) accumulation of the maximum reliable data on the primary gamma-transition intensities following resonance neutron capture on "filtered" beams;
- (b) measurement of cascade intensities with two and more quanta on beams of thermal and resonance neutrons:
- (c) measurement of spectra of two-step reactions like (particle, gamma-quantum) on accelerator beams with high energy resolution of particle registration. Besides, two possibilities enumerated above should be used in order to derive information from the gamma-cascades following emission of particle with excitation of high-lying levels of final nucleus.

These experimental data must be analyzed with accounting for potentially strong influence of nuclear structure on emission probability of reaction products.

#### 8. Conclusion

Modern experimental technique at correct (from the point of view of mathematical statistics and with exclusion of superfluous hypotheses) analysis of its data provided for possibility of detailed search for interaction process between fermion and boson components of nuclear matter. Potentially possible information can de obtained under conditions completely being absent in macrosystems (limited sizes, change in ratio of different type excitations, shell structure and so on).

#### REFERENCES

- 1. Vasilieva E.V., Sukhovoj A.M., Khitrov V.A., Phys. At. Nucl., 64(2) (2001) 153. (nucl-ex/0110017).
- 2. Sukhovoj A.M,. Khitrov, V.A., Physics of Paricl. and Nuclei, 36(4) (2005) 359.
- 3. Bohr A.,. Mottelson B.R, Nuclear structure, Vol. 1 -W.A. Benjamin, Inc. New York, Amsterdam, 1969.
- 4. Axel P., Phys. Rev., 126(2) (1962) 671-683.
- 5. Brink D. M., Ph. D. thesis, Oxford University (1955).
- 6. Vonach H., Proc. IAEA Advisory Group Meeting on Basic and Applied Problems of Nuclear Level Densities, (New York, 1983), INDC(USA)-092/L, (1983), P.247.
- 7. Zhuravlev B.V., Bull. Rus. Acad. Sci. Phys., 63 (1999) 764.
- 8. Boneva S.T., Khitrov V.A., Sukhovoj A.M., Nucl. Phys., A589 (1995) 293.
- Reference Input Parameter Library RIPL-2. Handbook for calculations of nuclear reaction data. IAEA-TECDOC, 2002. <a href="http://www-nds.iaea.or.at/ripl2">http://www-nds.iaea.or.at/ripl2</a>.
- 10. Solov'ev V.G., Fiz. Elem. Chastits At. Yadra, 3(4) (1972) 770.
- 11. Kadmensky S.G., Markushev V.P., Furman W.I., Sov. J. Nucl. Phys., 37 (1983) 165.
- 12. Dilg W., Schantl W., Vonach H., Uhl M., Nucl. Phys., A217 (1973) 269.
- 13. Strutinsky V.M., Proc. of Int. Conf. Nucl. Phys., Paris, 1958. P. 617.
- 14. Sukhovoj A.M., Furman W.I.,, Khitrov V.A, // Proc. of the XV International Seminar on Interaction
- of Neutrons with Nuclei, Dubna, May 2007, E3-2007-9, Dubna, 2007, -P. 92.
- 15. Sukhovoj A.M. Khitrov V.A., Physics of Paricl. and Nuclei, 37(6) (2006) 899.
- 16. Rejmund F., Ignatyuk A.V., Junghans A.R., Schmidt K.-H., Nucl. Phys., A678 (2000) 215.
- 17. Mughabghab S.F. // Neutron Cross Sections BNL-325. V. 1. Parts A, Ed. By Mughabghab S.F., Divideenam M., and Holden N.E.// (N.Y., Academic Press, 1984).

Mughabghab S.F., Neutron Cross Sections, V.1, part B, Ed. by Mughabghab S.F., (N.Y., Academic Press, 1984).

- 18. Sukhovoj A.M. Khitrov, V.A., JINR preprint E3-2005-196, Dubna, 2005.
- 19. Khitrov V.A., Li Chol, Sukhovoj A.M., Proc. of the XI International Seminar on Interaction of Neutrons with Nuclei, Dubna, May 2003, E3-2004-9, Dubna, 2004, -P. 98. (nucl-ex/0404028).
- Sukhovoj A.M., Khitrov V.A. et al., Proc. of the XIII International Seminar on Interaction of Neutrons with Nuclei, Dubna, E3-2006-7, Dubna, 2006, P.

Sukhovoj A.M., Khitrov V.A. et al., ibid., P. 72.

Sukhovoj A.M., Khitrov V.A.et al., ibid., P. 64.

Khitrov V. A., Sukhovoj A. M., Grigoriev E. P. Proceedings of the Eleventh International Symposium on Capture Gamma-Ray Spectroscopy and Related Topics, Pruhonice, 2002, World Scientific, 2002, Ed. by J. Kvasil, P. Ceinar, M. Krticka, P. 718.

Sukhovoj A.M., Khitrov V.A., Grigor'ev E.P., INDC(CCP)-432, Vienna, 2002,pp. 115-132.

- 21. Porter C.F., and Thomas R.G., Phys. Rev., 104(2) (1956) 483.
- 22. These proceedings, P. .
- 23. von Egidy T. et al., Phys.Rev. C 20 (1979) 944.

# PARAMETERS OF DISTRIBUTION OF THE PRIMARY GAMMA-TRANSITION INTENSITIES FOLLOWING RESONANCE NEUTRON CAPTURE AND SOME PROPERTIES OF COMPOUND NUCLEI $^{157,159}\mathrm{Gd}$

#### A.M. Sukhovoj, V.A. Khitrov

Joint Institute for Nuclear Research, 141980, Dubna, Russia

#### Abstract

The re-analysis of the published experimental data on the primary gamma-transition intensities following neutron capture in different groups of neutron resonances in  $^{156,158}\mathrm{Gd}$  has been performed. There are determined the most probable values of sum of E1 and M1 primary transitions, numbers of excited by them levels of both parities, ratios of radiative strength functions k(M1)/k(E1), dispersions of deviations of random values of intensities from the average and ratios of mean intensities of primary transitions to levels J=5/2 with respect to analogous data for J=1/2 and 3/2 (capture of the 24 keV neutrons) in narrow excitation energy intervals.

All the data on level density and sums of radiative strength functions confirm the presence of clearly expressed step-like structure in level density below 3 MeV and general trend in change in strength functions as changing primary gamma-transition energy. Variations of distribution dispersions and, especially, ratio k(M1)/k(E1) (or k(E1)/k(M1)) at changing excitation energy point to strong change in structure of these nuclei above 1.0-1.5 MeV.

As in neighboring isotopes  $^{156,158}$ Gd, the shape of energy dependence of k(M1) + k(E1) considerably differs as changing nuclear mass. This can be due to dependence of gamma-decay process on structure of neutron resonance and/or levels excited by gamma-transitions. The dilemma appeared can be solved only in direct experimental search for structure of neutron resonances in region of their energy of about two nucleon pairing energy in nuclei of corresponding mass.

#### 1 Introduction

Density of excited levels  $\rho$  and emission probability  $\Gamma$  of any nuclear reaction product following neutron resonance  $\lambda$  decay are the main sources of experimental information on properties of nuclear matter and practically important nuclear-physics constants. This stipulates for necessity of their determination with maximum possible accuracy.

However, the  $\rho$  and  $\Gamma$  values cannot be determined for main mass of nuclei excited in  $(n,\gamma)$  reaction in direct experiments: mean spacing D between levels is comparable with or much less than a resolution (FWHM) of existing spectrometers. Correspondingly, these parameters can be extracted only from the spectra measured with "bad" resolution. Only one-step reactions were mainly used for this aim. Obtaining of information on  $\rho$  and  $\Gamma$  from gamma-spectra of two-step reaction was started only in the last time [1]. Comparison of shape of functional dependence of the obtained in this way values of  $\rho = f(E)$  and radiative strength functions  $k = \Gamma_{\lambda}/(E_{\gamma}^{2}D_{\lambda}A^{2/3}) = \phi(E_{\gamma})$  with the data of one-step reactions (spectra of evaporated nucleons, different gamma-spectra) points to

their principle incompatibility. It appears itself in presence [1] or lack of abrupt changes in determined parameters. This operation allows one to determine sources of systematical errors, estimate their values and reveal the region of maximum discrepancy between the data of different experiments.

Analysis of the most sufficient sources of systematical errors [2] and their transfer coefficients onto errors of parameters in practically realized case of two-step reaction (two simultaneously emitted gamma-quanta) showed that even maximum possible errors of the  $\rho$  and  $\Gamma$  values (obtained from two-step reaction) cannot explain discrepancy for one- and two-step reactions.

Nevertheless, necessity of additional testing a method for determination of  $\rho$  and  $\Gamma$  from two-step reactions calls no doubts. At present, such test can be performed only in model-less analysis of the primary gamma-transition intensities from reaction  $(\overline{n}, \gamma)$  (capture in "averaged" resonances).

Possibility to obtain new information from these data is caused by the use by authors of experiments of unnecessary for analysis ideas of "statistical" mechanism of gamma-decay process and abstract form of distribution law of arbitrary gamma-transition intensity deviation in individual resonance from mean value. The shape of approximating function and concrete results of analysis of rather limited set of strongly fluctuating data are given in [3]. More general variant of analysis is described in [4].

# 2 Experimental data

In the isotopes under consideration <sup>157,159</sup>Gd were measured the primary transition intensities following resonance neutron capture with mean energies of 2 and 24 keV; there are also data for <sup>159</sup>Gd for both capture of neutrons in resolved resonances and on beam with cadmium filter. Experimental data cover maximum level excitation energy diapason for even-odd deformed nuclei and allow one to get maximum possible and completely independent information on the desired gamma-decay parameters.

In two last cases s-neutrons are mainly captured, but capture of p-neutrons must be taken into account at  $E_n=2$  and 24 keV. According to [5], ratio between available in that time values of strength functions of s- and p-neutrons does not exceed 0.08 for  $E_n=2$ , but is grater than 1 for 24 keV. Therefore, the following analysis should account for excitation of resonances with spins 1/2, 3/2 and different parity only for the data  $E_n=24$  keV. This means that the averaged intensity of the primary dipole gamma-transitions to levels 5/2 depends on ratio between strength functions  $S_0$ ,  $S_1$  and that it must be varied at determination [4] of distribution parameters of the random intensity deviations from mean value. In principle, level density with spin 5/2 in deformed nuclei must be bigger than corresponding sum for spins 1/2, 3/2 (as it approximately follows from known functional dependences  $\rho = f(J)$ ). In case of lower neutron energy, there was adopted hypothesis of equal intensity of primary gamma-transitions with near energy and the same multipolarity to levels with spins 1/2, 3/2.

This assumption can be mistaken for strongly differing structure of wave functions of excited levels with different spin. According to modern microscopic nuclear models, amplitude of gamma-transition is determined by a set of quasiparticle and phonon components. Their contribution depends on wave functions of both decaying and excited levels (simplified expression for matrix element of gamma-transition in even-odd nucleus is given for example, in [6]).

## 3 Required parameters of analysis

Examples of random intensity distributions in integral form for their different  $N_{\gamma}$  values in given level excitation energy interval, ratios k(M1)/k(E1) of strength functions of E1- and M1-transitions, dispersions of distributions  $\sigma^2 = 2/\nu$  and registration threshold of peak in spectrum are given in [4] for the case of excitation of resonances with the only spin value.

Introduction of additional parameter (ratio between mean intensities of primary gamma-transitions to levels 5/2 and corresponding data for levels 1/2, 3/2) in the case of resonance with two spin values weekly influences stability of approximation and sensitivity of this process to variation of initial values of fitted parameters. This result was tested for the case when mean intensities in two different groups differed, practically, by a factor 2.

# 4 Results of analysis

Experimental cumulative sums of relative intensities  $\langle I_{\gamma}/E_{\gamma}^3 \rangle$  are presented in figs. 1,2 together with their best approximations. As an example, there are used the data for  $E_n=2$  keV. Due to negligible contribution of p-neutron capture, approximation takes into account only two distributions – E1- and M1-transitions following decay of resonances with spins 1/2. Experimental distributions for  $E_n=24$  keV are superposition of four distributions – two distributions mentioned above and one more pair corresponding to gamma-transitions between resonances with J=3/2 and final levels with J=5/2. Its mean intensity relatively to gamma-transition intensities to levels J=1/2, 3/2 is found equal  $\approx 0.44$  for both isotopes (but with some larger dispersion of values for <sup>159</sup>Gd).

All the data are presented so that the expected total intensity of gamma-transitions lying below registration threshold corresponds to the most probable value of cumulative sum for zero intensity.

Precision in determination of parameters of approximating curve at low energy of final levels  $E_i$  must get worse due to inequality of level densities with different parity. Most probably, this increases error of extrapolation by approximating curve to zero intensity of gamma-transition. In practice, overestimation of the  $N_{\gamma}$  values seems to be more probable.

The best values of fitting parameters  $R_k = k(M1)/k(E1)$  and  $\nu$  are presented in figs. 3 and 4. Main part of data in fig. 3 corresponds to the case k(M1)/k(E1). In potentially possible case  $k(E1) \leq k(M1)$ , some portion of the data shown in these figures corresponds to alternatively determined ratio k(E1)/k(M1). These cases cannot be revealed without the use of additional experimental information. Noticeable change in  $R_k = k(M1)/k(E1)$  and  $\nu$  at  $\approx 1$  MeV points to considerable change in structure of isotopes under study at this excitation energy. As it is seen from figure 4, fluctuations of random intensities to final levels of <sup>159</sup>Gd with spins 1/2, 3/2, from the one hand, and 5/2, from the other hand, are described by distributions with rather different values of  $\nu$ . This fact has, in

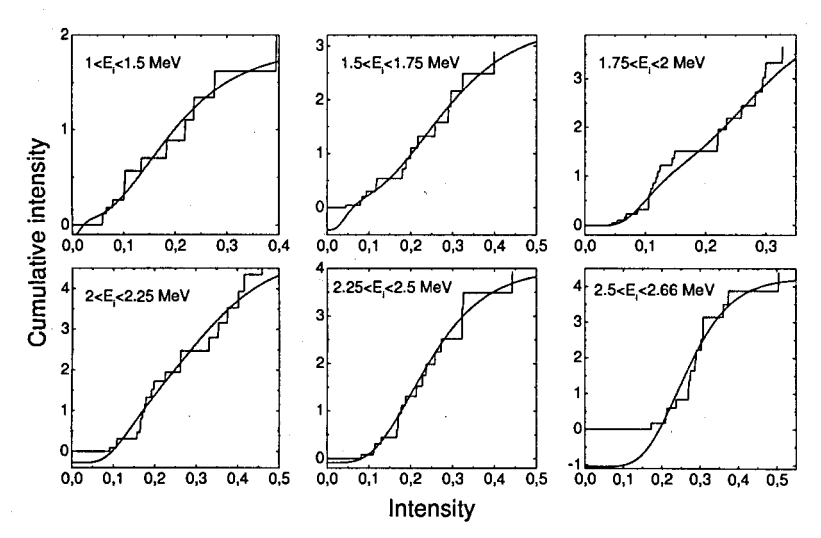


Fig. 1. The experimental cumulative sum of reduced intensities  $\langle I_{\gamma}/E_{\gamma}^{3} \rangle$  for <sup>157</sup>Gd - histogram. Smooth curve corresponds to the best approximation. Excitation energy intervals of cascade final levels  $E_{i}$  are given in figure. Experimental data for neutron energy  $\approx 2$  keV.

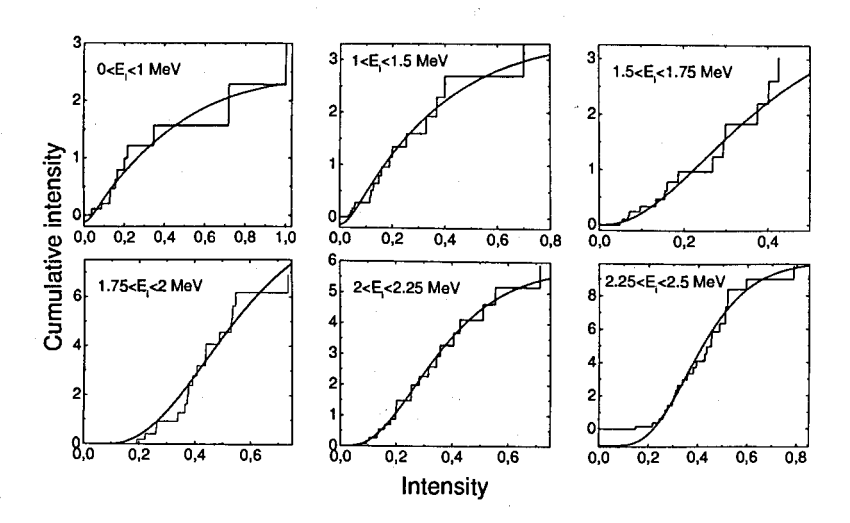


Fig. 2. The same, as in Fig. 1, for <sup>159</sup>Gd.

principle, the following interpretation:

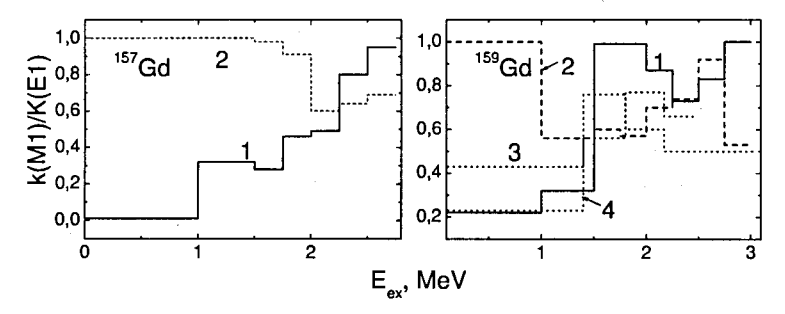


Fig. 3. The best values of ratios k(M1)/k(E1) (or k(E1)/k(M1)) for different energy of levels excited by dipole gamma-transitions in  $^{157,159}$ Gd. Line 1 represents data for  $E_n \approx 2$  keV, line 2 - for  $E_n \approx 24$  keV. Line 3 - data for  $E_n > 1$  eV, line 4 - data for isolated resonances

- (a) distinction in structure of decaying neutron resonances with different spin and parity;
- (b) amplitude of corresponding gamma-transitions is determined by components of wave functions which differ (see, for example, [9]) in number of phonons and degree of their fragmentation;
- (c) different structure and degree of fragmentation of the levels excited by primary gamma-transitions.

In principle, one cannot exclude possibility of presence of some specific systematical uncertainty which explains this effect. But, there is required realistic explanation for its selectivity with respect to resonance spins. Unreality of existence of assumed uncertainty brings to considerable conclusion: there are not grounds to exclude possible appearance of the different  $\nu$  values for gamma-transitions with different multipolarity to final levels

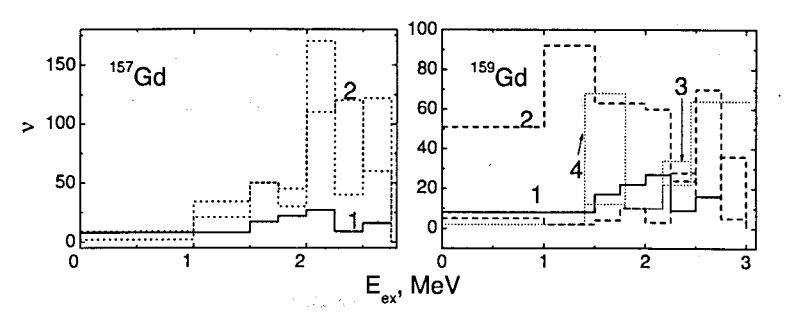


Fig. 4. The same, as in Fig. 3, for parameter  $\nu$  for <sup>157,159</sup>Gd.

with different spin. The data in figs. 3.4 unambiguously point to evident change in structure of wave functions of final levels below and above  $\approx 1$  MeV.

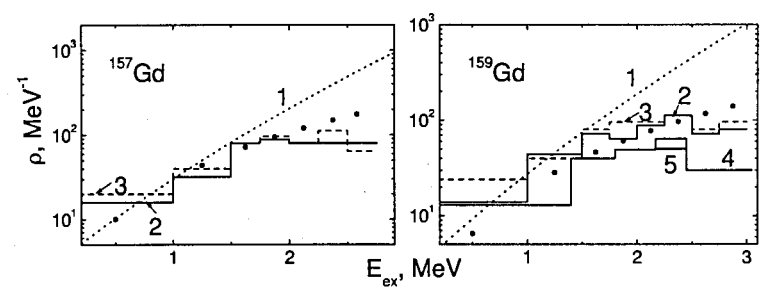


Fig. 5. Different data on level density in  $^{157,159}$ Gd. Dotted curves 1 represent results of calculation within model [16]. From the data for  $E_n \approx 2$  – histogram 2;  $E_n \approx 24$  keV – histogram 3. Points - the best fit of data for  $E_n \approx 2$  within model [14] for  $K_{coll}$ =const. Histogram 4 shows data for  $E_n > 1$  eV, histogram 5 - for isolated resonances.

The best values of level density  $\rho = \sum_{J,\pi} N_{\gamma}/\Delta E$  and sums of radiative strength functions  $\sum \langle I_{\gamma} \rangle / \langle E_{\gamma}^3 N_{\gamma} \rangle$  are shown in figs. 5, 6. Normalization of intensities and strength functions in both [7] and [8] was performed for five (from six) data sets.

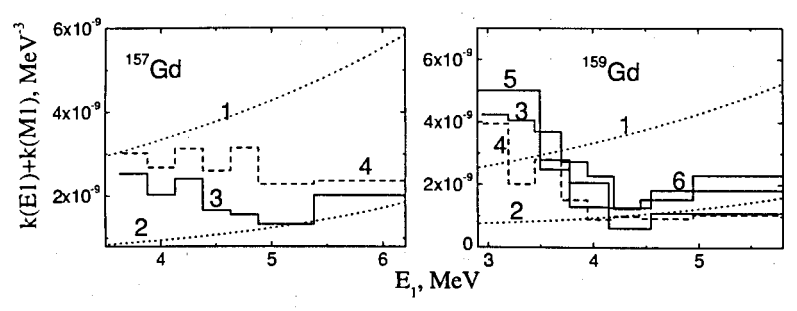


Fig. 6. Different data on radiative strength functions of the primary gamma-transitions in  $^{157,159}$ Gd. Dotted curve 1 shows results of calculation according to model [17]; dotted curve 2 – calculation within model [18] in sum with k(M1) = const. From the data for  $E_n \approx 2$  – histogram 3;  $E_n \approx 24$  keV – histogram 4. From the data for  $E_n > 1$  eV – histogram 5; isolated resonances – histogram 6.

Because intensities of gamma-transitions following "filtered" neutron capture are given in [7, 8] in relative units then corresponding strength functions in figs. 5, 6 are combined with each other under assumption of their approximate equality for final levels  $E_i < 1$  MeV.

The most probable approximated  $N_{\gamma}$  values from capture spectra of 2 keV and 24 keV neutrons in <sup>158</sup>Gd below 1.0 and above 2.5 MeV exceed "resonance" values, practically, by a factor of 2 (and some less - in other excitation energy intervals).

#### 4.1 Some sources of systematical errors

Absolute minimum of  $\chi^2$  for all the used sets of intensities is achieved, practically, for the only value of  $N_{\gamma}$ , if the value of this variable equals  $\sim 5$ . Change in this parameter by  $\pm 1$  brings usually to considerable increase in  $\chi^2$ .

This allows one not to account for possibility of considerable (for example, more than 10-20%) uncertainty in determined level density caused by chosen conditions of approximation (excluded inequality of level densities with different parity).

Main problems in determination of nuclear parameters and their systematical errors are, most probably, caused by:

- (a) the use of assumptions on shape of the random intensity deviations from mean value and
- (b) possible presence of significant systematical errors in sets of analyzed intensities [7, 8].
- 1. The Porter-Thomas distribution allows very significant random partial widths. But fluctuations of the measured gamma-transition intensities  $I = \Gamma_{\lambda i}/\Gamma_{\lambda}$  are always limited in their maximum value by positive correlation between partial and total radiative widths of decaying level. This results in some overestimation of number of degrees of freedom  $\nu$  determined by approximation and its dependence on intensities included in approximation of cumulative sums. For instance, there is region of values  $I_{\gamma}/(E_{\gamma}^3) > 0.4$  for  $1 < E_i < 1.5$  MeV shown in Fig. 1. Intensities in the performed analysis were normalized so that their maximum value did not exceed  $\sim 50\%$  of approximation region for the majority of data sets.
- The main error of analysis can be related only to "loss" of gamma-transitions whose intensities do not exceed threshold value and/or mistaken identification of quanta ordering in gamma-cascades.

Probability of overlap of two peaks corresponding to near-lying levels was estimated in [10]. As it follows from the data presented by authors, this effect is small enough and, most probably, cannot explain significant (several times) discrepancy between level density determined by us and its prediction in the frameworks of the Fermi-gas model. Moreover, this overlapping in the chosen presentation of experimental data increases rate of growth of cumulative sums and, most probably, overestimates the  $N_{\gamma}$  value obtained. There could be essential uncertainty caused by even and considerable loss of some part of observed peaks corresponding to intense primary transitions due to groping of levels in near-lying (spacing of about 1-2 keV) multiplets. But this possibility is not predicted by modern nuclear theory. Experimental data of nuclear spectroscopy also do not point to existence of numerous multiplets of neighboring levels with spins 1/2 and 3/2 in even-odd compound nuclei.

3. It is also possible that the gamma-transitions in the all or greater part of chosen intervals of of primary transition intensities (with the width of some hundreds keV) have different mean values. Moreover, probability of relatively low-intensity gamma-transitions

quickly (but smoothly) increases as decreasing their intensity. In principle, this effect can be caused by mechanism of fragmentation [9] of different states over neighboring levels of a nucleus.

Apparently, only this hypothesis can be alternative explanation of "step-like" structure in level density in performed here analysis. This hypothesis can be applied to the determined according to [1, 11] level densities under the following conditions: main part of levels (with the same  $J^{\pi}$ ) below  $\sim 0.5B_n$  must not be excited by primary gammatransitions; some Cooper pairs of nucleons must break simultaneously at small as compared with  $B_n$  nuclear excitation energy. One cannot suggest other possibility for precise calculation of the two-step gamma-cascade intensities in the investigated even-odd nuclei.

#### 4.2 Interpretation of the obtained results

The most important physics information on structure of excited levels below  $\approx 0.5B_n$  can be derived from coefficient of collective enhancement of level density  $K_{\text{coll}}$ :

$$\rho(U, J, \pi) = \rho_{\rm qp}(U, J, \pi) K_{\rm coll}(U, J, \pi). \tag{1}$$

In accordance with modern notions,  $K_{\rm coll}$  determines [12] degree of increase in density of pure quasiparticle excitations  $\rho_{qp}(U,J,\pi)$  in deformed nucleus due to its vibrations and rotation. One can accept in the first approach that, to a precision of small constant, it equals coefficient of vibrational enhancement of level density  $K_{\rm vibr}$ .

On the whole, this coefficient is determined by change in entropy  $\delta S$  of a nucleus and redistribution of nuclear excitation energy  $\delta U$  between quasiparticles and phonons at nuclear temperature T:

$$K_{\text{vibr}} = exp(\delta S - \delta U/T).$$
 (2)

Now there is a possibility for unambiguous experimental determination [13] of breaking threshold  $E_N$  for the first and following Cooper pairs, value and shape of correlation functions  $\delta_N$  of nucleon pair number N in heated nuclei. The main uncertainty of  $E_N$  is caused by the lack of experimental data on function  $\delta_N = f(U)$ , the secondary - by uncertainty of one-quasiparticle level density g in model [14]. So, three different model dependent approximations of level density in large set of nuclei ([13] and [15]) predict threshold  $E_2$  for five-quasiparticle excitations which differs by a factor of 1.5-2.0.

In practice, we used the second variant of notions of the Cooper pair correlation function in heated nucleus [13] for estimation of the  $K_{\rm vibr}$  value from approximation of the data [7, 8]. The values  $\delta_1 = 1.02$  MeV, g = 9.95 MeV<sup>-1</sup> were used in calculation. Densities of three-quasiparticle levels (multiplied by the "best"  $K_{\rm vibr} = const$  value) calculated for the breaking threshold of the first Cooper pair of nucleons  $E_1 = 0$  MeV are given in fig. 7. Its concrete values for minimal  $\chi^2$  are equal to 9.6 and 6.3 for <sup>157</sup>Gd and <sup>159</sup>Gd, respectively. The assumption on energy independence of  $K_{\rm vibr}$  at low excitation energy is evidently unreal (see fig. 7).

Parameter  $K_{\text{coll}}$ -1 determined from comparison between calculated in this way density of three-quasiparticle excitations (J = 1/2, 3/2) and its most probable experimental value is compared with calculated value  $\delta_1$  in Fig. 7.

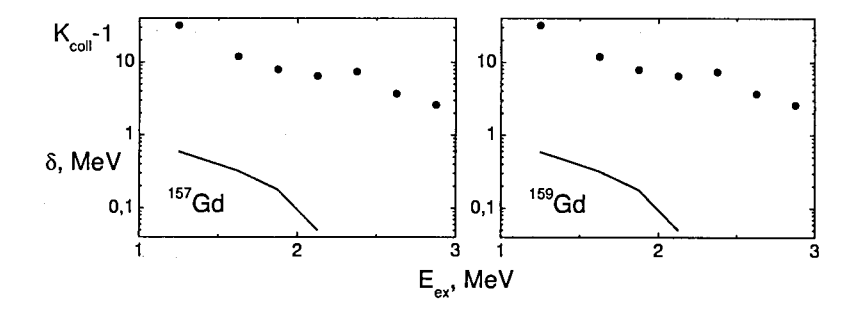


Fig. 7. Points show coefficient of collective enhancement of level density, curve represents the values of parameter  $\delta_1$  used in [13, 15] for calculation of partial density of three-quasiparticle levels.

In the excitation energy interval below  $\approx 2$  MeV is observed considerable correlation of this coefficient with the  $\delta_1$  value from [15] and from the second variant of analysis [13]. Decrease in correlation at higher excitation energy can be related to significant contribution of five-quasiparticle excitations in function  $\rho_{qp}(U,J,\pi)$  and/or to smaller than it is adopted in [13, 15] rate of decrease of function  $\delta_1$  at U > 1.8 MeV.

Analysis of experimental data presented above in common with the data [1, 11] points to necessity of experimental search for neutron resonance structure in the energy interval  $E_n$  of about 1-2 MeV and more. Figure 6 show both general properties of radiative strength functions in isotopes under consideration and their evident difference in region below  $\sim 0.5 B_n$ .

Analogous variations of energy dependence of radiative strength functions in both nuclei of neighboring elements and isotopes are also demonstrated by analysis of the two-step cascade intensities. If these changes are completely or to a great extent determined by difference in ratio between quisparticle and phonon components of the neutron resonance wave functions then extrapolation of the regularity established in [15] for expected difference of breaking threshold of two neighboring Cooper pairs  $E_{N+1} - E_N \approx 2\delta$  can be spread and into the region above  $B_n$ . Therefore, one can expect cyclic change in structure of excited resonances with period of about 2 MeV for heavy nuclei with  $\delta \sim 1$  MeV.

Moreover, this effect in even-odd isotopes of rear earth elements can appear itself as change in ratio between intensities of the primary transitions with energy  $E_1=3-4$  MeV and  $E_1>B_n-1$  MeV.

The data presented allow the following conclusions:

- 1. Nuclei  $^{157,159}$ Gd, excited in the  $(\bar{n},\gamma)$  reaction by the 2 keV and 24 keV neutrons demonstrate the same properties as those revealed earlier for about forty nuclei from the mass region  $40 \le A \le 200$ : step-wise structure in level density and local strengthening of radiative strength functions of the primary gamma-transitions to the levels of this structure.
- 2. Abrupt change in structure of levels in the excitation energy region about 1.0-1.5 MeV. It manifests itself in considerable increase of the k(M1)/k(E1) values and in strong difference between their distribution and normal distribution of random gamma-transition amplitudes.

- 3. These experimental ratios k(M1)/k(E1) can be used for obtaining of simpler values of the E1- and M1-transition strength functions and data on the ratio between density of levels with different parity in the frameworks of methods [1, 11].
- 4. Main part of the primary gamma-transitions observed in the  $(\bar{n}, \gamma)$  reaction corresponds, probably, to excitation of levels with large and weakly fragmented phonon components of wave functions.
- 5. The data on the most probable  $N_{\gamma}$  values obtained for different intervals of neutron energy allow one to consider practically negligible dependence of the determined level density on  $E_n$ . Besides, influence of nuclear resonance structures results in considerable change in shape of the deviation distribution of the gamma-transition intensities from its mean value even in the narrow interval of nuclear excitation energy considered here.

#### 5 Conclusion

Analysis of the available data on the primary gamma-transition intensities from  $(\overline{n},\gamma)$  reaction in compound nuclei <sup>157,159</sup>Gd showed step-like structure in density of their levels and increase in radiative strength function of transitions to levels in region of this structure, at least, for primary dipole gamma-transitions. Id est, it confirmed main conclusions of [1, 11] and pointed to necessity to reveal and remove systematical experimental errors in alternative methods for determination of only level density [19] and simultaneous determination of all the parameters of cascade gamma-decay [20, 21]. The most important problems at experimental determination of level density and emission probability of reaction product become both correct accounting for influence of level structure on emission probability of nuclear evaporation and cascade gamma-quanta in investigations of nuclear reactions on accelerator beams and considerable decrease in systematical errors of experiment.

The best estimations of dispersion (parameter  $\nu$ ) of the random intensity fluctuations strongly differ from the mean values predicted in [22]). This allows one to assume that the wave functions of levels excited by primary transitions contain considerable components of weakly fragmented nuclear states which are more complicated than one- or three-quasiparticle states. Approximation of the obtained level density by model [14] confirms the fact of considerable ( $\approx 10$  times) increase of level density due to excitations of mainly vibration type [15]. Comparison of the data presented in figs. 5,6 with those obtained from intensities of two-step cascades permits one to make preliminary conclusion that the abrupt change in structure of decaying neutron resonances, at least, in their energy interval  $\approx 24$  keV is not observed. There is no reason to wait principle change in the determined according to method [1, 11] level density and energy dependence of the primary transition radiative strength functions from resonance to resonance. Further decrease of errors of these nuclear parameters determined from intensities of the two-step gamma-cascades undoubtedly requires reliable estimation of function  $k(E_{\gamma}, E_{ex})$  practically in all energy diapason of levels excited at thermal neutron capture.

#### References

- [1] E. V. Vasilieva, A. M. Sukhovoj, V. A. Khitrov, Phys. At. Nucl., 64, 153 (2001).
- V. A. Khitrov, Li Chol, A. M. Sukhovoj, in: XI International Seminar on Interaction of Neutrons with Nuclei, Dubna, May 2003, E3-2004-9, (Dubna, 2004), p. 98;
   V. A. Khitrov, Li Chol, A. M. Sukhovoj, nucl-ex/0404028.
- [3] A. M. Sukhovoj, V. A. Khitrov, Phys. Atomic Nuclei, 62, 19 (1999).
- [4] A. M. Sukhovoj, Physics of Atomic Nuclei, 71, 1907 (2008).
- [5] G.W. Reich, Proc. of the 3th International Symposium on Capture Gamma-Ray Spectroscopy and Related Topics, Upton, 18-22 September 1978 /Ed. R.E.Crien, W.R.Kane, Plenum Press, N.Y. and London, p. 105.
- [6] S.T. Boneva et al., Yad. Fiz., 49, 944 (1989).
- [7] J. Kopecky, M. Uhl, R.E. Chrien, Phys. Rev. 47(1), 312 (1993).
- [8] G. Granja, S. Pospisil, S.A. Telezhnikov, R.E. Chrien, Nucl. Phys. A729, 679 (1984).
- [9] L.A. Malov, V.G. Soloviev, Yad. Fiz., 26, 729 (1977).
- [10] V.L. Stelts, R.E. Chrien, M.K. Martel, Phys. Rev. C, 24(4), 1419 (1981).
- [11] A.M. Sukhovoj, V.A. Khitrov, Physics of Particl. and Nuclei, 36(4), 359 (2005).
- [12] Reference Input Parameter Library RIPL-2. Handbook for calculations of nuclear reaction data. IAEA-TECDOC, 2002. http://www-nds.iaea.or.at/ripl2. Handbook for Calculation of Nuclear Reactions Data, IAEA, Vienna, TECDOC-1034, 1998.
- [13] A. M. Sukhovoj, V. A. Khitrov, Preprint Nº E3-2005-196, JINR (Dubna, 2005).
- [14] V. M. Strutinsky, in Proc. of Int. Conf. Nucl. Phys., (Paris, 1958), p. 617.
- [15] A.M. Sukhovoj, V.A. Khitrov, Physics of Paricl. and Nuclei, 37(6), 899 (2006).
- [16] W. Dilg, W. Schantl, H. Vonach, M. Uhl, Nucl. Phys. A 217, 269 (1973).
- [17] P. Axel, Phys. Rev. 126, 671 (1962).
- [18] S. G. Kadmenskij, V. P. Markushev, V. I. Furman, Sov. J. Nucl. Phys., 37, 165 (1983).
- O.T. Grudzevich et.al., Sov. J. Nucl. Phys. 53, 92 (1991).
   B.V. Zhuravlev, Bull. Rus. Acad. Sci. Phys. 63 123 (1999).
- [20] G. A. Bartholomew et al., Advances in nuclear physics 7, 229 (1973).
- [21] A. Schiller et al., Nucl. Instrum. Methods A 447, 498 (2000).
- [22] C. F. Porter, R. G. Thomas, Phys. Rev. 104, 483 (1956).

# POSSIBILITY OF EXPERIMENTAL DETERMINATION OF RELIABLE PARAMETERS OF THE COMPOUND-STATE GAMMA-DECAY AND SOME ERRORS OF ANALYSIS: <sup>96</sup>Mo AS AN EXAMPLE

#### A.M. Sukhovoj, V.A. Khitrov

Joint Institute for Nuclear Research, 141980, Dubna, Russia

Comparison between potential possibilities and inevitable systematic errors of one- and two-step reactions for obtaining of maximum reliable data on level density and radiative strength functions after decay of excited levels of complicated nuclei has been performed. It was shown that the use for this aim of two-step reactions instead of one-step reactions provides for potential possibility to decrease systematical errors of mentioned nuclear parameters, as minimum, by several times.

### 1 Introduction

Level density  $\rho$  and radiative strength functions  $k=f/A^{2/3}=\Gamma/(E_{\gamma}^2D_{\lambda}A^{2/3})$  of cascade gamma-transitions following decay of high-lying levels  $(E_{ex}>5-10~{\rm MeV})$  for main portion of excited nuclei can be determined experimentally only from solution of reverse task – from the spectra of cascade gamma-decay measured with "bad resolution". There is standard task for mathematical analysis. Usually, it has infinite number of possible solutions. But, the interval of the possible  $\rho$  and k values can be both infinite or strongly limited by experimental conditions. In the first case, determination of  $\rho$  or k is impossible without applying additional information, in the second – it is possible to determine the small enough region of the  $\rho$  and k values which reproduce experimental spectra with the value  $\chi^2/f < 1$ . In the second variant it is appeared, as minimum, possibility to exclude from consideration some nuclear models which do not provide required precision in reproduction of experimental data.

Such models of  $\rho$  and k inevitably appeared by theoretical analysis of experimental data obtained earlier with large systematical errors. The latter unambiguously follows from comparison of  $\rho$  and k values determined in experiments of different types. The primary problem in this comparison and following selection of nuclear models is realistic estimation of systematical uncertainties of the data under consideration.

## 2 Experiments of different type

Qualitative difference in potential possibilities to get reliable data on  $\rho$  and k is caused, first of all, by the type of experiment. The usual (below – one-step) experiment corre-

sponds to registration of given reaction product and, main, to comparison between probability distribution of its emission and tested reaction notions independently on probable yield of other products.

Two-step experiment assumes both measurement and comparison of the measured and calculated with the tested functions  $\rho = \psi(E_{ex})$  and  $k = \phi(E_{\gamma})$  emission probability of two correlated reaction products. There can be two gamma-quanta or particle and gamma-quantum. The function shape for probability distribution of their registration with the determined parameters in one- and two-step reactions is different. Just this difference causes different value of systematical uncertainties of measured nuclear parameters and high resulting reliability of their values in two-step reaction.

The reason for considerable discrepancy between achieved precision in determination of experimental data on  $\rho$  and k is easily revealed at comparison between one- and two-step reactions. In the first case, determination of these nuclear parameters is performed usually from the spectra whose S amplitudes are described by expression like  $S \propto \rho k/\sum(\rho k)$ . Registration probability  $B_r$  of the next reaction product (here – gamma-quanta to given final levels) has another form of dependence on the same parameters:  $B_r \propto k/\sum(\rho k)$ . This leads to principle change in values of systematical errors  $\delta \rho$  and  $\delta k$  – decrease of their values by several times as compared with one-step reactions.

## 3 One-step reaction

Authors [1] performed re-analysis of their experimental data (practically – one-step reactions ( ${}^{3}\text{He}, {}^{3}\text{He}'\gamma$ ), ( ${}^{3}\text{He}, \alpha\gamma$ )) and changed small portion of results presented earlier.

On the whole, principle discrepancy between physical picture of eascade gamma-decay obtained in Oslo and Dubna remains. Characteristic feature of the first data set – smooth change in level density as changing excitation energy; sharp changes in nuclear properties are absent. Any correlation between level density and emission probability of gamma-quanta is not reported.

In the second case is observed alternative picture of processes occurring in nucleus.

Approximation of level density [2] by Strutinsky model [3] and sum of radiative strength functions by semi-phenomenological dependence [4] gives the following picture of gamma-decay:

- (a) level density below neutron binding energy  $B_n$  is determined by quantity of excited quasi-particles breaking threshold of 3-5 nucleon pairs. This number depends on shape of energy dependence of the nucleon pair correlation function in heated nucleus. Main portion of excited levels below  $\approx 0.5 B_n$  is caused by nuclear phonon excitations and (for deformed nuclei) by their rotation. This result qualitatively coincidences with the data on coefficients  $K_{\rm coll}$  of collective enhancement of level density presented in file [5];
- (b) sum of radiative strength functions of E1- and M1-transitions is described very well by superposition of model [6] and local "peak" structure. The latter has maximum value in

region of levels whose wave functions contain large few-quasi-particle components or large phonon components (excitation energy region with  $K_{\rm coll} \gg 1$ ) with the "tail" potentially decreasing as decreasing gamma-transition energy. Moreover, functional dependence [6] has the weight  $w \sim 1/K_{\rm coll}$  and, correspondingly, less nuclear temperature T. Parameters w and T depend on parity of nucleon number in nuclei studied up to now.

Therefore, there is urgent necessity in further analysis of systematical errors of different methods for determination of  $\rho$  and k. In [7] is demonstrated that change in total intensity of two-step cascades by  $\pm 25\%$  from the value obtained in experiment does not lead to principle change in form of determined  $\rho$  and k values. The use of hypothesis [8, 9] instead of experimental function  $k(E_{\gamma}, E_{\rm ex})$  overestimates the obtained level density, most probably, not less than by two times (the values of k are underestimated, respectively). The other ordinary systematical errors have minor value. On the whole, difference between the pictures of gamma-decay obtained in different experiments cannot be related mainly to systematical errors of method [10].

Necessity, direction and considerably larger volume of required re-analysis in [1], as it should be expected, are caused by inaccurate subtraction of Compton background (and other backgrounds) in each experimental total gamma-spectrum and errors of normalization of all the spectra to the same number of decays.

Unfortunately, authors of [1] did not performed quantitative analysis of systematical errors and, main, coefficients of their transfer to the determined parameters. In particular, relative normalization of total gamma-spectra was done with the use of experimental multiplicity of coincidences. As it follows from the works published by Oslo group, probable discrepancy between its value and mean number of gamma-quanta in cascade following decay of levels with excitation energy  $E_{cx}$  was not investigated. Nevertheless, determination of systematical errors of the obtained  $\rho$  and k requires one to estimate possible errors of the measured intensity and, main, coefficients of their transfer to the "first generation spectra". And then – to the determined parameters  $\rho$  and k.

## 3.1 Error transfer and possibility to estimate its coefficients for one-step reaction

Qualitative notion on the considered values can be obtained in different ways:

1. Direct comparison between "raw" and "primary" spectra presented in the same scale. (Normalization of these spectra relative to their high-energy parts can be performed unambiguously). This allows one easily to estimate required precision in determination of intensity of total gamma-spectra following decay of levels lying in region of neutron binding energy (and lower) for any nucleus studied in Oslo. For the low-energy primary gamma-transitions (for example,  $E_{\gamma}\approx 1-2$  MeV), relative error of subtracted Compton background of raw-spectrum must not exceed  $\sim 0.01$ . (It is obtained at rather optimistic estimation of required precision in determination of the primary gamma-transition intensities - 10% and exceeding of "raw" spectrum above the "primary" one only  $\sim 10$  times at low energy of gamma-quanta).

Therefore, inevitable and different components of background (independently on their nature) and any distortion at registration of gamma-quanta by scintillation detector must be small enough (i. e., their contribution in low-energy part of total spectrum must be noticeably less than  $\sim 1\%$ ). In the other case they must be determined independently on main experiment, at least, with the same precision.

2. Calculation of total gamma-spectra for different model functions of  $\rho$ , k and following comparison of differences  $\Delta S_{ij}^{cal}$  with corresponding values of  $\delta \rho_{ij}$  and  $\delta k_{ij}$  for any possible pairs of  $\rho$  and k.

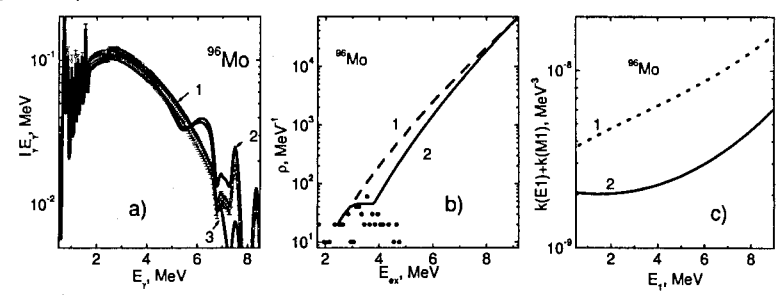


Fig. 1a). 4 variants of the calculated total gamma-spectra in  $^{96}$ Mo. Points with errors – calculation for models [6] and [11], curve 1 - [8, 9]+[11], curve 2 - [6] and step-like level density from Fig.1b), curve 3 - [8] and step-like structure. Fig. 1b). Points – total number of levels in known decay scheme [12], curve 1 - [11], curve 2 – level density with step-like structure. Fig. 1c). Curve 1 - data [8], curve 2 - [6] together with k(M1) =const.

In Fig. 1a) are presented four total gamma-spectra for  $^{96}$ Mo calculated within two models of level density and two models of radiative strength functions shown in Fig. 1b and Fig. 1c), respectively. For convenience of comparison, calculated spectra are presented in form  $S = I_{\gamma}E_{\gamma}$ . For one spectrum there are given errors of calculation which are equal to 10%. As it is shown below, the total gamma-spectrum can be presented by sum of spectra of the irst generation gamma-transitions depopulating low-lying levels. Id est, it follows from the fact of small difference between model calculation in low-energy part of spectrum that the required total error in determination of total gamma-spectra in method [13], most probably, must be considerably less than 10%.

3. Calculation of spectra h of primary gamma-transitions for different excitation energy of studied nucleus and given parameters  $\rho$ , k with folding of these functions in total gamma-spectra S according to expression:

$$S_i = h_i + \sum_{l} (h_l S_l). \tag{1}$$

The following distortion of spectra  $S_i$  by different errors d and reconstruction of distorted values of  $h_i$  by means of reverse to (1) procedure:

$$h_i = S_i d_i - \sum_l (h_l S_l d_l) \tag{2}$$

allow easy modeling of error transfer of total gamma-spectra to the errors of the primary gamma-transition spectrum. Necessity and possibility of effective search for error transfer of the total gamma-spectra to the primary transition spectra was first investigated and suggested in [14].

(a) Identical analysis for gamma-decay of  $^{96}$ Mo excited levels shows, for example, that [1] "unexpected enhancements in the radiative strength functions (RSF) of low energy gamma-ray..." is, probably, inevitable consequence of ordinary systematical errors in normalization of the total gamma-spectra. For instance, at linear distortion of their area by coefficient  $d=1+d_{max}((B_n-E_{ex})/B_n)$  in energy interval of decaying levels from 9 MeV to ground state. There were tested two variants of distorting function  $(d_{max}=10\%$  and  $d_{max}=-10\%$ ). The results are presented in Fig. 2. Most probably, this estimation of possible systematical error  $d_{max}=\pm10\%$  is optimistic and underestimated by several times. This conclusion was made on the ground of dispersion of experimental multiplicity of gamma-quanta presented in [15]. Just this parameter of gamma-decay is used for relative normalization of the total gamma-spectra by group from Oslo.

Moreover, double overestimation of intensity of the primary transition spectrum is observed at the primary transition energy of about 1 MeV for the nuclear excitation energy  $E_{ex} = 9$  MeV (Fig. 2). Analogous overestimation is regularly present and at lower excitation energy  $E_{ex}$ . This error quickly increases at the less than 1 MeV primary transition energy  $E_{1}$ . At higher energy – changes sign and magnitude. Transfer coefficients of these errors to the determined level density and radiative strength functions strongly exceed analogous values in analysis of two-step cascade intensities [7] due to difference of functional dependences on  $\rho$  and k of experimentally measured distributions.

(b) There are no doubts in difference of shapes and areas of incoming in (2) gamma-spectra following depopulation of levels of the same energy but excited by primary gamma-transitions from higher-lying  $(S_i)$  levels or in result of the nucleon product emission of nuclear reaction  $(S_l)$ .

This is caused by both difference in energy dependence of the primary E1- and M1transitions (directly observed in method [10]) and widening of spin interval excited by dipole gamma-transitions. The method for determination of corresponding error is unknown.

However, it should be taken into account that the values of analyzed errors and coefficients of their transfer to values of level density and radiative strength functions must be determined numerically for the worst cases.

(c) Multi-parametric fitting is usually performed using the method suggested for the first time by Gauss and then developed by other mathematicians for the case when corresponding system of equations is singular or close to singular. The method consists in the following: the value of vector-column X consisting from n parameters is determined (for example, [16]) in the vicinity of their actual values for k+1 iteration by the matrix equation

$$X_{k+1} = X_k - (J^T G J)^{-1} J^T G S(X_k),$$
(3)

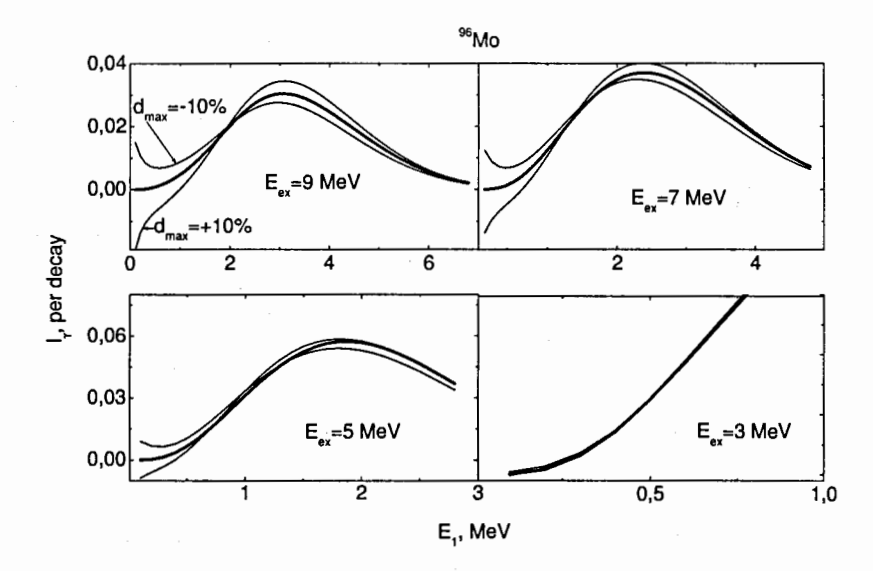


Fig. 2. Solid curve – model calculation of the primary gamma-transition intensity in  $^{96}$ Mo. Two thin curves show its change for linear overestimation (underestimation) of area of total gamma-spectra for different energy  $E_{ex}$  of decaying levels.

where G is the matrix of weights, the Jacobi matrix J and corresponding transposed matrix  $J^T$  are the matrixes of derivatives from function  $S(E_\gamma)$  with respect to the desired radiative strength function k of transition and number  $\rho$  of levels in a given energy interval  $\Delta E$  of corresponding spectrum. S is the vector-row of m experimental points in all spectra involved in fitting of parameters. It is obvious that eq. (3) has a solution (unique) only upon condition of existence of covariant matrix  $C = (J^T G J)^{-1}$ . Otherwise, process (3) is realized using some type of regularization. Existing programs of multi-parameter fitting can find some arbitrary solution of system in case when system of equations is degenerated.

In the case considered here [1], matrix C is degenerated [17] even at the use of all available spectroscopic information (known level density in two excitation energy points, total radiative width in vicinity of  $B_n$  and ratio k(M1)/k(E1) near  $B_n$ ).

As a consequence, iterative process for search of maximum of likelihood function requires one to use regularization (increasing of diagonal elements of matrix C), which does not distort direction along gradient of the likelihood function.

Compulsory limitation of any elements of corrective vector  $\delta X/X$  for unknown  $\rho$  and k by relative value P in limits  $0.01 \le P \le 0.2$  (expression (17) in [13]) at each iteration deflects this vector from the maximum of the likelihood function. Authors [13] did not present proof for convergence of the process under conditions listed above. Therefore, one can conclude that the maximum of likelihood function was not achieved.

As it follows from accumulated experience of determination of function parameters

(presented in textbooks on mathematical statistics), they should be determined at maximal variation of initial values of level density and radiative strength functions. Under conditions of degenerated matrix, maximum of likelihood function cannot be the only. Conclusion completely contradicts algorithm [13].

(c) High sensitivity and very large volume of accumulated information on two-step reaction  $(n,2\gamma)$  [10] allows one to get principally new information on structure of nuclei of any type in considerably wider excitation energy interval than it is available for classical nuclear spectroscopy. Hence, reliable parameters of gamma-decay can be obtained only under condition of accounting for the strongest violation of the Axel-Brink hypothesis for gamma-transitions to the levels with different ratio between vibrational and quasi-particle components. It is regularly and easily revealed experimentally as very significant enhancement in cascade population of levels in region of step-like structure (nuclear excitation energy – several MeV) in investigation of two-step cascades. It should be noted, that accounting for probable dependence  $k(E1) + k(M1) = f(E_{\gamma}, E_{ex})$  simultaneously decreases discrepancy between the calculated and experimental total gamma-spectra also [18]).

Analysis [19] showed principle discrepancy between shape of experimental intensity of two-step cascades in  $^{57}$ Fe, for example, and that calculated with the use of the data on the  $(^{3}He, ^{3}He'\gamma)$  reaction. The analysis was performed with accounting for all requirements of mathematical analysis and mathematical statistics.

## 4 Two-step reaction

The term "two-step" reaction assumes, in general, experimental measurement of product of partial cross-sections for two successive products of nuclear reaction in case when spectrometer resolution is enough for observation of individual peaks, or sum of their intensities over excitation energy region of intermediate levels - at bad resolution. Besides, there is possible registration of charged particle and following gamma-quantum. Reaction  $(n, \gamma \alpha)$  studied early in FLNP JINR also belongs to class of two-step reactions.

Naturally, it is necessary to account for possibility of significant systematical error in strength function of low-energy primary gamma-transitions determined in analysis. This error can be due to incorrectness of hypotheses used for experimental data analysis and, correspondingly, can lead to incorrect parameterization of model [6] obtained on this basis. (For example, at considerable increase in  $\alpha$ -widths relative to the average.) Most probably, there is the main problem for analysis of two-step reactions and source of main systematical uncertainties in nuclear parameters obtained from them. Main sources of errors in processing of the two-step cascade intensities were analyzed in [14] and detailed in [19].

The used in [10] main principles and algorithms for the two-step cascade intensity analysis were developed in functional analysis and mathematical statistics and completely correspond to their basis notions. Practically revealed sources of systematical errors and problems which should be solved by analysis of two-step cascade intensities are the following:

- 1. The assumption [8, 9] on absence or weak influence of nuclear structure on its main parameters—level density and emission probability of gamma-quanta with the same energy but different energies of nuclear excitations is obviously mistaken.
  - 2. The existence of false solutions of reversed task considered here is inevitable.
- 3. There is necessary to take into account the strongest correlation between both different desired parameters and parameters of the same type (but for different nuclear excitation energy).
- 4. Non-linearity of error transfer coefficients of the measured spectra and their change at increasing (decreasing) error of experiment determines the width of interval for the possible  $\rho$  and k values for different systematical errors of cascade intensities and and vice versa.

These statements are based on modern theoretical ideas, the set of available experimental data and general methodological scientific principles.

#### 1. There are:

- a) Analysis of fragmentation of nuclear states of different complexity [20] showed strong irregularity of this process. At any nuclear excitation energy, wave functions of levels can contain large components of different type. They can be in matrix elements of gamma-transitions and penetration coefficients of nuclear surface for nucleon products of nuclear reaction. This contradicts main postulates of "statistical" model of nucleus.
- b) The same conclusion follows from coefficients of vibrational enhancement of level density [5] in the region of neutron binding energy and estimation of parameters of the primary gamma-transition intensity distribution in reaction  $(\bar{n}, \gamma)$ . The achieved level of experiment and modern mathematics apparatus allows its treatment without the use of this obsolete postulate.
- c) Only the comparison between the parameters of nuclear reaction obtained in this way and theoretical ideas can give objective picture of processes occurring in nucleus.
- 2. Because simultaneous extraction of  $\rho$  and k from untransformed experimental spectra of two-step reactions always gives some set of false solutions. Region of their values must be minimal at registration of different products at the first and second steps of reaction. But, it very strongly increases at registration of two gamma-quanta with lifetime of intermediate level in femtosecond diapason by any known spectrometers of gamma-coincidences.

In consequence, experimental spectra of the  $(n,2\gamma)$  reaction can be reproduced with  $\chi^2/f < 1$  by infinite number of the level density and radiative strength functions – on gamma-quantum energy and structure of levels connected by gamma-transition. Moreover, ratio between the obtained maximal and minimal values of  $\rho$  and k can exceed some tens [14].

Very essential reduction of interval of their possible values in the  $(n, 2\gamma)$  reaction requires one to determine the portion of the primary transition intensity in arbitrary

energy interval of cascade gamma-transitions in vicinity of chosen energy  $E_{\gamma}$ . This task can be solved [21] with acceptable error by accounting for shape of line (changes in intensity and number of registered cascades) of primary gamma-transition with different energy  $E_1$ .

3. Any change in function  $\rho$ , for example, precisely reproducing experimental spectra results in adequate change of the same value for other excitation energy or/and strength functions k. This correlation is realized through the total radiative widths of initial and intermediate cascade levels. Such correlation is clearly observed in method [10] for all the nuclei studied in Dubna. This follows from the fact that in experiments with even ordinary detectors is observed some tens percent of the total intensity of the primary gamma-transitions

$$I_{\gamma\gamma}(E_1) = \sum_{\lambda,f} \sum_{i} \frac{\Gamma_{\lambda i}}{\Gamma_{\lambda}} \frac{\Gamma_{if}}{\Gamma_{i}}.$$
 (4)

The analysis performed, for example, in [22, 23, 24] ignores strong correlation between intensity of any caseade with other gamma-quanta. Therefore, comparison only of central parts of the experimental spectra with different variants of model calculation by discrepancy at the ends of spectra guaranties absolute unreliability of the made conclusion.

4. Applicability of some set of the  $\rho$  and k models for reproducing experimental cascade intensity by means of criterion  $\chi^2$  was estimated without accounting for significant nonlinear coefficients of error transfer of experimental spectrum to errors of parameters. They significantly differ from unit. In this situation, the width of confidence interval for errors of tested level density and radiative strength functions can be unlimited large at least in some cases.

The examples of the two-step cascade intensity analysis in  $^{57}$ Fe,  $^{172}$ Yb,  $^{163}$ Dy and  $^{198}$ Au performed without accounting for mentioned above specific of two-step reaction  $(n, 2\gamma)$  can be found in [22, 23, 24]. Accounting for this specific [19, 14, 25] gives significantly different data on both level density and radiative strength functions and does not contradicts our data for other nuclei.

Nucleus <sup>96</sup>Mo is not exclusion, as well.

## 4.1 Grounded and ungrounded conclusions at analysis of experiment

Necessity in estimation of ground of experimental conclusion unambiguously follows from two examples:

- a) comparison between results of different experiments at test of the Bohr-Mottelson [26] (or Axel-Brink) hypothesis of independence of reverse reaction cross-sections on wave function structure of excited level of final nucleus and
  - b) logic in choice of conclusion on the nuclear process picture at presence of infi-

nite number of possible parameter values concentrated in final interval of their possible magnitudes.

1. Extraction of level density from spectra of one-step reactions is impossible without the use of hypotheses of independence of reverse reaction cross-section on excitation energy of final nucleus. Corresponding error of any adopted hypothesis is directly transformed into unknown systematical uncertainty in determination of  $\rho$ .

This problem is not so important for two-step reactions. As it was shown in analysis of change in cascade population of levels of studied nucleus below  $0.5B_n$  [10], deviation of cross-section from general trend at different nuclear excitation energy in reaction  $(n, 2\gamma)$  has different sign. Qualitatively, the effect of sign-changeable cycling in deviation of cross-sections from averaged dependence can be interpreted in frameworks of theoretical conclusions about regularities of fragmentation process of states with different numbers of quasi-particles and phonons. So, inapplicability of the Axel-Brink hypothesis for gammaquanta is partially smoothed in the value of the total radiative width of the cascade intermediate level by items of different sign. On the other hand, experimental data allow one to account to the fist approach for considerable enhancement in k(E1) + k(M1) for the secondary cascade transitions to the levels lying below the break threshold of the second Cooper pair of nucleons.

This means that the conclusion [27] on justice of hypothesis [26] is not grounded. I. e., existing experimental data do not permit one to exclude possibility of strong correlation between partial cross-sections of gamma-transitions and evaporated nucleons for given excitation energies of final nuclei.

2. Analysis of published results on study of two-step reaction  $^{95}$ Mo $(n, 2\gamma)$  demonstrates another aspect which should be taken into account in order to obtain reliable conclusion about the studied picture of processes occurring in nucleus.

So, impossibility to reproduce experimental intensity of two-step cascades in limits of their total experimental error with the use of any model notions of  $\rho$  and k or data of other experiments is absolute argument for their more or less mistakenness. This is true within uncertainty of other existing notions of gamma-decay process. For instance, there is idea of independence of decaying mode of excited levels on way of their excitation.

But, correspondence between calculation and experiment (moreover, in limited interval of gamma-transition energy) cannot be a proof for justice of the tested  $\rho$  and k. This is due to their potential coincidence with one of false solution from one hand and owing to impossibility to guess experimental values of  $\rho$  and k - from other hand.

## 5 Principles of two-step cascade analysis in <sup>96</sup>Mo

The goal of analysis suggested here is determination of the most reliable  $\rho$  and k values for given isotope (independently on other opinions concerning this point).

Unique (and not realized in [28, 29]) possibility for this aim is provided by experimental data on two-step cascades measured in Řež. But, obtaining of reliable data is impossible without formulation of conditions and postulates of analysis providing its maximal reliability:

1. Cascade intensity is described by the function whose arguments have infinite number of possible values. However, all these values are physically limited by final interval of possible magnitudes for any energy of excitation and gamma-transition:

$$\rho_{min} < \rho < \rho_{max} 
\Gamma_{min} < \Gamma < \Gamma_{max}.$$
(5)

Therefore, the region of their possible values can be determined by mathematical methods without using of model notions about  $\rho$  and /or k. But, this can be done only under condition that the ratio between strength functions of primary and secondary gamma-transitions of the same energy and multipolarity is set on basis of some hypotheses or experimental data. This statement is easily tested using any algorithm of search for random solution of system of equations (4) even at its spreading onto functional dependence for eascades with reverse ordering of primary and secondary gamma-transitions of considered energy. Of course, it is necessary to set maximally different initial values for iterative process and, it is desirable, out of the region (5) of its determined maximal and minimal values.

- 2. On the ground of experiments performed earlier, it must be assumed that the cascade intensity depends on the wave function structures of its three levels. If this statement is false for given nucleus then objective analysis must demonstrate their independence.
- 3. The analysis must use all inherent to experiment possibilities. Therefore, it is necessary to use the only found up to now possibility [10] to estimate degree of functional dependence of strength functions on energy (i.e., structure of wave function) of decaying level.

If nucleus <sup>96</sup>Mo is exclusion from this rule, and the Axel-Brink hypothesis is applicable and for it then experiment must show in limit of errors the independence of wave functions on nuclear structure:  $k(E_{\gamma}, E_{ex}) = k(E_{\gamma})$ .

## 6 Results of analysis of two-step cascade intensities in <sup>96</sup>Mo

As earlier, authors of [28, 29] used for proof of their point of view comparison between central parts of some experimental spectra (corrected by efficiency of easeade registration) for choice of some variant of model values of  $\rho$  and k. In their opinion, the tested variants describe the compound-state gamma-decay adequately to the experiment.

Practical use of the analysis principles enumerated above does not correspond to this conclusion completely.

In analysis of the experimental data performed by us were used the following nuclear parameters: density of levels with  $J^{\pi}=2,3^+$  at  $B_n=9.154$  MeV corresponds to spacing

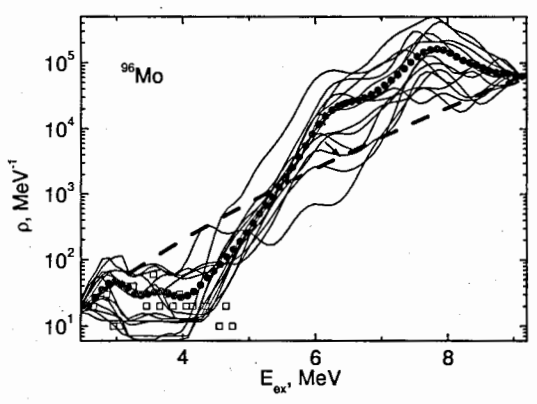


Fig. 3. Curve 1 – model values [11], thin curves represent the best random functions of the density of intermediate cascade levels reproducing  $I_{\gamma\gamma}$  in Fig. 5, 6 with practically the same values  $\chi^2/f < 1$ . Solid points show their mean value. Squares present data from [12].

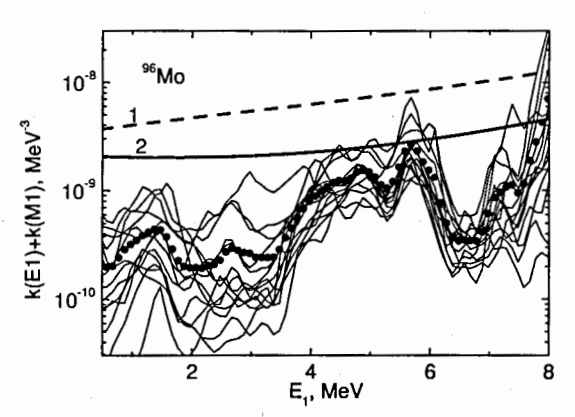


Fig. 4. Curve 1 - k(E1) from model [8], curve 2 - [6] in sum with k(M1) =const. Thin curves represent the best random functions reproducing  $I_{\gamma\gamma}$  in Fig. 5, 6 with practically the same values  $\chi^2/f < 1$ . Solid points show their mean value.

between them D=55 eV. Below 2.5 MeV were used experimental scheme of levels and modes of their decay. Level density excited according to model [11] by primary dipole transitions is presented in Fig. 3 by curve 1. It corresponds to nuclear parameters enumerated above. Analysis in frameworks of this model gives level density at the lowest and highest nuclear excitation energy. It is fixed equality of level density with different parity at  $B_n$ . Their ratio below neutron binding energy is free parameter.

The total radiative width of neutron resonances was taken equal to  $\Gamma_{\gamma}=160$  meV, ratio k(M1)/k(E1)=0.256 for  $E_{\gamma}=6.8$  MeV. The threshold of fitted spectra was taken equal to 0.9 MeV for correspondence with [1]. The ratio of capture number in compound state with  $J=2^+$  to the total number of captures was accepted equal to  $\sigma_{J}$ =50 and 66%. This variation was performed for possible compensation of error in determination of spins (and capture cross-sections) in under-threshold resonances [30].

The functions presented in Fig. 1b) and 1c) were used as initial values of  $\rho$  and k in some part of calculation. And obviously unreal their values were used in other part of calculation.

As it was already mentioned in [7, 19, 25], the use of experimental spectra with indefinite ratio between intensities of the primary and secondary transitions in vicinity of the primary gamma-transition energy  $E_{\gamma} = E_1$  or  $E_{\gamma} = E_2$  increases region of the possible  $\rho$ and k values by 1-2 order as compared with the used by us [10] analysis. This is observed in figs. 3 and 4 (there is given for  $\sigma_J = 66\%$ ). Some decrease in dispersion of the found  $\rho$  and k values can be achieved by the use of experimental data on primary transition intensities of the most strong cascades. This is effectively in near-magic nuclei and, in principle, allows one to reject clearly false "bump" which appears itself in Fig. 4 about  $E_1 = 1.5$  MeV in some variants of calculation. This problem is solved automatically in experimental data processing within the method [10] if only the quanta ordering in the most intense cascades is determined by means of apparatus of nuclear spectroscopy with errors not exceeding some percents. However, possibility of mistaken determination of quanta ordering in cascades with their intermediate level energies below 3-4 MeV in the considered isotope with relatively low level density is practically unreal. Principle discrepancy in results of approximation with variants  $\sigma_J = 50\%$  and  $\sigma_J = 66\%$  in spectra of possible  $\rho$  and k functions is not observed. Pure E2-transitions were not considered in approximation; actually, the data in Fig. 4 may contain mixture of dipole and quadrupole transitions.

The cascade intensity spectrum is given in [29] only for four summed energies. Therefore, just these data were used in our fitting of spectra. Results of approximation of summed intensity of central parts for 11 spectra by random functions (figures 3 and 4) are presented in Fig. 5. Resulting dispersion in calculated data presented in this figure for maximal excitation energies can be stipulated by both errors in normalization of spectra and errors in the used in calculation values of their spin and parity.

Anti-correlation between  $\rho$  and k results in fact that the level density functions with their maximum values correspond to strength functions with the least values (it directly follows from condition  $\Gamma_{\gamma} = \text{const}$ ).

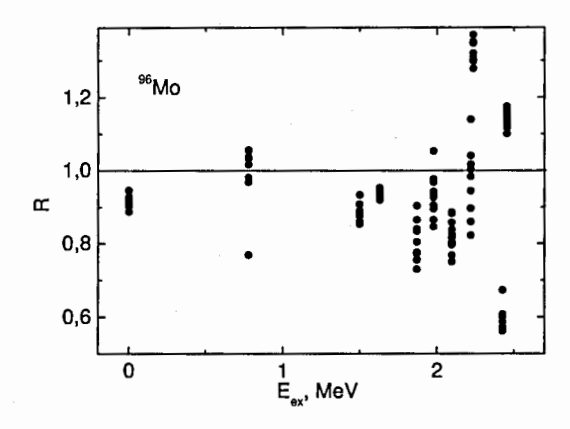


Fig. 5. The ratio between calculated and experimental intensities for central parts of 11 spectra for random functions presented in figs. 3 and 4.

### 7 Conclusion

- 1. Description of the experimental intensity of two-step cascades to a precision of experiment is impossible in frameworks of many existing model notions and experimental data.
- 2. Approximation of cascade intensity to the ground (phonon-less), one-phonon ( $E_{ex}=778$ ) states and two-phonon doublet ( $E_{ex}=1625+1629$ ) keV reflects, probably, influence of wave function structure of cascade final level on its intensity. Local "bump" in region of the primary transition energy  $\approx 4$  MeV determines the shape of their energy dependence and summed intensity of each cascade.
- 3. More precise data on  $\rho$  and k can be obtained only by application of methods [21, 10] to the experimental data from Rez. Uncertainty in determination of dependence (4) of cascade intensities on on energy of their primary transitions within the method [21] at given statistics, resolution and background will be considerably less than error in normalization of absolute intensity  $I_{\gamma\gamma}$ .
- 4. Spectroscopic data can permit one to determine cascade population of levels in  $^{96}$ Mo up to the excitation energy not less than 4.5 MeV. It is not excluded that this is quite enough for observation of increase in strength functions of secondary transitions to the levels lying in region  $E_{ex} \approx 4$  MeV.
- 5. The shapes of energy dependences for  $\rho$  and k repeat, in the average, analogous data for other nuclei step-like structure, strengthening of k to the levels in its region not only for primary but, probably, also for secondary cascade transitions, and noticeable decrease in low-energy region of primary transitions  $E_1 < 3.5 \text{ MeV}$ .

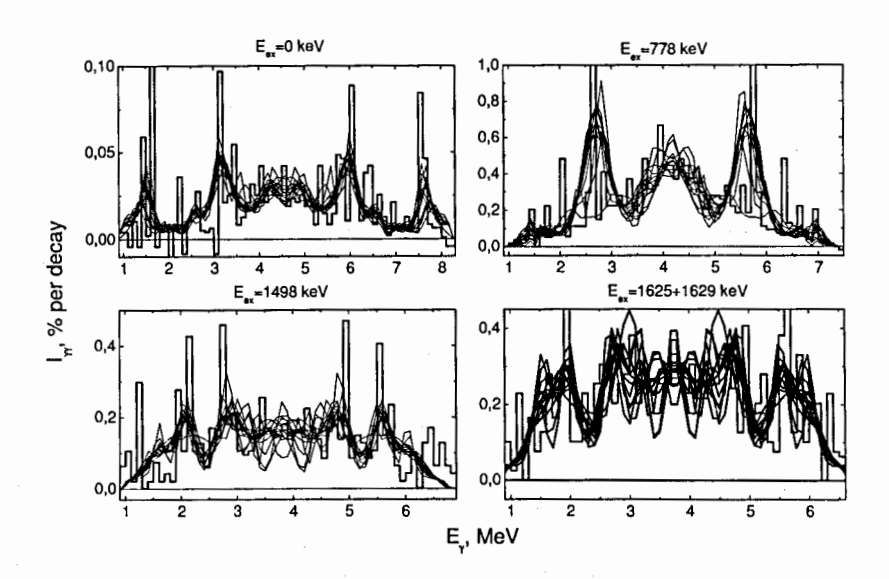


Fig. 6. Histogram – experimental intensity of two-step cascades for the levels  $E_{ex}$  (summed over the intervals of 100 keV). Lines – variants of the calculation with random level density and radiative strength functions presented in figures 3 and 4. Normalization of experimental and calculated spectra corresponds to that adopted in [29], i.e., corresponds to summed intensity of all possible two-step cascades 200% per decay.

- 6. The method used in Oslo needs in realistic estimation of systematical errors of the measured spectra and their coefficient transfer to the determined  $\rho$  and k values. It is not excluded that the required precision of experiment estimated here cannot be achieved in existing variant of the experiment even in principle.
- 7. Most probably, its authors would be able to obtain reliable enough data by the use of two-step reaction "charged particle + gamma-quantum to low-lying level".

## References

- [1] M. Guttormsen et al., http://arXiv.org/abs/nucl-ex/0801.4667.
- [2] Sukhovoj A.M., Khitrov V.A., Physics of Paricl. and Nuclei, 37(6) (2006) 899. http://www1.jinr.ru/Pepan/Pepan-index.html (in Russian)
- [3] V. M. Strutinsky, in Proc. of Int. Conf. Nucl. Phys., (Paris, 1958), p. 617.
- [4] Sukhovoj A.M., Furman W.I., Khitrov V.A. In: XV International Seminar on Interaction of Neutrons with Nuclei, Dubna, May 2007, E3-2008-26, Dubna, 2008, p. 92.
- [5] Reference Input Parameter Library RIPL-2. Handbook for calculations of nuclear reaction data. IAEA-TECDOC, 2002. http://www-nds.iaea.or.at/ripl2.
- [6] S.G. Kadmenskij, V.P. Markushev, V.I. Furman, Sov. J. Nucl. Phys. 37 (1983) 165.
- [7] Khitrov V.A., Li Chol, Sukhovoj A.M., In: XI International Seminar on Interaction of Neutrons with Nuclei, Dubna, May 2003, E3-2004-9, Dubna, 2004, p. 98. http://arXiv.org/abs/nucl-ex/0404028.
- [8] P. Axel, Phys. Rev. 1962. **126(2)**, (1962) 671.
- [9] Brink D. M., Ph. D. thesis, Oxford University (1955).
- [10] A.M. Sukhovoj, V.A. Khitrov, Phys. Particl. and Nuclei, 36(4) (2005) 359. http://www1.jinr.ru/Pepan/Pepan-index.html (in Russian)
- [11] W. Dilg, W. Schantl, H. Vonach, M. Uhl, Nucl. Phys. A217 (1973) 269.
- [12] http://www.nndc.bnl.gov/nndc/ensdf.
- [13] A. Schiller et al., Nucl. Instrum. Methods Phys. Res. A447 (2000) 498.
- [14] Khitrov V.A., Li Chol, Sukhovoj A.M., XII International Seminar on Interaction of Neutrons with Nuclei, Dubna, May 2004, E3-2004-169, Dubna, 2004, p. 438. http://arXiv.org/abs/nucl-ex/0409016.
- [15] J.H. Degnan et al., Phys. Rev. C 5, (1972) 836.

- [16] Aleksandrov L., JINR Communications P5-7259 (1973).
- [17] Khitrov V.A., Sukhovoj A.M., Pham Dinh Khang, Vuong Huu Tan, Nguyen Xuan Hai, In: XI International Seminar on Interaction of Neutrons with Nuclei, Dubna, 22-25 May 2003, E3-2004-9, p.107.
- [18] Sukhovoj A. M., Khitrov V. A. et al., in XIII International Seminar on Interaction of Neutrons with Nuclei, Dubna, May 2006, JINR E3-2006-7, (Dubna, 2006), p. 56, ibid., p. 72, Sukhovoj A.M., Khitrov V.A., Pham Dinh Khang, et al. ibid., p. 64, Khitrov V.A., Sukhovoj A.M., Grigoriev E.P. in Proceedings of the Eleventh In-

ternational Symposium on Capture Gamma-Ray Spectroscopy and Related Topics, Pruhonice, September 2-6, 2002, (World Scientific, 2002), Ed. by J. Kvasil, P. Cejnar, M. Krticka, p. 718,

- A. M. Sukhovoj, V. Khitrov, E. P. Grigor'ev, INDC(CCP), Vienna 432, 115 (2002).
- [19] Sukhovoj A.M., Khitrov V.A., Li Chol, Pham Dinh Khang, Vuong Huu Tan, Nguyen Xuan Hai, In: XIII International Seminar on Interaction of Neutrons with Nuclei, Dubna, May 2006, E3-2006-7, Dubna, 2006, p. 72. http://arXiv.org/abs/nuclex/0508007.
- [20] Malov L.A., Solov'ev V.G., Yad. Phys., 26(4) (1977) 729.
- [21] Boneva S.T., Khitrov V.A., Sukhovoj A.M., Nucl. Phys. A589 (1995) 293.
- [22] A.V. Voinov et al., Phys. Atomic Nuclei 67, (2004)1866
- [23] A. Voinov et al., Phys. Rev. Lctt. 93, (2004) 142504
- [24] F.Bečvar et al., Phys. Rev. C 52(3) (1995) 1278. M. Krtička et al., in: Pros. of XII inter. Symp. of Capture gamma-ray spectroscopy and related topics, ed. by Woehr A., Abrahamian A., AIP, 2006, p. 563.
- [25] Sukhovoj A.M., Khitrov V.A., Crawford B.E., Stephenson S.L., In: XV International Seminar on Interaction of Neutrons with Nuclei, Dubna, May 2007, E3-2008-26, Dubna, 2008, p. 134.
- [26] O. Bohr, B.R. Mottelson, Nuclear Structure, Vol. 1 (Benjamin, NY, Amsterdam, 1969).
- [27] A. Voinov et al., http://arXiv.org/abs/nucl-ex/0704.0916.
- [28] M. Krtička and F. Bečhvář, J. Phys. G:Nucl. Part. Phys. 35 (2008) 014025.
- [29] M. Krtička et al., PoS(PSF07)024, http://pos.sissa.it/cgi-bin/reader/conf.cgi?confid=44.
- [30] S. F. Mughabghab, Neutron Cross Sections BNL-325. V. 1. Parts A, edited by S. F. Mughabhab, M. Dividcenam, N. E. Holden, (N.Y., Academic Press, 1984).

## RADIATIVE CAPTURE OF THERMAL AND RESONANCE NEUTRONS, MAIN PARAMETERS OF THE GAMMA-DECAY PROCESS AND PROPERTIES OF THE 174 YE NUCLEUS

#### A.M. Sukhovoj, V.A. Khitrov

Joint Institute for Nuclear Research, 141980, Dubna, Russia

#### Abstract

The re-analysis of the data published on the primary gamma-transition intensities following capture of 2 keV neutrons in  $^{173}{\rm Yb}$  have been performed. Distribution of dispersion of these intensities with respect to mean value was approximated over different energy intervals of the primary gamma-transitions. This allowed one to estimate independently on other experimental methods the expected numbers of levels of both parities for spins J=1-4 and possible total sum of partial widths for primary electric and magnetic dipole gamma-transitions to the levels with excitation energy up to 4 MeV. The determined level densities and summed radiative strength functions confirm peculiarities of analogous data derived from the two-step  $\gamma$ -cascade intensities following thermal neutron radiative capture in nuclei from the mass region  $40 \le A \le 200$  and permits one to estimate sign and magnitude of their systematical uncertainties. The latter can be due only to very strong dependence of radiative strength functions of cascade gamma-transitions to lower-lying levels on their structure.

#### 1. Introduction

Analysis of the two-quantum cascade intensities following thermal neutron capture [1] in large set of nuclei showed a presence of strongly appeared itself step-like structure with the width of 2 MeV in density of nuclear levels  $\rho$  below  $\approx 0.5B_n$ . The further development of this method [2] resulted in additional confirmation of the fact of strong dependence of partial widths  $\Gamma_{if}$  of not only primary but also following  $\gamma$ -transitions on excitation energy of nuclear levels f in the region of mentioned above structure. Accounting for this circumstance considerably decreased level density determined according [2] with respect to results [1].

The methods [1,2] belong to the class of inverse tasks (determination of unknown parameters of functions measured experimentally) and, therefore, require maximum possible test and revealing all the sources of systematical errors). There must be solved the problem of discovering probable dependence of the obtained according to [1,2] parameters of  $\gamma$ -decay of highly-excited levels on energies of neutron resonances  $\lambda$  and possible influence of their structures on parameters of the reaction under study.

Intensities  $I_{\gamma\gamma}$  of two-step cascades to any group of low-lying levels in arbitrary nucleus are determined by radiative strength functions k of their primary and secondary transitions in combination with level densities of both parities for fixed spin window. Functional relation between them is non-linear. Therefore, the region of multitude of the possible  $\rho$  and  $k = f/A^{2/3} = \Gamma_{\lambda y}/E_{\gamma}^3A^{2/3}D_{\lambda}$  values precisely reproducing experimental spectra is always limited [1] by finite intervals of values for both parameters. This interval is narrow enough under condition that the ratio between partial widths  $\Gamma$  of primary and secondary  $\gamma$ -transitions of the same multipolarity was set for total interval of their possible energies and nucleus excitation energy on the grounds of additional experimental information [2] or some hypotheses [3,4]. Just nonlinear relation between  $\rho$  and k with  $I_{\gamma\gamma}$  allows one to get the mentioned parameters of  $\gamma$ -decay from the only experiment with acceptable uncertainty. Only this approach provides one to get the  $\rho$  and k values with the least (as compared with the other existing methods) systematical errors [5].

By now, experimental measurements of  $I_{\gamma\gamma}$  were performed only for thermal neutron capture. The accumulated experimental data allowed determination of the  $\rho$  and k values for 42 nuclei [1] (only in the frameworks of the usually used hypothesis [3,4] on independency of radiative strength functions on nuclear excitation energy). Besides, these data were obtained for two tens of these nuclei with relatively realistic (but partial) accounting for function  $k(E_{\gamma}, E_f)$ , experimentally estimated below excitation energy  $E_f$ -4 MeV [2]. This circumstance and obviously observed dependence of cascade intensities on structures of all three levels (including initial compound-state) [6] caused necessity to obtain new experimental data on  $\rho$  and k from other experiments on investigation of gamma-decay.

At present, search for influence of the initial compound state structure on gamma-decay process is the first-turn task of experiment. Really this can be done in analysis of the experimentally measured primary gamma-transitions following capture of "filtered" neutrons with energy 2 MeV. The authors of corresponding experiments [7] practically used their data only for determining spin and parities of excited levels on the base of notions of the limit "statistical" theory of gamma-decay. I. e., in the frameworks of hypotheses of independency of k(E1) and k(M1) on structure of any decaying ( $\lambda$ ) and excited (f) levels nuclear levels and applicability of the Porter-Thomas distribution [8] for describing random deviations of gamma-transition partial widths in arbitrary interval of their mean values. There are no experimental grounds for hypotheses [3,4,8] for the data like [7] (concrete nucleus, a given set of primary gamma-transition intensities). Therefore, analysis method must take into account possibility of complete non-execution of assumptions mentioned above.

Quite enough basis for the analyses suggested below are the following statements:

the experimental values of  $\rho\Delta E$  and sum  $\Gamma_{\lambda f}$  can be determined with acceptable errors by extrapolation of the measured experimentally distribution of random intensities of gammatransitions to zero threshold of their registration;

averaging of fluctuations of the primary gamma-transition widths over initial compoundstates decreases their dispersion independently on extent of truth of hypothesis [8]. I. e., any set of gamma-transition intensities from  $(\bar{n},\gamma)$  reaction can be described by  $\chi^2$ -distribution with unknown number v of degrees of freedom. (In the other words – it is close to normal distribution with dispersion  $\sigma^2 \approx 2/v$ ). Corresponding method was developed and tested on large set of data on two-step cascade intensities in [9].

The Porter-Thomas distribution correctly describes random fluctuations of partial widths of tested gamma-transitions only when their amplitudes are described by normal distribution with zero mean. That is why, they must be a sum of a large number of items with different signs and the same order of magnitudes. This condition is to be fulfilled if wave functions of levels connected by gamma-transition contain a big number of items of different signs and equal order of magnitude. Matrix element for amplitude of gamma-transition must have only these components.

## 2. Main aspects of modern theoretical notions of the compound-state gamma-decay

On the whole, existing theoretical concepts, for example, Quasiparticle-Phonon Nuclear Model (QPNM) [10,11] call doubts in applicability of enumerated above so primitive ideas of gamma-decay. In particular, the studied in frameworks of QPNM regularities of fragmentation of states with different complexity [12] directly point to presence of items with large components of wave functions in the primary gamma-transition amplitudes. First of all, this concerns wave functions of excited levels [13, 14], but it is not excluded that wave functions of decaying compound-states (neutron resonances) also have [10] large phonon, in particular, components. This directly points to potential possibility of

rather considerable violations of the Porter-Thomas distribution. These violations can appear themselves in limited [12] energy intervals of final levels and change dispersion of real distribution with respect to [8] in any side. Ratio between absolute values of items in amplitude of any gamma-transition and their signs for the data like [7] are unknown. Therefore, the analysis of experimental data suggested below must take into account a possibility of strong dependence of the primary transition partial widths on structure and, correspondingly, energy of excited levels and cover all the possible spectrum of their random deviations from the mean value.

#### 3. Specific of experimental data from $(\overline{n}, \gamma)$ reaction

In the experiments performed in BNL and later in Kiev were investigated different nuclear-targets. But for the analysis presented below was chosen even-odd nuclear-target <sup>173</sup>Yb. This choice is caused by both the maximum primary gamma-transitions energy interval [7] and presence of determined in [1] level densities and primary gamma-transition strength functions. This nucleus is also very good for both search for discrepancy of general trend for energy dependencies of  $\rho$  and k(E1)+k(M1) revealed earlier at thermal neutron capture in neighboring nuclei [1, 2] and estimating systematical uncertainty of method [1]. The latter is completely determined by errors in the performed by now experiments on measuring thermal neutron capture spectra and insufficient set of the data obtained.

Even-even (odd-odd) nucleus has two possible spins of resonances. Therefore, analysis of intensities in this case requires one to introduce and then to determine maximal number of parameters. Even-odd compound nuclei represent particular case of the problem under consideration.

The width FWHM=850 eV of filtered neutron beam with 2 keV energy in performed experiments is determined by interference minimum in total cross-section of scandium. The mean spacing between neutron resonances in  $^{173}$ Yb equals 7.8 keV, and dispersion  $\sigma^2$ =2/v of their expected distribution in very rough approach can be estimated by value of ~0.05 (v ≈40).

It is assumed in analysis that all the distributions of the primary gamma-transition intensities from reaction  $(\bar{n}, \gamma)$  have only the following unknown parameters:

- (a) the mean reduced intensity  $< I_{\gamma}^{\text{max}} / E_{\gamma}^{3} > \text{ of gamma-transitions exciting levels } J=2,3;$
- (b) the portion  $B = \langle I_{\gamma}^{min} \rangle / \langle I_{\gamma}^{max} \rangle$  of the reduced gamma-transition intensity to levels J=1,4 with respect to their intensity to levels J=2,3;
- (c) the independent on spins of the levels excited by the primary gamma-transitions ratio  $R_k = k(M1)/k(E1)$ ;
- (d) the expected and equal numbers  $N_{\gamma}$  of gamma-transitions to levels to J=2,3 and J=1.4:
  - (e) as well as the dispersion  $\sigma^2$ , measured in units of number of degree of freedom v.

Naturally, these parameters are to be determined independently for each energy interval of the primary gamma-transitions. Statistical uncertainties in determination of the experimental  $\langle I_{\gamma}/E_{\gamma}^3 \rangle$  values increase experimental dispersion  $\sigma^2$  of distribution and decrease the v value. It is assumed that their relative systematical errors in each energy interval are practically equal. Of course, this notion assumes that, in limits of the excitation energy intervals  $\Delta E \approx 200\text{-}300$  keV, the structures of compound-state and all excited levels

connected by gamma-transition weakly influence the  $\langle I_{\gamma}/E_{\gamma}^3 \rangle$  values of the gamma-transitions of the same type populating these levels.

Both approximation and interpretation [6] of the experimental data on the k(E1)+k(M1) values and results of experimental determination of structures of low-lying nuclear levels show that this assumption can contain considerable uncertainty (especially for wide energy intervals of the primary gamma-transitions under study). But, maximum

precision in determination of the most probable  $N_p$ , B,  $R_k$ , v and  $\langle I_p^{\text{max}} \rangle$  values can be achieved, in principle, by recurrent optimization of energy intervals of the primary gammatransitions where these parameters are determined.

One more problem is related to small size of set and difference in number of electric and magnetic dipole primary gamma-transitions in given intervals  $\Delta E$ . Therefore, it is necessary to introduce and to fix in analysis some assumption on numbers of levels of positive and negative parities in given excitation energy interval of a nucleus. Below is used hypothesis of equality of numbers of electric and magnetic gamma-transitions. In practice, there is possible variation of their ratio for any given excitation energy interval. The problem of difference of level densities with different parities disappears in the case of  $R_k \approx l$ , maximum error of determination of  $N\gamma$  for  $R_k \approx 0$  corresponds to transitions with the least intensities and insignificantly distorts the desirable sum  $\sum \langle I_{\gamma}^{\max} \rangle / E_{\gamma}^{3}$ . Error of approximation in intermediate variant will be determined, first of all, by difference in level densities of positive and negative parities, i. e., it will decrease when increases excitation energy (as it is predicted in the whole by modern theoretical calculation of this nuclear parameter [15]).

Approximation of a mixture of two types of random values with different mean parameters by any distribution cannot determine their belonging to one or another type without the use of additional information. But accounting for known fact that the magnetic gamma-transitions to the lowest levels are by order of magnitude less than electrical transitions, one can extrapolate inequality  $R_k = k(M1)/k(E1) < 1$  up to excitation energy of studied nuclei where  $R_k = 1$ . But it is not excluded that at higher excitation energy k(M1)/k(E1) > 1.

Strength functions of p-neutrons in ytterbium isotopes are many times less than strength functions of s-neutrons. The former in actinides exceeds [16] strength function of s-neutrons by a factor of 1.5-2.0. Authors [17] estimated, that portion of capture of 2 keV p-neutrons equals approximately 15%. If one does not account for possible appearance of some number of the primary dipole gamma-transitions to levels J=0 and J=5 following capture of p-neutrons, then this capture leads, most probably, to change in the  $R_k$  values for different energies of excited levels and corresponding increase in v. That is why, small number of p-neutron captures in p-neutr

Distributions of the random  $\langle I_{\gamma}^{\text{max}} \rangle / E_{\gamma}^{3}$  were approximated by analogy with [9] for cumulative sums in function of increasing values of intensities.

## 4. Results of analysis

Experimental distributions of cumulative sums of reduced intensities of the primary gamma-transitions  $\sum I_{\gamma}/E_{\gamma}^{3} = F(\langle I_{\gamma}/E_{\gamma}^{3} \rangle, N_{\gamma}, \nu, R_{k})$  calculated for different values of concrete parameters are presented in Fig. 1 (only for one from two possible for given nucleus

sets of spins of final levels). As it is seen from the figure, one can hope for obtaining quite reliable estimations of parameters  $N_{\gamma}$ ,  $R_{k}$ , v u  $< I_{\gamma}>$  with acceptable errors of about 10% or some bigger.

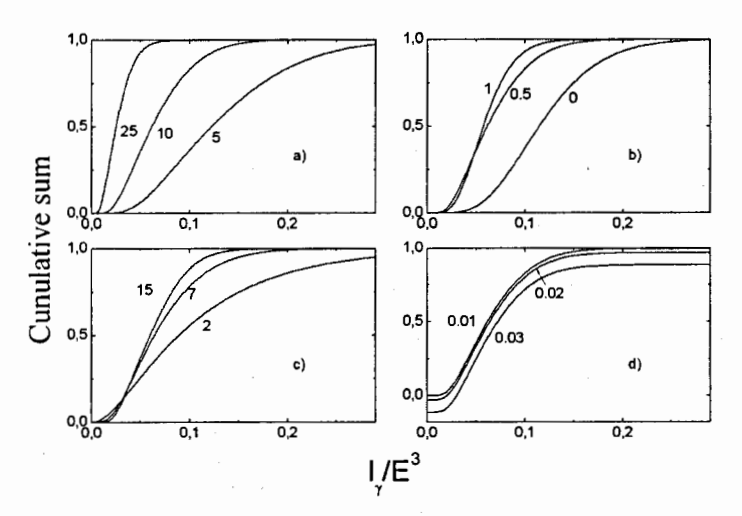


Fig. 1. Variations of dependence of cumulative sum of intensity on cascade intensity for: (a) – number of gamma-transitions, (b) – ratio  $R_k$ , (c) - value of v, (d) – registration threshold of gamma-transition. The values of varied parameters are given in figures. The values of other parameters correspond to the set:  $N_v=10$ ,  $R_k=0.5$ , v=10 and zero registration threshold of gamma-quantum.

It can be see from Fig. 1(a) that cumulative sum of intensities must be determined for excitation energy interval of even-odd nucleus containing  $N_{\gamma} \sim 5\text{-}10$  gamma-transitions and two times more – for even-even nucleus. Their bigger quantity cannot provide for good sensitivity at determining the most probable expected number of gamma-transitions for zero threshold of experiment. In the case of their less quantity, a discreteness of experimental cumulative sum becomes essential.

It is seen from Fig. 1(b) that there is possible to determine the  $R_k=k(M1)/k(E1)$  values in interval from 0 to ~0.5 with acceptable reliability and reveal a fact of closeness of the k(M1) and k(E1) values. Fig. 1 demonstrates possibility of precise enough determination of expected dispersion for given set of experimental intensities for  $v\approx10$  or less.

One can expect that the precision in determination of the registration threshold of gamma-transition intensity is high enough and error of its determination can be ignored. But, it can be done only at correspondence between experiment and adopted hypotheses of distribution shape of random intensities of the primary gamma-transitions. At presence of functional dependence of the primary gamma-transition intensities on some "hidden" parameter, the maximum errors, most probably, are possible for approximated values of the most probable number of gamma-transitions  $N_y$  and their expected deviation  $\delta N_y$  from the mean value. Modern nuclear theory does not consider this possibility. There are no experimental data on existence of "hidden" dependence, as well. Below it is not taking into account.

Experimental relative intensities  $\langle I_{\gamma}^{\text{max}} / E_{\gamma}^{3} \rangle$  together with their best approximation are given in Fig. 2. The data are presented so that the expected sum of intensity of gamma-

cascades lying below detection threshold corresponds to the most probable value of cumulative sum for  $\langle I_r^{\text{max}} / E_r^3 \rangle = 0$ .

Precision of determining parameters of approximating curve at small excitation energy of final levels  $E_f$  must additionally get worse due to inequality of level densities of different parity. Most probably, this increases error of extrapolation to zero intensity of gammatransition. In practice, this can result in overestimation of  $N_y$ . Comparison between approximated value of this parameter and known number of levels with spins 1-4 points [18,19] to overestimation of the  $\sum N_y$  value below  $E_i$ =2.6 MeV by a factor of 1.5-1.6.

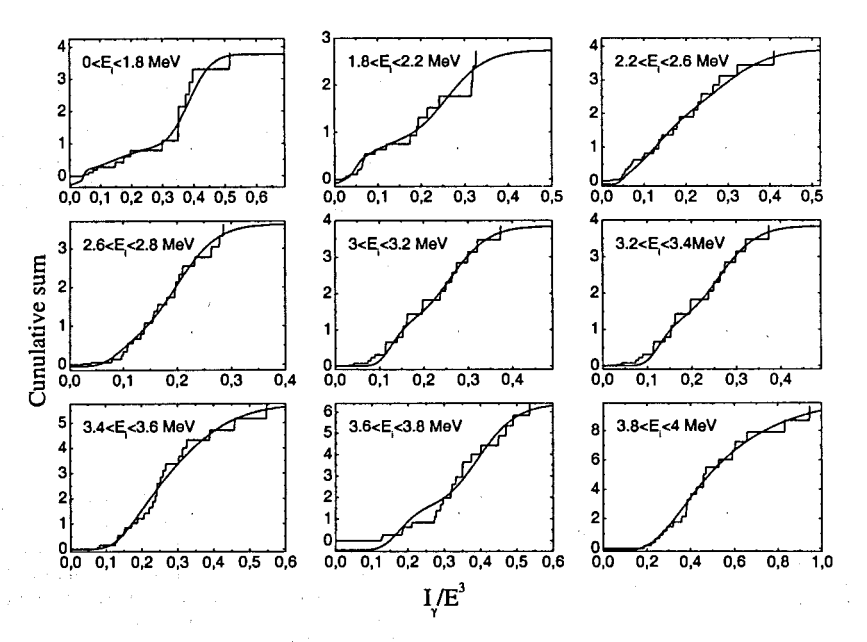


Fig. 2. Experimental value of cumulative sum of reduced experimental intensities  $\langle I_y/E_y \rangle$  for <sup>174</sup>Yb - histogram. Smooth curve represents the best approximation. Excitation energy intervals  $E_i$  of final levels are shown in figures.

The best values of fitting parameters v and  $R_k$  are given in figs. 3 and 4. Noticeable change in these approximation parameters for  $E_i > 2.5$  MeV points to considerable change in structure of even-odd isotope under consideration in given excitation energy region.

The best values of level density  $\rho = \sum_{J,\pi} N_{\gamma} / \Delta E$  and sums of radiative strength functions  $\sum \langle I_{\gamma} \rangle / E_{\gamma}^3 N_{\gamma}$  are shown in figs. 5 and 6. Intensities and strength functions in both [1] and [7] were normalized to absolute values.

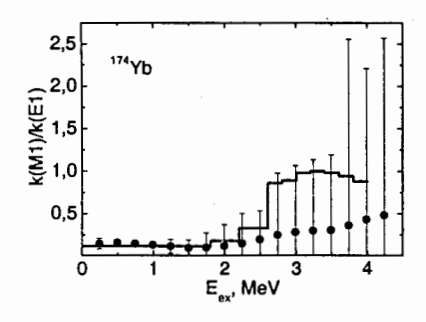


Fig. 3. The ratio k(M1)/k(E1) for different energy of levels excited by dipole primary gamma-transitions — histogram. Points with errors show interval of possible values of ratios  $R_k$ =0.5 from the data [1].

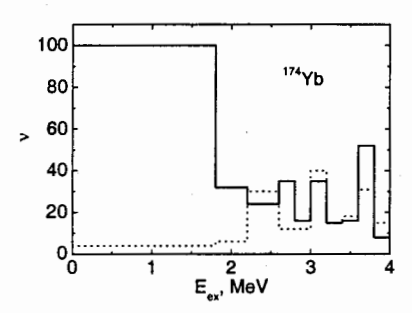


Fig. 4. The best values for dispersion of random intensities of the primary gamma-transitions to levels with different spins. Solid histogram represents values of parameter v for gamma-transitions to levels wit J=2,3, dashed histogram – to final levels with J=1,4.

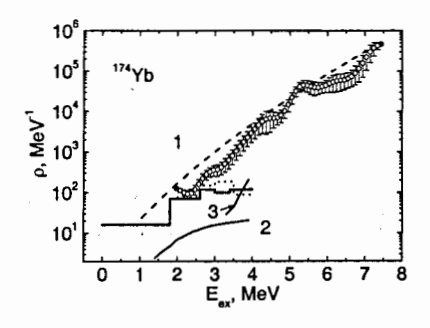


Fig. 5. Experimental and model values of level density in <sup>174</sup>Yb. Curve 1 represents level density calculated within model [20], curve 2 shows expected density of two-quasiparticle levels for their appearance threshold 1 MeV, curve 3 – density of four-quasiparticle levels for threshold 3.1 MeV. Solid histogram corresponds to the best approximation of data [7], dotted histogram shows data [9], points with errors represent data [1].

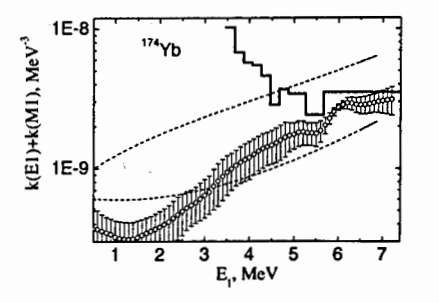


Fig. 6. The sums of radiative strength functions for the best approximation of the data [7] – histogram. Dashed curves represent predictions of models [3,21] in sum with k(M1)=const. Points with errors represent data [1].

Physically important information on structure of levels in the interval of their excitation from ~2 to ~4 MeV can be extracted from the coefficient of collective enhancement of level density:

$$\rho(U,J,\pi) = \rho_{ap}(U,J,\pi)K_{coll}(U,J,\pi). \tag{1}$$

According to modern notions,  $K_{coll}$  determines [22] degree of enhancement of density of purely quasiparticle excitations  $\rho_{qp}(U,J,\pi)$  of deformed nucleus due to its rotation and vibrations. One can accept in the first approach that in narrow excitation energy interval and very narrow spin window considered here, parameter  $K_{coll}$  is approximately equal to coefficient  $K_{vibr}$  of vibrational enhancement of level density. In general form, the latter is determined by change in nuclear entropy  $\delta S$  and re-distribution of nuclear excitation energy  $\delta U$  between quasiparticles and phonons at temperature of a nucleus T:

$$K_{vibr} = exp(\delta S - \delta U/T).$$
 (2)

Available experimental data on level density and model notions of it do not allow unambiguous and reliable determination of the  $K_{vibr}$  value for arbitrary nuclear excitation energy U even for zero systematical error in determination of function  $\rho(U,J,\pi)$ .

Unfortunately, there was not found possibility for unambiguous experimental determination [23] of breaking threshold  $E_N$  of the first, second and following Cooper pairs, value and form of correlation functions  $\delta N$  of nucleons pair number N in heated nuclei. The main uncertainty of  $E_N$  is caused by lack of experimental data on function  $\delta_N = f(U)$ , the secondary – by ambiguity of density of two-quasiparticle levels in model [24]. So, according to three different model ideas, the threshold  $E_2$  of appearance of four-quasiparticle excitations was found to be equal to 1.7, 3.2 [23] and 3.4 MeV [25]. It is most likely [22] that the breaking threshold of the secondary Cooper pair  $\approx 3.3$  MeV has the least systematical uncertainty. In this case, good estimation for  $\rho_{qp}(U,J,\rho)$  will be density of two-quasiparticle excitations calculated in accordance with [24]. The  $K_{coll}$ -1 value obtained is shown in Fig. 7. There is observed significant correlation of this coefficient with the value of  $\delta_I$  from [25] and from the second variant of analysis [22] in the excitation energy interval  $\approx 2.0 - 3.1$  MeV. Decrease in correlation coefficient at higher excitation energy can be related to both significant contribution of four-quasiparticle excitations in function  $\rho(U,J,\pi)$  and less than it is adopted in [22, 25] velocity of decrease of function  $\delta_I$  at U>3 MeV.

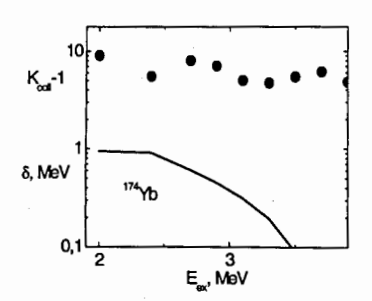


Fig. 7. Comparison of coefficient of collective enhancement of level density and correlation function of nucleon pair in  $^{174}$ Yb. Circles show coefficient of collective enhancement of level density, curve – values of the  $\delta_I$  parameter used in [25] for calculation of partial density of two-quasiparticle levels.

The data presented allow the following conclusions:

1. In the <sup>174</sup>Yb nucleus excited in  $(\overline{n}, \gamma)$  reaction with neutron energy of  $\approx 2$  keV are observed the same properties which were revealed for approximately four tens of nuclei from the mass region  $40 \le A \le 200$ : step-like structure in level density and significant local enhancement of radiative strength functions of the primary gamma-transitions to corresponding low-lying levels. The data on these parameters of cascade gamma-decay obtained in [1], most probably, contain significant errors: level density in the region 2.5 to 4.0 MeV (or wider) is overestimated, as minimum, by several times.

Strength functions are accordingly underestimated. Most probable, these errors are caused by significant increase in strength functions of the secondary cascade gammatransitions to the levels of step-like structure. This effect was revealed and reproduced in calculation [2] in some neighboring even-even nuclei in form of significant increase in cascade population of levels lying above 3-4 MeV (or lover by the  $\delta$ -value – in odd nuclei).

- 2. In the excitation energy region about 2.0-2.5 MeV occurs abrupt change in level structure. It appears itself in considerable increase of the k(M1)/k(E1) values and in strong difference of distribution of random gamma-transition amplitudes from normal one.
- 3. Experimental ratios k(M1)/k(E1) can be used for obtaining more unambiguous values of radiative strength functions for E1- u M1-transitions and data on relation between level densities of different parity in the frameworks of methods [1,2].
- 4. The main part of the primary gamma-transitions observed in  $(\bar{n}, \gamma)$  reaction corresponds, probably, to population of levels with large and weakly fragmented phonon components of wave functions.

#### 5. Conclusion

Analysis of available experimental data on intensities of the primary gammatransitions following 2 keV neutron capture in compound nucleus 174Yb demonstrated presence of step-like structure in level density and increase in radiative strength functions of transitions to levels in region of this structure, at least, for the primary dipole transitions. I. e., it confirmed main conclusions of [1,2] and simultaneously showed necessity to reveal and remove systematical experimental errors in alternative methods of determination only of level density and all other parameters of cascade gamma-decay. That is why, two problems become the most important - correct accounting for influence of level structure on probability of nuclear evaporation and emission of cascade gamma-quanta in investigation of nuclear reactions on beams of accelerators as well as considerable decrease of systematical errors of experiment. Comparison of the data presented in figs. 5 and 6 with the obtained intensities of two-step gamma-cascades allows preliminary conclusion that sharp change in structure of decaying neutron resonances, at least, in interval of their energies of ≈2 keV is not observed.

#### REFERENCES

- 1. Vasilieva E.V., Sukhovoj A.M., Khitrov V.A., Phys. At. Nucl. 64(2) (2001) 153. (nucl-ex/0110017).
- 2. Sukhovoj A.M,. Khitrov V.A., Physics of Paricl. and Nuclei, 36(4) (2005) 359.
- 3. Axel P., Phys. Rev. 126(2). (1962) 671.
- 4. Brink D. M., Ph. D. thesis, Oxford University (1955).
- 5. Khitrov V.A., Li Chol, Sukhovoj A.M., Proc. of the XI International Seminar on Interaction of Neutrons with Nuclei, Dubna, May 2003, E3-2004-9, Dubna, 2004, P. 98. (nucl-ex/0404028).

- 6. Sukhovoj A.M., Furman W.I., Khitrov V.A., Proc. of the XV International Seminar on Interaction of Neutrons with Nuclei, Dubna, May 2007, E3-2007-9, P. 92.
- 7. Granja C., Pospisil S., Chrien R.E., and Telezhnikov S.A., Nucl. Phys., A757 (2005) 287.
- 8. Porter C.F., and Thomas R.G., Phys. Rev., 104(2) (1956). 483.
- 9. Sukhovoi A.M, Khitrov V.A., 62 (1999) 19.
- 10. Solov'ev V.G., Fiz. Elem. Chastits At. Yadra, 3(4) (1972) 770.
- 11. Solov'ev V.G.., Theory of atomic Nuclei: Quasiparticles and Phonons -Institute of Physics Publishing, Bristol and Philadelphia, 1992.
- 12. Malov L.A., Solov'ev V.G. Yad. Phys., Vol. 26(4) (1977) 729.
- 13. Malov L.A., Meliev F.M., and Soloviev V.G., Z. Phys., A320(3) (1985) 521.
- 14. Gareev F.A., Ivanova S.P., Solovev V.G., Fedotov S.I., Fiz. Elem. Chastits At. Yadra, 4(2) (1973) 357.
- 15. Vdovin A.I. et al., Fiz. Elem. Chastits At. Yadra, 7(4) (1076) 952.
- 16. Mughabghab S.F. // Neutron Cross Sections BNL-325. V. 1. Parts A, Ed. By Mughabghab S.F., Divideenam M., and Holden N.E.// (N.Y., Academic Press, 1984) Mughabghab S.F., Neutron Cross Sections, V.1, part B, Ed. by Mughabghab S.F., (N.Y., Academic Press, 1984).
- 17. Chrien R.E. and Kopecky J., Nucl. Phys. A 414 (1984) 281.
- 18. http://www.nndc.bnl.gov/nndc/ensdf.
- 19. Belen'kii V.M.,. Grigor'ev E.P., Struktura slozhnukh yader. (Energoizdat, Moscow). 1987.
- 20. Dilg W., Schantl W., Vonach H., Uhl M., Nucl. Phys., A217 (1973) 269.
- 21. Kadmensky S.G., Markushev V.P., Furman W.I., Sov. J. Nucl. Phys. 37 (1983) 165.
- 22. Reference Input Parameter Library RIPL-2. Handbook for calculations of nuclear reaction data. IAEA-TECDOC, 2002. http://www-nds.iaea.or.at/ripl2.
- 23. Sukhovoj A.M. Khitrov V.A, JINR preprint E3-2005-196, Dubna, 2005.
- 24. Strutinsky V.M., Proc. of Int. Conf. Nucl. Phys., Paris, 1958. P. 617.
- 25. Sukhovoj A.M. Khitrov V.A., Physics of Paricl. and Nuclei, 37(6) (2006) 899.

# PARAMETERS OF CASCADE GAMMA-DECAY OF COMPOUND-NUCLEI <sup>146</sup>Nd, <sup>156</sup>Gd, <sup>172</sup>Yb, <sup>182</sup>Ta, <sup>184</sup>W, <sup>191</sup>Os, <sup>231,233</sup>Th, <sup>239</sup>U, <sup>240</sup>Pu FROM EXPERIMENTAL DATA OF REACTION $(\overline{n}, \gamma)$

### A.M. Sukhovoj, V.A. Khitrov

Joint Institute for Nuclear Research, 141980, Dubna, Russia

#### Abstract

Re-analysis of experimental data on primary gamma-transitions averaged over some energy intervals of neutron resonances has been performed. Approximation of their cumulative sums together with extrapolation of the obtained distribution to zero value allowed us to determine mean intensities of of E1- and M1-transitions, their probable number and total dispersion of intensity deviations from the mean value. The level density and sum of radiative strength functions determined in this way confirm main peculiarities of these nuclear parameters determined from intensities of the two-step gamma-cascades.

### 1 Introduction

Level density  $\rho$  and radiative strength functions  $k = \Gamma/(E_{\gamma}^3 D_{\lambda} A^{2/3})$  of the dipole primary transitions of the neutron resonance gamma-decay provided us with a considerable portion of experimental information on both nuclear properties on the whole and nuclear resonances – in particular.

Nevertheless, there is an urgent necessity in determination of these data in new independent experiments. The ground for this is principle incompatibility of experimental data on  $\rho$  and k(E1) + k(M1) obtained in two-step reaction  $(n, 2\gamma)$  [1, 2] with analogous data from one-step reactions like (p, n) [3, 4],  $(d, p\gamma)$  [5] and  $({}^{3}\text{He}, \alpha\gamma)$  [6].

Partial analysis of possible reasons for this discrepancy was performed, for example, in [7]. It results in the following statements:

- a) transfer coefficients of total errors in determination of partial cross-sections of twostep reactions onto errors of the parameters under determination are much less than those determined in one-step reactions like  $(d, p\gamma)$ , ( ${}^{3}\text{He}, \alpha\gamma$ ) due to other form of functional dependence between subjects "spectrum" and "parameters";
- b) the same concerns sensitivity of the determined parameters to degree of erroneous of hypothesis by Bohr-Mottelson [8] (Axel-Brink [9, 10]) for gamma-quanta) of independence of interaction cross-section of final reaction product in reverse reaction with the excited final nucleus.

In practice, error in absolute normalization of the two-step spectra by order of  $\pm 25\%$  changes the  $\rho$  and k(E1) + k(M1) values not more than by a factor of two [11] near  $E_{ex} \approx 0.5B_n$ . This is the largest systematical error in these experimental data. Analogous error of the total gamma-spectrum normalization for different excitation energies  $0 \le$ 

 $\Delta S/S \leq 1\%$  in one-step (according to the used analysis method) reaction  $(d, p\gamma)$  or  $(^3\text{He},\alpha\gamma)$  brings [12] to more than 100% errors in intensities of all the spectra of only primary gamma-transitions, at least, for  $E_{\gamma} \leq 0.5$  MeV. The coefficients of further transfer of the indicated error on the determined values of the parameters, until now, were not determined by anyone. It is possible to suggest in this situation, that  $\rho$  and k(E1)+k(M1) determined according to [6] have arbitrary systematical errors for different excitation and primary gamma-transitions energies.

Direct experimental verification of hypotheses [8, 9, 10] is impossible. But, the possibility of obtaining functionals directly depending on unknown partial cross-sections of reaction for excited target-nucleus was found in [2]. Cascade population of levels determined there for the majority of  $\approx 20$  nuclei up to excitation energy of  $E_{ex} \sim 3-5$  MeV cannot be reproduced in frameworks of Axel-Brink hypotesis. However, they can be easily enough reproduced under assumption of existing enhancement of primary and secondary gamma-transitions to the region of "step-like" structure in level density [1, 2].

Unfortunately, complete notion of the observed by this method function  $k(E1) + k(M1) = f(E_{\gamma}, E_{ex})$  cannot be obtained due to lack of experimental data. But, as it is seen from comparison between the results [13, 14] and the data [1, 2], violation of hypothesis [9, 10] is considerably larger than it was obtained in [2]. For this reason, level density obtained in [1, 2] can be overestimated by several times in excitation region  $\sim 0.5B_n$ . Most probably, this error gradually decreases at lower and higher excitation energy of nucleus under condition that the experimental data on density of low-lying levels and neutron resonances have significantly lesser errors. Strength functions k(E1) + k(M1) are, most probably, underestimated.

Due to this reason, authors [1, 2] performed independent model-free re-analysis of the experimental data from the  $(\bar{n}, \gamma)$  reaction in frameworks of only mathematical statistics with the least number of assumptions on parameters of small sets of the primary gamma-transition partial widths. It was obtained that the refusal from main postulates of "statistical" theory brings to conclusion which confirms main results of [1, 2].

## 2 Main principles of analysis

Capture of neutrons in "filtered" beams, for example, noticeably enough averages the gamma-transition partial widths in local resonances. This is true for nuclei with small enough spacing  $D_{\lambda}$  between neutron resonances. It is possible to observe experimentally the width  $\Gamma$  with relative statistical error  $\sigma$  if its value exceeds practically constant detection threshold L of experiment (in any given narrow interval of gamma-transition energy).

The portion of primary gamma-transitions of the same multipolarity and practically equal energy with  $\Gamma < L$  is determined by concrete form of deviation distribution of  $\Gamma$  from mean value in individual resonances and their effective number for neutron beam in experiment.

It follows from main statements of modern nuclear theory that the amplitude of gamma-transition between neutron resonance and low-lying level is determined by quasiparticle and phonon components in wave functions of both levels (see, for instance, [16]). Their concrete values are determined by fragmentation degree of the states like n quasiparticles and m phonons over nuclear levels at different excitation energy. In accordance with [17], this process is rather specific – strength of the fragmented state is distributed very irregularly. In many cases, its strength is fragmented over the levels lying near the initial position of non fragmented state.

In practice, this means that the  $\Gamma$  values must strongly and locally depend on structures of decaying and excited levels. Their dispersion relative to the average must be determined by number and value of the wave function components of these levels. Therefore, fluctuations of  $\Gamma/<\Gamma>$  cannot be described by universal distribution. Its deviation from the generally adopted Porter-Thomas distribution [18] must be determined in every case experimentally. Practically, it is adopted in analysis (see [13]) that the sum of dispersions of experimental statistics uncertainty and "nuclear fluctuations" is equal to  $\sigma^2=2/\nu$  with unknown parameter  $\nu$ .

The second assumption of analysis is that the gamma-transitions of the same multipolarity with energy of about some hundreds keV have the same mean value. In principle, this assumption can be mistaken and, for instance, mean widths of all the gamma-transitions involved in the set under analysis can belong to some rather wide interval of possible values. Moreover, the probability of given mean value may increases as decreasing  $<\Gamma>$ .

This possibility is to be investigated experimentally. Real width distribution around the average determines reliability of both data presented below and conclusions of [1, 2].

## 3 The most reliable values

The values of level density and radiative strength functions of primary gamma-transitions obtained by analogy with [13] are presented in figs. 1–4. The distribution of cumulative sums of reduced intensities for the analyzed nuclei [19] - [28] and parameters of approximating curve have no principle difference with that given in [13, 14, 15]. Therefore, they are not presented in this work.

The gamma-decay parameters of nuclei determined in [1, 2] are compared with results of two different in principle methods of analysis. Accounting for results of theoretical analysis [17] (possible dependence of the wave function components of levels determining  $\Gamma$  on energy of neutron resonances) one can conclude that the discrepancy between results of two methods of analysis mentioned above is less than their difference from the data [4, 6].

It follows, first of all, from observation of "step-like" structure in level density in both methods [1, 2, 13] and close to zero or negative derivative  $d(k(E1) + k(M1))/dE_1$  for the same excitation region of nucleus. Id est, the local peak in sum of strength functions must be more or less clearly expressed.

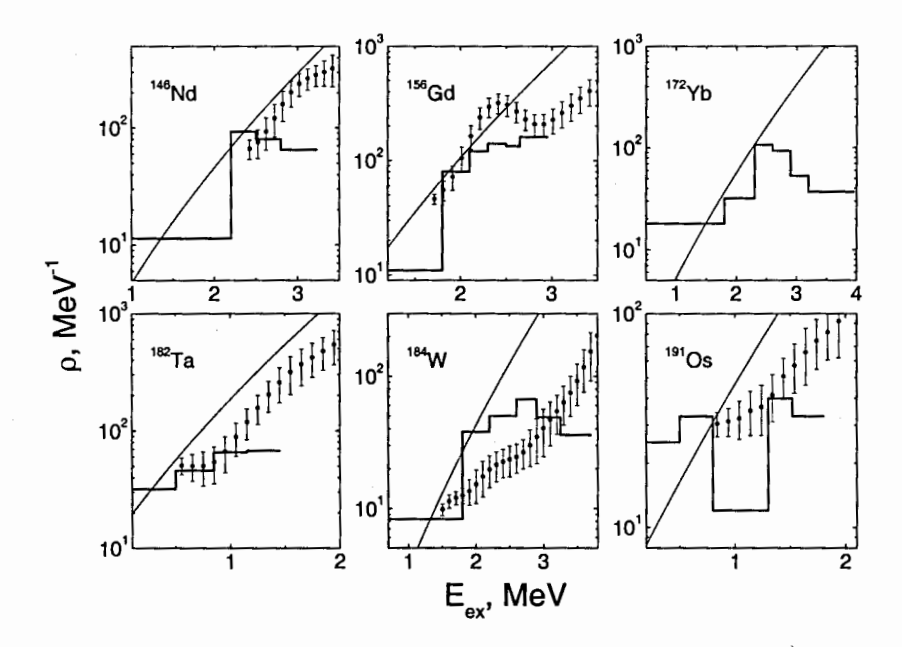


Fig. 1. Comparison of different data on level density for the <sup>146</sup>Nd, <sup>156</sup>Gd, <sup>172</sup>Yb, <sup>182</sup>Ta, <sup>184</sup>W and <sup>191</sup>Os nuclei. Curve represents the calculated within model [29] density of levels populated by the primary gamma-transitions. Results of presented analysis – histogram, points with errors – data [1] and [2].

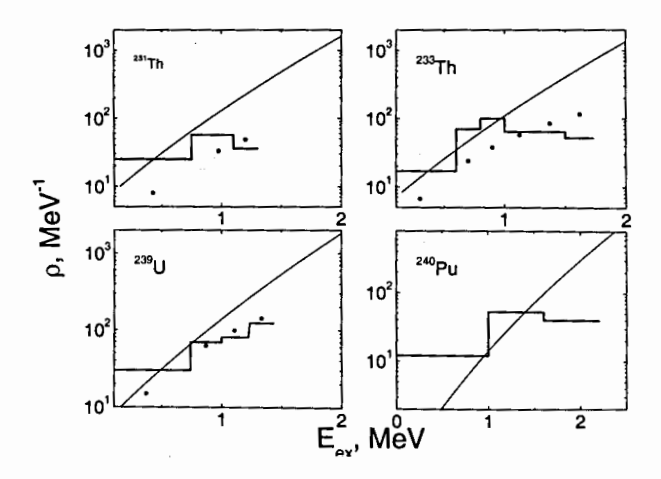


Fig. 2. The same, as in Fig. 1, for <sup>231,233</sup>Th, <sup>239</sup>U and <sup>240</sup>Pu. Points show approximation of the experimental data by density of two- or three-quasiparticle levels of model [31] with the independent on excitation energy coefficient of collective enhancement.

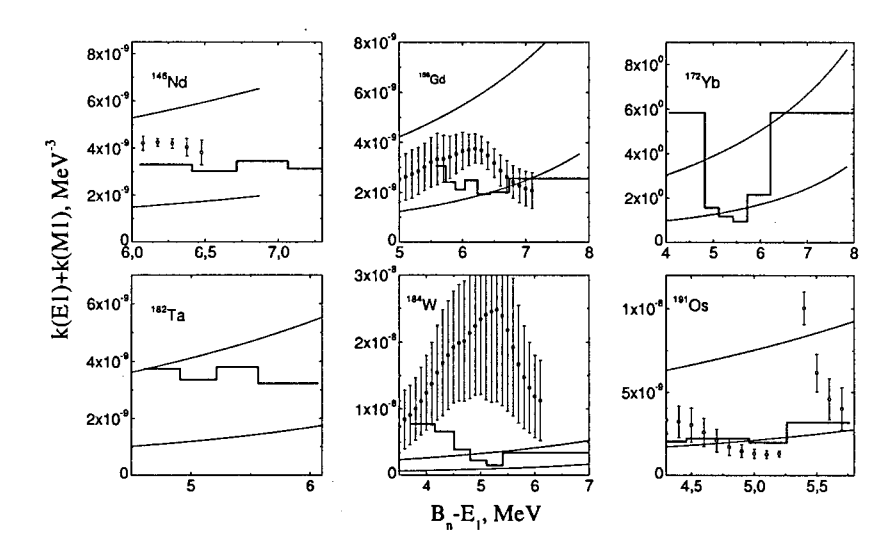


Fig. 3. The same, as in Fig. 1, for sums of the radiative strength functions. Results of analysis performed in this work are presented as histogram of relative values. Upper curve - [9], lower curve - [30] together with k(M1)=const. Points with errors show the data [1, 2].

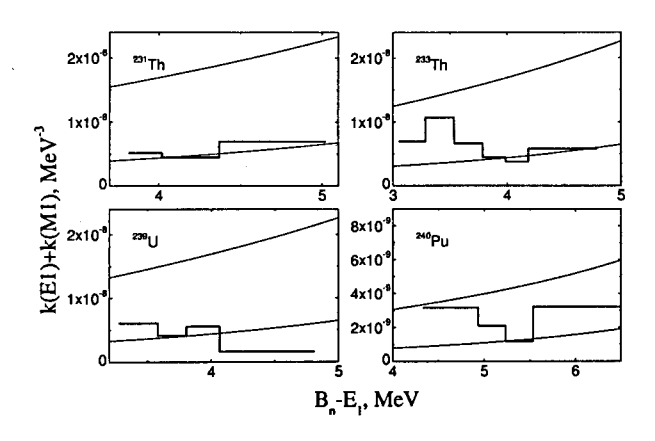


Fig. 4. The same, as in Fig. 3, for <sup>231</sup>Th, <sup>233</sup>Th, <sup>239</sup>U and <sup>240</sup>Pu.

The data presented in figs. 1, 2 confirm also conclusion on probable local increase in density of vibration type levels in the region of the nucleon pairing energy for a nucleus of a given mass. The shape of this dependence is presented in details in [13, 14, 15].

## 4 Conclusion

Unfortunately, energy interval of the primary gamma-transitions observed in experiment is considerably less than that for <sup>157,159</sup>Gd, <sup>174</sup>Yb and <sup>237</sup>U. Nevertheless, the data shown in figs. 1-4 bring to the following conclusion: notions of a nucleus as a system of non-interacting Fermi-gas and ideas of other analogous nuclear models [32] are insufficient for reproduction of modern experimental data.

### References

- Vasilieva E.V., Sukhovoj A.M., Khitrov V.A., Phys. At. Nucl. 64(2) (2001) 153, (nucl-ex/0110017)
- [2] A.M. Sukhovoj, V.A. Khitrov, Phys. Particl. and Nuclei, 36(4) (2005) 359.
- [3] Vonach H., Proc. IAEA Advisory Group Meeting on Basic and Applied Problems of Nuclear Level Densities, (New York, 1983), INDC(USA)-092/L, (1983), p.247.
- [4] Grudzevich O.T. et.al., Sov. J. Nucl. Phys. 53 (1991) 92.
   Zhuravlev B.V., Bull. Rus. Acad. Sci. Phys. 63 (1999) 123.
- [5] Bartholomew G.A. et al., Advances in nuclear physics, 7 (1973) 229.
- [6] Schiller A. et al., Nucl. Instrum. Methods, A447 (2000) 498.
- [7] These proceedings, p. .
- [8] Bohr A., Mottelson B.R., Nuclear structure, Vol. 1 (W. A. Benjamin, Inc. New York, Amsterdam, 1969).
- [9] Axel P., Phys. Rev., 126, 671 (1962).
- [10] Brink D. M., Ph. D. thesis, Oxford University (1955).
- [11] Khitrov V.A., Li Chol, Sukhovoj A.M., Proc. XI International Seminar on Interaction of Neutrons with Nuclei, Dubna, May 2003, E3-2004-9, 2004. Dubna, P.98, (nuclex/0404028).
- [12] Khitrov V. A., Sukhovoj A. M., Pham Dinh Khang et al., JINR preprint E3-2003-7, Dubna, 2003. Khitrov V.A., Sukhovoj A.M., Pham Dinh Khang et al., Proc. XI International

- Seminar on Interaction of Neutrons with Nuclei, Dubna, 22-25 May 2003, JINR E3-2004-9, (Dubna, 2004) p. 107.

  Whitney V.A. Sukherei A.M. Phom Diph Khong et al., puel or (0205006)
- Khitrov V.A., Sukhovoj A.M., Pham Dinh Khang et al., nucl-ex/0305006.
- [13] Sukhovoj A. M., Physics of atomic nuclei, 71 (2008) 1907.
- [14] These proceedings, p. 192.
- [15] These proceedings, p. 164.
- [16] Boneva S.T., Vasilieva E.V., Malov L.A. et al., Yad. Phys., 49 (1989) 944.
- [17] Malov L.A., Solov'ev V.G., Yad. Phys., 26(4) (1977) 729.
- [18] Porter C.F., Thomas R.G., Phys. Rev., 104 (1956) 483.
- [19] Kononenko et al., Izv AN SSSR, ser. fiz., 50(5) (1986) 883.
- [20] Litvinsky L.L. et al., Yad. Fiz., 58(2) (1995) 206.
- [21] Greenwood R.C., Reich C.W., Nucl. Phys. A, 252 (1975) 260.
- [22] Stelts M.L., Browne J.C., Phy. Rev., C16 (1977) 574.
- [23] Greenwood R.C., Reich C.W., Nucl. Phys. A,223 (1974) 66.
- [24] Casten R.F. et al., Nucl. Phys. A 285 (1977) 235.
- [25] White D.H. et al., Phys. Rev. C35 (1987) 81.
- [26] Jeuch P. et al., Nucl. Phys. A317 (1979) 363.
- [27] Chrien R.E., Kopecky J., Nucl. Phys. A414 (1984) 281.
- [28] Chrien R.E.et al., Nucl. Phys. A436 (1986) 205.
- [29] Dilg W., Schantl W., Vonach H., Uhl M., Nucl. Phys. 1973. A217. P.269.
- [30] Kadmenskij S.G., Markushev V.P., W.I. Furman, Sov. J. Nucl. Phys., 37 (1983) 165.
- [31] Strutinsky V.M., Proc. Int. Conf. Nucl. Phys., 1958, Paris, P.617.
- [32] Reference Input Parameter Library RIPL-2. Handbook for calculations of nuclear reaction data. IAEA-TECDOC, 2002. http://www-nds.iaea.or.at/ripl2.

## NUCLEAR INTERACTION DYNAMICS IN 56Fe(0,xn) REACTION

B.V. Zhurayley, N.N. Titarenko, V.I. Trykova

State Scientific Center of Russian Federation – Institute for Physics and Power Engineering, 249033 Obninsk, Kaluga Region, Russia

Neutron spectra and angular distributions in  $^{56}$ Fe( $\alpha$ ,xn) reaction have been measured at  $\alpha$ -particle energies of 12, 16, 18, 27, 45 MeV. The measurements were performed by time-of-flight fast neutron spectrometers on the pulsed accelerators. The analysis of the measured data have been carried out in the framework of equilibrium, preequilibrium and direct nuclear reaction mechanisms. The calculations are done using the exact formalism of the statistical theory as given by Hauser-Feshbach with the nuclear level densities of Ni isotopes, excited in this reaction, determined on the basis of new experimental data on the low-lying levels, the swave neutron resonance spacing and neutron evaporation spectra [1]. The contributions of equilibrium, preequilibrium and direct mechanisms of neutron emission has been studied in a wide energy range of  $\alpha$ -particles.

#### Introduction

Understanding of the nuclear interaction mechanisms is an overall objective of any nuclear reaction study. In spite of permanent interest to elaboration of fundamental approaches in the description of nuclear interaction in mega-electron-volt range of the energy, the complete understanding of nuclear reaction mechanisms yet it is not achieved. Accordingly the models are not developed, allowing to predict differential cross-sections of interaction with accuracy achievable in experiment. Three types of the interactions described by mechanisms of equilibrium, preequilibrium and direct processes are traditionally distinguished. The equilibrium mechanism of reaction is strictly enough formalized in Hauser-Feshbach model, however big uncertainties arise at modeling of nuclear level density. Analysis of a nonequilibrium part demands more clear split between preequilibrium emission of particles and direct processes, especially one-step, as a rule negligible in the preequilibrium mechanism. Study of the nonequilibrium neutron emission in (α,xn) reaction is represented a little bit easier other reactions with complex particles as in this case the probability of preliminary formation of α-particles is not considered, lack of Coulomb barrier in output channel makes neutron decay predominated one, and the neutron optical potential is most investigated.

In the present work differential cross-sections of  $^{56}$ Fe( $\alpha$ ,xn) reaction are measured at  $\alpha$ -particle energies of 12, 16, 18, 27, 45 MeV and analyzed within the framework of equilibrium, preequilibrium and direct mechanisms of interaction. The nuclear level densities of Ni isotopes, excited in this reaction, were determined on the basis of new experimental data on the low-lying levels, the s-wave neutron resonance spacing and neutron evaporation spectra [1].

### Experiment

Spectra and angular distributions of neutrons from  $^{56}$ Fe( $\alpha$ ,xn) reaction are measured at  $\alpha$ -particle energies of 12.3, 16.3, 18.3, 26.8, 45,2 MeV. The measurements of neutron spectra were performed by time-of-flight fast neutron spectrometers on the pulsed tandem accelerator at  $\alpha$ -particle energies of 12.3, 16.3 and 18.3 MeV in the angle range of (20-140) $^{0}$  [2] and on

150 cm cyclotron at  $\alpha$ -particle energies of 26.8 and 45.2 MeV in the angle range of  $(30\text{-}150)^0$  [3]. As a target were used the self-supporting metal foil with thickness of  $0.6 \text{ mg/cm}^2$  and  $2.6 \text{ mg/cm}^2$  and enrichment of 99.5 %. Neutrons were detected by the scintillation detector. For decreasing of the background it was placed in the massive shielding and electronic discrimination of gamma-rays was used. The detector efficiency was determined by measuring of the  $^{252}$ Cf prompt fission neutron spectrum, yields of monoenergetic neutrons from T(d,n), T(p,n), D(d,n) reactions and direct modeling of interaction of neutrons with organic scintillator. The neutron spectrum measurement procedure has been consisted in measuring with target and without it for the same  $\alpha$ -particle flux, registrated by the integrator of a current with Faradey-cup as a charge collector. The background was small in magnitude and practically uncorrelated over time. Typical angle-integrated neutron emission spectra and angular distributions of neutrons from  $^{56}$ Fe( $\alpha$ ,xn) reaction are presented in figs. (1-5). As the  $\alpha$ -particle energy increases, a high-energy component manifests itself in the neutron spectra, angular distributions of which are asymmetric, that are a typical indication of nonequilibrium processes in nuclear reactions.

#### Data analysis

For the calculation of an equilibrium part of differential cross-section of reaction we used Hauser-Feshbach mathematical formalism of statistical theory of the nuclear reactions [4], precisely taking into account laws of spin and parity preservation and also the characteristic of low-lying levels of a residual nucleus.

$$\frac{d^{2}\sigma(E_{0}, E_{2}, \theta)}{dE_{2}d\Omega} = \frac{1}{4K_{0}^{2}} \cdot \sum_{k,l_{1}} \sum_{l_{0}j,l_{2}j_{2}} \frac{2J_{1} + 1}{(2S_{0} + 1) \cdot (2J_{0} + 1)} \cdot B_{k}(l_{0}, S_{0}, j_{0}, J_{0}, J_{1}) \cdot \sum P_{k}(l_{2}, j_{2}, S_{2}, J_{2}, J_{1}) \times \tau \cdot \rho(E_{0} + Q_{\alpha,n} - E_{2}, J_{2}) \cdot P_{k}(\cos\theta),$$
(1)

$$\tau = \frac{T_{l_0 j_0}(E_0) \cdot T_{l_2 j_2}(E_2)}{\sum_{c} (\sum_{l,j} T_{l,j} + \sum_{l,j,J} \int_{U_c} T_{l,j} \cdot \rho(E_0 + Q_{\alpha,n} - E_2, J_2) \cdot dU}$$
(2)

$$B_k(l,S,j,J_f,J_i) = (-1)^{J_f-J_i-S} \cdot (2J_i+1) \cdot (2j+1) \cdot \left\langle l_0 l_0 \middle| K_0 \right\rangle W(J_i J_i j j ; K J_f) \cdot W(j j l l ; K S), \quad (3)$$

where:  $\langle l_0 l_0 | K_0 \rangle$  - Clebsch-Gordan coefficients,  $W(J_1 J_1 j_1 j_2 j_3 K_1 j_4)$  - Racah coefficients,  $P_k(\cos \theta)$  -Legendre polynomials,  $K_0$  - wave vector of particle,  $l_0, l_2, j_0, j_2, J_0, J_2, E_0, E_2$  - accordingly the orbital moments, spins of particles and nuclei, energy of particles in input and output channels,  $J_1$  - spin of compound nucleus,  $T_{lj}$  - transmission coefficients,  $\rho(E_0 + Q_{\alpha_n} - E_2, J_2)$  - nuclear level density,  $U = E_0 + Q_{\alpha_n} - E_2$  - excitation energy of residual nucleus.

Initial distribution of a compound nucleus on energy and angular moment is determined on the basis of optical model. Then distribution on energy and moment for a residual nucleus is calculated. For each kind of decay and all possible values of energy and moment relative probabilities of emission are calculated and on initial population and relative probability of emission particle emission spectra are determined. After probabilities of the parent nucleus decay are calculated, the obtained distribution of an affiliated nucleus becomes initial on the next step of decay. Spectra of the particles emited at equilibrium decay of a compound nucleus substantially are determined by level density of the residual nuclei excited in researched reaction. Therefore in calculations we used the data on level density of <sup>60</sup>Ni, <sup>59</sup>Ni, <sup>58</sup>Ni and <sup>57</sup>Ni determined on the basis of new experimental data on the low-lying levels, the neutron resonance spacing and neutron evaporation spectra [1]. Fig. 6 shows the level density of <sup>59</sup>Ni nucleus excited at the first step of neutron emission in <sup>56</sup>Fe(α,xn) reaction.

One can see that the description of the experimental data in the framework of the different model systematics differs markedly.

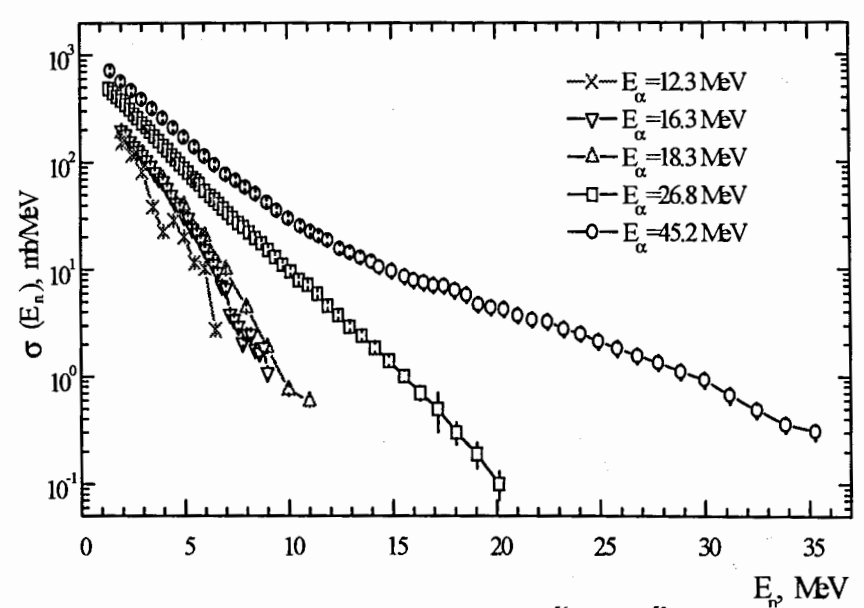


Fig.1. Angle-integrated neutron spectra from <sup>56</sup>Fe(α,xn)<sup>59</sup>Ni reaction.

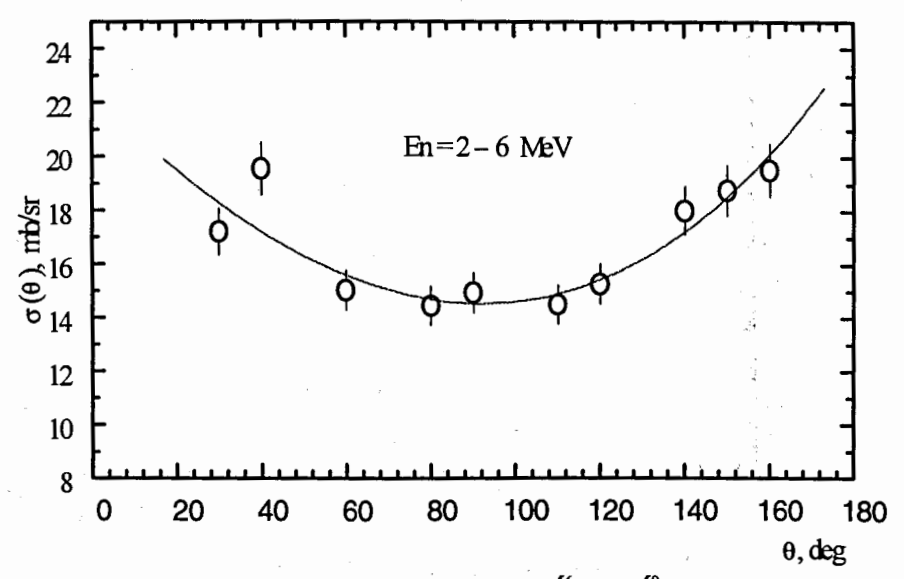


Fig.2. Angular distribution of neutrons from  $^{56}$ Fe( $\alpha$ ,n) $^{59}$ Ni reaction at E<sub>a</sub>=12,3 MeV. Curve - approximation data by Legendre polynomials.

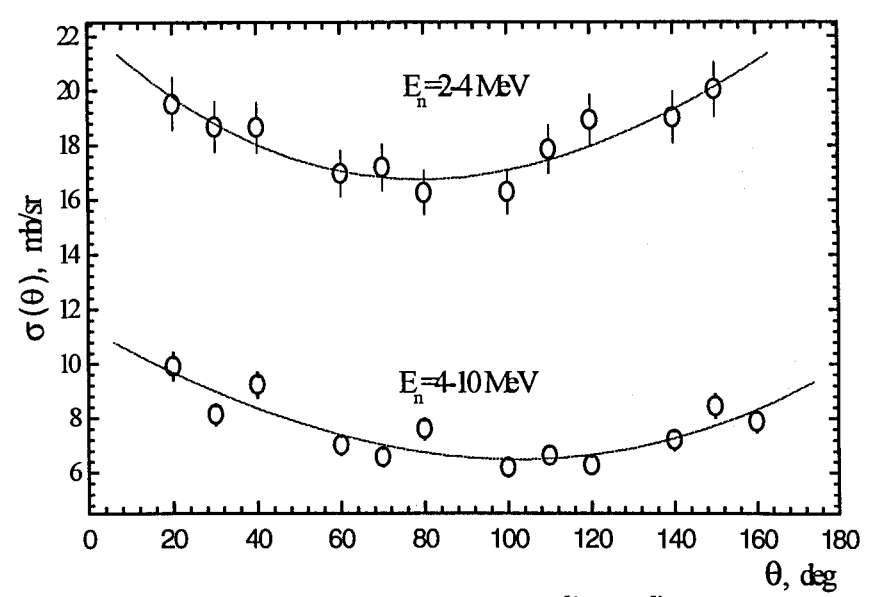


Fig.3. Angular distribution of neutrons from  $^{56}$ Fe( $\alpha$ ,n) $^{59}$ Ni reaction at  $E_a = 16.3$  MeV. Curve - approximation data by Legendre polynomials.

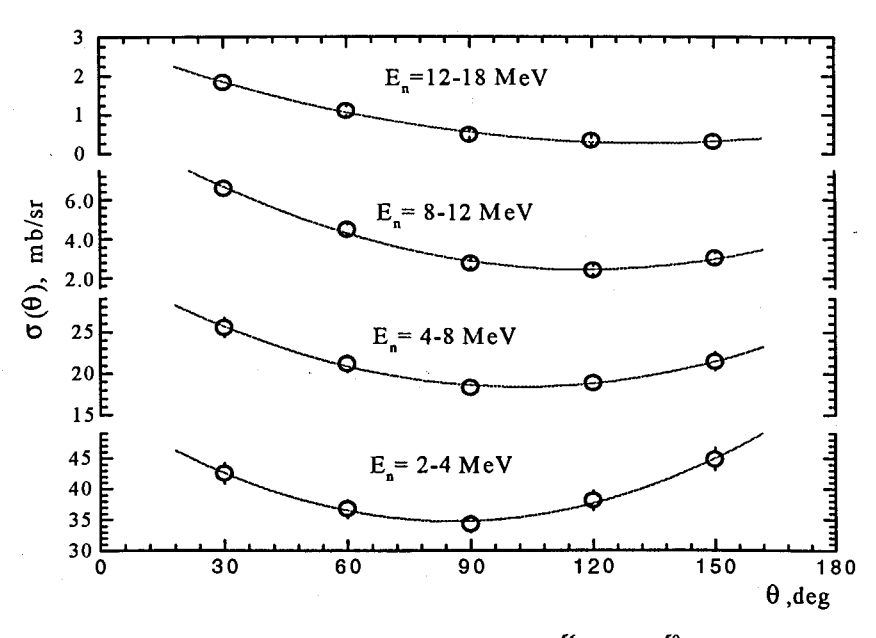


Fig.4. Angular distribution of neutrons from  $^{56}$ Fe  $(\alpha,xn)^{59}$ Ni reaction at  $E_a = 26.8$  MeV. Curve - approximation data by Legendre polynomials.

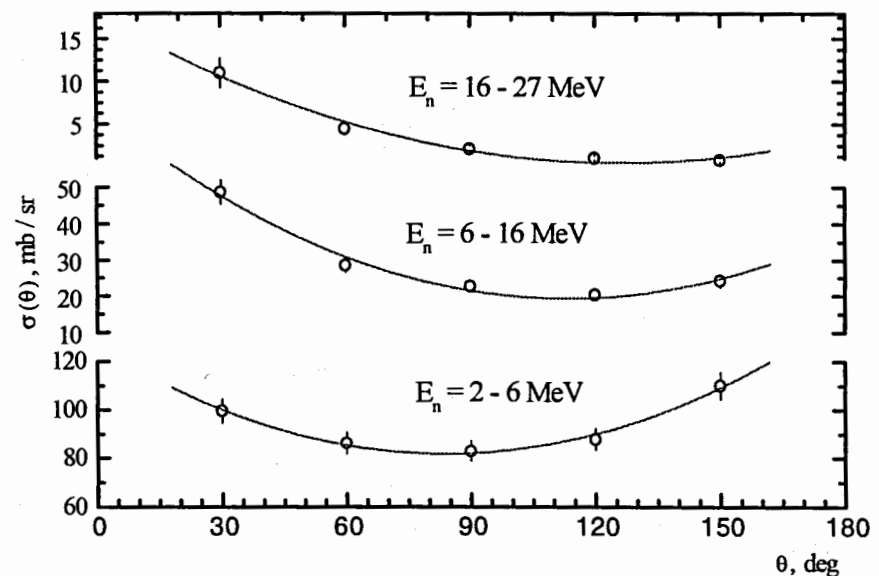


Fig. 5. Angular distribution of neutrons from  $^{56}$ Fe( $\alpha$ ,xn) $^{59}$ Ni reaction at  $E_a$  =45.2 MeV. Curve - approximation data by Legendre polynomials.

Calculations of preequilibrium neutron emission are executed in the framework of exciton model [5,6].

$$\frac{d\sigma(E_n)}{dE_n} = \sigma_a(E_o) \cdot \sum_{n=n_o}^{n_{max}} \lambda(n, E_n) \cdot \tau(n, E), \tag{4}$$

$$\lambda(n, E_n) = \frac{2s+1}{\pi^2 \cdot \hbar^3} \cdot \mu \cdot E_n \cdot \sigma_c(E_n) \cdot R \cdot \frac{\omega(p-1, h, U)}{\omega(p, h, E)}, \tag{5}$$

$$\omega(p,h,E) = \frac{g \cdot (g \cdot E - A_{p,h})^{n-1}}{p!h!(n-1)!},$$
(6)

where: s, µ, En - spin, reduced mass and neutron energy,

g - single particle state density (g=A/13),

 $\sigma_{\alpha}\!(E_0)$  - absorption cross-section of  $\alpha\text{-particles}$  by nucleus,

 $\sigma_c(E_n)$  - inverse reaction cross-section,

E and U - excitation energy, respectively, for composite and residual nuclei, n=p+h - exciton number of the system (p - particles, h - holes),

τ(n,E) - mean life-time of composite nucleus in n-exciton state.

R - factor, which is taking into account distinction of neutrons and protons in the internuclear cascade, was calculated in the assumption that in each pair interaction the proton and neutron are created with relative probabilities Z/A and N/A.

Aph - Pauli correction function.

In calculations are taken into account surface, shell structure and pairing effects. The initial exciton number " $n_0$ " is a parameter of model and we used a configuration 4p0h ( $n_0$ =4) in the assumption, that all  $\alpha$ -particles collapse on nucleons in a field of a nucleus-target. The quantity of the square of the average matrix element in model was 135.6 MeV<sup>2</sup>.

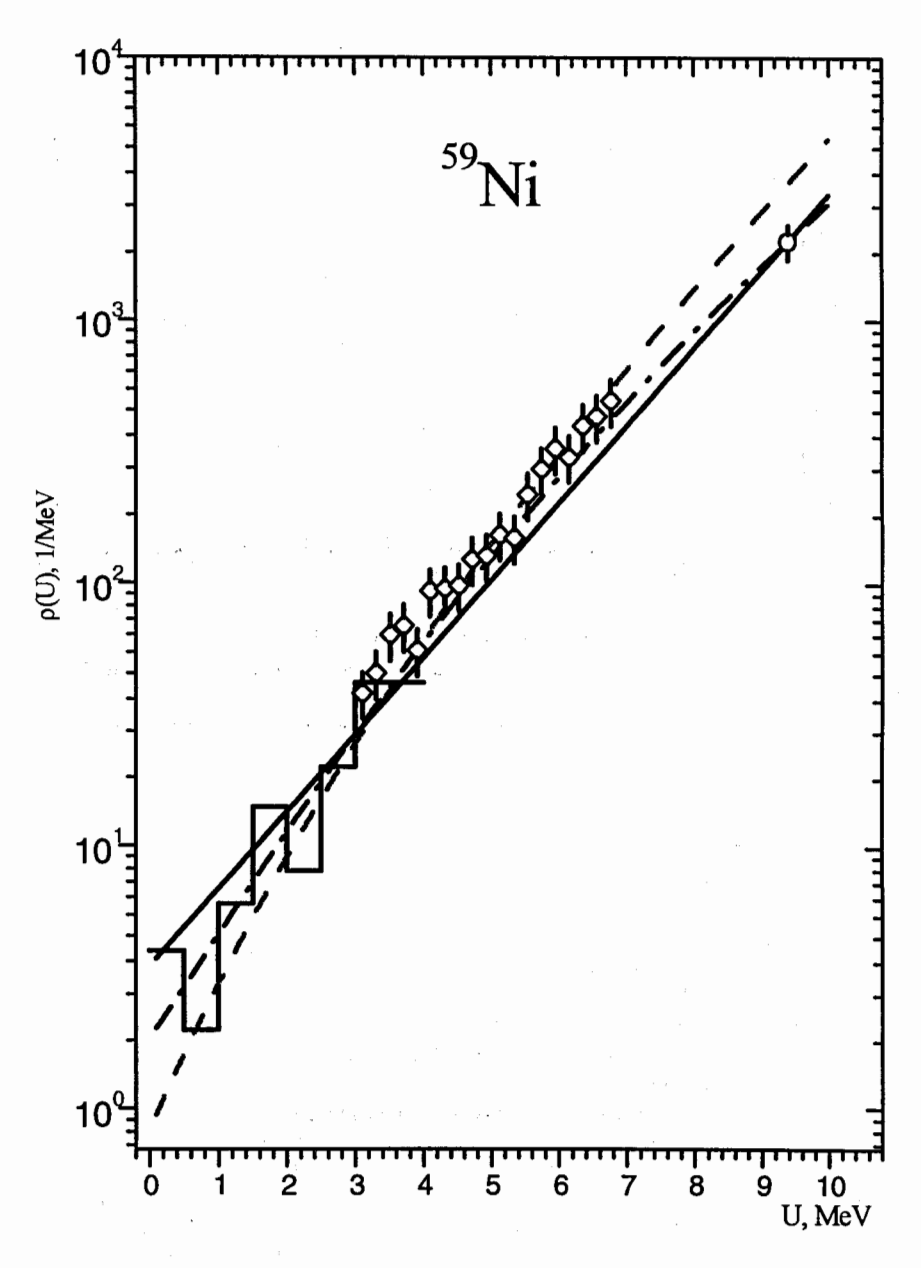


Fig. 6. Nuclear level density of the <sup>59</sup>Ni. ◊ - data obtained in our study from neutron evaporation spectra in <sup>59</sup>Co(p,n)<sup>59</sup>Ni reaction [1], histogram – low-lying level data, o - neutron resonance data. Curves are results of the calculations: dash-dotted - on the generalized model of a superfluid nucleus, dashed - on the back-shifted Fermigas model, solid - on the Gilbert-Cameron composite formula.

All calculations within the framework of optical-statistical models of equilibrium and preequilibrium decay of nucleus are carried out on modernized GNASH code [7], allowing to trace the decay of the excited compound nucleus with account of the emission of neutrons, protons,  $\alpha$ -particles and  $\gamma$ -quantums. For neutrons and protons the optical potential from work [8], for  $\alpha$ -particles - from work [9] and for deuterons - from work [10] was used.

For the full calculation of particle emission in nuclear reaction the separate direct interactions it is necessary to consider in addition to exciton model of preequilibrium emission [11]. At consideration of direct interaction effects it is important to know, what kinds of direct processes are taken into account in the framework of exciton model and to find independent ways of calculation of direct interactions which are not taken into account. In our case process of direct stripping of three nucleons of  $\alpha$ -particle and direct knockout process of neutron by  $\alpha$ -particle are not taken into account in the considered variant of exciton model, in which the initial stage of preequilibrium emission is ( $n_0$ =4, p=4, h=0), when  $\alpha$ -particle collapses on four nucleons in the field of a nucleus-target.

The general differential cross-section formula for continuum stripping reaction <sup>56</sup>Fe(α,n)<sup>59</sup>Ni is [11]

$$\frac{d\sigma(E_n)}{dE_n} = \frac{2s_n + 1}{2s_\alpha + 1} \cdot \frac{A_n}{A_\alpha} \cdot \frac{E_n \cdot \sigma_c(E_n)}{A_\alpha \cdot E_\alpha} \cdot K \cdot \left(\frac{A_\alpha}{E_\alpha + V_\alpha}\right)^{2n} \cdot \left(\frac{C}{A_{Ni}}\right)^n \cdot 0.0127 \cdot \omega(p, h, U), \quad (7)$$

where:  $s_n$ ,  $s_{\alpha}$  - spins of neutron and  $\alpha$ -particle,

 $A_n$ ,  $A_\alpha$ ,  $A_{Ni}$  - mass number of neutron,  $\alpha$ -particle and residual nucleus <sup>59</sup>Ni,  $E_\alpha$  -  $\alpha$ -particle energy,

 $V_{\alpha}$  - well depth ( $V_{\alpha}$ =12.5 $A_{\alpha}$ =50 MeV),

n - exiton number,  $n=A_{\alpha}-A_{n}=3$  (p=3, h=0),

ω(p,h,U) - accesible state density given by Eq (6).

The total residual state density however also takes into account more complex configurations that can be excited by stripping reaction [11].

Direct knock-out process of neutron by  $\alpha$ -particle also is not taken into account in the considered variant of exciton model. For the account of this mechanism we considered an  $\alpha$ -particle as cluster, exciting a neutron particle-hole pair in a nucleus-target ( $n_0$ =3, p=2, h=1), by analogy to how it is realized in works [11,12]. The differential cross-section for continuum knockout reaction is

$$d\sigma(E_n)/dE_n = const \cdot (2s_n + 1) \cdot \mu \cdot E_n \cdot \sigma_c(E_n) \cdot g_n \cdot g_\alpha \cdot (U - 1/2g_n - 1/2g_\alpha), \qquad (8)$$

where:  $g_n=N/13$ ,  $g_\alpha=A/208$ , the normalizing multiplier "const" was determined from the best fit of calculation and experimental data in a high-energy part of neutron spectra.

The cross-section of direct neutron sripping and knock-out processes are calculated separatly and cross-section of preequilibrium emission is overnormalized on their quantity.

#### Results

The tipical calculated according to the procedure described above neutron spectra from  $^{56}\text{Fe}(\alpha,xn)$  reaction at all investigated values of  $\alpha$ -particle energy are shown in figs.(7-11). The calculated and measured angle-integrated neutron spectra are in agreement as a whole within the limits of errors of measurements. In the table integrated cross-sections of equilibrium, preequilibrium, stripping, knock-out neutron emission and total cross-sections of reaction are presented also.

Table. Cross-sections of equilibrium, preequilibrium, stripping, knock-out neutron emission and total neutron emission cross-sections of <sup>56</sup>Fe(α,xn) reaction.

Eα, MeV	σ equil., mb	σ preeq., mb	σ strip., mb	σ knock., mb	σ total, mb
12.3	465	16	-	-	481
16.3	606	45	-	-	651
18.3	685	49	-	-	734
26.8	1443	77	49	39	1608
45.2	1994	249	54	25	2322

One can see that the neutron emission spectra from  $^{56}$ Fe( $\alpha$ ,n) $^{59}$ Ni reaction at  $\alpha$ -particle energies of 12.3, 16.3 and 18.3 MeV mainly are caused by the equilibrium neutron emission; contributions of the preequilibrium neutron emission are small (3-7%) and, practically, have not influence on the shape of the neutron spectra. At higher  $\alpha$ -particle energies ( $E_{\alpha}$ =26.8 and 45.2 MeV) the hard part of the angle-integrated neutron spectra ( $E_{n}$ >15 MeV) are associated, mainly, with nonequilibrium emission of neutrons and as, one can see from figs. 10 and 11, taking into account of the direct interaction processes (stripping and knock-out) allows reliably to describe the experimental data at these values of  $\alpha$ -particle energies both in the hard parts of the spectra and in the entire energy range of emitted neutrons. Though the cross-sections of the stripping and knock-out processes at  $\alpha$ -particle energy of 45.2 MeV put together about 3.5% from total neutron emission cross-section, the hard part of the observed neutron spectrum with  $E_{n} \ge 25$  MeV can be described only if these direct processes are taken into account in nuclear reaction mechanisms.

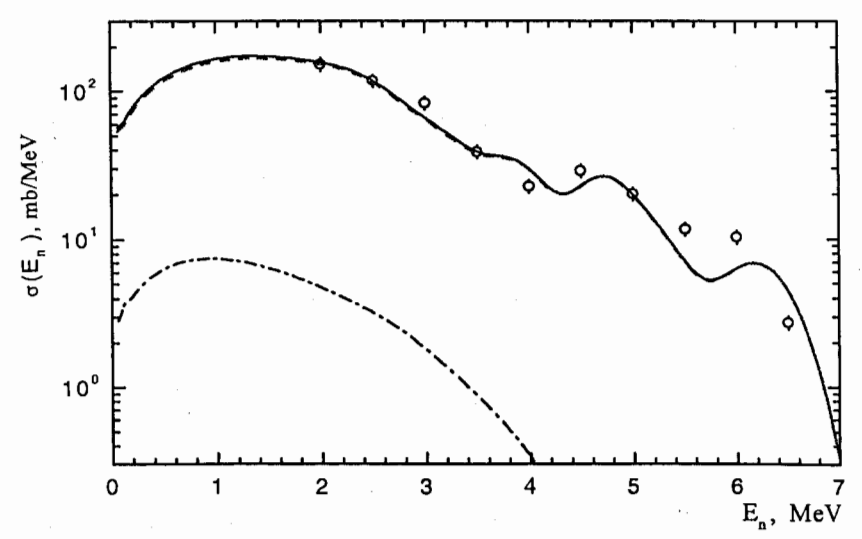


Fig.7. Neutron spectra from  $^{56}$ Fe  $(\alpha, n)^{59}$ Ni reaction at  $E_{\alpha} = 12.3$  MeV. o -experiment, curves - calculation: - - - - summary contribution: - - - - equilibrium emission, - - - - preequilibrium emission.

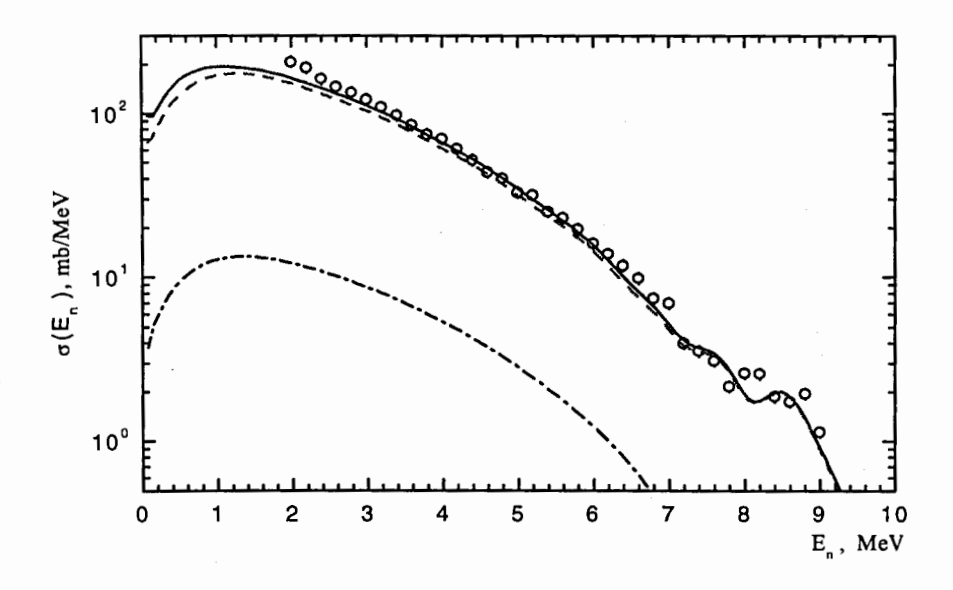


Fig. 8. Neutron spectra from  $^{56}$ Fe( $\alpha$ ,n) $^{59}$ Ni reaction at  $E_{\alpha}$  =16.3 MeV. Designations are the same as in Fig. 7.

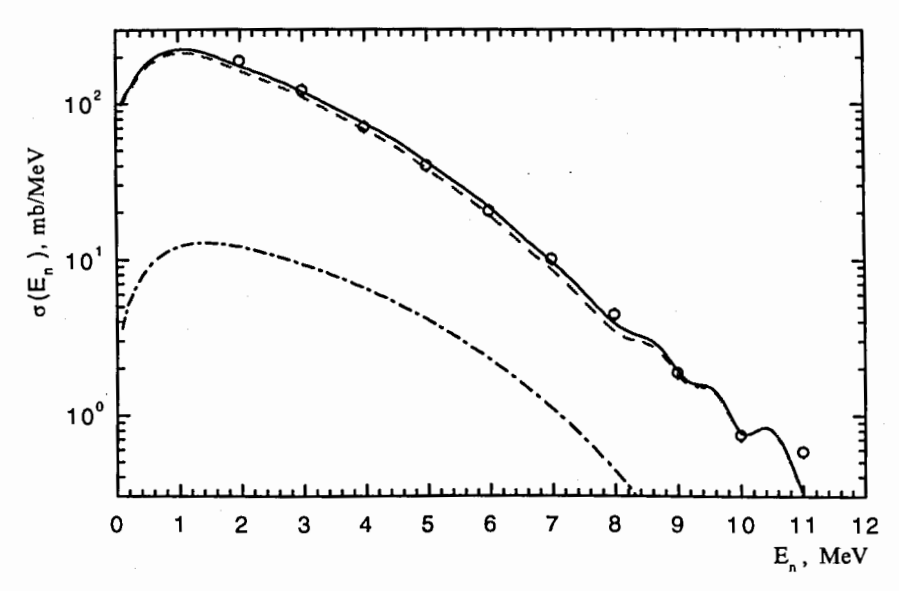
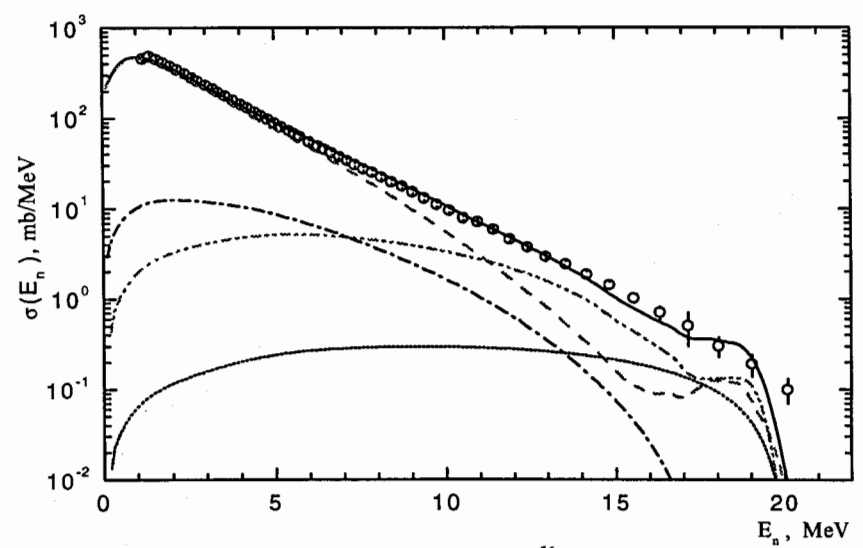


Fig.9. Neutron spectra from  $^{56}$ Fe  $(\alpha,n)^{59}$ Ni reaction at  $E_{\alpha} = 18.3$  MeV. Designations are the same as in Fig. 7.



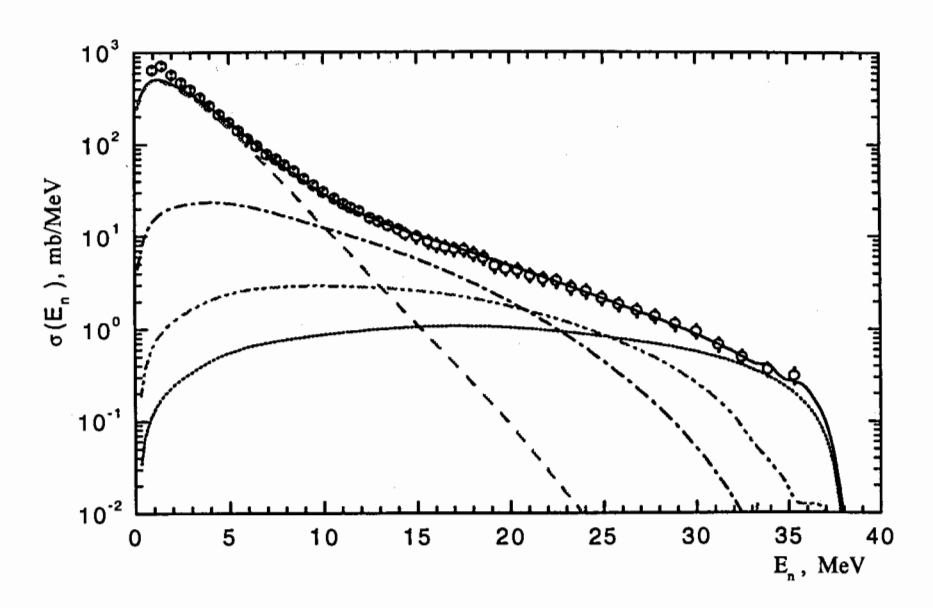


Fig.11. Neutron spectra from reaction  $^{56}$ Fe( $\alpha$ ,xn) at  $E_{\alpha}$  =45.2 MeV. Designations are the same as in Fig. 10.

#### Conclusion

The differential neutron emission cross-sections in  $^{56}\text{Fe}(\alpha,xn)$  reaction are measured at  $\alpha$ -particle energies of 12.3, 16.3, 18.3, 26.8, 45.2 MeV and are analysed within the framework of equilibrium, preequilibrium, direct stripping and knock-out mechanisms of the particle emission in nuclear reactions. The spectra of all four mechanisms of neutron emission are calculated and is shown, that the calculation results are in an agreement with the measured neutron spectra within the limits of measurement errors. Use of the new experimental data on the nuclear level density of  $^{59}\text{Ni}$ , excited on a first step of neutron emission in  $^{56}\text{Fe}(\alpha,xn)$  reaction, has allowed reliably to determine the contribution of equilibrium emission. Cross-sections of equilibrium, preequilibrium, direct stripping and knock-out neutron emission in reaction are determined at all investigated values of  $\alpha$ -particle energies. It is shown, that the cross-section of nonequilibrium emission is essentially increased with growth of  $\alpha$ -particle energy and at  $\alpha$ -particle energy of 45.2 MeV the hard part of the observed neutron spectrum with  $E_n > 15$  MeV is associated mainly with nonequilibrium emission of neutrons.

This work has been supported in part by the Russian Foundation for Basic Researches and Kaluga Scientific Center (grant 07-02-96400).

#### References:

- Zhuravlev B.V., Lychagin A.A., Titarenko N.N., Demenkov V.G., Trykova V.I., Grigoriev Yu.V., Doroshenko A.Yu. "Nuclear level densities of nickel isotopes". In Proceedings of Region Competition of Scientific Projects in Natural Sciences, Kaluga Scientific Center, in print.
- Zhuravlev B.V., Titarenko N.N., Trykova V.I. et al. Izv. AN, ser. fizicheskaya, 1999, v.63, №5, p. 959-967.
- 3. Zhuravlev B.V., Dovbenko A.G. Yadernaya Fizika, 1995, v.58(10), p.1731-1734.
- 4. Hauser W., Feshbach H. Phys. Rev., 1952, v.87, p.366
- Zhivopiszev F.A., Kebin E.I., Sukharevskij V.G. "Models of preequilibrium nuclear reactions", Moscow State University, 1987, p. 31
- 6. Kalbach C. Zeitschrift fur Physik A, 1977, v. 283, p. 401-411.
- P.G. Young, E.D. Arthur and M.B. Chadwick, in Proceedings of IAEA Workshop on Nuclear Reaction Data and Nuclear Reactors, Trieste, Italy, April 15 - May 17, 1996 (World Sci., Singapore, 1998), Vol.1, p.227
- 8. Koning A.J. and Delaroche J.D. Nucl. Phys. A, 2003, v. 713, p. 231.
- 9. Avrigeanu V., Hodgson P.E., Avrigeanu M. Phys. Rev. C, 1994, v.49, p. 2255.
- 10. Daehnick W.W., Childs J.D., Vrecelj Z. Phys. Rev. C, 1980, v. 21, p.2253.
- 11. Kalbach C. Users manual for PRECO-2000. Duke University, 2001, retrived from <a href="https://www.nndc.bnl.gov/nndcscr/model-codes/preco-2000/">www.nndc.bnl.gov/nndcscr/model-codes/preco-2000/</a>.
- 12. Biryukov N.S., Zhuravlev B.V. et al. Yadernaya Fizika, 1977, v.25(4), p.767-771.

# CROSS SECTION MEASUREMENT FOR THE $^{147}$ Sm(n, $\alpha$ ) $^{144}$ Nd REACTION AT E<sub>n</sub> = 5.0 AND 6.0 MeV

#### Yu. M. Gledenov, M. V. Sedysheva, V. A. Stolupin

Frank Laboratory of Neutron Physics, JINR, Dubna, 141980, Russia

#### G. Khuukhenkhuu

Nuclear Research Centre, National University of Mongolia, Ulaanbaatar, Mongolia

#### P. J. Szalanski

University of Lodz, Institute of Physics, Poland

Jiaguo Zhang, Li-an Guo, Hao Wu, Jinxiang Chen, Guoyou Tang, Guohui Zhang
State Key Laboratory of Nuclear Physics and Technology, Institute of Heavy Ion Physics,
Peking University, Beijing 100871, China

#### Abstract

Cross sections of the  $^{147}\text{Sm}(n,\alpha)^{144}\text{Nd}$  reaction were measured at  $E_n=5.0$  and 6.0 MeV. Experiments were performed at the 4.5 MV Van de Graaff accelerator of Peking University. Neutrons were produced through the  $D(d,n)^3\text{He}$  reaction with a deuterium gas target. A twin gridded ionization chamber was used as charged particle detector and two large area  $^{147}\text{Sm}_2\text{O}_3$  samples placed back to back were employed. Absolute neutron flux was determined by a small  $^{238}\text{U}$  fission chamber. Present cross section data are compared with existing results of evaluations and measurements.

#### 1. Introduction

 $^{147}$ Sm is a fission product nucleus. The Q value of the  $^{147}$ Sm(n, $\alpha$ ) $^{144}$ Nd reaction is as big as 10.13 MeV. Study of this reaction is important in astrophysics, in determination of the parameters of optical model potentials and in the research of nuclear reaction mechanisms. Several experimental and theoretical works have been done for this reaction [1-6], but existing measurements are only confined in the resonance and in 14 MeV neutron energy region. In the MeV neutron energy region, however, there is no experimental data up to now mainly due to the small cross section of this reaction and low intensity of neutron flux. Thus, for the  $^{147}$ Sm(n, $\alpha$ ) $^{144}$ Nd reaction cross section very large discrepancies exist among different

<sup>\*</sup>Project supported by National Key Project for Cooperation Researches on Key Issues Concerning Environment and Resources in China and Russia (2005CB724804), and by The Russian Foundation for Basic Research and National Natural Science Foundation of China (NSFC-RFBR 07-02-92104, 10575006, and 10811120014).

evaluated data libraries such as ENDF/B-VII, ENDF/B-VI, JENDL-3.3 and JEFF3.1.

Since the cross section of the  $^{147}\text{Sm}(n,\alpha)^{144}\text{Nd}$  reaction is small in the MeV neutron energy range and the sample should be thin enough to allow alpha particles to escape without too much straggling, it is necessary to use relatively large area samples for measurement. Furthermore, charged particle detector with large detection solid angle and high detection efficiency should be employed. By using a twin gridded ionization chamber and two large area  $^{147}\text{Sm}_2\text{O}_3$  samples, cross sections of the  $^{147}\text{Sm}(n,\alpha)^{144}\text{Nd}$  reaction were measured at  $E_n = 5.0$  and 6.0 MeV in the present work.

#### 2. Details of experiment

The experiment was performed at the 4.5 MV Van de Graaff accelerator of Peking University. The setup of our experiment is shown in Fig. 1 which mainly consists of three parts: neutron source, neutron flux detector and charged particle detector.

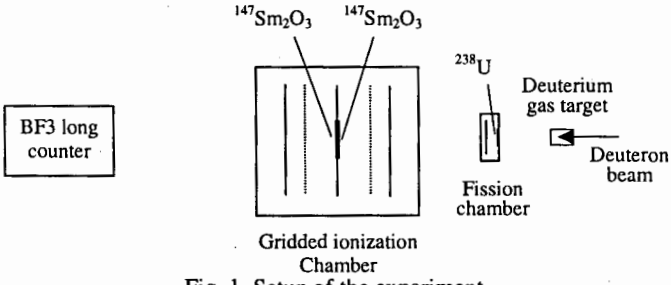


Fig. 1. Setup of the experiment.

In the present experiment, quasi-monoenergetic neutrons were produced through the  $D(d,n)^3$ He reaction with a deuterium gas target. The length of the gas cell is 2.0 cm and it was separated from the vacuum tube by a molybdenum foil 5.0  $\mu$ m in thickness. The pressure of the deuterium gas was 3.0 to 2.9 atm during experiment. The energies of the deuteron beam after accelerating before entering the molybdenum foil were 2.46 and 3.26 MeV. By Monte Carlo simulation the corresponding neutron energies were 5.0 and 6.0 MeV, with neutron spread 0.16 and 0.12 MeV, respectively.

A BF<sub>3</sub> long counter was used as the neutron flux monitor. The axis of the long counter was set along the beam line, and from the front side of the BF<sub>3</sub> long counter to the gas target was about 3.0 m. The absolute neutron flux was determined through a small parallel plate <sup>238</sup>U fission chamber with flowing Ar+3.73%CO<sub>2</sub> (a little more than 1.0 atm) as working gas. The abundance of the <sup>238</sup>U sample is 99.997%. The diameter of the round-shaped <sup>238</sup>U sample is 2.0 cm, and the weight is 547.2±7.1 µg. The <sup>238</sup>U sample was placed perpendicularly to the beam line, and the center of the sample was at 0° to the beam line. The distance from the <sup>238</sup>U sample to the center of the gas target was 3.4 cm.

A twin gridded ionization chamber was used as the charged particle detector. It is composed of two symmetry sections with a common cathode. The cylindrical-shaped chamber is made from aluminum and the thickness of the wall is 2.0 mm. The diameter and height of the chamber are 37.0 and 29.0 cm, respectively. The shape of the electrodes (one cathode, two

grids and two anodes) is rectangle. The center of the cathode was at  $0^{\circ}$  to the beam line, and the electrodes were perpendicular to the beam line. Two round-shaped  $^{147}\text{Sm}_2\text{O}_3$  samples with aluminum backings were set back to back on the common cathode. Thus, the alpha events were measured almost the entire  $4\pi$  solid angle.

The abundance of the enriched  $^{147}\mathrm{Sm}$  isotope in the sample was 95.3%. The thickness and diameter of each sample were 5.0 mg/cm² and 11.0 cm, and the thickness of each aluminum backing was 1.0 mm. The distances from the cathode to grid and from grid to anode of the twin gridded ionization chamber were 7.5 and 2.0 cm, respectively. The distance from the cathode to the center of the gas target was 35.0 cm. The working gas of the gridded ionization chamber was Kr + 2.27% CO<sub>2</sub>, and the gas pressure was 2.20 atm. High voltages applied to the cathode, grid and anode were -3400, 0 and +1700 V, respectively.

There were two removable compound alpha sources in the gridded ionization chamber for energy calibration and for adjustment and checking of the electronics system.

Block diagrams of electronics for alpha events measurement is shown in Fig. 2. Forward  $(0^{\circ} \sim 90^{\circ})$  and backward  $(90^{\circ} \sim 180^{\circ})$  direction alpha events were recorded simultaneously, and the cathode-anode two-dimensional spectra were obtained for forward and backward events, respectively.

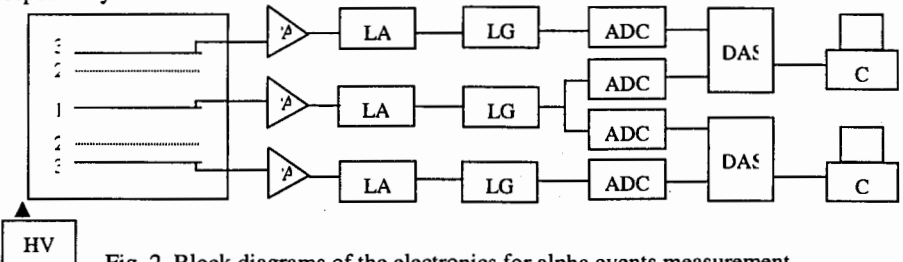


Fig. 2. Block diagrams of the electronics for alpha events measurement.

1-Cathode, 2-Grid, 3-Anode,

HV-High Voltage Divider, PA-Preamplifier, LA-Linear Amplifier, LG-Linear Gate Stretcher, ADC-Analog-to-digital Converter, DAS-Data Acquisition System, C-Computer

The number of forward and backward alpha events can be obtained from the cathode-anode two-dimensional spectra. During experiment, the anode spectra of the <sup>238</sup>U fission chamber were also recorded from which the number of the fission fragments can be derived.

The cross section of the  $^{147}\text{Sm}(n,\alpha)^{144}\text{Nd}$  reaction can be calculated from the following

formula: 
$$\sigma_{\alpha} = K\sigma_f \frac{N_{\alpha}}{N_f} \frac{N_{238U}}{N_{147.5m}}$$
 (1)

where  $\sigma_{\alpha}$  denote the cross section to be measured;  $\sigma_f$  is the <sup>238</sup>U(n,f) standard cross section at the same neutron energy taken from ENDF/B-VII library;  $N_{\alpha}$  and  $N_f$  are numbers of the alpha events from <sup>147</sup>Sm(n, $\alpha$ )<sup>144</sup>Nd reaction and fission fragments from <sup>238</sup>U(n,f) reaction, respectively;  $N_{238U}$  and  $N_{1475m}$  are the atom numbers of <sup>238</sup>U and <sup>147</sup>Sm in the samples, respectively; and K is the neutron flux density ratio on <sup>238</sup>U and <sup>147</sup>Sm<sub>2</sub>O<sub>3</sub> samples which can be calculated by

using Monte Carlo method according to the dimensions and positions of the samples and the gas target as well as the angular distribution of the  $D(d,n)^3$ He reaction. For  $E_n = 5.0$  and 6.0 MeV, the calculated values of K are 94.4 and 92.5 with relative uncertainty 3%, respectively.

The deuteron beam intensity was about 2.5  $\mu A$  during experiment. For  $E_n = 5.0$  and 6.0 MeV measurement, the beam time were about 28 and 22 h, respectively.

#### 3. Results and discussions

Fig. 3 is the forward direction cathode-anode two-dimensional spectrum for 6.0 MeV measurement.

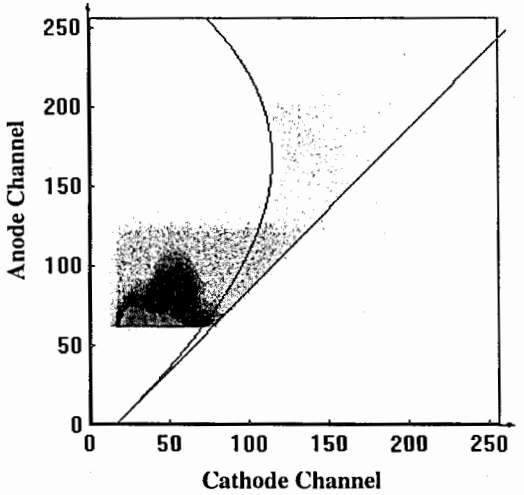


Fig.3. Two-dimensional spectrum of forward events at  $E_n$ =6.0 MeV.

One can see from Fig.3 that the counts corresponding to higher anode channels between the 0° line and the 90° line [7] are alpha events from the  $^{147}$ Sm(n,  $\alpha$ ) $^{144}$ Nd reaction. Those for lower anode channels distributed from 90° line to very low cathode channels are alpha events from working gas through (n, $\alpha$ ) reaction. Apparently, the number of alpha events from the  $^{147}$ Sm(n,  $\alpha$ )  $^{144}$ Nd reaction is much less than that from the working gas.

From the two-dimensional spectrum, one can get the anode spectrum of the alpha events between the  $0^{\circ}$  and the  $90^{\circ}$  lines, as shown in Fig. 4. The counts corresponding to higher anode channels are alpha events from the  $^{147}\mathrm{Sm}(n,\alpha)^{144}\mathrm{Nd}$  reaction. According to the fact that the two-dimensional spectrum of alpha events from the working gas is uniformly distributed along the cathode channel in Fig.3, the background from the working gas between  $0^{\circ}$  and  $90^{\circ}$  lines can be estimated by counting the equivalent region at the left side of the  $90^{\circ}$  line as the dash line shown in Fig.4. Then the number of alpha events with higher channels  $N_{\alpha 1}$  ( $\geq 130$  channel in Fig.4) can be obtained after background subtraction. Because of Coulomb barrier effect, higher energy alpha particles corresponding to the ground state and low energy excited states of  $^{144}\mathrm{Nd}$  are dominant, and those corresponding to higher excited states (lower energy alpha particles) should be much less.

In addition to the higher channel part, the anode spectrum of the measured alpha

particles should go continuously to lower channels until zero channel due to energy loss inside the sample although the number of low energy alpha particles is not many for the present experiment. Besides, since the <sup>147</sup>Sm<sub>2</sub>O<sub>3</sub> sample is 5.0 mg/cm<sup>2</sup> in thickness, some alpha particles can't go out and will be absorbed by the sample.

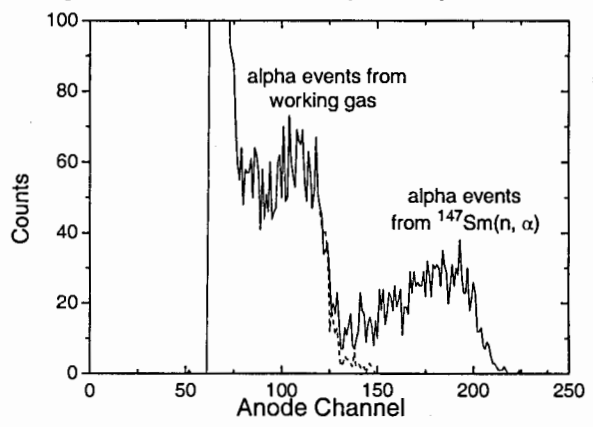


Fig. 4. Anode spectrum of forward events at  $E_n$ =6.0 MeV between 0° line and 90° line.

The ratio of the lower channel part together with the self absorption part of alpha particles over total alphas  $R_1$  can be estimated by Monte Carlo method. According to alpha stopping power in the sample, the measured ratio of forward/backward alpha events, and the fact that alpha particles corresponding to the ground state of <sup>144</sup>Nd are dominant, the ratios of lower channel part plus the self absorption part over total alphas were calculated. At  $E_n$ =5.0 MeV, the ratios are 6.6% and 9.7% for forward and backward alphas, respectively; and at En = 6.0 MeV, the ratios are 5.3% and 10.6% for forward and backward alphas. Error of the calculated ratio  $R_1$  is about 25%.

Total number of alpha events from the  $^{147}\mathrm{Sm}(n,\alpha)$   $^{144}\mathrm{Nd}$  reaction  $N_{\alpha}$  was obtained according to the measured alpha number  $N_{\alpha 1}$  and the calculated ratio  $R_1$ :

$$N_{\alpha} = N_{\alpha 1} / (1 - R_1) \tag{2}$$

Error of  $N_{\alpha 1}$  comes from statistics (2.5~5%) and uncertainty of background subtraction (3.5~5%). Total error of  $N_{\alpha}$  is 5.5~8.5%.

The number of fission fragments  $N_f$  was derived from the anode spectrum of the <sup>238</sup>U fission chamber. Fig. 5 is the anode spectrum of the fission chamber at 5.0 MeV.

Forward and backward cross section data can be calculated from equation (1). In addition, the forward/backward cross section ratio can be calculated. According to equation (1) the forward/backward cross section ratio equals the forward/backward alpha events ratio. Results of cross section data (forward plus backward) and forward/backward ratios in the laboratory reference system for the  $^{147}$ Sm(n, $\alpha$ ) $^{144}$ Nd reaction are listed in Table. 1. Error of the cross section comes from the uncertainties of the alpha event  $N_{\alpha}$  (5.5~8.5%), fission count  $N_f$  (2.5%),  $^{238}$ U and  $^{147}$ Sm<sub>2</sub>O<sub>3</sub> neutron flux density ratio K (3%),  $^{238}$ U fission cross section (1%), the atom number of  $^{147}$ Sm (1.5%) and  $^{238}$ U (1.3%). Total error is about 10%.

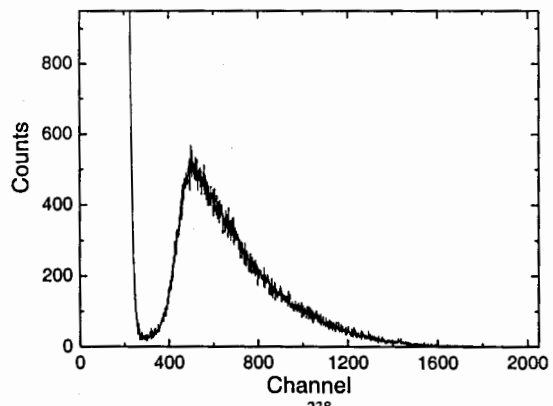


Fig. 5. The anode spectrum of the <sup>238</sup>U fission chamber at 5.0 MeV.

During data processing, corrections from the neutron flux attenuation through the 2-mm-thick aluminum wall of the chamber and through the 2-mm-thick aluminum backing of the two samples were carried out. According to the total neutron cross section data of aluminum taken from ENFD/B-VII, the correction factor from attenuation for 5.0 and 6.0 MeV neutrons through 2-mm-thick aluminum are 0.972 and 0.975, respectively.

Table 1: Cross sections of the <sup>147</sup>Sm(n,α)<sup>144</sup>Nd reaction and forward/backward ratios in the laboratory reference system.

E <sub>n</sub> / MeV	$\sigma_{n\alpha}$ / mb	forward/backward ratio
$5.0 \pm 0.16$	$0.23 \pm 0.02$	$1.65 \pm 0.17$
$6.0 \pm 0.12$	$0.28 \pm 0.03$	$2.54 \pm 0.25$

Present results of cross section are compared with existing evaluations and experiments in Fig. 6. Cross section data at 12.1, 14.1 and 18.2 MeV were obtained via integration of differential cross section data of Glowacka et al. [4].

As can be seen from Fig. 6 very large discrepancies exist among different evaluations, especially in the MeV neutron energy region. Our results are in agreement with the evaluation of ENDF/B-VII if the linear-logarithmic interpolation instead of linear-linear is applied from 0.45 to 7.0 MeV. This work is the first one to measure cross section of the  $^{147}\text{Sm}(n,\alpha)^{144}\text{Nd}$  reaction in the MeV neutron energy region and our results are very useful in determining the threshold behavior of the  $^{147}\text{Sm}(n,\alpha)^{144}\text{Nd}$  reaction. The forward/backward ratios of the  $^{147}\text{Sm}(n,\alpha)$  reaction are as large as 1.65 and 2.54 at 5.0 and 6.0 MeV which is an indication of direct reaction mechanism.

#### Acknowledgements

The authors acknowledge the crew of the 4.5 MV Van de Graaff accelerator of Peking University for kind help.

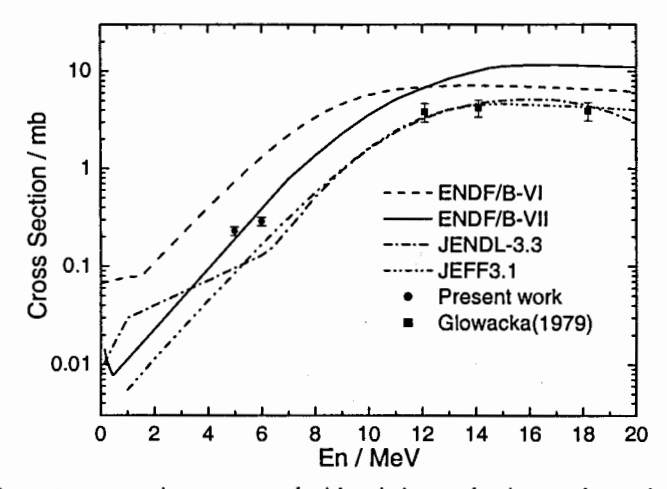


Fig. 6. Present cross sections compared with existing evaluations and experimental data.

#### References

- 1. N.P. Balabanov, Yu.M. Gledenov, P.H. Chol, Yu.P. Popov, V.G. Semenov. Total  $\alpha$ -widths of neutron resonances of <sup>147</sup>Sm and <sup>149</sup>Sm. Nucl. Phys. A 261 (1976) 35-44.
- E. Gadioli, S. Mattioli, W. Augustyniak, L. Glowacka, M. Jaskola, J. Turkiewicz. Structure
  effects in the spectra of α particles from the interaction of 12 to 20 MeV neutrons with
  samarium isotopes. Phys. Rev. C 43(4) (1991) 1932-1936.
- 3. Yu.M. Gledenov, P.E. Koehler, J. Andrzejewski, K.H. Guber, T. Rauscher.  $^{147}$ Sm $(n,\alpha)$  cross section measurements from 3 eV to 500 keV: Implications for explosive nucleosynthesis reaction rates, Phys. Rev. C 62 (2000) 042801.
- L. Glowacka, M. Jaskola, J. Turkiewicz, L. Zemlo, M.Kozlowski. Study of the <sup>147</sup>Sm(n,α)<sup>144</sup>Nd reaction induced by fast neutrons. Nucl. Phys. A 329 (1979) 215-223.
- 5. P.E. Koehler, Yu.M. Gledenov, T. Rauscher, C. Frohlich. Resonance analysis of  $^{147}$ Sm $(n,\alpha)$  cross sections: Comparison to optical model calculations and indications of nonstatistical effects. Phys. Rev. C 69 (2004) 015803.
- Yu.P. Popov, M. Przytula, R.F. Rumi, M. Stempinski, M. Frontasyeva. Investigation of α-decay of <sup>148</sup>Sm resonance states. Nucl. Phys. A 188 (1972) 212-224.
- N. Ito, M. Baba, S. Matsuyama, I. Matsuyama, N. Hirakawa. Large solid angle spectrometer for the measurements of differential (n,charged-particle) cross sections. Nucl. Instr. Meth. A 337(1994) 474-485.

#### THE SYSTEMATIC STUDY OF (n,p) CROSS

#### **SECTIONS FOR 18 AND 20 MeV**

<sup>1</sup>Khuukhenkhuu G., <sup>2</sup>Gledenov Yu.M., <sup>2</sup>Sedysheva M.V. and <sup>1</sup>Odsuren M.

<sup>1</sup>Nuclear Research Center, National University of Mongolia, Ulaanbaatar, Mongolia

<sup>2</sup>Frank Laboratory of Neutron Physics, JINR, Dubna, Russia

**Abstract:** The statistical model, Griffin's exciton model and PWBA are used for systematical analysis of (n, p) reaction cross sections at the 18 and 20 MeV neutrons.

#### 1. INTRODUCTION

Investigation of charged particle emission reactions induced by fast neutrons is important for both nuclear reactor technology and the understanding of nuclear reaction mechanisms. In particular, the systematic study of (n, p) reaction cross sections is necessary to estimate radiation damage due to hydrogen production, nuclear heating and transmutations in the structural materials of fission and fusion reactors. In addition, it is often necessary in practice to evaluate the neutron cross sections of the nuclides, for which no experimental data are available. Because of this, in last years we carried out the systematic analysis of known  $(n, \alpha)$  and (n, p) cross sections and observed so-called isotopic effect in the wide energy interval of neutrons for the broad mass range of target nuclei [1-3]. Also, some formulae for the systematic analysis of the fast neutron induced (n, p) reaction cross sections using the statistical model, exciton model and PWBA were obtained [4-6]. In this paper the systematic analysis of known (n, p) cross sections for 18 and 20 MeV neutrons using the theoretical model formulae is described.

### 2. THEORETICAL FORMULAE OF (n,p) REACTION CROSS SECTIONS

#### 2.1. Statistical Model

For fast neutrons using the evaporation and constant nuclear temperature models, semi-classical approach for an inverse reaction cross section and  $\Gamma \approx \Gamma_n$  approximation we can obtain the following formula for (n, p) cross section:

$$\sigma_{n,p}^{com} = C\pi (R + \hbar)^2 e^{-\kappa \frac{N-Z+1}{A}},$$
 (1)

where 
$$K = 4\xi \sqrt{\frac{A}{13.5(E_n + Q_{np})}}$$
 (2)

and 
$$C = \exp\left\{ZA^{1/6} \frac{2\gamma - 1}{\sqrt{13.5(E_n + Q_{np})}}\right\}$$
 (3)

Here: R, Z, N and A are the radius, the proton and neutron numbers, and the mass number of the target nucleus, respectively;  $\lambda$  is the wavelength of incident neutrons divided by  $2\pi$ ;  $\xi$  and  $\gamma$  are the constants of Weizsacker's formula;  $E_n$  and  $Q_{np}$  are the neutron and reaction energies, respectively. The parameters C and K in eq.(1) are usually determined by fitting to experimental cross sections. However, the parameters C and C can be obtained directly from eqs. (2) and (3).

So, from eqs. (2) and (3) it can be written that the parameters C and K are related as follows:

$$\ln C = \frac{Z}{A^{1/3}} \left( \frac{2\gamma - 1}{4\xi} \right) K. \tag{4}$$

Using the following designation 
$$B = \frac{Z}{A^{1/3}} \left( \frac{2\gamma - 1}{4\xi} \right)$$
 (5)

we can get following relation between the parameters C and K:

$$C = e^{BK} . ag{6}$$

#### 2.2. Exciton Model

In the framework of the pre-equilibrium nuclear reaction mechanism using the Griffin's exciton model we can write following expression for (n,x) cross section [5]:

$$\frac{d\sigma_{n,x}^{pre}}{dE_x} = \sigma_r(E_n) \sum_{n=n_0}^{n_{max}} \lambda_x(n, E_x) \tau(n, E). \tag{7}$$

Here:  $\sigma_r(E_n)$  is the total reaction cross section for neutrons;  $\lambda_x(n, E_x)$  is the emission rate from an n exciton state (n = p + h); p is the particle number; h is the hole number;  $\tau$  is the mean lifetime of an n-exciton state. We assume the probability of nucleon emission from state with n excitons  $\gamma_n \approx 0$  and depleting factor  $D \approx 1$ . Also, for the transition probability is used following approximation:

$$\lambda_n^+ >> \lambda_n^- >> \lambda_n^- . \tag{8}$$

Then, the cross section formula for (n, p) reaction can be obtained from eq. (7) as follows:

$$\sigma_{n,p}^{pre} = 68.3 \frac{\pi^6}{\hbar^2} R^2 \sigma_r(E_n) \frac{2M_p}{K_0 A} \frac{\left[ (E_n + Q_{np}) - V_p \right]^3}{(E_n + B_n)^3}, \tag{9}$$

where  $M_p$  is the mass of protons;  $K_0 \approx 400 \text{ MeV}^3$ .

#### 2.3. Plane Wave Born Approximation

The transition probability of a system from the initial state to the final one is given by

$$w = \frac{2\pi}{\hbar} \left| \int \Psi_f^* H \Psi_i \, d\tau \right|^2 \rho_f(E) \,, \tag{10}$$

where H is the perturbation operator;  $\rho_f(E)$  is the final states density;  $\Psi_i$  and  $\Psi_f$  are the wave functions for the initial and final states, respectively.

In the case of (n, p) reaction we use following approximations for the initial and final states of system [6]:

$$\Psi_i = U_i U_n \text{ and } \Psi_f = U_f U_p, \tag{11}$$

where  $U_i, U_f, U_n$  and  $U_p$  are the wave functions of the target nucleus, product nucleus, neutron and proton, respectively. Also, we assume the perturbation operator is equal to a constant:

$$H = C = const. (12)$$

The effect of the Coulomb field of nuclei was neglected as following

$$U_{i} \approx U_{i} \equiv U. \tag{13}$$

In the case of plane wave Born approximation (PWBA) for neutrons and protons from eqs. (10)-(13) can be written following formula for the (n, p) cross section

$$\sigma_{np}^{dir} = C_0 \pi R^2 \sqrt{1 + \frac{Q_{np}}{E_n}} \tag{14}$$

where  $C_0$  is the fitting parameter which can be interpreted as a proton emission probability in the asymptotic total cross section for  $E_n >> Q_{np}$ .

So, total (n, p) cross section is determined as following

$$\sigma_{np} = \sigma_{np}^{com} + \sigma_{np}^{pre} + \sigma_{np}^{dir}. \tag{15}$$

From eqs. (1), (9), (14) and (15) the parameter  $C_0$  is obtained as best fit to experimental data.

#### 3. ANALYSIS OF (n, p) CROSS SECTIONS

#### 3.1. Systematics of (n, p) cross sections

For  $E_n=18$  and 20 MeV the dependence of reduced (n,p) cross section on the relative neutron excess parameter is shown in Fig.1. From the theoretical line used eq.(1) and fitted to experimental data were obtained the parameters C and K which are given in Fig.1, also. These values and other data of the parameters C and K obtained for  $E_n=6$ , 8, 10, 13, 14.5 and 16 MeV [7] are given in Table 1.

The dependences of the parameters K and C on neutron energy are shown in Figs.2 and 3, respectively. The values of A,Z and  $Q_{np}$  are fitted as averaged and constant parameters for all isotopes and given in Figs. 2 and 3, also.

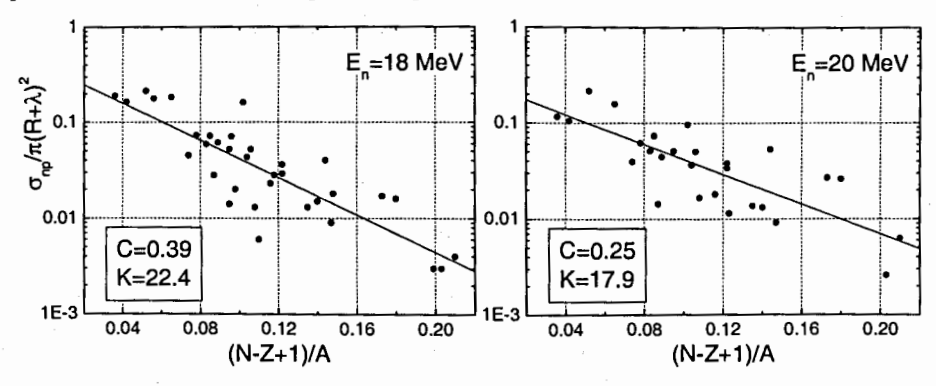


Fig.1. The dependence of reduced (n, p) cross sections on the relative neutron excess parameter (N-Z+1)/A for neutron energies 18 and 20 MeV.

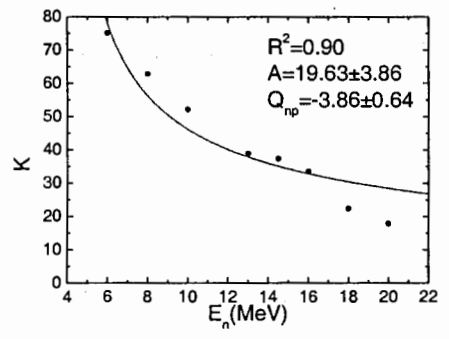


Fig.2 Energy dependence for parameter K.

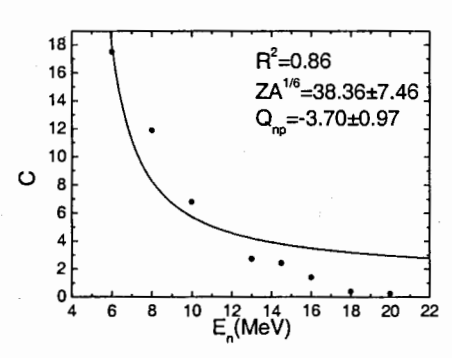
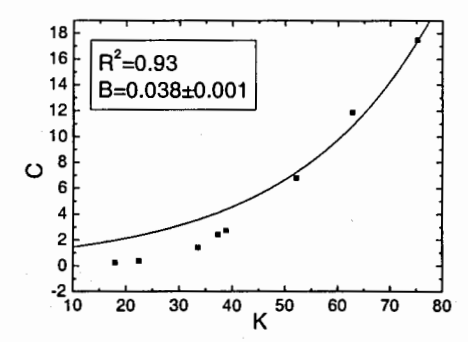


Fig.3 Energy dependence for parameter C.

Fig.4 shows the dependence between the parameters C and K. Here the solid squares are the fitted to experimental data values (table 1) and the solid curve is the theoretical. In addition, the fitted value for parameter B of eq.(5) is given in Fig.4.

Table 1.

E <sub>n</sub> (MeV)	K	C
6	75.2	17.5
8	62.8	11.9
10	52.1	6.80
13	38.8	2.74
14.5	37.3	2.43
16	33.5	1.42
18	22.4	0.39
20	17.9	0.25



**Fig.4** The relationship between the parameters C and K.

From Figs.2, 3 and 4 it can be seen that the fitted values of parameters C and K are satisfactorily described by the statistical model formulae (2), (3) and (4).

#### 3.2. Theoretical and experimental (n, p) cross sections

The comparisons of the absolute values for theoretical (n, p) cross sections calculated by statistical model, exciton model and PWBA with known experimental data at  $E_n=18$  MeV are shown as examples in Fig.5. It is seen that theoretical total (n, p) cross sections are in agreement with known experimental data (see Fig.5 d). Similar picture was obtained for  $E_n=20$  MeV (see Fig.6).

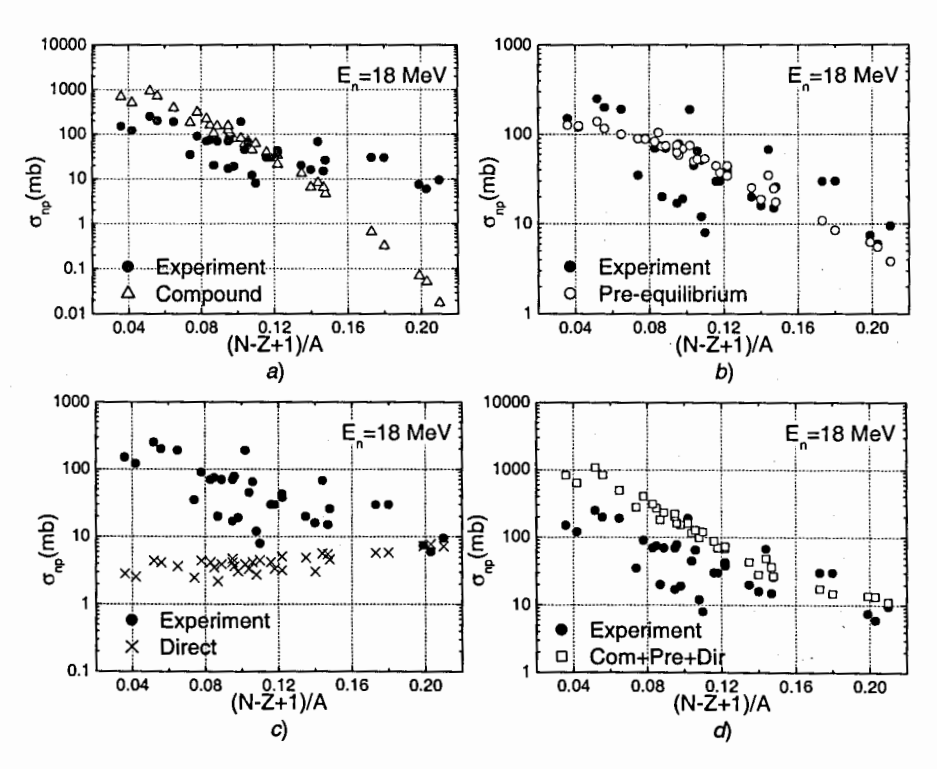


Fig. 5. Theoretical and experimental data of (n, p) cross sections at 18 MeV a) statistical model, b) exciton model, c) PWBA, d) total.

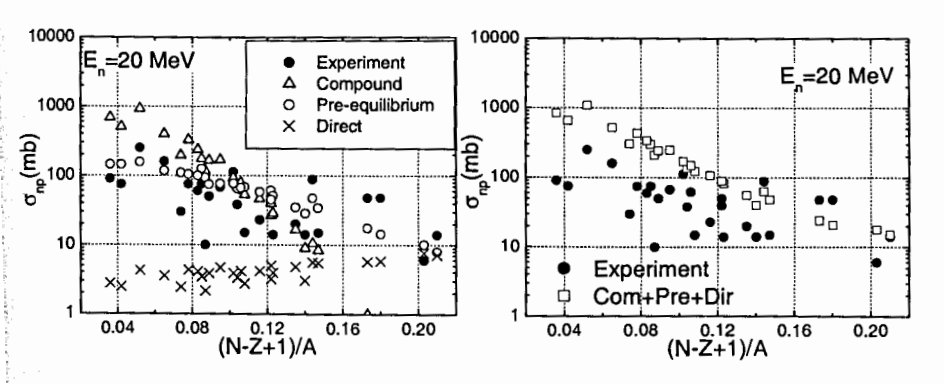


Fig.6. Experimental and theoretical total (n, p) cross sections at 20 MeV.

#### ACKNOWLEDGEMENT

This work was carried out in the framework of the "Nuclear Dynamics" proje supported by Mongolian Science and Technology Foundation.

#### REFERENCES

- G.Khuukhenkhuu, Yu.M.Gledenov, M.V.Sedysheva and G.Unenbat. JINR Communications, E3-93-466, 1993, Dubna.
- G.Khuukhenkhuu, Yu.M.Gledenov, M.V.Sedysheva and G.Unenbat. JINR Communications, E3-94-316, 1994, Dubna.
- G.Khuukhenkhuu, G.Unenbat, Yu.M.Gledenov and M.V.Sedysheva. In book: Proceedings of the International Conference on Nuclear Data for Science and Technology Trieste, 1997, Edited by G.Reffo, A.Ventura and C.Grandi, p.934.
- 4. G.Khuukhenkhuu, G.Unenbat, M.Odsuren, Yu.M.Gledenov, M.V.Sedysheva and B.Bayarbadrakh JINR Communication, E3-2007-25, Dubna, 2007.
- 5. G.Khuukhenkhuu, G.Unenbat, M.Odsuren, Yu.M.Gledenov, M.V.Sedysheva and B.Bayarbadrakh JINR Communication, E3-2007-26, Dubna, 2007.
- 6. G.Khuukhenkhuu, G.Unenbat, M.Odsuren, Yu.M.Gledenov, M.V.Sedysheva and B.Bayarbadrakh JINR Communication, E3-2007-27, Dubna, 2007.
- G.Khuukhenkhuu, Yu.M.Gledcnov, M.Odsuren, M.V.Sedysheva, B.Bayarbadrakh In book: Proceedings of the International Conference on Contemporary Physics, ICCP-IV, August 13-20, 2007, Ulaanbaatar, Mongolia, p.413

## POSSIBILITY OF SOME RADIONUCLIDES PRODUCTION USING HIGH ENERGY ELECTRON BREMSSTRAHLUNG

<u>Baljinnyam N.</u>, Belov A.G.<sup>1)</sup>, Ganbold G.<sup>2)</sup>, Gerbish Sh., Maslov O.D.<sup>1)</sup>, Shvetsov V.N.

<sup>1)</sup> Flerov Laboratory of Nuclear Reactions of the JINR, Dubna, Russia
<sup>2)</sup> Nuclear Research Center of NUM, Ulan-Bator, Mongolia

#### Abstract

The method of some radio nuclides production using high energy Bremsstrahlung of electron accelerators and determination of photonuclear reaction yield and specific activity for some radio nuclides is described. Photonuclear reaction yield and specific activity for some radio nuclides were determined for <sup>117m</sup>Sn, <sup>111</sup>In and <sup>195m</sup>Pt.

Based on the experimental data obtained at low energy ( $E_e$ -<30 M<sub>3</sub>B) electron accelerators as well as the microtron MT-25 (FLNR, JINR) with the power 0.5 kW, photonuclear reaction yields are estimated for some radio nuclides for the linear electron accelerator ( $E_e$ - = 75 MeV) of the IREN facility, FLNP JINR at irradiation of high purity platinum and tin metals.

#### INTRODUCTION

At present, the requirements for an acceptable radionuclide are still considerably high. The nuclear reactors and cyclotrons are mainly used for the radionuclide production. However, they are not able to produce all the required types of radio nuclides, therefore, electron accelerators as Linac and Microtron, that can be produced radio nuclides using the Bremsstrahlung, are suitable complements.

Properties of the radionuclide <sup>117m</sup>Sn are acceptable for clinical and therapeutic use: the short half-life of 13.6 days is necessary to minimize the patient exposure, the gamma emission of photons of 158.4 keV (84 %) for imaging, and abundance (116 %) of low energy (127-129, 152 keV) Auger and conversion electrons for delivering a high radiation dose to sites of a bony metastatic disease [1, 2]. Also the platinum radionuclide <sup>195m</sup>Pt can be used for cancer diagnosis and therapy.

The yields for a number of radio nuclides produced by the Bremsstrahlung beam irradiation were measured by different groups. Oka et al. [3] measured the yields of radio nuclides induced by the  $(\gamma, n)$  reactions with the 20 MeV Bremsstrahlung from a linac on 37 elements. Analogous measurements were performed at the Czech microtron by Randa et al. [4] with the 19 MeV Bremsstrahlung beam. Detailed measurements were also performed by Gerbish et al. [5] and Thiep et al. [6] at the microtron in Dubna, FLNR, JINR for practically all natural nuclides at different electron 14, 18 and 20 MeV energies. Properties and activity yields of radio nuclides obtained from photonuclear reaction data are based exclusively on experimentally obtained results for the majority of elements and are presented in book by Segebade et al. [7].

#### THE AIM OF THESE EXPERIMENTS

In the work will try to give some information on the possibility of application of the Bremsstrahlung beam of the linac of the new Intense REsonance Neutron pulsed source (IREN)

for fundamental and applied nuclear physics is being realized in the 2008 in Frank Laboratory Neutron Physics of JINR, Dubna.

#### ACCELERATOR

The methods of multielemental photon activation analysis (MPAA) and radionuclide production will be developed at the Linac of the IREN facility.

Some technical characteristics for the Linac of the IREN facility are as follows:

Maximum Energy of Electrons
Peak current
Pulse frequency
Electron burst width (FWHM)
Power
75 MeV
2.84 A;
50 Hz;
140 ns.
1,1 kWt

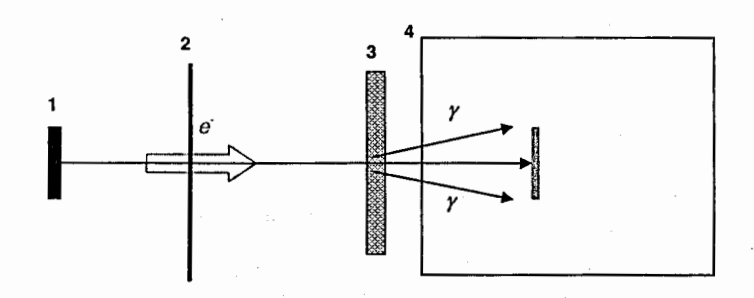


Fig 1. Simple geometry of radiation target by bremsstrahlung 1 - electron source; 2 - exit foil (~0,1-0,3 mm thick Ti); 3 - converter (W or Pt plate ~ 2,5 and 5 mm); 4 - target.

A water cooled tungsten or platinum target has been used for the Bremsstrahlung converter. The temperature on the surface of the W or Pt disk of the target must be lower than ~900 °C.

The preliminary methodical experimental investigation was carried out on the cyclic electron accelerator Microtron MT-25 of FLNR, JINR. The Microtron MT-25 was used as the Bremsstrahlung source to determine specific activities and yields of the photonuclear reactions. The 0.57~kW power irradiation targets of the Microtron MT-25 were operated with the electron beam -15  $\mu$ A current and 23.5 MeV energies. The results of methodical study are given in the present work.

#### EXPERIMENTAL PROCEDURE

To estimate the activity and yield of the radionuclide  $^{117m}Sn$ ,  $^{111}In$ ,  $^{195m}Pt$  production, the natural pure tin, platinum and enriched  $^{118}Sn$  (98.5 %) isotope have been irradiated at the Microtron MT-25 in Dubna, FLNR, JINR by the bremsstrahlung beam of 23.5, 22, 21, 20, 19 MeV with the current of  $13-14.5~\mu A$  during 1-2 h at the radial distance of 2 cm from the tungsten target (4 mm thick). For determination of photonuclear reaction specific activity and yields of Sn, Pt isotopes several experiments have been carried out:

Bremsstrahlung Energy, (Mev)	Elements	Mass of sample, (mg)	Irradiation time, hours
	Au - 1	5	
	Zr - 1	1,2	
23,5	Sn - 1	46,1	1
	Sn - 118 (9)	31,3	
	Cu - 1	49,5	
		6,2	
22	Zr - 2	0,6	1,5
1 22	Sn - 2	19,2	1,5
	Cu - 2	48,8	
		6.9	
1			
1 2			
21			1,5
			¥
1		12	
		5,5	
		4	
20		14	1,5
1			
1		1	
19	Sn - 5	37.4	1,5
1			-,-
		6.3	
1 a.a			
24,2			1,5
1			
	23,5	Energy, (Mev)  Au - 1  Zr - 1  23,5  Sn - 118 (9)  Cu - 1  Au - 2  Zr - 2  Sn - 2  Cu - 2  Au - 3  Zr - 3  Sn - 3  Cu - 3  Pt - 1  Sn - 112  Au - 4  Zr - 4  20  Sn - 4  Cu - 4  Pt - 2  Au - 5  Zr - 5  Sn - 5  Cu - 5  Pt - 5  Au - 6  Zr - 6	Energy, (Mev)    Au - 1

Activity of the irradiated high purity natural platinum, tin and enriched <sup>118</sup>Sn samples and monitors were measured by HP Ge detectors' of the gamma spectrometer of FLNP, JINR with the energy resolution of 2 keV at gamma line of 1332 keV for <sup>60</sup>Co radionuclide. To the monitors of the high energy electron's Bremsstrahlung flux were used pure metal foils of Au, Cu and Zr. Gamma lines of the radio nuclides, which are detected from samples and monitors [2, 4] have been given in Table 1.

Equation (1) and (2) were used for calculation of specific activity, yield and integrated cross section of the photonuclear reaction.

$$S = \Delta N \gamma \varepsilon = \phi_{ih} \sigma_{eff} \frac{N_A \theta w}{M} \left( 1 - e^{-\lambda t_{irr}} \right) e^{-\lambda t_d} \cdot \frac{\left( 1 - e^{-\lambda t_m} \right)}{\lambda} \cdot \gamma \varepsilon \tag{1}$$

$$\sigma_{\text{int}} = \frac{A_s \cdot M(E_{\text{max}} - E_{th})}{N_A \cdot \Phi_{th}}; [MeV \cdot b]$$
 (2)

#### Where:

S - net peak area

N<sub>A</sub> - Avogadro's number (mol<sup>-1</sup>)

θ - isotopic abundance of the target isotope (%)

 γ - gamma ray abundance (i.e. probability of the disintegrating nucleus emitting a photon of this energy, photons per disintegration).

w - Mass of the irradiated element (g)

M - Atomic mass (g.mol-1)

ε - Photo peak efficiency of detector (i.e. probability that an emitted photon of given energy will be detected and contribute to the photo peak in the spectrum).

 $\sigma_{eff}$  - effective cross-section (mb or  $10^{-27}\ cm^2)$ 

 $\phi_{th}$  - photon flux (cm<sup>-2</sup>. $\mu$ A<sup>-1</sup>.s<sup>-1</sup>)

λ - decay constant

 $t_{irr}$  - irradiation time (s)

 $t_d$  - decay time (s)

 $t_m$  - measuring time (s)

As - Specific Activity (Bq/mg)

E<sub>max</sub> - Irradiation energy (MeV)

E<sub>th</sub> - Reaction threshold energy (MeV).

Table 1. Nuclear data of TIN (Sn) and PLATINUM (Pt) radioisotopes.

Radionuclide and half-life	Main energy E <sub>r</sub> , keV	Intensity, %	Reaction	Threshold energy of reaction $E_{\gamma}$ , MeV	Abundance of target, %
<sup>117m</sup> Sn 13.6 d	158.40	84.00	<sup>117</sup> Sn (γ,γ') <sup>118</sup> Sn (γ,n) <sup>119</sup> Sn (γ,2n)	-0.32 -9.65 -16.13	7.5 24.01 8.58
117mSn 13.6 d	158.40	84.00	<sup>118</sup> Sn (γ,n)	-9.65	98.50
2.83 d	171.29 245.35	91.00 94.00	<sup>112</sup> Sn(γ,p)	-7.73	0.95
<sup>195m</sup> Pt 4.1 d	98.86 129.74	11.01	<sup>195</sup> Pt (γ,γ') <sup>196</sup> Pt (γ,n) <sup>198</sup> Pt (γ,3n)	-0.26 -8.18 -21.60	33.80 25.20 7.19

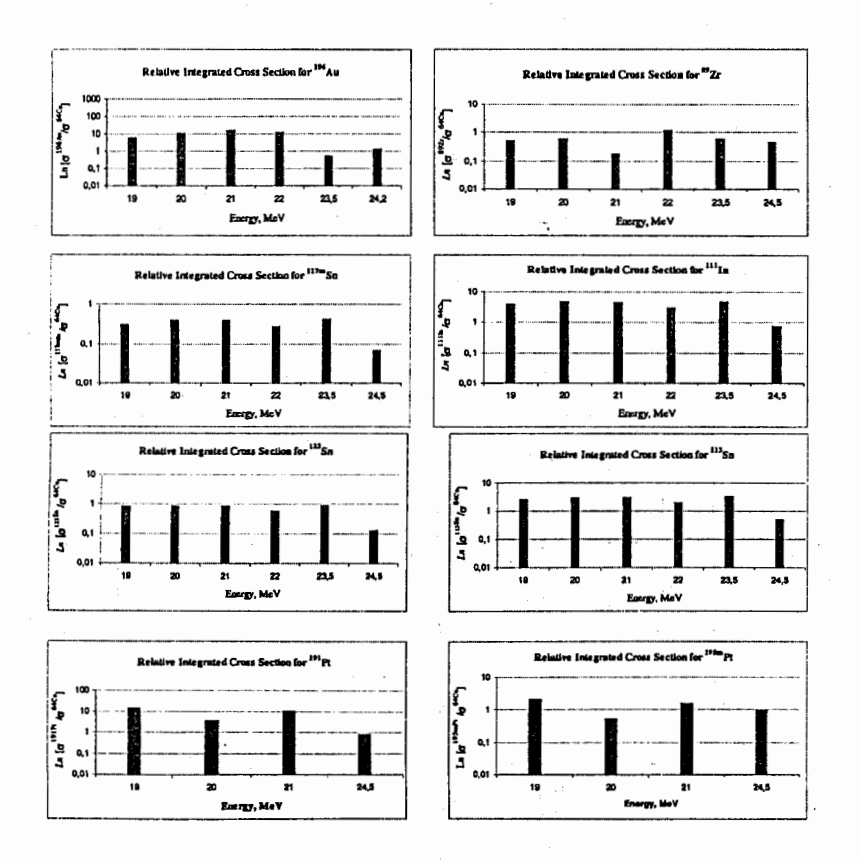
Radionuclide of this class is therapeutically and diagnostically useful in skeletal imaging and for the radiotherapy of bone tumors and other disorders [9-12].

From the measured gamma spectrum data the experimental photonuclear reaction activity and yield have been determined for radio nuclides <sup>117m</sup>Sn; <sup>111</sup>In and <sup>195m</sup>Pt. Their experimental values are shown in Table 2.

Table 2. Experiment's results of specific activity and yield for some radio nuclides.

Table 2. Experiment's results of specific activity and yield for some radio nuclides.							ies.	
No	Energy of Bremsstrahlung, Ey [MeV]	Element	Radio- nuclide	Specific activities A, [Bq/mg]	Yields Y. [Bq/ [µA mg h]	Isomer's Ratio R, [Ym/Yx]	Relative integrated cross section, $[\sigma'/\sigma^{64C_a}]$	
1	23.5	Sn – 1	<sup>117m</sup> Sn <sup>111</sup> In <sup>113</sup> Sn <sup>123</sup> Sn	8.17E+05 8.76E+06 7.01E+06 1.52E+06	5.45E+04 5.84E+05 4.68E+05 1.01E+05	0.09 0.116 0.54	0.44 5.1 3.46 0.93	
		Sn -118	117mSn	5.77E+05	3.85E+04		0.31	
2	22	Sn - 2	117mSn 111In 113Sn 123Sn	3.14E+05 3.15E+06 2.62E+06 6.17E+05	1.39E+04 1.40E+05 1.16E+05 2.74E+04	0.09 0.12 0.51	0.28 3.12 2.01 0.64	
3	3 21	Sn - 3	117mSn 111In 113Sn 123Sn	3.02E+05 3.30E+06 2.60E+06 6.02E+05	1.33E+04 1.47E+05 1.16E+05 2.68E+05	0.09 0.115 0.49	0.40 4.84 3.12 0.92	
		Pt - 1	195mPt 191Pt	6.56E+05 4.46E+06	2.92E+04 1.98E+05	0.15	1.63 10.77	
4	20	Sn - 4	117mSn 111In 113Sn 123Sn 195mPt	2.75E+05 2.99E+06 2.33E+06 5.07E+05	1.20E+04 1.30E+05 1.02E+05 2.21E+05	0.09 0.12 0.54	0.41 5.08 3.18 0.89	
	1	Pt - 3	19174	1.96E+05 1.30E+06	8.55E+03 5.70E+04	0.15	0.56 3.62	
5	19	Sn - 5	117mSn 111In 113Sn 123Sn	1.1E+05 1.25E+06 1.05E+06 2.49E+05	3.77E+03 4.29E+04 3.59E+04 0.85E+04	0.08 0.105 0.44	0.31 4.12 2.70 0.84	
			195mPt	4.04E+05 2.66E+06	1.38E+04 0.91E+05	0.15	2.23 14.6	
6	24.5	24.5	Sn – 6	117mSn 111In 113Sn 123Sn	9.73E+04 1.07E+06 8.69E+05 1.86E+05	4.11E+03 4.51E+04 3.67E+04 7.86E+03	0.09 0.11 0.52	0.07 0.78 0.54 0.14
		Pt - 6	195mPt	8.03E+05 6.95E+06	3.39E+04 2.93E+05	0.116	1.0 0.84	
		Sn-118	117mSn	5.43E+5	2.29E+4		0.06	

Fig. 3. The distribution of relative integrated cross section  $[\sigma^{s}/\sigma^{64Cu}]$  for some radio nuclides in irradiation energies of Bremsstrahlung.



#### DISCUSSION AND CONCLUSION.

- Results of the experiments have shown a possibility of the <sup>117m</sup>Sn, <sup>111</sup>In, <sup>195m</sup>Pt radionuclide production using the Bremsstrahlung of high energy electron accelerators. In case of irradiation of the natural pure tin, radioisotopes <sup>117m</sup>Sn and <sup>111</sup>In have been produced, which both are useful for medical purposes.
- The experimental yield of photonuclear reaction is several times higher than when an enriched <sup>118</sup>Sn (98.5 %) isotope is used in the target, and from the gamma spectrum can see

the gamma line of 158.4 keV of only one radionuclide <sup>117m</sup>Sn. The photonuclear reaction yields of the <sup>111</sup>In have been compared with the data determined in other works and they have sufficient coincidences.

- 3. The isomeric ratio of <sup>117m</sup>Sn was estimated from the experimental data of activities of 158.4 (<sup>117m</sup>Sn); 391.7 (<sup>113</sup>Sn) and 1089 (<sup>123</sup>Sn) keV energy gamma lines. The isomeric ratios for <sup>117m</sup>Sn were estimated and determined 0,114 ± 0.005 and 0,506 ± 0.038 for the radio nuclides <sup>113</sup>Sn, <sup>123</sup>Sn, correspondingly. A isomeric ratio for <sup>195m</sup>Pt determined 0.141± 0.005.
- The activities and yields of the <sup>117m</sup>Sn and <sup>111</sup>In radio nuclides will be (10 times) increased at the Bremsstrahlung beam of the Linac of the IREN facility, which is constructed in FLNP, JINR.
- In the Table 2. have shown the calculated specific activities, photonuclear reaction yields and relative integrated cross section for the radio nuclides (<sup>196</sup>Au, <sup>89</sup>Zr, <sup>117m</sup>Sn, <sup>111</sup>In, <sup>113</sup>Sn, <sup>123</sup>Sn, <sup>195m</sup>Pt and <sup>191</sup>Pt).
- 6. In Fig. 3 have given the histograms of distribution for relative integrated cross section of the above mentioned radio nuclides in absorption energies of Bremsstrahlung.
- 7. From the calculated integrated cross section can be determined isomeric ratio and  $\sigma(\gamma,n)/\sigma(\gamma,p)$  for Sn have find 0.088  $\pm$  0.004.
- From the results of experiments can concluded the possibility production more useful radio nuclides as well as <sup>117m</sup>Sn, <sup>111</sup>In, and <sup>195m</sup>Pt for nuclear medicine, science and technology using high energy Bremsstrahlung of electron accelerators.

#### REFERENCES

- S. C. Srivastava, et. al. Nuclear Medicine and Biology Advances, Ed., by C. Raynaud, vol.2, Pergamon Press, 1983, pp. 1635-1638.
- 2. S.C. Srivastava, et al. // Clinical Cancer Research 61, vol.4, January 1998, pp. 61-68.
- 3. Y. Oka, T. Kato, K. Nomura and T. Saito // Bull. Chem. Soc. Jap. 40 (1967) 575.
- 4. Z. Randa, V. Duchacek, M. Hradil. //Jaderna Energie 34 (1988) 365.
- 5. Sh. Gerbish, et. al. Communication of JINR, P6-91-123, Dubna, 1991.
- Tran Duc Thiep, Truong Thi An, Nguyen The Vinh, Phan Viet Cuong. Письма в ЭЧАЯ. 2007. Т. 4, № 5(141). С. 668-675.
- Segebade Christian; Weise Hans-Peter; George J Lutz. Photon Activation Analysis.// -Berlin; New York: Walter de Gruyter, 1988, pp. 161-310.
- A. F. Novogorodov, et. al. Simple method of high temperature separation <sup>111</sup>In from massive tin target. (in Russian), //Radiokhimiya, No.2, 1987, pp.254-258.
- 9. V. Levin, et. al. // Radiochem. Radioanal. Letters, 1981, vol. 49, No.2, p.111.
- 10. A. Malinin, et. al. // Radiochem. Radioanal. Letters, 1983, vol. 59, No.4, p.21
- 11. V.L. Aksenov, et. al. Proposal for the construction of the New intense resonance neutron source (IREN). Сообщение ОИЯИ, ЕЗ-92-110, Дубна, 1992.
- Sh. Gerbish, et. al. Application of the IREN facility for production of radionuclide. Russian), Communication of the JINR, P18-2006-116.

## Heavy metals and REE in bottom sediments and dreissenids of the Rybinsk reservoir

Goryaynova Z.I.<sup>1</sup>, Frontasyeva M.V.<sup>1</sup>, Pavlov S.S.<sup>1</sup>, Pavlov D.F.<sup>2</sup>

Frank Laboratory of Neutron Physics, Joint Institute for Nuclear Research, 141980, Dubna, Institute of Inland Water Biology, 152742, Borok, Yaroslavskay Region

The Rybinsk reservoir is the largest artificial water body in Europe and water supply of fresh water for Central Russia. This reservoir is affected by largest in Europe metallurgical plant situated in its northeast part in the town of Cherepovets. To assess the possible impact of this plant on the abiotic and biotic components of the reservoir ecosystem sediments and mollusk Dreissena polymorpha samples were collected in different compartments of the reservoir in 2005. A total of 33 elements including some heavy metals were determined in sediments, zebra mussel shells and soft tissues by means of NAA. High concentrations of some heavy metals were revealed in sediments, shells and soft tissues of zebra mussel in the close vicinity of metallurgical plant.

#### 1 Introduction

Heavy metals from industrial and urban discharges are deposited in different components of the aquatic ecosystem, such as water, sediments, soils and biota. All heavy metals are potentially harmful to most organisms at some level of exposure and absorption. Under certain environmental conditions, heavy metals may accumulate to a toxic concentration, and cause ecological damage. During the last decades mining and industrial production of rare earth elements increased drastically, which led to enlarged input of these elements into the environment, primarily water bodies.

The Rybinsk Reservoir, the largest artificial water body in Europe, is the main source of drinking water for the towns located along its cost-line. The greatest potential risk of environmental contamination to this man-made lake is posed by the town of Cherepovets with its steel producing plant, largest in Europe.

Bottom sediments represent a sink for suspended matter including organic and inorganic pollutants in the freshwater ecosystem. They are frequently used for determining the contamination level of the water ecosystem as well as for assessing risk of potential remobilization of pollutants into the ecosystem.

For biomonitoring purposes in the Rybinsk reservoir two species of bivalve mollusk (*Dreissena polymorpha* and *D. Bugensis*) were used. These mollusks are characterized by their sedentary life style (which unsure representativeness towards a given water body or its part), good filtration capacity and resistance to acute toxicity of pollutants (Klerks et al., 1997; Pavlov, Frontasyeva, 2005). Although dreissenids are considered as reliable bioindicators by many authors (Bervoets et. al., 2001), some investigators debate this fact (Wiesner et al., 2001). The latter study revealed that the mean concentrations of some heavy metals in soft tissues of the mollusks were 9, and in some cases 170 times lower than those in seston and bottom sediments. The authors suggest that dreissenids have great ability to detoxicate heavy metals, which diminishes their bioindicating importance. Bottom sediments in this context can serve as more trustworthy and simple indicators.

The aim of the study is first of all to determine chemical elements, including heavy metals and rare earth elements in tissues of the dreissenids and sediments in different compartments of the reservoir. This can make it possible to assess the contamination level of the reservoir as well as to evaluate the possibility of using dreissenids for monitoring fresh water ecosystems.

#### 2 Methods and materials

Sampling was carried out from research ships of the Institute of Inland Water Biology in 2005-2006 at different areas of the reservoir (Fig. 1). Sediment samples were collected using bottom sampler and dreissenids – using bottom drag.

Mollusk samples were frozen at -18°C for further sample preparation. Mollusks were dissected into a soft part and a shell being preserved separately.



Fig. 1. Study area with sampling sites

Both sediment and mollusk specimens were dried at 40 C<sup>0</sup> and then homogenized with the help of mortar and pastel. The specimens were packed into aluminum cups and polyethylene bags for long and short irradiation, respectively, and analyzed for elemental composition using instrumental epithermal neutron activation analysis (ENAA) at the IBR-2 reactor (JINR, Dubna).

The statistical analyses were performed using the software package Statistica 6.0 for Windows (Statsoft). P values <0.05 were considered statistically significant.

#### 3 Results and discussions

ENAA enabled identification of 31 elements in bottom sediments and zebra mussels.

Concentrations of such elements like scandium, vanadium, manganese, barium, lanthanum, samarium, hafnium, tantalum in the soft tissues of dreissenids differ insignificantly from those in the shell. La, Sm, Hf, Ta content in the soft tissues is no more than twice as much as their shell content, while Mg and Ba concentrations are a little higher in the shell. At the same time cobalt, nickel, zinc, selenium and bromine concentrations in the

soft tissues are 1-2 orders of magnitude higher than those in the shell, while strontium and calcium contents in the shell substantially exceed those in the soft tissues (Fig. 2 and 3). The last observed phenomenon is explained by the fact that calcium is a bulk material for a mineral matrix of the shell and strontium actively replaces calcium in this tissue.

Bottom sediments concentrations for most elements are one order of magnitude higher than those in the soft tissues of the mollusks. The reverse pattern is observed for Ca, Co, Ni and Zn, whose concentrations in the soft tissues differ from those in the sediments insignificantly, while Se and Br concentrations are ten times higher in the soft tissues than in the sediments (Fig. 2 and 3).

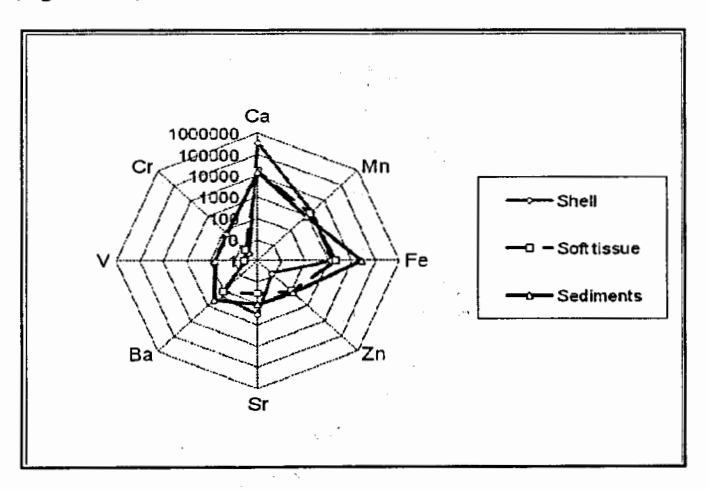


Fig. 2. Concentrations of some elements in the shell, soft tissue of the mollusks and bottom sediments (logarithmic csale)

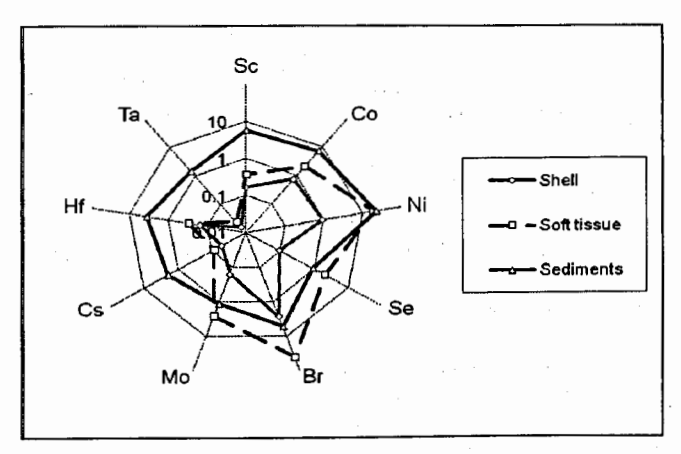


Fig. 3. Concentrations of some elements in the shell, soft tissue of the mollusks and bottom sediments (logarithmic csale)

This means that most elements consumed by the mollusk are not accumulated, but cleared from its body (Wiesner et. al., 2001). Such elemental pattern also demonstrates physiological importance of the above-mentioned elements being not toxicants but essential macro and micro components for the mollusk organism. However, it is well known that under strong anthropogenic contamination microelements can accumulate in an organism in concentrations exceeding their physiological levels. In such conditions the organism cannot control the processes of element consumption and excretion. Thus it may be suggested that the high concentrations of Zn, Co, Ni in the mollusk body are explained by the influence of Cherepovets metallurgical complex.

No significant spatial differences were revealed in shell and soft tissue concentrations for the majority of heavy metals except for zinc and cobalt, whose concentrations in the shell and soft tissues sampled in close vicinity of Cherepovets exceed those from the other sampling points (Fig. 4). Though absolute metal concentrations in soft tissues are higher than those in shells, the latter reflects anthropogenic contamination much better. Trace metal content in the mollusk body depends very much on numerous varying extraneous and intrinsic factors. As the element turnover in the shell is much slower, the shell reflects long-term input trends.

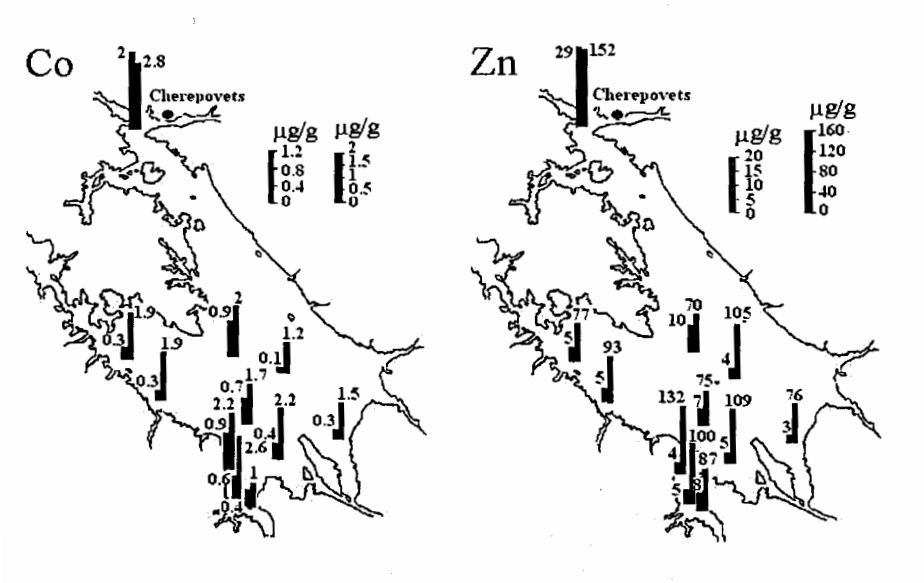


Fig 4. Spatial distribution of Co and Zn in the zebra mussel showing the element content in the soft tissue (left) and in the shell (right)

To establish the spatial distribution of heavy metals in the reservoir sediments cluster analysis was performed (Fig. 5). Clusterization was carried out on the basis of the concentrations of cobalt, nickel, zinc, antimony and tungsten normalized to scandium as a conservative element.

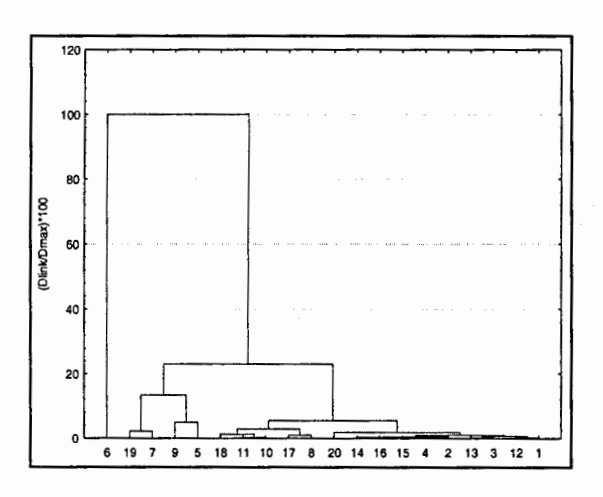


Fig. 5. Cluster analysis of bottom sediments. Hierarhical tree plot

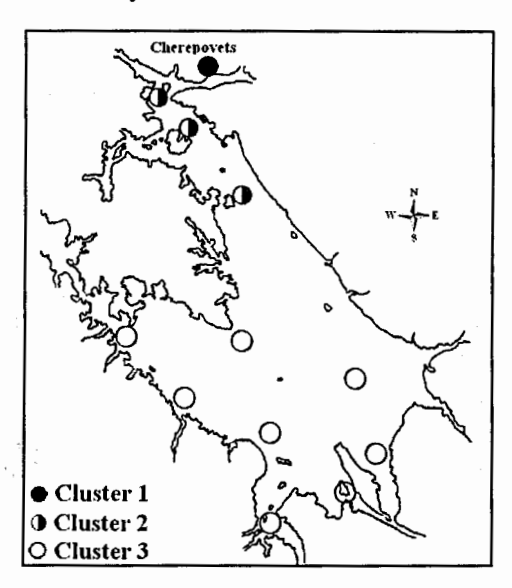


Fig 6. Results of clusterisation for some trace metal concentrations normalized to scandium in sediments from the Rybinsk Reservoir

The first cluster, represented by one sampling point, is characterized by extremely high heavy metal concentrations (Tab. 1). It is located in the Serovka River which is directly exposed to Cherepovets steel producing plant effluents. The second cluster is characterized by moderate heavy metal concentrations and the third cluster corresponds to relatively clean sites (Table 1). As it is evident from the map (Fig. 6), the area of the Cherepovets industrial complex influence is confined to the northeastern part of the reservoir whereas in the central part it is negligible.

Table 1. Mean concentrations of some metals in different sediment cluster (µg/g)

Cluster	Co	Ni	Zn	W	Sb
1	27.0	392.0	1870.0	18.0	6.0
2	10.0	31.0	198.0	3.0	0.8
3	3.2	8.3	27.5	1.0	0.1

#### 4 Conclusions

Our study confirmed that the steel producing complex in Cherepovets exerts negative influence on the reservoir ecosystem. Bottom sediments are reliable objects for monitoring heavy metals and rare earth elements in fresh water ecosystems. Mollusks and dreissenids, in particular, may serve as contamination indicators. Nonetheless, the shell composition reflects permanent source of anthropogenic pollution better than the soft tissue composition does. The feasibility of ENAA for freshwater monitoring has been shown.

#### References

- Bervoets L. et. al. Metal accumulation and condition of transplanted zebra mussel (Dreissena polymorpha) in metal polluted rivers. Department of Biology, Ecophysiology, Biochemistry and Toxicology Group, University of Antwerp., 2001.
- Klerks, P.L., P.C Fraleigh, J.E. Lawniczak. Effects of the exotic Zebra Mussel (Dreissena polymorpha) on the metal cycling in Lake Erie. Can. J. Fish. Aquat. Sci. 1997, Vol. 54. P. 1630-1638.
- Pavlov D. F., Frontasyeva M. V. Comparative chemical composition of two invasive dreissenids, Dreissena polymorpha and D. bugensis in the Rybinsk Reservoir (the Upper Volga basin, Russia) and assessment of invasion-related modification of exchange and balance of chemical elements in the reservoir ecosystem// Alien Species in Holarctic (Borok-2). Book of abstracts. Second Intern. Symp., Borok, Russia, 27 Sept. 1 Oct. 2005, Rybinsk-Borok, 2005, P. 126-127.
- Pavlov D. F., Frontasyeva M. V., Pavlov S. S., Pankratova Yu. Distribution of trace elements in freshwater ecosystem compartments of man-made Rybinsk Reservoir (Central Russia) using epithermal neutron activation analysis. Ovidius University Annals of Chemistry. 2005. 16. No 1, P. 72-75.
- Wiesner L., Günter B., Fenske C. Temporal and spatial variability in the heavy-metal content of Dreissena polymorpha (Pallas) (Mollusca: Bivalvia) from the Kleines Haff (northeastern Germany). Hydrobiologia, 2001, Vol. 443, No. 1-3, P. 137-145.

#### DETERMINATION OF MAJOR AND MINOR ELEMENTS IN SEDIMENTS OF SOME CENTRAL AND NORTHERN MONGOLIAN RIVERS USING INAA

Sh. Gerbish, N. Baljinnyam, G. Ganbold\*, G. Ganchimeg\*

\*- NUM, Ulan-Bator, Mongolia

#### Abstract

The sediment samples from rivers of the central and northern part of Mongolia were studied and the concentration of 41 elements (Na, Mg, Cl, K, Ca, Al, Sc, Ti, V, Cr, Mn, Fe, Co, Ni, Cu, Zn, As, Se, Br, Sr, Rb, Sr, Zr, Nb, Sb, Cs, Ba, La, Ce, Nd, Sm, Eu, Tb, Dy, Tm, Hf, Ta, W, Au, Hg, Th, U) was determined by instrumental neutron activation analysis using epithermal neutrons (ENAA) at the IBR-2 reactor, FLNP JINR, Dubna.

The obtained results of heavy metals and other trace elements in these samples were compared with the reference materials and other clean area data.

This work done under RFFI-Mongolia 08-05-90214 MONG\_a

#### INTRODUCTION

Many of the sediments in rivers, lakes, and oceans have been contaminated by pollutants and most of the contaminants were released years ago while other contaminants enter our water every day. Some contaminants flow directly from industrial and municipal waste dischargers, while others come from polluted runoff in urban and agricultural areas. Still other contaminants are carried through the air, landing in lakes and streams far from the factories and other facilities that produced them. The samples of sediments were collected from the Selenga inflow rivers, which are mainly contaminated by anthropogenic pollutants from industrial, urban and agricultural areas of Mongolia in 2002-2003 years. The sediment analysis of minor and trace elements must be useful to estimate sufficiently the pollution area and river's water. As the rivers flow they are carrying soil, sand, and sediment along with them. The sediments that rivers transport actually play quite an important role in shaping the environment and even in our own lives. When it rains, soil and debris from the surrounding land are eroded and washed into streams. From there, sediment particles ranging from as small as clay to as large as boulders flow along with the water.

#### 1. EXPERIMENTAL PROCEDURE

Monitoring studies of concentration of heavy metals and trace elements in the sediments of the Selenga inflow rivers are important for assessing the effect of contamination by pollutants from industrial, urban and agricultural areas. Sampling points of the sediment have been chosen from the rivers near the most industrial, urban and agricultural areas of the central and northern part of Mongolia (for example: the Tula river near Ulan-Bator, the Khara river near Darkhan and Khangal river near Erdenet) and are shown in Table 1.

After the thermal procedure the sediment powder samples were prepared for irradiation and analyzed at the IBR-2 reactor of FLNP JINR, Dubna, using thermal and epithermal neutrons.

The samples were irradiated in channels of the fast pulsed IBR-2 reactor, the flux parameters of neutrons at irradiation channels: the thermal neutron flux density was 1.1E+12 cm<sup>-2</sup> s<sup>-1</sup> and the fast neutron density was 1.4E+12 cm<sup>-2</sup> s<sup>-1</sup>. For the neutron flux density measurement, the gold foil was used [1-3]. Two kinds of analysis were performed: the long irradiation (for 100 h) in channel (Ch.1) was used to determine the elements associated with long-lived radio nuclides of elements (As, Cd, Ba, Br, Ce, Cs, Eu, Fe, Ni, La, Rb, Sb, Sc, Se, Sm, Th, U, Zn) and the short irradiation (for 20 min) in channel (Ch.2) was used for short-lived radio nuclides of elements (Al, Ca, Cl, I, K, Na, Mg, Mn, V, Cu).

Gamma-ray spectra were recorded 4-5 times using the gamma spectrometers with HP Ge detector. The cooling times of 5 and 10 min were chosen after the decay periods following the short irradiation and those of 5, 13, and 20 days for the long irradiation.

## 2. DISCUSSION AND CONCLUSION

Out of 41 determined elements biogenic or essential macro elements (Na, K, Mg, Ca, Cl) were found; biogenic or essential microelements (Fe, Cu, Zn, Mn, Cr, Se, Co, V, Ti, Ni, As); non-biogenic or other elements (Hg, Sb, Ba, Sr, Cs, Al, Rb, Zr, Nb, Au, Br, Sc, La, Tm, Hf, Ta, W, Th, U and some REE: such as Ce, Nd, Sm, Eu, Tb, Dy) were determined by INAA and shown in Table 2 and 3.

Heavy metals and trace elements in sediments of central and northern rivers have been accumulated from polluted industrial, urban and agricultural areas. The results of our study are important for assessing the effect of contamination pollutants and confirmed by the conclusions.

- We concluded that sediments of rivers are suitable and useful indicators for monitoring studies of environmental pollution of rivers.
- The Nuclear Analytical (INAA) Technique has the sensitivity and accuracy method for the heavy metals and trace element studies of the environments.
- From Table 2 and 3 one can see that contents of the elements Cr, Ti, V, Cu, As, Se and Sb are higher than in crust rocks [4].
- From Fig. 1 and 2 one can conclude that the accumulation of biogenic elements such as Na, Mg, Cl, K, Ca and Fe are higher in sediments No. 5, 9, and 10. Also, the microelements: Ti, V, Cu, Sb and Se have been found higher than others in samples of these sediments.
- It is shown that the main pathway of these (Ti, V, Cu, Se and Sb) elements to sediments No. 5, 9 and 10 is from the polluted area and the waste water of the rivers Khangal and Govil near the storage of Slag-heap tail [5].
- From Fig. 1 one can conclude that the accumulation of U and Th are higher in sediments
  No. 1, 2, 3, 13 and 7 near Ulan-Bator than other samples of sediments and it means that,
  the mean pollution sources of these elements are burning brown coal in power plants and
  heating systems.
- Results of studies of such kind will be important to determine biogenic or essential macro, micro and non-biogenic or other elements in sediment samples of rivers to determine the pollution sources.

#### REFERENCES

- M.V. Frontasyeva, S.S. Pavlov, Analytical investigation at the IBR-2 reactor in Dubna. Proceeding of the VII International Seminar on Interaction of Neutrons with Nuclei, Dubna, May 17-20, 2000, E3-2000-192, p.219-227, JINR(2000).
- Ganbold G. et al., Atmospheric deposition of trace elements around Ulan-Bator city studied by moss and lichen biomonitoring technique and INAA. Communication JINR E18-2005-113. Dubna, 2005.
- Ganbold G. et al., Assessment of hazardous impact on the pastured animals of non-ferrous industry in the town of Erdenet, Mongolia. Communication JINR E18-2006-176. Dubna, 2006.
- 4. B. Mason, Principles of Geochemistry, J. Wiley and Sons, New York, 1966.
- Gerbish Sh. et.al., Multielemental Photon Activation Analysis of Copper-Molybdenum Ores and its Products of Processing Using Microtron bremsstrahlung / Journal of Radioanalytical and Nuclear Chemistry, Articles Vol.138, No.2, (1993), pp. 503-511.

Table 1. Sampling places of the sediment samples

No	Name of rivers	Location
1	Tula	Ulan – Bator, (south part)
2	Dundgol	Peace bridge, Ulan – Bator
3	Selbe	Lion bridge, Ulan – Bator (central part)
4	Uliastai	Uliastai bridge, Ulan – Bator (east part)
5	Govil	Erdenet town
6	Soil	Erdenet town (central part)
7	Shariingol	Bridge, Selenga aimak
8	Kharaagol	Darkhan bridge, Darkhan
9	Khangal	Ulaantolgoi, Erdenet
10	Khangal	Erdenet bridge, Erdenet (central part)
11	Tula	Zaamar bridge, Central aimak
12	Tula	Ovoot bridge, Central aimak
13	Tula	Gachurt bridge, Ulan – Bator (east)
14	Tula	Altan Dornot, Zaamar, Central aimak

Table 2. Contents (mg/kg) in sediments of inflow rivers Selenga (Mongolia); (C± ΔC, %).

Elements	№ 1.	№ 2.	№ 3.	№ 4.	№ 13.	№ 11.	<b>№</b> 12.
Na	24800 (10)	16900(10)	18200 (10)	18100 (10)	28100 (10)	21400 (10)	21400 (10)
Mg	27900 (28)	32000 (28)	27900 (28)	23700 (13)	22900 (29)	30700 (29)	23600 (29)
Al	58900 (20)	80300 (20)	71500 (20)	67400 (20)	65700 (20)	70600 (20)	74000 (20)
CI	3.22 (33)	3.22 (33)	3.22 (33)	4.91 (33)	3.22 (33)	8.86 (33)	3.22 (33)
K	28000 (23)	23500 (23)	27400 (23)	23800 (23)	34600 (23)	26300 (23)	24200 (23)
Ca	48100 (33)	36000(33)	93500 (33)	21000 (33)	21200 (33)	30900 (33)	32600 (33)
Sc	9.98 (13)	12.1 (13)	9.60 (13)	5.90 (13)	4.00 (13)	8.51 (13)	4.35 (13)
Ti	4150 (41)	5110 (40)	4730 (42)	2950 (45)	2800 (42)	4120 (42)	4240 (41)
V	114 (21)	101 (22)	140 (20)	63.1 (24)	42.9 (29)	93.5 (22)	74.8 (23)
Cr	54.3 (23)	66.7 (24)	60.7 (23)	26.3 (24)	20.8 (20)	29.0 (25)	20.8 (20)
Mn	880 (6)	610 (6)	921 (6)	473 (6)	576 (6)	878 (6)	542 (6)
Fe	26200 (4)	31400 (5)	25200 (4)	18100 (4)	10500 (4)	21500 (4)	9460 (4)
Co	11.7 (11)	13.2 (11)	13.6 (11)	5.76 (11)	3.94 (12)	9.20 (11)	3.61 (12)
Ni	14.0 (27)	21.8 (23)	22.8 (23)	8.42 (30)	8.26 (28)	17.2 (23)	9.17 (26)
Cu	ND	ND	ND	ND	ND	ND	ND
Zn	97.7 (6)	120 (5)	160 (5)	63.9 (6)	31.5 (8)	57.3 (6)	20.6 (9)
As	14.0 (6)	7.61 (6)	20.7 (6)	7.16 (6)	8.72 (8)	10.2 (6)	3.58 (7)
Se	0.290 (25)	0.016 (14)	0.22 (27)	0.016 (17)	0.23 (23)	0.314 (25)	0.016 (17)
Br	7.06 (25)	6.28 (25)	12.2 (25)	1.96 (25)	6.3 (25)	7.42 (25)	1.62 (27)
Rb	74.1 (9)	102 (9)	72.4 (9)	84.2 (9)	67.1 (9)	63.4 (9)	49.6 (9)
Sr	316 (8)	318 (7)	310 (8)	309 (7)	192 (8)	214 (8)	183 (8)
Zr	315 (7)	345 (7)	176 (11)	203 (8)	181 (8)	227 (8)	248 (7)
Nb	22.3 (21)	23.7 (21)	13.2 (21)	14.7 (22)	10.9 (22)	16.7 (22)	16.4 (21)
Sb	2.38 (13)	2.41 (13)	3.29 (13)	2.06(13)	0.77 (15)	1.06 (14)	0.536 (16)
Cs	5.41 (13)	6.47 (13)	6.12 (13)	3.96 (13)	2.43 (13)	4.03 (13)	1.95 (14)
Ba	502 (8)	677 (8)	523 (9)	629 (8)	405 (9)	383 (8)	347 (8)
La	51.8 (7)	37.0 (7)	47.3 (7)	22.4 (7)	33.4 (7)	44.4 (7)	26.7 (7)
Ce	124 (11)	126 (11)	107 (11)	77.3 (11)	66.2 (11)	94.4 (11)	46.4 (11)
Nd	22.8 (32)	34.0 (19)	17.0 (38)	11.0 (47)	13.8 (37)	17.1 (35)	21.5 (25)
Sm	8.85 (7)	8.01 (7)	8.98 (7)	5.00 (7)	5.51 (7)	8.25 (7)	4.85 (7)
Eu	ND	1.09 (38)	ND	ND	0.588 (35)	0.346 (51)	0.626 (40)
Tb	0.679 (33)	0.828 (33)	0.604 (33)	0.516 (33)	0.380 (33)	0.591 (33)	0.386 (33)
Dy	6.40 (38)	6.37 (39)	9.96 (39)	3.83 (55)	5.67 (39)	5.12 (43)	5.93 (39)
Tm	ND	1.12 (8)	ND	0.601 (9)	ND .	ND .	0.549 (9)
Hſ	8.0 (8)	8.39 (8)	4.06 (9)	5.56 (8)	4.05 (8)	5.02 (8)	5.96 (8)
Та	0.99 (25)	- 1.17 (25)	0.74 (25)	0.76 (25)	0.51 (25)	0.76 (25)	0.61 (25)
W	11 (13)	9.73 (11)	13.9 (11)	5.40 (13)	4.2 (16)	5.17 (15)	3.94 (15)
Au	ND	0.012 (24)	0.047 (9)	0.003 ± 34	ND	ND	ND
Hg	ND	ND	ND	ND	ND	ND	0.076 (45)
Th	15.5 (10)	17.0 (10)	13.8 (10)	9.27 (10)	10.3(10)	10.9(10)	6.26(10)
U	10.5 (15)	8.13 (15)	12.4 (14)	4.19 (14)	9.98 (14)	7.41 (14)	5.01 (14)

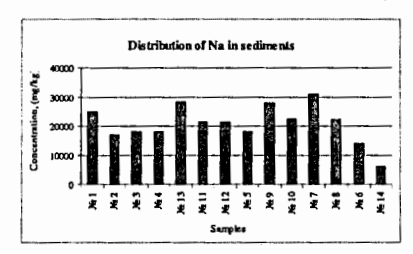
Note: ND - no detected

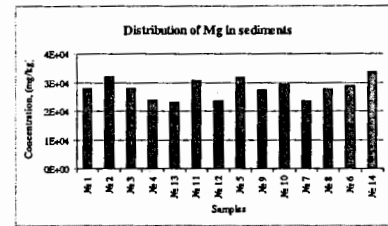
Table 3. Contents (mg/kg) in sediments of inflow rivers Selenga (Mongolia); ( $C\pm \Delta C$ ,%).

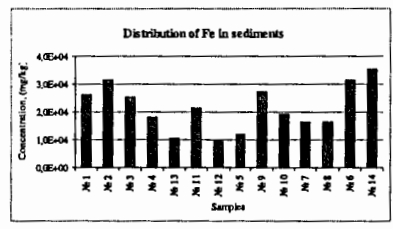
ts							
Elements	№ 5.	№ 9.	№ 10.	№ 7.	№ 8.	№ 6.	№ 14.
Na	18000 (10)	28000 (10)	22400 (10)	30900 (10)	22300 (10)	14000 (10)	6020 (10)
Mg	31800 (29)	27400 (28)	29400 (29)	23500 (13)	27700 (28)	28900 (28)	33800 (28)
Al	75400 (20)	76700 (20)	68200 (20)	61800 (20)	74700 (20)	61600 (20)	75200 (20)
Cl	13.1 (33)	5.76 (33)	12.1 (33)	3.22 (33)	4.36 (33)	5.00 (33)	3.22 (33)
К	20900 (33)	23600 (33)	21600 (23)	25500± 24	19800 (33)	19400 (33)	19700 (33)
Ca	99600 (33)	58200 (33)	53900 (33)	47300 (33)	44800 (33)	39500 (33)	33000 (33)
Sc	4.80 (13)	9.64 (13)	6.85 (13)	7.87 (13)	7.80 (13)	11.8 (13)	14.1 (13)
Ti	6510 (41)	7610 (40)	4260 (42)	4530 (41)	4830 (41)	5550 (40)	6240 (41)
v	143 (19)	165 (19)	98.6 (20)	81.8 (22)	88.6 (22)	120 (19)	137 (21)
Cr	32.5 (24)	56.1 (33)	37.7 (33)	20.8 (28)	42.6 (33)	58.1 (22)	20.8 (20)
Mn	900 (6)	831 (6)	611 (6)	628 (6)	684 (6)	839 (6)	863 (6)
Fe	12000 (4)	27100 (5)	19300 (4)	16300 (4)	16500 (4)	31500 (3)	35200 (3)
Co	5.90 (11)	9.48 (11)	8.76 (11)	5.81 (11)	5.84 (12)	13.0 (11)	15.3 (10)
Ni	13.5 (24)	15.4 (24)	13.9 (24)	9.30 (29)	8.24 (31)	20.7 (22)	41.5 (19)
Cu	1030 (53)	1510 (11)	1630 (28)	ND	ND	ND	ND
Zn	24.9 (11)	50.0 (7)	52.8 (6)	41.0 (7)	27.8 (9)	82.7 (6)	20.6 (9)
As	8.35 (6)	19.1 (6)	16.1 (6)	3.34(8)	5.50 (7)	9.53 (6)	50.5 (6)
Se	0.249 (33)	1.23 (25)	0.518 (24)	0.249 (24)	0.017 (33)	0.017 (17)	0.023 (21)
Br	9.54 (25)	4.86 (25)	2.68 (26)	3.52 (26)	1.93 (26)	7.02 (25)	0.324 (33)
Rb	27.7 (10)	51.1 (9)	42.9 (9)	49.7 (9)	61.0 (9)	68.3 (9)	71.9 (9)
Sr	176 (8)	385 (7)	351 (7)	283 (7)	291 (7)	371 (7)	125 (8)
Zr	111 (11)	330 (7)	197 (8)	482 (6)	514 (6)	312 (8)	205 (6)
Nb	8.01 (23)	22.4 (21)	14.7 (21)	31.8 (21)	32.9 (21)	16.7 (22)	16.4 (21)
Sb	0.414 (16)	1.85 (13)	2.70 (13)	0.37 (17)	0.66 (16)	1.18 (14)	1.27 (13)
Cs	1.51 (14)	1.90 (14)	1.63 (14)	2.03 (14)	2.35 (14)	3.58 (13)	1.95 (14)
Ba	226 (8)	452 (8)	453 (9)	412 (8)	451 (8)	579 (8)	425 (8)
La	31.2 (7)	35.6 (7)	23.7 (7)	44.8 (7)	30.7 (7)	30.6 (7)	29.6 (7)
Ce	42.9 (12)	81.1 (11)	54.8 (11)	80.8 (11)	83.4 (11)	97.0 (11)	84.8 (11)
Nd	ND	20.1 (33)	11.1 (42)	ND	17.8 (29)	21.2 (31)	25.6 (26)
Sm	7.08 (7)	8.17 (7)	4.91 (7)	8.47 (7)	7.29 (7)	7.13 (7)	7.13 (7)
Eu	ND	0.881 (37)	0.374 (66)	1.02 (32)	0.986 (34)	0.916 (38)	1.14 (26)
Тъ	0.283 (33)	0.541 (33)	0.382 (33)	0.626 (33)	0.661 (33)	0.687 (33)	0.622 (33)
Dy	6.89 (40)	6.05 (39)	7.21 (48)	5.99 (39)	3.83 (55)	6.54 (40)	6.48 (40)
Tm	ND	1.14 (8)	0.471 (9)	ND	0.776 (8)	0.771 (8)	0.638 (7)
Hf	2.43 (9)	7.69 (8)	4.97 (8)	11.1 (7)	12.0 (7)	2.43 (9)	4.75 (8)
Ta	0.343 (26)	0.787 (25)	0.537 (25)	1.01 (25)	0.922 (25)	0.965 (25)	0.719 (25)
w	3.68 (17)	.5.60 (14)	5.46 (14)	3.97 ± 18	4.40 (14)	3.89 (13)	5.61 (12)
Au	ND	ND	0.0083 (27)	ND	0.0033 (48)	ND	0.008 (21)
Hg	ND	ND	ND	ND	0.128 (40)	ND	0.076 (45)
Th	5.11 (10)	7.60 (10)	5.42 (10)	9.71 (10)	9.52 (10)	12.5 (10)	9.67 (10)
U	4.82 (15)	5.63 (15)	3.64 (15)	7.71 (14)	5.16 (14)	4.52 (14)	4.60 (14)

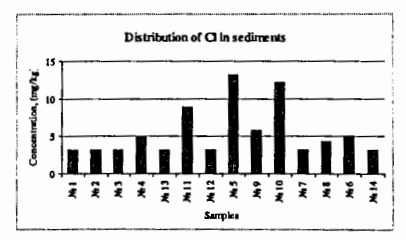
Note: ND - no detected

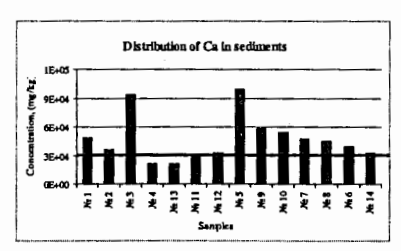
Fig. 1. Histogram of distribution for macro elements in sediments

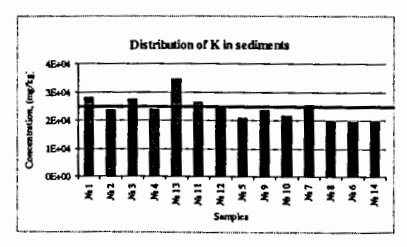


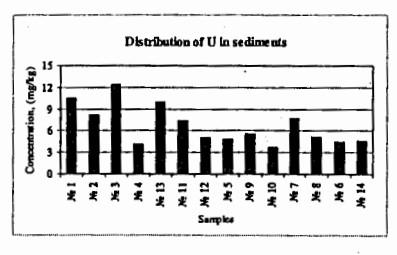












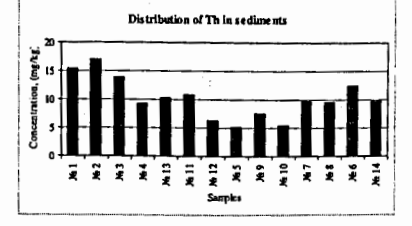
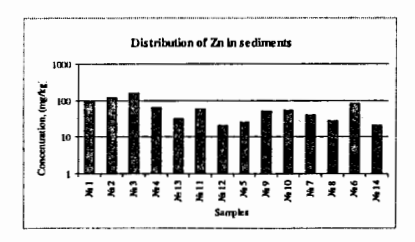
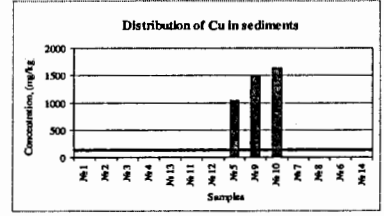
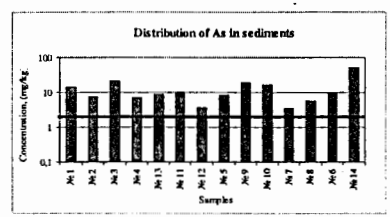
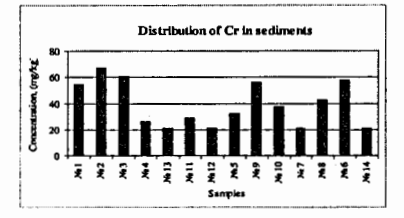


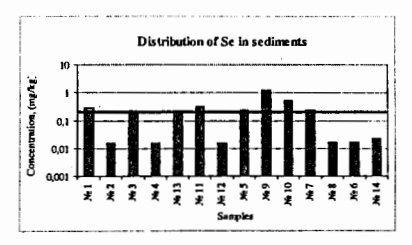
Fig. 2. Histogram of distribution for some micro elements in sediments

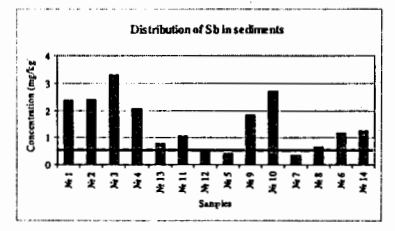


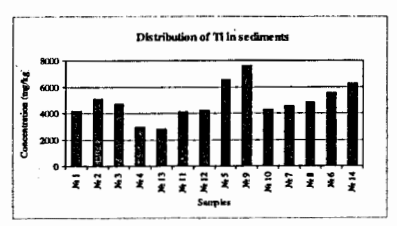


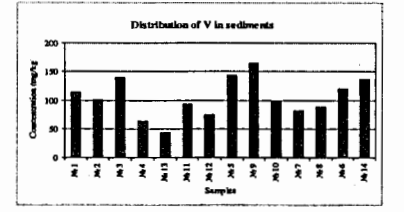












# WDXRS OF MINOR AND TRACE ELEMENT CONTENTS IN SOILS OF THE KHAMAR-DABAN MOUNTAIN RANGE

E. Grosheva<sup>1</sup>, D. Zaichick<sup>2</sup>, S. Lyapunov<sup>3</sup>, E. Schevchenko<sup>3</sup>

<sup>1</sup>Institute of Ecological Toxicology, Baikalsk 665932, Russia, e-mail: egrosheva@list.ru

<sup>2</sup>Moscow State Agricultural Academy, Moscow 127550, Russia

<sup>3</sup>Geological Institute of Russian Academy of Sciences, Moscow 109017, Russia

### Introduction

With consideration of predominating winds in the region, the Baikal Pulp-and-Paper Complex (BPPC) is likely to be a key source of industrial air emissions on the southern shore of the Baikal Lake to the North-East of the Baikalsk city. Indirect retrospective assessment of the regional pollution level is achievable through a survey focused on environment objects that accumulate chemical elements present in industrial air emissions. Such objects normally include topsoil, mosses, lichens, mushrooms, etc. Topsoil is a more appropriate subject for such surveys. Opposite to other environment components (air, water) where periodic self-treatment processes may occur, soil is an active acceptor of chemical contaminants and virtually has no inherent self-treatment ability. Contaminants are retained in soil for significantly longer time than in other biosphere components (mosses, lichens, mushrooms, etc.) - most likely eternally. Soil serves as a mighty absorber of many chemical elements. It retains them in topsoil, which is the most fertile soil layer. North-western slopes of Khamar-Daban mounts are most representative for regional BPPC impact assessment.

The range of chemical elements emitted to air by solid fuel burning is very diverse. Key air emission contaminants are: Al, As, Ca, Ce, Cl, Co, Cr, Cs, Cu, Eu, F, Fe, Hf, K, Mg, Mn, Mo, Na, Ni, P, Pb, Rb, S, Sb, Sc, Se, Si, Tb, Th, Ti, V, Yb, Zn, etc. <sup>1-4</sup> That is why for properly assessing a region's man-caused degree of pollution it is necessary to maximize the number of chemical elements that can be determined for study. These elements should obviously include top-priority toxicants. The existing Russian environmental standards for soils <sup>5</sup> identify 11 chemical elements, namely As, Cd, Cr, Cu, Hg, Mn, Ni, Pb, Sb, V, and Zn.

This research aims at a more detailed examination of the pollution level across the region to the north-east of BPPC caused by some chemical elements of industrial air emissions.

Topsoil samples were taken on the Khamar-Daban mounts to the North-East of BPPC at a height of about 1200 - 1500 m above sea level in two areas located 11 and 84 km away, respectively. The first sampling area (Area 1) is located on the Osinovsky bare mount in upper reaches of the Bolshaya Osinovka River 10 km away from the Baikal shoreline and in 11 km from BPPC. Five topsoil samples were taken in various points of slopes and top of the mount. Investigated samples were classified to mountain-tundra low-capacity soil, cedar elfin woods and reindeer, cowberry-reindeer or grass-reindeer mosses vegetation. The second sampling area (Area 2) is located on the Osinovsky bare mount in upper reaches of the Osinovka River 10 km away from the Baikal shoreline and in 84 km from BPPC. The area is

a part of the Baikal nature reservation and is located 3 - 5 km east from the Tankhoi city right opposite the Angara River heads in the West. Four topsoil samples were taken in various points of slopes and top of the mount. Investigated samples were classified to mountain-tundra low-capacity soil, moss and lichen vegetation.

# Experimental

<u>Samples</u>. For chemical element analysis soil samples were taken from topsoil 4 cm thick as an average mixed sample by the plastic knife and the plastic scoop. Soil samples were dried in the air in enclosed space at room temperature during a few days. Air-dry scattered soil samples were cleaned from roots, impurities, neoformations and sod, from which soil clods had been carefully shaken off. Then each sample was mixed, homogenized, mechanically ground using the porcelain mortar and sieved to <2 mm using nylon screening. Then a randomized 5 g weight portion of each sample was milled for 5 min using an "IB-micro" mill. This time was enough to reach about 200 mesh dispersion level controlled visually by comparing with the standards. The fine milled soil samples were poured into special dashboard capacities filled up to their edges.

<u>Standards</u>. Quality control of the developed procedure and analytical results was implemented in parallel by examining samples prepared from the IAEA international standard reference material (SRM) - IAEA Soil-7.

Analytical method. Instrumental wave-dispersive X-ray fluorescent analysis (WD-XRF) was used to determine contents of chemical elements. Mass fractions of Mo, Nb, Y, and Zr were measured using an ARF-6 analyzer with an Ag-tube. The same analyzer, but with a Mo-tube was used to determine contents of As, Ba, Br, Pb, Rb, Sr, Th, and U in the samples. Mass fractions of Co, Cr, Cu, Fe, Mn, Ni, Ti, V, and Zn in the soil samples were analyzed using a SPM-25 Quantometer equipped with a Rh-tube. Measurements with the ARF-6 analyzer were carried out twice. The duration of each measurement was 100 s. Measurements of 100 s duration were carried out once using the SPM-25 Quantometer. The  $K_{\alpha I}$ -lines were used to register intensities of characteristic X-rays of Ti, V, Cr, Mn, Fe, Co, Ni, Cu, Zn, As, Br, Rb, Sr, Y, Zr, Nb, Mo, and Ba, while the  $L_{\beta I}$ -lines were used to register intensities of X-rays of Pb, Th, and U. The sample matrix effect was account by noncoherent scattered  $K_{\alpha}$ -line of the X-ray tube.

<u>Calculations.</u> Standard program for calculations of an arithmetical mean (M), standard deviation (S.D.), and standard deviation of the mean (S.E.) was used for the statistical treatment of the results.

#### Results and discussion

The accuracy of the obtained results was estimated by determination of the element contents in samples of the IAEA Soil-7 international certified reference material. The Table 1 results show that application of instrumental WD-XRF analysis makes it possible to determine mass fractions of not less than 21 chemical elements in the soil samples. The relative errors of a single measurement of different element mass fractions vary within a rather wide range to be no more than 5% for Fe, Mn, Rb, Sr, Th, and Zr, 6% to 10% for Ba, Br, Co, Cr, Cu, Nb, Ni, Pb, Ti, V, and Zn, and above 10% for As, Mo and U. Coincidence of

the WD-XRF mean values of chemical element contents in the IAEA Soil-7 reference material with certificate data in the range of 95% confidential interval was obtained for 17 elements from 21. The only exclusion was the results of Fe (not certified), Mn, V, and U for which the difference between means of mass fraction were +31%, +19%, +48 and -38% respectively. Thus, a systematic error might be available only while determining Mn, V, and U contents by WD-XRF analysis. In general, good coincidence with certificate data indicates high accuracy of the used technique and the correctness of the obtained results.

Table 1. WD-XRF data of some minor and trace elements of the IAEA Soil-7 reference material compared to certified values

No	Element			Our results	
		Mean	95% confidence	Type*	Mean
			interval		
1	As, mg/kg	13.4	12.5-14.2	С	14
2	Ba, mg/kg	159	131-196	N	184
3	Br, mg/kg	7.0	3.0-10.0	N	8
4	Co, mg/kg	8.9	8.4-10.1	С	9
5	Cr, mg/kg	60	49-74	С	74
6	Cu, mg/kg	11.0	9.0-13.0	С	12
7	Fe, g/kg	25.7	25.2-26.3	N	33.6
8	Mn, mg/kg	631	604-650	С	750
9	Mo, mg/kg	2.5	0.9-5.1	N	3
10	Nb, mg/kg	12	7-17	N	10
11	Ni, mg/kg	26	21-37	N	22
12	Pb, mg/kg	60	55-71	С	55
13	Rb, mg/kg	51	47-56	С	51
14	Sr, mg/kg	108	103-114	С	107
15	Th, mg/kg	8.2	6.5-8.7	С	6.8
16	Ti, g/kg	3.0	2.6-3.7	N	3.4
17	U, mg/kg	2.6	2.2-3.3	С	1.6
18	V, mg/kg	66	59-73	С	98
19	Y, mg/kg	21	15-27	С	26
20	Zn, mg/kg	104	101-113	C	102
21	Zr, mg/kg	185	180-201	C	185

<sup>\*</sup> C - certified values, N - non-certified values

A considerable remoteness of Area 2 from BPPC (84 km), as compared to Area 1 (11 km), allows to assuming it as a checkpoint (background levels) in BPPC air emission impact assessment. The comparison of mean values in topsoil on the Osinovsky slopes in Areas 1 and 2 made for 19 chemical element mass fractions did not reveal any statistically valid increases (Table 2) with Y exclusion only. Moreover in soil of the mount top in Area 2 contents of such elements, as Sr and U, were correspondingly 1.18 and 1.67 times higher (statistically valid) than in Area 1 (Table 2).

The comparison of the obtained results with literature data makes it possible to conclude that mean contents of all 19 elements in Osinovsky topsoil are within the range characteristic of non-polluted soils on the territories of former USSR, CIS and across the world (Table 3).

Table 2. Means (M±S.D.) of chemical elements mass fraction in soils of slopes and tops in areas 1 and 2 (air-dried soil)

Element		Slopes			Tops	
	Areas 1	Areas 2	p<	Areas 1	Areas 2	p<
		Reservation	t-test		Reservation	t-test
As, mg/kg	<3.0	<3.0-3.1	-	3.6±0.4	4.3±0.1	-
Ba, mg/kg	325±49	355±120	-	395±7	400±14	-
Br, mg/kg	1.9±1.6	$2.8\pm2.7$	-	$2.6\pm0.1$	$3.4\pm0.6$	-
Co, mg/kg	$4.0\pm1.4$	$12.0\pm5.7$	-	$7.5 \pm 0.7$	$7.5 \pm 0.7$	-
Cr, mg/kg	51±4	52±34		86.0±15.6	$72.5 \pm 0.7$	-
Cu, mg/kg	16.5±6.4	38.5±26.2		$37.0\pm4.2$	37.0±2.8	-
Fe, g/kg	19.3±4.2	36.2±25.2	-	$44.0 \pm 2.0$	43.6±1.1	-
Mn, mg/kg	410±42	580±367	-	715±162	605±7	-
Ni, mg/kg	2.85±0.78	$3.50\pm0.28$	-	23.0±1.4	19.0±1.4	-
Pb, mg/kg	$4.0\pm0.1$	5.5±3.5	-	$7.5 \pm 0.7$	8.5±0.7	
Rb, mg/kg	54.5±9.2	82.5±14.8	-	$67.0 \pm 7.1$	80.5±0.7	-
Sr, mg/kg	125±35	155±7	-	165±7.1	195±7	0.05
Th, mg/kg	3.25±0.35	$3.25\pm3.18$	-	$6.35 \pm 0.92$	$6.80\pm0.14$	-
Ti, g/kg	5.75±0.35	$4.20\pm1.27$	-	5.75±1.06	$6.05 \pm 0.07$	
U, mg/kg	<1	<1-2.1	-	$1.35\pm0.07$	2.25±0.07	0.01
V, mg/kg	90.5±14,8	79.0±39.6	-	107±6	106±2	-
Y, mg/kg	24.0±1.4	17.5±6.4	-	22.0±1.4	13.0±1.4	0.01
Zn, mg/kg	31±4	32±13	-	22.0±4.2	15.5±0.7	-
Zr, mg/kg	195±7	145±35	-	205±57	215±7	-

The attained results provide evidence that the BPPC air emission total for the overall operation period did not induce any shifts in the chemical composition of soils in the adjacent region that would be beyond background (natural) values. However, this conclusion does not allow to generally rule out any impact from the BPPC operation on the chemical composition of regional soils but just defines a scale of such exposure. It is known that in nature there exist so-called biogeochemical provinces where either a deficit or excess of chemical elements in soils leads to human or animal diseases as well as suppresses plant growth. Development of understandings about "healthy soil" and optimum chemical element contents in soil is a challenging and multi dimensional endeavor. Available scientific literature offers only a few Russian and international references, which provide data on upper and lower limits of optimum chemical element contents in soils accompanied by rather convincing justification. 6,10-12,16,19,20 For 11 chemical elements (As, Cd, Cr, Cu, Hg, Mn, Ni, Pb, Sb, V, and Zn) the existing GOST (Russian State Standard) defines maximum permissible level

(MPL) or tentative permissible level (TPL) on the basis of a few soil characteristics (Table 4).<sup>5,21</sup> Among the 19 chemical elements, mass fraction of which were determined in soils of the Osinovsky mount, recommended ("Norm") or regulatory (MPL and TPL) data is available for only 10, namely for As, Co, Cr, Cu, Mn, Ni, Pb, Sr, V and Zn (Table 4). Mean mass fractions of these elements in Osinovsky topsoil fall within the optimum range and do exceed neither MPL nor TPL. Thus, soils of the Osinovsky bare mount are to be characterized as "healthy" and "non-toxic" in terms of chemical element contents.

Table 3. Comparison of the obtained results with the published data on chemical element mass fractions (median and range of means) in soils of the former USSR, CIS and globally (air-dried soil)

Element	Soils of the former	World's soils	Soils of Osinovsky
	USSR and CIS	(Bowen <sup>17</sup> ;	mountains
	(Russian	Ure & Berrow <sup>18</sup> and	
	references <sup>5,6-16</sup> )	Russian references <sup>5,6-16</sup> )	
	Range of means	Median & Range of means	Range of means
As, mg/kg	1 - 40	11.3 (0.1-194)	<3.0-4.3
Ba, mg/kg	<10 - 30000	568 (<1-10000)	325-400
Br, mg/kg	0.8 - 5.0	42.6 (0.27-850)	1.9-3.4
Co, mg/kg	0.4 - 90	12 (0.3-200)	4.0-12.0
Cr, mg/kg	8.0 - 614	84 (0.9-4000)	51.0-86.0
Cu, mg/kg	< 1.0 - 500	25.8 (<1-390)	16.5-38.5
Fe, g/kg	0.0003 - 3.9	3.2 (0.01-55)	19.3-44.0
Mn, mg/kg	10 - 7400	760 (<1-18300)	410-715
Ni, mg/kg	1.9 - 3000	33.7 (0.1-1520)	2.85-23.0
Pb, mg/kg	<1 - 3000	29,2 (<1-3000)	4.0-8.5
Rb, mg/kg	70 - 194	120 (1.5-1800)	54.5-82.5
Sr, mg/kg	1 - 3500	278 (1-3500)	125-195
Th, mg/kg	0.04 - 22	14 (0.04-72)	3.25-6.80
Ti, g/kg	0.0006 - 1.5	0.51 (0.000017-3.4)	4.20-6.05
U, mg/kg	0.4 - 1.4	2.18 (0.1-14)	<1-2.25
V, mg/kg	3.0 - 700	108 (0.8-1000)	79.0-107
Y, mg/kg	5.8 - 50	27.7 (5-250)	13.0-24.0
Zn, mg/kg	0.5 - 7000	59.8 (1.5-7000)	15.5-32.0
Zr, mg/kg	100 - 870	345 (<10-3000)	145-215

## Conclusion

1. It was shown that the instrumental WD-XRF analysis allowed determining with high accuracy mass fractions up to 21 chemical elements such as As, Ba, Br, Co, Cr, Cu, Fe, Mn, Mo, Nb, Ni, Pb, Rb, Sr, Th, Ti, V, U, Y, Zn, and Zr in the air-dried soil samples even at the natural (uncontaminated) levels. This method is non-destructive, i.e. non-utilizing a sample under study. To prepare a sample for the analysis, it should only be dried and mill. The

method is very express (only 1 to 2 min is required for an element determination) combined with high enough sensitivity, reproducibility, and accuracy of the results. The whole process of the analysis can be partially or even fully automated. The equipment required for the analysis is comparatively cheap, fully autonomous and compact.

Table 4. Comparison of mean mass fractions of chemical elements in Osinovsky mounts soils with maximum permissible and tentative permissible levels (MPL and TPL) adopted for soils in Russia and existing limits for "normal" soil

(air-dried soil)

Element	"Norm"*			MPL & TPL <sup>5,21</sup>	Soils of
	Kovalsky <sup>11</sup>	Thornton <sup>19</sup>	Ilin <sup>20</sup>	(1;2;3)**	Osinovsky
	Rovaisky	Thornton	11111		mountains
As, mg/kg	-	<5-40	<15 - 20	2.0 (2, 5, 10)	<3.0-4.3
Ba, mg/kg	-	-	-	-	325-400
Br, mg/kg	-	-	'	-	1.9-3.4
Co, mg/kg	7 - 30	-	7 - 20	-	4.0-12.0
Cr, mg/kg	-	15 - 300	<200	100	51.0-86.0
Cu, mg/kg	15 - 60	2 - 60	<25	55 (33, 66, 132)	16.5-38.5
Fe, g/kg	-	=	-	-	19.3-44.0
Mn, mg/kg	400 - 3000	-	400 - 800	1500	410-715
Ni, mg/kg		2 - 100	<40	85 (20, 40, 80)	2.85-23.0
Pb, , mg/kg		10 - 150	<50	32(32, 65, 130)	4.0-8.5
Rb, mg/kg	-	-	-	-	54.5-82.5
Sr, mg/kg	<600	-	<600 - 1000	•	125-195
Th, mg/kg	-	-	-	=	3.25-6.80
Ti, g/kg	-	-	-	-	4.20-6.05
U, mg/kg	-	-	-	-	<1-2.25
V, mg/kg	-	-	<200	150	79.0-107
Y, mg/kg	-	-	-	-	13.0-24.0
Zn, mg/kg	30 - 70	25 - 200	10 - 70	100(55, 110, 220)	15.5-32.0
Zr, mg/kg			*	-	145-215

<sup>\* -</sup> normal levels of "health soil"

- 2. The attained results evidence that the BPPC air emission total for the overall operation period did not induce any shifts in the mean contents of 19 elements of soils in the adjacent region that would be beyond background (natural) values.
- 3. Soils of the Osinovsky bare mount are to be characterized as "healthy" and "non-toxic" in terms of chemical element contents.
- 4. The results of expert assessment do not fully rule out the availability of any impact of the BPPC on the regional soils but just define a scale of such exposure. For high precision evaluation of the impact of BPPC on region's soils, a series of researches on regular-basis

<sup>\*\* -</sup> MPL & TPL (1;2;3) - maximum permissible limit (MPL) or tentative permissible limit (TPL) of sand and subsand (1), acid (2), loam and clay (3) soils respectively

with 2 -3 year frequency are needed. Such researches are in plan of the Institute of Environmental Toxicology as the issue of BPPC shutdown still remains open and the Complex continues its operation.

#### References

- 1- N.K. NOVIKOVA, V.A. KNIZHNIKOV, Gigiena i Sanitaria, 3 (1985) 47.
- 2- S.M. SOKOLOV, Gigiena i Sanitaria, 9 (1986) 17.
- 3- V.A. BOLSHAKOV, N.M. KRASNOVA, T.I. BORISOCHKINA, V.G. GRAKOVSKY, Airtechnogenic Pollution of Soils by Heavy Metals: Sources, Scale, Recultivation, Soil Institute of RAS, Moscow, 1993.
- 4- M.A. RAUF, M. IKRAM, N. J. AYUB, Trace and Microprobe Techniques, 20 (2002) 91.
- M.M. OVCHARENKO, Heavy Metals in the Soil-plant-fertilizer System, Moscow, 1997.
- 6- A.P. VINIGRADOV, Geochemistry of Rare and Scattered Chemical Elements in Soils, USSR Academy of Science, Moscow, 1957.
- 7- V.A. CHERNOV, K.V. VERIGINA, Yu.I. DOBRITSKAYA, O.A. VADKOVSKAYA, E.G. MARKOVA, in: Trace Elements in Agriculture and Medicine, Riga, 1959, p. 91.
- 8- Y.I. DOBRITSKAYA, E.G. ZHURAVLEVA, L.P. ORLOVA, M.G. SHIRINSKAYA, in: Trace Elements in Agriculture and Medicine, Agricultural Literature, Kiev, 1963, p. 391.
- 9- P.N. SAVINA, in: Trace Elements in Agriculture and Medicine, Vol. 2., Ulan-Ude, Russia, 1966, p. 100.
- 10-N.I. KHLEBNIKOV, News of Academy of Medical Sciences of the USSR, 2 (1963) 3.
- 11- V.V. KOVALSKI, R.I. BLOKHINA, I.I. NIKITINA, in: Trace Elements in Medicine, Ivano-Frankovsk, 1969. p. 47.
- 12-V.V. KOVALSKI, in: Trace Elements in Medicine, Issue 6, Zdorovie, Kiev, 1975, p. 3.
- 13-N.G. ZYRIN, A.I. OBUKHOV, Spectrum Analysis of Soils, Plants and other Biological Objects, Moscow State University, Moscow, 1977.
- 14-S.K. PRASAD, Integrated Instrumental Analysis of the Environmental Objects, Ph.D. Thesis, Moscow, 1992.
- 15- V.V. SNAKIN, A.A. PRISYAZHNIKOVA, Sci. Total Environ., 256 (2000) 95.
- 16-S.I. TOMA, I.Z. RABINOVICH, S.G. VELIKSAR, Trace Elements and the Harvest, Shtiintsa, Kishinev, 1980.
- 17-H.J.M. BOWEN, Environmental Chemistry of the Elements, Academic Press, London, 1979.
- 18- A.M. URE, M.L. BERROW, Envir. Chem., 2 (1982) 94.
- THORNTON, in: Trace Elements in Environmental History, Springer-Verlag, Berlin, 1988, p. 135.
- 20- V.B. ILJIN, Heavy Metals in the Soil-plant System, Nauka, Novosibirsk, 1991.
- 21- Normative Documents on the Control of Heavy Metals in Soils, TSINAO, Moscow, 1995.

# NEUTRON ACTIVATION ANALYSIS OF TRACE ELEMENT CONTENTS IN THE CROWNS OF HUMAN PERMANENT TEETH

V. Zaichick

Medical Radiological Research Centre of RAMS, Koroleva str., 4, Obninsk, 249020, Russia, e-mail: yezai@obninsk.com

#### Introduction

The apatite phases of teeth can apparently be affected by trace element incorporation into teeth with effects on the physicochemical properties<sup>1-4</sup>. It is the reason why deficiency or excess of F, Sr, Mn, Fe and some other trace elements is one of the factors which determines the degree of susceptibility of caries and other dental diseases.<sup>5,6</sup> So, chemical element analysis of teeth expands the knowledge of etiology of dental diseases and may be apply for diagnostic, therapeutic and preventive purposes. Furthermore, teeth have been suggested as dose monitors for the exposure of human body to elements concentrated in calcified tissues.<sup>7,8</sup> In accordance with it teeth are used in an occupational medicine and environmental health studies.<sup>9-12</sup> Moreover, a chemical element analysis of human teeth are often used in paleoanthropology for dietary and environment reconstruction, assessment of the social and economic status of human groups.<sup>13-18</sup> It developed that for efficient application of teeth analysis in all above-mentioned directions it is necessary to know the normal levels and age-related changes of teeth trace elements in large scale.

There are several reviews and text in regard to trace elements of teeth, using chemical analysis techniques and instrumental methods. 1,2,5,19-22 However, the majority of these data are based upon non intact teeth but separated tissues of teeth such as enamel, dentin or cement. It was shown that samples are contaminated some trace elements from stainless steel tools during the separation. 23,24 In most cases, teeth samples are treated with solvents in order to remove organic matrix, and are then ashed and acid digested. There is evidence that by these methods some chemical elements are lost, their relationship also being affected. 25,26

In the present study the effect of age on Co, Eu, Fe, Hg, Sb, Sr, and Zn mass fraction in crown of permanent teeth were analyzed with two objectives. The first objective was to use intact teeth. The second objective was to perform measurements on crown – the only part of teeth available for *in vivo* examination.

### Experimental

Samples of human permanent teeth were obtained at postmortems, from intact cadavers (24 males, with ages from 16 to 55 years) within 24 hours of death. Each death had resulted from trauma, due to automobile accidents, falls, shootings, knifings, hanging, acute alcohol poisoning, and freezing. Mainly molars and premolars were extracted. The crowns contacted with the stainless steel surgical instruments were clean by the alcohol moist gauze tampons. A tool made of titanium was used to cut and to scrub soft tissue and blood off the

roots. After separating the crown from root with a titanium knife, samples were freeze dried until constant mass was obtained. The crowns were used in the study only.

To determine concentrations of the elements by a relative way, biological synthetic standards (BSS) prepared from phenol-formaldehyde resins in the Institute of Physics, Georgian Academy of Sciences specifically for INAA were used<sup>27</sup>. The BSS were 4 mm diameter tablets weighing about 30 mg. Corrected certified values of BSS element contents were reported by us before<sup>28</sup>. The tooth crown samples, ten CRM IAEA H-5 (Animal Bone) and SRM NIST 1486 (Bone Meal) subsamples weighing about 50-100 mg, together with SSB tablets were wrapped separately in a high-purity aluminum foil washed with rectified alcohol beforehand and put into a nitric acid-washed quartz ampoule. To arrange reference material samples and standards in the quartz ampoule, they were distributed among tooth crown samples along the whole ampoule length. This enabled correcting an influence of neutron flux non-uniformity in the reactor channel. The quartz ampoule was soldered, positioned in a transport aluminum container and exposed to 20-hour neutron irradiation in a vertical channel with neutron flux 1.7·10<sup>12</sup> n·cm<sup>2</sup>·s<sup>-1</sup>. Seven days after irradiation samples were reweighed and repacked.

The measurement of each sample was made twice, 7-10 and 40-60 days after irradiation. The second measurements started 40 days after irradiation due to the high intensity of  $^{32}P$   $\beta$ -particles ( $T_{1/2}$ =14.3 d). To reduce  $^{32}P$   $\beta$ -particles background, a combined lead-cadmium-copper-aluminum filter was used. The duration of the first and second measurements was 10 min and 10 hours, respectively. The gamma spectrometer included an HPGe detector (GEM 15180P, ORTEC, relative efficiency 15%) and a MAA combined with a PC (ASPRO-NUC) was used. The spectrometer provided resolution 1.8 keV on the  $^{60}Co$  1332 keV line. Processing of gamma spectra and computations of chemical element mass fractions in the examined samples were carried out using ASPRO software package<sup>29</sup>.

Irradiation, expose and measurement times as well as the sample-detector distance were regarded optimum in terms of providing feasibility of simultaneous measurement for the maximum number of elements with acceptable statistical error for each of them. A dedicated computer program of NAA mode optimization was used for preliminary estimation of these parameters<sup>30</sup>.

# Results

Radionuclides and some of their characteristics used for INAA of Ag, Ce, Co, Cr, Cs, Eu, Fe, Gd, Hf, Hg, Mo, Rb, Sb, Sc, Se, Sr, Ta, Tb, Th, Yb, Zn, and Zr contents in tooth crown and reference material samples are given in Table 1.

Table 2 shows our results for ten sub-samples of CRM IAEA H-5 Animal Bone and SRM NIST 1486 Bone Meal reference material and the certified values of this material.

Table 3 gives some statistical parameters of trace element contents in the intact tooth crown of healthy men such as arithmetic mean, standard deviation, standard error of mean, minimal and maximal values, median, percentiles with 0.025 and 0.975 levels.

Finally, Table 4 presents the comparison of our and reference data of trace element contents in human teeth.

Table 1. Nuclear reactions and some characteristics of radionuclides used for INAA of crowns of human permanent teeth

Element	Nuclear reaction	Radionuclide	Half-life	γ-energy used
	100			keV
Ag	<sup>109</sup> Ag (n, γ)	110mAg	250.0 d	658, 1384
As	' <sup>3</sup> As (n, γ)	′⁰As	1.12 d	559
Au	<sup>19</sup> 'Au (n, γ)	<sup>198</sup> Au	2.7 d	412
Ba	$^{130}$ Ba(n, $\gamma$ )	<sup>131</sup> Ba	11.52 d	216, 373, 496
Br	°'Br(n, γ)	82Br	1.47 d	698, 777, 1044
Cd	114Cd(n, γ)	115Cd	2.2 d	336
Ce	<sup>140</sup> Ce(n, γ)	<sup>141</sup> Ce	32.5 d	145
Co	<sup>3</sup> Co(n, γ)	°°Co	5.64 y	1173, 1332
Cr	<sup>30</sup> Cr(n, γ)	<sup>51</sup> Cr	27.8 d	320
Cs	133Cs(n, γ)	134Ce	2.05 y	796
Eu	<sup>131</sup> Eu(n, γ)	152Eu	13.6 y	1408
Fe	<sup>3°</sup> Fe(n, γ)	<sup>59</sup> Fe	45.6 d	1099, 1292
Gd	<sup>132</sup> Gd(n, γ)	<sup>151</sup> Gd	120 d	154
Hf	<sup>180</sup> Hf(n, γ)	<sup>181</sup> Hf	42.4 d	482
Hg	$^{202}$ Hg(n, $\gamma$ )	<sup>203</sup> Hσ	46.91 d	279
La	$^{139}La(n, \gamma)$	. <sup>140</sup> T.a	1.68 d	487, 816, 1595
Lu	'''Lu(n, γ)	17/ <b>T</b> 11	6.74 d	208
Nd	<sup>140</sup> Nd(n, γ)	14/Nd	11.02 d	91
Rb	δ <sup>5</sup> Rb(n, γ)	<sup>86</sup> Rh	18.66 d	1076
Sb	<sup>121</sup> Sb(n, γ)	<sup>122</sup> Sb	2.74 d	564
	<sup>123</sup> Sb(n, γ)	<sup>124</sup> Sh	60.9 d	1691
Sc	<sup>43</sup> Sc(n, γ)	<sup>46</sup> Sc	83.89 d	889, 1121
Se	′*Se(n, γ)	<sup>/5</sup> Se	120.4 d	136, 265, 401
Sm	$^{132}Sm(n, \gamma)$	153Sm	1.96 d	103
Sr.	°4Sr(n, γ)	∞Sr	64.8 d	514
Ta	'°'Τa(n, γ)	182Ta	115 d	1221
Tb	<sup>139</sup> Tb(n, γ)	100Th	72.3 d	879, 966
Th	<sup>232</sup> Th(n, γ)		27.0 d	312
U	<sup>230</sup> U(n, γ)	$^{239}U(\beta \rightarrow ^{239}Np)$	23.5 m (2.36 d)	228, 278
Yb	''*Yb(n, γ)	175Vh	4.19 d	396
Zn	$^{\circ 4}$ Zn(n, $\gamma$ )	vo/n	245.7 d	1115
Zr	<sup>94</sup> Zr(n, γ)	95Zr	65.5 d	724, 757

Table 2. INAA data of trace elements of CRM IAEA H-5 Animal Bone and SRM NIST 1486 Bone Meal (mg/kg on dry weight basis)

Element	nent CRM IAEA H-5		Own results	SRM NI	ST 1486	Own results
	Mean	Type*	Mean±S.D.	Mean	Type*	Mean±S.D.
Ag	-	-	< 0.02	-	-	< 0.02
As	0.013	N	< 0.1	0.006	N	< 0.1
Au	-	-	< 0.01	-	-	< 0.01
Ba	72±28	С	<100	-	-	270
Br	3.6	N	<10	-	-	<10
Cd	0.023	-	<2	0,003	N	<2
Ce	-	-	< 0.03	-	-	< 0.03
Co	0.25	N	0.56±0.25	-	-	$0.11\pm0.02$
Cr	2.56	N	<0.8	-	-	< 0.9
Cs	-	-	< 0.05	-	-	< 0.06
Eu	-	-	< 0.015	-	-	< 0.02
Fe	79±11	C	85±17	99±8	C	93±11
Gd	-	-	< 0.25	-	-	< 0.25
Hf	-	-	< 0.04	-	-	< 0.04
Hg	0.008	N	< 0.01	-	-	< 0.01
La	-	_	< 0.05	-	-	< 0.05
Lu	-	-	< 0.003	-	-	< 0.003
Nd	-	-	< 0.1	-	-	< 0.1
Rb	1.07	N	<1.0	-	-	< 0.9
Sb	0.024	N	<0,02	-	-	< 0.02
Sc	-	-	< 0.001	-	-	< 0.001
Se	0.054	N	< 0.05	0.13	N	< 0.05
Sm	-	-	< 0.01	-	-	< 0.01
Sr	96±17	С	103±9	264±7	С	263±10
Ta	-	-	< 0.08	-	-	< 0.08
Tb	-	-	< 0.005	-	-	< 0.006
Th	-	-	< 0.05	-	-	< 0.05
U	-	-	< 0.07	-	_	< 0.07
Yb	-	-	< 0.03	-	-	< 0.03
Zn	89±15	C	86±7	147±16	C	153±29
Zr	-	-	<0.2	_	-	<0.2

<sup>\* &</sup>quot;C" - certified values, "N" - non-certified values

Table 3. Some statistical parameters of trace element contents in the intact crowns of human permanent teeth of healthy men (mg/kg on dry weight basis)

Element	Mean	SD	SEM	Min	Max	Med	Per0.025	Per0.975
Ag	< 0.02	-	-	-	-	-	-	-
As	< 0.1	-	-	-	-	-	-	-
Au	< 0.01	-	-	-	-	-		-
Ba	<100	-	-	-	-	-	-	
Br	<10	-	-	-	-	-	-	•
Cd	<2	-	-	-	-	-	-	-
Ce	< 0.02	-	-	-	-	-	-	-
Co	0.0030	0.0032	0.0012	0.00045	0.0098	0.0021	0.00053	0.00882
Cr	< 0.3	-	-		-	-	-	-
Cs	< 0.02	-	-	< 0.002	0.056	-		-
Eu	0.00081	0,00056	0,00023	0,00030	0.00161	0,00057	0,00031	0,00158
Fe	4.67	3.13	1.10	2.43	11.1	3.72	2.43	10.4
Gd	<0.1	-	-	-	-	-	-	-
Hf	< 0.03	-	-	-	-	-	-	-
Hg	0.00053	0.00041	0.00020	0.00021	0.00113	0.00040	0.00022	0.00108
La	< 0.05	-	-	-	-	-	-	-
Lu	< 0.003	-	-	-	-	-	-	-
Nd	< 0.1	-	-	-	-	-	-	-
Rb	<0.6	-	-	-	-	-	-	-
Sb	0.022	0.011	0.007	0.012	0.035	0.020	0.012	0.034
Sc	< 0.0009	-	-	-	-	-	-	-
Se	< 0.04	-	-	-		-	-	-
Sm	< 0.01	-	-	-	-	-	-	-
Sr	198	200	40	31.7	860	108	38.5	746
Ta	< 0.007	-	-	-	-	-	-,	-
Tb	< 0.01	-	-	-	-	-	-	-
Th	< 0.05	-	-	-	-	-	-	-
U	< 0.07	-	-	-	-	-	-	-
Yb	< 0.03	-	-	-	-	-	-	-
Zn	136	50.2	11	42.6	285	136	60.4	246
Zr	<0.7	-	-		-	-	-	-

M -mean

SD - standard deviation

SEM - standard error of mean

min – minimal value

max - maximal value

Med - median

Per0,025 - percentile with 0,025 level

Per0,975 – percentile with 0,975 level

Table 4. Mean, range of means or upper level of chemical element contents (mg/kg on dry weight basis) in the enamel or dentin according to data from the literature in comparison with our data for crowns of human permanent teeth (superscripted number in the column headings designate reference number)

Element	Element From review of Cutress <sup>7</sup>		Our	Our review		
	Mean or rang	ge of means	Mean or ran	Mean or range of means		
	enamel	dentin	enamel	dentin	crown	
Ag, mg/kg	0.005-1.11	0.005-17	0.0049-10.9	0.004-2.18	< 0.02	
As, mg/kg	< 0.02-0.07	٠_	<0.007->10	11-111	< 0.1	
Au, μg/kg	0.0001 - 0.11	0.03-0.07	0.0001-0.11	< 0.0004-0.07	< 0.01	
Ba, mg/kg	2.1-125	129	2.1-125	129	<100	
Br, mg/kg	1.1-33.8	4-114	0.45->100	4-114	<10	
Cd, mg/kg	0.04-14.9	-	0.026-14.9	0.086-0.097	<2	
Ce, mg/kg	-	-	0.07	-	< 0.02	
Co, mg/kg	0.0002-34.3	0.0003-32	0.0002-37.3	0.00034-33	0.0030	
Cr, mg/kg	0.004-6.4	0.005-2.0	0.003-28	0.005-6.6	< 0.3	
Cs, mg/kg	0.04	-	0.04	-	< 0.02	
Eu, μg/kg	-	-	< 0.04	-	0.00081	
Fe, mg/kg	2.77-338	2.0-110	2.77-876	2.0-110	4,67	
Gd, mg/kg	-	-	< 0.08	-	<0.1	
Hf, mg/kg	-	-	< 0.08	-	<0:03	
Hg, mg/kg	<0.11-2.6	-	0.02-86	0.18-1.03	0.00053	
La, mg/kg	0.004-0.005	-	0.004-0.005	-	< 0.05	
Lu, mg/kg	-	-	< 0.02	_	< 0.003	
Nd, mg/kg	0.045-0.050	-	0.045-0.050	-	< 0.1	
Rb, mg/kg	0.41-73	6-69	0.39-73	5.6-69	<0.6	
Sb, mg/kg	0.001-0.96	0.7	0.012-1.0	0.1-2.7	0.022	
Sc, µg/kg	0.0007	-	0.0007-53	20-71	< 0.0009	
Se, mg/kg	0.01-1.47	0.3-0.5	0.004-14.5	0.07-4.9	< 0.04	
Sm, mg/kg	-	-	< 0.08	-	< 0.01	
Sr, mg/kg	76.2-286	64-570	14.5-610	64-256	198	
Ta, mg/kg	-		< 0.1	-	< 0.007	
Tb, mg/kg	< 0.005	-	< 0.005	-	< 0.01	
Th, mg/kg	-	-	-	-	< 0.05	
U, μg/kg	-	-	< 0.02-0.03	_	< 0.07	
Yb, mg/kg	< 0.01	-	< 0.01	-	<0.03	
Zn, mg/kg	126-740	160-2200	64-1670	148-1860	136	
Zr, mg/kg	0.08-1.8	-	0.07-175	-	<0.7	

#### Discussion

Of 6 (Ba, Br, Fe, Pb, Sr, Zn) and of 3 (Fe, Sr, Zn) trace elements with certified values for the CRM IAEA H-5 and the SRM NIST 1486 reference materials respectively, we determined contents of Fe, Sr, and Zn (Table 2). Mean values for these elements were in the range of 95% confidence interval. Mean values and 95% confidence intervals of Co, Cr, Hg, Rb, Sb, and Se were reported for CRM IAEA H-5, although those were not certified<sup>31</sup> (Table 2). Of these elements, a good agreement was obtained for Sb and Se. Mean contents obtained for Co, Cr, and Hg appeared to be considerably lower than the appropriate values of Parr's report<sup>31</sup>. Good agreement with the certified data of CRM IAEA H-5 and SRM NIST 1486 reference materials indicate an acceptable accuracy of the results obtained in the study of trace elements of the teeth as shown in Table 3.

The mean values and all selected statistical parameters were calculated for 7 (Co, Eu, Fe, Hg, Sb, Sr, and Zn) trace elements (Table 3). The contents of these trace elements were measured in all or majority part of teeth samples. The contents of Cs were determined in a few samples of collection only. The upper limit of mean for the elements was found as the normalized sum of all individual contents and detection limits. The contents of Ag, As, Au, Ba, Br, Cd, Ce, Cr, Gd, Hf, La, Lu, Nd, Rb, Sc, Se, Sm, Ta, Tb, Th, U, Yb, and Zr were lover of detection limits in all samples.

The obtained means for Co, Fe, Sb, Sr and Zn, as shown in Table 4, agree well with ranges of the mean values cited by other researches for teeth. <sup>1,2,5,19-22</sup> The Eu and Hg means are two orders of magnitude lower than range of previously reported data. The upper limit of mean for Ce, Cs, Hf, Lu, Sm, and Ta are some lower than of previously reported results (Table 4).

Statistically significant age difference is shown for none of the studied trace elements. It conforms well to the data by Little et al.<sup>32</sup> (Fe, Sr, Zn), Derise and Ritchey<sup>5</sup> (Fe), Nixon et al.<sup>33,34</sup> (Hg, Sb), Brudevold et al.<sup>35</sup> (Zn), and Steadman et al.<sup>36</sup> (Sr). On the contrary the negative Sr-, Zn- and positive Co-, Se-age correlation in teeth have been observed by Derise and Ritchey.<sup>5</sup>

Our data for Co, Eu, Fe, Hg, Sb, Sr, and Zn mass fractions in intact crown of permanent teeth may serve as indicative normal values for male residents of the Russian Central European region.

#### References

- 1- N. L. DERISE, S. J. RITCHEY, A. FURR, J. Dent. Res., 53 (1974) 847.
- 2- M. E. J. CURZON, T. W. CUTRESS (Eds.), Trace Elements and Dental Disease. PSG-John Wright, Boston, 1983.
- 3- M. KORAY, Y. ÖNER-IYIDOGAN, M. SOYMAN, F. GÜRDÖL, J. Trace Elements Med. Biol., 10 (1996) 255.
- 4- R. Z. LEGEROS, M. A. MIRAVITEI, G. B. QUIROLGICO, M. E. J. CURZON, in: Calcified Tissues 1976. Leeds, 1977, p. 362.
- 5- N. L. DERISE, S. J. RITCHEY, J. Dent. Res., 53 (1974) 853.
- 6-B. E. DAVIES, R. J. ANDERSON, Experimentia, 43 (1987) 87.
- 7- L. F. ALTSHULLER, D. B. HALAK, B. H. LANDING, A. R. KEHOE, J. Pediatr., 60 (1962) 224.

- 8- L. M. SHARON, Perspect. Biol. Med., 32 (1988) 124.
- 9-L. M. ALEXANDER, A. HEAVEN, H. T. DELVES, J. MORETON, M. J. TRENOUTH, Arch. Environ. Health, 48 (1993) 392.
- 10- M. BARANSKA-GADIOWSKA, M. KAMINSKI, K. OWCARCZAK, Z. KABZA, Czas. Stomatol., 41 (1988) 406.
- 11- K. BERCOVITZ, D. LAUFER, Archs. Oral. Biol., 35 (1990) 895.
- 12- P. BLOCHI, I.M. SHAPIRO, L. SOULE, A. CLOSEI, B. REVICH, Appl. Radiat. Isot., 49 (1998) 703.
- 13- A. ATTRAMADAL, J. JONSEN, Acta Odontol. Scand., 36 (1978) 97.
- 14- L. BALUSZYNSKA, K. SZOSTEK, E. HADUCH, in: 3rd International Symposium on Trace elements in human: New Perspectives. (Eds.: S. Ermidou-Pollet, S.Pollet). Athens, Greece, 2001, p.364.
- P. BUDD, J. MONTGOMERY, J. EVANS, M. TRICKETT, Sci. Total Environ., 318 (2004) 45.
- 16- E. GLEN-HADUCH, K. SZOSTEK, H. GLAB, J. Phys. Antropol., 103 (1997) 201.
- 17- P. GRANDJEAN, P. J. JORGENSEN, Environ. Res., 53 (1990) 6.
- 18- H. V. KUHNLEIN, D. M. CALLOWAY, Am. J. Clin. Nutr., 30 (1977) 883.
- 19- T. W. CUTRESS, in: Trace Elements and Dental Diseases (Eds.: M. E. Curson, T. W. Cutress). PSG-John Wright, Boston, 1983, p.33.
- T. MOLLESON, in: Trace Elements in Environmental History (Eds.: G. Grupe, B. Herrmann). Springer-Verlag, Berlin, 1988, p. 67.
- 21- G. S. NIXON, Caries Res., 3 (1969) 60.
- 22- N. D. PRIEST, F. L. VAN DE VYVER (Eds.), Trace metals and Fluoride in Bones and teeth. CRC Press, Boca Raton, Floride, 1990.
- 23- A. R. BRYNE, L. KOSTA, Sci. Total Environ., 10 (1978) 17.
- 24- G. S. NIXON, M. D. LIVINGSTON, H. SMITH, Arch. Oral Biol., 11 (1966) 247.
- 25- M. D. GRYNPAS, K. P. PRITZKER, R. G. V. HANCOCK, Biol. Trace Elem. Res. 13 (1987) 333.
- 26- V. ZAICHICK, Trace Elements in Medicine, 5 (2004) 17.
- 27- L. M. MOSULISHVILI, M. A. KOLOMI'TSEV, V. Yu. DUNDUA, N. I. SHONIA, O. A. DANILOVA, J. Radioanal. Chem., 26 (1975) 175.
- 28- V. ZAICHICK, Fresenius. J. Anal. Chem., 352 (1995) 219.
- 29- V. P. KOLOTOV, V. V. ATRASHKEVICH, J. Radioanal. Nucl. Chem. Articles, 193 (1995) 195.
- A. M. KORELO, V. ZAICHICK, in: Activation Analysis in Environment Protection, JINR, Dubna, 1993, p.326.
- 31- R. PARR, Inter-comparison of minor and trace elements in IAEA Animal Bone (H-5), Progress Report No.1, Vienna, 1982.
- 32- M. F. LITTLE., L. T. STEADMAN, Arch. Oral. Biol., 11 (1966) 273.
- 33- G. S. NIXON, G. D. PAXTON, H. SMITH, J. Dent. Res., 44 (1965) 654.
- 34- G. S. NIXON, M. D. LIVINGSTON, H. SMITH, Caries Res., 1 (1967) 327.
- 35- F. BRUDEVOLD, L. T. STEADMANN, M. A. SPINELLI, B. H. AMDUR, P. GRON, Archs. Oral Biol., 8 (1963) 135.
- 36- L. T. STEADMAN, F. BRUDEVOLD, F. A. SMITH, J. Am. Dent. Assoc., 57 (1958) 340.

# ROLE OF NUCLEAR ANALYTICAL METHODS IN THE ENVIRONMENTAL HEALTH ELEMENTOLOGY

V. Zaichick<sup>1</sup>, S. Ermidou-Pollet<sup>2</sup>, S. Pollet<sup>2</sup>

<sup>1</sup>Medical Radiological Research Center of Russian Academy of Medical Sciences, 249020 Obninsk, Kaluga Region, Russia, e-mail: vezai@obninsk.com

<sup>2</sup>Department of Biochemistry, Medical School, University of Athens, Greece

#### Introduction

Study of changes in the content of chemical elements in an organism at all levels of its organization in response to changes of environmental conditions and detection of the role of chemical elements in the etiology and pathogenesis of different diseases is one of the subjects of new scientific discipline – Medical Elementology (from Lat. "medicina" and "elementum"). <sup>1-6</sup> It is possible to call this part of Medical Elementology as the Environmental Health Elementology.

The science, by its definition, is a sphere of human activity whose functions include the development and theoretical ordering of objective knowledge about reality. The direct purposes of science are the description, explanation and prediction of processes and phenomena, which are the subject of its study, based on the laws discovered by the scientific process. As a rule, various scientific disciplines are characterized, first of all: 1 - by the subject of study and its corresponding name; 2 - by accepted postulates; 3 - by research methods; 4 - by methods of quality control and processing of the obtained information; 5 - by terms and definitions.

# Subject of study

What is the subject of the study of Medical Elementology? Tracing basic historical stages of the development of medicine, one can detect a clear regularity - from the whole to more and more detailed, originally primary, i.e. elementary components (organism  $\rightarrow$  systems, organs, tissues  $\rightarrow$  cells and subcellular structures  $\rightarrow$  biological molecules). The next step in the study of living organisms was investigation of the atomic level, or the level of chemical elements. From here it is possible to formulate the fundamental propositions about the subject matter of Medical Elementology.

1. Study of regularity of content and distribution of chemical elements in the human organism, its systems, organs, tissues, fluids, cells, subcellular structures and molecules under conditions of permanent contact and exchange with the environment, with regard to gender, race, nationality, physiological rhythms, profession, social status, household traditions and harmful habits of the individual;

- 2. Determination of the role and the degree of chemical element participation in the normal structure and function of an organism at all levels of its organization during conception, formation, maturity and ageing, in conditions of permanent contact and exchange with the environment:
- 3. Study of changes in the content of chemical elements in an organism at all levels of its organization in response to changes of environmental conditions, or to extreme loads or external influences, as well as in various pathological conditions;
- 4. Detection of the role of chemical elements in the etiology and pathogenesis of different diseases as well as the efficacy of using chemical elements for corrections of dysfunctions and treatment.

It follows from this, probably not quite full, definition of the research aims, that the basic objects of study in the new scientific discipline are chemical elements and human organism condition that exist in continuous and intimate contact with the environment. From here it follows that the name of this new scientific field - "Medical Elementology" is quite relevant.

# Postulates of Medical Elementology

Collected knowledge allows the basic postulates of Medical and Biological Elementology to be formulated. The following six postulates are offered for discussion and acceptance.

- 1. Presence of chemical elements. The Biosphere, including all separated habitats, contains all the natural chemical elements have been found on the Earth (at present 90 of 109 known elements, the remaining 19 being human made). All living organisms, including humans, continuously absorb from the environment some portions and species of the medium from which they derive products necessary for their life. From this it follows that organism's tissues and fluids contain all the chemical elements available on the Earth.
- 2. Differential homeostasis. In all living organisms, including humans, differential homeostasis of chemical elements is carried out, i.e. at all levels of their organization (the internal environs, organs, tissues, cells, etc.) the content of chemical elements is maintained at certain levels. These levels can change with age and under the influence of various exogenous and endogenous factors, within, however, the certain ranges and limits. Differential homeostasis is a cause of irregularity in distribution and of difference in exchange velocity of chemical elements in organs, tissues, fluids and other structural formations of the organism.
- 3. Chemical element involvement. The processes of phylogenesis and ontogenesis began and continue under the conditions of permanent contact of living organisms with the chemical elements of their inhabitancies. Therefore none of the Earth's chemical elements can be considered as indifferent or insignificant for an organism and to be defined as an alien, or xenobiotic (from Greek: "xenos" foreign, "biotos" life).
- 4. Usefulness (essentiality, benefit) of chemical elements.

  How many of the 90 naturally occurring elements are essential to life? This question has a long story no less, at least, than from 1713 year (detection of Fe in blood) up to nowadays. After almost three centuries of increasingly refined investigation, the question still can't be answered

with certainty. A lot of the criteria for essentiality were proposed by various authors – from very hard to very formal.

In the strictest sense a chemical element can be classified as essential if its absence in an organism is incompatible with life. This criterion, although logically correct, is too restrictive because it is impossible to induce true "zero" concentrations in any system. So-called "zero" concentration depends on the analytical capabilities and it changes with time. It is very hard criterion and its application would hinder rather than advance element's essentiality research. Avogadro number is  $6.02 \cdot 10^{23}$  atoms in 1 mole of substance. The best detection limit of the contemporary analytical methods for chemical element contents in biological substances is on the level between  $10^{-12} - 10^{-14}$ . So, it means that in 1 mole of all biological substances no less than  $10^9 - 10^{11}$  atoms are out of our control. It is quite enough if remember that biological reactions may be very sensitive.

More realizable in experimental practice the criteria for essentiality include the postulate that withdrawal of an essential elements from the body must induce reproducibly the same structural abnormalities and impairment of the biological functions, regardless of species studied and that this abnormalities must be always accompanied by pertinent specific biochemical changes, reversible or preventable by supplementation. Such kind of criteria is some softer but the definition of "impairment of a biological function" is left rather vague. Also undefined is the nature of the biological function that might be impaired in a deficiency. Therefore almost any function is acceptable including behavioral functions.

Schroeder<sup>7</sup> has proposed definition of essentiality that is based mainly on occurrence and metabolism, but not on function. It is very formal criteria. But the absolutely formal criteria has been created by Liebscher and Smith.<sup>8</sup> They postulated that essential chemical elements in a population study of its contents in tissues and fluids should exhibid a "normal" distribution curve, while nonessential elements should have a "log-normal" distribution. It is interest to mark that as an example of nonessential elements they used "log-normal" distribution of As.

As usual at present researches of essentiality of chemical elements use the combinations of a few requirements. The next list of requirements for essentiality is generally accepted9:

- The organism can neither grow nor complete its life cycle in the absence of the element.
- The element cannot be replaced completely by any other element.
- The given element has direct influence on the organism and is involved in its metabolism.
- The element is present in tissues of different animals at comparable concentrations.
- Its withdrawal produces similar physiological or structural abnormalities regardless of species.
- Its presence reverses or prevents those abnormalities. These abnormalities are accompanied by specific biochemical changes that can be remedied or prevented when the deficiency is checked.

This list includes almost all uncertainties that were considered above.

The great previous experience shows that it is impossible to give strict definition of essentiality useful in the experimental study. The irremovable uncertainties of definition are the reason why the determination of essential or non-essential characters of some chemical elements constitutes a field of intense discussions. <sup>10</sup> It is clear that question will be closed with the

understanding of the mechanism of chemical element action on the physiological, biochemical and chemical levels.

There is the other point of view on subject of trace element essentiality. The huge variety and specificity of biochemical reactions occurring in living organisms allow us to assume that Nature in its Majesty used all available means for their implementation, including the whole set of chemical elements. Such characteristics as "useful" or "useless" for this or that chemical element are determined only by the extent of our knowledge about the degree of its involvement in biochemical processes. We witness how new gained knowledge constantly extends the number of biologically "useful" chemical elements (Fig. 1). With such tendency in 50-70 years all 90 naturally occurring elements will be recognised as essential.

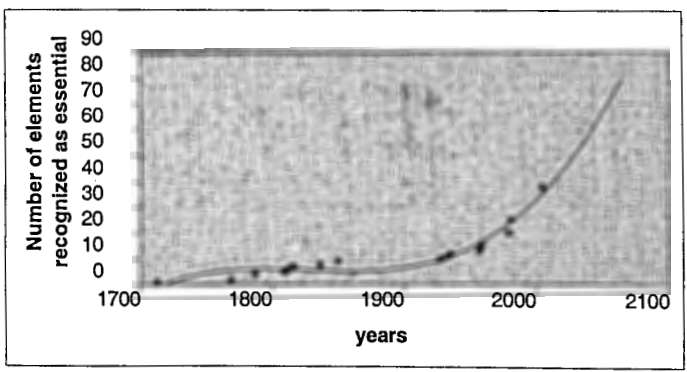


Fig. 1. Discovery of chemical elements requirements for the living organisms. The data of reviews Schwarz<sup>11</sup>, Todhunter<sup>12</sup>, Egger et al. <sup>13</sup>, Mertz<sup>14,15</sup>, Anke<sup>16</sup> were used.

5. Harmfulness (toxicity, harm impact) of chemical elements. Useful (essential) or harmful (toxic) action of a chemical element is determined only by the amount of its content in an organism. Paracelsus was right (Paracelsus, the real name is Philippus Theophrastus Bombastus von Hohenheim, 1493-1541), when he concluded, that nothing in nature is a poison - any natural substance is turned into poison only by its dose (quantity). Figs. 2a and 2b illustrate this postulate.

6. Combinatorial (collective, mutual) impact of chemical elements. As well as in absolute amounts, the recombination of chemical elements in their common summation has an important influence on an organism's condition. It is associated with a synergistic, antagonistic or indifferent interactions of many chemical elements. Mosaic combinations of chemical element content are formed by specific combinations of exogenous (biogeochemical peculiarities of environment, ethnic preferences in foods and so on) and endogenous (genetic heredity, acquired diseases etc.) factors.

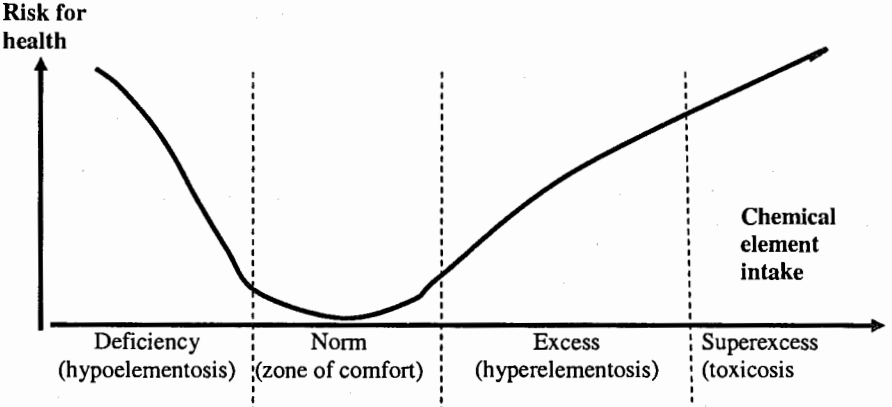


Fig. 2a. This figure illustrates the sense of this postulate. The curve of conventional risk for health versus chemical element intake has at least 4 zones: deficiency (hypoelementosis), norm (zone of comfort), excess (hyperelementosis), and superexcess (toxicosis). The minimum of the curve indicates the range where an organism enjoys its best conditions (zone of comfort).

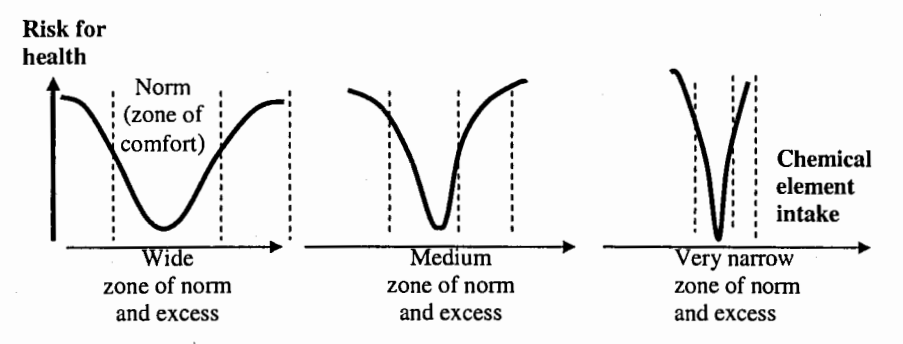


Fig. 2b. The minimum of the curve of conventional risk for health indicates the range where an organism enjoys its best conditions (zone of comfort). The wider this range the less likely it will be disturbed by an external influence. It is clear from this why there is an historical definition of some chemical elements as toxic. These elements are characterized by very narrow zones of "norm" and "excess" and, therefore it is easy to pass from the zone of comfort to the zone of toxicity.

#### Research methods

The basic information unit in Medical and Biological Elementology is the quantitatively expressed content of a chemical element in a studied biological object. The presence of chemical elements is inherent for all objects, alive or lifeless, and hence it is not specific for living organisms only. Only their quantity, ratios and nature of changes in levels of content during their development and existence can be specific. However only in the last decades of the 20<sup>th</sup> century there appeared really quantitative and metrologically sound (quality assured) methods for analysis of chemical elements in biological objects which allowed to start studying the content of a large number of chemical elements in the human organism, practically at all levels of its organization. Among these methods, it is necessary first to mention spectral methods such as atomic absorption spectrophotometry (AAS), inductively coupled plasma atomic emission spectrometry (ICPES) and inductively coupled plasma mass spectrometry (ICPMS), and nuclearphysical methods - neutron activation analysis (NAA), X-ray fluorescent analysis (XRF), proton induced X-ray emission (PIXE), proton induced gamma emission (PIGE), synchrotron radiation induced X-ray fluorescent (SRXRF). Their combination in an instrumental variant (without preliminary concentration or separation) allows the determination of up to 60 or more chemical elements that present in biological samples.

Application of nuclear-physical methods not only expands the number of chemical elements accessible to estimation, but also opens additional unique opportunities to study biological objects. These methods do not demand destruction and utilization of a sample. They also avoid the possibility of additional introduction of chemical elements into the sample or losses of chemical elements during the sample preparation. These features make nuclear-physical methods among the most reliable ones and give them the referent status. Besides that, as the sample remains intact, nuclear-physical methods can be successfully combined with other analytical methods. Besides estimation of total quantities of chemical elements, such nuclearphysical methods as electron probe X-ray fluorescent microanalysis (EPXRMA), proton induced X-ray emission (PIXE) and ion probe microscopy based on secondary ion mass spectrometry (SIMS) also provide the capability to investigate chemical elements' distribution by their morphological structures. The absolute prerogative of nuclear-physical methods is the possibility of measuring the content of some chemical elements in the human organism in vivo. Current developments in neutron activation and X-ray fluorescent analysis already allow the content of elements such as H, C, N, O, Na, P, Cl, K, Ca, Zn, Sr, Cd, I, Pb to be determined in vivo, either in the whole body, or in certain organs and tissues. There are theoretical and technological preconditions for significant expansion of in vivo methods in the near future.

Any additional methods of analysis should necessarily be combined with the basic methods for research carried out in the field of Medical and Biological Elementology. As additional methods it is possible to list/include: all existing inorganic, biological and bioinorganic chemistry methods of separation and identification of various biosubstrates and macromolecules; all epidemiological, physiological and clinical methods of estimation of health state both for a population as a whole and also at the level of an individual organism, its organs, systems, tissues, cells and subcellular structures; all fundamental experimental and ecological methods used for investigation of biota - animals (mostly mammalians), plants, micro-organisms, bacteria etc.

# The quality control methods and processing of the acquired information

The definition of a science underlines the necessity of obtaining an objective knowledge. The criterion of knowledge objectivity is fine reproducibility of research results. In analytical chemistry a special system of measures of analytical quality control was developed to guarantee required reproducibility of results. This complex provides regular intra-laboratory monitoring of quality and inter-laboratory or external control, as well as the obligatory usage of national or international standard or certified reference materials (SRM or CRM). Unfortunately, the necessity of carrying out these actions in the field of Medical and Biological Elementology is not always carried out in practice.<sup>3,5</sup>

This conclusion is well-illustrated by the following historical example. In the late 1970s/early1980s the IAEA, concerned by poor reproducibility of chemical element analysis in biological samples, decided to develop a number of actions for assessing measurement quality including the development of standard reference materials (SRM) from natural biological substances. For this purpose large amount of certain biological materials (for example, human hair, animal blood and tissues, etc.) were dried, homogenized, packaged, and sent to key analytical laboratories of the world for the quantitative analysis of chemical element content. Analyses of the same element from the same biological sample, received from various laboratories differed by many mathematical orders. 17-19 Such divergence of results testified to the extremely pitiable condition of analytical practice and stimulated many countries to establish national and international centres especially aimed at developing a wide nomenclature of standard reference samples, including biological ones; and to providing different analytical laboratories with these reference materials. Therefore, to guarantee reproducibility of results obtained by different laboratories and to ensure valid comparison of data, it is necessary for the investigational practice of Medical and Biological Elementology for laboratories to make obligatory monitoring of the quality of analytical results.

Another difficulty in obtaining objective knowledge in medical elementology concerns the dependence of chemical element content of biological objects on many exogenous (environment) and endogenous (health condition, age, gender, physiological rhythms, nationality, individual habits etc.) factors. A review of the literature on the chemical element content of the hair and blood of healthy humans clearly demonstrates how strong an influence these factors can have.<sup>3,5</sup>

A failure to account for the main exogenous and endogenous factors, together with low analytical quality, generates data with a high dispersion of values that hampers objective estimation and practical application of measured information. In order always to allow for the influence of the main factors and, as far as possible, to account for the role of numerous secondary influences, it will be necessary to adopt the following measures:

- i) to regulate methodological approaches to planning full-scale and experimental research, depending on their scales, aims and tasks,
- ii) to unify methods of obtaining, storaging and preparating samples of each kind of biological object, having rejected the old technological methods, inevitably leading to distortion of results in estimating content of chemical elements.

#### Definitions and terms

Many terms, historically existing in various scientific disciplines and used in medical elementology, have no exact definitions or are generally wrong or unhelpful:

- 1) Examples of terms not having exact definitions macro-, micro- and ultramicroelements, trace elements, traces, biological elements, biotics, atomovites, heavy metals, metals of life, essential elements, toxic elements.
- 2) <u>Examples of wrong terms</u> biogenic elements, mineral elements, xenobiotic elements, and essential heavy metals.
- 3) Examples of wrongly used terms, i.e. the terms having strict definitions, but occupied in other scientific disciplines minerals, bioindicators, biomonitoring.

Therefore it is necessary to conduct a revision of the terms in use and to remove all ambiguous and incorrect definitions. <sup>1.3,5</sup> It is also necessary to give precise formulations to all basic concepts.

#### References

- 1. V. ZAICHICK, N.A.AGADZHANJAN, Vestnik vosstanovitelnoi medicini, 9 (2004) 19.
- V. ZAICHICK, Sophie ERMIDOU-POLLET, S. POLLET, Proceedings Book of the 5<sup>th</sup> International Symposium on Trace Elements in Human: New Perspectives. Athens, 2005, p. 24.
- 3. V. ZAICHICK, Radioanal. Nucl. Chem., 269 (2006) 303.
- V. ZAICHICK, Sophie ERMIDOU-POLLET, S. POLLET, Trace Elements and Electrolytes, 24 (2007) 69.
- 5. V. ZAICHICK, Rima NAGINIENE, Metals in the Environment, Vilnus, 2007, p. 116.
- V. ZAICHICK, Trace Element Speciation in Biomedical, Nutritional and Environmental Sciences, Helmholtz Zentrum München, Neuherberg, 2008, p. 58
- H.A. SCHROEDER, J.J. BALASSA, J. Chronic. Dis., 19 (1966) 573.
- 8. K. LIEBSCHER, H. SMITH, ARCH. ENVIRON. HEALTH., 17 (1968) 882.
- 9. C.T. HOROWITZ, J. Trace Elem. Elect. Health Dis., 32 (1988) 135.
- Sophie ERMIDOU-POLLET, S. POLLET, Proceedings Book of the 2<sup>nd</sup> International Symposium on Trace Elements in Human: New Perspectives. Athens, 1999, p. 609.
- K. SCHWARZ, Nuclear Activation Techniques in the Life Sciences. Vienna, IAEA, 1972, p. 3.
- 12. E.N. TODHUNTER, Nutrition Reviews. 34 (1976) 353.
- 13. V.E. EGGER, D. MEISSNIR, L.H. SCHMIDI, E. GLAIZII, Zbl. Pharm., 17 (1978) 680.
- 14. W. MERTZ, Biol. Trace Elem. Res. 1 (1979) 259.
- 15. W. MERTZ, Science, 213 (1981) 1332.
- Anke M.K. Elements and their Compounds in the Environment. 2-nd Eddition. Weinheim: WILEY-VCH Verlag GmbH&Co.KgaA, 2004, p. 305.
- 17. R. PARR, Report No 2, IAEA, Vienna, 1980.
- 18. S.B. M'BAKU, R. PARR, J. Radioanal. Chem., 69 (1982) 171.
- 19. R. PARR, Progress Report No 1, IAEA, Vienna, 1982.

# SYMMETRIES AND SPIN-ANGULAR CORRELATIONS IN NEUTRON INDUCED REACTIONS: ELASTIC. RADIATIVE AND FISSION CHANNELS

Barabanov A.L.

Kurchatov Institute, Moscow 123182, Russia

#### Abstract

This is a review of the most important results and new proposals on study of spin-angular correlations in the interaction of slow neutrons with medium and heavy nuclei. Special attention is given to spin-angular correlations sensitive to violations of fundamental symmetries - spatial parity and time reversal invariance. Other nuclear characteristics that may be obtained in measurements of spin-angular correlations are also discussed.

## 1. Introduction

Spin-angular correlations in neutron induced reactions arise due to interference of partial waves (carriers of definite angular momenta) and are sensitive to any mechanisms influencing these waves. Therefore from the beginning of 1950th years spin-angular correlations are actively used as a tool of studying those terms in Hamiltonians of strong, weak and electromagnetic interactions which depend on angular momenta (spins). In particular, forces breaking fundamental symmetries, spatial parity (P) and time reversal invariance (T), are of this type.

However, each of reactions, (n,n),  $(n,\gamma)$  and (n,f), initiated by neutrons, has special features. The purpose of the report is to present the current situation with measurement of different spin-angular correlations in neutron reactions and to discuss their importance.

The report is devoted mainly to the interaction of slow neutrons (s-, p- and d-waves) with medium and heavy nuclei. Thus there are three types of processes in the interaction of slow neutrons with nuclei: elastic scattering, capture with emission of  $\gamma$  quantum (radiative capture) and fission (if target nuclei are heavy enough). Besides it is possible to study a total cross section by neutron transmission through the target. According to the optical theorem the total cross section is determined by the amplitude of elastic scattering on the zero angle. Therefore all the effects connected with transmission are actually determined by the elastic channel.

All four possible channels of neutron-nucleus interaction are listed in Figure 1.

# 2. What there is spin-angular correlation?

Let us address to Figure 1 to explain what spin-angular correlation means. In an entrance channel of nuclear reaction there are two colliding particles (for example, a neutron and a nucleus), each of which, generally speaking, has a spin - s and I. The momentum k the incident particle is represented also.

# Channels:

Total cross section (elastic due to optical

theorem): n + N

• Elastic scattering:  $n + N \rightarrow n + N$ 

Radiative capture: n + N → γ + N' (+ γ')

• Fission:  $n + N \rightarrow N_1 + N_2 (+ N_3)$ 

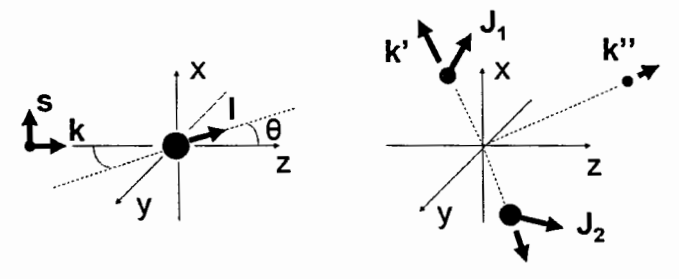


Figure 1

In an exit channel there are at least two particles ( $\mathbf{k}'$  is their relative momentum) which fly away from one another. For example, it can be the elastic scattered neutron and recoil nucleus. Or the  $\gamma$  quantum and recoil nucleus; the nucleus, being in an excited state, can emit a second  $\gamma$  quantum represented in the Figure 1 as a third particle in the exit channel (with the momentum  $\mathbf{k}''$ ). Two particles in the exit channel can be also two fragments from nuclear fission, while the third particle can be  $\alpha$  particle in ternary fission, or  $\gamma$  quantum emitted by one of the fragments. Besides the momenta, the particles in the exit channel possess, generally speaking, the spins -  $\mathbf{J}_1$  and  $\mathbf{J}_2$  (the spin of the third particle is not represented to simplify the Figure).

Thus, it is possible to put the question, what is the probability of the process at which spins and momenta of colliding and formed particles have the certain directions. Calculation of such probability is calculation of the spin-angular correlation.

One should note, however, that the arrows representing momenta of the particles in the Figure 1, really are showing the momenta, because the momentum direction can be fixed exactly. At the same time the direction of a particle spin cannot be fixed, because only one projection of the spin (on an axis of quantization) is defined. Therefore the arrows representing the spins, in fact are showing the axes of orientation of particle spins. For simplicity, however, we will name the directions of axes of spin orientation the spin directions.

# Simplest spin-angular correlation: angular distribution of γ quanta

$$\begin{array}{c|c}
 & z \\
M & p_{\gamma} \\
\theta & p_{\gamma} \\
\hline
 & \gamma \text{ quantum}
\end{array}$$

$$\begin{array}{c|c}
 & J M \\
\hline
 & Y \\
\hline
 & J_f M_f$$

$$d w (\theta) \sim \sum_{M_f} |\langle J_f M_f | \hat{V} | J M \rangle|^2 \sim a + b \cos^2 \theta + \dots$$

Figure 2

As an example of the simplest spin-angular correlation, let us consider the angular distribution of  $\gamma$  quanta that are emitted by a quantum system (by atom or nucleus) in a transition  $|J\rangle \to |J_f\rangle$  (see Figure 2). Orientation of spin J with respect to an axis z is determined by a distribution over projections M of the spin on the axis. Let the initial projection M be fixed, while a final projection  $M_f$  is out of interest. Then, as shown in Figure 2, summation over  $M_f$  should be performed at the calculation of the angular distribution dw(0). Generally, the additional summation over M is needed with the weights describing the initial distribution over M. In any case the angle  $\theta$  is the angle between the momentum  $p_\gamma$  of  $\gamma$  quantum and the axis z of spin orientation.

If parity is conserved, only even degrees of  $\cos \theta$  enter into the angular distribution (as shown in Figure 2). Parity violation was just found in 1957 as a

contribution of linear term ( $\sim \cos \theta$ ) into the angular distribution of electrons with respect to polarized spins of  $\beta$  decaying nuclei  $^{60}$ Co [1].

Thus, the orientation of spin J of a particle with respect to the fixed axis z is determined by the distribution over projection M of the spin on the axis. Two typical situations are shown in Figure 3: polarization and alignment. Ensemble of particles is named polarized along the axis z if the population  $n_M$  of substate with the projection M of the spin on this axis monotonously grows with an increase of M. On the other hand, pure alignment takes place when there is the equality:  $n_M = n_M$ . The parameters describing polarization,  $p_1(J)$ , and alignment,  $p_2(J)$ , are expressed via the first and second moments,  $\langle M \rangle$  and  $\langle M^2 \rangle$ , of the distribution  $n_M$ , as shown in Figure 3. Higher moments, as a rule, have no practical value.

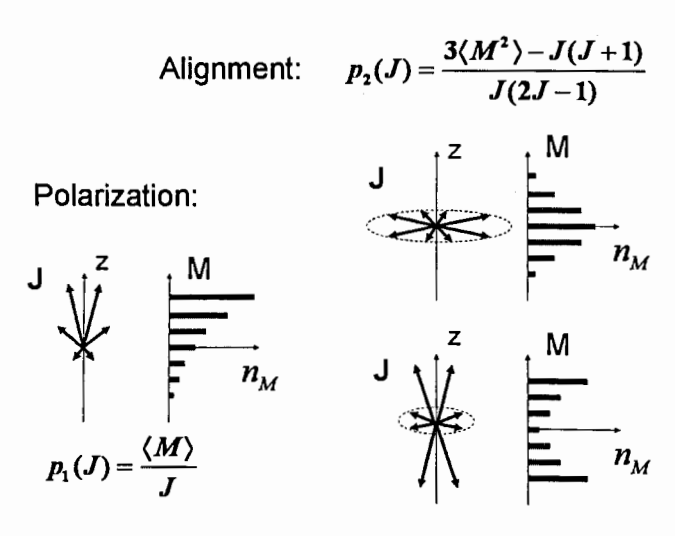


Figure 3

Of course, in the real experiment it is difficult to fix at once directions of many vectors. As a rule, the directions of only two vectors are fixed (herewith explicit or implicit summation over directions of all other vectors is performed). If one of these vectors is the momentum of a particle in the exit channel (with respect to some other vector) one says not about spin-angular correlation but, simply, about angular distribution. Correlations of three vectors are studied in the most advanced experiments.

Combination of these vectors may be rather unexpected. For example, last decade a T odd correlation of three vectors in ternary fission was actively discussed. These vectors are spin of the incident neutron, momentum of the light fragment and momentum of the  $\alpha$  particle (or, generally, third particle in the fission). This correlation will be discussed in the end of the report.

# 3. Fundamental symmetries and spin-angular correlations

Let us pass now to the main question - why studying of spin-angular correlations is of interest? Let us address to Figure 4. Obviously, the spin-angular correlations is a natural tool of studying of any characteristics related to spins. The simplest point is measurement of spins and parities of quantum levels or spin dependence of level density. Some similar things will be discussed later. The other clear point is study of spin dependent forces, such as spin-spin, spin-orbital and tensor interactions. So, in particular, the model explaining the T odd correlation in ternary fission by specific spin-orbital forces in the exit channel is described in Section 8.

# Goal: spin-angular correlations is a tool of studying of any characteristics related to spins

- · Spins and parities of levels, level density...
- · Interactions: spin-spin, spin-orbit, tensor...
- Fundamental symmetries: P (after 1956) and T (mainly after 1964):

Parity Violating (PV),  $\sim \sigma p$ ,  $\pi$ -,  $\rho$ -,  $\omega$ -mesons Time Violating Parity Violating (TVPV),  $\sim \sigma r$ ,  $\pi$ -mesons Time Violating Parity Conserving (TVPC),  $\sim rp$ ,  $\rho$ -mesons

# Figure 4

However, the sensitivity of spin-angular correlations to violation of fundamental symmetries – spatial parity (P) and time reversal invariance (T) - are of principal interest. The existence of such sensitivity is clear because the forces breaking fundamental symmetries depend somehow on spins (on angular momenta).

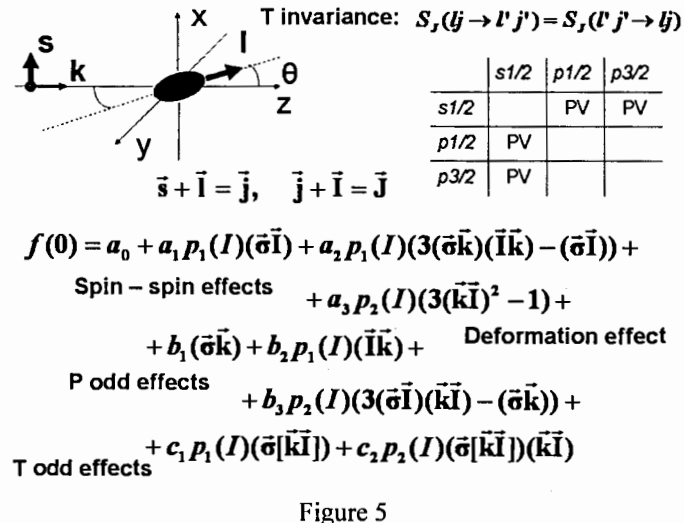
In fact, as it was told above, P invariance violation has been established in 1957 just by means of the elementary P odd correlation of spin and momentum in  $\beta$  decay. After 1964, when CP violation was found [2], searches of T non-

invariant spin-angular correlations in nuclear reactions and decays have begun. These searches had no success till now, probably, simply because accuracy of the experiments was not sufficiently high.

Thus, nothing definite is known so far about forces breaking T invariance. Therefore two possibilities should be considered. If T non-invariant forces violate parity, they are TVPV interactions (T Violating P Violating). Or, on the contrary, they keep parity, and their name is TVPC interactions (T Violating P Conserving).

# 4. Spin-angular correlations in the total cross section

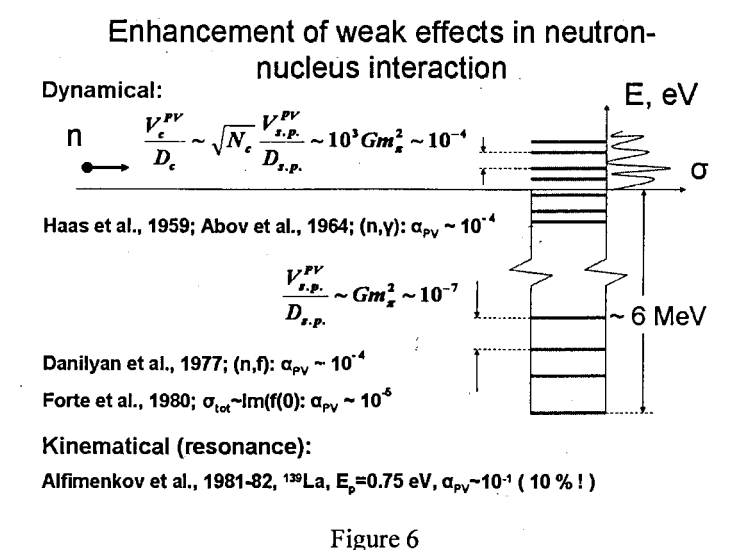
We address to the amplitude of elastic scattering of neutron by nucleus on the zero angle - f(0). There are only three vectors in our disposal - spin s and momentum k of the incident neutron and spin I of the target nucleus. Assuming. that velocities are small (thus, only s- and p-waves participate), and that the neutrons are polarized, while the nuclei are both polarized and aligned, we receive the required amplitude presented in Figure 5.



I shall note at once, that the full structure (eight spin-angular correlations) has been written out only in the middle of 1980th years (see, e.g., [3, 4] and references therein). I shall notice, that the terms with factors "a" are caused by

spin-spin and tensor forces, terms with factors "b" are due to parity violating (PV) forces whereas two last terms with factors "c" - 3-fold and 5-fold correlations - are non-zero, only if there is a violation of S matrix symmetry with respect to the main diagonal, that means the T violation.

I'd like to draw the attention to the fact that up to now from the specified eight correlations only two were investigated in the interaction of slow neutrons with nuclei. They are, first, spin-spin correlation, (sI), that is of great practical importance (it is used for polarization of neutrons by their transmission through polarized targets - see, e.g., [5]) and, secondly, the simplest P odd correlation of neutron spin and momentum, (sk). Discovery [6] of this P odd correlation in the beginning of 1980th years or, more accurately, the fact of its large enhancement, have stimulated revealing of all other terms in the amplitude of elastic scattering on the zero angle.



Let us stop in more detail on the enhancement. Some explanations are given in Figure 6. Neutron resonances are highly excited nuclear states. Distances between them are of the order of 10 eV that is much less than a typical distance (~1 MeV) between low lying states of nuclear spectrum. Therefore, if a mixing of the low lying states by PV forces is of the order of 10<sup>-7</sup>, then the same mixing of neutron resonances may be much larger. Explicit expression for the

corresponding enhancement factor of the scale of 10<sup>3</sup> that is named dynamical, is presented in Figure 6 (see, e.g., [7, 8]).

Dynamical enhancement has been predicted in [9], and then confirmed in the beginning of 1960th years in radiative capture of neutrons [10]. Later the similar enhancement was found for the P odd effects in nuclear fission [11] and in the elastic channel [6]. All these measurements were performed for thermal neutrons.

But in the same time, in the beginning of 1980th years, it has been realized [12, 13], that it is possible to receive an additional kinematical (or resonance) enhancement on 3 orders of magnitude in p-wave resonances. Then it has been checked up (and confirmed) in Dubna for <sup>139</sup>La nucleus [14]; in 1990th years the similar P odd effects at the level of 10 % have been found for <sup>232</sup>Th nucleus in Los Alamos [15].

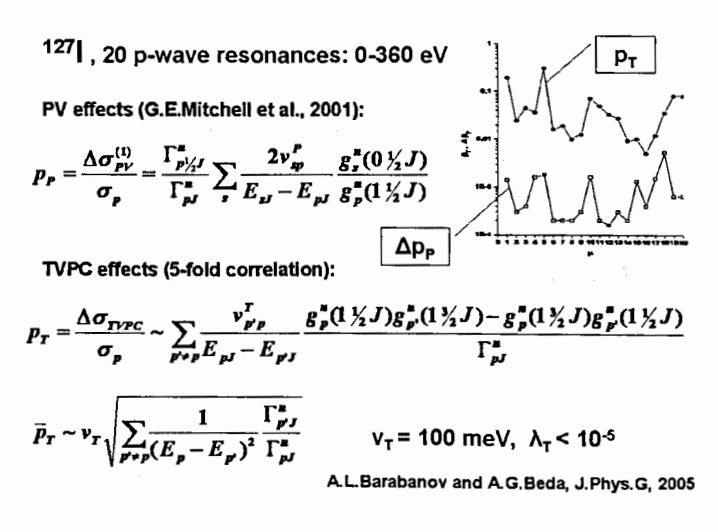


Figure 7

Later it has been shown [16, 17] that the same factors of enhancement -dynamical and kinematical (resonance) - should exist for T non-invariant effects in p-wave resonances. Thus, searching TV forces by means of measurement of 3-fold, (s[kI]), and 5-fold, (s[kI])(kI), correlations in the amplitude of elastic scattering on the zero angle is of great perspective. Notice that the 3-fold correlation is P odd, therefore it is sensitive to hypothetical TVPV forces. At the

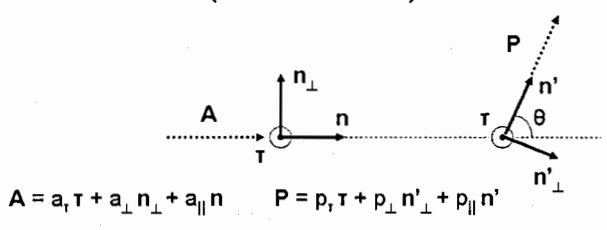
same time the 5-fold correlation is P even, thus its measurement is a way to search for TVPC interactions.

Recently we have pointed out [18] the new opportunities for searching TVPC forces in the interaction of polarized neutrons with aligned nuclei <sup>127</sup>I. In Figure 7 the expression is presented that defines the asymmetry p<sub>T</sub> of the total cross section caused by 5-fold correlation. We have estimated this asymmetry in the assumption that the characteristic matrix element v<sub>T</sub> of p-wave resonance mixing by hypothetical TVPC forces is equal to 100 meV that is approximately one order of magnitude lower than the current direct limit on this matrix element. In Figure 7 the results for p<sub>T</sub> are presented for 20 p-wave resonances of <sup>127</sup>I nucleus found in Los Alamos at P odd effects study.

P odd effects  $p_P$  surpassing statistical errors  $\Delta p_P$  were found only in some of these p-wave resonances. However, due to similarity of proposed experiment (searching for TVPC effects) and performed experiment (investigation of PV effects), it is natural to expect that statistical errors of both measurements (proposed and performed) would be approximately identical in any p-wave resonance. Thus, comparison of the expected TVPC effects  $p_T$  and the measured statistical errors  $\Delta p_P$  is done in Figure 7. It is seen that the proposed experiment will allow to improve at least by one order of magnitude the existing limitation on TVPC forces (at the best it will allow to discover TVPC forces).

Searching for TVPV forces in elastic scattering (including coherent) of polarized neutrons on non-oriented nuclei

(P - A theorem)



T invariance:  $p_1 = a_1$ ,  $p_{\perp} = a_{\perp}$   $p_{||} = a_{||}$ 

A.L.Barabanov and V.R.Skoy, Nucl. Phys. A, 1998

Figure 8

# 5. Spin-angular correlations in elastic scattering

One of the consequences of T invariance is the P-A theorem for elastic scattering that relates vectors of polarization **P** and asymmetry **A** (analyzing power). If T invariance holds, then the equalities exist between components of the specified vectors. These equalities are presented in Figure 8 (see, e.g., [19] and references therein). Thus, check of these relations is the test of T invariance.

One can show that the check of the equalities will testify the presence of TVPV forces if the components considered lay in a plane of reaction (in a plane of Figure). In this sense such test is similar to the search of 3-fold correlation in the total cross section. However, polarization of the target nuclei is needed for measurement of 3-fold correlation, while the check of the P-A theorem can be performed without nuclear polarization.

Searching for TVPV forces in elastic scattering (including coherent) of polarized neutrons on non-oriented nuclei (P – A theorem)

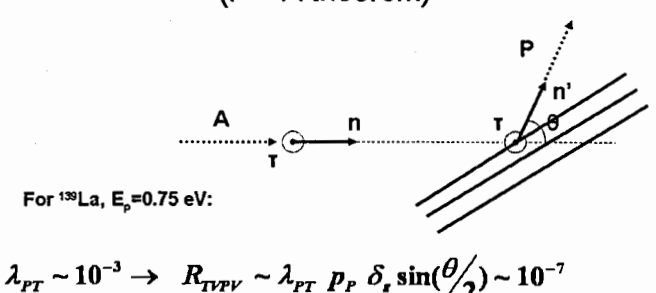


Figure 9

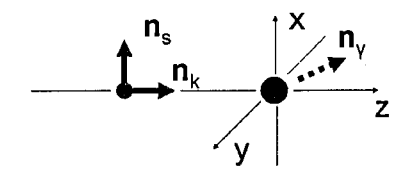
The principal disadvantage of the check of the P-A theorem is low intensity of elastic scattered neutrons. The situation may be improved by the use of coherent Bragg scattering. This variant of experiment was first proposed in [20] and is shown in Figure 9. The estimates have been obtained in [19] for relative violation  $R_{\text{TVPV}}$  of equalities (imposed by the P-A theorem) for given scale of TVPV forces.

# 6. Spin-angular correlations in radiative capture

Let us pass to radiative capture of slow neutrons. If we take into account only three vectors,  $\mathbf{n}_s$ ,  $\mathbf{n}_k$  and  $\mathbf{n}_\gamma$  - along the neutron spin s, the neutron momentum  $\mathbf{k}$  and the  $\gamma$  quantum momentum  $\mathbf{p}_\gamma$ , as well as only P even correlations, we obtain "fore-aft" (FA) and "left-right" (LR) asymmetries of emission of  $\gamma$  quantum (see, e.g., [21, 22] and references therein). They are caused by interference of two channels of the reaction, one of which is induced by neutron s-wave, while another - by neutron p-wave. The situation is presented in Figure 10. Curiously, however, there is a sensitivity to the forces breaking T invariance, more accurately, to TVPC forces.

Really, let us pass to Figure 11. For the sake of simplicity we consider the case when the reaction amplitudes in both channels can be presented in the Breit-Wigner form. Then, for example, "fore-aft" asymmetry,  $A_I(E)$ , goes to zero in the same point  $E_p$  where the p-wave cross section reaches the maximum. Herewith the reality of the amplitudes is assumed owing to the presence of T invariance.

«Ordinary» (P and T invariant) spin-angular correlations in (n,γ) reaction in a p-wave resonance are sensitive to p1/2- and p3/2-contributions, negative s-wave resonances and TVPC forces



$$\frac{d\sigma_{ny}(\vec{n}_{y}, E)}{d\Omega} = A_{0}(E) + A_{1}(E)(\vec{n}_{y}\vec{n}_{k}) + B_{1}(E)(\vec{n}_{y}[\vec{n}_{z}, \vec{n}_{k}]) + \dots$$

Figure 10

If, however, T invariance is violated, the neutron and radiative amplitudes have phases. As a result the zero-point of the "fore-aft" asymmetry shifts a little from the position  $E_{\rm p}$  of the p-wave resonance as it is presented in Figure 12.

$$f_{s}(E) = \frac{g_{r}^{s}(0)/2)g_{r}^{r}}{E - E_{r} + i\Gamma_{r}/2}$$

$$f_{g}(E) = \frac{g_{r}^{s}(0)/2)g_{r}^{r}}{E - E_{p} + i\Gamma_{p}/2}$$

$$\frac{d\sigma_{xy}(\vec{n}_{y}, E)}{d\Omega} = A_{0}(E) + A_{1}(E)(\vec{n}_{y}\vec{n}_{k}) + B_{1}(E)(\vec{n}_{y}[\vec{n}_{s}, \vec{n}_{k}]) + \dots$$

Near p-wave resonance:

$$A_1(E) \sim \text{Re}\left(f_p^*(E)\left(f_{p_2^{1/2}}(E) - \frac{1}{\sqrt{2}}f_{p_2^{1/2}}(E)\right)\right) \sim \frac{E - E_p}{(E - E_p)^2 + \Gamma_p^2/4}$$

Figure 11

In Figure 13 the formula for the energy shift  $\Delta E_p$  is presented together with the Dubna data [23, 24] on "fore-aft" and "left-right" asymmetries for the reaction  $n+{}^{117}$ Sn near the p-wave resonance with the energy  $E_p=1.33$  eV. It has been shown [25] that the similar data [26] for the reaction  $n+{}^{113}$ Cd near the p-wave resonance with the energy  $E_p=7$  eV lead to the same scale of limitation on TVPC forces as the other experiments performed in this time. Notice that no more strong restrictions have appeared until now.

Near p-wave resonance:

$$A_1(E) \sim \text{Re}\left(f_{p/2}^*(E)\left(f_{p/2}(E) - \frac{1}{\sqrt{2}}f_{p/2}(E)\right)\right) \sim \frac{E - E_p - \Delta E_p}{(E - E_p)^2 + \Gamma_p^2/4}$$

In the presence of TVPC forces:  $\Delta E_p \neq 0$ 

Figure 12

In fact, the study of the "fore-aft" and "left-right" asymmetries in the radiative capture [23, 24, 26] had been made not for investigation of T invariance (limitation on TVPC forces was a by-product). The main purpose was measurement of  $p_{1/2}$  and  $p_{3/2}$  contributions into the p-wave resonances. The formula for the "fore-aft" asymmetry  $A_1(E)$  presented in Figures 11 and 12 clearly shows that this asymmetry should be sensitive to the ratio between the specified contributions.

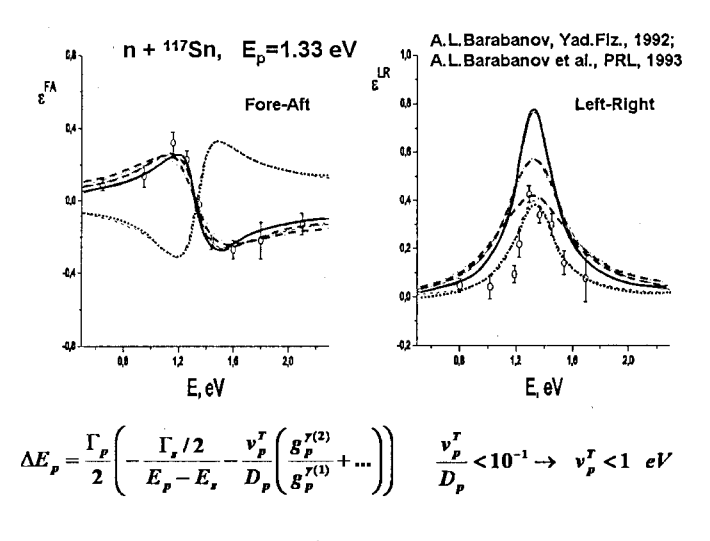


Figure 13

The results, however, were strange for both nuclei: <sup>117</sup>Sn and <sup>113</sup>Cd. Let us take for definiteness the data for <sup>117</sup>Sn. If we choose parameters of the p-wave resonance from the fitting of the "fore-aft" asymmetry, then the description of the "left-right" asymmetry is unsatisfactory (solid curves in Figures 13 and 14). But, on the contrary, the parameters that are found from the fitting of the "left-right" asymmetry give very bad description of the "fore-aft" asymmetry (dotted curves in Figures 13 and 14). All these calculations were performed for the "standard" parameters of the s-wave resonances among which the negative resonance is dominating.

I have assumed [22], that the source of the problem is not the p-wave but the negative s-wave resonance. Its "standard" parameters, probably, are not true. I have shown that more accurate description of both measured asymmetries may be achieved by means of shifting the s-wave resonance with respective change of its neutron width (dashed curves in Figures 13 and 14). The experiments were proposed to check this hypothesis (they are not performed so far).

Thus, spin-angular correlations in the reaction  $(n,\gamma)$  may be used not only for checking fundamental symmetries but also for studying positions and other parameters of neutron resonances (including negative).

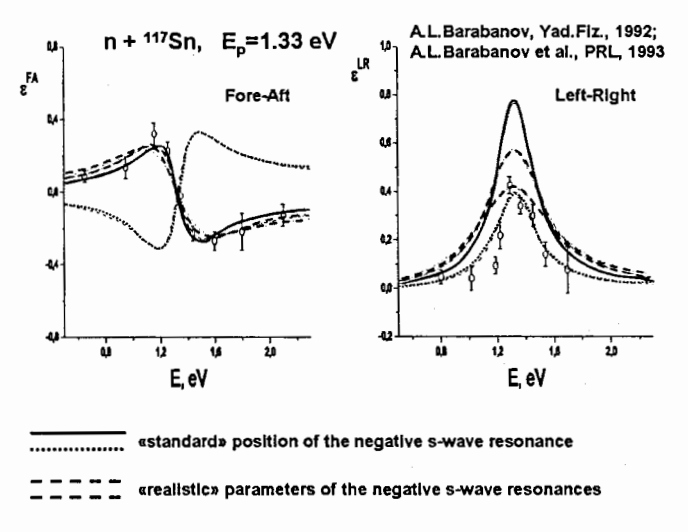


Figure 14

# 7. Spin-angular correlations in nuclear fission

Similar situation takes place for correlations in the reaction (n,f). There is, however, a serious difference between fission and radiative capture. As a rule, a certain exit channel is separated in the reaction  $(n,\gamma)$  - a quantum state of the nucleus that emits the  $\gamma$  quantum. At the same time summation over a huge number of exit channels is performed in fission - over differing quantum states of fragments (formed in highly excited states). Thus, there is a question: why spin-angular correlations that are, generally speaking, very sensitive to quantum numbers of final states, do not vanish in summation over the huge number of fission final states?

O. Bohr [27] has answered this question in 1950th years. He related the angular distribution of fragments (the simplest spin-angular correlation) with distribution of fission probability over the states with certain projection K of the nucleus spin J on the deformation axis at the barrier. This result is illustrated in Figure 15. Slightly later V.M. Strutinsky has shown [28], that after scission the number K transfers into the total helicity (the projection of the total spin F of both fragments on the fission axis). The identity of this quantum number for all fission final state provides the "survival" of spin-angular correlations in summation over the huge number of final states.

Consistent description of P even and P odd spin-angular correlations in (n, f) reaction with the use of the (|K|, $\Pi$ ) representation (K – helicity,  $\Pi$  – parity)

A.L.Barabanov and W.I.Furman, Z.Phys.A, 1997; Czech.J.Phys., 2003

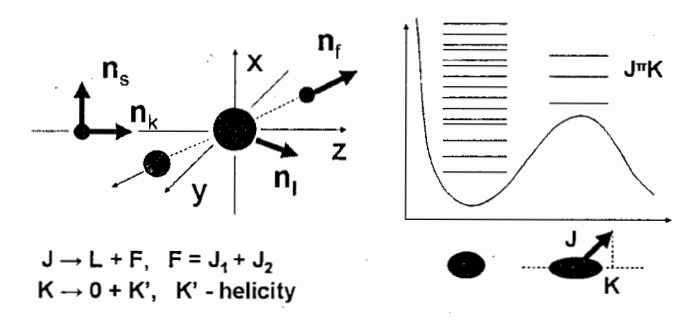


Figure 15

Differential cross section of nuclear fission induced by slow polarized neutrons

Figure 16

Explicit expression for the differential cross section of fission of nonoriented target nuclei by polarized neutrons is presented in Figure 16. It is obtained in the assumption that only neutron s-waves and interference of s- and p-waves are of importance. We see the terms related to P odd (PV) correlations as well the "fore-aft" (FA) and "left-right" (LR) correlations. Exactly as in the reaction  $(n,\gamma)$ , these correlations are caused by the interference of amplitudes describing the states with opposite parities. But the operator of helicity does not commutate with the operator of spatial inversion. Thus, the usual representation of helicity does not allow to describe the fission final states with certain parity.

# «Fore-Aft» and «Left-Right» correlations in nuclear fission at «one-level» approximation

$$\frac{d\sigma_{f}}{d\Omega} = \frac{1}{4\pi} \left( \sigma_{f}^{0} + \frac{\pi}{k^{2}} \sum_{J_{i} \in 20} q(jKJ_{r}J_{p}) \operatorname{Im} \left( S_{J_{r}}(0\frac{1}{2} \to K\Pi_{r}) S_{J_{p}}^{*}(1j \to K\Pi_{p}) \times \right) \right) \times \left( (\vec{n}_{f}\vec{n}_{k}) - i\beta_{j} p(\vec{n}_{f}[\vec{n}_{k}\vec{n}_{r}]) \right) \times \left( (\vec{n}_{f}\vec{n}_{k}) - i\beta_{j} p(\vec{n}_{f}\vec{n}_{k}) \right) \times \left( (\vec{n}_{f}\vec{n}_{k}) - i\beta_{j} p(\vec{n$$

Figure 17

To solve this problem we have introduced [29, 30] a new representation in which final states of two fragments are determined by the modulus of helicity, |K|, and by the parity,  $\Pi$ . In the framework of this formalism we have obtained explicit expressions for all terms in the differential fission cross section. Resonance overlapping was accurately taken into account. It is of great importance for heavy nuclei, because distances between neutron resonances for such nuclei are rather small.

It is interesting to consider the simplified case when it is possible to use the one-resonance approach both in s- and p-wave neutron channels. Results for P even spin-angular correlations are presented in Figure 17. Earlier similar results in the specified assumption have been obtained by O.P. Sushkov and V.V. Flambaum [31] in the framework of O. Bohr's hypothesis (without helicity representation). Notice that in our formulas the fission amplitudes have no phases. Thus, our approach implies essentially smaller number of free parameters.

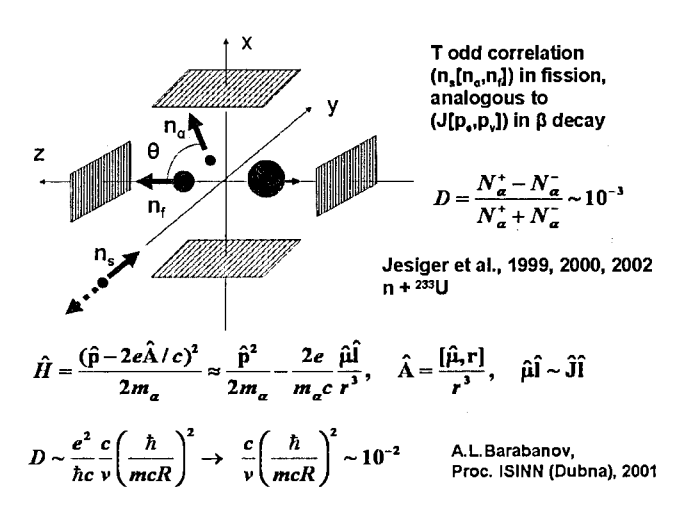


Figure 18

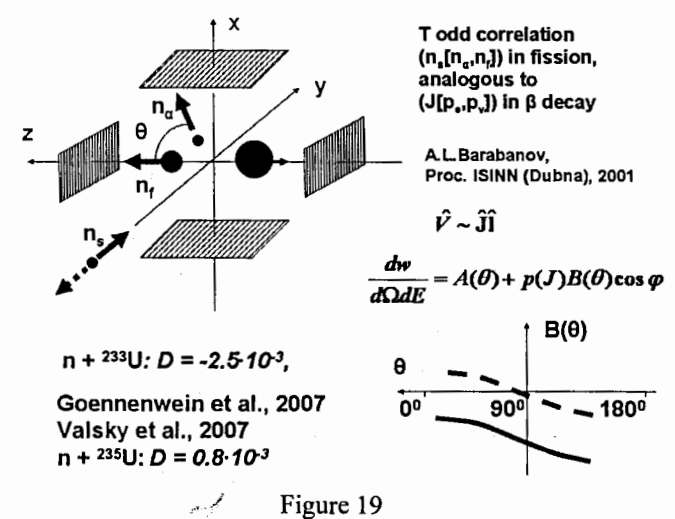
## 8. T odd correlation in ternary fission

At last, let us discuss the T odd correlation in ternary fission. Three unit vectors are of importance here,  $\mathbf{n}_s$ ,  $\mathbf{n}_f$  and  $\mathbf{n}_\alpha$  - along spin of the incident neutron, momentum of the light fragment and momentum of the third particle (e.g., the  $\alpha$  particle). The scheme of experiment is presented in Figure 18. The asymmetry of  $\alpha$  particle emission upwards and downwards of the scale  $10^{-3}$  has been found in fission of  $^{233}$ U nuclei by thermal polarized neutrons [32,33].

Similar correlation,  $(J[p_e,p_v])$ , is subject of searches in  $\beta$  decay of free neutrons and nuclei where its detection will give the evidence for T invariance violation. It is known, however, that electromagnetic interaction in the final state may induce a false effect, fortunately, very insignificant. Up to now searches of the specified 3-fold correlation in  $\beta$  decay gave neither true, nor false effect.

However, in the final state of the fission reaction besides the electromagnetic interaction, there is the strong interaction between particles. A model of the interaction that leads to the required asymmetry has been proposed [34]. The main point of this model is the interaction between the spin of fissioning nucleus and the orbital momentum of  $\alpha$  particle, i.e. specific spin-orbital interaction. The corresponding nuclear forces surpass electromagnetic forces at least by two orders of magnitude. Thus, they are strong enough to provide the observable effect.

The formula describing the asymmetry of  $\alpha$  particle emission upwards  $(\phi=0^0)$  and downwards  $(\phi=180^0)$  depending on the angle  $\theta$  between the momenta  $p_\alpha$  and  $p_f$  has been derived [34]. Its general form is presented in Figure 19. Arguments in favor of smooth dependence of the factor  $B(\theta)$  on the angle  $\theta$  have been proposed.



Notice that for  $^{233}$ U target nuclei [32, 33] no significant dependence of the factor  $B(\theta)$  (of "the correlation coefficient D" - in terms of the authors of [32, 33]) on the angle  $\theta$  was found. Furthermore, this fact was interpreted as an argument against the spin-orbital interaction in the final state: "... in case of the spin-orbit interaction is at work, the correlation coefficient D should have opposite signs for the angles smaller or larger than the average angle  $83^{0}$ ... However,... experiment clearly tells that the correlation coefficient D is independent from the emission angle of the TP [third particle]. The spin-orbit interaction thus appears to be ruled out ..." [33]. But in fact, the results of the measurements [32, 33] may correspond to the behavior  $B(\theta)$  that is presented in Figure 19 by the solid curve.

However, in recent searches of the T odd correlation for  $^{235}$ U target nuclei [35, 36], it was discovered that the correlation coefficient D really has opposite signs for the angles smaller or larger than the average angle  $83^{\circ}$ ! In the model of spin-orbital interaction it may be explained by the behavior B( $\theta$ ) that is presented in Figure 19 by the dashed curve. Obviously, herewith the total asymmetry (the coefficient D) should be small, and it is really the case for  $^{235}$ U target nuclei.

#### 9. Conclusion

Possible subjects of future studies of spin-angular correlations in neutronnucleus interaction are presented in Figure 20. Searching for 3-fold and 5-fold correlation in the total cross section would give new information about the magnitude of TVPV and TVPC forces breaking T invariance. Searches of P odd and P even correlation are also of great perspective because new data on neutron resonances, fission and radiative channels as well as on PV nuclear forces may be obtained.

Conclusion: future studies of spin-angular correlations in neutron-nucleus interaction

- Searching for T invariance violation (TVPV and TVPC forces): 3- and 5-fold vector correlations in total cross section
- Energy dependence of P odd and P even spin-angular correlations in (n,n), (n,γ) и (n,f) reaction to study:
  - 1) negative resonances;
  - 2) correlations of p1/2- and p3/2-waves;
  - 3) fission channels (JΠK);
  - 4) PV mixing of s- and p-wave resonances...

# Figure 20

This work was supported in part by the grant NS-3004.2008.2.

#### References

- 1. C.S. Wu, E. Ambler, R.W. Hayward, D.D. Hoppes and R.P. Hudson. Phys. Rev., 1957, V. 105, P. 1413.
- 2. J. Christenson, J.W. Cronin, V.L. Fitch and R. Turlay. Phys. Rev. Lett., 1964, V. 13, P. 138.
- 3. A.L. Barabanov. Yad. Fiz., 1986, V. 44, P. 1163 (in Russian) [Sov. J. Nucl. Phys., 1986, V. 44, P. 755].
  - 4. A. L. Barabanov. Nucl. Phys. A, 1997, V. 614, P.1.
- 5. V.P. Alfimenkov and L.B. Pikelner. EChAYa, 1995, V. 26, P. 1524 (in Russian) [Phys. El. Part. At. Nucl., 1995, V.26].
- 6. M. Forte, B.R. Heckel, N.F. Ramsey, K. Green, G.L. Greene, J. Byrne and J.M. Pendlebury. Phys. Rev. Lett., 1980, V. 45, P. 2088.

- 7. O.P. Sushkov and V.V. Flambaum. UFN, 1982, V. 136, P. 3 (in Russian) [Sov. Phys. Usp., 1982, V. 25, P. 1].
- 8. V.E. Bunakov and L.B. Pikelner. Prog. Part. Nucl. Phys., 1997, V. 39, P. 337-392.
- 9. R. Haas, L.B. Leipuner and R.K. Adair. Phys. Rev., 1959, V. 116, P. 1221.
- 10. Yu.G. Abov, P.A. Krupchitsky and Yu.A. Oratovsky. Phys. Lett., 1964, V. 12, P. 25.
- 11.G.V. Danilyan, B.D. Vodennikov, V.P. Dronyaev, V.V. Novitskii, V.S. Pavlov and S.P. Borovlev. Pis'ma ZETF, 1977, V. 26, P. 197 (in Russian) [JETP Lett, 1977, V. 26, P. 186].
- 12. O.P. Sushkov and V.V. Flambaum. Pis'ma ZETF, 1980, V. 32, P. 377 (in Russian) [JETP Lett., 1980, V. 32, P. 352].
  - 13. V.E. Bunakov and V.P. Gudkov. Z. Phys. A, 1981, V. 303, P. 285-291.
- 14. V.P. Alfimenkov, S.B. Borzakov, Vo Van Thuan, Yu.D. Mareev, L.B. Pikelner, A.S. Khrykin and E.I. Sharapov. Pis'ma ZETF, 1982, V. 35, P. 42 (in Russian) [JETP Lett., 1982, V. 35, P. 51].
- 15. S.L. Stephenson, J.D. Bowman, B.E. Crawford, P.P.J. Delheij, C.M. Frankle, M. Iinuma, J.N. Knudson, L.Y. Lowie, A. Masaike, Y. Matsuda, G.E. Mitchell, S.I. Penttila, H. Postma, N.R. Roberson, S.J. Seestrom, E.I. Sharapov, Y.-F. Yen and V.W. Yuan. Phys. Rev. C, 1998, V. 58, P. 1236.
- 16. V.E. Bunakov and V.P. Gudkov. Pis'ma ZETF, 1982, V. 36, P. 268 (in Russian) [JETP Lett., 1982, V. 36, P. 328].
  - 17. V.E. Bunakov. Phys. Rev. Lett., 1988, V. 60, P. 2250.
- 18. A.L. Barabanov and A.G. Beda. J. Phys. G: Nucl. and Part. Phys., 2005, V. 31, P. 161.
  - 19. A.L. Barabanov and V.R. Skoy. Nucl. Phys. A, 1998, V. 644, P. 54.
- 20. A.L. Barabanov and V.L. Kuznetsov. Phys. Lett. B, 1989, V. 232, P. 151; 1990, V. 244, P. 580 (Errata).
  - 21. V.V. Flambaum and O.P. Sushkov. Nucl. Phys. A, 1985, V. 435, P. 352.
- 22. A.L. Barabanov. Yad. Fiz., 1992, V. 55, P. 2421 (in Russian) [Sov. J. Nucl. Phys., 1992, V. 55, P. 1513].
- 23. V.P. Alfimenkov, S.B. Borzakov, Vo Van Thuan, Yu.D. Mareev, L.B. Pikelner, I.M. Frank, A.S. Khrykin and E.I. Sharapov. Pis'ma ZETF, 1984, V. 39, P. 346 (in Russian) [JETP Lett., 1984, V.39].

- 24. V.P. Alfimenkov, S.B. Borzakov, Yu.D. Mareev, L.B. Pikelner, A.S. Khrykin and E.I. Sharapov. Kratkie soobscheniya OIYaI N 10-85, Dubna, 1985, P. 19 (in Russian).
- 25. A.L. Barabanov, E.I. Sharapov, V.R. Skoy and C.M. Frankle. Phys. Rev. Lett., 1993, V. 70, P. 1216.
- 26. V.P. Alfimenkov, S.B. Borzakov, Yu.D. Mareev, L.B. Pikelner, V.R. Skoy, A.S. Khrykin and E.I. Sharapov. Yad. Fiz., 1990, V. 52, P. 927 (in Russian) [Sov. J. Nucl. Phys., 1990, V.52].
- 27. A. Bohr. Proceedings of the International Conference on the Peaceful Uses of Atomic Energy, V. 2. United Nations, N.Y., 1956, P. 151.
  - 28. V.M. Strutinsky. ZETF, 1956, V. 30, P. 606 (in Russian).
  - 29. A.L. Barabanov and W.I. Furman. Z. Phys. A, 1997, V. 357, P. 411.
- 30. A.L. Barabanov and W.I. Furman. Czechoslovak journal of Physics, Supplement B, 2003, V. 53, P. B359.
- 31.O.P. Sushkov and V.V. Flambaum. UFN, 1982, V. 136, P. 3 (in Russian) [Sov. Phys. Usp., 1982, V. 25, P. 1].
- 32. P. Jesinger, A. Koetzle, A.M. Gagarski, F. Goennenwein, G. Danilyan, V.S. Pavlov, V.B. Chvatchkin, M. Mutterer, S.R. Neumaier, G.A. Petrov, V.I. Petrova, V. Nesvizhevsky, O. Zimmer, P. Geltenbort, K. Schmidt and K. Korobkina. Nucl. Instr. Meth. A, 2000, V. 440, P. 618.
- 33.P. Jesinger, A. Koetzle, F. Goennenwein, M. Mutterer, J. von Kalben, G.V. Danilyan, V.S. Pavlov, G.A. Petrov, A.M. Gagarski, W.H. Trzaska, S.M. Soloviev, V.V. Nesvizhevsky and O. Zimmer. Yad. Fiz., 2002, V. 65, P. 662 [Phys. At. Nucl., 2002, V. 65, P. 630].
- 34.A.L. Barabanov. In: Neutron Spectroscopy, Nuclear Structure, Related Topics (Proc. of the 9-th Int. Seminar on Interaction of Neutrons with Nuclei, Dubna, 2001), JINR, E3-2001-192, Dubna, 2001, P. 93; arXiv: 0712.3543 (nucl-th).
- 35.F. Goennenwein, M. Mutterer, A. Gagarski, I. Guseva, G. Petrov, V. Sokolov, T. Zavarukhina, Yu. Gusev, J. von Kalben, V. Nesvizhevsky and T. Soldner. Phys. Lett. B, 2007, V. 652, P. 13.
- 36. G.V. Valsky, A.S. Vorobiev, A.M. Gagarsky, I.S. Guseva, F. Goennenwein, T.A. Zavarukhina, Yu.N. Kopach, D.O. Krinitsyn, M. Mutterer, G.A. Petrov, V.I. Petrova, V.E. Sokolov and O.A. Scherbakov. Izv. RAN, Ser. fiz., 2007, V. 71, P. 368 (in Russian).

# THE ROTATION OF THE FISSIONING COMPOUND NUCLEUS IN REACTIONS INDUCED BY POLARIZED NEUTRONS

Bunakov V.E.<sup>1</sup>, Kadmensky S.G.<sup>2</sup>

PNPI, Gatchina 188300, <sup>2</sup>Voronezh State University, Voronezh 39

#### 1.Introduction.

In our previous papers [1-3] we developed the theory which explained the earlier observed (see e.g. [4]) T-odd correlation of the type:

$$\vec{\sigma}_n[\vec{k}_{LF}\cdot\vec{k}_{\alpha}]$$

in ternary fission induced by polarized neutrons. Here  $\vec{\sigma}_n$  is the neutron spin, while  $\vec{k}_{LF}$  and  $\vec{k}_{\alpha}$  are the momenta of the light fragment and the ternary particle (usually alpha) emitted in ternary fission. This correlation, which was called TRI-correlation, was described by the differential cross-section of the type:

$$\frac{d^2\sigma}{d\Omega_{LF}d\Omega_{\alpha}} = B_0 + D \cdot \vec{\sigma}_n [\vec{k}_{LF} \cdot \vec{k}_{\alpha}] \tag{1}$$

The experimental geometry was chosen in such a way that the directions of the unit vectors  $\vec{\sigma}_n$  and  $\vec{k}_{LF}$  were parallel to the y and z axes, while the vector  $\vec{k}_{\alpha}$  varied in the (x,y) plane. The effect measured was defined as:

$$D = \frac{\sigma_+ - \sigma_-}{\sigma_+ + \sigma_-} \quad , \tag{2}$$

where  $\sigma_{+}$  and  $\sigma_{-}$  stand for the differential cross-sections with the neutron beam positive and negative helicities. The magnitude of the effect for the <sup>233</sup>U target was about -3·10<sup>-3</sup>. It is important to point that this magnitude and the sign of the effect were practically independent of the angle  $\theta$  between the vectors  $\vec{k}_{LF}$  and  $\vec{k}_{\alpha}$  in a wide range of angles around  $\theta \approx 90^{\circ}$ .

However, the recent measurements [5] for the  $^{235}$ U target demonstrated the existence of the new effect, which was called ROT. Contrary to the TRI, this effect does not change with the inversion of either  $\vec{k}_{LF}$  or  $\vec{k}_{\alpha}$  but changes its sign in the vicinity of  $0\approx90^{\circ}$ . This effect is rather well reproduced [6] in the classical trajectory calculations of the alpha-particle emission in the rotating Coulomb field of the fission fragments with the angular momentum of about few h, equal to the total spin J of the polarized fissioning nucleus  $^{236}$ U which appears after the absorption of the polarized neutron by the target nucleus. The rotation of alpha particles slightly lags behind the rotation of the outgoing fragments' motion axis (Coriolis effect). This leads to the shift of the whole alpha angular distribution with respect to this axis. The inversion of the neutron helicity causes the inversion of the compound-nucleus polarization direction and, therefore to the inversion of the system's rotation direction. This leads to the shifts of the alpha-particle angular distributions in the opposite directions. The difference of the angular distributions for the opposite helicities causes the effect observed. It was possible to reproduce the experimental effect with the angular shift about 0.1°.

It is well known that the classical trajectory calculations of the alpha angular distributions in ternary fission without the rotation of the decaying system reproduce the experimental data fairly well because the motion of alphas in the Coulomb fields of the fragments is quasiclassical. However in ref. [6] the rotation of the system was taken into account in the trajectory calculations for the first time. Its success is quite surprising because the results of these calculations seem to contradict the uncertainty relation for the system's angular momentum and the angle  $\theta$  of its rotation in the plane perpendicular to it:

$$\Delta J \cdot \Delta \theta \Box \hbar$$
 (3)

In the case considered the nuclear angular momentum was of the order of few h units. Therefore one should expect the uncertainty of the rotation angle to be  $\Delta\theta$  | 1 radians. As pointed above, the trajectory calculations gave the value  $0.2^{0}\approx0.003$  radian in full contradiction to (3). Besides this, the expression used in [6] for the angular velocity of the rotating system was quite contradictory. These contradictions will be considered below.

## 2. Contradictions in the initial conditions of the trajectory calculations

The effective angular velocity of the fissioning system's rotation was estimated in [6] as:

$$\vec{\Omega} = \vec{P}(J) \frac{R}{\Im} ,$$
 (4)

where  $\Im$  is the moment of inertia of the fissioning system and P(J) is the compound-nucleus polarization, resulting from the absorption of the neutron with polarization  $p_n$ :

$$P(J) = \begin{cases} \frac{2I+3}{3(2I+1)} p_n \equiv \frac{J+1}{3J} p_n & for \quad J = I+1/2 \\ -\frac{1}{3} p_n & for \quad J = I-1/2 \end{cases}$$
 (5)

Ex. (5) does not take into account the axial symmetry of the deformed fissioning nucleus which therefore possess the additional quantum number K of its spin projection on the symmetry axis. At low excitation energies close to the fission barrier this nucleus fissions through only one-two transition states with fixed K values.

This axially symmetrical deformation was taken into account in ref. [6] by introducing into eq.(4) of the quantity R, which was named in [6] "the angular momentum of the nuclear collective rotation" and related to the values of the total nuclear spin J and its projection K on the nuclear symmetry axis as:

$$R = \hbar \sqrt{J(J+1) - K^2} \tag{6}$$

It was assumed that this vector  $\vec{R}$  was directed along the vector of the neutron beam polarization so that the rotation of the symmetry axis takes place in the plane perpendicular to the neutron polarization vector  $\vec{P}_n$  directed along the y axis. The direction of the light fragment emission (i.e. the direction of the nuclear symmetry axis) coincides then with z axis. This shows that the introduction of vector  $\vec{R}$  is questionable even in the classical approach. Indeed with our (and experimental) choice of the axes  $R = J_y$  while  $K = J_z$ . If K = 0

then the whole nuclear spin J is caused by the collective rotation. Thus  $R=J\hbar$  in contradiction to (6). If  $K\neq 0$  then

the direction of the collective rotation vector  $\vec{R}$  (and, therefore the direction of the angular velocity vector  $\vec{\Omega}$ ) can not coincide with the direction of the fissioning nucleus polarization vector because:

$$\vec{J} = \vec{R} + \vec{K}$$
in contradiction to (4) and (6).

In the quantum approach the inconsistencies of Eqs. (4)-(6) are even more evident because the vector components  $J_y$  and  $J_z$  do not commute (the corresponding eigenvalues can not be measured simultaneously). One might only introduce the new operator  $\hat{R}^2$  of the angular momentum squared  $\hat{R}^2$  defined as:

$$\hat{R}^2 = \hat{J}_x^2 + \hat{J}_y^2 = J^2 - J_z^2 \tag{8}$$

Exactly this was done by Bohr and Mottelson [7] to whom the authors of [6] refer. The eigenvalue of this operator is

$$R(R+1) = J(J+1) - K^{2}$$
(9)

in contradiction to (6). Exactly this eigenvalue enters the well-known expression for the collective energy:

$$E_{rot} = \frac{\hbar^2}{2\Im_{\perp}} (J(J+1) - K^2), \tag{10}$$

which is given in [7]. By comparing this formula with the expression for the rotation energy of the rigid rotator with the symmetry axis along the z axis and the moments of inertia  $\Im_x = \Im_y = \Im_\perp$ :

$$E_{rot} = \frac{1}{2} \Im_{\perp} (\Omega_x^2 + \Omega_y^2) , \qquad (11)$$

one might obtain the expression for the square of the rotation velocity in the plane (x,y):

$$\Omega_{\perp}^{2} = (\Omega_{x}^{2} + \Omega_{y}^{2}) = \frac{\hbar^{2} R(R+1)}{\Im_{\perp}^{2}}$$
 (12)

This allows to obtain the expression:

$$\Omega_{\perp} = \sqrt{\Omega_x^2 + \Omega_y^2} = \frac{\hbar}{\Im_{\perp}} \sqrt{R(R+1)} = \frac{\hbar}{\Im_{\perp}} \sqrt{J(J+1) - K^2}$$
 (13)

which resembles the Eqs. (4)-(6). However the angular momentum of the collective rotation R is defined not by Eq. (6), but rather by the solution of the quadratic equation (9). The direction of this momentum in the (x,y) plane (and, therefore the direction of the rotation velocity vector) remains undefined and, in complete agreement with quantum mechanics, can not coincide with the y axis, as supposed in [6].

Thus the expressions (4)—(6) for the angular velocity which were used in ref.[6] are invalid both in classical and in quantum approaches. Eq. (5) for the polarization of the fissioning system does not take into account the specific features of the low-energy fission causing the existence of the K quantum number. The attempt to correct this drawback by the introduction of the quantity (6) is physically meaningless and leads to the contradictions both with classical and quantum mechanics.

# 3. The correct quantum approach to the rotation of the polarized fissioning nucleus

We had seen that quantum mechanics does not allow to define the eigenvalues of the two angular momentum projections  $J_z=K$  and  $J_y$  at the same time, while our physical problem demands this. Strictly speaking, in quantum mechanics we can define only the eigenvalues of the square of the spin operator and of its projection on one given axis, but can not speak about the direction of the spin vector in space. However, by averaging over the ensemble of

particles we can simultaneously define all the three components  $P_i = \frac{\langle J_i \rangle}{J}$  of the

polarization vector with unlimited accuracy (for instance, the rotation angle of the neutron polarization was measured in [8], which was equal to  $10^{-6}$  radians). The ensemble -averaged quantities  $< J_i >$  are usually obtained with the aid of the density matrix  $\rho_{MM}^J$ . Actually the average value <A> of any spin operator  $\hat{A}$  for the system with the fixed spin J and its projection M can be defined as:

$$\langle A \rangle = \sum_{MM'} \rho_{MM'}^J A_{M'M} = Sp(\rho A),$$
 (14)

where the matrix element

$$A_{M'M} = \langle \Psi_{JM'} | \hat{A} | \Psi_{JM} \rangle \tag{15}$$

is defined with the aid of the system's wave function  $\Psi_{JM}$ , and

$$Sp\rho = 1$$

The Eq. (5) can be obtained in this way for the compound nucleus resonance with the fixed values of J and M, which appeared after the absorption of the polarized neutron. Mind that, as is well known, neutron resonances in deformed nuclei possess no definite value of the K quantum number, as a result of the complete K-mixing caused by the dynamical enhancement of the Coriolis interaction [9,10]. Therefore for isolated resonances, induced by polarized neutrons their decay into various neutron and gamma channels is governed by the factor (5). However for sufficiently low neutron energies the saddle- point in the fission channel selects only one-two values of K corresponding to the lowest collective excitations. The probability of this selection is defined by the quantity

$$|b_{sK_s}^{J_s}|^2 = |a_{sK_s}^{J_s}|^2 |c_{sK_s}^{J_s}|^2$$
 (16)

where  $|a_{sK_s}^{J_s}|^2$  is the probability to find the component  $K_s$  in the s-resonance wave –

function. Due to the complete K-mixing  $a_{sK_s}^{I_s}$  has random sign and the average value

$$<(a_{sK_s}^{J_s})^2>=(2J_s+1)^{-1}$$
 (17)

 $|c_{sK_s}^{J_s}|^2$  is the transmission probability of this K-value from the resonance s via the

transition state with  $J_s$ ,  $K_s$  to the scission point. One can assume that  $|c_{sK_s}^{J_s}|^2 \approx 1$  for one fixed value of  $K_s$  and is approximately zero for all the other values.

Thus we obtain the polarized fissioning system with the fixed values of J, M and K, caused by the absorption of the polarized neutron. With our choice of coordinates the nuclear symmetry axis coincides with z, while the neutron beam is polarized along y-axis. Now we can find the averaged values of all the 3 components of the nuclear spin for a given value of K using the above equations (14), (15) and the known wave function  $\Psi_{MK}^J$  of the deformed fissioning nucleus (see e.g. [7]):

$$\Psi_{MK}^{J} = \sqrt{\frac{2J+1}{16\pi^2}} \left[ D_{MK}^{J}(\omega) \Phi_K(q) + (-1)^{I+K} D_{M,-K}^{J}(\omega) \Phi_{\overline{K}}(q) \right]$$
(18)

Using now the definition of the average spin projections on the i=(x, y, z) axes:

$$< J_i(K) > = \sum_{MM} \rho_{MM}^J < \Psi_{MK}^J |\hat{J}_i| \Psi_{MK}^J >$$
 (19)

and the expression for the density matrix (see [1]

$$\rho_{MM}^{J} = \frac{1}{2(2I+1)} \left[ \delta_{MM} + i p_n A(J,J) (C_{J1M1}^{JM} + C_{J1M-1}^{JM}) \right]$$
 (20)

$$A(J,J) = \left(\sqrt{\frac{J}{2(J+1)}} \delta_{J,J_{<}} - \sqrt{\frac{J+1}{2J}} \delta_{J,J_{>}}\right)$$
 (21)

· we obtain:

$$\langle J_{x}(K) \rangle = \langle J_{z}(K) \rangle = 0$$
 , (22)

$$\langle J(K) \rangle = \langle J_y(K) \rangle = \frac{g_{KJJ}}{2} p_n \hbar$$
 (23)

Here

$$g_{K_s J_s J_s} = \frac{J_s (J_s + 1) - I(I + 1) + 3/4}{J_s} \cdot \frac{J_s (J_s + 1) - K_s^2}{(J_s + 1)}$$
and 
$$J_s = \begin{cases} I + 1/2 = J_> \\ I - 1/2 = J_< \end{cases}$$
, while *I* is the target spin.

and 
$$J_s = \begin{cases} I + 1/2 = J_{>} \\ I - 1/2 = J_{<} \end{cases}$$
, while *I* is the target spin

Thus we obtained a result (see (22)-(23), which is quite unexpected from the classical point: Even for  $K\neq 0$  the average projection  $\langle J_z \rangle$  (as well as  $\langle J_x \rangle$ ) equals to zero. This is the purely quantum result, caused by the fact that the wave-functions (18) contain the contributions of K and (-K) with equal weights (i.e. the rotation eigenstates are always doubly-degenerate in the sign of K, as seen from (10)). The only non-zero component of the average spin vector is its projection on the y-axis (i.e. on the direction of the neutron beam polarization), which is perpendicular to the nuclear symmetry axis z. Therefore for the fixed K-value the total spin of the deformed fissioning nucleus is polarized along the direction of the neutron beam polarization and its polarization is given by:

$$P(J,K) = \frac{\langle J(K) \rangle}{J} = \frac{g_{KJJ}}{2J} p_n$$
 (25)

Now we can estimate the angular velocity of the rotation around this axis using the expression:

$$\omega_q(J,K) = \frac{\langle J(K) \rangle}{\Im},\tag{26}$$

which gives:

$$\omega_{q}(J_{s}, K_{s}) = \frac{g_{K_{s}J_{s}J_{s}} \cdot \hbar}{2\Im} \mathbf{p}_{n} = \begin{cases} \frac{J_{s}(J_{s}+1) - K^{2}}{J_{s}} \frac{\hbar}{2\Im} \cdot \mathbf{p}_{n} & \text{for} \quad J_{s} = I + 1/2 \\ -\frac{J_{s}(J_{s}+1) - K^{2}}{(J_{s}+1)} \frac{\hbar}{2\Im} \cdot \mathbf{p}_{n} & \text{for} \quad J_{s} = I - 1/2 \end{cases}$$
(27)

If several transition states contribute to fission (i.e. if several values  $|c_{sK_{-}}^{J_{s}}|^{2}$  in (16) are nonzero), then:

$$\omega_q^{eff} = \sum_{K_s} |b_{sK_s}^{J_s}|^2 \, \omega_q(J_s, K_s)$$
 (28)

If all the K-values contribute equally (i.e. if all the coefficients  $|b_{sK_s}^{J_s}|^2 = |a_{sK_s}^{J_s}c_{sK_s}^{J_s}|^2$  equal their average value  $(2J_s+1)^{-1}$ ), then the polarization P(J,K) of eq.(25) is averaged over all the K-values and

$$\frac{1}{(2J+1)} \sum_{K} P(J,K) = P(J) \quad , \tag{29}$$

where P(J) is defined by (5). This is exactly what applies to the non-fission channels of the neutron resonance decay. One can say that the use of Eq.(5) means averaging over all the possible directions of the deformed nucleus symmetry axis. However, if the coefficient  $|c_{sK_s}^{J_s}|^2$  equals to 1 for only one K-value (as it often happens in fission channel), then one should use (25), (27) instead of (5), (4).

# 4. On the absolute values and signs of the TRI and ROT effects

The main physical difference between our approach and the one used in [6] lies in the fact that the rotation angular velocity vector is defined not by the angular momentum R whose direction can not be defined, but rather by the polarization vector  $\vec{P}(J,K)$  of the fissioning nucleus whose all the three components are defined by Eqs. (22)—(25). Exactly this classical character of the polarization vector removes all the contradictions connected with the uncertainty relation (3) and allows to measure simultaneously the ensemble-averaged vector  $<\vec{J}(K)>$  and the system's rotation angle in the plain perpendicular to it. As mentioned above, the rotation of the polarization vector can be measured with the precision higher than  $10^{-6}$  radians. No wonder that we can measure the rotation angle of the polarized system with the precision higher than  $0.1^{0}$ . Comparing our Eq. (27) for the angular velocity  $\Omega_{q}(J,K)$  with the empirical Eqs. (4)—(6) used in ref. [6] we see that the ratio

$$\frac{\Omega_q(J,K)}{\Omega} = \frac{3}{2} \frac{\sqrt{J(J+1) - K^2}}{J+1}$$
 (30)

varies for J=3,4 in the interval from 0.5 to 1.3. Thus one might expect that in the case of the strong isolated resonance when the interference effects can be neglected, the results of the classical calculations of [6] might be correct to within this factor even if the K-values of the transition states are unknown or when the results of their definition by the different methods differ considerably, as in the case of <sup>236</sup>U fission [11].

Much more significant might be the purely quantum effects of the resonance interference which can not be taken into account in the classical approach. The unified quantum description of TRI and ROT effects [3,12] gives the following expression for the polarization dependent part of the ternary particle angular distribution:

$$\frac{d^{2}\sigma^{Cor}}{d\Omega_{\alpha}d\varepsilon} = \frac{p_{n}\pi}{2(2I+1)k_{n}^{2}} \sum_{ss',J_{s}J_{s}:cK_{s}} |h_{s}^{J_{s}}| |h_{s}^{J_{s}'}| |b_{sK_{s}}^{J_{s}}b_{s'K_{s}}^{J_{s}'}\Gamma_{cK_{s}}\sqrt{(2J_{s}+1)(2J_{s'}+1)} \times 
\times g_{K_{s}J_{s}J_{s'}} |A_{c}^{0}| \{\vec{\sigma}_{n}[\vec{k}_{LF}\cdot\vec{k}_{\alpha}]F_{odd} + \vec{\sigma}_{n}[\vec{k}_{LF}\cdot\vec{k}_{\alpha}](\vec{k}_{LF}\cdot\vec{k}_{\alpha})F_{even}\} , \quad (31)$$

Here the factor 
$$h_s^{J_s} = \frac{\sqrt{\Gamma_{sn}^{J_s}}}{E - E_s^{J_s} + i\Gamma_s^{J_s}/2} = |h_s^{J_s}| \exp\{i\delta_{sJ_s}\}$$
 (32)

shows the resonance energy-dependence of the cross-section and the fission width through the transition state  $(J_s, K_s)$  into the channel c:

$$\Gamma_{sJ_s,cK_s} = |b_{sK_s}^{J_s}|^2 \Gamma_{cK_s}$$
(33)

is defined by the above coefficients  $b_{sK_s}^{J_s} = a_{sK_s}^{J_s} c_{sK_s}^{J_s}$  of Eq. (16).

The amplitudes  $A^0(\theta, \varepsilon)$  of alpha – particles' angular and energy ( $\varepsilon$ ) distribution for the ternary fission of the unpolarized nucleus is:

$$A_c^{\ 0}(\theta,\varepsilon) = \sum_l |d_{cl}(\varepsilon)| \exp\{i\delta_{cl}(\varepsilon)\} Y_{l0}(\Omega_\alpha) = |A_c^0(\theta,\varepsilon)| \exp\{i\delta_c^0\},$$

while the functions  $F_{odd}$  and  $F_{even}$  define the contributions to (31) from the odd and even values of the alpha's angular momentum and therefore the values of TRI and ROT effects:

$$F_{odd} = |d_{c1}^{Cor}(\varepsilon)| a_1 \sin(\delta_{sJ_ss'J_{s'}} + \delta_{c1}^{Cor}(\varepsilon) - \delta_c^0(\theta, \varepsilon)) + + |d_{c3}^{Cor}(\varepsilon)| a_3 \sin(\delta_{sJ_ss'J_{s'}} + \delta_{c3}^{Cor}(\varepsilon) - \delta_c^0) (\mathbf{k}_{LF} \cdot \mathbf{k}_{\alpha})^2 + \dots$$
(34)

$$F_{even} = \left| d_{c2}^{Cor}(\varepsilon) \right| b_1 \sin(\delta_{sJ_ss'J_{s'}} + \delta_{c2}^{Cor}(\varepsilon) - \delta_c^0(\theta, \varepsilon)) + \\ + \left| d_{c4}^{Cor}(\varepsilon) \right| b_2 \sin(\delta_{sJ_ss'J_{s'}} + \delta_{c4}^{Cor}(\varepsilon) - \delta_c^0) (\mathbf{k}_{LF} \cdot \mathbf{k}_{\alpha})^2 + \dots$$
(35)

One can see that Eq. (31) contains contributions not only from the terms with s=s' (which correspond to the isolated resonances) but also from the interference terms with  $s\neq s'$ . The signs of these interference terms are random due to the random signs of the coefficients

$$b_{sK_s}^{J_s}=a_{sK_s}^{J_s}c_{sK_s}^{J_s}$$
 , while the magnitudes of the "non-diagonal" quantities  $g_{K_sJ_sJ_s}$  differ

from those of the "diagonal" ones (24), which define the angular velocities of the system's rotation for isolated resonances. Unfortunately the analysis carried out in [11] shows that the approximation of isolated resonances is invalid in the case of <sup>236</sup>U fission. The interference terms' influence is especially strong for the neutron energies between the resonances—exactly in the region where the experiments [4,5] were done.

Another important consequence of the resonance interference is the appearance of the additional phase shifts:

$$\delta_{sJ,s'J,\cdot} = \delta_{sJ,\cdot} - \delta_{s'J,\cdot} \tag{36}$$

in the sin arguments of the functions  $F_{odd}$  and  $F_{even}$  which define the relative magnitudes and signs of the TRI and ROT effects. The experimentally observed difference in the relative values and signs of the effects for two U isotopes should be explained by the difference of the quantities (36).

#### 5. Summary

We have shown that the classical trajectory calculations [6] (especially if they are done with the correct quantum initial conditions (27), (28)) might describe the experimental ROT effect with good accuracy in the case of strong isolated resonances. We have also derived the formula for the polarization of the deformed compound-nucleus with the fixed values of the

quantum numbers J and K. This new expression should be used in the description of the fission reaction induced by the low-energy polarized neutrons.

In the case of the strongly overlapping neutron resonances the influence of the quantum interference effects might be quite strong. Therefore the classical trajectory calculations might reproduce only the order of magnitude of the effect and could not define the correct relative sign and magnitude of the TRI and ROT effects.

#### References.

- 1. V. Bunakov, S. Kadmensky. Phys. At. Nucl. V.66, 2003, p.1846.
- 2. V. Bunakov, S. Kadmenski, L. Rodionova. Izvestia RAS (phys.) V.69, 2005, p.614.
- 3. V. Bunakov, S. Kadmenski. Izvestia RAS (phys.) V.71, 2007, p.364.
- 4. Jessinger P., Kotzle M., Gagarski A. et.al. Nucl. Instum. Methods. 2000. V. A440. P.618.
- 5. Goennenwein F., Mutterer M., Gagarski A. et.al.. Phys. Lett. 2007. V.B652. P.13.
- 6. I.S.Guseva and Yu. Gusev. Proc. Int. Sem. ISINN-14, Dubna JINR, 2007, p.101-108.
- 7. A.Bohr, B.Mottelson. Nuclear Structure. V.2. Benjamin, N-Y. 1974.
- 8. Forte M., Heckel B., Ramsey N. et.al. Phys. Rev. Lett. 1980. V.45. P.2088.
- 9. S.Kadmensky, V.Markushev, V.Furman. Sov. Journ. Nucl. Phys. 1981. V.35. P.300.
- S.Kadmensky, V.Markushev, Yu.Popov, V.Furman. Sov.Journ. Nucl. Phys. 1984. V.39.
   P.7.
- 11. Yu. Kopach et al. Phys. At. Nucl. V.62, 1999, p.840.
- 12. V.E. Bunakov, S.G. Kadmensky, S.S. Kadmensky. Phys. At. Nucl. V.71, 2008, p.1917.

# THE MECHANISM OF EXCITATION OF GIANT RESONANCES IN NUCLEAR FISSION AND T-ODD CORRELATIONS FOR PRESCISSION GAMMA-QUANTA

V.E. Bunakov<sup>1</sup>, S.G.Kadmensky<sup>2</sup>, S.S.Kadmensky<sup>2</sup>

Petersburg Nuclear Physics Institute, Gatchina, 188300, Russia
 Voronezh State University, Voronezh, University Square, 1, Russia

Abstract: In the framework of the quantum fission theory the conditions are investigated for the appearance and the observation of the pre-scission gamma-quanta which are emitted by the fissioning nucleus before its scission. It is shown that these conditions are fulfilled for the gamma-decay of the giant electric isovector dipole resonances whose excitation is caused by the non-adiabatic character of the nuclear collective motion at the final stages of its pre-scission evolution. The analysis is carried of the energy and angular distributions for these quanta emitted by the unpolarized nuclei. T-odd correlations are also studied in the angular distributions of these quanta emitted in the fission reactions induced by the polarized cold neutrons. The similarity of these correlations are shown to the T-odd ROT-correlations which were discovered earlier for the ternary fission alpha-particles.

#### 1. Introduction

T-odd TRI correlations were discovered [1] in the angular distribution of the products of <sup>233</sup>U ternary fission induced by the cold polarized neutrons. They could be described by the expression:

$$\frac{d^2 \sigma^{(TRI)}}{d\Omega_{LF} d\Omega_3} = A \vec{\sigma}_n \left[ \vec{k}_{LF}, \vec{k}_3 \right], \tag{1}$$

where  $\vec{\sigma}_n$ ,  $\vec{k}_{LF}$ ,  $\vec{k}_3$  are the unit vectors directed along the neutron polarization vector and the wave vectors of the light fragment and the ternary particle (predominantly alpha), respectively. A few years later another T-odd correlation was discovered [2,3] in ternary fission of  $^{2.5}$ U

$$\frac{d^2 \sigma^{(ROT)}}{d\Omega_{LF} d\Omega_3} = A' \bar{\sigma}_n \left[ \vec{k}_{LF}, \vec{k}_3 \right] \left( \vec{k}_{LF}, \vec{k}_3 \right), \tag{2}$$

which was named ROT and interpreted [4] in terms of classical mechanics as the result of the fission fragments' emission by the rotating fissioning system.

The description of these effects in the framework of quantum theory was given in [5-7] which considered the influence of the fissioning system rotation on the angular distribution of the ternary fission products. This rotation causes the appearance of Coriolis interaction in the internal coordinate system between the orbital momentum  $\vec{l}_3$  of the ternary particle and the nuclear total spin  $\vec{J}$ . An important role was demonstrated of the neutron resonances' interference which causes the damping of either even or odd orbital moments  $\vec{l}_3$  thus strengthening either TRI- or ROT-correlation, respectively.

In ref [8] the analogous ROT-effect was found for gamma quanta emitted in binary fission of <sup>235</sup>U induced by the polarized neutrons. The angular dependence of the effect was similar to the ROT effect for alpha particles while its magnitude was about 10<sup>-4</sup>.

In the present paper we shall use the approach of [5-7] to show that this latter effect could be explained by the T-odd asymmetry in the angular distribution of the pre-scission gammas emitted in binary fission induced by the polarized neutrons.

#### 2. Giant resonances in the fissioning nuclei and the pre-scission quanta

It was shown in ref [5-7] that the polarized neutron capture by the target nucleus leads to the excitation of neutron resonances in the first potential well of the compound nucleus. The nuclear fission is caused by the evolution of the resonance wave functions during the system's motion along the axially symmetric deformation mode. This evolution ends at the scission point by the transition of these wave functions into those of the fission modes  $\Psi_K^{JM}$ . The non-adiabatic character of this motion might lead to the excitation of the system's states which emit the pre-scission gammas. The typical time for the system's transition from the exterior saddle-point to the scission point is  $\tau_0 \approx 10^{-21} \mathrm{s}$ . Therefore, in order to make these gammas observable it is necessary that the life-times  $\tau_\gamma$  of those excited states should be of the same order as  $\tau_0$ . This means that their gamma widths  $\Gamma_\gamma = \hbar/\tau_\gamma$  should be of the order of 1 MeV. So large widths are characteristic only for the collective vibrations of the giant electric isovector dipole resonance (GDR) type. The typical energy of these resonances is  $E_0 = 80A^{-1/3} \mathrm{MeV}$ . However, in the axially-symmetric deformed nuclei these resonances split into two components corresponding to the vibrations along the long and the short axes of the system. The magnitude of this splitting is defined [9] by the expression:

$$\Delta E \approx E_0 \beta_2 \,, \tag{3}$$

where  $E_0 \approx 12 \,\text{MeV}$  for U isotopes and  $\beta_2$  is the quadrupole deformation parameter.

There are two possibilities to excite GDR in the fissioning nucleus. If its neck has not completely developed and the nucleus still conserves its ellipsoidal shape the GDR involves all the nucleons (in order to conserve total parity and the projection K of the total spin on the symmetry axis this resonance should be built on the excited state with negative parity and K'=K quantum number). Since the typical deformation of the heavy fissioning nuclei at the last stages before scission  $\beta_2 \approx 1$ , the energy of the lowest GDR component with spin's projection  $\nu = 0$  onto fissile nucleus symmetry axis might be quite low  $(E_{\nu=0} \approx (4-5) \,\text{MeV})$ . If the system's neck is already well developed and the pre-fragments appear the simultaneous excitation of two GDR's of the pre-fragments is possible caused by their mutual Coulomb However, the maximal deformation values  $\beta_2$  of the fragments with  $A_1 \approx A_2 \approx A/2$  do not exceed 0.3. Therefore the characteristic GDR energies of the fragments are rather large ( $E_{\nu=0}\approx 14$  MeV). The spectral analysis [10] of the gammas which follow the fission of <sup>235</sup>U shows the almost exponential decrease by 4 orders of magnitude in the energy range between  $E_{\nu} \approx 0.5$  MeV and  $E_{\nu} \approx 8$  MeV. One should expect that this decrease would continue at higher energies. This seems to cancel the case of the two GDR excitations of the pre-fragments and leaves us only with the first possibility - GDR excitation of the whole fissioning nucleus.

### The wave functions of the fissioning system which emit the pre-scission gammaquanta

The wave function of the fission mode  $\Psi_K^{JM}$  for the deformed axially symmetric fissioning nucleus can be written [9] as:

$$\Psi_{K}^{JM} = \sqrt{\frac{2J+1}{16\pi^{2}}} \left\{ \left[ D_{MK}^{J}(\omega) \chi_{K}(\xi) + (-1)^{J+K} D_{M-K}^{J}(\omega) \chi_{\overline{K}}(\xi) \right] (1 - \delta_{K,0}) + (4) + \sqrt{2} D_{M0}^{J}(\omega) \chi_{0}(\xi) \delta_{K,0} \right\}.$$

In order to describe the pre-scission gamma emission we shall introduce the vector spherical function [11]:

 $\vec{Y}_{jl\mu}(\Omega_{\bar{r}}, \vec{s}) = \left\{ Y_{lm}(\Omega_{\bar{r}}) \vec{e}_{lt}(\vec{s}) \right\}_{i\mu} , \qquad (5)$ 

where  $\vec{e}_{lt}(\vec{s})$  is the spin function which depends on the spin variables  $\vec{s}$  of the  $\gamma$ -quantum and its projection t ( $t=0,\pm 1$ ) on the Z-axis of the laboratory system;  $Y_{lm}(\Omega_{\vec{r}})$  is the spherical function which depends on the solid angle  $\Omega_{\vec{r}}$  of the quantum radius-vector  $\vec{r}$  and corresponds to the orbital momentum l and its projection m on Z-axis.. The curly brackets in (5) means the vector addition of the spin and the angular momentum of the quantum forming its total momentum  $\vec{j}$ .

One can use Wigner's transformation relating  $\vec{Y}_{jl\mu}(\Omega_{\vec{r}},\vec{s})$  of (5) to the vector spherical function  $\vec{Y}_{jl\eta}(\vec{s}')$  in the co-ordinate system K' where the vector  $\vec{r}$  defines the Z' axis direction and which realizes the helicity representation [9]:

$$\vec{Y}_{jl\mu}(\Omega_{\vec{r}},\vec{s}) = \sum_{n=1} D_{\mu n}^{j} (\Omega_{\vec{r}}) \vec{Y}_{jln}(\vec{s}'). \tag{6}$$

Here  $D^j_{\mu\eta}(\Omega_{\vec{r}})$  is the generalized spherical function which depends on the Euler's angles connected with the radius-vector  $\vec{r}$ ;  $\vec{Y}_{jl\eta}(\vec{s}')$  is the vector spherical function in the K'coordinate system:

$$\vec{Y}_{jl\eta}(\vec{s}') = \left(\frac{2j+1}{4\pi}\right)^{1/2} C_{j1-\eta\eta}^{l0} \vec{e}_{1\eta}(\vec{s}'). \tag{7}$$

Introduce now the vector potential  $\vec{A}_{jl\mu}(x)$  (where  $x \equiv \vec{r}, \vec{s}$  are the photon co-ordinates), which is normalized by the unit photon flux in the  $\vec{r}$  direction [11]:

$$\vec{A}_{jl\mu}(x) = \left(\frac{kc}{2\pi\hbar}\right)^{-1/2} k\left(n_l(kr) + ij_l(kr)\right) \vec{Y}_{jl\mu}(\Omega_{\vec{r}}, \vec{s}) i^l. \tag{8}$$

Here  $j_l(kr)$  and  $n_l(kr)$  are the Bessel and Neuman spherical functions while k is the modulus of the photon wave vector. Then the vector potentials  $\vec{A}_{\lambda l \mu}(x)$  corresponding to electric  $(\lambda = E)$  and magnetic  $(\lambda = M)$   $\gamma$ -quanta have the form:

$$\vec{A}_{\lambda j \mu}(x) = \begin{cases} -\sqrt{2} \sum_{l} C_{j1-11}^{l0} \vec{A}_{jl\mu}(x) \delta_{j,l} &, \lambda = M, \\ -\sqrt{2} \sum_{l \neq j} C_{j1-11}^{l0} \vec{A}_{jl\mu}(x) &, \lambda = E. \end{cases}$$
(9)

In general the Hamiltonian H' for the interaction of the electro-magnetic radiation with the atomic nucleus can be represented as [11]:

$$H' = -\frac{1}{c} \int \vec{Aj} d\tau \ . \tag{10}$$

Here  $\vec{j}$  is the density operator of the convectional and spin currents in the nucleus;  $\vec{A}$  is the vector potential of the electro-magnetic field. The integration is carried over all the nuclear coordinates  $\tau$ .

The fission mode wave function (4) after the emission of the  $\gamma$ -quantum transforms into the wave function  $\tilde{\Psi}_{K}^{JM}$  of the system which consists of the daughter nucleus plus the photon. Its asymptotic form for large r ( $r > R_A$ , where  $R_A$  is the nuclear radius) is:

$$\tilde{\Psi}_{K}^{JM} = \sum_{\alpha} \left\{ \Psi_{K}^{J'M'} \vec{A}_{\lambda j \mu} \right\}_{JM} \sqrt{\frac{\Gamma_{\gamma \alpha}^{JK}}{\hbar}}, \tag{11}$$

where  $\sqrt{\Gamma_{\gamma\alpha}^{IK}}$  is the partial width amplitude for the gamma decay of the fissioning nucleus into the channel  $\alpha$ :

$$\sqrt{\Gamma_{\gamma\alpha}^{JK}} = -\sqrt{\frac{\pi}{2\hbar}} \left( \frac{1}{2\pi ck} \right) \left\langle \left\{ \Psi_{K}^{JM} \tilde{\tilde{A}}_{\lambda j\mu} \right\}_{JM} \left| \vec{j} \right| \Psi_{K}^{JM} \right\rangle,$$

(12)

where potential  $\tilde{A}_{\lambda j\mu}$  differs from  $A_{\lambda j\mu}$  (8) by substitution of the function  $\left(n_l(kr)+ij_l(kr)\right)$  to the function  $j_l(kr)$ . Now one can show that in the long-wave approximation  $(kR_A <<1)$  the total width  $\Gamma_{\gamma E1}^{JK}$  of the electric dipole gamma decay is:

$$\Gamma^{JK}_{\gamma E1} = \sum_{J'K'} \Gamma^{JK}_{\gamma E1J'K'} = \Gamma^0_{\gamma K}.$$

(13)

Here the summation goes over the quantum numbers of the final states, while  $\Gamma^0_{\gamma K}$  is defined by the equation:

$$\sqrt{\Gamma_{\gamma K}^{0}} = -\sqrt{16\pi k} \left( \frac{k}{3!!} \right) \left\langle \chi_{K} \left| Q_{10}^{0} \right| \chi_{K} \right\rangle. \tag{14}$$

Here  $Q_{1K_1}^0$  is the electric dipole moment operator of the nucleus in the intrinsic coordinate system.

## The angular distribution of the pre-scission gamma-quanta emitted by the unpolarized fissioning nucleus

In order to describe the angular distribution of the pre-scission electric dipole quanta one can use Eq. (11), which can be written as:

$$\tilde{\Psi}_{K}^{JM} = \sum_{J'K'} \left\{ \Psi_{K'}^{J'M'} \vec{A}_{E1\mu} \right\}_{JM} \sqrt{\Gamma_{\gamma E1J'K'}^{JK}} . \tag{15}$$

With the use of Eqs. (8), (6) one can obtain the following expression for the vector potential  $\vec{A}_{F_{1}}(x)$ :

$$\vec{A}_{E1\mu}(x) = \sqrt{\frac{3}{4\pi}} \sum_{\eta=\pm 1} D_{\mu\eta}^{1}(\Omega_{\vec{r}}) \vec{e}_{1\eta}(\vec{s}') B(r),$$
(16)

where function B(r) is defined as:

$$B(r) = -\left(\frac{kc}{2\pi\hbar}\right)^{-1/2} 2\sum_{l\neq i} \left(C_{1-1-1}^{l0}\right)^{2} k\left(n_{l}(kr) + ij_{l}(kr)\right) i^{l}.$$
(17)

Now the wave function  $\tilde{\Psi}_{K}^{JM}$  of Eq. (15) can be written in the form:

$$\tilde{\Psi}_{K}^{JM} = \sum_{\eta=\pm 1} \sqrt{\frac{3}{4\pi}} D_{0\eta}^{1}(\Omega_{\bar{r}}^{1}) \bar{e}_{1\eta}(\bar{s}^{1}) \left(\frac{2J+1}{16\pi^{2}}\right)^{1/2} B(r) \times \left\{ D_{MK}^{J}(\omega) \chi_{K}(\xi) + (-1)^{J+K} D_{M-K}^{J}(\omega) \chi_{\bar{K}}(\xi) \right\} \sqrt{\Gamma_{\gamma K}^{0}}.$$
(18)

The fission fragments are emitted along the nuclear symmetry axis. Therefore if one chooses the Z-axis of the laboratory system to be directed along the light fragment momentum then the solid angle  $\Omega'_{\bar{r}}$  in (19) will coincide with the solid angle  $\Omega_{\bar{r}}$  which defines the direction of gamma emission with respect to the direction of the light fragment momentum.

With the help of Eq. (18) one can find the current density of the pre-scission gammas for  $r \to \infty$  and obtain the following expression for their angular distribution normalized by the total width  $\Gamma_{rK}^{0}$ :

$$\frac{d\Gamma_{\gamma K}(\Omega_{\bar{r}})}{d\Omega_{\bar{r}}} = \sum_{n=\pm 1} \frac{3}{4\pi} \left| D_{0\eta}^{1}(\Omega_{\bar{r}}) \right|^{2} \Gamma_{\gamma K}^{0} = \frac{3}{4\pi} \Gamma_{\gamma K}^{0} \sin^{2}\theta_{\bar{r}}. \tag{19}$$

We see that this angular distribution has a well - defined maximum in the direction perpendicular to the light fragment momentum when  $\theta_{\bar{r}} = \pi/2$ .

This expression holds irrespective of whether the emitting compound nucleus is polarized or not.

Now one can apply the technique of refs. [5-7] to obtain the differential cross section for the  $(n,\gamma)$  fission reaction with the emission of the pre-scission gamma :

$$\frac{d\sigma_{n\gamma}}{d\Omega_{\vec{r}}} = \frac{4\pi}{k_n^2} F^0(\Omega_{\vec{r}}),\tag{20}$$

where

$$F^{0}\left(\Omega_{\vec{r}}\right) = \sum_{sJ_{s}s'J_{s'}K_{s}} D_{K_{s}}^{sJ_{s}s'J_{s'}} \Gamma_{\gamma K_{s}}^{0} B_{K_{s}}^{sJ_{s}s'J_{s'}}, \tag{21}$$

$$D_{K_s}^{sJ_ss'J_{s'}} = b_{sK_s}^{J_s} b_{s'K_s}^{J_{s'}} \left| h_s^{J_s} \right| \left| h_s^{J_{s'}} \right|, \tag{22}$$

$$h_s^{J_s} = \frac{\sqrt{\Gamma_s^{J_s}}}{E - E_s^{J_s} + \frac{i\Gamma_s^{J_s}}{2}} = \left| h_s^{J_s} \right| e^{i\delta_{sJ_s}},$$

(23)

 $B_{K_s}^{sJ_ss'J_{s'}} = \delta_{J_s,J_{s'}} \frac{1}{16\pi^2} \frac{3}{4\pi} \sin^2 \theta_{\vec{r}} \frac{(2J_s + 1)}{2(2I + 1)} \cos \delta_{sJ_ss'J_{s'}}, \tag{24}$ 

and  $\delta_{sJ_s,s'J_s'} = \delta_{sJ_s} - \delta_{s'J_{s'}}$ , *I* is the target spin.

The direct measurement of the pre-scission gammas' angular distribution is complicated by the background of the much more intensive "statistical" gammas emitted by the thermalised fission fragments. Therefore in order to prove the existence of the pre-scission gammas one should investigate also the correlation effects which might be either larger or of the same scale as the analogous correlations for the statistical gammas. A good example of such effects is the T-odd correlation in the angular distributions of the pre-scission quanta emitted in fission reaction induced by the cold polarized neutrons which is caused by the influence of the polarized compound nucleus rotation on the angular distribution of the emitted quanta.

# 5. T-odd asymmetry in the angular distribution of pre-scission quanta

We shall study the influence of the polarized compound nucleus rotation on the angular distribution of the pre-scission quanta by introducing into the Hamiltonian the term  $H_{\text{Cor}}$  [9] coming from the Coriolis interaction of the total nuclear spin  $\vec{J}$  with the total momentum  $\vec{j}$  of the pre-scission quantum:

$$H_{\text{Cor}} = -\frac{\hbar^2}{2J_0} (J_+ j_- + J_- j_+), \tag{25}$$

where

$$J_{\pm} = (J_{x'} \pm iJ_{y'}), \ j_{\pm} = (j_{x'} \pm ij_{y'}),$$
(26)

and x', y' indicate the axes in the intrinsic coordinate system. The symbol  $\mathcal{F}_0$  means the moment of inertia of the fissioning system which evolves from the compound nucleus moment of inertia at the scission point up to the value  $M_c R^2$  for  $R \to \infty$  ( $M_c$  is the reduced mass for the fission channel c. The action of the operators  $J_{\pm}$  on the function  $D^J_{MK}(\omega)$  which describes the collective rotation of the whole system and of the operators  $j_{\pm}$  on the function  $D^1_{0\eta}(\Omega'_{\vec{r}})$  describing the angular distribution of the pre-scission quanta is defined as:

$$J_{\pm}D_{MK}^{J}(\omega) = \left[ \left( J \pm K \right) \left( J \mp K + 1 \right) \right]^{1/2} D_{M(K\mp 1)}^{J}(\omega) , \qquad (27)$$

$$j_{\pm}D_{0n}^{1}(\Omega_{\vec{r}}) = \sqrt{2}D_{(\pm 1)n}^{1}(\Omega_{\vec{r}}).$$
 (28)

By using the technique of ref. [5] one can take into account the influence of the Coriolis interaction on the fission mode wave function  $\Psi_K^{JM}$  by adding to it (in the region where the pre-scission quanta and the daughter nucleus are already formed) the wave function  $\Delta \tilde{\Psi}_K^{JM}$ :

$$\Delta \tilde{\Psi}_{K}^{JM}(x) = \sum_{m=\pm 1, \eta=\pm 1} \left\{ D_{MK+m}^{J}(\omega') \chi_{K}^{i} b_{KJ}^{m} + (-1)^{J+K} D_{M(-K+m)}^{J}(\omega') \chi_{K}^{i} b_{-KJ}^{m} \right\} \times \sqrt{\frac{2J+1}{16\pi^{2}}} D_{m\eta}^{1}(\Omega'_{r}) \vec{e}_{1\eta} \sqrt{\Gamma_{\gamma K}^{0}} \alpha^{\text{Cor}} B(r) \sqrt{2} \sqrt{\frac{3}{4\pi}},$$
(29)

where

$$b_{KJ}^{+1} = b_{-KJ}^{-1} = \sqrt{(J-K)(J+K+1)}; \ b_{KJ}^{-1} = b_{-KJ}^{+1} = \sqrt{(J+K)(J-K+1)}$$
 (30)

and

$$\alpha^{\text{Cor}} = \frac{k^2}{\hbar^2 c} \int_{R_A}^{\infty} \tilde{B}(r) \left( -\frac{\hbar^2}{2J_0} \right) B(r) r^2 dr .$$

Here the quantity  $\tilde{B}(r)$  is defined by Eq. (17) with the substitution of the function  $j_l(kr)$  instead of the quantity  $(n_l(kr)+ij_l(kr))$ . After adding the function  $\Delta \tilde{\Psi}_K^{JM}(x)$  to the unperturbed function  $\tilde{\Psi}_K^{JM}(x)$  of Eq. (18) one can find the current density of the prescission quanta  $\vec{j} = \vec{j}^0 + \Delta \vec{j}$ . Performing the integration over the internal co-ordinates  $\xi$  of the daughter nucleus one obtains the first-order correction  $F^{(1)}(\Omega_{\vec{r}})$  to the quantity  $F^0(\Omega_{\vec{r}})$  of (21) which defines the cross-section  $\frac{d\sigma_{n\gamma}}{d\Omega_{\vec{r}}}$  of Eq. (20). Thus we obtain the

additional term  $\frac{d\sigma_{n\gamma}^{cor}}{d\Omega_{\bar{r}}}$  to the cross-section coming from the Coriolis interaction. This term is defined by the non-diagonal part of the spin density matrix  $\rho_{MM}^{J_sJ_s}$  which is proportional to the neutron polarization  $p_n$ . Therefore  $\frac{d\sigma_{n\gamma}^{Cor}}{d\Omega_{\bar{r}}}$  is defined by the Eqs. (20-23) with the quantity  $B_K^{sJ_ss^*J_s}$  of Eq. (24) substituted by:

$$\left(B_{K_{s}}^{sJ_{s}s'J_{s'}}\right)^{\text{Cor}} = \left(\frac{1}{8\pi^{2}}\right)\alpha^{\text{Cor}} \frac{3}{4\pi} \frac{\sqrt{(2J_{s}+1)(2J_{s'}+1)}}{2(2I+1)} g_{K_{s}J_{s}J_{s'}} p_{n} \sqrt{2} \times \sum_{n=\pm 1} \left[D_{-1\eta}^{1}(\Omega_{\vec{r}}) - D_{1\eta}^{1}(\Omega_{\vec{r}})\right] D_{0\eta}^{1*}(\Omega_{\vec{r}}) \sin \delta_{sJ_{s}s'J_{s'}}, \tag{32}$$

where

$$g_{K_{s}J_{s}J_{s}} = A(J_{s}, J_{s}) \left[ \sqrt{(J_{s} + K_{s})(J_{s} - K_{s} + 1)} C_{J_{s} 1(K_{s} - 1)1}^{J_{s} \cdot K_{s}} - \sqrt{(J_{s} - K_{s})(J_{s} + K_{s} + 1)} C_{J_{s} 1(K_{s} + 1) - 1}^{J_{s} \cdot K_{s}} \right],$$
(33)

$$A(J_{s},J_{s'}) = \delta_{J_{s},J_{s'}} \left( \sqrt{\frac{J_{s}}{2(J_{s}+1)}} \delta_{J_{s},J_{s'}} - \sqrt{\frac{J_{s}+1}{2J_{s}}} \delta_{J_{s},J_{s}} \right) - \sqrt{\frac{2J_{s}+1}{2J_{s}}} \delta_{J_{s},J_{s'}+1} + \sqrt{\frac{2J_{s}+1}{2(J_{s}+1)}} \delta_{J_{s},J_{s'}-1},$$
(34)

$$J_{>} = I + 1/2, \qquad J_{<} = I - 1/2.$$

The component of the angular distribution of pre-scission quanta arising from the neutron polarization is:

$$J\left(\Omega_{\vec{r}}\right) = \sum_{n=+1} \left[ D_{-1\eta}^{1}\left(\Omega_{\vec{r}}\right) - D_{1\eta}^{1}\left(\Omega_{\vec{r}}\right) \right] D_{0\eta}^{1*}\left(\Omega_{\vec{r}}\right). \tag{35}$$

This expression can be reduced to the form:

$$J(\Omega'_{\vec{r}}) = -C_{11-10}^{20} \left[ Y_{2(-1)}(\Omega'_{\vec{r}}) - Y_{21}(\Omega'_{\vec{r}}) \right] \sqrt{\frac{4\pi}{5}} (-1) C_{11-11}^{20} 2 = -\frac{1}{\sqrt{2}} \sin 2\theta_{\vec{r}} \cos \varphi_{\vec{r}}.$$
(36)

Thus the expression for the polarization-dependent addition to the differential cross-section is:

$$\frac{d\sigma_{n\gamma f}^{Cor}}{d\Omega_{\bar{r}}} = \frac{p_n}{2(2I+1)k_n^2} \sum_{ss',J_s,J_{s'}} |h_{s'}^{J_s}| |h_{s'}^{J_{s'}}| |b_{sK_s}^{J_s}| b_{s'K_s}^{J_{s'}}| \Gamma_{\gamma K_s}^0 \sqrt{(2J_s+1)(2J_{s'}+1)} \times g_{K_sJ_sJ_{s'}} \left( -\frac{3\alpha^{Cor}}{8\pi^2} \right) \sin 2\theta_{\bar{r}} \cdot \cos \varphi_{\bar{r}} \cdot \sin \delta_{sJ_s s'J_{s'}}.$$
(37)

One can see from Eq. (36) that the part of the angular distribution connected with the collective rotation of the polarized nucleus is defined by the spherical functions  $Y_{2,\pm 1}$  coming from the even value l=2 of the angular momentum. As shown in [7] for the case of T-odd correlation of alpha particles, this means that the T-odd correlation for the pre-scission gammas are only of the type of the ROT-effect.

Eq. (37) shows that this correlation appears only in the case of the neutron resonances interference when the value  $\delta_{sJ_ss'J_{s'}} \neq 0$ . Since the pre-scission gammas are observed on the strong background of statistical quanta with rather small anisotropy, the angular dependence of the asymmetry coefficient  $D_{\nu}(\Omega_{\Gamma})$  is of the form:

$$D_{x}(\theta_{z}) = A\sin 2\theta_{z} \,, \tag{38}$$

which is close to that observed in ref. [8].

In order to estimate the coefficient  $D_{\gamma}$  for the pre-scission quanta one can use the qualitative classical picture which was applied in ref. [4] to the case of the alpha particles' ROT asymmetry. Consider the rotating nucleus emitting electric dipole quanta. Their angular distribution without rotation should be (19):

$$P(\theta) = B\sin^2\theta \,\,\,\,(39)$$

where  $\theta$  is the angle between the nuclear symmetry axis and the direction of the gamma emission. However the nucleus rotates with the angular velocity  $\omega \approx 2 \cdot 10^{19}\,\text{l/s}$  while emitting the pre-scission quanta and manages to turn since the initial moment of this emission through the angle:

$$\theta_0 = \omega \tau + \alpha \quad , \tag{40}$$

where au is the pre-scission gamma emission time and lpha is the rotation angle of the system after scission, which was estimated in [4] as  $\alpha \approx 3 \cdot 10^{-3}$ . Therefore the angular distribution for the rotating nucleus in the laboratory system is:

$$P_{+}(\theta) \approx B \sin^{2}[\theta \pm (\omega \tau + \alpha)] \approx B\{\sin^{2}\theta \pm (\omega \tau + \alpha)\sin 2\theta\}$$
 (41)

Here the subscript  $\pm$  defines the polarized neutron helicity (i.e. the direction of nuclear rotation). Therefore the numerator of the asymmetry coefficient  $D_r$  is:

$$P_{\perp}(\theta) - P_{\perp}(\theta) = B(2\omega\tau + 2\alpha)\sin 2\theta . \tag{42}$$

Taking the emission time of the GDR gammas to be  $\tau \approx \hbar/\Gamma \approx 10^{-21}$ s, we obtain  $(2\omega\tau+2\alpha)\approx 4\cdot 10^{-2}$ .

$$(2\omega\tau + 2\alpha) \approx 4 \cdot 10^{-2} \tag{43}$$

Dividing this quantity by twice the number of statistical gammas one obtains for the magnitude of the ROT asymmetry effect the value  $B \cdot 2.5 \cdot 10^{-3}$ .

The analysis [10] of gamma spectrum following the <sup>235</sup>U fission by thermal neutrons shows that the number B of quanta per fission in the range of  $E_{\nu}$ =4-6 MeV is about 0.1. This seems to be in agreement with the experimental value 10<sup>-4</sup> obtained in ref. [8].

#### 6. Summary

Our studies of the possible T-odd asymmetry for the pre-scission gammas carried in the framework of the quantum theory of fission allow to obtain the angular dependence and the magnitude of the asymmetry coefficient  $D_{\gamma}$  in agreement with experiment [8]. In order to make the final conclusions about the existence of the pre-scission quanta one should investigate the possibility to obtain the T-odd correlation with the statistical quanta, its magnitude and angular dependence.

This work was supported by the grants of RFBR (№03-02-16853) and INTAS.

#### References.

- 1. P. Jessinger, A. Kotzle, A.M. Gagarski et.al., Nucl. Instrum. Methods. A440, 2000, p.618.
- 2. G. Val'sky, A. Vorobiev, A. Gagarski et.al.. Izvestia RAN, 71, 2007, p. 368.
- 3. F.Goennenwein, M. Mutterer, A. Gagarski et al. Phys. Lett. B 652, 2007, p. 13.
- 4. I. Guseva, Yu. Gusev. Proc. of ISINN-14, Dubna JINR, 2007, p.101 -108.
- 5. V. Bunakov, S. Kadmensky. Phys. At. Nucl. V.66, 2003, p.1846.
- 6. V. Bunakov, S. Kadmenski, L. Rodionova. Izvestia RAS (phys.) V.69, 2005, p.614.
- 7. V.E. Bunakov, S.G. Kadmensky, S.S. Kadmensky, Phys. At. Nucl. V.71, 2008, p.1917.
- 8. G. Danilyan. Phys.At.Nucl. V.71, 2008 (in press).
- 9. A.Bohr, B.Mottelson. Nuclear Structure (Benjamin, NY, 1974) V.2.
- 10. F.Maienschein, R. Peele, W.Sobel, T.Love. Proc. of II Internat. Conference on Peaceful Uses of Atomic Energy. Geneva, 1958. (United Nations, N-Y, 1958).
- 11. A.Lane, R.G..Thomas. Rev. Mod. Phys. V.30, 1958, p.25.

# LOW-ENERGY SCATTERING OF A POLARIZED NEUTRON ON A POLARIZED PROTON

V.L.Lyuboshitz, <u>V.V.Lyuboshitz</u>\*)

Joint Institute for Nuclear Research, 141980 Dubna, Moscow Region, Russia \*) E-mail: Valery, Lyuboshitz@iinr.ru

The spin structure of the amplitude of s-wave elastic scattering of a slow neutron on a free proton is considered. The formula for effective cross-section of scattering of a slow polarized neutron on the polarized proton target is obtained, and it is shown that, in the effective cross-section, the amplitudes of triplet (total spin S=1) and singlet (total spin S=0) scattering are summed up incoherently. In doing so, the maximum value of integral cross-section  $\sigma_{max} \approx 37.1$  barn corresponds to the antiparallel orientations of spins of the totally polarized neutron and proton ( $\mathbf{P}_n \mathbf{P}_p = -1$ , where  $\mathbf{P}_n$  and  $\mathbf{P}_p$  are the polarization vectors), whereas the minimal magnitude of cross-section  $\sigma_{min} \approx 3.64$  barn is observed in the case of parallel orientation of spins ( $\mathbf{P}_n \mathbf{P}_p = +1$ ).

The low-energy scattering of polarized neutrons is also analyzed. Taking into account the identity effect, the s-wave scattering of neutrons is possible only in the singlet state. According to the isotopic invariance, one could expect that the amplitude of s-wave scattering of two neutrons must coincide, with the precision of (1+3)%, with the singlet amplitude of neutron scattering on the proton. Nevertheless, in fact the scattering lengths take the values  $b^{(np)} = -a^{(np)}(0) = -23.7$  fm and  $b^{(nn)} = -a^{(nn)}(0) = -17.0$  fm; so, we have  $|b^{(np)}/b^{(nn)}| \approx 1.4$ . However, the concept of "isotopic invariance" is applicable rather to the interaction potential than to the scattering amplitude. Analysis shows that, if the modulus of amplitude is large as compared with the range of force action, the magnitude of scattering amplitude becomes very sensitive to the parameters of potential. Within the model of spherical rectangular well, the change of depth or width of the well by several per cent leads to the substantial change of scattering length.

**1.** Amplitude of the elastic s-wave scattering of a slow neutron on a free proton has the following structure:

$$\hat{f}(k) = a_t(k)\hat{P}_t + a_s(k)\hat{P}_s \quad , \tag{1}$$

where  $a_t(k)$  is the amplitude of triplet scattering, corresponding to the total spin of the neutron-proton system equaling 1,  $a_s(k)$  is the amplitude of singlet scattering, corresponding to the total spin of the (np) system equaling 0, k is the modulus of nucleon momentum in the c.m. frame,

$$\hat{P}_{t} = \frac{3\hat{I}^{(1)} \otimes \hat{I}^{(2)} + \hat{\sigma}^{(1)} \otimes \hat{\sigma}^{(2)}}{4} , \qquad \hat{P}_{s} = \frac{\hat{I}^{(1)} \otimes \hat{I}^{(2)} - \hat{\sigma}^{(1)} \otimes \hat{\sigma}^{(2)}}{4}$$
(2)

are the operators of projection onto the triplet states and the singlet state, respectively, satisfying the relations:

$$\hat{P}_{t}^{2} = \hat{P}_{t}$$
,  $\hat{P}_{s}^{2} = \hat{P}_{s}$ ,  $\hat{P}_{s}\hat{P}_{t} = \hat{P}_{t}\hat{P}_{s} = 0$  (3)

( In Eq. (2):  $\hat{I}^{(1)}$ ,  $\hat{I}^{(2)}$  are two-row unit matrices,  $\hat{\sigma}^{(1)} = \{ \hat{\sigma}_x^{(1)}, \hat{\sigma}_y^{(1)}, \hat{\sigma}_z^{(1)} \}$  and  $\hat{\sigma}^{(2)} = \{ \hat{\sigma}_x^{(2)}, \hat{\sigma}_y^{(2)}, \hat{\sigma}_z^{(2)} \}$  are vector Pauli operators ).

Relations (3) can be easily verified using the matrix equality:

$$(\hat{\sigma}^{(1)} \otimes \hat{\sigma}^{(2)})^2 = 3\hat{I}^{(1)} \otimes \hat{I}^{(2)} - 2\hat{\sigma}^{(1)} \otimes \hat{\sigma}^{(2)} \qquad . \tag{4}$$

Formula (1) may be also rewritten in the form:

$$\hat{f}(k) = c(k)\hat{I}^{(1)} \otimes \hat{I}^{(2)} + d(k)\hat{\sigma}^{(1)} \otimes \hat{\sigma}^{(2)} \qquad , \tag{5}$$

where

$$c(k) = \frac{3a_t(k) + a_s(k)}{4}$$
,  $d(k) = \frac{a_t(k) - a_s(k)}{4}$ 

According to the experimental data, at zero energy:

$$a_t(0) = -5.38 \text{ fm}$$
;  $a_s(0) = +23.6 \text{ fm}$ ;  $c(0) = 1.89 \text{ fm}$ ;  $d(0) = -7.27 \text{ fm}$ .

By definition, the scattering lengths are:  $b_{(s,t)} = -a_{(s,t)}(0)$ .

Introducing the operator of permutation of spin projections [1,2]:

$$\hat{P}_{exch}^{(1,2)} = \frac{1}{2} [\hat{I}^{(1)} \otimes \hat{I}^{(2)} + \hat{\sigma}^{(1)} \otimes \hat{\sigma}^{(2)}] \qquad , \tag{6}$$

one can get easily convinced in the validity of the following equalities as well:

$$\hat{P}_{exch}^{(1,2)}\hat{P}_t = \hat{P}_t\hat{P}_{exch}^{(1,2)} = +\hat{P}_t \quad , \quad \hat{P}_{exch}^{(1,2)}\hat{P}_s = \hat{P}_s\hat{P}_{exch}^{(1,2)} = -\hat{P}_s \quad . \tag{7}$$

In accordance with Eq. (7), the eigenvalues of the operator  $\hat{P}_{exch}^{(1,2)}$  are equal to (+1) for the three triplet states and to (-1) for the singlet state.

2. The total cross-section of elastic scattering of slow polarized neutrons on a polarized proton target amounts to:

$$\sigma^{(n,p)} = 4\pi \operatorname{tr}(\hat{f}(k)\hat{\rho}^{(1,2)}\hat{f}^{+}(k)) = 4\pi \operatorname{tr}(\hat{f}(k)\hat{f}^{+}(k)\hat{\rho}^{(1,2)}) \quad , \tag{8}$$

where the amplitude  $\hat{f}(k)$  is determined according to Eq. (1),

$$\hat{\rho}^{(1,2)} = \frac{1}{4} (\hat{I}^{(1)} + \mathbf{P}_{n} \,\hat{\sigma}^{(1)}) \otimes (\hat{I}^{(2)} + \mathbf{P}_{p} \hat{\sigma}^{(2)})$$
(9)

is the 4-row spin density matrix of the neutron and proton,  $\mathbf{P}_n = \langle \hat{\mathbf{\sigma}}^{(1)} \rangle = tr(\hat{\mathbf{\sigma}}^{(1)} \, \hat{\boldsymbol{\rho}}^{(1,2)})$  and  $\mathbf{P}_p = \langle \hat{\mathbf{\sigma}}^{(2)} \rangle = tr(\hat{\mathbf{\sigma}}^{(2)} \, \hat{\boldsymbol{\rho}}^{(1,2)})$  are respective polarization vectors for the neutron and proton .

Taking into account the equalities (2), we have :

$$tr(\hat{P}_{t}^{2}\hat{\rho}^{(1,2)}) = tr(\hat{P}_{t}|\hat{\rho}^{(1,2)}) = \frac{3 + \mathbf{P}_{n}\mathbf{P}_{p}}{4} , tr(\hat{P}_{s}^{2}\hat{\rho}^{(1,2)}) = tr(\hat{P}_{s}|\hat{\rho}^{(1,2)}) = \frac{1 - \mathbf{P}_{n}\mathbf{P}_{p}}{4} ,$$
$$tr(\hat{P}_{t}\hat{P}_{s}|\hat{\rho}^{(1,2)}) = 0 . \tag{10}$$

As a result, we obtain:

$$\sigma^{(np)} = 4\pi \left\{ |a_t(k)|^2 \frac{3 + \mathbf{P}_n \mathbf{P}_p}{4} + |a_s(k)|^2 \frac{1 - \mathbf{P}_n \mathbf{P}_p}{4} \right\} =$$

$$= 4\pi \left\{ \frac{3|a_t(k)|^2 + |a_s(k)|^2}{4} + \frac{|a_t(k)|^2 - |a_s(k)|^2}{4} (\mathbf{P}_n \mathbf{P}_p) \right\} . \tag{11}$$

We see that, in the effective cross-section, the contributions of triplet and singlet scattering are summed up incoherently. In doing so, the quantities

$$W_t = \frac{3 + \mathbf{P}_n \mathbf{P}_p}{4} , \quad W_s = \frac{1 - \mathbf{P}_n \mathbf{P}_p}{4}$$
 (12)

determine the respective relative fractions of the triplet states and the singlet state for the (np) system with the polarization vectors  $\mathbf{P}_n$  and  $\mathbf{P}_p$ .

In the case when at least one of the nucleons is unpolarized, as well as when the nucleon polarization vectors are mutually orthogonal ( $\mathbf{P}_n \mathbf{P}_p = 0$ ), the integral cross-section of s-wave elastic neutron scattering on the proton at zero energy equals:

$$\sigma_0 = \pi \left( 3a_t^2(0) + a_s^2(0) \right) \approx 20.4 \text{ barn}.$$

The maximum value of the effective cross-section corresponds to the antiparallel orientation of spins of the totally polarized proton and neutron  $(\mathbf{P}_n \mathbf{P}_p = -1)$ :

$$\sigma_{max} = 2\pi (a_t^2(0) + a_s^2(0)) \approx 37.1 \text{ barn},$$

and the minimal value of the effective cross-section – to the parallel orientation of spins  $(\mathbf{P}_n \mathbf{P}_p = +1)$ :

$$\sigma_{min} = 4\pi a_1^2(0) \approx 3.64 \text{ barn}.$$

3. Let us remark that the amplitude of s-wave scattering of slow neutrons, defined in the front hemisphere of solid angles, is as follows, taking into account their identity [3]:

$$f^{(nn)}(k) = a_s^{(nn)}(k)\hat{P}_s - a_s^{(nn)}(-k)\hat{P}_{exch}^{(1,2)}\hat{P}_s = 2a_s^{(nn)}(k)\hat{P}_s =$$

$$= a_s^{(nn)}(k)\frac{\hat{I}^{(1)} \otimes \hat{I}^{(2)} - \hat{\sigma}^{(1)} \otimes \hat{\sigma}^{(2)}}{2} . \tag{13}$$

In doing so, the integral cross-section of elastic scattering equals:

$$\sigma^{(nn)} = 2\pi |a_s^{(nn)}(k)|^2 (1 - \mathbf{P}_1 \, \mathbf{P}_2) , \qquad (14)$$

where  $P_1$ ,  $P_2$  - neutron polarization vectors.

Indeed, owing to the equality [2,3]:

$$(-1)^{L+S} = 1$$
 , (15)

where L is the orbital momentum and S is the total spin of two identical particles, the s-wave neutron-neutron scattering – as well as the s-wave scattering of any two identical particles with spin 1/2 – is possible only in the singlet state .

Taking into account the isotopic invariance, one could anticipate that the amplitude of neutron scattering on the proton, corresponding to the total spin of the (np) system S = 0 (singlet amplitude  $a_s^{(np)}(k)$ ) must coincide with the neutron-neutron scattering amplitude  $a_s^{(nn)}(k)$ , which can be singlet only. However, in fact these amplitudes are essentially different: the singlet length of (np) scattering is  $b_s^{(np)} = -23.7$  fm, whereas the respective length of (nn) scattering equals  $b_s^{(nn)} = -17.0$  fm. This is due to the fact that, under the condition when the scattering amplitude substantially exceeds in modulus the range of force action, the scattering length becomes very sensitive to the depth and width of the interaction potential [4]. In this case, the concept of isotopic invariance is applicable namely to the interaction potential, but not to the scattering amplitude: the potentials of neutron-proton and neutron-neutron interaction should be approximately the same, differing by not more than (2 ÷ 3) %. Nevertheless, this small difference leads to the difference of respective amplitudes by several tens per cent, which looks like a spurious violation of isotopic invariance.

**4.** The further analysis will be performed within the model of a rectangular well with depth  $V_0$  and width  $r_0$ . In this model, the phase of s-wave scattering  $\delta_0(k)$  is determined by means of the conjunction of logarithmic derivatives of wave functions inside and outside the well [3]. This gives:

$$k \operatorname{ctg}(kr_0 + \delta_0(k)) = \chi(k) \operatorname{ctg} \chi(k) \quad , \tag{16}$$

where

$$\chi(k) = \sqrt{\frac{2mV_0}{\hbar^2} + k^2} \qquad , \tag{17}$$

m is the reduced mass.

In doing so,

$$\operatorname{ctg}(kr_0 + \delta_0(k)) = \frac{\operatorname{ctg} \delta_0(k) - \operatorname{tg} kr_0}{1 + \operatorname{ctg} \delta_0(k) \operatorname{tg} kr_0} . \tag{18}$$

As it is known, the amplitude of s -wave scattering is connected with the phase  $\delta_0(k)$  by the relation:

$$\frac{1}{a(k)} = k \operatorname{ctg} \delta_0(k) - ik \tag{19}$$

Substituting Eqs. (18) and (19) into formula (16), we obtain:

$$\frac{1}{a(k)} = \frac{\chi(k) \operatorname{ctg}(\chi(k) r_0) + k \operatorname{tg} k r_0}{1 - \frac{\operatorname{tg} k r_0}{k} \chi(k) \operatorname{ctg}(\chi(k) r_0)} - ik \qquad (20)$$

Hence, the scattering length is

$$b = -a(0) = -\frac{\lg(\chi_0 r_0)}{\chi_0} + r_0 \qquad , \tag{21}$$

where

$$\chi_0 = \chi(0) = \sqrt{\frac{2mV_0}{\hbar^2}} \quad . \tag{22}$$

In the framework of the effective radius theory [3]:

$$\frac{1}{a(k)} = -\frac{1}{b} + \frac{1}{2} r_{eff} k^2 - ik \qquad (23)$$

Expanding the right-hand side of Eq. (20) over the powers of  $k^2$  and taking into account that  $\chi(k) = \chi_0 + \frac{k^2}{2\chi_0}$ , we obtain formula (21) for the scattering length and the following value of the effective radius:

$$r_{eff} = 2 r_0 (1 - \chi_0 r_0 \operatorname{ctg}(\chi_0 r_0))^{-1} +$$

+ 
$$\left[\frac{\operatorname{ctg}(\chi_0 r_0)}{\chi_0} - \frac{r_0}{\sin^2(\chi_0 r_0)} + \frac{2}{3}r_0^3\chi_0^2\operatorname{ctg}^2(\chi_0 r_0)\right](1 - \chi_0 r_0\operatorname{ctg}(\chi_0 r_0))^{-2}$$
. (24)

It follows from Eq. (21) for the scattering length that at  $\chi_0 r_0 \approx \frac{\pi}{2}$  (tg  $(\chi_0 r_0) >> 1$ ) the values of scattering length are very sensitive to the magnitudes of depth and width of the potential well.

Indeed, let us introduce the characteristics of the potential well for the proton and neutron in the singlet state, corresponding to the data on the amplitude of singlet (np) scattering:

$$V_{0(s)}^{(np)} = 14.524 \text{ fm} ; r_{0(s)}^{(np)} = 2.5458 \text{ fm} .$$

In this case  $(\chi_0 r_0 = 1.506$ ,  $tg(\chi_0 r_0) = 15.47 >> 1$ ), calculations using Eqs. (21), (24) give:

$$b_s^{(np)} = -23.6 \text{ fm}$$
,  $r_{eff(s)}^{(np)} = 2.66 \text{ fm}$ .

When decreasing the depth of the potential well by 3 % only ( $V_0^{(nn)} = 14.084 \text{ MeV}$ ), the calculation according to Eqs. (21), (24) at the same width of the potential well leads to the values:

$$b_s^{(nn)} = -17.1 \text{ fm}, \quad r_{eff(s)}^{(nn)} = 2.72 \text{ fm}.$$

In doing so,  $\left|b_s^{(np)}\middle/b_s^{(nn)}\right| = 1.38$ , whereas the effective radius changes insignificantly.

Now let the depth of the potential well take the initial value ( $V_0^{(nn)} = 14.524 \text{ fm}$ ), and let us decrease the width of the well by 1.5 % ( $r_{0(x)}^{(nn)} = 2.49 \text{ fm}$ ). Then the calculation using Eq. (21) leads to the value  $b_x^{(nn)} = -16.8 \text{ fm}$ .

So, we see that, despite the substantial difference of the singlet amplitudes of (np) and (nn) scattering, for the respective potentials the isotopic invariance really holds: the parameters of potentials coincide with the precision of  $(1.5 \div 3)$  %.

# 5. Summary

- 1. The spin structure of the amplitude and effective cross-section of scattering of a slow neutron on a proton target is analyzed.
- 2. The comparison of the (np) scattering amplitude with the neutron-neutron scattering one is performed.
- 3. It is shown that, in the conditions when the modulus of scattering length consi-derably exceeds the range of interaction, the value of scattering length becomes very sensitive to the characteristics of potential.
- 4. In this connection, the concept of isotopic invariance is related rather to two-nucleon interaction potentials than to nucleon-nucleon scattering amplitudes.

# References

- V.L. Lyuboshitz and M.I. Podgoretsky. Yad. Fiz. 60, 45 (1997)
   [ Phys. At. Nucl. 60, 39 (1997) ] .
- V.L. Lyuboshitz. Proceedings of the XXXIV Winter School of Petersburg Nuclear Physics Institute. Physics of Atomic Nucleus and Elementary Particles, Saint-Petersburg (2000), p. 402.
- 3. L.D. Landau and E.M. Lifshitz. Quantum mechanics. Nonrelativistic theory (in Russian). Nauka, Moscow, 1989, §§ 61, 62, 132, 138.
- 4. G. Bethe and F. Morrison. *Elementary Nuclear Theory* (in Russian). IIL, Moscow, 1958, § 13.

# ROT - effect in Binary Fission Induced by Polarized Neutrons

- G.V. Danilyan <sup>1</sup>, P. Granz <sup>2</sup>, V.A. Krakhotin <sup>1</sup>, F. Mezei <sup>2</sup>, V.V. Novitsky <sup>1,3</sup>, V.S. Pavlov <sup>1</sup>, M. Russina <sup>2</sup>, P.B. Shatalov <sup>1</sup>, T. Wilpert <sup>2</sup>.
- Alikhanov Institute for Theoretical and Experimental Physics (ITEP), Moscow, Russia
- 2. Hahn-Meitner Institut (BENSC, HMI), Berlin, Germany
- 3. Frank Laboratory of Neutron Physics, (FLNP, JINR), Dubna, Russia

# Introduction

Recently a small shift has been observed in the angular distribution (AD) of light charged particles (LCP) emission relative to the fission axis in ternary fission of <sup>235</sup>U nuclei induced by cold polarized neutrons at ILL HFR [1]. The authors explained this effect as a result of the rotation of the fissile nuclei around the nuclear spin and called it the "ROT-effect". The shift of AD of LCP is an apparent effect, which appears due to the summation of radial and tangential velocities of fission fragments; the trajectories of the fragments become hyperbolae instead of straight lines and direction of deviation of the trajectory from a straight line depends on the direction of fissile nucleus rotation. In experiment, AD is measured relative to so called fission axis defined by the trajectory of fragment while in reality it is formed relative to the deformation axis.

ROT-effect should become apparent also in binary fission accompanied by other particles. From this reason we performed an experiment at the BENSC HMI BER-II reactor to search for the ROT-effect in  $^{235}$ U(n, $\gamma$ f) - reaction induced by cold polarized neutrons. It's well known that the fission process is accompanied by the emission of gamma-quanta. The main part of these gamma's is irradiated by excited fragments, while another part can be emitted by the fissile nuclei at the scission moment or before the scission (rupture of the neck). In the last case the shift angle should include the additional small angle defined by the turning of the deformation axis during the time interval  $\tau$ . Of course,  $\tau$  must be much less than the fissile nucleus period of revolution, otherwise the ROT-effect will be washed out. This part of gamma's will be referred to as pre-scission gamma's (PscG).

The experiment has been arranged similarly to experiment [1]. The difference was in the particles detected in coincidence with the fission fragment. It was LCP of ternary fission in the experiment [1], and it was PscG from binary fission in our

experiment. The asymmetry of the coincidence count rates between pulses from gamma-quanta and from fission fragments detectors with respect to the direction of the fissile nuclei polarization,

$$R = \{N_1(\theta) - N_2(\theta)\}/\{N_1(\theta) + N_2(\theta)\}$$
 (1)

is proportional to the angle of shift. Here  $N_1(\theta)$  and  $N_2(\theta)$  are count rates at opposite directions of the neutron beam polarization, and  $\theta$  is the angle between gamma-quantum and fission fragment detectors.

# Experiment

The cold polarized neutron beam passes through a thin Al window into the cylindrical fission chamber filled with isobutane at pressure of 8 mbar (Fig.1). The two sided target of <sup>235</sup>U (40 mg in total) evaporated on a thick Zr substrate with dimensions 4x10 cm is mounted on the axis of the chamber along the longitudinally polarized neutron direction. Two multi-wire low proportional counters (MWPC) to detect fission fragments were disposed on both sides of the target at of 7.5 cm distance. Both detectors are connected in parallel and they don't distinguish between light and heavy fragments. The gamma-ray detectors are arranged outside the fission chamber at 25 cm distance from the center of the target. They consist of plastic scintillator and photomultiplier (PMT). We used plastic scintillators with the aim to search for the ROT effect not only for PscG, but also for the so called scission neutrons (ScN). They also can be used as a trigger to see the shift of their angular distribution relative to the fission axis if this distribution is not the isotropic. To distinguish between the

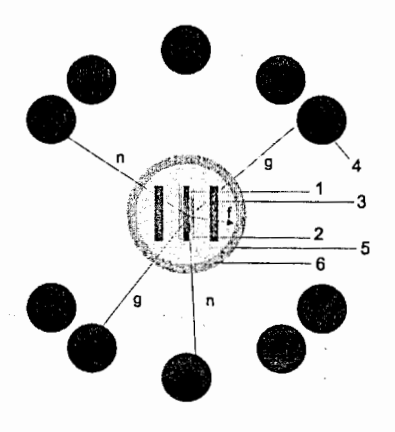


Fig. 1. The cross-section of the experimental setup, with the GND's placed at ±35°, ±57° and ±90°. 1 – <sup>235</sup>U double-sided target; 2 – longitudinally polarized neutron beam; 3 – fission fragments' detectors (multiwire proportional counters); 4 – gamma-quanta and neutrons detectors (plastic scintillator and photomultiplier); 5 – isobutane C<sub>4</sub>H<sub>10</sub> at pressure 8 mbar; 6 – fission chamber (stainless steel)

gamma pulses and the prompt fission neutron (PFN) pulses from PMT we used the time-of-flight technique. We used the pulses from the fragment detectors (FD) as start pulses, while pulses from gamma/neutron detector (GND) were used as stop. The GND are mounted at the angles 0,  $\pm \pi/8$ ,  $\pm \pi/4$ ,  $\pm 3\pi/8$ ,  $\pm \pi/2$ ,  $\pm 5\pi/8$ ,  $\pm 3\pi/4$ ,

 $\pm 7\pi/8$ , and  $\pi$ , relative to the average fission axis defined by fission fragment detectors. The plane formed by the vectors of the gamma/neutron momentum and the momentum of the fragment is orthogonal to the longitudinally polarized neutron beam direction. The polarization of the neutron beam is reversed every 0.5 second. We have measured counts rate under the gamma-peak and under the peak of PFN for both directions of neutron beam polarization (Fig. 2). The asymmetry R of the counts rate (eq. 1) is calculated on-line.

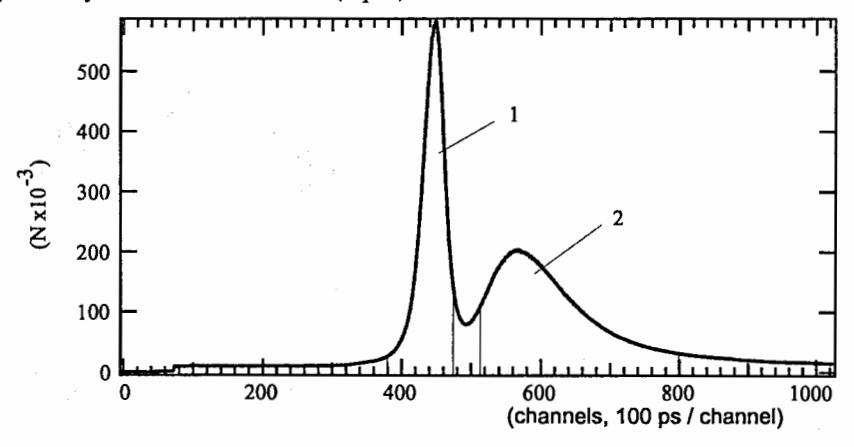


Fig. 2. Time-of-flight spectrum of the coincidence between pulses from gamma/neutron and fission fragment detectors.

1 - The prompt fission gamma-ray events

2 - The prompt fission neutrons events.

# Results

The first results of the ROT-asymmetry measurements performed on the instrument V-13 BER-II reactor of BENSC HMI were presented in [2]. Averaging the ROT-asymmetry results for PscG for symmetric combinations of the detectors, we obtained for 3 angles between GND and fission axis the next values:

$$R_{\gamma}(35^{\circ}) = (+1.5 \pm 0.4) \cdot 10^{-4}$$

$$R_{\gamma}(57^{\circ}) = (+2.3 \pm 0.4) \cdot 10^{-4}$$

$$R_{\nu}(90^{\circ}) = (-0.2 \pm 0.6) \cdot 10^{-4}$$

For the ScN there was no significant asymmetry, although the statistical error is larger compared to the results for PscG.

The new measurements in the geometry described above resulted in more accurate values:

$$R_{\gamma}(0) = (-0.1 \pm 0.3) \cdot 10^{-4}$$

$$R_{\gamma}(\pi/8) = (+0.8 \pm 0.2) \cdot 10^{-4}$$

$$R_{\gamma}(\pi/4) = (+1.5 \pm 0.2) \cdot 10^{-4}$$

$$R_{\gamma}(3\pi/8) = (+0.7 \pm 0.3) \cdot 10^{-4}$$

$$R_{\gamma}(\pi/2) = (-0.3 \pm 0.3) \cdot 10^{-4}$$

The main result of this experiment is, of course, the observation of pre-scission, scission or post-scission gamma-rays which are "time markers" for the scission moment. The origin of this radiation is not known yet. To get some information relating to the mechanism of the radiation we performed measurements of the dependence of the ROT-asymmetry on gamma-rays energy using NaI(Tl)-detectors as well as the angular dependence of the ROT-asymmetry. The preliminary results are shown in Fig. 3 and 4. Angular dependence of the ROT-asymmetry does not contradict with the assumption that radiation is the dipole irradiation. As to the energy of gamma-rays, it's evident that it differs from the spectrum of gamma-rays emitted by excited fragments.

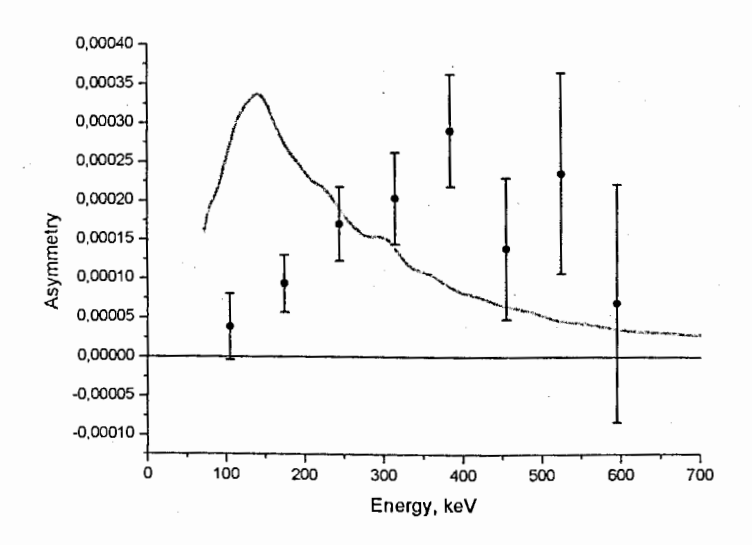


Fig. 3. Energy dependence of ROT-effect.

Dots – energy dependence of ROT-asymmetry (angle 45°) Curve – corresponding experimental  $\gamma$ -ray energy spectrum

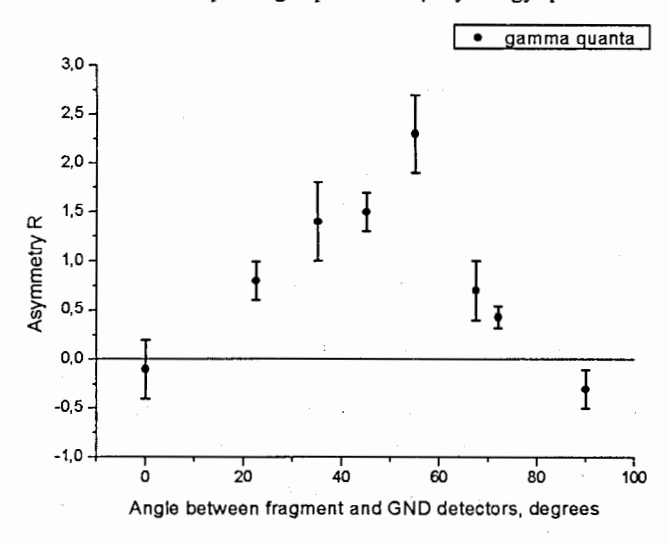


Fig. 4. Angular dependence of ROT-effect.

# Discussion

In the reaction  $^{235}$ U(n, $\gamma$ f), soft gamma-rays can be emitted by the transitions between excited states in the first wall of the compound nucleus. The life time of the compound nucleus measured from the gamma-quanta transition is of the order of  $10^{-14}$  s. In this case the time interval between gamma-quantum radiation and the scission is much larger then the characteristic rotational time of the nucleus, so the fissile nucleus can make about  $10^5$  revolutions before scission. Therefore the average ROT-effect in this process will be washed out. The transitions between the states of the second wall of the potential barrier can produce the very fast soft radiation. The time of the descent from saddle point to scission is of the order of  $10^{-21}$  –  $10^{-20}$  s. So, at this stage of the fission the trigger gamma's can be also generated. It's impossible to exclude the possibility to generate the radiation during the fragments acceleration time like the bremsstrahlung. It can be the E1-irradiation of highly deformed light fragment very soon after neck rupture (giant resonance) as well as the radiation accompanied the transition of highly deformational state of light fragments to the normal deformational state.

# Conclusion

This experimental work revealed the existence of asymmetry in the angular distribution of pre-scission gamma radiation (so called ROT-effect) in the binary nuclear fission process. Our observation implies the discovery of a new kind of electromagnetic radiation accompanying the fission. This is very important for theoretical considerations of the fission dynamics. From the practical point of view it opens new perspectives. The magnitude of the ROT-effect depends on the projection of the fissile nucleus spin on the deformation axis, i.e., on the K value. According to the O.Bohr's theory of nuclear fission K is one of main quantum numbers of quasi-stationary state at the saddle point, which defines the fission channel. For a fission channel with K = 0 the ROT-effect should be maximal, while for a channel with K = I the ROT-effect does not exist at all. Therefore, the measurement of the dependence ROT-effect on the neutron energy in the wide resonance region can give information about effective Kvalue in different neutron resonances. The observation of ROT-effect in (1) as well as in this work is the definite indication that the fission of <sup>235</sup>U by slow neutrons take place from the rotational state. And finally it should be taken into account that AD relative the "fission axis" of LCP or gamma-rays in fission of <sup>235</sup>U by unpolarized slow neutrons is wider than true AD respect to deformation axis.

# Acknowledgements

We should like to thank to the aid of HMI and ITEP staff, in particular to Werner Graf and to Yuri Belov. Our thanks to RFBR (grant 07-02-01095) and FANI for financial support of this work. We also are indebted to K. Diederichsen for linguistic work on this paper.

# References

- A.Gagarski, I.Guseva, F.Gönnenwein, et al. XIV International Seminar on Interaction of Neutrons with Nuclei, Dubna (2006), Abstracts volume, p. 33.
- G.V. Danilyan, P. Granz, V.A. Krakhotin, F. Mezei, V.V. Novitsky, V.S. Pavlov, M. Russina, P.B. Shatalov, T. Wilpert. Physics Letters B, 2009, to be published.

# DETAILED STUDY OF THE EFFECTS FOLLOWING FROM ROTATION OF THE SCISSIONING NUCLEI IN TERNARY FISSION OF <sup>235</sup>U BY COLD POLARIZED NEUTRONS ("ROT" AND "TRI" EFFECTS)

A.Gagarski <sup>a</sup>, G. Petrov <sup>a</sup>, I. Guseva <sup>a</sup>, T. Zavarukhina <sup>a</sup>, F. Gönnenwein <sup>b</sup>, M. Mutterer <sup>c</sup>, J. von Kalben <sup>c</sup>, W. Trzaska <sup>d</sup>, M. Sillanpää <sup>d</sup>, Yu. Kopatch <sup>c</sup>, G. Tiourine <sup>f</sup>, T. Soldner <sup>g</sup>, V. Nesvizhevsky <sup>g</sup>

<sup>a)</sup> PNPI RAS Gatchina, Russia; <sup>b)</sup> University of Tübingen, Germany; <sup>c)</sup> Technical University Darmstadt, Germany;

d) University of Jyväskylä, Finland; f) KRI, St. Petersburg, Russia;

e) Frank Laboratory, JINR, Dubna, Russia; g) ILL, Grenoble, France

# 1. Introduction

Since 1998 angular correlations in ternary nuclear fission induced by polarised neutrons at thermal energies were intensively studying by our collaboration. Recently reactions have been of particular interest where the neutron beam hitting the target is polarised longitudinally and the detectors for fragments and ternary particles are mounted in a plane perpendicular to the neutron beam. The angular distribution for one of the fission fragments (FF) and ternary particles (TP) at given neutron spin ( $\sigma$ ) can be written as:

$$W(p_{FF}, p_{TP}) \sim (1 + D \cdot \sigma \cdot [p_{FF} \times p_{TP}]) \cdot W_0(p_{FF}, p_{TP})$$
 (1)

with  $W_0(p_{FF},p_{TP})$ — the basic conventional correlation being independent of neutron spin between the momenta of FF and TP;  $p_{FF},p_{TP}$ — momentum of one of the FFs (usually the light FF is taken as a reference) and the TP;  $\sigma$ — neutron spin; and D— coefficient measuring the size of the triple correlation  $\sigma \cdot [p_{FF} \times p_{TP}]$ .

In experiments with  $^{233}$ U and  $^{235}$ U as the targets it was observed that the angular distribution of ternary particles relative to the momentum of the light fragment (LF), being roughly Gaussian, exhibits a slight variation at the relative level ~  $10^{-3}$  upon flipping the neutron spin relative to the plane  $(p_{FF}, p_{TP})$  formed by LF and TP momentums [1,3]. It was proposed to distinguish between two types of change of the TP angular distribution when flipping neutron spin. One type is "SCALING" where with spin flip the shape and the position of the angular distribution remains unchanged, but the total probability for TPs to move towards one or the other hemisphere of the  $(\sigma, p_{LF})$ -plane becomes asymmetric. We call this the TRI effect. The second type of change is "SHIFT" when with spin flipping the angular distribution is shifted in angular position without changing the total probability in hemispheres. This is called the ROT effect. In the terms of the formula (1) the TRI effect corresponds to the case when D coefficient is constant over angle. While the ROT effect will obviously give rise to a pronounced angular dependence of D on the angle between LF and TP.

The ROT effect is traced to a collective rotation of the partially polarized fissioning nucleus around its polarization direction <u>during the acceleration phase of TPs</u>. This hypothesis was corroborated by trajectory calculations [2]. One can suppose that the TRI effect could be due to the rotation affecting other degrees of freedom in the nucleus <u>before</u> rupture. At this stage the inertia forces arising in the rotating scissioning system "break" axial symmetry in the neck region and can help the "latent" TPs to "decide" to which hemisphere they will be emit-

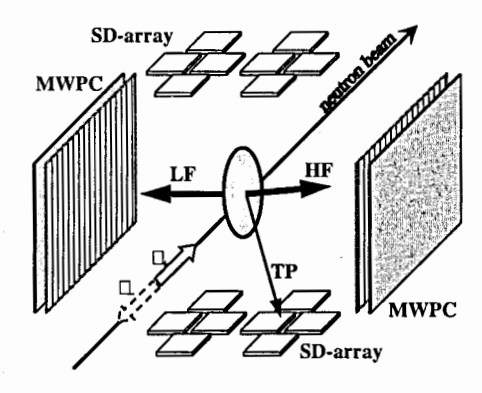


Fig. 1. Sketch of layout of experiment.

ted. The effect of rotation at this stage will not depend on the TP emission angle relative to the LF, because the specific TPs angular distribution is not yet settled.

As follows from the previous experiments, in  $^{233}$ U(n,f) the TRI effect is dominant, while in  $^{235}$ U(n,f) the ROT effect is better pronounced.

For the new experiment performed in 2007 it was suggested to analyze more thoroughly the angular asymmetry (1) in a dedicated study of the reaction <sup>235</sup>U(n,f). From the experimental side it was mandatory to improve on the angular resolution for the detection of fission fragments and TPs. By measuring the dependence of the

asymmetry coefficient over angle between LF and TP with better resolution it should become feasible to differentiate reliably both TRI effect, which does not depend on TP angle, and the ROT effect whose essence is its angular dependence. (In the work [3], where the ROT effect was discovered, the asymmetry was measured only for two angles 68° and 112° with poor angular resolution determined by the detectors sizes ~50°)

# 2. Experiment

The experiment was performed on the cold polarized neutron beam PF1 (intensity  $\sim 10^9 \text{ n/s} \text{ Gm}^2$  and polarization  $\sim 95\%$ ) of the Institute Laue-Langevin (Grenoble).

The general scheme of the setup was similar to one we had in all our previous experiments. It is shown in Fig. 1. The neutrons were polarized along the beam axis. The fissile target with diameter of the active spot ~8 cm is located at the centre of the assembly and oriented nearly parallel to the beam axis. Approximately 5 mg of <sup>235</sup>U (uranium tetra fluoride) were evaporated as a thin layer of ~100 \mathbb{L}g/cm^2 on a thin titanium foil (~100 \mathbb{L}g/cm^2) transparent to the FFs. Low-pressure position sensitive multi-wire proportional counters (MWPC) are used for registration of FFs. They are mounted a distance ~12 cm apart from the target plane and serve as stop detectors for the FFs. The size of the MWPCs is ~14×14 cm². Two arrays of surface barrier silicon detectors (SD) with 8 diodes each are placed ~ 12 cm away from the target for registration of the TPs at the axis perpendicular to MWPCs. The SD arrays are covered by ~25 \mathbb{Tm} aluminium foil against damaging by FFs. The target and all detectors assembly are placed in a ~40 litres chamber filled with ~10 mbar of CF4 counting gas for MWPC operation.

In these experiments one should, as a minimum request, achieve an identification of 'light' and 'heavy' FFs. It can be readily done relying on momentum conservation and measuring times-of-flight of two complementary FFs. In the time-of-flight method the start time mark was provided by the TP detector arrays and stop signals for coincident FFs were derived from the MWPCs. The time resolution was  $\sim 1$  ns. The two measured FFs times should be corrected for the TP flight time from the target to the detector, which can be found from the measured TP energies ( $E_{TP}$ ) and the distance from the fission point to the diodes having been hit. The fission position on the target is determined quite accurately by using the coordinates of FFs from the position sensitive MWPCs to reconstruct the fission axis. Knowing coordinates, tim-

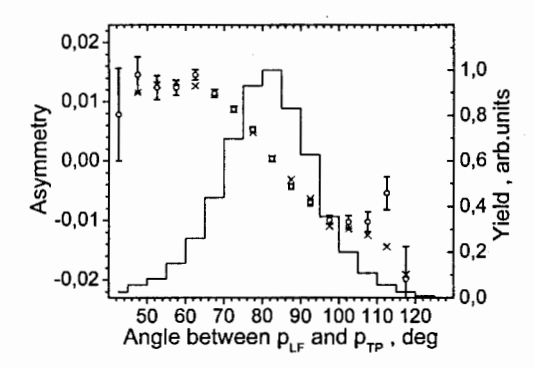


Fig. 2. Angular dependence of the experimental asymmetry for the reaction <sup>235</sup>U(n,f) – open points, left scale; angular distribution of TP emission – histogram, right scale; results of ROT+TRI model fit for the asymmetry – crosses. For details see the text.

ing and  $E_{TP}$ , all angles between vectors together with the mass of the light fragment  $(M_{LF})$  and the total FFs kinetic energies  $(E_{FF})$  are calculated event-by-event in the off-line analysis. The estimated resolutions for the LF mass are  $\square M_{LF} \sim 8$  a.m.u and for the FFs energy  $\square E_{FF} \sim 30$  MeV. The coordinate information from the MWPCs together with granulation of the silicon diodes arrays provides angular resolution  $\sim 10^\circ$ .

The experimental value of the asymmetry is defined as follows:

$$A_{i} = \frac{N_{i}^{+} - N_{i}^{-}}{N_{i}^{+} + N_{i}^{-}},$$
 (2)

where  $N_i^{+/-}$  are count rates of the LCP-FF coincidences. The index i means different selection criteria on

recorded parameters of the fission event, such as angles,  $E_{TP}$ ,  $M_{LF}$ ,  $E_{FF}$  and others, while (+/-) indicates the direction of the neutron spin being flipped periodically (~1 Hz) by a spin flipper device. It is easily shown, that the experimental asymmetry A is proportional to D, the proportionality factor in  $A \sim D$  accounting for experimental factors such as neutron polarization, accidental background, solid angles of registration etc.

The dependence of the experimental asymmetry A in eq. (2) on the angle between LF and TP is presented in Fig. 2 (open dots). The data are corrected for finite neutron polarization, background of accidental coincidences and geometrical efficiency. The corrected angular distribution of TPs is shown on the same figure as a histogram. The experimental asymmetry as a function of angle  $\vartheta$  between LF and TP was fitted with a model function constructed on the basis of the hypothesis that, in the general case, the asymmetry is the sum of ROT and TRI effects:

In this formula  $Y(\vartheta)$  is the experimental (averaged over two spins) angular distribution and  $Y'(\vartheta)$  its derivative. The first and second term on the RHS in (3) corresponds to the ROT and TRI asymmetry, respectively. Obviously, the ROT asymmetry originating from angular shifts depends on the shape of the angular distribution  $Y(\vartheta)$  and it is proportional to the normalized derivative  $Y'(\vartheta)/Y(\vartheta)$ . The TRI asymmetry is constant over angle. The asymmetry is then described with two free parameters:  $S_{ROT}$  – the angular shift between TP distributions for the two spin polarizations and  $D_{TRI}$  – the relative difference in total probabilities for TPs emitted towards the upper (lower) hemisphere for the two spin directions.

In Fig. 2 the results of the fit based on eq. (3) are indicated by crosses. Evidently the ansatz in eq. (3) describes the experiment very well. The values obtained for the fitting parameters are

$$S_{ROT} = 0.215^{\circ} \pm 0.005^{\circ}$$
 and  $D_{TRI} = (+1.7 \pm 0.2) \times 10^{-3}$ .

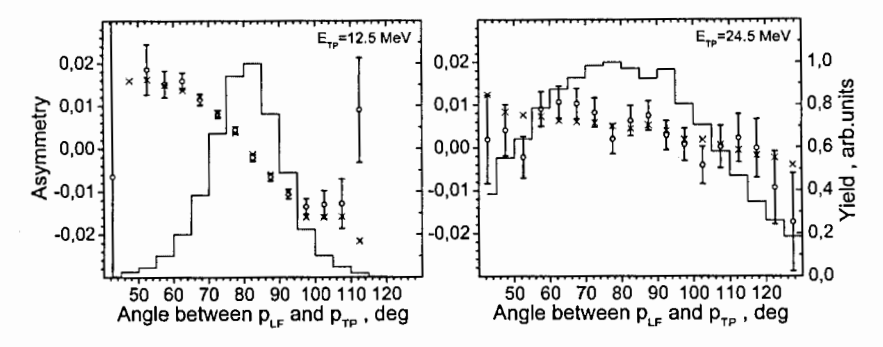


Fig. 3. Angular dependences of the experimental asymmetry and the fit results for two slices on  $E_{TP}$ : 12.5 $\pm$ 1.5 MeV and 24.5 $\pm$ 1.5 MeV. Designations are the same as on the Fig.2. For comments see the text.

For a more detailed study of the asymmetries the ternary events were sorted into bins of selected fission products parameters such as:  $E_{TP}$ ,  $M_{LF}$  (as a fraction of the compound nuclear mass), and  $E_{FF}$ . The binned data were evaluated following the same procedure as described above. In spite of the fact that the angular distributions of TPs vary strongly with the energies of TPs and the masses and energies of FFs, the results of the fits were always satisfactory. On Fig. 3 the results of the fits for two bins of  $E_{TP}$ , 12.5±1.5 MeV and 24.5±1.5 MeV, with narrow and wide angular distributions respectively, are shown as an example.

In the way described the ROT shifts and TRI coefficients were obtained separately as a function of the above fission observables. In Fig.4 the values obtained for the fitting parameters  $S_{ROT}$  and  $D_{TRI}$  are plotted versus  $E_{TP}$ ,  $M_{LF}$  and  $E_{FF}$ .

For the ROT effect our semi-classical model [3] was verified by comparing the new detailed experimental data with results of trajectory calculations of alpha particle emission from rotating fissioning nuclei. To estimate the effective rotational momentum of the compound system, the ratio  $\square(J=4^-)$  /  $\square(J=3^-)$  of the cold neutron capture cross-sections was taken to be 1.8, according to [5]. In a first approach only two fission channels (J,K) = (4,0) and (J,K) = (3,2) were taken into account. The results of trajectory calculation are shown by squares in Fig. 4 [2]. One can see, that the calculations not only reproduce very well the experimental average value of ROT effect, but also the calculated dependencies of the ROT shift on measured parameters agree, at least qualitatively, with the experimental trends.

For the TRI asymmetries, however, we still have no theoretical model which is capable to give quantitative predictions and the experimental data are still a challenge for interpretation.

#### 3. Conclusion

The main conclusion of the present experiment is that at the present level of experimental accuracy we can describe the changes of angular distributions of TPs relative to the LF for opposite spin polarizations of the compound nucleus by only two parameters: the angular shift  $S_{ROT}$  and the scaling  $D_{TRI}$  of the total probability distribution without change of its Gaussian-like shape. The characteristic parameters of both effects were obtained as a function of TP

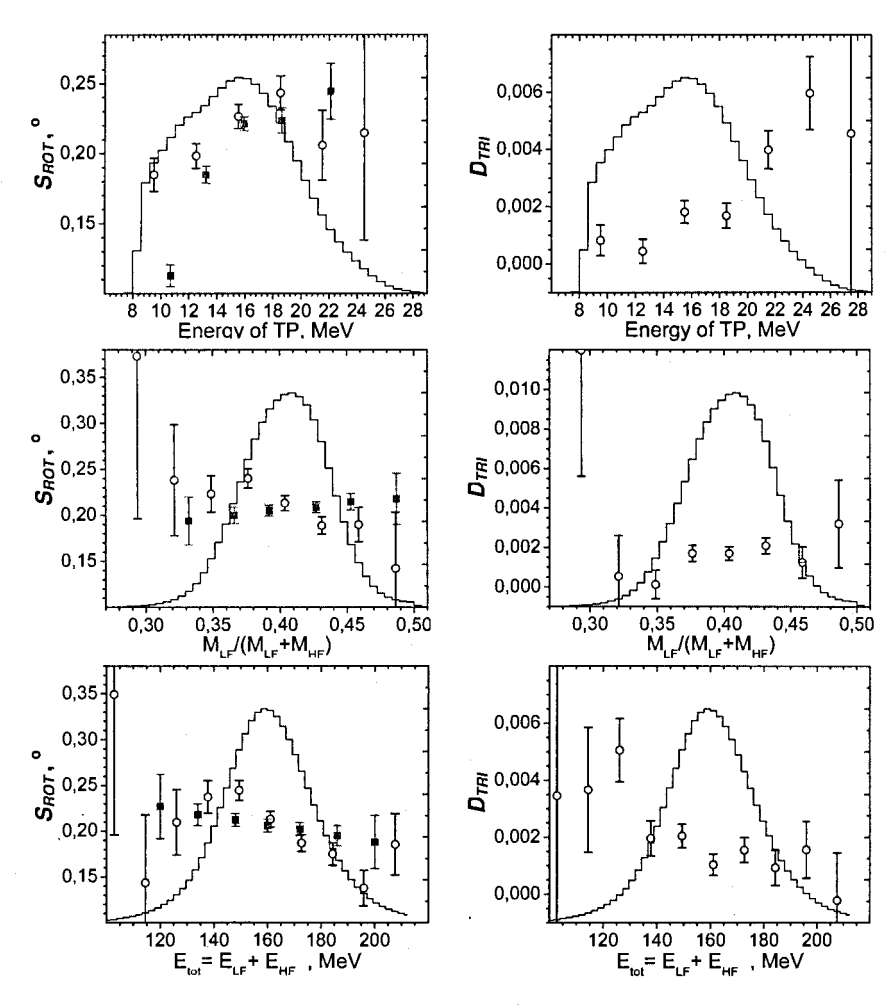


Fig. 4. Dependences of  $S_{ROT}$  (left) and  $D_{TRI}$  (right) on  $E_{TP}$ ,  $M_{LF}$ ,  $E_{FF}$ . Open dotes – experimental data, filled squares – result of trajectory simulations for ROT effect. See the text.

energy, FF mass and the total FF kinetic energy. It was demonstrated that despite of the smallness of both effects they are well measurable with spin the flip technique on an intense neuron beam.

Obviously, the ROT and TRI effects depend on many parameters of the fission process – such as the collective characteristics of transition states, the overlap of neutron resonances, the

structure of scission configurations, the dynamics, etc. The high sensitivity of the ROT effect was clearly demonstrated in our trajectory calculations [2,4]. Since both effects are closely related to the fission mechanism, their study is thought to be a valuable and sensitive tool for exploring the fission process.

In more detail the general status of ROT and TRI effect studies, their perspectives and possible applications are discussed in a further report at this conference [4].

# 4. Acknowledgements

This work was performed with the financial support of the foundations RFBR/Moscow (grant 06-02-16668-a) and INTAS/Bruxelles (grant 6417). The authors thank the members of the ILL technical services, who have done the utmost for making these experiments possible.

#### References

- 1. P. Jesinger et al., Nucl. Instr. Methods, A440 (2000), 618
  - P. Jesinger et al., Yad. Fiz., 65 (2002), 662 [Phys. At. Nucl., 65 (2002), 630]
  - A. Gagarski et al., Proc. Int. Seminar ISINN-12, Dubna, Russia, 2004, 255
- I. Guseva, Yu. Gusev, Izvestiya RAN: Ser. Fiz., 71 (2007), 382 [Bull. of the RAS: Physics, 71 (2007), 367]
  - I. Guseva, Yu. Gusev, Proc. Int. Seminar ISINN-14, Dubna, 2006, 101
- 3. F. Goennenwein et al., Phys. Lett. B, 652 (2007),13
  - A. Gagarski et al., Proc. Int. Seminar ISINN-14, Dubna, 2006, 93
- 4. G. Petrov et al., Proc. Int. Seminar ISINN-16, Dubna, 2008, these proceedings
- 5. Yu. Kopach et al. Yad. Fiz., 62 (1999), 812 [Phys. At. Nucl., 62 (1999), 840]

# TRI- and ROT-effects in ternary fission as a new way of investigating fission dynamics at low excitation energies

G.A. Petrov<sup>1</sup>, A.M. Gagarski<sup>1</sup>, I.S. Guseva<sup>1</sup>, F. Goennenwein<sup>2</sup>, M. Mutterer<sup>3</sup>, V.E. Bunakov<sup>1</sup>

- <sup>1</sup> St. Petersburg Nuclear Physics Institute of Russian Academy of Sciences, Gatchina, 188300 Russia
- <sup>2</sup> Physikalisches Institut, Universitaet Tuebingen, D 72976 Germany
- 3 Technische Universitaet Darmstadt, D-64289 Germany

#### 1.Introduction

It is common knowledge that angular distributions of fission products may be used effectively for investigating the so-called transition states at the barrier of the fission process induced by energetic light and/or heavy ions and y-rays /1,2/. These investigations demonstrated for several different fission reactions not only the existence of transition states of the fissioning compound system near the barrier top, but some more general characteristics were obtained as well. Based on the analysis of experimental data it was suggested that the fissioning system in these transition states is axially symmetric with quantum numbers for total spin J and its projection on the nuclear symmetry axis K. It was further argued that these numbers are conserved from the transition shape onwards. Fission probability was assumed to be proportional to the number of open (J, K) channels of the fissioning nucleus in its movement from the top of the barrier to the rupture point along the different valleys of the potential energy surface /3/. As a result, the configuration of the system at the rupture point, its excitation energy, and the resulting mass-energy distributions of the fission fragments may be very different for different nuclei. In addition to this, the barrier heights at the entrance to potential energy valleys may in principle be different as well /3/. Of course this overall picture of the fission dynamics in the passage of a deformed system through fission barriers and in its subsequent descent from the barrier top to the rupture point requires the investigation of further more fine details. The main still open questions are the fraction of the energy liberated in the descent process being dissipated into internal excitation, and the collective kinetic energy of the scissioning system near the rupture point. The available information on these important questions is rather contradictory and, as a rule, has been obtained rather indirectly.

Near the end of the last century, in addition to conventional measurements of fission fragment angular distributions for reactions induced by energetic particles /1/ and in continuation of experiments with oriented nuclei and polarized neutrons P-even and P-odd angular correlations in binary fission (see e.g. /4/), T-odd angular correlations in ternary fission induced by polarized low energy neutrons were discovered and contributed to the transition state investigations /5,6.7/. The angular distribution of fission fragments is described by

 $W(\Omega) - I + \alpha_{PNC}(\sigma_n \cdot P_r) + \alpha_{PC} \cdot \sigma_n \cdot [P_f \times P_n] + D_{TRI} \cdot \sigma_n \cdot [P_f \times P_\alpha] + D_{ROT} \cdot \sigma_n \cdot [P_f \times P_\alpha] \cdot (P_r P_\alpha).$  (1) Here  $\sigma_n$ ,  $P_f$ , and  $P_\alpha$  are unit vectors directed along neutron polarization and linear momenta of fission fragment and ternary particle, respectively. The coefficients  $\alpha_{PNC}$ ,  $\alpha_{PC}$ ,  $D_{TRI}$ , and  $D_{ROT}$  are the asymmetry coefficients for Parity-Non-Conservation, parity conserving Left-Right asymmetry and the two T-odd TRI- and ROT-effects, respectively. The latter two asymmetries were discovered in ternary fission with additional emission of light particle.

It could be shown in /8,9/ that the coefficients  $\alpha_{PNC}$  and  $\alpha_{PC}$  are expected to be very small  $(10^{-3}-10^{-4})$  yet closely connected with the transition states' properties, in particular, with the J and K values. It should be pointed out that non-vanishing coefficients D do not imply time reversal invariance to be violated. Instead both, statistical and quantum-mechanical dynamical models were proposed emphasizing the role played by the interplay of fragment spin and the orbital momentum of ternary particles and, most important, collective rotations of the

scissioning compound steering the emission probabilities of the light charged particles in ternary fission /6,10/. The coefficients  $D_{TRI}$  are determined in the framework of a statistical model by level densities and moments of inertia of spherical fission fragments, and by the split between fragments of the excitation energy and polarization of the scissioning system /6/. On the other hand, the values of  $D_{ROT}$  are determined mainly by the J and K values and the relationship between ternary fission fragment and light charged particle velocities near the rupture point of the fissioning system /11/.

Experimental values of D<sub>TRI</sub> and D<sub>ROT</sub> coefficients reveal a marked dependence on fragment masses and kinetic energies, and on the energies of the light charged particles. Such peculiarities in the behavior of the coefficients open new possibilities to answer some interesting questions of fission dynamics. The main results of investigations on P-odd and P-even interference effects were published earlier in the works /12-15/. Here we are presenting and shortly discussing the first results obtained in the studies of T-odd angular distributions of light charged particle emission in ternary fission and some conclusions about fission dynamics obtained from the data analysis in the framework of a rotational model of the fissioning system /11/.

# 2. Current status of experimental investigations of TRI- and ROT-effects in ternary fission induced by cold polarized neutrons

The average values of T-odd asymmetry coefficients  $D_{TRI}$  for the  $\alpha$ -particles and tritons in ternary fission of  $^{233,\,235}$ U,  $^{239}$ Pu, and  $^{245}$ Cm induced by cold polarized neutrons are presented in Table I /16,17/. In all cases the average T-odd asymmetry coefficients are calculated as normalized differences of the two LCP angular distributions for mutually opposite directions of neutron polarization (spin flip technique). It should be noted that in the first experiments the existence of two distinct T-odd effects was not known.

Table I. Average asymmetry coefficients for different fissioning nuclei with the spins J

	Target / D>	<sup>233</sup> U	<sup>235</sup> U	<sup>239</sup> Pu	<sup>245</sup> Cm
	coefficient	J = 2, 3	J = 3, 4	J = 1, 0	J = 2, 3
	$< D_{\alpha} > 10^{-3}$	$-(3.9 \pm 0.1)$	$+(1.7\pm0.2)$	$-(0.15 \pm 0.23)$	$+(1.30\pm0.48)$
1	<d<sub>t&gt;·10<sup>-3</sup></d<sub>	$-(2.9 \pm 0.5)$	+ (0.90 ± 0.6)	-	-

The polarization of compound states after capture of polarized cold neutrons ( $P_n \sim 95\%$ ) by fissile targets with spin I may be estimated by the following simplified expressions:

$$P(J^+) = (2I+3)/([3(2I+1)] \cdot P_n \text{ for } J^+ = (I+1/2) \text{ and } P(J^-) = -1/3 \cdot P_n \text{ for } J^- = (I-1/2)$$
 (2)

The complicated structure of compound nuclei at excitation energies of about 6 MeV makes it difficult to get experimental values of T-odd asymmetry coefficients for individual compound states. Therefore the values <D> in Table 1 contain the contributions to the effect from all the nearby resonances with different compound-states spins  $J^{(t)} = (I \pm 1/2)$ .

This seems to be a possible reason for the scattering of experimental data in Table I both as to magnitudes and signs. Another interesting result presented in Table I lies in the fact that the T-odd asymmetry values for the  $\alpha$ -particles and tritons are equal at the limit of accuracy in spite of the difference in particle spins and, probably, also orbital momentum. This fact was successfully explained by theory /18/.

First explanations of experimental results were given in a statistical model of V. Bunakov et al. /6/. In this model the probability of ternary fission is proportional to the density of final states of the system after LCP emission. Assuming that the fragments being deformed at scission have their spins oriented perpendicular to the deformation (fission) axis the level density is

$$\rho_i(A_i, E_{xi}^{sc}, M) \sim \exp[2\sqrt{a_i(E_{xi}^{sc} - \hbar^2 M_i^2 / 2Z_i)}] \approx \exp[2\sqrt{a_i E_{xi}^{sc}} \cdot (1 - \hbar^2 M_i^2 / 4Z_i E_{xi}^{sc})], \quad (3)$$

where  $A_i$ , and  $E_{xi}^{w}$  are atomic number and fragment excitation energy,  $M_i$  is the projection of total momentum  $J_i$  on a given axis, and  $Z_i$  is the moment of inertia of spherical fragments. As seen from expression (1) the magnitude of the T-odd asymmetry effect peaks at mutually orthogonal vectors  $\sigma_n$ ,  $P_i$ , and  $P_{\alpha}$ . In such a configuration the orbital momentum of the light

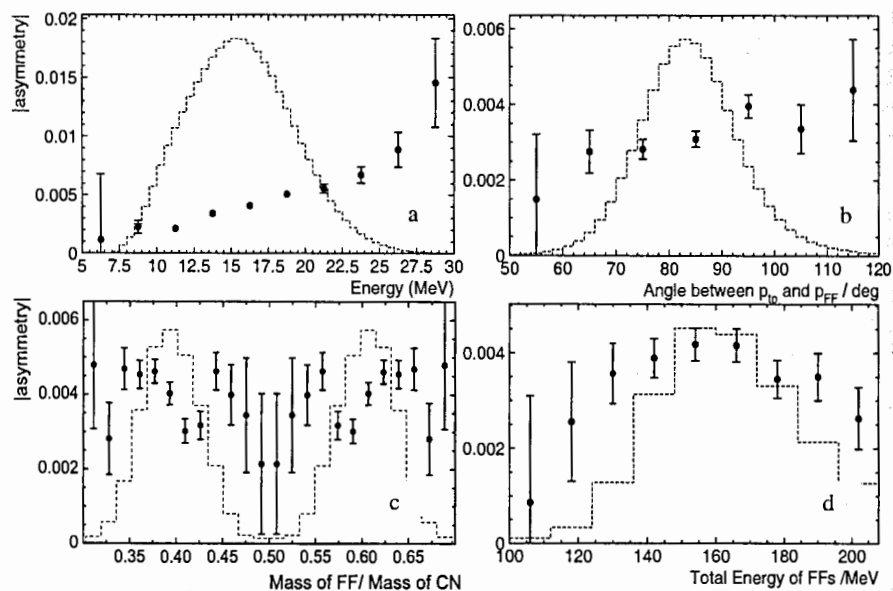


Fig.1. The modulus |D| of the correlation coefficient as a function of: ternary particle (TP) energy (a), mass of the fission fragment (FF) normalized to the mass of the compound nucleus (CN) (b), angle of TP's emission relative to the light FF (c), total kinetic energy of the FFs (d).

particle may be directed alternatively along or against the polarized compound nucleus spin. As a result  $M_{final} = (M \pm l_{\alpha})$ , so the LCP emission probability increases or decreases depending on the mutual direction of the momenta  $l_{\alpha}$  and J:

$$D_i(J^{\pm}) \approx \frac{\hbar^2 M_i l_\alpha \sqrt{a_i}}{Z_i \sqrt{E_{ii}^{sc}}} \mu_i P(J^{\pm}) \quad \text{and} \quad D \sim 1/\sqrt{6 - 0.2 E_{\alpha}^{kin}}$$
 (4)

Here  $a_i$  and  $\mu$  are level density parameters and factors characterizing the transfer of compound nucleus polarization to the fragments, respectively, while  $Z_i$ ,  $E_{xi}^{sc}$ , and  $E_{\alpha}^{kin}$  are the fragment inertia parameter, excitation energy of the fragments at the rupture point and ternary particle kinetic energy.

The observed dependences of the modulus of T-odd asymmetry coefficients on different parameters of the ternary  $^{233}$ U fission process are presented in Fig.1. The histograms show experimental angular, mass and energy distributions of fission products. Quite evidently there is a dip in the fragment mass dependence of the asymmetry coefficient |D| in the region of doubly magic masses where the level density is low (see eq. 4). Likewise the dependence of the asymmetry |D| on the kinetic energies of light particles and fission fragments is in qualitative agreement with eq. (4). In addition, a slight increase of |D| for increasing emission angles of the ternary particles relative to the fission axis is observed.

In 2005 further investigations of T-odd asymmetries in ternary fission <sup>235</sup>U revealed a pronounced dependence of the T-odd asymmetry on the emission angle of the light particle.

To explain this new and unexpected effect, called ROT-effect in contrast to the TRI-effect discussed above, the hypothesis was proposed that the fissioning compound is rotating around its direction of polarization /5/. It is relatively easy to understand that such a rotation can induce a shift of the angular distributions of ternary particles. The shift is wobbling back and forth when the compound polarization direction changed by neutron spin flipping. For angular distributions assumed having Gaussian shapes centered around 90° relative to the fission axis, the difference between two shifted distributions varies with the cosine of the angle. It is important to point out that the ROT-effect (shift of Gaussians) can exist together and independently of the TRI-effect which corresponds to differences of yields (areas of Gaussians) under reversal of polarization.

A comparison of experimental results on the angular dependence of the ROT-effect in  $^{233}$ . U ternary fission is presented in Fig.2. In the case of  $^{235}$ U ternary fission, experimental data are compared with the results of an evaluation where a small TRI-effect (assumed to be independent of angle (dashed line)) and a pronounced ROT-effect (crosses) are superimposed. The size of the ROT-effect is calculated as the difference in yield (normalized to the sum) for two shifted angular distributions depicted as histogram. The fit is excellent indicating that the angular shift  $2\Delta = 0.215(5)^{\circ}$  between two distributions is very small. By contrast, for the  $^{233}$ U(n,f) reaction the TRI-effect is large and the ROT-effect is still smaller than for the companion reaction  $^{235}$ U(n,f).

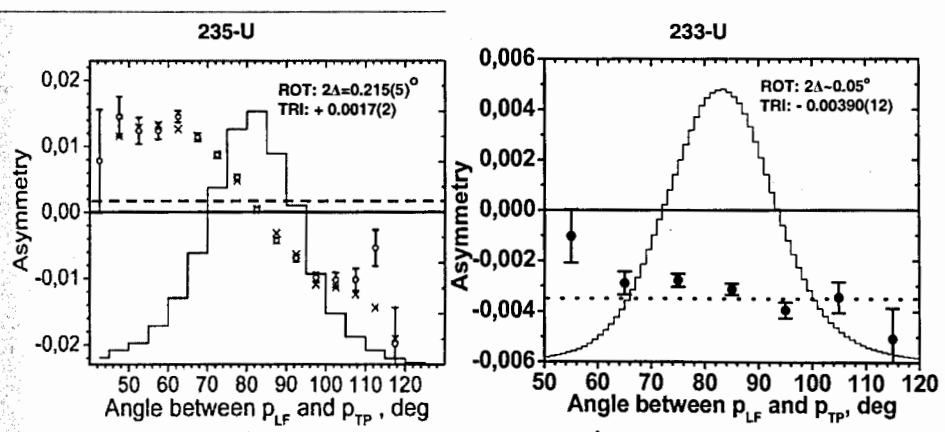


Fig. 2. T-odd asymmetry effects in <sup>253</sup>, <sup>255</sup>U ternary fission as a function of emission angle of the third particle. Histograms show the angular distributions of the third particle. Dotted lines show the absolute values of the TRI-effects in <sup>233</sup>, <sup>235</sup>U ternary fission.

To support the experimental findings trajectory calculations for fission fragments and ternary particles were performed for a rotating nucleus undergoing ternary fission. The initial conditions for the trajectory calculations of reaction products flying apart after scission of the rotating compound nucleus were chosen under the condition to describe properly the particles' angular and energy distributions observed in experiments. This means that the third particle was born in between the two fission fragments ( $d \approx 20$  fm for for  $M_H/M_L = 1.44$ ) and with the initial energy inside the interval (0.1 - 1.3) MeV. It is important to point out that in estimating the rotation velocity of the fissioning system we used the ensemble averaged value  $\langle J(K) \rangle$  of the total spin projection on the polarization axis which depends on K and was obtained in ref. /20-21/. In the trajectory calculations the (J,K) spin values of the transition states enter as free parameters. In case of the  $^{235}U(n,f)$  reaction, for example, the compound

spin J takes on the values J=3 or J=4 and the K-values are running from K=0 to K=J. Calculation results are given in Fig. 3 for this reaction. In view of the convincing fit of the ROT asymmetry in terms of a shift angle  $2\Delta$ , the dependence of the ROT asymmetry on ternary particle and fragment mass and energy is not described by a  $D_{ROT}$  coefficient following eq. (I) but as a shift angle  $2\Delta$ . As seen in Fig. 3 the ROT angle depends indeed on the above parameters.

A striking feature in Fig. 3 is the strong dependence of the calculated angular shifts on the (J,K) values adopted. In the Figures 3a through 3c it is obvious that a combination of (J,K) = (3,2) with (J,K) = (4,0) gives a much better description of angular shifts as a function of ternary particle and fragment energy and fragment mass than the combinations (J,K) = (3,0) with (4,2).

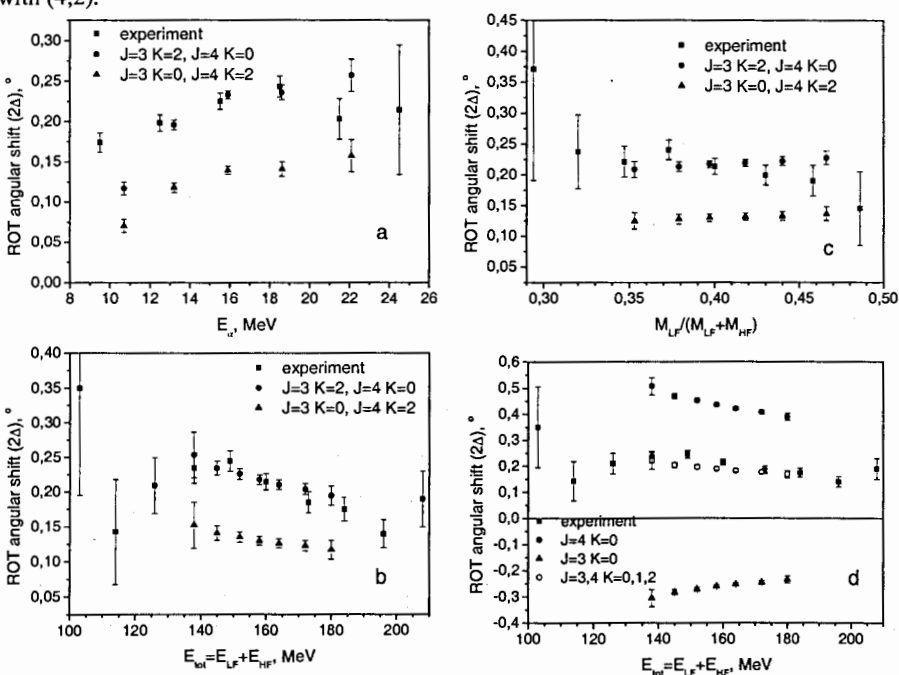


Fig.3. ROT angular shift in the reaction 235U(n,f) as a function of the ternary particle kinetic energy (a), total fragment kinetic energy (b), and normalized masses of light fragment (c) in comparison with results of trajectory calculations performed for two possible sets of J = 3, 4 and different K values. In Fig.3 (d) the ROT angular shift is presented as a function of total fragment kinetic energy in comparison with the results of trajectory calculations performed separately for J = 3 and J = 4 values and with combination J and K obtained in the work /19/ where the fission cross section was investigated with an oriented target of  $^{235}$ U and a polarized resonance neutron beam.

It demonstrates the sensitivity of the ROT effect on transition state properties. This is even more clearly evident in Fig. 3d where the transition states (J,K) = (4,0) and (J,K) = (3,0) yield completely different predictions even differing in sign for the ROT angle. But the comparison of Figs 3b and Fig. 3d also reveals ambiguities in the spectroscopy of transition states since the combinations (J,K) = (3,2) with (J,K) = (4,0) and the set with J = 3 and 4, and K = 0, 1 and 2 taken from ref. /19/ reproduce the experimental data equally well. Nevertheless, it is surprising that a variety of experimental data may be successfully explained with a simple semi-classical hypothesis of a rotating fissioning compound that continues to rotate beyond

scission. It should be noted, however, that after scission the rotation comes very quickly to a virtual stop within a few 10<sup>-21</sup> s because the moment of inertia of the rotation explodes when the fragments are flying apart.

A quantum theory of this phenomenon /20/ has shown that the above quasiclassical approach is not based on too crude assumptions and, anyhow, today is the only possibility to get quantitative estimations. It was pointed out, however, that for a more detailed analysis, in future work it will be necessary to take into account the possibly strong influence of interference effects from neighboring resonances.

Summarizing all the aforesaid one can state that the discovery and the first detailed investigations of relatively small P-odd and P-even interference effects as well as TRI- and ROT-effects of T-odd asymmetry in ternary fission open the way to quite new and interesting investigations of low energy fission dynamics. Of course both, the statistical accuracy and the resolution for mass, energy and angles of fragments and ternary particles should be improved. As to the trajectory calculations they should be refined by taking into account more parameters of low energy fission. In particular the calculated trend of the dependence of the ROT effect on fragment mass is for the moment opposite to experiment. Very probably this is simply due to a not appropriate choice of scission configurations as a function of mass split. In the following chapter some possible ways of immediate investigations of T-odd asymmetry effects are briefly recalled /21/.

# 3. Puzzles of T-odd asymmetry effects and tasks for investigations

One of the main questions is to understand why two very similar uranium isotopes <sup>233,235</sup>U exhibit a quite different behavior as to T-odd asymmetry effects in ternary fission. As seen from inspecting Fig.2 and Table I the magnitudes of TRI- and ROT-effects are very different in these isotopes. The authors of /20/ pointed out that the reason for this difference is due to different phase factors of the interfering neighboring neutron resonances. In any case it seems to be important to clarify this question. It is evident that the most direct way to answer this question would be T-odd effect measurements for isolated resonances with well-known spins.

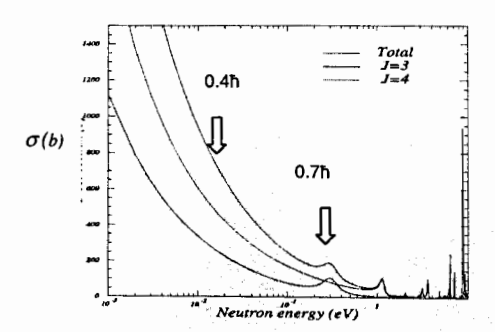


Fig.4. Partial fission cross-sections: total (upper curve), for spin J = 3 (lower curve) and J = 4 (middle). Arrows show the estimates of "averaged" spin values at the energy of cold neutrons (0.4h) and the 0.3 eV resonance  $^{236}U^{*}$  (0.7h). The estimates have been obtained with formula (5).

However, for the time being due to the low intensity of polarized neutrons in the resonance energy region such studies are not feasible. But, in principle, one can also perform comparative measurements of TRI- and ROT-effects for two energy intervals with different but well-known mixtures of resonances with different spins (Fig.4).

In such experiments the "averaged" value <J> of the polarized spin of the system, which defines the angular rotation velocity, might for interfering (I+1/2) and (I-1/2) states be roughly estimated as:

$$\langle J \rangle = [(\sigma_{J_{+}} \cdot P_{J_{+}} \cdot J_{+} + \sigma_{J_{-}} \cdot P_{J_{-}} \cdot J_{-})]/(\sigma_{J_{+}} + \sigma_{J_{-}}),$$
 (5)

where  $\sigma_1$  and  $P_1$  are partial cross-sections and polarizations. An example for the <sup>235</sup>U target is shown in Fig.4. In this case one can at any rate check the validity of the semi-classical trajectory calculations ones more.

Another possibility for studies of T-odd asymmetries with definite spins of transition states of the fissioning nucleus without having to apply the approximate expression (5) consists in the use of a polarized fissile <sup>235</sup>U target and a high intensity polarized cold neutron beam. The main difficulties of such a method are connected with the necessity to use rather complicated cryogenic equipments.

Investigations may also be performed with specially selected pairs of fissile nuclei such as presented in Table II.

Table II. Main parameters of fissile targets with similar transition state properties of compound systems, formed after cold neutron capture.  $E_0$ -energy of the nearest low-lying resonances.

Parameter Target	E <sub>0</sub> (eV)	J	2gΓ <sub>n</sub> (meV)	Γ (meV)	Γ <sub>f</sub> (meV)
Target 233U (I=5/2)	- 3.92	-	-		557
	1.35	(+2)	0.165	60	553
<sup>241</sup> Pu (I=5/2)	-0.16	-	-	_	103.4
	0.258	+3	0.055	-	75
<sup>235</sup> U (I=7/2)	-1.4	-4	-	-	200
	0.29	-3	0.0032	-	98
<sup>245</sup> Cm (I=7/2)	-0.25		-	-	220
	0.85	-	0.102		800
<sup>239</sup> Pu (I=1/2)	-0.576	+0	-	-	290
	0.296	+1	0.108	102	60

The majority of resonance spin values **J** given in the table are either unknown or not reliable. But interestingly there are two pairs of target nuclei with the same spins. One may therefore anticipate that the ratios of TRI to ROT effect could be similar for both nuclei of a pair. Thus one might expect to observe for the pair ( $^{233}$ U -  $^{241}$ Pu) relatively large TRI- but small ROT-effects as this is observed in  $^{233}$ U. An opposite situation might be obtained for the pair ( $^{235}$ U -  $^{245}$ Cm) with a small TRI- but large ROT-effect. Besides, in the compound system  $^{246}$ Cm\* the excitation energy following neutron capture is much higher above the barrier top than in its partner  $^{236}$ U\*. By contrast, in the pair ( $^{233}$ U -  $^{241}$ Pu) these heights are close to each other.

The fissile target  $^{239}$ Pu is interesting because only one type of polarized transition states with spin J=1 can be formed after the capture of polarized slow neutrons. The capture probabilities for J=0 and J=1 states are close to each other. As one can see from Table I, the TRI-effect in  $^{239}$ Pu ternary fission was not observed, but it does not mean that the ROT-effect is absent as well! If this effect should be observed in ternary fission of  $^{239}$ Pu there will be a unique chance to pin down the (J,K) values for the J=1 state. It means that one can learn much more about the mechanism of T-odd asymmetry effects.

# 4. Conclusion

The modern methods of fission investigations are characterized by multi-parameter measurements of angular, mass, and energy distributions of all or at least of the most interesting reaction products. Among them, the distinguishing feature of T-odd asymmetry

effects is the relative smallness of the magnitude to be measured as a function of fission parameters. But at the same time, the quantities measured (in our case asymmetry coefficients) turn out to be highly sensitive to most important characteristics of fission dynamics, such as fission fragment velocities just near the rupture point, configuration of the scissioning system and properties of transition states.

Of course, for the full and successful realization of all possibilities presented by the T-odd asymmetry effects it is necessary to have available high fluxes of resonance polarized neutrons and to make use of modern methods of registration and spectrometry of fission fragments, neutrons and  $\gamma$ -radiation at counting rates of up to  $10^6$  sec<sup>-1</sup>.

In conclusion, the authors are grateful to the ILL staff for running the High Flux Reactor with the Cold Polarized neutron beams PF1 and especially PF1B, to the staff of JINR for running the IBR-30/LUE-40 with Resonance polarized neutron beams, and to all colleagues for fruitful discussions. The work has been supported by numerous grants of RFBR, grants from ISF, and INTAS grants (99-0229 and 03-51-6417).

# References:

- 1. R. Vandenbosch and I. Huizenga. In "Nuclear Fission", Academic Press, 1973, p. 197.
- A.Goverdovsky et al. Yad. Fiz. 56 (1993) 40.
- U. Brosa et al. Z.Phys. A310 (1985) 177 and A335 (1986) 241.
- 4. Yu. Kopatch, A. Popov, V.Furman et al. Particles & Nuclei.32 (2001) 204
- 5. A. Gagarski, I. Guseva, G. Petrov, F. Goennenwein et al. Preprint-PNPI-2656, 2006, Russia
- 6. V. Bunakov, F. Goennenvein, P. Jesinger, M. Mutterer, G. Petrov. Bull. RAS. 67 (2003) 624
- F.Goennenwein, M.Mutterer, A.Gagarski, I.Guseva, G.Petrov et al Phys. Lett. B652 (2007) 13.
- 8. P. Sushkov and V. Flambaum. Usp. Fiz. Nauk. 136 (1982) 3
- 9. V. Bunakov and V. Gudkov. Nucl. Phys. A 401 (1983) 93.
- 10. V. Bunakov, S. Kadmensky. Phys. At. Nucl. 668 (2003) 1846.
- 11. I.S.Guseva and Yu. Gusev. Proc. Int. Sem. ISINN-14, Dubna JINR, 2007, p 101
- V.P. Alfimenkov, , L.B. Pikelner, V.R. Skoy, M.I. Tsulaya, A.M. Gagarski, I.S. Guseva, S.P. Golosovskaya, I.A. Krasnoschekova, G.A. Petrov, V.I. Petrova, A.K. Petukhov, Yu.S. Pleva, V.E. Sokolov, G.V. Val'ski et al. Nucl. Phys. A645 (1999) 31
- Alfimenkov V.P., Chemikov A.N., Gagarski A.M., Golosovskaya S.P., Guseva I.S., Krasnoshchekova I.A., Lason L., Mareev Yu.D., Novitsky V.V., Petrov G.A., Petrova V.I., Petukhov A.K., Pikelnre L.B., Pleva Yu.S., Sokolov V.E., Tsulaya M.I., Tsulaya V.M. Physics of Atomic Nuclei. 63 (2000) 539
- 14. Gagarski A.M., Guseva I.S., Golosovskaya S.P., Krasnoschekova I.A., Petrova V.I., Petrov G.A., Petukhov A.K., Pleva Yu.S., Sokolov V.E., Alfimenkov V.P., Chernikov A.N., Lason L., Mareev Yu.D., Novitski V.V., Pikelner L.B., Skoy V.R., Tsulaya M.I., Soloviev S.M. . Preprint PNPI of RAS, NP-32-1999, n. 2317.
- A.M. Gagarski, I.S. Guseva, I.S. Krasnoshchekova, G.A. Petrov, V.I. Petrova, A.K. Petukhov, Yu.S. Pleva, V.E. Sokolov, V.P. Alfimenkov, N.A. Bazhnov, A.N. Chernikov, W.I. Furman, Yu D. Mareev, V.V. Novitski, L.B. Pikelner, T.I. Pikelner, A.B. Popov, M.I. Tsulaya, A.L. Barabanov and S.M.Soloviev. Proc. Intern. Seminar ISINN-10, Dubna, 2003, p.184.
- Gagarski A., Goennenwein F., Gusena I., Jesinger P., Mutterer M., Petrov G., Petrova V. et al. IX International Seminar ISINN-9, Dubna, JINR, 2001, p 214
- Gagarski, G.Petrov, T.Zavarukhina, F.Goennenwein, P.Jesinger, M.Mutterer et al. Int Sem. ISINN-12., Dubna, JINR, 2004, p 255
- 18. V. Bunakov, S. Kadmenski, L. Rodionova. Bull. RAS (phys.) 69 (2005) 614.
- 19. Yu. Kopach et al. Phys. At. Nucl. 62 (1999) 840.
- 20. V.E. Bunakov, S.G. Kadmensky, S.S. Kadmensky. Phys. At. Nucl. 71 (2008) 1917
- G. Petrov, A. Gagarski, I.Guseva, Yu. Kopatch, et al. Phys. Atom. Nucl. 71. (2008) 1149

# THE ESTIMATION OF SCISSION NEUTRON PARAMETERS FROM N-F AND N-N ANGULAR CORRELATIONS IN <sup>235</sup>U(n<sub>th</sub>,f) REACTION

I.S. Guseva, A.M. Gagarski, V.E. Sokolov, G.A. Petrov, D.O. Krinitsin, G.V. Val'ski, A.S. Vorobyev, O.A. Scherbakov

Petersburg Nuclear Physics Institute of Russian Academy of Sciences Gatchina, Leningrad District, 188300, Russia

#### Abstract

With the aim to investigate the process of neutron emission two experiments on studying of neutron-fragment and neutron-neutron angular correlations in <sup>235</sup>U(n<sub>th</sub>,f) reaction were carried out in PNPI recently [1,2].

The neutron spectra for different angles as well as the angular dependences of neutron-fragment and neutron-neutron coincidence rates from these experiments were compared with the results of calculations based on Monte-Carlo method. In process of calculation it was assumed that the major part of fission neutrons evaporates from fully accelerated fragments but a fraction of total number of fission neutrons can be emitted isotropically in the laboratory system.

From the comparison of experimental data connected to both n-f and n-n angular distributions simultaneously with the results of Monte-Carlo calculations it was concluded that about 7% of total number of neutrons in  $^{235}U(n_{th},f)$  reaction are emitted isotropically and probably can be attributed to "scission neutrons" arising just at the rupture moment. The form of this component corresponds to Weisskopf distribution with temperature parameter T $\approx$ 1 MeV.

It is reliably established that most of prompt neutrons are evaporated during the fission process by fully accelerated fragments. This conclusion is based on the fact that instead of isotropic neutron distribution in laboratory system of reference, a considerable increase of neutron yield is observed in the direction of the light fragment motion and in the opposite direction. In the former case a part of neutrons emitted from heavy fragment is small and the total spectrum is very close to the neutron spectrum produced by the light fragment. On the other hand at 180° the contribution of neutrons from the light fragment is negligible and the neutron spectrum is shaped by the heavy fragment.

The peculiarity of neutron spectra at these angles can be used to determine the neutron spectra in the centre-of-mass for the light and heavy fragment, respectively, and corresponding temperature parameters. It is known the form of neutron spectrum in the centre-of-mass of each fragment is very close to Maxwellian distribution. On the base of obtained temperature parameters and taking into account final velocities of accelerated fragments one can calculate the neutron yield in any direction of the lab-system.

The results of calculations for angular distributions in the reaction <sup>235</sup>U(n<sub>th</sub>,f) performed in the frame of neutron emission from fully accelerated fragments show the difference between experimental data and calculated curve [3]. Such discrepancy can be minimised if one supposes that a fraction of total number of fission neutrons can be emitted isotropically in laboratory system of reference. It is assumed that the neutrons of isotropic component can appear just after the rupture point (so-called "scission" neutrons). The contribution of isotropic component evaluated by Skarsvag is about 15%. But this value is still under question because in the literature we can find a lot of different results for similar estimations.

As state above, now we have our own experimental data on neutron-fragment angular distributions in slow-neutron-induced fission of <sup>235</sup>U [1]. To describe these distributions and evaluate the contribution of isotropic component it is necessary to have neutron spectra in fragment centre-of-mass. With this object in mind we also used experimental neutron spectra at zero and 180 degrees in laboratory system of frame. Although the shape of neutron spectra in fragment centre-of-mass is very close to Maxwellian distribution, it was decided to use direct numerical values of neutron spectra obtained with the help of Jackobian transformation.

The anisotropy of neutron emission due to the presence of angular momentum of fission fragments was also taken into account [4]. In process of calculation were used energy dependences of angular anisotropy for the light and heavy fission fragments with the most probable masses. The solid curves in the figure 1 demonstrate the results of Monte-Carlo calculations of neutron emission anisotropy for both fragments. These estimations were performed with averaged initial angular momentum 7 (for light) and 8 (for heavy) fragments, respectively. The dashed curves show corresponding neutron spectra, whose shapes determine the value of averaged anisotropy for each fragment. They were estimated as 6.3% for light and as 9.5% for heavy fragment, respectively.

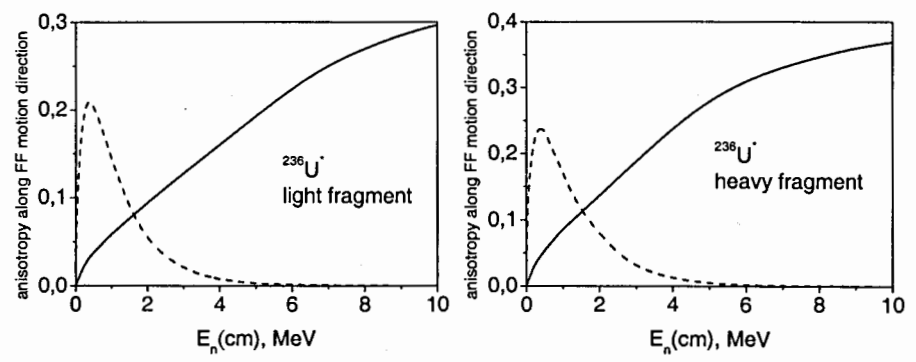


Fig.1. Anisotropy of neutron emission for light and heavy fragments (solid lines). The dashed curves show corresponding neutron spectra in fragment centre-of-mass.

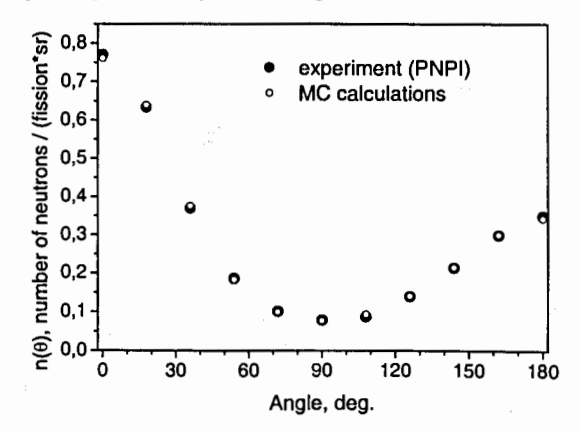
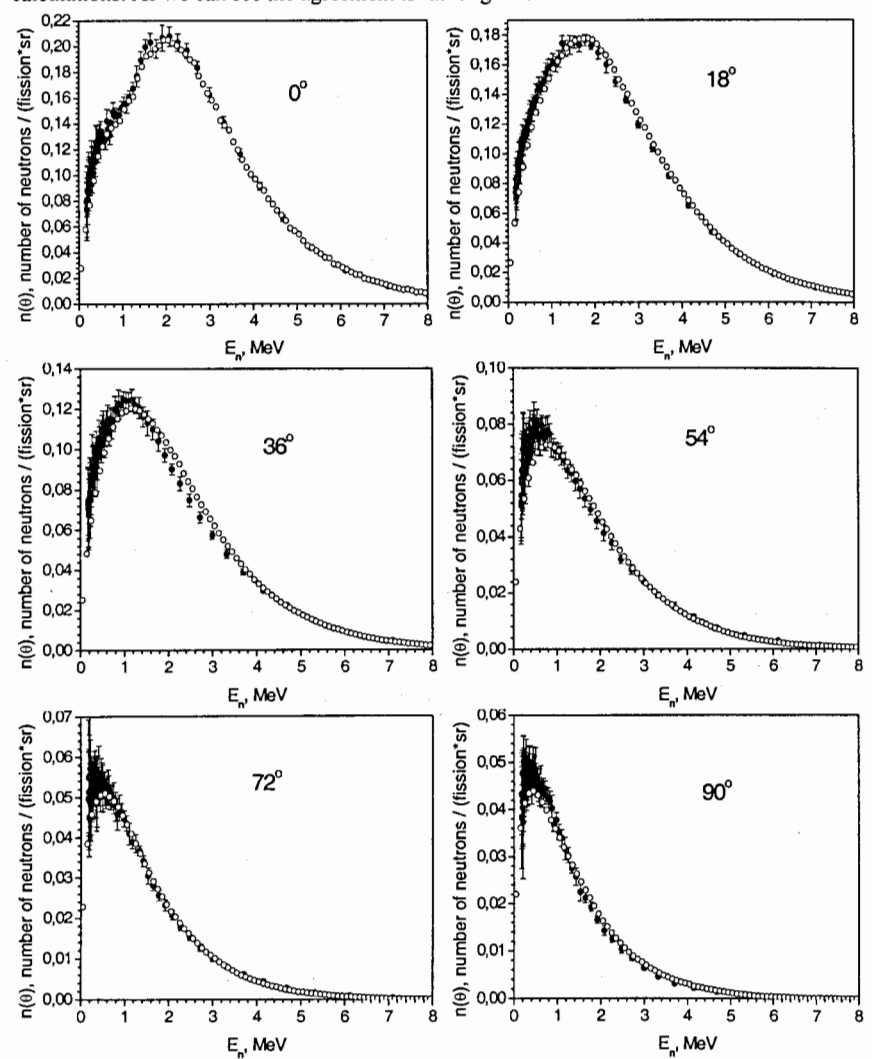


Fig.2. Experimental data and the result of MC calculations for energy integrated angular dependence of neutron yields.

Finally together with neutrons evaporated from fully accelerated fragments we also had to add 7% of neutrons concerned with isotropic component to describe the angular distribution of neutron yields. The energy distribution for this component was assumed Weisskopf form with temperature 1 MeV.

The figure 2 shows experimental data and calculated results integrated over all values of neutron energy.

The next eleven illustrations in the figure 3 demonstrate more detailed picture, namely: experimental neutron spectra at different angles and corresponding results of Monte-Carlo calculations. As we can see the agreement is rather good.



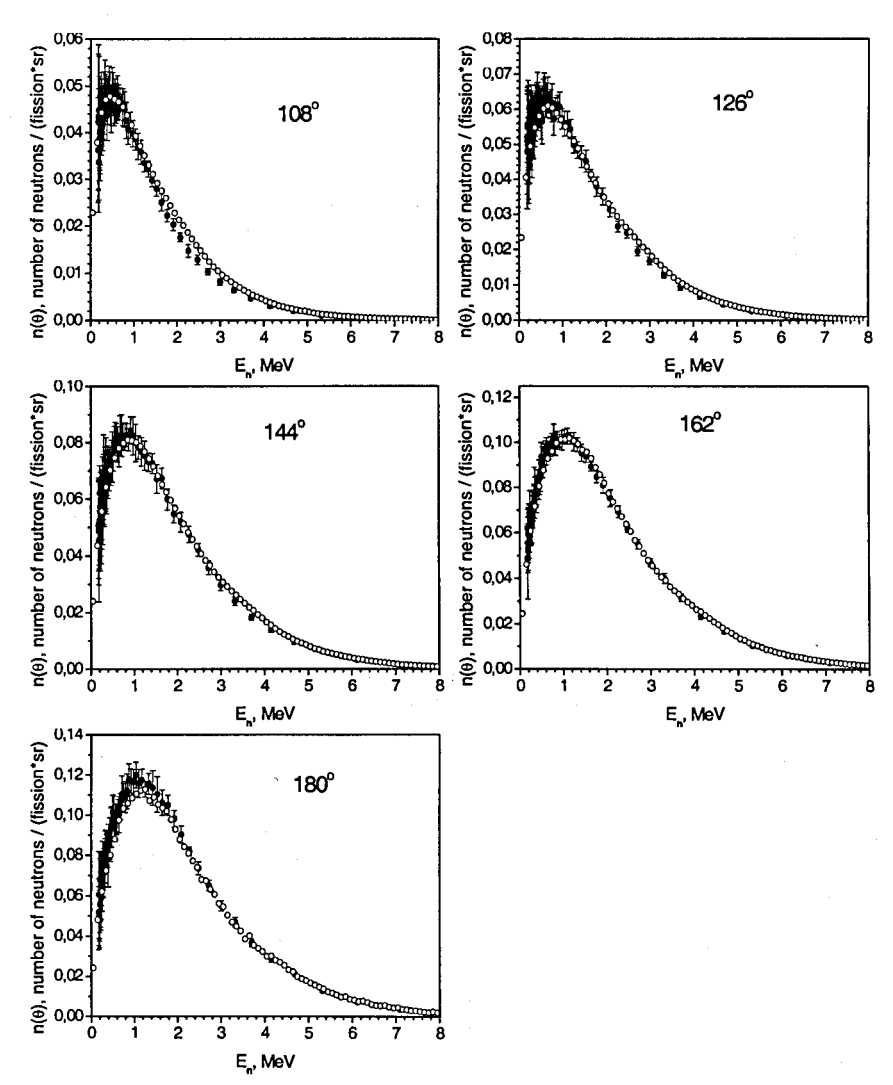


Fig.3. The comparison of experimental neutron spectra at different angles ( $\bullet$ ) observed in the reaction <sup>235</sup>U(n<sub>th</sub>,f) and corresponding results of Monte-Carlo calculations ( $\circ$ ).

With the aim to investigate the process of neutron emission the coincidences between prompt neutrons from fission can be also used. With this design the measurements of neutronneutron correlations in slow neutron induced fission of <sup>235</sup>U were realised recently in PNPI [2].

In our experiment the angular dependences of n-n coincidences integrated over all neutron energy values were measured for six different energy thresholds. This allowed us to get some

information not only about the contribution of additional component but also concerning its energy distribution.

Since the thresholds of the detecting device were set by the scale graduated against  $\gamma$ -rays, the true values of the neutron energy thresholds were obtained in process of corresponding time-of-flight spectrum fitting. Every time-of-flight spectrum consists of  $\gamma$ - $\gamma$ , n-n and  $\gamma$ -n components. The first two components are in the middle of the measured spectrum (see Fig.3 in [5]). Especially the scopes of  $\gamma$ -n component determine the neutron energy threshold.

Then neutron-neutron angular distribution was calculated for each neutron energy threshold. These calculations were based on the same assumptions as for description of neutron-fragment angular correlations. At the first stage of this calculation it was simulated neutron emission from both fragments with the addition of the necessary contribution of scission neutrons, namely 7%.

The averaged total multiplicity of emitted neutrons was taken as 2.42. The actual number of neutrons evaporated by each fragment was chosen randomly by two-dimensional Gaussian distribution with experimentally defined covariance and known ratio of averaged fragment multiplicities. We have got this ratio and neutron spectra in fragment centre-of-mass due to neutron-fragment experiment.

It was taken into account the presence of neutron emission anisotropy concerned with the angular momentum of each fragment.

In process of calculation were used final velocities of the light and heavy fission fragments with the most probable masses.

The Weisskopf form of energy distribution with temperature parameter 1 MeV for scission neutron spectrum was assumed.

Thus all input data for calculations were obtained from neutron-fragment angular correlations and we had no free parameters (including parameters of isotropic component) to describe n-n angular distributions.

The figure 4b demonstrates the Monte-Carlo predictions of n-n angular distributions in slow neutron induced fission of <sup>235</sup>U for our six neutron energy thresholds. All angular dependences were normalized to one at 90°. As we can see the ratio between maximal and minimal values of n-n angular correlation depends very significantly on neutron energy threshold. For maximal value of energy threshold, namely 2030 MeV, this proportion is twice as much than for lowest one.

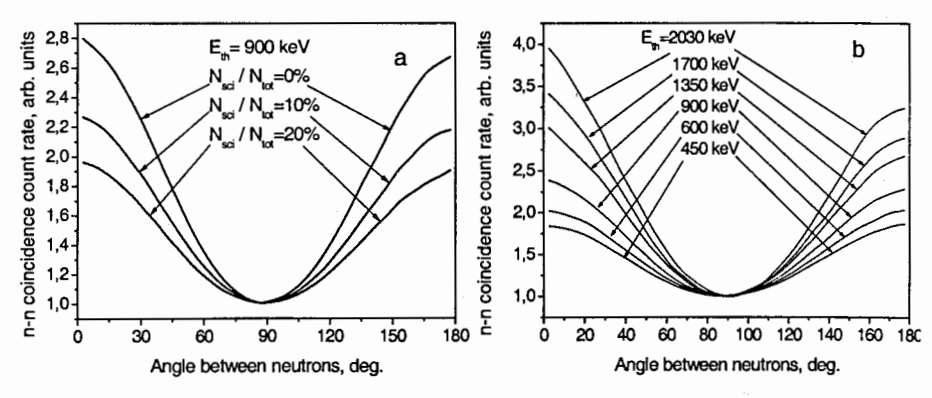


Fig.4. The influence of scission neutron contribution (a) and neutron energy threshold (b) on describing of n-n angular distributions.

We can compare calculated results with experimental data of neutron-neutron angular distributions. The next 6 pictures in the figure 5 represent such distributions for different neutron energy thresholds. As we can see our calculations are in a good agreement with experimental results.

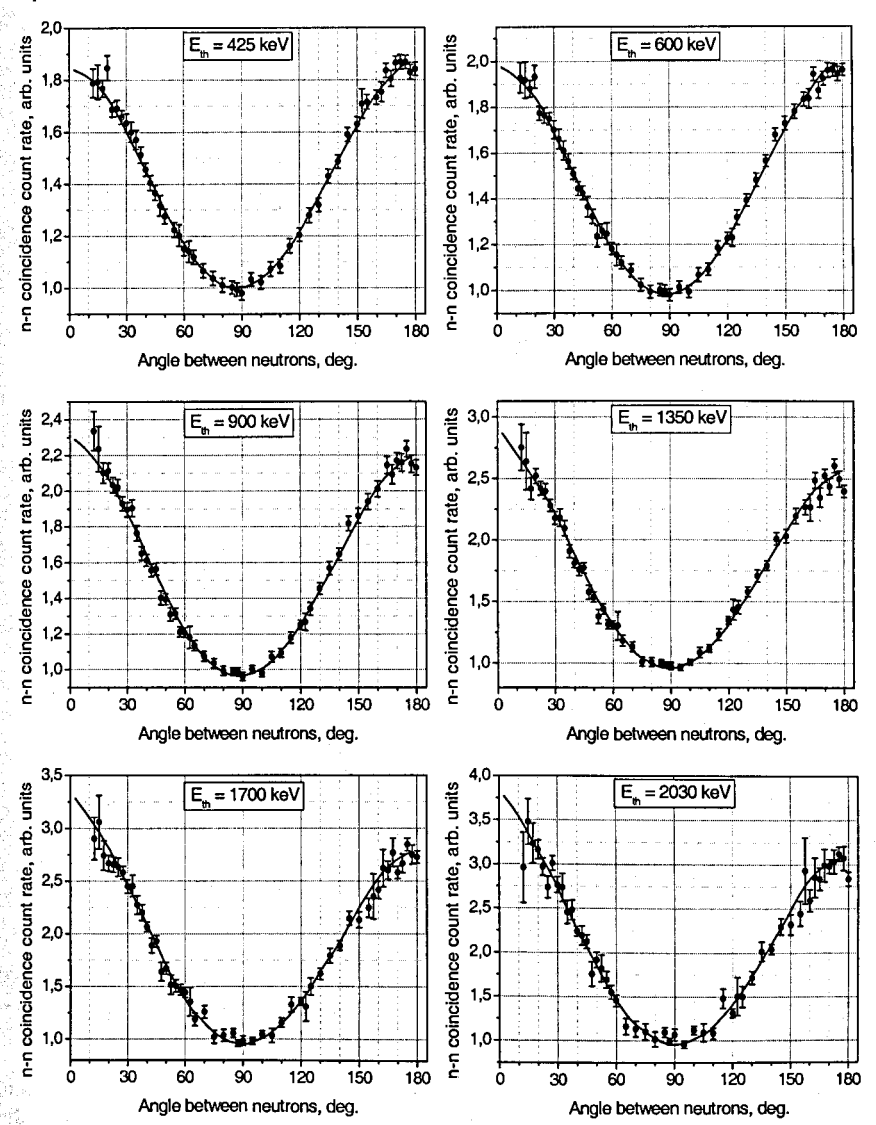


Fig.5. The comparison of experimental data and results of MC calculations for n-n angular correlations in the reaction  $^{235}U(n_{th},f)$ .

The figure 6 demonstrates the sensitivity of calculated values for n-n coincidence count rate to scission neutron contribution. It may be seen that all experimental data are practically bounded by two lines: with 5% and 9% contributions of isotropic in laboratory system component. This allowed us to evaluate the contribution of scission neutrons as (7±2)% for total number of emitted neutrons.

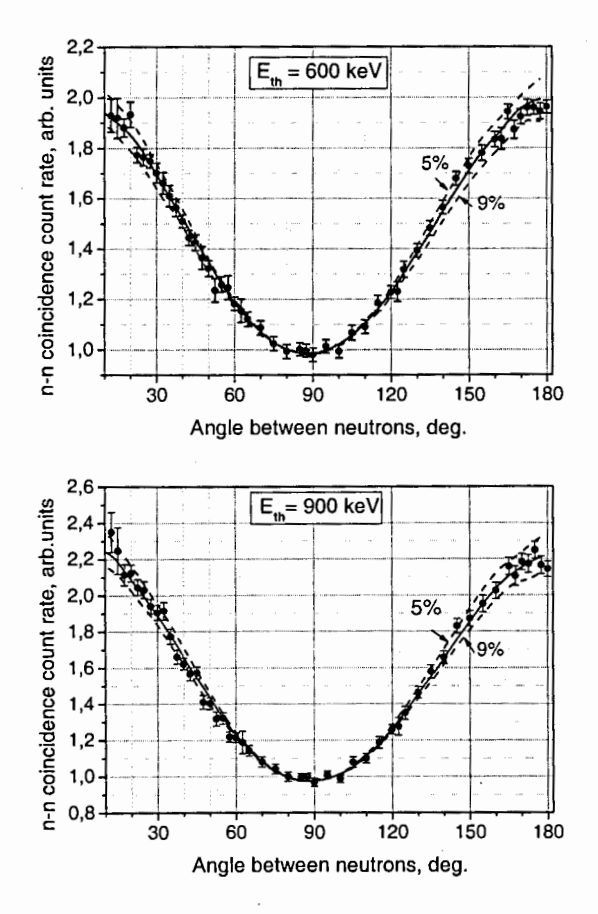


Fig.6. The sensitivity of calculated values for n-n coincidence count rate to scission neutror contribution. The solid curve corresponds to 7% of isotropic component, the dashed lines – 5% and 9%.

As a part of the previous report in proceedings of ISINN-15 [5] was the evaluation of scission neutron component using experimental data of Franklin [6]. These data also correspond to n-n angular distribution in slow neutron induced fission of <sup>235</sup>U but they were obtained only for three neutron energy thresholds. These data give us another result, namely 15%. Now we have an opportunity to compare both experimental data (Franklin and PNPI connected practically with the same energy thresholds.

But before this it is necessary to recall how n-n angular distributions depend on the contribution of isotropic component and on neutron energy threshold. The two figures 4a and 4b demonstrate mentioned relations. As we can see the more the part of scission neutrons and lower energy threshold are supposed the planer calculated curve is.

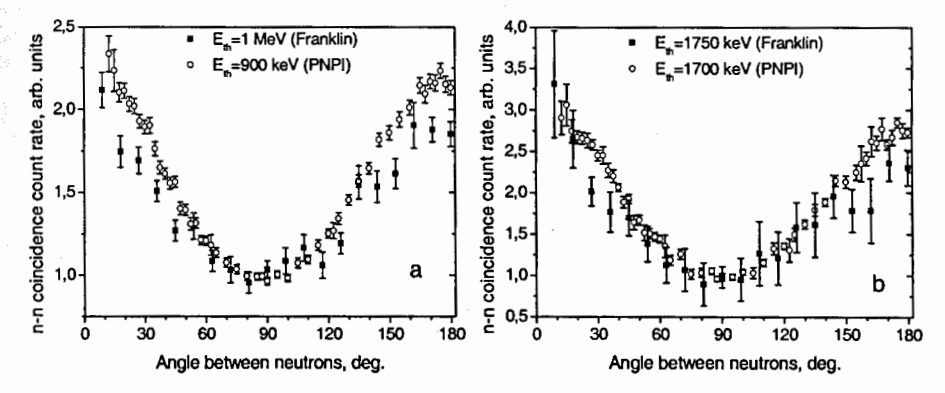


Fig.7. The comparison of our experimental data on n-n angular correlations with experimental data obtained by Franklin.

Let's go back to experimental data comparison. The figures 7a and 7b show n-n angular distributions for neutron energy thresholds near 1 MeV (a) and about 1.75 MeV (b). All data were normalised at 90 degrees. As we can see positions of our data are systematically above although they must be slightly below than Franklin's data if all neutron energy thresholds were right estimated. We are sure that our determination of energy threshold is correct but we do not know how this value was obtained by Franklin. Perhaps the discrepancy between energy threshold estimations is the reason of different values for isotropic component.

#### Conclusions:

Both experimental data (corresponded to n-f and n-n angular distributions) in slow neutron induced fission of <sup>235</sup>U can be well reproduced by Monte-Carlo calculations assuming neutron evaporation from fully accelerated fragments with the addition of (7±2)% isotropic component. The form of energy distribution of isotropic component is N~E·exp(-E/T) with T=1 MeV. During the calculation anisotropy of neutron emission due to the presence of fragment angular momentum was taken into account.

#### References:

- 1. V.E.Sokolov et al., ISINN-15, Abstracts, Dubna, p.46 (2007).
- 2. K. Skarsvag, K. Bergheim, Nucl. Phys. 45 (1963) 72.
- V.E.Bunakov, I.S.Guseva, S.G.Kadmenski, G.A.Petrov ISINN-13, p.293 (2005), Izv.Ross.Akad.Nauk, Ser.Fiz., 2006, vol.70, no. 11, p.1618.
- 4. I.S.Guseva, A.M. Gagarski, G A.S. Vorobyev et al., Preprint PNPI №2753 (2008).
- 5. V.A. Petrov, V.E. Sokolov, G.V. Val'ski ISINN-15, p.266 (2008).
- 6. C.B. Franklyn, C.Hofmeyer and D.W.Mingay, Phys. Lett. 78B (1978) 564.

# Left-right and angular asymmetry of fission neutron emission

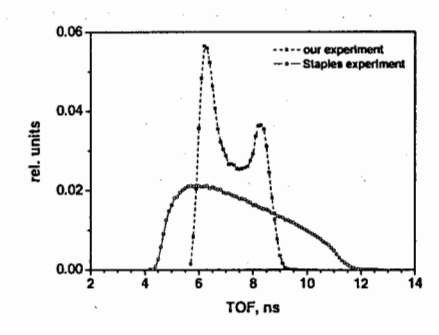
Kornilov N.V., Hambsch F.-J., Fabry I., Oberstedt S. EC-JRC-IRMM, B-2440 Geel, Belgium Simakov S.P.

Forschungszentrum Karlsruhe, Institute for Reactor Safety, D-76021 Karlsruhe Germany

Following a recommendation of the NEA Working Party on Evaluation cooperation (WPEC) [1] the prompt fission neutron spectrum (PFNS) was measured at ~ 0.5 MeV incident neutron energy.

# 1. Experimental procedure and results

Three experiments were carried out at the 7 MV Van de Graaff accelerator of the IRMM in Geel, Belgium, using the fast neutron time-of-flight technique. A pulsed proton beam of about 1.0 - 1.5 ns FWHM at 1.25 - 2.5 MHz repetition rate and 0.2 - 0.8  $\mu$ A average current was used. Mono-energetic neutrons of 0.52 MeV average energy were produced using the  $^7\text{Li}(p,\,n)$  reaction. A metallic  $^{235}\text{U}$  sample (93.15 % enrichment, 161.28 g) and a similar sized lead sample were applied for foreground and background measurements, respectively.



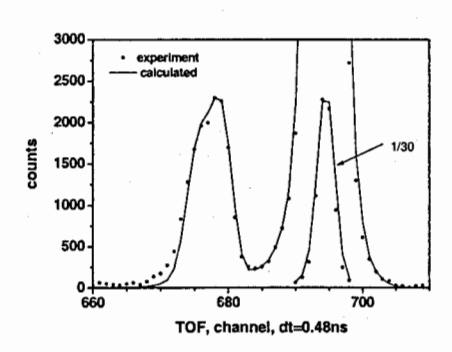


Fig. 1. Comparison between the TOF distribution of the input neutrons inside the sample for the present experiment (full symbols) and the one of Ref. [6] (open symbols). The data are from a Monte Carlo simulation.

Fig.2 Prompt-gamma ray peaks measured by detector R90 (Jan08 run). The threshold is 1.2 MeV. The channel width is 0.47 ns. The convoluted result is also given. The target gamma-rays (left) peak gives the detector resolution and proton pulse width. The prompt fission gamma-rays give the total time resolution including neutron spread inside the sample (Fig. 1).

In a first run (Jul06) an angular dependent effect was found. The neutron yield is  $\sim$  10% higher and the average secondary neutron energy  $\sim$  80 keV higher at 120 degree compared to 90 degree. The result was discussed at the Nice ND2007 conference [2]. This unusual finding stimulated new investigations to verify and to estimate the nature of this effect. In a second experiment (Apr07) we used three identical neutron detectors at a flight path of 2.24  $\pm$  0.01 m placed at 90, 150 and 120 degrees. The distance from the neutron production target to the sample was  $\sim$  8 cm.

In a third experiment (Jan08) the same detectors were applied. Two of them were placed at 90 degree to the left and right side relative to the proton beam direction. The third detector was at 150 degree at the right side. Flight paths were of  $2.25 \pm 0.01$  m. The sample was placed at  $8.5 \pm 0.2$  cm from the neutron target (0 position) and was moved also along the axis between detectors R90 and L90 at  $\pm 3$  cm and  $\pm 7$  cm. The plus sign means that the sample was moved towards the R90 detector and the minus sign in opposite direction towards the 90L detector. The third detector can see the sample only in the 0-position. Results for the sample in the 0-position only are discussed in this report. In every experiment the neutron detectors were shielded against direct and room-scattered neutrons.

Table 1. Average energies of the PFNS for all angles and runs. The letters shows left-L and right-R sides of the detector relative to the proton beam,  $\Delta E = 0.010$  MeV.

Angle,	<e>, MeV</e>	<e>, MeV</e>	<e>, MeV</e>
degree	Jul06	Apr07	Jan08
R90	2.004	2.002	2.021
L90			2.007
L120	2.076	2.050	
R150		2.026	1.975

The traditional pulse-shape analysis was applied to reduce the gamma-ray background. A small Pilot-U scintillator was used as a proton pulse shape monitor. The data were collected in list mode for offline analysis. The detector efficiencies were measured relative to the <sup>252</sup>Cf standard spectrum. A specially designed low mass, fast ionization chamber [3] was put at the place of the U-sample keeping the same geometry as during the experiments. The energy spectra were corrected for detector efficiency, for neutron multiple scattering in the sample, and for time resolution. A detailed description of the experimental procedure will be published elsewhere [4].

The pulse mode operation of the VdG was not the same during these experiments. The FWHM was  $\sim 1$  - 1.5 ns in all experiment. However, some tailing did exit which could not be removed completely. The worst tailing was observed during the Jul06 experiment. The best beam quality was realized during the third experiment, with a FWHM  $\sim 1$  ns and a FW(1/1000)M < 10 ns. We recalculated the time resolution correction for the measured

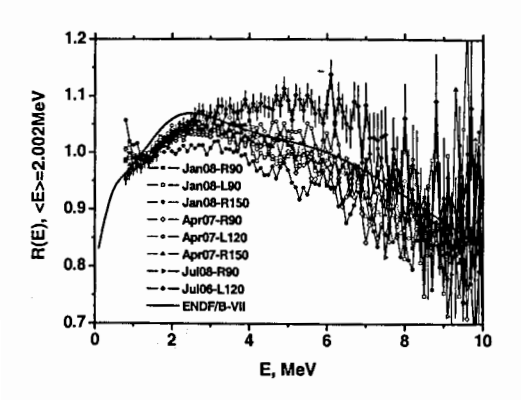


Fig. 3. Comparison between all of our results (full symbols). The ENDF/B-VII spectrum is given as a full inc.

spectra from Jul06 published before [2, 5]. An additional energy dependence in the neutron detector efficiency at E > 4 MeV has been taken into account, too. This factor slightly reduced the PFNS in the energy range 5 - 8 MeV and the average secondary neutron energy by up to ~ 15 keV for the first run.

The time resolution of the TOF spectrometer consists of the following components: detector resolution, pulse shape of the accelerator and neutron

distribution inside the sample. The last factor is very important. Fig. 1 shows the TOF intensity distribution of the incident neutrons inside the sample for our experiment compared to the one in Ref. [6]. Clearly the double peaked intensity structure of our ring shaped sample is visible in contrast to the very broad distribution of the very large sample (7.7 cm diameter) of Ref. [6]. This factor together with a shorter flight path (1.63 m) in spite of a very short proton burst of 0.6 ns in Ref. [6] is very important for data comparison. Therefore, the experimental data of Ref. [6] were corrected for this time resolution assuming the same contribution of the detector resolution as in our experiment. The present experimental time resolution together with the calculated dependences including all factors is given in Fig. 2.

The experimental PFNS were normalized to unity and the average secondary neutron energy was calculated. A Maxwellian spectrum was fitted in the energy range of 0.7 - 1.5 MeV and 9 - 11 MeV to the measured spectrum and an extrapolation to zero and to 20 MeV was done. Based on our detailed analysis of all incorporated corrections and possible uncertainties, we conclude that the average energy is estimated with an accuracy of  $\pm 0.010$  MeV. The average energies measured in all experiments are given in Table 1.

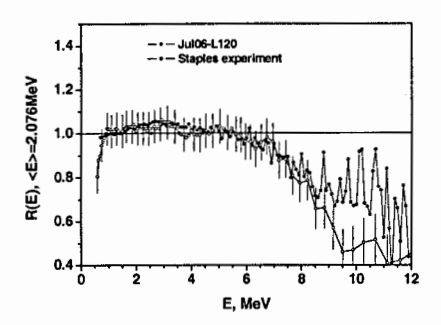
The PFNS at all investigated angles and for all runs are shown in Fig. 3 as a ratio to a Maxwellian distribution with the average energy  $\langle E \rangle = 2.002$  MeV.

The following peculiarities may be highlighted:

1. The data demonstrate the variety of the spectrum shape. A difference exists not only for various detector angles but for detectors at 90 degree placed at left and right sides (see Jan08 90R, 90L in Fig 2 and Tables 1, 2);

Table 2. Average spectral ratios <R> = N(E,90R)/N(E,90L) and their errors for different energy intervals.

E <sub>1</sub> -E <sub>2</sub> , MeV	$\langle R \rangle \pm \delta R$	E <sub>1</sub> -E <sub>2</sub> , MeV	$\langle R \rangle \pm \delta R$
0.8 - 2	$0.999 \pm 0.003$	5-6	$1.009 \pm 0.005$
2 - 3	$1.010 \pm 0.002$	6-8	$1.051 \pm 0.006$
3 - 4	$1.020 \pm 0.005$	8 – 10	$0.970 \pm 0.032$
4 - 5	$1.034 \pm 0.004$		



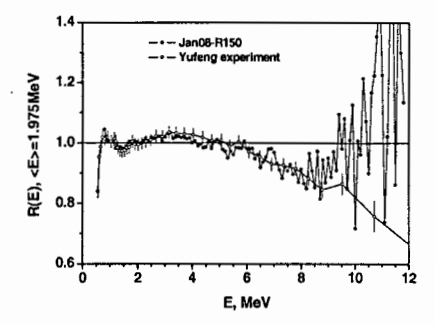
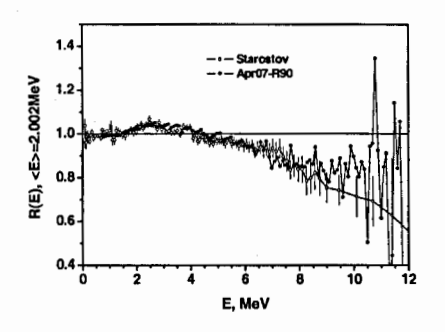


Fig. 4. Comparison between our result (Jul06 L120 detector) and data from Ref. [6].

Fig.5. Comparison between our result (Jan08, R150 detector) and data from Ref. [7].

- 2. The normalized spectra are fixed at low and high energies (see Fig. 3). The integrals between 1.3 2.3 MeV and 8 10 MeV are constant. The standard deviations of 8 spectra are 0.2% and 3%, respectively;
- 3. Among these data one may find a result which agrees perfectly with an old experiment or evaluation.

A comparison between the different experiments and literature values are given in Figs. 4-8. The spectra measured at thermal energy were normalized to a Maxwellian with reduced average secondary energy -  $\langle E_{th} \rangle$  =  $\langle E_{0.5} \rangle$  \* 0.995.



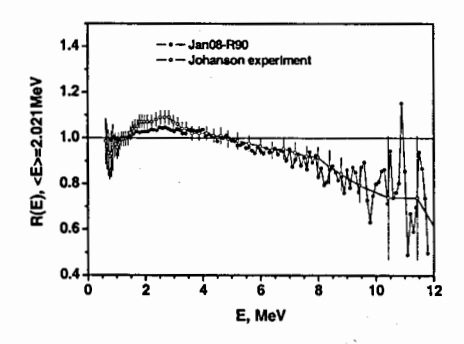
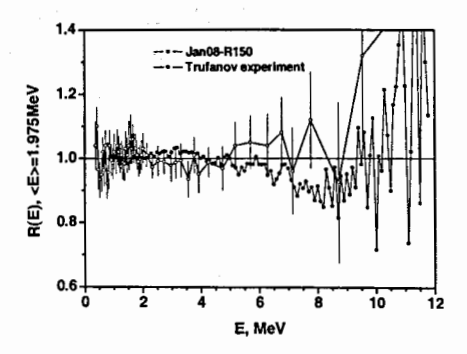


Fig. 6. Comparison between our result (Jul06, R90 detector) and data from Ref. [8].

Fig. 7. Comparison between our result (Jan08, R90 detector) and data from Ref. [9] corrected with multiple scattering and angular distribution from the T(p,n) reaction taken from Drosg's evaluation [10].



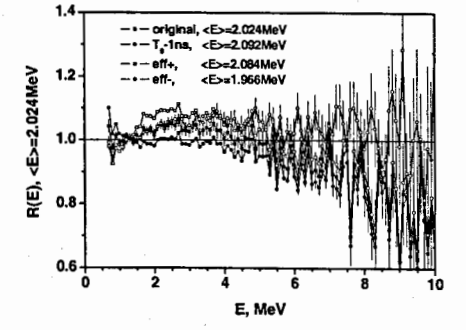


Fig. 8. Comparison between our result (Jan08, R150 detector) and data from Ref. [11].

Fig. 9. The original spectrum and the ones estimated using different perturbation factors as given in the legend.

Before starting any scientific discussion about the nature of this strange behavior of the PFNS one should answer the main question: is this a real effect or an experimental artifact?

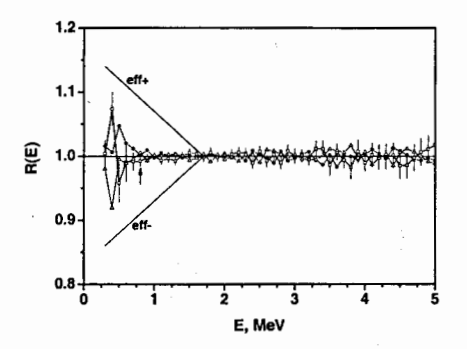
# 2. Possible experimental problems

The experiments were carried out relative to the standard  $^{252}$ Cf spectrum measured in the same experimental conditions. Therefore a lot of systematic uncertainties such as: flight path, uncertainties in the time channel width, a possible time reference shift ( $T_0$  value) connected with the detector operation, a distortion of the spectrum due to scattering in the collimator are drastically reduced or even canceled.

The shift of  $T_0$  versus pulse height was investigated. After an additional correction as a function of pulse height, the shift was < 0.1 ns (ADC channel width was 0.117 ns).

We investigated a possible change of the <sup>252</sup>Cf spectrum due to different emission angles of the neutrons relative to the electrode plates in the ionization chamber. The ionization chamber was rotated relative to its vertical axis and the neutron spectra were measured by two detectors at 90, and 120 degrees [4]. No influence was found.

The spectrum shape may be distorted due to the proton pulse shape (VdG pulse mode operation) and a possible mistake in the time resolution correction. In this case the high energetic part of the spectrum (most sensitive to the time resolution) should be distorted. Since we observe the same integrals for the energy interval 8-10 MeV this argument is not valid. In addition, this factor is common for all detectors and cannot explain the observed difference between them.



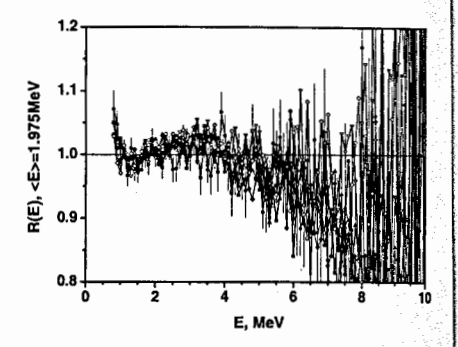


Fig. 10. The ratio of the detector efficiencies to the average value measured during the Jan08 experiment at the beginning, in the middle and at the end of the experiment. The distortion factors are shown by the full line. An arrow shows the cut-off energy in the data analysis.

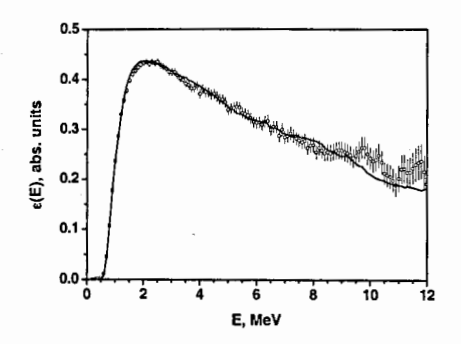
Fig.11. The spectra measured by the R150 degree detector during the Jan08 run.

So the most sensitive factor is the stability of the detectors and the correct estimation of the  $T_0$  value. The detector efficiency might be arbitrary changed in between the Cf and U measurements. As one can see in Fig. 2 the prompt fission peak (the zero time  $(T_0)$  is

determined relative to the prompt peak position) is very well separated from the main component due to prompt gamma rays from the target and  $T_0$  can be deduced with an accuracy of  $\sim 0.1$  ns. In addition to provide a measured difference between the spectra we should shift  $T_0$  in the opposite direction depending on the neutron detector.

We simulated the influence of both factors. The results are given in Fig. 9. We calculated the spectrum with the nominal parameters, with a shifted  $T_0$  by 1 ns and with a distorted detector efficiency by the function  $1 \pm 0.1 * (1.7 - E)$ , E < 1.7 MeV. The influence of these factors may provide an effect comparable with the data spread shown in Fig. 3, the average secondary energy varied by  $\pm 70$  keV. However, a shift of  $T_0$  by 1 ns changed the integral in the energy range 8 - 10 MeV by 28 % which is  $\sim 10$  times higher then the real data spread in Fig. 3, so we can also exclude this. Another possibility would be that the distortion factor is connected with instabilities of the threshold and neutron-gamma discrimination parameters. The detector efficiencies were measured before, in the middle, and after the U run in each experiment. The U-spectra shown in Fig. 3 are sums of several (5-7) runs measured during 10 - 20 hours, so the direct comparison of the separate spectra may answer this question about the detector stability. According to the results given in Figs. 10, 11 there is no evidence for a detector instability which may provoke the change in the measured results. In addition the detector efficiencies are in very good agreement with calculated results using the NEFF7 code [12], see Fig. 12.

These arguments are valid for each of the experiments, and the present conclusion is that we measured a real effect and no experimental artifact!



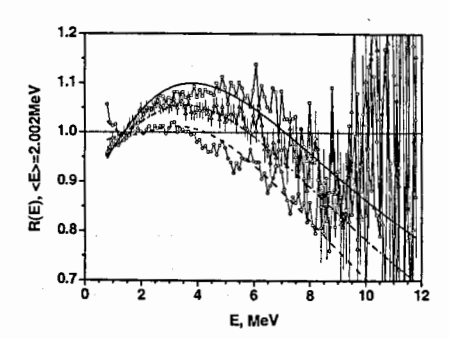


Fig. 12. The efficiency of one detector (Jan08, R150 detector) measured relative to <sup>252</sup>Cf and calculated with the NEFF7 code (full line).

Fig.13. Some experimental data and their description with a "3 source model". Dashed line -  $\zeta = 0.6$ , dashed-dotted line -  $\zeta = 0.4$ , full line -  $\zeta = 0.2$  (for details see text).

# 3. What does this experimental fact mean?

On the basis of the above discussion one may conclude that a factor exists which has a rather strong influence on the PFNS shape and asymmetry effects but was not fixed in our investigations and in all available experiments performed during the long history of fission investigations. One may assume that this factor is the neutron polarization. In the preparation stage of any PFNS experiment it was assumed that this factor is not important or by definition should be equal to zero. If this explanation is true, the transmission mechanism of the

information from the incident neutron to the secondary fission neutron should be found. The only possibility might be scission neutron emission, a fast process without formation of the compound nucleus. This may provide the link between the incident neutron and the secondary fission neutron. We should have in mind that three particles (two fission fragments and a scission neutron) are emitted at the same time which complicates the problem a lot.

The information about scission neutron emission is very poor. It was estimated in Ref. [13] that the probability of fission with scission neutron emission is ~ 40 % (which corresponds to a total of 15 % in total multiplicity), that the spectrum of scission neutrons consists of a low (~ 0.8 MeV) and a high (~ 2.5 MeV) energy components. In Ref. [14] evidence was given that scission neutrons are emitted by fission fragments with high total kinetic energy (TKE) (compact system). From the results of this paper we may estimate a high energy limit in the spectrum for scission neutron emission of ~ 8.5 MeV. The question is now, which parameters should be changed to provide the variety of results given in Fig. 3.

In case of scission neutron (SCN) emission, fission neutrons should be emitted from three sources:

1. Neutrons from fragments after fission of the compound nucleus A+1

$$N_{A+1}(E) = (1-\alpha) \cdot W_{A+1}(E) , \qquad (1)$$

where  $\alpha$  is the share of scission neutron emission and  $W_{A+1}$  is the spectrum which describes the neutron emission from accelerated fragments;

2. Neutrons from accelerated fragments after fission of the nucleus A, which is formed after the emission of one SCN:

$$N_{\Lambda}(E) = \alpha \cdot (\nu - 1) \cdot W_{\Lambda}(E) / \nu . \tag{2}$$

3. Scission neutrons itself:

$$N_{**}(E) = \frac{\alpha}{\nu} \cdot E \cdot \left( \frac{\varsigma}{T_1^2} \exp\left( -\frac{E}{T_1} \right) + \frac{1-\varsigma}{T_2^2} \exp\left( -\frac{E}{T_2} \right) \right), \tag{3}$$

where  $\zeta$  is the share of the low energy component and  $\nu$  is the neutron multiplicity.

The spectra  $W_A$ ,  $W_{A-1}$  were calculated with a Watt distribution for light and heavy fragments with masses  $A_h = 140$  and  $A_1 = A-140$ . The ratio of the neutron multiplicity for light and heavy fragments was  $v_1/v = v_1/v = 0.5$ . Temperature parameters were found based on the Fermi-gas relation and the thermal-equilibrium assumption with an additional correction of cor = 0.9 for the excitation of the heavy fragment  $U_h = U_{0h} \cdot \text{cor}$  [13]. The level density parameter was calculated as a = A/c, c = 8.4, TKE = 170.5 MeV, v = 2.45.

The equation for  $N_{\rm scn}(E)$ , and the corresponding parameters  $T_1$ ,  $T_2$  were taken from Ref. [13] introducing minor corrections:  $T_1 = 0.4$  MeV,  $T_2 = 1.35$  MeV. Changing only  $\zeta$  from  $\zeta = 0.2$  to  $\zeta = 0.6$  allowed us to describe the spectrum shape with reasonable accuracy from the highest average secondary neutron energy  $\langle E \rangle = 2.070$  MeV to the lowest  $\langle E \rangle = 1.967$  MeV (Fig.13). The spectrum with  $\zeta = 0.31$  extrapolated to thermal energy describes the integral experiments. The average ratio of the calculated cross sections to the experimental ones (Ref. [15], IRDF-2002) is  $\langle R \rangle = C/E = 0.997 \pm 0.008$ . The average energy of the PFNS at thermal energy is  $\langle E \rangle = 2.038$  MeV.

#### 4. Conclusion

In conclusion, a very unusual result, not observed before was found in the present investigation. Presently, there is no model, able to explain this result. We may assume that a different mechanism of the fission process and of neutron emission should be incorporated.

For the moment we may only conclude, that the measured effect is not an experimental artefact. We should assume the existence of an additional factor (parameter), for example the neutron polarisation which may be responsible for the measured peculiarities. However, we did not demonstrate the direct link between this unknown parameter and the fission neutron spectrum, the left-right and angular asymmetry. At present we can not answer the very important question, why the parameters of prompt fission neutrons changed so drastically and what is happening inside nuclear reactors.

So, new experimental efforts are urgently needed. It seems experiments with polarised thermal neutrons would be very interesting.

We would also like to thank the Van de Graaff accelerator team C. Chaves de Jesus, G. Lövestam, T. Gamboni, W. Geerts and R. Jaime Tornin for the high-quality pulsed beam.

#### References

- 1. Madland D.G., ISBN-92-64-02134-5, NEA/WPEC-9, 2003.
- 2. N.V. Kornilov, F.-J. Hambsch, I. Fabry, et al., *Proc. of the Int. Conf for Nucl. Data for Sci. and Tech.*, ND2007, Nice, France, Apr 2007, to be published.
- 3. N.V.Kornilov, F.-J. Hambsch, S. Oberstedt et al., JRC-IRMM, Neutron Physics Unit, Scientific report 2005, p. 67
- 4. N.V. Kornilov, F.-J. Hambsch et al., Internal report GE/NP/01/2007/02/14.
- 5. N.V.Kornilov, F.-J. Hambsch, S. Oberstedt et al., JRC-IRMM, Neutron Physics Unit, Scientific report 2006, p. 37.
- 6. P. Staples, J. J. Egan, G. H. R. Kegel, A. Mittler and M. L. Woodring, Nuclear Physics A591 (1995) 41.
- 7. W. Yufeng et al., Chin. J. Nucl. Phys. 11 (1989) 47. EXFOR32587.
- 8. B.I. Starostov et al., Nejtronnaja Fizika (6-th Conf. for Neutron Phys., Kiev. 1983), 1984. T.2. C.285,290, 294, EXFOR 40871, 40872, 40873.
- 9. P.I. Johansson, B. Holmqvist, Nucl. Sci. Eng. 62 (1977) 695.
- 10. M.Drosg, http://www-nds,org/drosg2000.html.
- 11. A.M. Trufanov et al., J. Nucl. Phys. 57 (1994) 606.
- 12. G. Dietze, H. Klein, PTB-ND-22 Report (1982).
- 13. N.V. Kornilov et al., Phys. of At. Nucl. 62 (1999) 209 and Nucl. Phys. A686 (2001) 187.
- 14. N.V.Kornilov, F.-J. Hambsch, A.S. Vorobyev, Nucl. Phys. A789 (2007) 55.
- 15. K.I. Zolatorev, INDC(NDC)-448, 2003, 25.

# EXOTIC HIGH NEUTRON MULTIPLICITY MODES IN 252Cf(sf)

Yu.V. Pyatkov<sup>1, 2</sup>, A.N. Tyukavkin<sup>2</sup>, D.V. Kamanin<sup>2</sup>, O.V. Falomkina<sup>2, 3</sup>, J.E. Lavrova<sup>1</sup>, I.I. Falomkin<sup>3</sup>, Yu.P. Pyt'ev<sup>3</sup>, E.A. Sokol<sup>2</sup>, E.A. Kuznetsova<sup>2</sup>

<sup>1</sup>Moscow Engineering Physics Institute, Moscow, Russia
 <sup>2</sup>Joint Institute for Nuclear Research, Dubna, Russia
 <sup>3</sup>Moscow State University, Moscow, Russia

Abstract. The structures presumably linked with collinear multicluster decay (CMD) of <sup>252</sup>Cf nucleus become visible in the mass-mass distribution of fission fragments gated by neutrons detected in coincidence. A reliability of the structures observed was estimated using Hough transformation. Analysis shows that CMD mode in question manifests itself as isotropic source of multiplicity ~ 4. Alternative treating is also possible that moving source of multiplicity 9 is decisive for the effect. Another exotic "collimated" neutron source is discussed as well.

#### INTRODUCTION

Some years ago in the frame of the program of studying of a new type of nuclear transformation called by us as collinear cluster tripartition (CCT) or more precisely collinear multicluster decay (CMD) bearing in mind our recent results obtained in this field [1], the experiment was performed aimed at measuring of neutrons correlated with unusual decay channel [2]. We expected one of the CMD modes to be an isotropic neutron source of high multiplicity. A special designed neutron detector based on <sup>3</sup>He counters was used in order to reveal this mode. All in all 140 neutron counters were located as a belt surrounded <sup>252</sup>Cf source in orthogonal to the mean fission axis plane (fig.1). Six modules of FOBOS spectrometer in each arm were used for measuring of fission fragments (FF) masses.

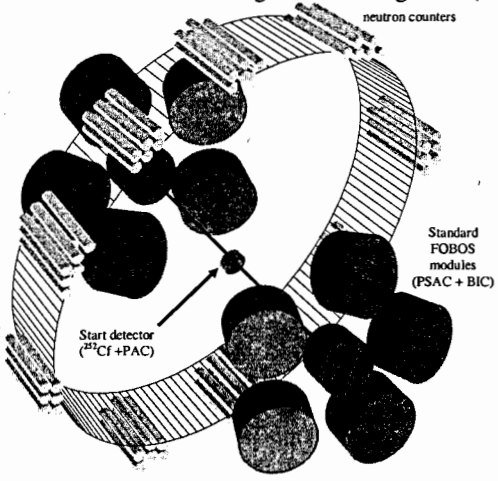


FIGURE 1. Sketch of the experimental setup used for registration of neutrons emitted in the CMD channel in coincidence with fission fragments.

# EXPERIMENTAL RESULTS UNDER ANALYSIS

Probability distribution for number of detected neutrons in a time gate started by fission event is shown in fig. 2. The spectrum predicted by the model of the neutron detection channel [2] is shown as well for comparison. As can be referred from the figure the model gives an adequate description of the experimental curve up to number of detected neutrons amounts to five. The yields at higher multiplicities forming a "tail" in the spectrum are underestimated in the model, which accounts only "conventional" neutrons originated likely uniquely from binary fission. Thus some unusual neutron source could give rise to the "tail" observed. We shell try to estimate characteristics of this source below.

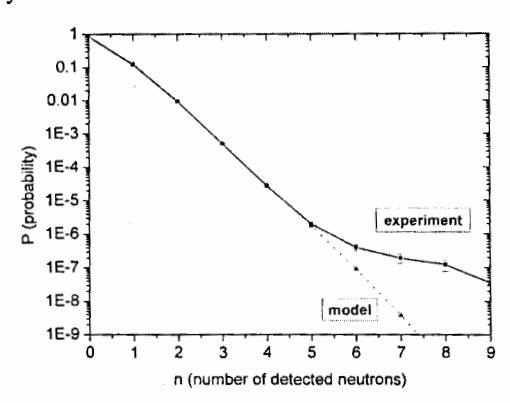


FIGURE 2. Experimental probability of detecting of fixed number of neutrons emitted in a single fission event.

Next interesting feature noted in [3] is connected with the FF mass-mass distributions obtained under condition that fixed numbers of neutrons were detected in selected fission event. Corresponding distribution when two or more neutrons were detected is shown in fig. 3. It seems the points below the "thickening" in the upper part of the figure presented a diffused edge of the locus of conventional binary fission form regular structures consisting of lines to be parallel to the coordinate axes (Ma,Mb=const) or tilted to them at 45°. Evidently the line tilted at 45° reference to abscissa corresponds to the condition Ms=Ma+Mb=const. Perpendicular line (-45° reference to abscissa axis) if it goes through the points Ma=Mb makes evident sense. Let us imagine that we deal with ternary nuclear system looks like a chain. If the middle partner of the chain exports equal number of nucleons from its body to two adjacent clusters their masses form the line parallel to the Ma=Mb line in the mass-mass plot. One observes such line if a middle cluster is missed for detection. Using additional selection by the fragments velocities i.e. Va≈Vb we revealed a rectangle bounded by known magic numbers (fig. 3a).

Something similar was obtained while  $n\ge 3$  (where n is a number of detected neutrons) selection rule was applied (fig. 4).

The yields of unusual points (below the locus of binary fission) forming in fact the structures discussed amount to  $1.28*10^{-4}$  and  $2.5*10^{-5}$  for distributions in fig. 3 and fig. 4 respectively.

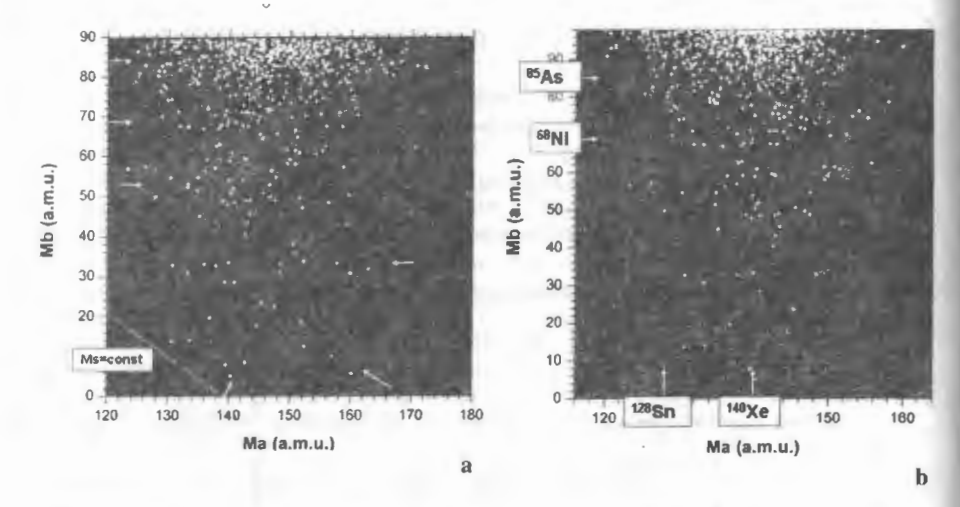


FIGURE 3. Mass-mass distribution of the FF under condition that two or more neutrons were detected in fission event selected (a). The same distribution but only events where  $Va \approx Vb$  are shown

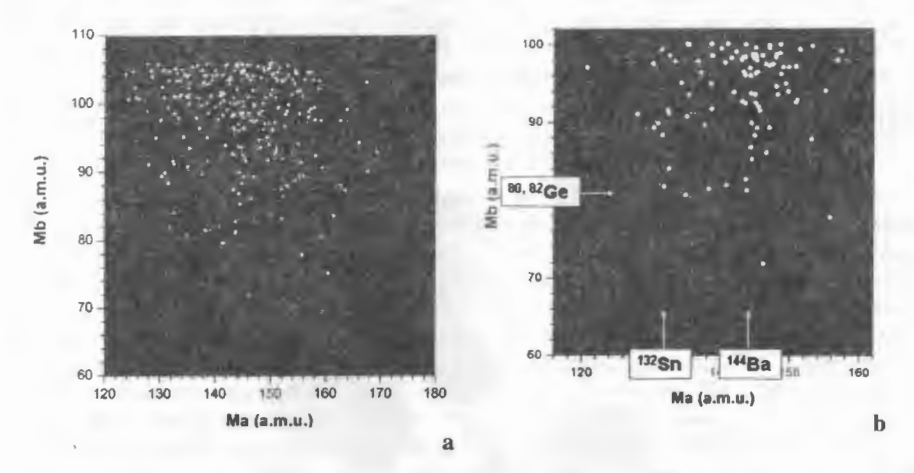


FIGURE 4. Mass-mass distribution of the FF under condition that three or more neutrons ( $n \ge 3$ ) were detected in fission event selected (a). The same distribution but only events where  $Va \approx Vb$  are shown (b).

It should be stressed that the structures seen in figs. 3, 4 manifest themselves clearly only in one spectrometer arm namely in this looking to the baking of the Cf source. Similar effect we have already noted as the "bump" structure in the FF mass-mass distributions originated both from <sup>252</sup>Cf (sf) and <sup>235</sup>U(n<sub>th</sub>, f) [4, 5] (fig. 5). Events selection sensitive to the nuclear charge of the fragments let us to suppress substantially a background under the bump (fig. 5b). Internal structure of the bump consists of tilted ridges Ma+Mb=const and these to be parallel

to the coordinate axes (i.e. Ma=const, Mb=const) are vividly seen in this case. Just the latter straight lines prove to constitute the rectangles in figs. 3b, 4b.

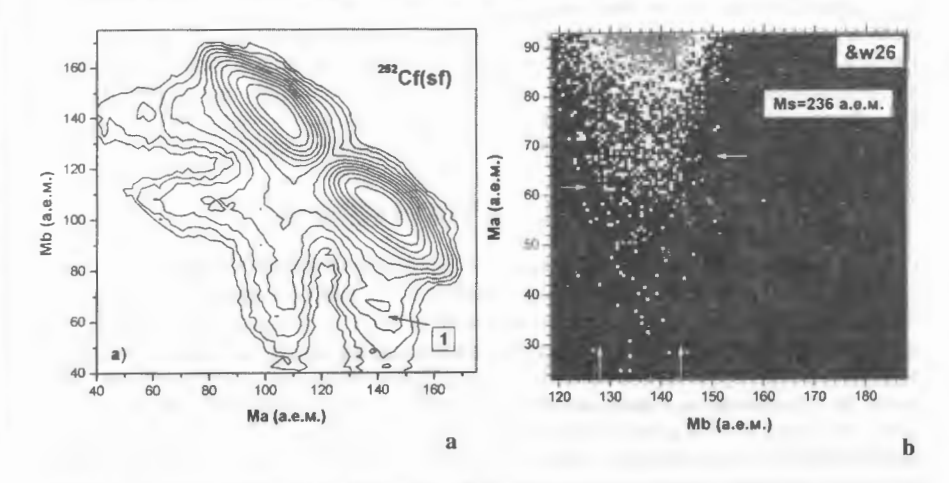


FIGURE 5. "Bump"-structure in the FF mass-mass distribution originated from <sup>252</sup>Cf (sf) (a) (bump is marked by the arrow) and <sup>235</sup>U(n<sub>th</sub>, f) (b). In the latter figure arrows point at the internal structures in the bump namely ridges Ma+Mb=const (tilted at 45° reference abscissa axis) and Ma, Mb=const.

# RELIABILITY OF THE STRUCTURES REVEALED

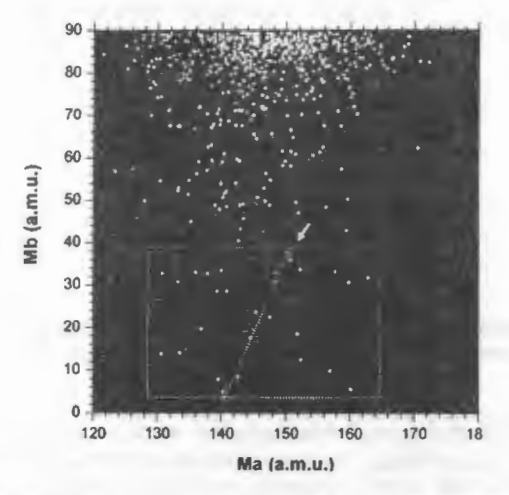


FIGURE 6. Region (rectangle) and image (the line marked by the arrow) chosen for testing a reliability of the structures under analysis. See text for details.

A natural question arises whether the structures at hand really make sense i.e. they are not random sequence of points. In order to answer the question a following simulation was performed. A formal algorithm (Hough transformation [4]) was used for recognition of a line. For instance, inside the rectangle shown in the fig. 6 only one line (marked by the arrow)

united nine points was find. Let us estimate a probability of random realization of the line of such length and tilted to the abscissa axis at arbitrary angle. We generated a sequence of random matrices bounded by the rectangle included precisely the same number of points as this in the initial distribution. Each matrix was processed with the Hough algorithm in order to search for the line mentioned above. Among one hundred matrices analyzed only two of them provided positive answer. In other words, a probability of random realization of the line under discussion is about 2%. Absolutely clear that more complicated structure such as rectangle (fig. 3, 4) is much less probable as randomly assembled image.

## CMD AS A NEUTRON SOURCE

Let us estimate real neutron multiplicity corresponding to the multibody decays under discussion basing on the model of the neutron registration channel worked out [2]. The modes manifested themselves via decay events where more then two neutrons were detected. An increased number of neutrons (just to remind- corresponding total mean value is substantially less of a unit, see fig.1) could be due to some different reasons. Firstly, it could be binary fission. In this case the structures originate simply from a random grouping of experimental points originated from scattered fragments. As was shown above it is extremely unlikely. Secondly, the structures associate with at least ternary fission. Let us suppose that neutrons are emitted from accelerated fragments moving with the velocities typical for conventional binary fission. Corresponding spectra for some fixed numbers of emitted neutrons are presented in fig. 7. Using the slope of the experimental curve as a criterion one can try to choose the best among the model spectra. The curve looked for corresponds to multiplicity 9.

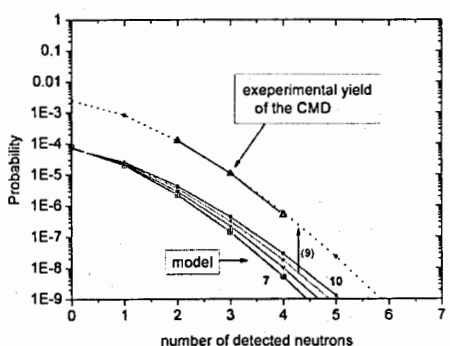


FIGURE 7. Comparison of the neutron yields associated with CMD and model spectra for neutrons emitted from the accelerated fission fragments. Model neutron multiplicities are varied in the range 7÷10neutrons.

Let come to hypothesis that an isotropic neutron source is linked with the structures in question. The results of modeling of such situation are compared with the experimental data in fig. 8. The best agreement is observed for the curve corresponding to four neutrons emitted. Summing up the yields over all this curve one can obtain a total yield of the CMD mode stands behind, namely,  $Y \sim 10^{-3}$ / binary fission being in line with this ( $\sim 2*10^{-3}$ ) obtained earlier for the bump in the mass-mass distribution (fig. 5a).

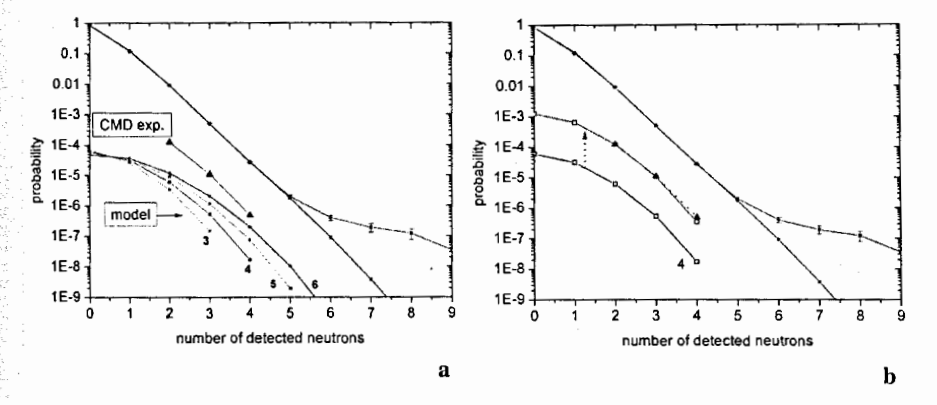


FIGURE 8. Comparison of the CMD mode yields with modeling of the isotropic neutron sources of different multiplicities (marked near curves) (a). Each curve is normalized arbitrary to the total yield 10<sup>4</sup>. The model curves provided best agreement with the experiment (b).

Due to the "graphical quality" (clearness) of the structures in fig.3, 4 it is believed a background in the effect region to be less than 20% or in other words we suppose that at the worst only each fifth point in the effect region relates to the background. In its turn the background amounts to scattered fragments of conventional binary fission. Thus according to the assumptions put forward the curve which describes the background should be congruent to the global experimental spectrum P(n) evidently linked with binary fission but shifted to the point 0.2 P<sub>eff</sub>(2) (the yield of the effect for the abscissa n=2). It is precisely the recipe used to draw the curve marked by the label "background" in fig. 8.

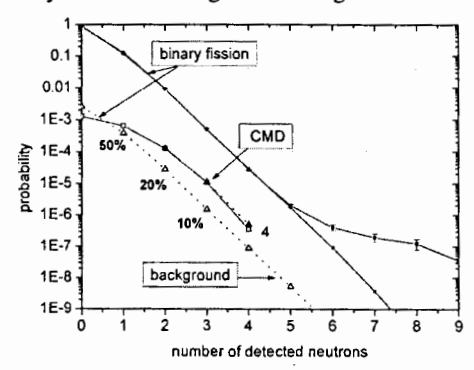


FIGURE 9. Estimation of the background in the region of CMD manifestation.

Having the curve obtained in such a manner we can estimate a contribution of the background in all the range of the detected neutrons. As can be referred from the figure one half of the events when one neutron was detected are due to the background, for three detected neutrons corresponding portion does not exceed 10%. These numbers give an idea why the structures linked with CMD become visible only at increased number of the detected neutrons ( $n\geq 2$ , 3).

#### **EXOTIC NEUTRON SOURCE?**

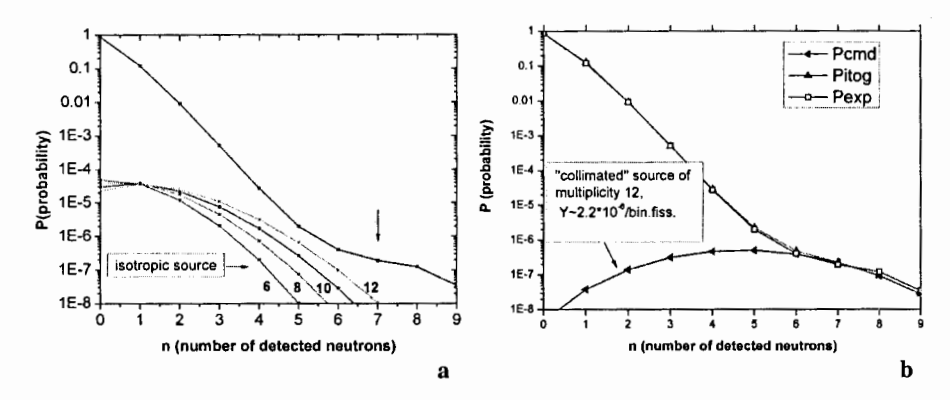


FIGURE 10. Fitting of the "tail" (marked by vertical arrow) in the experimental P(n) spectrum. Even isotropic neutron sources of high multiplicity show spectra being too far from the "tail" by the slope (a). "Collimated" neutron source of multiplicity twelve provides the best description of the "tail" (b).

In order to estimate at least roughly parameters of the neutron source delivers the "tail" in the experimental P(n) spectrum (fig. 10) we try as it was done above to fined suitable candidate among isotropic sources of different multiplicities but failed. Really, the spectrum even for multiplicity twelve has absolutely different slope (fig. 10a). The problem is solved if one supposes neutron registration efficiency to be 40% and multiplicity twelve (fig. 10b). It is rather astonishing result bearing in mind that total geometrical efficiency of neutron detectors (neutron belt) is only 19% (but from  $4\pi$ ). In other words the source in question should be collimated in the plane perpendicular to the fission axis. It could be "hot spot" between two fragments right after scission. We are going to verify this exciting conclusion in forthcoming experiment.

#### ACKNOWLEDGMENTS

This work has been supported in part by CRDF, grant MO-011-0.

#### REFERENCES

- Yu. Pyatkov et al., 6<sup>th</sup> International Conference on Dynamical Aspects of Nuclear Fission "DANF2006", Smolenice Castle, Slovak Republic, 2-6 October 2006. Conference proceedings, World Scientific Publishing Co. Pte. Ltd., 2008, p. 248-258.
- 2. D.V. Kamanin et al., Physics of Atomic Nuclei, 66 (2003) 1655.
- 3. Yu.V. Pyatkov et al., Physics of Atomic Nuclei, 66 (2003) 1631.
- 4. Yu.V. Pyatkov et al., Romanian Reports in Physics, 59, No. 2, (2007) 569-581.
- D.V. Kamanin et al., Preprint JINR PI5-2007-182, Dubna 2007 (rus).
- 6. http://homepages.inf.ed.ac.uk/amos/hough.html

# MEASURING OF THE FRAGMENTS NUCLEAR CHARGES AT THE MINI-FOBOS SPECTROMETER

A.N. Tyukavkin<sup>1</sup>, Yu.V. Pyatkov<sup>1,2</sup>, D.V. Kamanin<sup>1</sup>, Yu.N. Kopach<sup>1</sup>, A.A. Alexandrov<sup>1</sup>, I.A. Alexandrova<sup>1</sup>, S.B. Borzakov<sup>1</sup>, Yu.N. Voronov<sup>1</sup>, S.V. Denisov<sup>1</sup>, G.L. Efimov<sup>1</sup>, V.E. Zhuchko<sup>1</sup>, N.A. Kondratiev<sup>1</sup>, E.A. Kuznetsova<sup>1</sup>, Yu.E. Lavrova<sup>2</sup>, S.V. Mitrofanov<sup>1</sup>, Ts. Panteleev<sup>1</sup>, V.S. Salamatin<sup>1</sup>, I.P. Tsurin<sup>1</sup>

<sup>1</sup>Joint Institute for Nuclear Research, Dubna, Russia <sup>2</sup>Moscow Engineering Physics Institute, Moscow, Russia

Abstract. Method of measuring and calibration of fission fragments nuclear charges is described. The nuclear charge was determined by measuring of the drift time of a track formed after stopping of a fragment in the gas-volume of the high aperture ionization chamber. This method was applied at the MiniFOBOS spectrometer in the experiment aimed at studying of the <sup>235</sup>U(n<sub>th</sub>, f) reaction. The experiment was performed at the IBR-2 beam in FLNP of the JINR. The nuclear charge proves to be important additional parameter for reliable identification of the collinear multicluster decay products [1] searched for.

#### EXPERIMENTAL SETUP

MiniFOBOS setup (fig. 1) is a double armed time-of-flight-energy spectrometer based on the standard detector modules (fig.2) of the  $4\pi$ - spectrometer FOBOS. Each detector module used consists of position-sensitive avalanche counter (PSAC) and an axial big ionization chamber (BIC) which registered the full energy of the fragments. The drift time of a track formed after stopping of a fragment in the gas-volume of the BIC is known to be linked with the fragment nuclear charge [2]. Corresponding parameter was measured as a time difference between PSAC signal and the signal from the Frisch grid of the BIC.

Specially designed start-detector represents symmetrical avalanche counter (SAC) with an internal target (fig. 3). An active layer of the target was prepared by evaporation of  $100 \,\mu g/cm^2$  of  $^{235}$ U isotope on Al<sub>2</sub>O<sub>3</sub> backing of  $50 \,\mu g/cm^2$  thick.

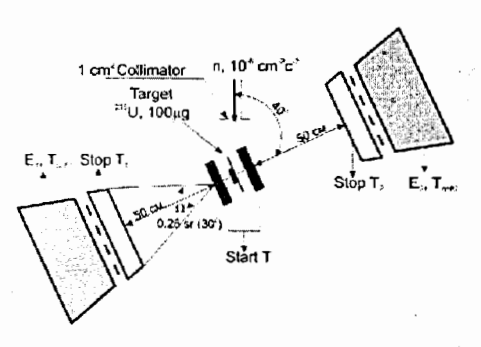


FIGURE 1. Scheme of the experimental setup

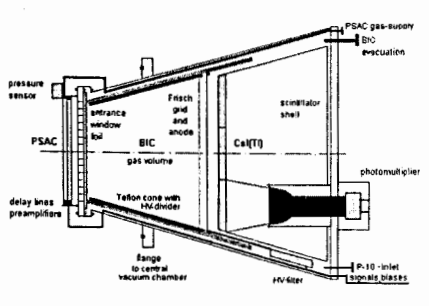


FIGURE 2. Detector module of MiniFOBOS spectrometer

# THE NUCLEAR CHARGE CALIBRATION PROCEDURE DEVELOPED

The parameterization of a fragment range in a gas volume was successfully applied in Ref. [3].

The range of a particle can be expressed as

$$R = L - D \cdot V_{drift}, \tag{1}$$

where L – is the distance between entrance window and Frisch grid, D – drift time of a track,  $V_{drift}$  – drift velocity of electrons forming the track.

The Bohr-Wheeler [4] relation was applied for description of a particle range:

$$R = \beta \sqrt{EM} Z^{-2/3}, \tag{2}$$

where E - is the energy of fission fragment (FF), M - FF mass, Z - FF nuclear charge.

Fragment momentum can be expressed as:

$$P_{BIC} = \sqrt{1.923EM} \,. \tag{3}$$

Using expressions (1-3) one can obtain:

$$D = \alpha - \beta \cdot P_{BIC} \cdot Z^{-2/3} + \gamma M + \delta E, \tag{4}$$

where  $\alpha$ ,  $\beta$ ,  $\gamma$ ,  $\delta$  are the parameters to be calculated.

Thus one need a parameter vector  $Y(\alpha,\beta,\gamma,\delta)$  for calculating the FF Z-value basing on formula (4):

$$Z = \left(\frac{\beta \cdot P_{BIC}}{\alpha - D_{-}\exp + \delta E}\right)^{3/2}.$$
 (5)

An algorithm for calculation of vector Y (Z – calibration procedure) starts from generation of matrix "Drift time – energy in BIC" (fig.3) using experimental data for the fixed Mtt value (FF mass obtained in the frame of the velocity-velocity method).

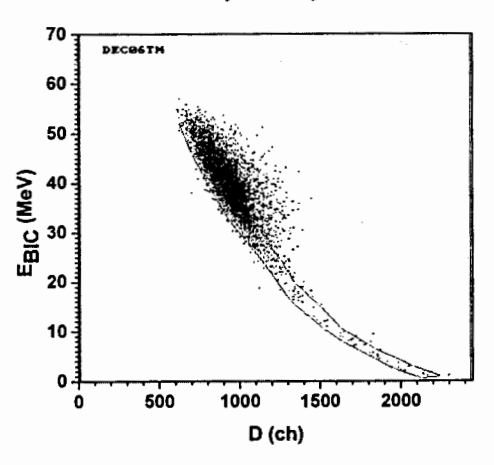


FIGURE 3. "Drift time vs. energy in BIC" dependence for the FF having fixed Mtt mass = (97±1) a.m.u.

A "tail" of the main locus in the figure is due to the FF scattered on the supporting grid of the BIC. Selected Mtt value is corrected in order to take into account emitted neutrons (fig. 4),

in other words, mean post-neutron mass value is obtained which is used for calculation of the FF momentum  $P_{BIC}$  in the BIC.

At the next step one obtains the (<D\_exp> vs.P<sub>BIC</sub>) dependence by means of averaging of D\_exp values at each momentum value. Simultaneously Z- value is calculated for each event involved in the distribution in fig. 3 using current parameters vector Y. This vector is changed in the frame of the procedure based on the MINUIT minimization code [6] in order to minimize purpose function which represents the quadratic difference between both experimental and calculated curves  $D(P_{BIC})$  and <Z> for Mtt mass selected for calibration. Reference Z values are calculated according  $Z_{ucd}$ -hypothesis within the corrections from [7] (fig. 5).

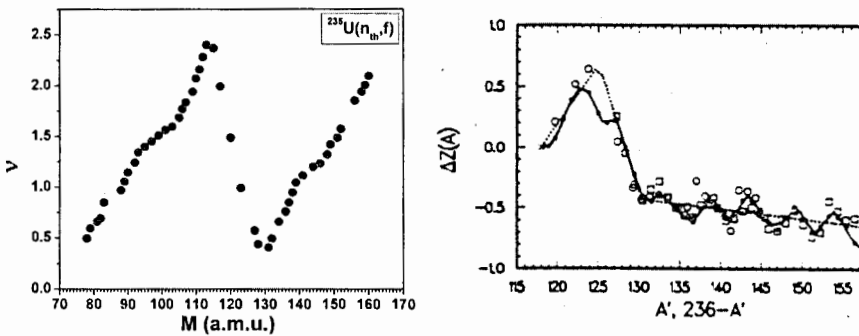


FIGURE 4. Average number of neutrons vs. pre-neutron mass for the reaction <sup>235</sup>U(n<sub>th</sub>f) [5].

**FIGURE 5.** Corrections to the FF Z-value calculated according  $Z_{ucd}$  hypothesis [7].

The scheme of the Z-calibration code is presented below (fig. 6).

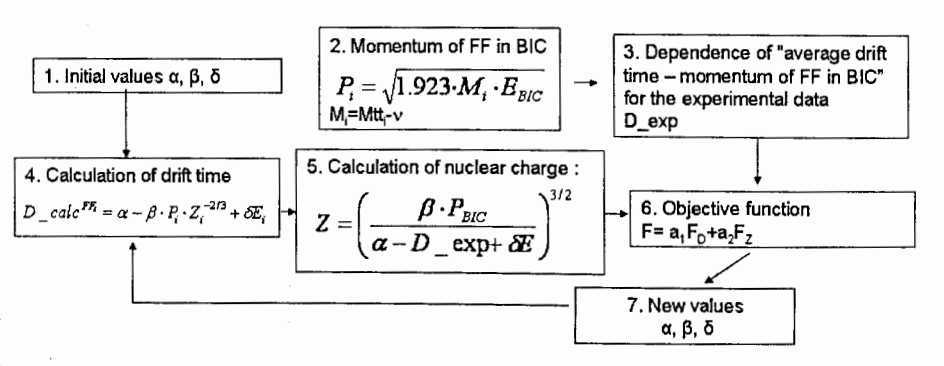


FIGURE 6. Scheme of the Z-calibration code developed.

#### TESTING OF THE CALIBRATION PROCEDURE

In order to test the calibration procedure developed simulations based on the quasiexperimental data were performed. The following parameters similar to the experimental ones were used for generation of the model data:

- -the BIC is filled by Ar at a pressure of 11 kPa;
- -the distance between entrance window and Frisch grid is equal to 26 cm;
- -the temperature is 19°C;
- -the density of the gas is equal to 1.85\*10<sup>-4</sup> g/cm<sup>3</sup>.

The range of the particles was calculated using computer code SRIMM 2006 [8] with PRAL algorithm (Projected Range Algorithm, J.P. Biersack [9]).

Table 1. The charges and energies of the fragments tested.

Z	6	8	10	15	20	23	32	34	37	51	55
E, MeV	1-15	1-30	1-30	1-30	1-30	1-40	1-50	1-60	1-45	1-25	1-20

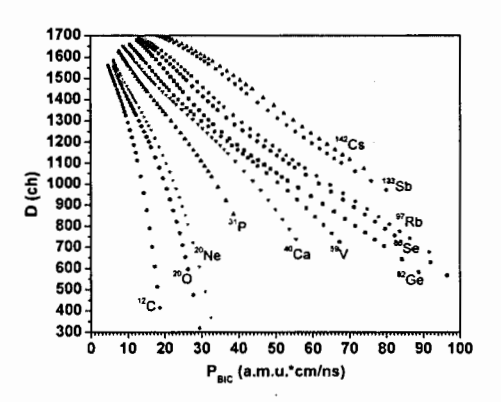


FIGURE 7. "Drift time vs. momentum of the FF in the BIC" model dependences obtained by the SRIMM code.

As can be referred from the figure the curves D(P) have rather complicated shape varying smoothly while nuclear charge is changed. Comparison of the calculated D(P) dependences with model and experimental are shown in fig.8a and fig.8b respectively. From the figures we observe that calibration proposed gives quite satisfactory description of both model end experimental data for typical fission fragments of the light mass peak in wide energy range. An agreement of the calculated D(P) dependences with the data for heavy fragments is much worse (fig. 9), especially for the model data. Likely it shows on miscalculations of the heavy ions ranges by SRIM code in this region.

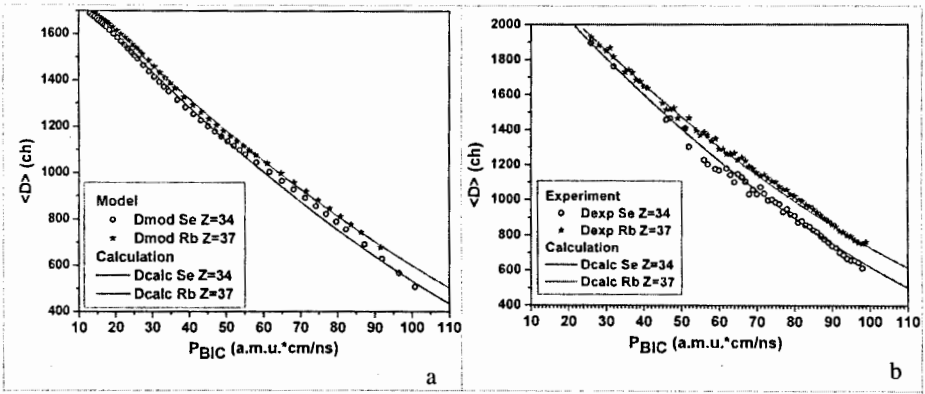


FIGURE 8. Comparison of the calculation with the modeling (a) and the experimental (b) data for FFs with masses 88 and 97 a.m.u.

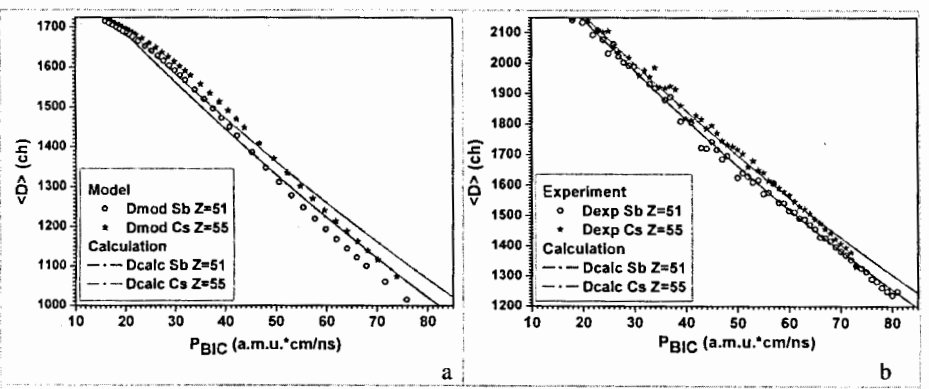


FIGURE 9. Comparison of the calculation with the modeling (a) and the experimental (b) data for FFs with masses 133 and 142 a.m.u.

## LIMIT OF LIGHT IONS

In our previous experiments devoted to searching for collinear multicluster decays we observed fragments of different masses including light ions. It was interesting whether parameterization (4) is suitable for estimation nuclear charges of light ions as well. Corresponding results are shown in figs. 10, 11. One can refer from the figures that the calculated curves are shifted reference to model (quasi-experimental) ones approximately on two charge units.

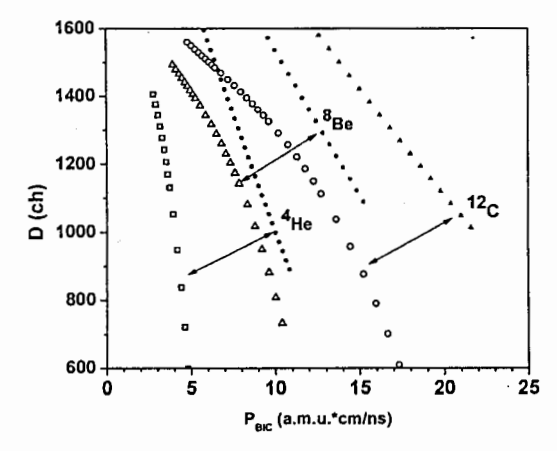


FIGURE 10. Comparison of simulated data (empty symbols) with calculations based on expression (4) for <sup>4</sup>He, <sup>8</sup>Be, <sup>12</sup>C ions.

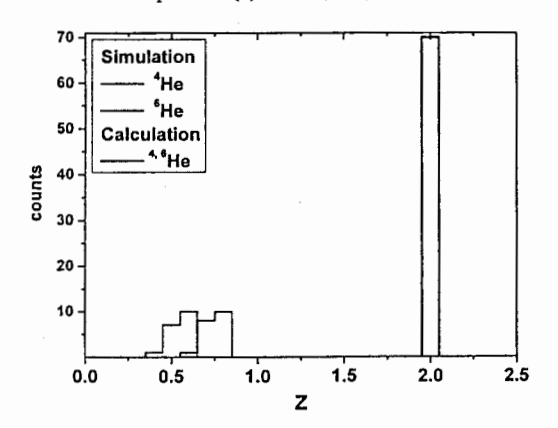


FIGURE 11. Comparison of simulated data with the results of calculation based on expression (4) for <sup>4,6</sup>He ions.

Table 2. Parameters of the nuclear charge spectrum of the FFs from the reaction  $^{235}\text{U}(n_{th},\,f)$ .

	MiniF	Lang et al [10]		
	Modul 1	Modul 2	Lang et al [10]	
<z>, light FF peak</z>	38.18	38.22	37.92	
FWHM	6.45	7.06	5.43	
<z>, heavy FF peak</z>	52.26	53.02	53.92	
FWHM	10.43 10.71		5.43	

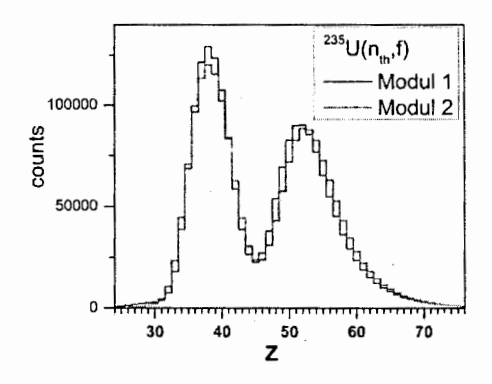


FIGURE 12. Nuclear charge spectrum of the FF from the reaction <sup>235</sup>U(n<sub>th</sub>, f) (shown separately for each spectrometer arm)

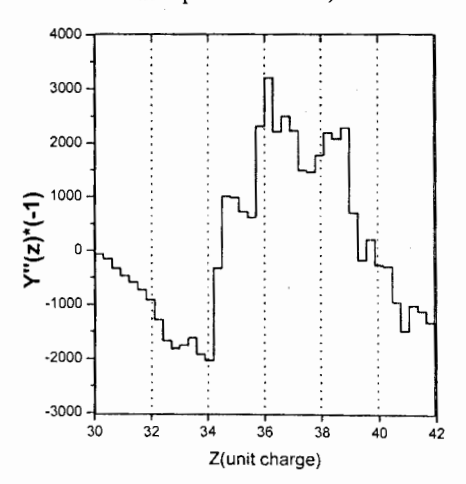


FIGURE 13. Second derivative of nuclear charge spectrum multiplied by factor (-1).

# CONCLUSION

Measuring of the fission fragments nuclear charges proves to be more complicated experimental problem in comparison with measuring of energy. Charge resolution depends crucially from both electric field uniformity and permanency of the mass of the gas in the volume of the ionization chamber. Necessary conditions were provided in our experiments at the miniFOBOS spectrometer. Special calibration procedure was developed for calculation of the FF nuclear charge which depends from the parameters measured in the experiment. Simulation showed that the approach developed satisfactory works in a wide range of the FF's energies but gives a little bit shifted values for very light ions.

#### ACKNOWLEDGMENTS

This work has been supported in part by CRDF, grant MO-011-0 and the grant of the Department of Science and Technology of South Africa

## REFERENCES

- Yu.V.Pyatkov et al., "New results in studying of the collinear cluster tripartition of the <sup>252</sup>Cf nucleus", Preprint JINR, Dubna, E15-2004-65, April 14, 2004
- 2. A. Oed. et al., NIM 205 (1983) 451.
- 3. S.L. Podshibyakin, Yu.V. Pyatkov et al. "Pribori I Technika Experimenta" No. 1, 1992, p.66-68.
- Yu.P. Gangrskii, B.N. Markov, V.P. Perelygin, "Registraciya I spectrometriya oskolkov deleniya". M.: Energoatomizdat, 1981.
- 5. V.F. Apalin et. al. Nucl. Phys. 71 (1965) 553
- 6. MINUIT http://wwwasdoc.web.cern.ch/wwwasdoc/WWW/minuit/minmain/minmain.html
- 7. A.C. Wahl, Atomic Data and Nucl. Data Tables 39 (1988) 1
- J.F. Ziegler "The Stopping and Range of Ions in Matter", vol. 2-6, Pergamon Press, 1977-1985. (http://www.srim.org).
- 9. J.P. Biersack, NIM 182/183 (1981) 199-206.
- 10. W. Lang et al., Nucl. Phys. A345 (1980) 34.

# A STATISTICAL ANALYSIS OF REGIONAL OIL IMPACTS ON ENVIRONMENT

C. Oprea a, M. V.Gustova a, O. D. Maslov a, A.I. Oprea a, P. J. Szalansky b

Joint Institute for Nuclear Research, Frank Laboratory of Neutron Physics, Departament of Experimental Nuclear Physics, Joliot-Curie 6 str. 6, 141980 Dubna, Russian Federation
 Lodz University, Faculty of Physics and Applied Informatics, Lodz, Poland

#### Abstract

The analytical work consisted of the measuring of the concentrations of 25 chemical elements (i. e. Ca, K, Ti, V, Cr, Mn, Fe, Ni, Cu, Zn, Pb, As, Se, Br, Rb, Sr, Y, Zr, Nb, Sb, I, Cs, Ba, La, Ce) in soils and water river sediment from the region of oil refinery complex Vega in the town of Ploiesti, Romania. The analyses were carried out on the grain fractions < 2 mm by using the X-ray fluorescence method.

Further the results were used to develop an approach for incorporating information on chemical availability in soils and river into risk assessment and risk-based decision making.

#### Introduction

In terms of the amounts of substances released, the oil pollution may have harmful effects on soil-plant ecosystems, all of them being related to human health. The oil pollutants can originate from a single point source presenting a local character as well as they can be released by mixed diffuse or punctual sources. Furthermore, to the level of ecosystem pollution contribute both local pollutants and those transported over long distances.

Emission estimates have long been basic tools for soil quality assessment. Usually emission data from specific test sources as well as continuous emission monitors are used as input information for developing emission control strategies. The literature data on soil contamination surveys by different monitoring techniques encounter a substantial difference between the estimates derived using different methods. Several projects related to the long-range atmospheric transport of trace heavy metals are carried out by environmental international/national organizations.

One of the task forces in the fields of long-range transport and deposition of heavy metals is to perform integrated assessment model calculations on heavy metal emissions in the all regions.

# Common aspects for local soil contamination

Several changes of soil quality occur when soil is exposed to different impact levels. The contaminated sites include sites at different levels of environmental and human health impacts, ranging from minor to relevant significant effects. Some common key aspects can be identified:- The contamination deriving from point sources, mainly waste disposal, industrial and military activities, and accidents.- The major local impacts of contaminated soil breed health problems due to direct contact with contaminated soil and use of contaminated groundwater, that imply the necessity to restrict some uses of the land.- The sustainable use of agriculture land supposes the mapping of soil parameters that result in regular network grid monitoring of the average extent of pollutant impacts on soil.

# Indicators for oil pollution

In the past years a preliminary list of indicators for soil contamination from oil localized and diffuse sources was identified and reviewed using the comparable data sets availability and quality. The development of oil pollution indicators for diffuse soil contamination follows the general scheme from the Figure 1.

# Data collection approach

The problem is the choice of the kind of sites (i.e. petrol stations) to be included.

The approach employed for data collection used in our researches implied an overall indicator to assess the number of sites that had been investigated to an acceptable standard for their use. More detailed stages of the process could introduce double counting of sites; depending on how often information was collected and updated.

Importance and data availability of this indicator were considered high. Some work has already been carried out in the monitored area. Unfortunately no clear distinction between different local sources of emission is possible.

The Ploiesti town region has been identified as one of oil contaminated zones. It is a highly industrialized town and also a petrochemical town, as presents several oil refineries.

To all samples collected in area of the Vega oil refinery (20x20 km<sup>2</sup>), one to three locations has to be contributing to each sampling location. The spots were further categorized by groups in relation with the downwind distance from the oil smelter complex.

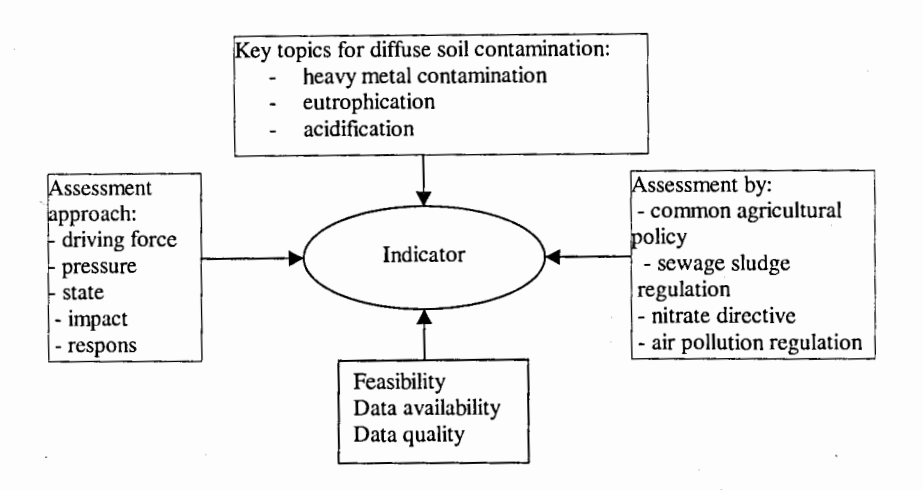


Figure 1. General scheme of the oil pollution indicators (EEA, 2002)

#### Results and discussion

The measured concentrations of 25 chemical elements (i. e. Ca, K, Ti, V, Cr, Mn, Fe, Ni, Cu, Zn, Pb, As, Se, Br, Rb, Sr, Y, Zr, Nb, Sb, I, Cs, Ba, La, Ce) for 52 categorized locations sampled in the Vega oil refinery area were determined. The average values of heavy metals were found for each spot category (Table 1). Ti, V, Cr, Mn, Fe, Ni, Cu, Zn, Pb, As, Se, Sb and Ba decrease in the following order of the distance from the refinery location: 1 km > 10 km > 20 km. The heavy metals levels as determined in river sediments of the Teleajen river were lower than those found at 1 km from the plant, but higher than those recorded at 20 km far from the plant. Their distribution point for the oil refinery discharges as source of those elements in the river. Concentrations of other elements vary since of the natural variability of the environment (Table 1).

Table 1. The mean elemental concentrations (% at) for different categories of sampling locations

	Av. conc., %							
Element	Soil, 1km	Soil,10 km	Soil, 20 km	River sediment				

K	7.3±1.0	3.9±1.2	0.99±0.15	≤0.85
Ca	0.7±0.2	2.1±0.5	4.2±0.5	3.1±0.4
Ti	0.99±0.15	0.68±0.12	≤0.15	0.42
V	≤0.19	≤0.12	≤0.05	≤0.07
Cr	0.25±0.01	0.08±0.02	≤0.06	0.1±0.03
Mn	0.12±0.04	≤0.03	≤0.014	≤0.05
Fe	3.17±0.03	2.19±0.03	1.78±0.03	2.51±0.03
Ni	0.033±0.010	0.027±0.009	≤0.009	0.015±0.004
Cu	0.061±0.009	0.037±0.006	0.017±0.004	0.048±0.009
Zn	0.039±0.006	0.019±0.006	0.013±0.006	0.015±0.006
Pb	0.024±0.003	0.015±0.003	0.0086±0.0029	≤0.004
As	0.016±0.003	≤0.003	≤0.003	0.009±0.001
Se	0.011±0.002	0.007±0.002	0.004±0.001	-
Br	0.007±0.002	0.006±0.002	0.006±0.002	0.013±0.002
Rb	0.0169±0.0012	0.0061±0.0013	0.0059±0.0012	0.013±0.008
Sr	0.0645±0.0009	0.0146±0.0010	0.0100±0.0008	0.02180±0.0011
Y	0.0055±0.0008	0.0067±0.0009	0.0021±0.0008	0.0066±0.0010
Zr	0.0255±0.0008	0.0256±0.0008	0.0235±0.0008	0.0019±0.0008
Nb	0.0019±0.0006	0.0025±0.0007	0.0009±0.0002	0.0021±0.0007
Sb	0.0036±0.0013	0.0034±0.0014	-	0.0050±0.0008
I	0.0043±0.0012	0.0032±0.0013	0.0048±0.0010	0.0015±0.0008
Cs	0.0038±0.0013	0.0022±0.0012	0.0018±0.0012	0.0031±0.0012
Ba	0.0588±0.0016	0.0517±0.0017	0.00762±0.0016	0.0685±0.0017
La	0.0036±0.0013	0.0035±0.0013	0.0020±0.0012	≤0.0013
Ce	0.0058±0.0016	0.0106±0.0015	0.0054±0.0012	0.0106±0.0014

R-mode factor analysis (Table 2), used to determine correlations among the measured elements, confirmed that elements Cu, Zn, As and Pb contribute to an overall pollution factor (F1). Concentrations V, Ni and Pb are strong correlated each other in the factor F2 assigned to petrol refining source. The factor F3 is mostly loaded with bedrock elements as Ca and Se.

The results for the all heavy metals, mainly for the three elements of major concern (V, Ni and Pb) show a proportional variation with the downwind distance approximated with a linear decrease of element concentration away from the source of pollution.

Table 2. R-mode factor analysis loadings

Metal	Factor 1	Factor 2	Factor 3

K	0.75	0.47	0.36
Ca	-0.78	0.39	0.75
Ti	0.91	0.30	-0.14
Cr	0.90	-0.17	0.07
Mn	0.78	0.25	-0.09
Fe	0.88	0.15	-0.02
Ni	0.86	-0.84	-0.08
V	0.47	-0.73	-0.03
Cu	0.45	-0.49	-0.20
Zn	0.54	-0.13	-0.06
As	-0.43	-0.47	-0.17
Se	0.77	0.38	0.72
Sb	0.73	0.07	0.04
Ba	0.49	0.25	-0.28
Pb	0.51	-0.82	0.19
Eigenvalue	4.17	2.35	0.48
Variance	0.44	1.81	0.16

#### Conclusions

It has been shown that the XRF analysis can be efficiently used for the screening of surface soil and river sediment elemental composition over local areas. The survey showed that in the monitored area bordering the Vega oil refinery complex there are zones with significantly elevated concentrations of Ni, Pb and V and other heavy metals as As, Cr, Cu, Fe, Sb and Zn linked to anthropogenic activities in the oil and hard industry.

Data for the indicator "progress in the management of contaminated sites" seems to be more accessible and it was further developed.

#### References

- 1. Cevik, U., S. Kaya, B. Ertugral, H. Balts, S. M. Karabidak. 2007. K-shell X-ray fluorescence cross-sections and intensity ratios for some pure metals at 59.5 and 123.6 keV. Nucl Instrum Methods B 262:165.
- 2. Gonzales-Fernandez, O., I. Queralt, M. L. Carvalho, G. Garcia. 2007. Elemental analysis of mining wastes by energy dispersive X-ray fluorescence (EDXRF). Nucl Instrum Methods B 262:81.

- 3. EEA, 2001a. Proposal for a European soil monitoring and assessment framework. Tech. rep. 61/2000.
  - 4. European Commission, 2002. Towards a strategy for soil protection. COM 179 final.
- 5. Nedelcu M., C. Oprea, C. Podina, D. Cupsa, I. A. Oprea, A. Teusdea, I. Burca. *Impact of hazardous substances in/on soil. Research reports.* 37<sup>th</sup> Annual meeting of ESNA, Sept. 10-14, 2007, JINR (in press).
- 6. Oluwole, A. F., O. Ajayi, J. O. Ojo, F. A. Balagun, I. B. Obioh, J. A. Adejumo, O. J. Ogunsola, A. Adepetu, H. B. Olaniyi, O. I. Asubiojo. 1994. *Characterization of pollutants around tin mining and smelting operations using EDXRF*. Nucl Instrum Methods A 353:499.
- 7. Oprea C., A. Mihul. 2007. *Oil pollution in relation with land use. Research reports*. 37<sup>th</sup> Annual meeting of ESNA, Sept. 10-14, 2007, JINR (in press).
- 8. Orescanin, V., L. Mikelic, S. Lulic, G. Pavlovic, N. Coumbassa. 2007. Seasonal variations in the concentrations of selected heavy metals and radionuclides in Sava River sediments upstream and downstream of NPP Krsko. Nucl Instrum Methods B 263:85.
- 9. Randa, Z., J. Kucera, L. Soukal. 2001. Possibilities of simultaneous determination of lead and thallium in environmental and biological samples by microtron photon activation analysis with radiochemical separation. J Radioanal Nucl Chem 248 1:149.

# IMPACT EVALUATION OF THE TOXIC AND BIOLOGIC ACTIVE ELEMENTS CONSUMED THROUGH FOOD CROPS ON THE CONSUMER'S HEALTH USING NUCLEAR METHODS AND NEURAL NETWORK TECHNIQUE

C. Oprea, O. D. Maslov, M. V.Gustova, A. G. Belov, A.I. Oprea JINR, Dubna, Russian Federation

#### A. Mihul

Bucharest University, Bucharest, Romania

V. Loghin, C. Nicolescu, G. Gorghiu Valahia University, Tirgoviste, Romania

#### Abstract

The main goal of the present research is to determine the extent to which industrial element pollutants are transferred to the crops. This will be achieved by using nuclear and related techniques, but also multivariate process to determine levels, pathways, and fate of toxic and non-toxic bioactive elements.

At the Flerov Laboratory of Nuclear Reactions (FLNR) were conducted experiments using gamma activation - at the microtron MT-25, and X-ray fluorescence analysis. The preliminary measurements effectuated in 2008 have shown that these methods are suitable for analyzing of different agricultural crop samples.

The heuristic determination of abnormal patterns by univariate statistical methods was performed. Further, in order to interpret the concentration data, multivariate statistical process was implemented using a variety of neural network techniques.

#### Introduction

Environmental pollution is a complicated issue. Since there are strict national and international regulations on the amount of contaminant allowable in different environmental media, models have been designed to determine the degree of pollution. The environmental data are collected by active or passive monitoring and analyzed by means of various methods including first principles, feature extraction and pattern recognition, and also neural networks.

Recent studies focusing on the preservation of our environment have shown, on a global scale, the considerable potential of analytical techniques and multivariate process as tools to understand the interrelationships existing between different environmental components.

This research investigates the potential application of neural network technology to forecast the concentrations of industrial pollutants beyond the origin source in relation with agricultural lands. Various solutions including mathematical algorithms implemented as software were used.

#### **Neural Networks**

A neural network is based on the working of the brain. The network is fed inputs and outputs and it tries to work out any connections or relationships between the two.

Since neural networks incorporate non-linear components they are suitable for modeling non-linear systems as weather systems and environmental conditions. Due to the complex nature of the variables associated with air modeling and the large array of non-linearity imposed by meteorological conditions and physical landscapes the neural network serves as a potential alternative to conventional air dispersion and regression type models.

The calculations of a neural network yield in the following way. In a multi-layer neural network model, the way complex behavior is simulated by the processing element, which is a software neuron, or node. The combined information is compared to a threshold and/or modified by a transfer function and then sent as output, which becomes input for any other processing nodes connected downstream. Given the correct data whose output is correlated with each input – a neural network is able to self-organize and subsequently predict an output for any input.

# Example: Neural network modeling of crop pollution in the Tirgoviste region

The aim of this example is to show how neural network modelling was used in the Tirgoviste region to assess the main pollution agents in crops in comparison with tree leaves. Samples of cabbage lettuce and leaves of acacias (Robinia pseudacacia) trees grown in different locations of the local monitoring net were used in this investigation.

Accurate determination of trace concentration levels is an important task in agricultural sciences and their applications. Photon activation analysis (IPAA) supplemented by the X-ray fluorescence analysis using the  $^{109}$ Cd (E $\gamma$ =22.16 keV) and  $^{241}$ Am (E $\gamma$ =59.57 keV) radioisotop

irradiation sources offered a reliable approach of providing a rapid multielemental analysis of various samples in ppm range, supposing as well the preservation of the samples.

Suggested analytical techniques were found as appropriate to measure concentrations of heavy metals in vegetation samples.

Suggested methodology mostly gives lower concentrations than in standard samples, high concentrations can be received in 1-2 cases from 5 for Cr, V, Ni.

Only 48.3% and 70% of standard concentrations are determined for Cd and Pb using the above methodology. Maximum determined concentrations of Cd and Pb were 64% and 76% from standards.

# Neural network modelling by the Levenberg - Marquard algoritm

One of the major limitations of current methods of biological detection of exposure to hazardous environmental agents is their inability to detect long-term exposures, and exposures occurred in the past. In the current study we examined the potential of a neural network bioassay that is based on the hypothesis that organism of the exposed leaves contains a toxic factor.

The Levenberg - Marquard algoritm is adopted as training method; the run is stopped once the squared error on the validation dataset begins to increase. To test the model, weather forecasts were fed into the model 24 hours in advance and the pollution levels were checked. The run showing the lowest squared error is selected as optimal and then simulated on the testing set (Figs. 1 - 2).

To study the correlations (Fe - Co) - (Ti - V) a neuronal 2 - 7 - 2 simulation was performed. As training values the first 15 data sets and as test values the last 8 data sets were used. The best approximations for linear function (R = 0.922, R = 0.960) are presented in the Figures 1 and 2.

A component of Fe, Co, Ti and V characterized a general pollution agent in crops and tree leaves connected with urban anthropogenic activity of Tirgoviste town.

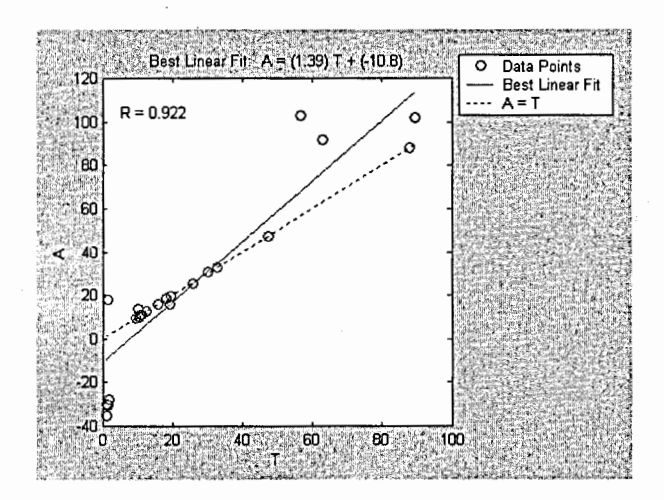


Fig. 1. Graphical representation of the experimental points versus regression line – Best Linear Fit – etalon line (A = T) for Ti concentration in cabbage lettuce leaves in the neuronal model adopted (Fe – Co) – (Ti)

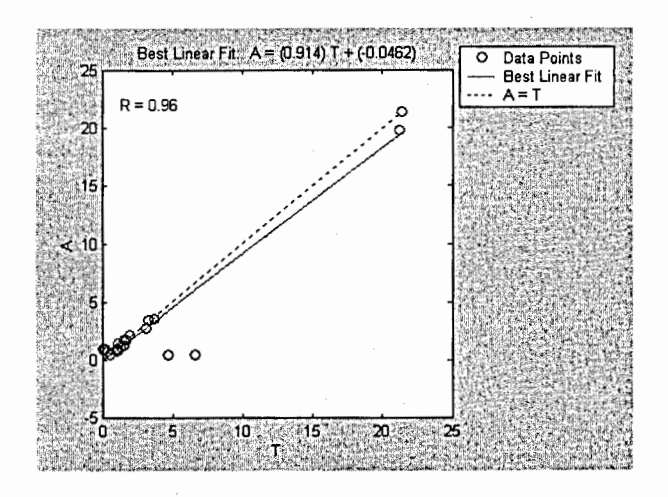


Fig. 2. Graphical representation of the experimental points versus regression line – Best Linear Fit – etalon line (A = T) for V concentration in tree leaves in the neuronal model adopted (Fe – Co) – (V)

#### Conclusions

It was obtained a good analytical recovery for most metals. The crops provided their capacities as biomonitors, but less than tree leaves.

We have shown that a neural network can reproduce output nearly identical to that produced by existing biomonitoring approaches. Furthermore, the results demonstrate the potential of the proposed methodology to detect environmental exposures long after they have occurred. It was notified the further decline heavy metal concentrations in tree leaves between 2000 and 2005; for crops, the situation is still unknown

#### References

- 1. Bishop, C.M., 1995. Neural networks for pattern recognition. Clarendon Press, Oxford.
- 2. Dare, P. and Saleh, H. A., 2000. GPS networks design: logistics solution using optimal and near-optimal methods. Journal of Geodesy, 74, 467.
- 3. Deb, K., 2001. Multi-objective Optimisation using Evolutionary Algorithms. Chichester: Wily & Sons, Ltd.
- 4. Oprea Cristiana, et al., 2005. Analysis of the pollution agents through neural network algoritms. *Eurisy* Conference "Integration of the New EU Member Countries into the GMES Programme", Warsaw, Poland, 12-14 December 2005, pp 8.
- 5. Oprea Cristiana, et al., 2005. Modeling the human health and environmental impacts status at Targoviste city area using neural network algorithms. *Eurisy* Conference "Integration of the New EU Member Countries into the GMES Programme", Warsaw, Poland, 12-14 December 2005, pp 10.
- 6. Oprea, C. D., Pincovschi, Eu., 2003. The assessment of pollution in the area of Turnu Magurele affected by fertilizers plant. Romanian Reports in Physics, 55, 2, 111.
- 7. Pantelica, A., Oprea C., et al., 2004. Contamination of crop vegetation with trace elements from a fertiliser plant: an INAA study. Vincent Guinn Memorial Issue of Journal of Radioanalytical and Nuclear Chemistry, Kluwer Academy, 262, 1, 111.
- 8. Rosenblatt, F., 1958. The perceptron: A probabilistic model for information storage and organization in the brain. Psychological Review, 65, 386.
- 9. Rumelhart, D. E. and McClelland, J. L., 1986. Parallel distributed processing: explorations in the microstructure of cognition, Vol. 1, Cambridge, MA: MIT Press.

- 10. Saleh, H., 1999. A Heuristic Approach to the design of GPS Networks. Ph.D. thesis, School of Surveying, University of East London, UK.
- 11. Zorriassatine, F., Tannock J.D.T., 1998. A review of neural networks for statistical process control. J. Intell. Manuf. 9, 209.
- 12. Wilson, D.J.H., Irwin, G.W., Lightbody G., 1997. Neural networks and multivariate SPC. Proceedings of the IEE/InstMC Colloquium on Fault diagnosis in Process Systems 97/174, London, April 1997, pp. 15.

# COMPARISON OF INORGANIC CHEMICAL CONSTITUENTS OF DIFFERENT HERBAL MEDICINES

C. Oprea<sup>1</sup>, M.V. Gustova<sup>1</sup>, O.D. Maslov<sup>1</sup>, A.G. Belov<sup>1</sup>, A.I. Oprea<sup>1,2</sup>, C. Pirvutoiu<sup>1,2</sup>, D. Vladoiu<sup>1,2</sup>

\*\*Joint Institute for Nuclear Research (JINR), Dubna 141980, Russian Federation

\*\*Paucharest State University, 76900, Bucharest, Romania\*\*

#### Abstract

The microconstituents and also some minor- and macroelements in seven medicinal plants, namely Achillea millefolium, Chelidonium majus, Cynara scolymus, Hypericum perforatum, Tilia cordata, Matricaria recutita, and Urtica, were determined. The above medicinal plant species were used for the experiments as they are an important source of drug with many pharmaceutical effects as well as bioaccumulators of the trace heavy metals and other bioactive chemicals.

The analytical work consisted of the measuring of the elemental concentrations of inorganic specific constituents using instrumental gamma-activation analysis in suite with X-ray fluorescence technique.

Further the results were used to develop an approach for incorporating information on biochemical availability in herbal medicines into practical anthropogenic use.

#### Introduction

The medicinal plants studied in this work have been administrated currently to cure some diseases in Romania and abroad. Diet is the main source of trace elements. Although the efficacy of herbs for curative purposes is often accounted for in terms of its organic constituents, it has been established that there exists a relationship between the chelating of metals and some chemotherapeutic agents. Herbs can interact directly or indirectly with body chemistry. The chemical compounds of these herbs are mainly responsible for the curative properties. It is known that there is a significant role of trace elements when treating various diseases. The absorption of their active constituents into the blood can influence the body system and these chemical constituents present in the plant are responsible for their curative aspect. Many essential elements play an important role in the plant metabolism products of

plant cells. Few studies have been reported about the elemental composition of medicinal plants. The goal of this work was to determine the availability of essential trace elements in commonly used medicinal plants in Romania and their possible correlation from one medicinal herb to another one.

#### Materials and methods

# Sample collection

For each type of herbal medicine, an average sample was prepared by mixing of the 6 samples collected from an area of  $50 \times 50 \text{ m}^2$ . Medicinal plants were purchased in the dried form of root, bark and leaf from local herbalists. Others were collected from national botanical parks situated in the Romanian Carpathians. Each plant was washed extensively in drinking water as to remove superficial dust and then dried by an IR lamp for one day. Prior to analysis the samples were dried at room temperature one month and later 48 hours at  $40^{\circ}$ C and then homogenely melted into fine powder in an agate mortar. The fresh/dry mass ratios calculated for herbal material were about 5.78 - 6.32.

## **Analytical methods**

A highly sensitive γ activation method based on the (γ, n) reactions and gamma-ray spectrometry (IGAA) for measuring the elemental concentrations in environmental samples is applied. The powdered samples were packed in polyethylene vials into duplicate. A packet consisting of 10 cassettes with samples and standard samples was irradiated by gamma-rays for 5 h together with flux monitors by a photon flux of 24 MeV at the MT-25 microtron (FLNR, JINR). For the irradiation there was a 7% difference in the flux factors between the upper and lower positions of the container. The overall integrated flux over a 5 hours irradiation is practically constant. The spectra calibration by the use of <sup>226</sup>Ra source was done.

Complementary the replicate samples were investigated by X-ray fluorescence analysis (XRF). The spectra of the characteristic X-ray lines were recorded by a Si(Li) X-ray detector having a thickness of 3 mm and an area of 30 mm2. The measured energy resolution of the detector system was 200 eV FWHM at the 5.9 keV Mn  $K_{\alpha}$  line. Another components are the Be window of the detector, the glass sample holder and the protections of Pb and Ag to

absorb the Compton scattering effect. Photons of 22.1 KeV from the 109Cd annular source and photons of 59.57 keV from the <sup>241</sup>Am annular source were used for excitation of the target X-rays. An Al shield was used in the case of each source to suppress the low-energy photons emitted from the radioisotope. The geometry of <sup>109</sup>Cd source was normally versus detection direction and that of <sup>241</sup>Am source was such that the incident direction was situated at 530 versus the detection direction.

The analysis of the measured spectra were performed using the SPM software developed in FLNR using a nonlinear least squares fitting routine which approximates characteristic X-ray peaks with Gaussian curves of various types of background depending on the spectrum region and calculates intensities of X-ray peaks.

#### Results and discussion

A total of 34 elements have been determined in the 7 medicinal plants commonly used in Romania using IGAA and XRF (Table 1). Elemental contents vary in a wide range, in some cases even by an order of magnitude (Figure 1). It can be observed that mean concentrations of Cu, Mn, Rb and Zn are in amounts >10  $\mu$ g/g whereas of Cr and V are in amounts >1 $\mu$ g/g. Toxic elements as As, Cd, Hg and Sb, are present in quartiles below the permissible limits.

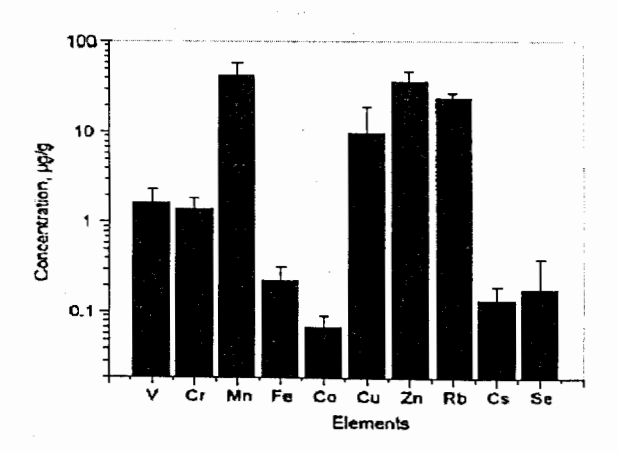


Figure 1. Variation in mean concentration of essential trace elements in medicinal plants

Table 1. Some elemental concentrations in medicinal herbs (% at)

	LT1	LT2	LT3	LT4	LT5	LT6	LT7
K	3.8±0.6	3.1±0.5	3.1±0.5	2.0±0.6	1.9±0.5	4.4±0.7	4.2±0.5
Ca	1.5±0.3	2.5±0.3	2.8±0.3	2.6±0.3	3.1±0.3	6.1±0.4	0.6±0.3
Ti	0.168±0.080	0.372±0.070				0.207±0.074	
V					0.15±0.04		
Mn	T	0.037±0.010		0.055±0.012	0.041±0.012	0.086±0.015	0.042±0.010
Fe	0.172±0.009	0.192±0.008	0.091±0.009	0.439±0.010	0.040±0.009	0.079±0.010	0.077±0.008
Ni	T		0.0116±0.0030	0.0140±0.0036		0.0160±0,0036	0.0090±0.0033
Cu	0.0198±0.0028	0.0102±0.0026	0.0114±0.0026	0.0267±0.0031	0.0116±0.0027	0.0074±0.0024	
Zn	0.0126±0.0023	0.0132±0.0023	0.0054±0.0026	0.0104±0.0026	0.0221±0.0026	0.0107±0.0028	0.0060±0.0020
Pb	0.0015±0.0008	0.0018±0.0008	0.0017±0.0009	0.0029±0.0010		≤0.0012	
Se	≤0.0005	Sec.	0.0013±0.0005	0.0023±0.0006			0.0009±0.0004
Br	0.0062±0.0004	0.0012±0.0004	0.0012±0.0005	0.0195±0.0005		0.0016±0.0004	
Rb	0.0011±0.0003	0.0013±0.0003	0.0009±0.0003	0.0041±0.0004	0.0033±0.0003	0.0014±0.0004	0.0012±0.0003
Sr	0.0037±0.0003	0.0047±0.0003	0.0072±0.0003	0.0092±0.0003	0.0054±0.0003	0.0185±0.0003	0.0042±0.0003
Y	0.0010±0.0003	0.0008±0.0003	≤0.0003	0.0009±0.0003	≤0.0004	≤0.0003	
Zr	0.0025±0.0003	0.0009±0.0002	≤0.0003	0.0064±0.0003	≤0.0005	0.0018±0.0003	≤0.0005
Nb	≤0.0002	≤0.0002		0.0008±0.0002			
Mo						0.0006±0.0003	0.0005±0.0002
Pd				0.0008±0.0003			
Ag			0.0016±0.0003			≤0.0004	
Cd						≤0.0004	
In	0.0015±0.0004		0.0006±0.0004	0.0011±0.0003	0.0028±0.0005	≤0.0004	
Sn	0,0009±0.0003			0.0008±0.0003		≤0.0004	0.0027±0.0004
Sb							0.0010±0.0004
Cs		0.0018±0.0004					
Ba	0.0023±0.0004	0.0059±0.0005	0.0035±0.0004	0.0079±0.0004	0.0008±0.0004	0.0033±0.0005	0.0024±0.0005
La		≤0.0003	≤0.0003	0.0027±0.0004	≤0.0003	≤0.0004	0.0018±0.0005
Ce	1		0.0019±0.0004	0.0027±0.0004	≤0.0005		

Bar plots of the all essential trace elements V, Cr, Mn, Fe, Co, Cu, Zn, Rb, Cs and Se exhibit large variations with Co (being in least amount) and Mn (the highest). This variation in elemental concentrations may be explained by the differential uptake by the plant from the soil or due to inherent nature of the plant species grown in that region.

There are interrelationships of various elements in plant species (Figure 2). K/P ratio exhibits a mean value of  $8.5\pm0.55$  and lies in the range 6.73-10.2. Also, Cu and Zn (r=0.74) exhibit consistent correlationship, indicating a suitable balance of biochemical processes and consequently potentially contributing to a good health.

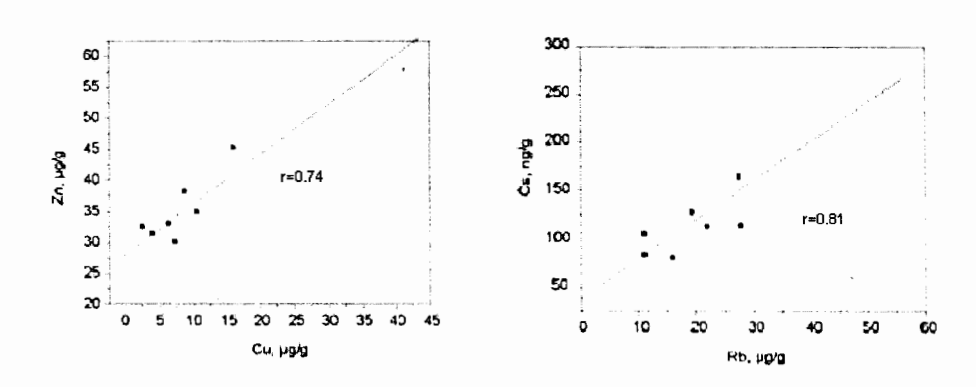


Figure 2. Correlations Zn - Cu and Cs - Rb in Achillea millefolium

Experimental data obtained for the minor, essential and toxic elements content in medicinal herbs can be used to evaluate their potentiality for the improvement of human health.

#### Conclusion

Leaves, roots, fruits and seeds of seven medicinal plants have been analyzed for 5 minor (Na, K, Ca, Mg and P) and 21 trace (s, Ba, Br, Cd, Ce, Co, Cr, Cs, Cu, Eu, Fe, Hg, La, Mn, Ni, Pb, Rb, Sb, Sc, Se, Sm, Th, V and Zn) elements by IGAA and XRF.

Results show that the application of the combination of the two analytical methods allows a realistic determination of the elemental content of the investigated herbal medicines with good detection limits and accuracy for the low level concentrations. The present work

will be developed into an approach between elemental content as therapeutic probability as well as when they are used as basic materials for the development of drugs for the pharmaceutical industry.

# References

- 1. Rajurkar, N.S., Pardeshi, B.M., 1997. Appl. Rad. Isot., 48, 1059.
- 2. Rajurkar, N.S., Pardeshi, B.M., 1998. Appl. Rad. Isot., 49, 773.
- 3. Zlokazov, V.B., 1975. Nucl Instrum Methods, 130 (2), 543.

# ASYMMETRY EFFECTS IN THE 19F(p,α) REACTION

A. I. Oprea, C. D. Oprea

Frank Laboratory of Neutron Physics – JINR 141980 Dubna, Russian Federation

Abstract. In this work we try to obtain the asymmetry effects (forward – backward, left – right and parity non conservation) using the model of the mixing states of the compound nucleus with opposite parities in the two level approximation as the authors already did in the case of the (n,p) reaction on <sup>35</sup>Cl and <sup>14</sup>N. This task is more complicated than in the case of the (n,p) reaction because the partial proton widths in the entrance cannel are practically unknown like the alpha widths in the exit channel. Also for the proton incident energy about a half of MeV the mechanism of the reaction is not well established. For this incident energy if we accept that the reaction is passing through the compound nucleus are a lot of resonances close to each other.

In [1] was evaluated an asymmetry effect for this reaction and it was of order of 10<sup>-3</sup>. This value is in good agreement with experimental evaluated. The weak matrix element was evaluated of order of 0.8 eV and this value is higher than the predicted expected value [1].

- 1. Introduction. The main goals to obtain the asymmetry effects like forward backward, left – right and parity non conservation in the  $^{19}\text{F}(p,\alpha)^{16}\text{O}$  reaction. In this reaction it is forming the compound nucleus  $^{20}\text{Ne}$ . This nucleus has two close resonance  $E_P = 1620 \text{ keV}$ ,  $J_p^{\pi} = 3^{-1}/2$  (P – state) and E<sub>S</sub>=1680 keV,  $J_s^{\pi} = 3^{+1}/2$  [2]. It is expected as results of interference of these resonance to have the mentioned asymmetry effects. It is proposed to use the formalism of the the mixing states with opposite parities of the compound nucleus [3], [4], [5]. As is suggested in [6] with the help of the experimental values of the indicated asymmetry effects in the two level approximation, it is possible in principle to extract the matrix element of the weak internucleon interaction in the compound nucleus. These procedure (in the two level approximation) was already realized by authors for the (n,p) reaction on the <sup>35</sup>Cl and <sup>14</sup>N [7], [8]. [9]. Taking into account the above it is of interest to evaluate theoretically the asymmetry effects in the  $^{19}F(p,\alpha)^{16}O$  reaction and to try to measure also experimentally these effects. To realize these it is necessary an accurate analyze of the reaction. From [2] we see that the widths for protons and alpha particles are practically unknown. These parameters can be evaluated using some theoretical assumptions but will be better to obtain them from experimental data on elastic scattering of protons and alpha particles on <sup>19</sup>F. In [1] the asymmetry in the differential cross section is evaluated,  $(6.6\pm2.4)\cdot10^{-3}$ , in the <sup>19</sup>F(p, $\alpha$ )<sup>16</sup>O reaction with proton energy E=670 keV and the weak matrix element obtained from the asymmetry is  $\langle P | H_w | S \rangle \approx 0.8 \,\text{eV}$ .
- 2. Theoretical background. The model of the mixing states of the compound nucleus with the same spin and opposite parities will be used to obtain the asymmetry effects and in the beginning only two resonance will be taken into account. These resonance have the same spin and opposite parities and it is a necessary condition to observe asymmetry effects. To evaluate the asymmetry effects we write first the amplitude of the (n,p) reaction. [3-7]. The relations (1), (2) are the amplitudes conserving the spatial parity and the relations (3), (4) represent the amplitudes non conserving the parities. The reaction takes place by formation of

the compound nucleus and the compound nucleus has definite properties as for example spin, resonance energy and parity etc. More detailed about the theoretical background can be found in the references at the end of the paper. We will continue with the amplitudes of the (n,p) reactions {3-5].

$$f_{1} = -\frac{1}{2k}C(I, I_{z}, a, a_{p}; J_{s}, J_{sz})C(I', I_{z}, 0, a_{\alpha}; J_{s}, J_{sz}) \frac{T_{s}^{p}T_{s}^{\alpha^{*}}}{(E - E_{s}) + i\frac{\Gamma_{s}}{2}}Exp(-i\varphi_{0})$$
 (1)

$$f_{2} = -\frac{2\pi}{k} \sum_{\substack{j_{R}, j_{RZ}, v_{R} \\ j_{P}, j_{PZ}, v_{P}}} C(I, I_{z}, j_{p}, j_{pz}; J_{P}, J_{Pz}) C(I, v_{p}, \frac{1}{2}, a_{p}; j_{p}, j_{pz}) \cdot$$

$$C(I', I'_{z}, j_{\alpha}, j_{\alpha}; J_{P}, J_{Pz})C(1, \nu_{p}, 0, a_{\alpha}; j_{\alpha}, j_{\alpha}) \frac{T_{P}^{\rho}(j_{p})T_{P}^{\alpha^{*}}(j_{\alpha})}{(E - E_{P}) + i\frac{\Gamma_{P}}{2}}.$$
(2)

$$Y_{1\nu_{p}}^{*}(\overrightarrow{n_{p}})Y_{1\nu_{\alpha}}(\overrightarrow{n_{\alpha}})Exp(-i\varphi_{1})$$

$$f_{3} = -\frac{\sqrt{\pi}}{k} W_{SP} \sum_{j_{\alpha}, j_{\alpha z}, \nu_{\alpha}} C(I, I_{z}, \frac{1}{2}, a_{p}; J_{S}, J_{Sz}) C(I', I'_{z}, j_{\alpha}, j_{\alpha z}; J_{P}, J_{Pz})$$

$$C(1, \nu_{\alpha}, 0, a_{\alpha}; j_{\alpha}, j_{\infty}) = \frac{T_{S}^{n} T_{P}^{p^{\bullet}}(j_{\alpha})}{(E - E_{P} + i\frac{\Gamma_{P}}{2})(E - E_{S} + i\frac{\Gamma_{S}}{2})}$$

$$(3)$$

$$Y_{1\nu_{\alpha}}(\vec{n_{\alpha}})Exp(-i\varphi_{1})$$

$$f_{4} = -\frac{\sqrt{\pi}}{k} W_{SP} \sum_{j_{n}, j_{nz}, \nu_{n}} C(I', I'_{z}, 0, a_{\alpha}; J_{S}, J_{Sz}) C(I, I_{z}, j_{p}, j_{pz}; J_{P}, J_{Pz}) C(1, \nu_{p}, \frac{1}{2}, a_{p}; j_{p,}j_{pz})$$

$$\frac{T_{S}^{\alpha r} T_{P}^{\rho}(j_{p})}{(E - E_{S} + i \frac{\Gamma_{S}}{2})(E - E_{S} + i \frac{\Gamma_{S}}{2})} Y_{1\nu_{p}}^{*}(\vec{n_{p}}) Exp(-i\varphi_{0})$$
(4)

3. Asymmetry coefficients. The asymmetry coefficients are an efficient tool for the studying the properties of the compound nucleus, the reaction mechanism and the parity non conservation effects in nuclear reactions. The expressions of the studied effects with correspond angular correlation are presented above.

The asymmetry effects can be interpreted as interferences between amplitudes of reactions. The forward backward effect is a result of the  $f_1$  and  $f_2$  amplitudes with unpolarized neutrons and the left right asymmetry is also the result of the interference between the same amplitudes but with transversal polarized neutrons. These first two as it is possible to see not include the weak interaction and they only the strong nuclear interaction. The parity non conservation effect is a result of the interferences between  $f_1$  and  $f_2$  and  $f_4$  this effect

includes the weak interaction. Usually the parity non conservation effect is about two or three order of magnitude lower than the forward backward and left right effects.

Forward – backward effect and angular correlation.

$$\alpha_{FB} = \frac{W(\theta = 0) - W(\theta = \pi)}{W(\theta = 0) + W(\theta = \pi)}$$
(5)

$$W(\theta) \sim 1 + \alpha(n_p \cdot n_{\alpha}) \tag{5.1}$$

Left -right effect.

$$\alpha_{LR} = \frac{W\left(\theta = \frac{\pi}{2}, \phi = \frac{3\pi}{2}\right) - W\left(\theta = \frac{\pi}{2}, \phi = \frac{\pi}{2}\right)}{W\left(\theta = \frac{\pi}{2}, \phi = \frac{3\pi}{2}\right) + W\left(\theta = \frac{\pi}{2}, \phi = \frac{\pi}{2}\right)}$$
(6)

$$W(\Omega) \sim 1 + \alpha_{LR} \stackrel{\rightarrow}{\sigma} \cdot (n_{p} \times n_{\alpha})$$
 (6.1)

Parity non - conservation effect.

$$\alpha_{PNC} = \frac{W(\theta = \frac{\pi}{2}, \phi = 0) - W(\theta = \frac{\pi}{2}, \phi = \pi)}{W(\theta = \frac{\pi}{2}, \phi = 0) + W(\theta = \frac{\pi}{2}, \phi = \pi)}$$

$$(7)$$

$$W(\Omega) \sim 1 + \alpha_{PNC} (\vec{\sigma}_{p} \cdot \vec{n}_{\alpha})$$
 (7.1)

**4. Discussion.** The same procedure as in the (n,p) reaction will be fulfilled for the  $^{19}F(p,\alpha)$  reaction. As both particle (incident and emergent) are charged it is necessary to determine the appropriate coulombian (and not only) phase shifts. It is necessary also an experimental and l or theoretical evaluation of the proton and alpha widths. As for the proton energy about 1 MeV near the two mentioned resonances are also other resonances. Will be evaluated the influence of the other resonances and open channels to see the availability of the two level approximation suggested in [1]. It is proposed an experiment to evaluate the forward – backward, left – right and parity non conservation asymmetry in the  $l^{19}F(p,\alpha)^{16}O$  reaction and some further measurements to evaluate the proton and alpha widths necessary to obtain the asymmetry effects.

#### References.

- [1] G. A. Lobov, Neytronnaya Fizika, vol. 3, pag. 428, Moskva, 1984 (in Russian)
- [2] Mughabghab S.F., Divadeenam M., Holden N.E. Neutron Cross Sections. NY, Academic Press, 1981, v.1.
- [3] O. P. Sushkov, V. V. Flambaum, Uspekhi Fizicheskih Nauk, Vol 136, Issue 1, 1982
- [4] V. V. Flambaum, O.P. Sushkov, Nucl. Phys. A412, p. 3, 1984
- [5] V. V. Flambaum, G. F. Gribakin, Prog. Part. Nucl. Phys. Vol. 35, p. 423, 1995
- [6] S. V. Zenkin, N. A. Titov, Preprint Π-0367,Institute for Nuclear Researches of Russian Academy of Sicence, Moscow, 1984 (in Russian)
- [7] Gledenov Yu.M., Machrafi R., Oprea A.I., Salatski V.I., Sedyshev P.V., Szalanski P.I., Vesna V.A., Okunev I.S., Nucl. Phys., 1999, v. A 654, p.943c.

- [8] Short Report of the most important scientific results of JINR in 2004, 2005-8, Dubna, 2005 (in Russian)
- [9] A.I. Oprea, C. Oprea, Yu. M. Gledenov, P. V. Sedyshev, Proceedings on the Fifteen International Seminar on Interaction of Neutron with Nuclei (ISINN-15), 15-19 May 2007, Dubna, p. 296, ISBN 5-9530-0169-X.

# PHOTON NEUTRON ACTIVATION ANALYSIS OF THE SEA LETTUCE ALGAE FROM THE BLACK SEA, ROMANIA

C. Oprea<sup>1</sup>, M.V. Gustova<sup>1</sup>, O.D. Maslov<sup>1</sup>, A.G. Belov<sup>1</sup>, I.A. Oprea<sup>1,2</sup>, I. Ion<sup>3</sup>, M.G. Nedelcu<sup>4</sup>, C. Pirvutoju<sup>1,2</sup>, D. Vladoju<sup>1,2</sup>

<sup>1</sup>Joint Institute for Nuclear Research (JINR), Dubna 141980, Russian Federation

<sup>2</sup>Bucharest State University, 76900, Bucharest, Romania

(3)ICPE-CA, Bucuresti, Romania

(4)Univ. of Bucharest, Faculty of Chem., Dept. of Radiochemistry

#### Abstract

Trace element contents of the sea lettuce algae collected from the Romanian littoral by photon neutron activation analysis were determined. The trace heavy metal concentrations in marine algae samples were  $2.5 - 29.4 \,\mu\text{g/g}$  for As,  $1.5 - 3.5 \,\mu\text{g/g}$  for Cd,  $3.2 - 11.7 \,\mu\text{g/g}$  for Co,  $0.7 - 8.5 \,\mu\text{g/g}$  for Cr,  $2.4 - 21.9 \,\mu\text{g/g}$  for Cu,  $201 - 350 \,\mu\text{g/g}$  for Fe,  $0.15 - 0.18 \,\mu\text{g/g}$  for Hg,  $15 - 85 \,\mu\text{g/g}$  for Mn,  $1.2 - 18.3 \,\mu\text{g/g}$  for Pb, and  $15 - 24 \,\mu\text{g/g}$  for Zn. The presence of different heavy metals released into the Black Sea through the Danube River waters are of anthropogenic origin, proceeding from industrial and farmer wastes and bilge oil from ships and also from air pollution influenced the algae's growth and their contents. The Sea lettuce algae are consumed for human diet.

#### Introduction

Sea lettuce (*Ulva lactuca*) is a deep green sea vegetable with a distinctive flavor and aroma. It is bright green algae composed of lobed, ruffle-edged leaves that are coarse and sheet-like and resemble a leaf of lettuce. The leaves may appear flat, thin, broad, and often rounded or oval. Its leaves are often perforated with holes of various sizes. Almost no stalk exists at the point of attachment, and no true roots are present. When dried by the sun, its color can range from white to black. Among the most familiar of the shallow water seaweeds, sea lettuce is often found in areas of exposed rocks and in stagnant tide pools. Sea lettuce has also been recorded at depths of 75 feet or more

It thrives in brackish water with organic enrichment. It thrives in polluted water without being effected by it from a quality point of view. The semi permeable membranes (cell wall) do stop most types of harmful organic materials including bacteria. If brown or red seaweed grow in the same environment it would be toxic.

It is very high in iron and protein (similar to dulse), and is high in iodine, aluminum, manganese and nickel as well (Table 1). Like dulse and most of our sea veggies, sea lettuce provides considerable amounts of dietary fiber (31%). Since the Black Sea veggies are low temperature dried in the sun, sea lettuce enzymes are still active. The sustainable harvesting and handling of the sea lettuce is certified organic by environmental agencies and the sea crop samples are tested for heavy metal, chemical, and microbiological contaminants.

Table 1. The average composition of sea lettuce

Component	Mean conc.
Protein	18-24 %
Carbohydrates	40-45 %
Magnesium	2-3 %
Sodium	1-2 %
Fat	1-2 %
Potassium	0.7-1 %
Calcium	7000-8000 ppm
Iron	870-1370 ppm
Manganese	300-350 ppm
Iodine	200-250 ppm
Vitamin	A, C, B3, B12

Tolerant of nutrient loading that would suffocate many other aquatic plants, sea lettuce can actually thrive in moderate levels of nutrient pollution. Their growth is stimulated by the presence of other pollutants. Then the sea lettuce is used as an indicator species to monitor pollution trends. The density and location of this alga can often indicate the presence of high amounts of nutrients.

Photon neutron activation method is a multielemental technique used in some environmental studies, using a microtron as primary excitation source.

In the present paper, some samples of Sea lettuce as the pollution indicators of the Black Sea Romanian littoral, which is a marine ecosystem greatly affected by natural and human causes, were characterized by the photon neutron activation method.

# Experimental

# Sample collection and preparation

Sea lettuce samples were collected from the littoral area of the seven touristic locations situated on the Black Sea Romanian coast, namely Mangalia (A1), Costinesti (A2), Eforie Sud (A3), Eforie Nord (A3\*), Constanta (A4), Mamaia (A4\*) and Navodari (A5) (Figure 1). Samples were recorded in 1m<sup>2</sup> quadrates from at least 6 sites from each locality and then combined in one collective sample. At this step of the research performing only a primary evaluation and in order to assure a spatial extent of the data, the samples from Mamaia and Eforie Nord were further excluded.

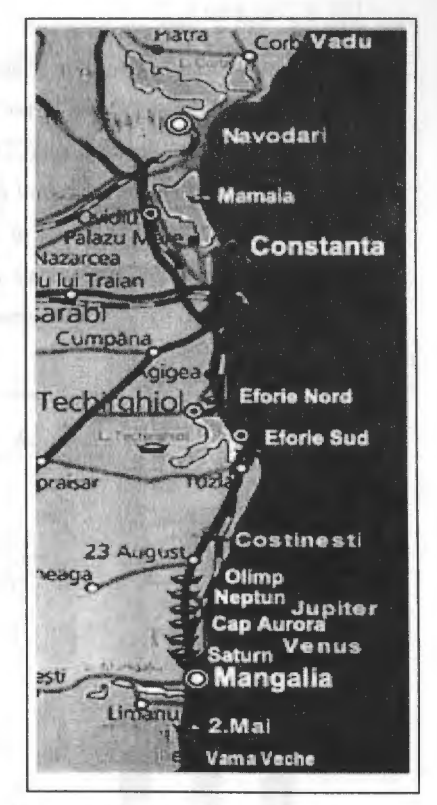


Figure 1. Map showing the sampling sites

Prior to analytical measurements, the sea lettuce samples were carefully cleaned from all shells, dead material and attached litter, and washed with distilled water; then were let to dry at room temperature on a filter paper, later were kept at 40°C for 48 hours in thermostat until constant weight and were finely powdered in an agate mortar.

# Analytical methodology

Photon neutron activation analysis is a sufficiently sensitive method of elemental analysis using a compact electron accelerator – the MT-25 microtron of the Flerov Laboratory for Nuclear Reactions of the Joint Institute for Nuclear Research (FLNR, JINR). The accelerated electrons are extracted from the microtron to a stopping target to produce γ rays or

are directed into a uranium-beryllium converter to produce neutrons. The scheme of the MT-25 microtron is presented in the Figure 2.

Samples of 2 g were placed in polyethylene cassettes. Then a packet consisting of 10 cassettes with samples and etalons (CII-3 standard material) was irradiated by 24 MeV electron beam for 4 h. Measurements of the induced activity were performed with the help of a HPGe detector with a resolution less of 2.0 keV at the line of 1333 keV. Short lived isotopes were recorded by 5 min measurements after 1.5 h cooling, and the medium and long-life isotopes were determined by 1h measurements after 1, 5 and 10 days of cooling, respectively.

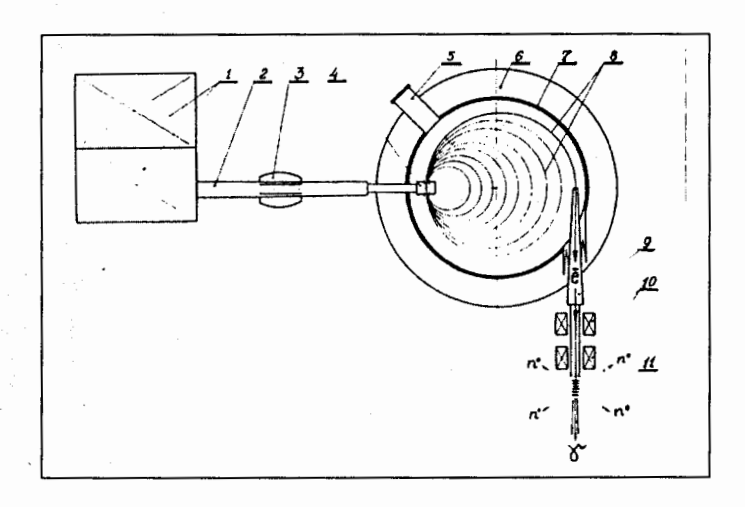


Figure 2. Scheme of the microtron MT - 25. (1 - system of high frequency; 2 - wave channel; 3 - ferrite isolator; 4 - resonator; 5 - vacuum system; 6 - magnet; 7 - vacuum camera, 8 - orbits of accelerated electrons; 9 - exit of electron beam; 10 - magnet, focusing electron beam; 11 - brake target).

Calculating the peak areas from the  $\gamma$  spectrum by the SPM software developed in FLNR, the amounts of elements in a sample was determined by using the relative method.

#### Results and discussion

The variation in the trace heavy metal concentrations in marine algae samples as obtained by the photon neutron activation analysis was as follows:  $2.5 - 29.4 \,\mu\text{g/g}$  for As, 1.5

 $-3.5 \mu g/g$  for Cd,  $3.2 - 11.7 \mu g/g$  for Co,  $0.7 - 8.5 \mu g/g$  for Cr,  $2.4 - 21.9 \mu g/g$  for Cu,  $201 - 350 \mu g/g$  for Fe,  $0.15 - 0.18 \mu g/g$  for Hg,  $315 - 385 \mu g/g$  for Mn,  $1.2 - 18.3 \mu g/g$  for Pb, and  $15 - 24 \mu g/g$  for Zn.

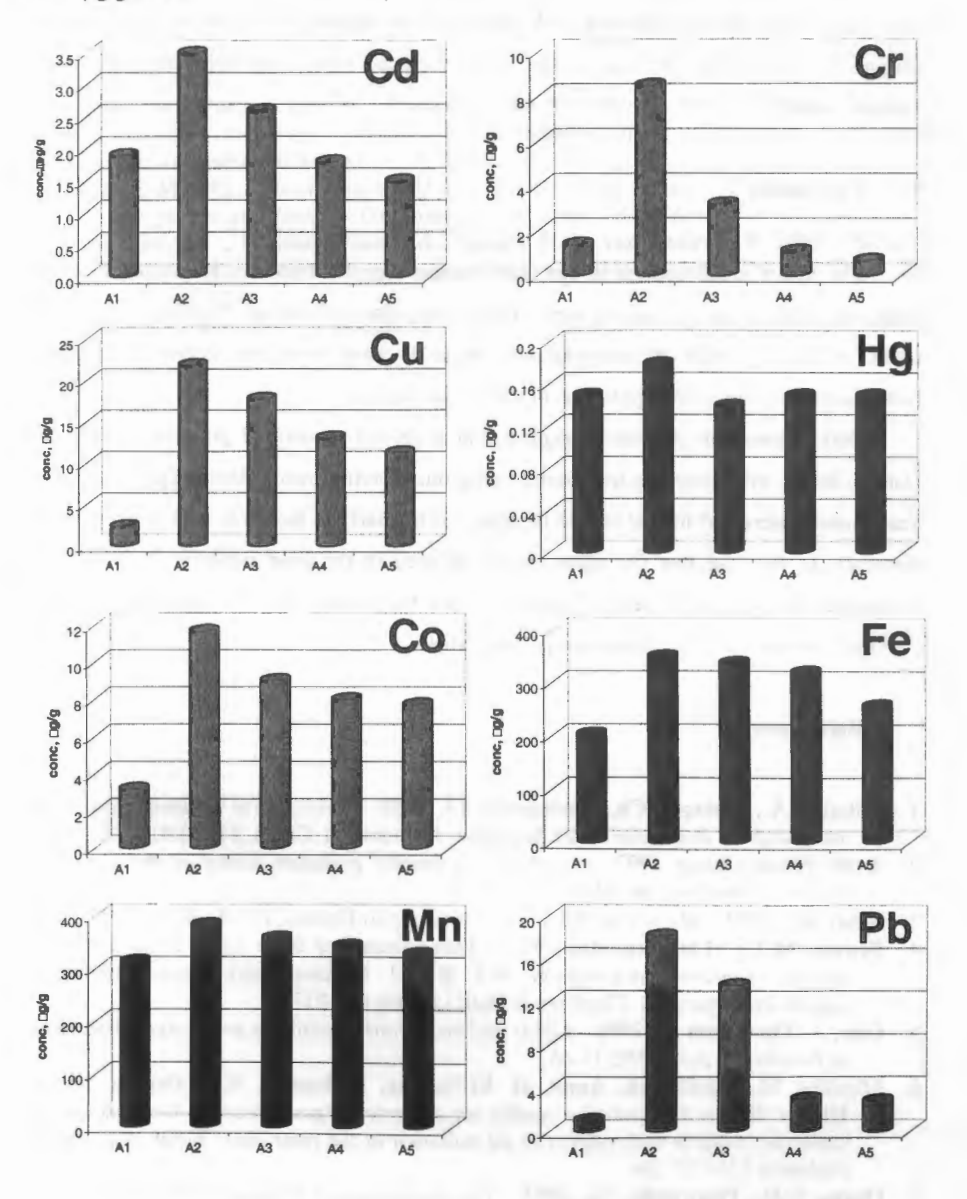


Figure 3. Spatial variation of the heavy metals in sea lettuce

The highest values for the Costinesti and Eforie Sud sampling locations were determined. Large volumes of sea lettuce found on the littoral of the Costinesti and Eforie Sud localities and also the elevated levels of heavy metals indicate high levels of pollution of the two spots. The spatial variations of the most significant heavy metals were examined (Figure 3). The general behavior of the values recorded shows a gradient along the coastal marine current.

#### Conclusion

The heavy metal content in sea lettuce algae samples from the Romanian Black Sea coast was studied for the second time. The results obtained during the present research in terms of heavy metals bio-accumulation of algae show that *Sea lettuce* is a reliable bioindicator for heavy metal pollution of the coastal waters.

Data reported in this study suggest that a greater amount of pollution comes from Danube Basin, with respect to the natural background environment. Marine algae of the Black Sea coastal waters and littoral should be analyzed regularly in Romania with respect of toxic elements. In the case that the algae should be used in the food industry, it should to be monitored the content of heavy metals in such by-products and to establish the proper ("clean") areas in order to collect non polluted algae.

# References

- 1. Mihai, S.A.; Hurtgen Ch., Georgescu, I.I. 1999 Radioactive accumulation in alga samples from Romanian Black Sea coast. J. Radioanal. Chem. 242(2):419-422.
- 2. Avril, Siung-Chang 1997 A review of marine pollution issues in the Caribbean. Environ. Geochem. and Health, 19:44-55.
- 3. Belov AG. 1993 Microtron MT-25. Scientific report Dubna, Д15-93-80: 12-19.
- Brown, M.T.; M.H. Depledge 1998 Determinants of trace metal concentrations in marine organisms. In:Langston, W.J. & M.J. Bebiano (eds), Metal metbolism in aquatic environments. Chapman & Hall, London:185-217.
- 5. Guy, A. Thompson Jr. 1996 Lipids and membrane function in green algae. Biochimica et Biophysica Acta 1302:17-45.
- Mostafa, M.; El-Sheekh, Amal, H. El-Naggar, Mohamed, E.H. Osman, Ayman, Hieder 2000 – Comparative studies on the green algae Chlorela homosphaera and Chlorela vulgaris with respect to oil pollution in the river Nile. Water, Air, and Soil Pollution 124:187-204.
- 7. Oprea, C.D.; Pincovschi, Eu. 2003 The assessment of pollution in the area of Turnu Magurele affected by fertilizers plant. Rom. Rep. in Phys. 55(2):111-115.

- 8. Oprea, C. D.; Mihul Al. 2003 Accumulation of specific pollutants in various media in the area affected by a petrochemical center. Rom. Rep. Phys. 55(2):82-90.
- 9. Oprea, C.D.; Mihul, Al. 2003 R-mode factor analysis applied to the exploration of air pollution in the South of Romania. Rom. Rep. in Phys. 55(2):91-110.
- 10. Oprea Cristiana, Alexandru Mihul, Ioana Ion, Madalina Nedelcu 2007 Danube pollution contributing to eutrophication of the Romanian Black Sea Coast. Horticulture series 50:5p.
- 11. Susan M., Coelho; Jan W., Rijstenbil and Murray T., Brown 2000 Impacts of anthropogenic stresses on the early development stages of seaweeds. J. of Aquatic Ecosys. Stress and Recovery 7:317-333.
- 12. Tuzen, M 2002 Determination of trace metals in sea lettuce (Ulva lactuca) by atomic absorption spectrometry. Fresenius Env. Bulletin, 11(7), 405:409.
- 13. van Netten C., Hoption Cann S.A., Morley D.R., van Netten J.P. 2000 Elemental and radioactive analysis of commercially available seaweed. The Sci. Total. Env., 255, 169, 175.
- 14. Villares R., Puente X., Carballeira A. 2002 Seasonal variation and background levels of heavy metals in two green seaweeds. Env. International, 119, 79, 90.

# **ISINN-16 Program**

Wednesday, 11.06.08

Neutron facilities, UCN

Belushkin A.V. Director of FLNP, Meeting Opening

Masuda Ya. He-II spallation UCN source.

Altarev I., Frei A., Gutsmiedl E., Paul S., Schrekenbach K., Stoepler R. Status of the UCN source project at FRM-II reactor.

Lychagin E. Storage of Very Cold Neutrons in bottles. First experimental results.

UCN, Fundamental properties of the neutron

Nesvizhevsky V. Observation of neutron quantum states in the field of centrifugal forces.

Frank A.I., Geltenbort P., Jentschel M., Kulin G.V., Kustov D.V., Nosov V.G., and Strepetov A.N. Acceleration matter effect in neutron optics: first observation and investigation.

Crawford B.E. On the coincidence measurement in the YAGUAR nn-experiment.

**Furman W.** Current status of the experiment on neutron-neutron scattering at the reactor. YAGUAR, Snezhinsk.

# Fundamental properties of the neutron, fundamental symmetries

Lyuboshitz V.V. and Lyuboshitz V.L. Low-energy scattering of a polarized neutron on a polarized proton.

Skorkin V.M. Dipole shift of neutron scattering resonances.

Vasiliev V.V. Neutron lifetime dependence on decay asymmetry.

Fedorov V. Test experiment for the neutron EDM search by crystal-diffraction method.

**Voronin V.** Diffraction enhancement and new way to measure neutron electric charge and the ratio of inertial to gravitational mass.

Nikolenko V.G., Okunev I.S., Parzhitski S.S., Sinyakov A.V., Tchuvilsky Yu.M. Is it possible to study pt-noninvariant effects with no coincidence scheme using thermal neutron source?

Sedyshev P.V. Measurement of the P-odd asymmetry of  $\gamma$ -quanta from the  $^{10}B(n,\alpha)^7Li^*$  -> Li(g.st.) reaction at heightened frequency of neutron polarization switching.

# Thursday, 12.06.08

#### Nuclear structure

von Egidy T. Nuclear level densities and spin distributions.

Algin E. Level Densities and Thermal Properties of 56-57 Fe.

Zhuravlev B.V., Titarenko N.N., Trykova V.I. Nuclear interaction dynamics in  $^{56}$ Fe( $\alpha$ ,xn) reaction.

Sukhovoj A.M., Furman W.I., Khitrov V.A. Status and problems of experimental study of excited nucleus superfluidity.

Grigoriev Yu.V., Pavlova O.N. Alekseev A.A., Berlev A.I., Koptelov E.A.,

Mezentseva Zh.V. Measurements of neutron transmissions and cross sections on the TOF spectrometers of Moscow meson factory.

Wang Tao Feng, Ranman M. S., Lee Man Woo, Kim Kyung-Sook, Kim Guinyun, Zhu Li Ping, Lee Xia, Xia Hai Hong, Zhou Zu Ying, Oh Young Do, Cho Moo-Hyun, Ko In Soo and Namkung Won Measurement of the Total Neutron Cross-Sections and Resonance Parameters of Natural Molybdenum and Niobium.

Yurevich V.I. Study of neutron emission in high-energy reactions with lead target.

**Zhang G.** Cross section measurement for the  $^{147}$ Sm(n,a) $^{144}$ Nd reaction at E<sub>n</sub> = 5.0 and 6.0 MeV.

Zhang G., Tang G. Measurement of cross sections of the <sup>6</sup>Li(n,t)<sup>4</sup>He reaction from 1.2 to 2.5 MeV.

**Koyumdjieva N.** Evaluation of <sup>232</sup>Th cross sections and self-shielding factors in the unresolved resonance region (4-140) keV.

Panteleev Ts., Borzakov S.B., Panteleev-Simeonova L. On the possibility of experimental measurement of the deformation of nuclei in excited states.

Abdurashitov J.N., Gavrin V.N., Matushko V.L., Shikhin A.A., Vetretenkin I.E., Yants V.E., Nico J.S., Thompson A.K. The development of segmented high resolution fast neutron spectrometer.

#### Parallel session

# Nuclear Analytical Methods in the Life Sciences

**Duliu O.** Instrumental Neutron Activation Analysis Applied to Environmental and Geological Studies.

Frontasyeva M.V. Trace element atmospheric pollution in the Balkans studied by the moss technique, ENAA and AAS.

Gerbish Sh. Insrumental neutron activation analysis for sediments of the central and northern mongolian rivers.

Nyamsuren Baljinnyam, Gerbish Shovoodoi. Possibility of production of some radionuclides using bremsstralung of high energy electrons.

Pantelica A. A retrospective review of JINR – IFIN-HH collaborative projects based on NAA.

Karadzhinova A. Air pollution studies in Bulgaria using moss biomonitoring technique, NAA and AAS.

# Friday, 13.06.08

#### Fission-1, Theory-1

Gagarski A. Detailed study of the effects following from rotation of the scissioning nuclei in ternary fission of <sup>235</sup>U by cold polarized neutrons ("ROT" and "TRI" effects).

Petrov G., Gagarski A., Guseva I., Gonnenwein F. and Bunakov V. TRI- and ROT-effects in ternary fission as a new way of low energy fission dynamics study.

Danilyan G.V. ROT-effect in binary fission.

**Karpechin F.F.** Neutron-resonance mixing through the electron shell in  $(n, \gamma\alpha)$  reaction; Right-left asymmetry of radiation from fission fragments.

Bunakov V.E., Kadmensky S.G. The rotation of the fissioning compound nucleus in reactions induced by polarized neutrons.

#### Theory-2

Bunakov V.E., Kadmensky S.G., Kadmensky S.S. The mechanism of excitation of giant resonances in nuclear fission and t-odd correlations for prescission gamma-quanta. Barabanov A.L. Symmetries and spin-angular correlations in neutron induced reactions: elastic, radiative and fission channels

Nureddin Turkan, Ismail Maras The missing points in calculations of electromagnetic transitions by using the code PHINT: an example on doubly even palladium nuclei.

#### Parallel session

# Nuclear Analytical Methods in the Life Sciences

Zaichick V., Ermidou-Pollet S., Pollet S. Role of nuclear analytical methods in the environmental health elementology.

Zaichik V. Neutron activation analysis of trace element contents in the crowns of human permanent teeth.

Maslov O.D. Multielemental and radionuclides content of moshrooms growing in the forest ecosystem.

**Culicov O.** Instrumental neutron activation analysis: interlaboratory comparison based on short-lived isotopes.

Korokin A.Zh. Assessment air pollutions level in urban areas by using bioindication.

#### Saturday 16.06.08

#### Fission-2

Guseva I.S., Gagarski A.M., Petrov G.A., Sokolov V.E., Krinitsin D.O., Valsky G.V., Vorobyev A.S., Scherbakov O.A. The estimation of scission neutron parameters from n-f and n-n angular correlations in  $^{235}$ U(n<sub>th</sub>,f) reaction.

Vorobyev A. Measurements of angular and energy distributions of prompt neutron emission from thermal induced fission.

Hambsch F.-J. <sup>235</sup>U(n,f) prompt fission neutron spectrum.

Hambsch F.-J., Zeynalov Sh., Oberstedt S., Fabry I. Fission fragment mass dependent prompt neutron emission investigation for resonance neutron induced fission of <sup>235</sup>U and for <sup>252</sup>Cf(sf).

Calviani M. Fission cross section measurements of actinides at CERN n\_TOF facility.

Kamanin D.V. Experimental evidences of clustering in thermal fission of <sup>235</sup>U.

Pyatkov Yu.V., Tjukavkin A.N., Kamanin D.V., Sokol E.A., Kuznetsova E.N. Exotic high neutron multiplicity modes in <sup>252</sup>Cf(sf)

Maslov V.M. Neutron capture by fissile targets.

# Poster session Thursday, 13.06.08

Grosheva E., Zaichick D., Lyapunov S., Schevchenko E. Wave-dispersive X-ray spectrometry of minor and trace element determination in soils of the Khamar-Daban mountain range.

Krmar Miodrag. Neutron induced activity in low background gamma spectroscopy systems. Pankratova Yu., Gundorina S. Identification of metal emissions from adjacent point sources in Northern Norway using moss biomonitoring and factor analysis.

Ostrovnaya T. Air pollution studies in Greece using the passive moss biomonitoring and neutron activation analysis.

A.I. Pantelica, C.R. Badita Low background gamma-ray spectrometry on environmental samples at GammaSpec laboratory of IFIN-HH.

Blagoeva E. I., Gustova M.V., Maslov O. D., Marinova S., Filippov M.F. Heavy metal determination in soils collected near the crossroads in the Plovdiv city, Bulgaria.

<u>Bulavina D.A., Maslov O.D.,</u> Gustova M.V. Determination of microelements and radionuclides in mushrooms of the forest ecosystems.

<u>C. Oprea</u>, O.D. Maslov, M.V. Gustova, A.G. Belov, A.I. Oprea, A. Mihul, V. Loghin, C. Nicolescu, G. Gorghiu. Industrial risk assessment of the toxic and biologic active elements on agriculture crops using nuclear methods and neural network technique.

<u>C. Oprea, A. Velichkov</u>, A.I. Oprea, D.V. Filosofov. The perturbation of the  $\gamma$ - $\gamma$  angular correlations for HFI and biological researches.

A. I. Oprea, C. Oprea, P.V. Sedyshev. Asymmetry effects in the  $^{19}F(p,\alpha)$  reaction.

C. Oprea, M. V.Gustova, O.D. Maslov, A.G. Belov, A.I. Oprea. IGAA and XRF analysis of Sea lettuce algae samples.

M. V.Gustova, C. Oprea, O. D. Maslov, A.I. Oprea, A. G. Belov. Comparison of inorganic chemical constituents of different herbal medicines.

<u>C. Oprea</u>, M.V. Gustova, O. D. Maslov, <u>A. I. Oprea</u>, A. G. Belov. A statistical analysis of regional oil impacts on environment.

Popesku I.V., Stihi C., Gheboianu A., Radulescu C., Belc M., Frontas'eva M.,

Culikov O. Atomic Absolution Spectroscopy and Neutron Activation Analysis methods applied in environmental studies using mosses as bioindicators.

Anicic M. Active moss biomonitoring of trace elements with *sphagnum girgensohnii* moss bags in relation to atmospheric bulk deposition in Belgrade, Serbia.

<u>Krivopustov M.I.</u> Investigation of Spatial Distribution of Fission Rate of Natural Uranium Nuclei in the Blanket of Elektro - Nuclear Setup "Energy plus Transmutation" at Nuclotron Proton Beam at Energies 1.5 GeV.

<u>Krivopustov M.I.</u> Topics on Creation of Accelerator Driven Systems and Investigation of Transmutation of Radioactive Waste of Nuclear Energetic at Synchrophasotron and Nuclotron Protons and Deuterons Beams (10-years of Dubna Experience).

Voronin V. Neutron volumetric test of a high perfect crystal quality.

Matsumiya R. Development of the He-II spallation UCN cryostat and UCN Storage Experiment.

Roccia. R&D on Hg magnetometry for the nEDM experiment at PSI.

Okunev I.S., Parzhitski S.S., Sinyakov A.V., Tchuvilsky Yu.M., Study of pt-noninvariant effects with radioactive sources

Sukhovoj A.M., Khitrov V.A. Main parameters of the gamma-decay process and the property of nucleus <sup>174</sup>Yb from the radiative capture of slow neutrons.

**Sukhovoj A.M., Khitrov V.A.** Distribution of parameters of the primary γ-transition intensities following resonance neutron capture and some properties of the <sup>157,159</sup>Gd compound nuclei.

Khafizov R.U., Tolokonnikov S.V., Solovei V.A., Kolhidashvili M.R. Status of the experiments on radiative branch of decay.

Kim G.N., Khandaker M. U., Kim K., Lee M. W., Kim K. S., Cho Y.S., and Lee Y.O. Production cross section of residual radionuclides by proton-induced reactions on <sup>nat</sup>Cd and <sup>nat</sup>Fe.

Soroko Z.N., Sukhoruchkin S.I., Sukhoruchkin D.S. Compilation of neutron resonance parameters NRF-3.

Alexandrov Yu. A., Oprea C., Oprea A.I. Determination of n-e length from neutron diffraction on a tungsten isotopic mixture in magnetic field.

Mitsyna L.V., Nikolenko V.G., Parzhitski S.S., Popov A.B., Samosvat G.S. Neutronelectron scattering length extraction from the neutron diffraction data measured on noble gases.

Tyukavkin A. Measuring of the fragment nuclear charges at the MINI-FOBOS spectrometer. Svirikhin A. Neutron barell" at the focal plane of the VASSILISSA separator.

Sedysheva M. The systematic study of (n,p) cross-sections for 18 and 20 MeV neutron energy.

A. I. Oprea, C. Oprea, P.V. Sedyshev. Asymmetry effects in the  $F(p,\alpha)$  reaction. Oprea I.A. A Monte Carlo Simulation of the Asymmetry Coefficients Measurements in the (n,p) reaction.

Oprea I.A. Statistical Model Evaluation of the cross section in  $(n, \alpha)$  reaction on  ${}^{\alpha}$ Zn.

#### Научное издание

# NEUTRON SPECTROSCOPY, NUCLEAR STRUCTURE, RELATED TOPICS XVI International Seminar on Interaction of Neutrons with Nuclei Proceedings of the Seminar

# НЕЙТРОННАЯ СПЕКТРОСКОПИЯ, СТРУКТУРА ЯДРА И СВЯЗАННЫЕ ВОПРОСЫ

XVI Международный семинар по взаимодействию нейтронов с ядрами  $\mathit{Труды}$  семинара

Ответственный за подготовку сборника к печати А. М. Суховой.

Сборник отпечатан методом прямого репродуцирования с оригиналов, предоставленных оргкомитетом.

E3-2009-33

Подписано в печать 13.04.2008. Формат 60 × 90/16. Бумага офсетная. Печать офсетная. Усл. печ. л. 27,13. Уч.-изд. л. 51,04. Тираж 180 экз. Заказ № 56533.

Издательский отдел Объединенного института ядерных исследований 141980, г. Дубна, Московская обл., ул. Жолио-Кюри, 6. E-mail: publish@jinr.ru www.jinr.ru/publish/